

# **Small hydroxy-9,10-anthraquinones and their complexes as effective anticancer drugs**

**Thesis submitted for the degree of  
Doctor of Philosophy (Science)  
of Jadavpur University**

**Under the supervision of  
Prof. Saurabh Das**

**By  
MOULI SAHA**



**Department of Chemistry  
Jadavpur University  
Kolkata - 700 032  
India**

**2022**



যাদবপুর বিশ্ববিদ্যালয়  
কলকাতা-৭০০ ০৩২, ভারত



\*JADAVPUR UNIVERSITY  
KOLKATA-700032, INDIA

FACULTY OF SCIENCE : DEPARTMENT OF CHEMISTRY : INORGANIC SECTION

### CERTIFICATE FROM THE SUPERVISOR

This is to certify that the thesis entitled “**Small hydroxy-9,10-anthraquinones and their complexes as effective anticancer drugs**” submitted by Ms. Mouli Saha who got her name registered on *14<sup>th</sup> October, 2015* for the award of Ph.D.(Science) degree of Jadavpur University, is absolutely based upon her own work done under my supervision at the *Department of Chemistry, Jadavpur University, Kolkata-700032* and that neither this thesis nor any part of it has been submitted for either any degree/diploma or any other academic award anywhere before.

*Saurabh Das* 07/06/2022

(Signature of Supervisor and date with official seal)

*Dr. Saurabh Das*

Professor

Department of Chemistry  
Jadavpur University  
Kolkata - 700 032

\*Established on and from 24th December, 1955 vide Notification No. 10986-Edn/IU-42/55 dated 6th December, 1955 under Jadavpur University Act, 1955 (West Bengal Act XXXIII of 1955) followed by Jadavpur University Act, 1981 (West Bengal Act XXIV of 1981)

দূরভাষ : ২৪১৪-৬৬৬৬/৬১২৪/৬৬৬৬/৬৪২৪/৬৪৪০ প্রসারণ : ২৪৬২

Website : www.jadavpur.edu

Phone : 2414-6666/6194/6643/6495/6443 Extn. 2469

দূরবার্তা : (৯১)-০৩৩-২৪১৪-৬৪১৪/২৪১০-৭১২১/২৪১৪-৬২১০

E-mail : registrar@admin.jdvu.ac.in

Fax : (91)-033-2414-6414/2413-7121/2414-6210





**JADAVPUR UNIVERSITY**  
KOLKATA-700 032  
MARK SHEET

NO. PHCW/1701/

(For Ph.D Course Work)

Results of the	PH.D. COURSE WORK EXAMINATION, 2016
In	SCIENCE held in NOVEMBER, 2016
Name	MOULI SAHA
Examination Roll No.	PHDCHEM16236

Course Name / Subject	Credit Hr.(c <sub>i</sub> )	Marks	Grade
COMPULSORY UNITS :: EX/CHEM/PHD/A & B RESEARCH METHODOLOGY & REVIEW OF RESEARCH WORK	4	81	A
ELECTIVE UNITS :: EX/CHEM/PHD/I-1 :: APPLICATION OF SPECTROSCOPIC STUDIES IN CHEMICAL RESEARCH EX/CHEM/PHD/I-2 :: MATERIALS, CATELYSES & ELECTROCHEMICAL STUDIES EX/CHEM/PHD/P-3 :: BIOPHYSICAL CHEMISTRY & SURFACE CHEMISTRY EX/CHEM/PHD/I-4 :: SINGLE CRYSTAL X-RAY STR. SUPRAMOLECULAR CHEM.& DFT COMPUTN.	4	73	B


Total Marks : 154 (out of 200 )

SGPA: 9.50

Remarks: P

Prepared by :  Checked by : 

Date of issue : 07-02-2017

  
Controller of Examinations



## DECLARATION

I do, hereby declare, that the work embodied in the thesis entitled “**Small hydroxy-9,10-anthraquinones and their complexes as effective anticancer drugs**” submitted for the award of Doctor of Philosophy (Ph. D.) in Science is the completion of studies carried out by me under the supervision of Dr. Saurabh Das at the Department of Chemistry, Jadavpur University. The work is original and has not been submitted in part or full for either any equivalent degree/diploma or any other academic award elsewhere.

In keeping with the general practice of reporting scientific observations, due acknowledgements have been made wherever the work described was done, taking active assistance of a laboratory that has an expertise in that particular field of investigation.

Mouli Saha

Research Fellow

Department of Chemistry

Jadavpur University

Kolkata-700032

India





**Dedicated to my  
parents**



## **Acknowledgement**

First and foremost, praises to the Almighty for showering His blessings throughout my journey in this doctoral programme. This journey is truly a life-changing experience which would not have been possible without the support and guidance I received from many people.

I would like to express my heartfelt gratitude to my Ph. D supervisor Prof. Saurabh Das for his magnanimous support and expert guidance all through the period of my research. His knowledge and vision in the specific area of the research work inspired me during discussions that guided me to achieve my goal. I am grateful to him because without his sincere interest and dynamic supervision, this would not have been possible.

I am especially thankful to Prof. Muktipada Sinha, Head, Department of Education, Jadavpur University who always stood by me during ups and downs of my research pursuit and motivated me all along. His continuous encouragement, constructive suggestions and mental support made this journey a lot easier than what it could have possibly been.

I acknowledge the support of UGC for the generous financial aid in terms of 'Rajiv Gandhi National fellowship' for conducting this research uninterruptedly.

I also wish to express my gratitude to the present Head, Department of Chemistry, Jadavpur University, Prof. Swapan Kumar Bhattacharyya and all former HoDs, during whose tenure I performed this work, for the continuous support I received from them, in times of need.

I convey my gratitude to Prof. Subenoy Chakraborty, Dean, Faculty Council of Science and all members of staff at the faculty office for the cooperation I received from them.

No words are enough to acknowledge the help received from Prof. Sanjay Kumar of the Department of Physics, Jadavpur University with regard to solving the structures of

complexes prepared by me. I wish to sincerely thank his research scholar Dr. Soumen Singha for helping me evaluate the structures.

I would be failing in my duty if I do not convey my gratitude to Prof. Parimal Karmakar of the Department of Life Science and Biotechnology, Jadavpur University for his help regarding studies performed on different cell lines. I am thankful to his research scholars Swagata Majumder, Deblina Ghosh and Swarupa Sarkar for their cooperation in this regard.

I am grateful to Prof. Shouvik Chattopadhyay of the Department of Chemistry for his constant support and encouragement during my research work. I received valuable suggestions from him and support with regard to instrumental facilities.

Special thanks are also due to Prof. Sujoy Baitalik, for kindly providing me the near-infrared spectrum of the prepared complexes, to Prof. Tapan Kumar Mondal and Prof. Mahammad Ali, all from the Department of Chemistry, Jadavpur University for the support received related to mass spectrometry analysis. I am grateful to their respective scholars also in this regard.

I express my gratitude and respect to all my teachers at the Department of Chemistry, Jadavpur University, who taught me during my graduation and post-graduation days and who directly or indirectly provided me inspiration, valuable suggestions during the course of this study.

I am extremely thankful to Chandika Prasad Ghosal, who has given me unstinting support in writing my thesis, whenever needed.

I am grateful to lab seniors, Dr. Piyal Das, Dr. Ramesh Chandra Santra, Dr. Durba Ganguly, Dr. Bitapi Mandal for their encouraging and motivating guidance.

Heartfelt thanks are due to Mr. Tanmay Saha and Ms. Promita Nandy with whom I worked in the laboratory and their company will always be remembered. I wish to also thank Dr. Sourav Roy who helped me a lot during my research work.

Heartfelt thanks go out to Liton Mallick, Suraj Bhattacharyya, Wasim Akram Khan, Bijoy Krishna Panda and Krishna Sarkar whose constant love and support kept my spirit high, motivated me to remain confident and achieve my goal.

I am grateful to all staff members of the “Research Section” and “Ph D cell” of our University, non-teaching staff members of the Department of Chemistry, Jadavpur University for the cooperation they extended to me.

Last but not least, I am grateful to my parents Mr. Shyamapada Saha and Mrs. Sutapa Saha for their unconditional loving support all along my academic career. Their moral and spiritual support enabled me to pursue this study. I also express my thanks to my beloved sister Ms. Soujanya Saha for her support and prayers.

Date:

Place:

Mouli Saha  
Research Fellow  
Department of Chemistry  
Jadavpur University  
Kolkata-700032  
India



## List of Abbreviations used

DHA	:	Alizarin or QHH* or 1, 2-dihydroxy-9,10-anthraquinone
Mn(QH) <sub>2</sub>	:	Mn <sup>II</sup> complex of Alizarin
CA	:	Carminic Acid
XRD	:	X-Ray Diffraction
DFT	:	Density Functional Theory
HOMO	:	Highest Occupied Molecular Orbital
LUMO	:	Lowest Unoccupied Molecular Orbital
MLCT	:	Metal to ligand charge transfer
LLCT	:	Ligand to ligand charge transfer
UV-Vis	:	Ultraviolet-Visible Spectroscopy
IR	:	Infrared spectroscopy
FTIR	:	Fourier-transform infrared spectroscopy
MS	:	Mass spectrometry
CV	:	Cyclic Voltammetry
DMF	:	Dimethyl formamide
DMSO	:	Dimethyl sulfoxide
TBAB	:	Tetra n-butyl ammonium bromide
DNA	:	Deoxyribonucleic acid
RNA	:	Ribonucleic Acid
c t DNA	:	Calf thymus DNA
TRIS	:	2-Amino-2-hydroxymethyl-propane-1,3-diol
B-H equation	:	Benesi-Hildebrand equation

EtBr	:	Ethidium bromide
HPLC	:	High Performance Liquid Chromatography
ROS	:	Reactive Oxygen Species
MPTP	:	Mitochondrial permeability transition pore
DMPO	:	5, 5-dimethyl-1-pyrroline-N-oxide
DHE	:	Dihydroethidium
MTT	:	3-(4, 5-dimethylthiazol-2-yl)-2,5-diphenyltetrazolium bromide
NADH	:	Nicotinamide Adenine Dinucleotide-Hydrogen
SOD	:	Superoxide Dismutase
NADPH	:	Nicotinamide adenine dinucleotide phosphate
ADP	:	Adenosine diphosphate
ATP	:	Adenosine triphosphate
HBSS	:	Hanks balanced salt solution
NAC	:	N-acetylcysteine
DCFDA	:	2',7' -dichlorofluorescein diacetate
DCF	:	Dihydrodichlorofluorescein



## Abstract

Cancer is a leading cause of death the world over and is currently on the rise. To counter the growing menace, chemotherapy, radiotherapy in combination with surgery are used as modes of treatment. Anthracyclines are chemotherapeutic drugs used against leukemia, lymphoma, cancer of the breast, the bladder, endometrium, the lungs, the ovaries, stomach, thyroid and in certain sarcomas. They impart cytotoxicity in multiple pathways of which that involving the presence and/or generation of ROS is significant. They are good DNA binding agents capable of intercalating DNA and deforming its three-dimensional structure. Drugs of this family also inhibit replication of DNA by interfering with the activity of DNA topoisomerase, pivotal in damaging cells and leading to their death. However, a major limitation of anthracyclines is their severe and chronic toxicity, significant being cardiotoxicity. Hydroxy-9,10-anthraquinones that form the core of anthracyclines are reduced to semiquinone by electrons being assisted by several enzymes. This results in a sequence of reactions culminating in the formation of reactive oxygen species (ROS) like the superoxide radical anion, hydrogen peroxide etc. ROS produced have beneficial activity owing to its role in cell killing. At the same time, they are responsible for toxic side effects, cardiotoxicity as mentioned already being of a serious concern. Another major problem with anthracyclines is their high cost. Through this study, an attempt was made to see if hydroxy-9, 10-anthraquinones, the core of anthracyclines, or their modified forms that are less costly could become effective substitutes of anthracyclines. This would then benefit many economically challenged communities. Anthraquinone being the functional unit in anthracyclines or in their analogues, therefore like in case of anthracyclines, the hydroxy-9,10-anthraquinones would also be cardiotoxic, unless of course ROS is regulated. Hence, modification of anthracyclines or their simpler analogues is important and one way to modify them would be to form metal complexes. Studies have

earlier shown complexes of this category of drugs are able to modulate formation of semiquinone which in turn regulate generation of reactive oxygen species (ROS).

In the research carried out, simpler analogues of anthracyclines like alizarin and carminic acid were chosen.  $Mn^{II}$  complexes of alizarin and carminic acid and  $Co^{II}/Co^{III}$  complexes of alizarin were prepared and characterized to investigate their ability to either modulate formation of semiquinone or realize their ability to bind to DNA against that known for standard anthracyclines or hydroxy-9, 10-anthraquinones. In the absence of single crystals, that are rare for the hydroxy-9, 10-anthraquinone ligands owing to planarity, structures were elucidated by computational techniques. Both complexes and parent molecules were investigated for their ability to affect nucleic acid bases or DNA in a free radical pathway. Experiments were also performed on both types of cell lines (carcinoma and normal) using hydroxy-9, 10-anthraquinones and their complexes.

Interaction of complexes with calf thymus DNA under varying conditions of ionic strength, pH and temperature reveal complexes address aspects of limitations of hydroxy-9,10-anthraquinones if compared with anthracyclines. The studies reflect on the requirements for a drug that is relatively simple in comparison to anthracyclines for use in cancer chemotherapy. For example, an increased affinity of the complex towards DNA and the fact that its binding constant values do not decrease with either an increase in pH or decrease in ionic strength of the medium are positive aspects of complex formation. This is unlike simpler analogues of anthracyclines where a comparatively lower binding constant value under different conditions was reported earlier, a fact that would seriously affect drug action on cancer patients if one were to use simpler analogues. Since fluctuation of pH in body fluids of cancer patients is expected owing to use of various drugs, coupled with varied approaches employed in treating cancer patients, the findings on DNA binding for complexes were an important aspect of this investigation. An attempt was also made to realize the influence of pKa values of simpler

analogues (alizarin and purpurin) on the evaluation of contributions of different forms of compounds used towards overall binding to DNA that has substantial medicinal applications particularly if the complex interferes with cancer cells through binding with DNA.

Another important aspect of the study was to use the prepared  $Mn^{II}$  and  $Co^{II}$  complexes of hydroxy-9, 10-anthraquinones to generate reactive species electrochemically by either one-electron or two electron reduction under aerated or de-aerated conditions to find out what happens when similar species are generated on anthracyclines that are used as drugs following reduction by any electron donating group present in a biological electron-transport chain. Behavior of generated reduced species in solution, their stability etc., were studied but more importantly what was followed is interaction of such electrochemically generated species with nucleic acid bases or calf thymus DNA to have an idea of the extent of damage such one-electron reduced species of quinone (semiquinone) or two-electron reduced species (quinone-dianion) might have on biological targets. Such electrochemical reduction experiments were achieved by maintaining a glassy carbon electrode at a constant potential (the reduction potential of the compound under investigation), maintaining either nucleic acid bases or calf thymus DNA in the immediate vicinity of such generation of reduced species. Such studies help to throw light on the mechanism by which compounds affect DNA. It was seen hydroxy-9,10-anthraquinones were generally more effective in causing damage to nucleic acid bases or to DNA in the free radical pathway and that under above mentioned conditions complexes were at a disadvantage. However, interesting aspect is that if all factors are considered together, complexes were more effective than hydroxy-9,10-anthraquinones from which they were prepared, on different carcinoma cell lines. Hence, despite being at a disadvantage in the free radical pathway, owing to decreased semiquinone formation, confirmed by decreased semiquinone generation in transfer of electrons from NADH to molecular oxygen in NADH dehydrogenase assay, complexes performed better. This means

complexes have other attributes that make up for a loss in activity in the free radical pathway. Hence, with an expected check on cardiotoxicity and that complexes do not ultimately compromise on drug efficacy, observed through experiments on HeLa, Hep G2, SIHA and PC3 (carcinoma cells) and WI 38 lung fibroblast normal cells, it may be said metal complexes of hydroxy-9,10-anthraquinones may be considered viable alternatives of anthracyclines as anticancer agents.

Another important aspect of the study was the interaction of chosen compounds and their complexes with ROS present within cells. This was studied on different cell lines using the H<sub>2</sub>DCFDA assay. It was found complexes exhibit increased ROS within a particular cell line in comparison to hydroxy-9, 10-anthraquinones that would be utilised to kill cells i.e. show greater cytotoxic activity in comparison to hydroxy-9, 10-anthraquinones. In a way, the study on “ROS present within cells” helped in explaining findings of the MTT assay. Performance on several cancer cells and on normal WI 38 lung fibroblast cells revealed complexes were more effective on carcinoma cells than on normal cells, an important finding with regard to complex formation of hydroxy-9, 10-anthraquinones.

Last, but certainly not least, the aspect of cost would also be addressed through this study since complexes are far less costly than anthracycline drugs that are in use.

## Content

	Page No.
Chapter 1: Introduction	1-10
Chapter 2: A review on anthracycline based anticancer agents and the simpler hydroxy-9, 10-anthraquinones as promising anticancer agents	11-38
Chapter 3: Reactive Oxygen Species and their measurement	39-56
Chapter 4: Chemical modification of nucleic acid bases and DNA	57-80
Chapter 5: Genesis and Scope	81-92
Chapter 6: Experimental: Materials and Methods	93-118
Chapter 7: Importance of pKa in an analysis of the interaction of compounds with DNA	119-138
Chapter 8: Characterization of a Mn(II) complex of alizarin suggests attributes, that explain superior anticancer activity: A comparison with anthracycline antibiotics	139-194
Chapter 9: A Cobalt <sup>II</sup> /Cobalt <sup>III</sup> complex of alizarin analyzed from the stand point of DNA binding, ROS generation and anticancer drug prospecting	195-238
Chapter 10: Comparing chemical, biophysical and biochemical attributes of anthracyclines as anticancer agents using carminic acid and its Mn <sup>II</sup> complex	239-264
Chapter 11: Free radical induced activity of alizarin and its Mn <sup>II</sup> complex on biological targets through <i>in situ</i> electrochemical generation of semiquinone	265-288
Chapter 12: Conclusion	289-296



# CHAPTER 1

## Introduction





The progress of civilization has brought along with it a series of developments that are not only unhealthy but disastrous at times. The pollution of earth, water and air as consequences of our striving for a better life invites threats to our constant search for well-being. In general, we are exposed to chemicals present in the environment virtually everywhere, at home, at the workplace, during transportation. Chemicals have acute as well as chronic effects which could be prevented if they are properly stored or handled. The process of deforestation to accommodate a growing population, the pollution of rivers with industrial wastes, the use of pesticides for better agricultural produce, use of chemicals as preservatives in food – all these practices are apparently considered to have beneficial effects on human life. They do, but at the same time they take their toll on human health. Similarly, technological development and a sense of urgency in modern times have joined hands to snatch away leisure, recreation and interpersonal communications from our daily life. Work pressure and a growing demand from the external world are giving rise to tension, anxiety and stress in our lives. Consequently, people are becoming abject victims of depression, loneliness and various kinds of mental disorders. Thus, the yearning for more and more material comfort is gradually landing us in situations where people are shattered equally in body and mind.

The growth of the deadly disease cancer is the fallout of this predicament. We hardly bother to take into account the fact that we ourselves are responsible for our health-related problems. For example, a rise in cancer cases is a consequence of the use of nitrates in food.<sup>1,2</sup> The large-scale use of chlorofluorocarbons is a reason why the ozone layer is depleted causing a rise in UV-radiation at the ground level that could lead to skin cancer, cataract in the eyes and also cause harm to the immune system in both humans and animals.<sup>3,4</sup> Thus, it has become a challenging task for us to put up a sustained fight for the prevention of cancer. It is a fast-growing disease that destroys a person both physically and economically. People from low income families, find it extremely difficult to carry on with the prolonged expensive

## ***Chapter 1: Introduction***

---

treatment that this dreadful disease has to offer. According to a report, cases of cancer in India, increased at an average annual rate of 1.1-2 per cent from 2010-2019. Deaths due to cancer went up at an average rate of 0.1-1 per cent in the same period.<sup>5,6</sup>

Over the past few decades, both industry as well as a large section of the population is becoming aware of the damaging effects of some of the facts mentioned above. A lot of effort is on all over the world to enhance our knowledge on cancer. Effective methods of controlling the disease have been achieved in the area of drug development. So far, chemotherapy and radiotherapy combined with surgery has proved to be the most significant strategy of treating the disease. However almost all chemotherapeutic drugs have an associated short-term or long-term toxicity for which the patient suffers from loss of hair, nausea, vomiting, irregular heartbeats and several forms of sexual dysfunctions.<sup>7-9</sup> Sometimes, toxic side effects become so severe that it overwhelms the drug's efficacy and the patient eventually dies not due to the disease but for adverse or toxic side effects. Hence, there is a growing need to find other ways of treating cancer that takes care of such toxic side effects to a reasonable extent without compromising much on efficacy. Platinum drugs (*cis-platin*) are important chemotherapeutic agents known for their established anti-cancer activity.<sup>10-12</sup> Similarly, anthracyclines are another prominent class of chemotherapeutic agents. Daunorubicin, the first of the anthracyclines developed led to others of that family that includes doxorubicin (adriamycin), epirubicin, idarubicin, amrubicin, aclarubicin and other analogues.<sup>13-15</sup> Anthracyclines form strong intercalation complexes with DNA which inhibit DNA and RNA synthesis; a dominant mode of their anticancer activity. Anthracyclines are also reduced enzymatically to semiquinone that donates an electron to molecular oxygen reducing it to superoxide radical anion ( $O_2^{\bullet-}$ ) with the semiquinone being oxidized to the original quinone.<sup>16</sup> Thus the redox cycle leads to formation of reactive oxygen

species (ROS) that are beneficial but also responsible for toxic side effects. Cardiotoxicity is the most common and relevant form of toxicity imparted by anthracyclines which limit their effectiveness.<sup>17,18</sup> The semiquinone radical initiates release of iron from the iron-storage protein ferritin that leads to an increase in free intracellular Fe<sup>2+</sup> and subsequent formation of hydroxyl radicals. This can initiate lipid peroxidation which is associated with anthracycline induced cardiotoxicity.<sup>19,20</sup> Such complications are increasingly becoming a global problem as they most often take away the good aspects of the drug. To prevent life-threatening cardiotoxicity, a careful monitoring of the generation of reactive oxygen species has become extremely essential so that cardiotoxic side effects are reduced and therapeutic efficacy not compromised. Literature says, anthracyclines have a strong chelating tendency towards metal centres that enable them to be more promising anticancer agents having efficacy better than free anthracyclines.<sup>21</sup> Formation of metal complexes of anthracyclines greatly influences the toxicity imparted by them.<sup>22,23</sup> Upon complex formation, the anthraquinone moiety is significantly modified and this decreases the toxicity of the drugs considerably. They not only have electron acceptor properties, but are also capable of participating in redox reactions, particularly in case of iron and copper, transforming into a more reactive state. Since metal ions are good binding agents for cellular target DNA, complex formation of such molecules result in better DNA targeting. At the same time complexes are less cardiotoxic.<sup>24,25</sup>

Another aspect related to anthracyclines that require serious consideration particularly with regard to the use of drugs in developing and underdeveloped countries is their high cost.<sup>26,27</sup>

If simpler analogues like hydroxy-9,10-anthraquinones (the core of anthracyclines), the unit responsible for anticancer activity, are considered then the advantage of using simple molecules could be realized. This would make the drugs less costly. These could be better penetrating agents as well, able to cross cell membrane barriers easily; an important criteria for effective cellular uptake.<sup>28</sup> It would therefore be important to see if hydroxy-9,10-

## ***Chapter 1: Introduction***

---

anthraquinones and their metal complexes participate in electron transfer processes in the same way as reported for anthracyclines.<sup>29,30</sup>

A review on anthracycline based anticancer drugs and their simpler analogues (hydroxy-9,10-anthraquinones) is provided in **Chapter 2**. Generation of reactive oxygen species (ROS) plays a vital role during treatment with anticancer drugs. Hence, reactive oxygen species and some of the techniques that are used for their measurement is reviewed in **Chapter 3**. **Chapter 4** deals with the aspect of nucleic acid base and DNA damage using various stimuli in the absence and presence of sensitizer molecules. Pyrimidine bases are generally used in studies in aqueous solution for reasons of solubility to act as model biological targets to enable the monitoring of base damage. Chemical modifications of both pyrimidine and purine bases are discussed in **Chapter 4**.

### **References:**

- [1] M. Karwowska, A. Kononiuk. 2020. Nitrates/Nitrites in Food-Risk for Nitrosative Stress and Benefits. *Antioxidants (Basel)*. 9, 241.
- [2] P. J. Weyer, J. R. Cerhan, B. C. Kross, G. R. Hallberg, J. Kantamneni, G. Breuer, C. F. Lynch. 2001. Municipal drinking water nitrate level and cancer risk in older women: The Iowa Women's Health Study. *Epidemiology*. 12:327–338.
- [3] T. Sivasakthivel, K. K. S. K. Reddy. 2011. Ozone Layer Depletion and Its Effects: A Review. *International Journal of Environmental Science and Development*. 2
- [4] J. W. Eaton. 1995. UV-Mediated Cataractogenesis: A Radical Perspective. *Doc Ophthalmol*. 88: 233-242.

- [5] S. Rajpal, A. Kumar, W. Joe. 2018. Economic burden of cancer in India: Evidence from cross-sectional nationally representative household survey, 2014. *PloS one*. <https://doi.org/10.1371/journal.pone.0193320>
- [6] R. L. Siegel, K. D. Miller, A. Jemal. 2019. CA: A Cancer Journal for Clinicians. *Cancer statistics*. 69: 7–34.
- [7] S. Boussios, G. Pentheroudakis, K. Katsanos, N. Pavlidis. 2012. Systemic treatment-induced gastrointestinal toxicity: incidence, clinical presentation and management. *Ann Gastroenterol*. 25:106-118.
- [8] N. Gegechkori, L. Haines, J. J. Lin. 2017. Long-Term and Latent Side Effects of Specific Cancer Types. *Med Clin North Am*. 101:1053-1073.
- [9] A. Pitman, S. Suleman, N. Hyde, A. Hodgkiss. 2018. Depression and anxiety in patients with cancer. *BMJ*. doi:10.1136/bmj.k1415
- [10] S. Dasari, P. B. Tchounwou. 2014. Cisplatin in cancer therapy: molecular mechanisms of action. *European journal of pharmacology*. 740:64–378.
- [11] A. Kozubík. 2008. Novel Anticancer Platinum(IV) Complexes with Adamantylamine: their efficiency and innovative chemotherapy strategies modifying lipid metabolism. *Metal-Based Drugs*. 1–15. doi:10.1155/2008/417897
- [12] R. G. Kenny, C. J. Marmion. 2019. Enhancing the therapeutic potential of Platinum-based anticancer agents by incorporating clinically approved drugs as ligands. *Metal-based Anticancer Agents*. 1-30. DOI: 10.1039/9781788016452-00001.
- [13] G. Laurent, J.P. Jaffrézou. 2001. Signaling pathways activated by daunorubicin. *Blood*. 98:913-924.

- [14] A. Di Marco, M. Gaetani and B. M. Scarpinato. 1969. Adriamycin (NSC-123,127): a new antibiotic with antitumoral activity. *Cancer Chemother. Rep.* 53:33-37.
- [15] D. Mavroudis, A. Alexopoulos, N. Ziras, N. Malamos, C. Kouroussis, S. Kakolyris, S. Agelaki, K. Kalbakis, N. Tsavaris, A. Potamianou, G. Rigatos, V. Georgoulas. 2000. Front-line treatment of advanced breast cancer with docetaxel and epirubicin: A multicenter phase II study. *Annals of Oncology* 11: 1249-1254.
- [16] I. Müller, D. Niethammer, G. Bruchelt. 1998. Anthracycline-derived chemotherapeutics in apoptosis and free radical cytotoxicity (Review). *Int J Mol Med.* 1:491-494.
- [17] T. Šimunek, M. Štirba, O. Popelová, M. Adamcová, R. Hrdina, V. Geršl. 2009. Anthracycline-induced cardiotoxicity: Overview of studies examining the roles of oxidative stress and free cellular iron. *Pharmacol Rep.* 61:154–171.
- [18] P. Angsutararux, S. Luanpitpong, and S. Issaragrisil. 2015. Chemotherapy-induced cardiotoxicity: Overview of the roles of oxidative stress. *Oxid Med Cell Longev.* 2015:795602. doi: 10.1155/2015/795602.
- [19] M. S. Horenstein, R. S. Vander Heide, T. J. L'Ecuyer. 2000. Molecular basis of anthracycline-induced cardiotoxicity and its prevention. *Mol Genet Metab.* 71:436-44.
- [20] S. Hrelia, D. Fiorentini, T. Maraldi, C. Angeloni, A. Bordoni, P. L. Biagi, G. Hakim. 2002. Doxorubicin induces early lipid peroxidation associated with changes in glucose transport in cultured cardiomyocytes. *Biochimica et Biophysica Acta (BBA) - Biomembranes.* 1567: 150-156.
- [21] A. Jabłońska-Trypuć, G. Świdorski, R. Krętowski, W. Lewandowski. 2017. Newly synthesized Doxorubicin complexes with selected metals-synthesis, structure and anti-breast cancer activity. *Molecules (Basel, Switzerland).* 22:1106.

- [22] C. Santini, M. Pellei, V. Gandin, M. Porchia, F. Tisato, C. Marzano. 2014. Advances in copper complexes as anticancer agents. *Chem. Rev.* 114: 815–862.
- [23] H. Beraldo, A. Garnier-Suillerot, L. Tosi, F. Lavelle. 1985. Iron(III)-Adriamycin and Iron (III)-Daunorubicin complexes: physicochemical characteristics, interaction with DNA, and antitumor activity. *Biochemistry.* 24: 284-289.
- [24] V. A. Rao. 2013. Iron chelators with topoisomerase-inhibitory activity and their anticancer applications. *Antioxidants & Redox Signaling.* 18: 955-930.
- [25] M. M. L. Fiallo, A. Garnier-Suillerot, B. Matzanke, H. Kozlowski. 1999. How Fe<sup>3+</sup> binds anthracycline anti tumour compounds: The myth and the reality of a chemical sphinx. *Journal of Inorganic Biochemistry.* 75: 105–115.
- [26] M. Siddiqui, S. V. Rajkumar. 2012. The high cost of cancer drugs and what we can do about it. *Mayo Clinic proceedings.* 87:935–943.
- [27] S. Dewilde, K. Carroll, E. Nivellet. 2020. Evaluation of the cost-effectiveness of dexrazoxane for the prevention of anthracycline-related cardiotoxicity in children with sarcoma and haematologic malignancies: a European perspective. *Cost Eff Resour Alloc.* <https://doi.org/10.1186/s12962-020-0205-4>
- [28] N. J. Yang, M. J. Hinner. 2015. Getting across the cell membrane: an overview for small molecules, peptides, and proteins. *Methods Mol Biol.* 1266:29-53.
- [29] C. A. Tsipis, E. G. Bakalbassi, V. P. Papageorgiou, M. N. Bakola-Christianopo. 1982. Structure and bonding of mononuclear and homobinuclear chelates of some divalent metal ions with the ligand 1,8-dihydroxyanthraquinone. *Can. J. Chem.* 60:2477- 2483.

## *Chapter 1: Introduction*

---

[30] L. D. Pettit, J. Ueda, E. Morier-Teissier, N. Helbecque, J. L. Bernier, J. P. Henichart, H. Kozłowski. The coordination of copper(II) to 1-hydroxy-4-(glycyl-histidyl-lysine) – anthraquinone; a synthetic model of anthraquinone anti-cancer drugs. *Journal of Inorganic Biochemistry*. 45:203-210.



# CHAPTER 2

**A review on anthracycline based anticancer agents and the simpler hydroxy-9,10-anthraquinones as promising anticancer agents**



At the present moment cancer is one of the leading causes of death throughout the world. With an increase in the incidence of cancer, discovery and development of anticancer agents are key focus of several pharmaceutical companies around the world. Hence, a search for anticancer drugs is extremely important and the research in this perspective is ever growing. Since the end of the nineteenth century, *cis-diamminedichloroplatinum* also known as Peyrone's chloride or more popularly as *cis* platin is a highly successful platinum-based antitumor agent, extensively used clinically against various types of human cancers affecting the ovary, bladder, head, neck etc.<sup>1,2</sup> In late 1960s, while carrying out experiments to probe effects of an electric field on bacterial growth, Barnett Rosenberg and his colleagues observed that bacterial proliferation stopped when they were placed in an electric field where platinum electrodes were being used. This led to an understanding that the platinum-based compound (*cis* platin) could be responsible for anti-proliferative action.<sup>1</sup> Since 1972, *cis* platin was made available as a research drug from the National Cancer Institute in the USA and launched in the demesne of medicinal applications in 1978.<sup>3</sup> Although it demonstrates extremely good anti-cancer activity, this goodness does not come without adverse effects; in fact it moves hand in hand with efficacy. This fact that is identified with regard to the clinical use of *cis* platin is a common problem encountered with most drugs. Use of *cis* platin revealed nephrotoxicity, ototoxicity, neurotoxicity, myelosuppression, nausea and vomiting.<sup>3,4</sup> To eliminate these side effects, a variety of platinum based anticancer agents were researched upon. In the process, several drugs were obtained that were different from the classical *cis*platin analogues.<sup>4,5</sup> In the early 1980s, carbo-platin was proposed to be the second most clinically important platinum analogue, essentially recommended to minimize the toxicity of *cis*platin-based chemotherapy. Although carboplatin was therapeutically equivalent to *cis*platin, it offered additional benefits of reduced gastro-intestinal effects, negligible nephrotoxicity and less frequent nausea and vomiting.<sup>5,6</sup> To overcome limitations

antagonised with the mechanism of action and resistance from *cisplatin* and carboplatin, oxaliplatin was subsequently considered as a distinct platinum-based compound showing better anti-tumour activity on *cisplatin*-resistant tumours.<sup>7,8</sup> However, the most common problems associated with platinum based anticancer drugs being their toxicity, development of less toxic clinical drug candidates became an urgent need of the time. Approximately around this time, medicinal chemists confronted with the discovery of another class of anticancer drugs, *the anthracyclines*, that had a hydroxy-9,10-anthraquinone at its core.<sup>9, 10</sup> Keeping some of the facts mentioned above in mind, this chapter provides an overview on some naturally occurring anthracyclines, their discovery, mechanism of action, therapeutic efficacy and some serious drawbacks.

### **2.1. Anthracyclines and anticancer activity:**

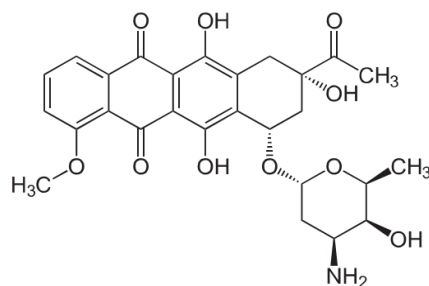
Anthracycline antibiotics are a class of clinically useful chemical agents listed with the World Health Organisation's (WHO) model list of essential medicines.<sup>11,12</sup> Primarily recognized for their antibacterial activity, it is only after analysing their therapeutic value regarding antitumor activity that they were developed as antitumour agents. Discovery of two compounds daunorubicin (daunomycin) and doxorubicin (hydroxyl daunomycin) from *Streptomyces peucetius varcaesitue* is considered a milestone in antibiotic history over production techniques that showed extensive antitumor activity against several human cancer.  $\beta$ -rhodomycin **II**, separated from *Streptomyces purpurascens* by Brockmann and Bauer was the first anthracycline whose structure was demonstrated. Afterwards, Arcamone and colleagues isolated a red coloured compound from *Streptomyces sp.* as rhodomycin B.<sup>13,14</sup> Although anthracyclines are vigorously effective against a number of human malignancies acute leukaemia, lymphoma, breast cancer, to name a few, their potential is limited, owing to their associated cardiac-toxicity. The cardiovascular side effects of the two classical drugs doxorubicin and daunorubicin gradually became vivid on cancer patients. There being no

potent treatment for dose dependent cardiotoxicity caused by anthracyclines, efforts are being made to look for analogues that match the efficacy of anthracyclines and have less toxic side effects.

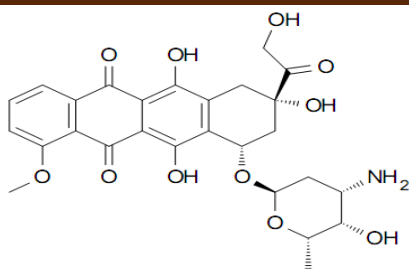
## **2.2. Anthracyclines: Varieties and/or derivatives**

Nearly a hundred analogues of the first two anthracyclines doxorubicin and daunorubicin have been synthesized and/or characterized. Anthracyclines share a tetracyclic aglycone structure with one or more deoxy sugar units, mostly belonging to L-hexopyranoside series consisting of an aminosugar.<sup>15</sup> The quinone moiety present assume significant clinical importance.<sup>16</sup> This large growing family of anthracyclines now include over 2,000 analogues. Following are some of the common anthracyclines used in the treatment of cancer today.

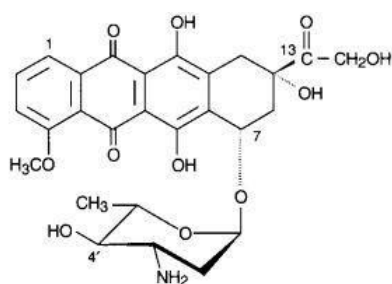
- ❖ **Daunorubicin:** This molecule is one of the major antitumor agents substantially used in treatment of acute myeloid leukemia (AMLs).<sup>17</sup>



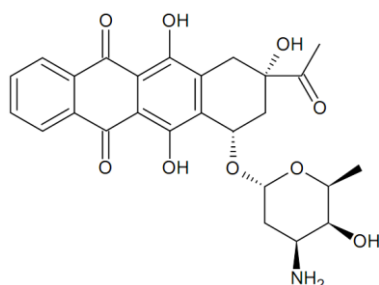
- ❖ **Doxorubicin:** Doxorubicin is correlated chemically to daunorubicin and can be separated from it by paper or thin layer chromatography. The outstanding anti-malignancy properties of doxorubicin was highlighted by Di Marco *et al.*<sup>18</sup> Intercalation into DNA by the molecule helps to deform DNA; the molecule is also involved in the production of reactive oxygen species that in turn damage DNA either at the site of the nucleic acid bases or at sugar residues by the free radical pathway.<sup>19</sup>



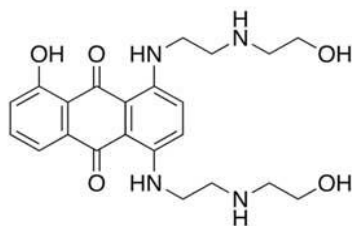
- ❖ **Epirubicin:** Epirubicin was found to be less cardiotoxic than doxorubicin and may be considered the most effective regimens in metastatic breast cancer (MBC)<sup>20,21</sup>



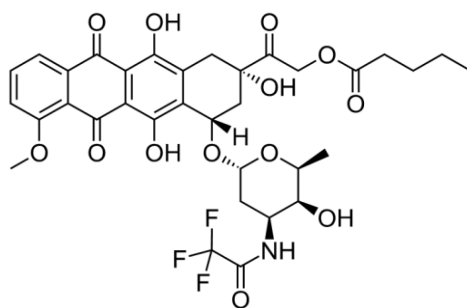
- ❖ **Idarubicin:** Idarubicin (particularly in combination with cytarabine) is an effective alternative to other anthracyclines in the treatment of acute myelogenous leukaemia, and there are evidences that it is also less cardiotoxic than other anthracyclines.<sup>22,23</sup>



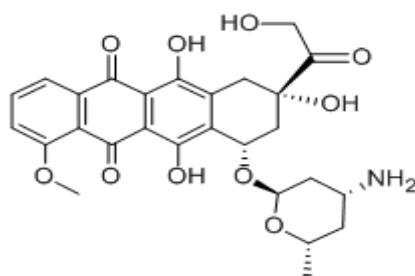
- ❖ **Mitoxantrone:** Mitoxantrone, an anthracenedione antineoplastic agent, is a type II topoisomerase inhibitor disrupting DNA synthesis and DNA repair. It is also a validated agent for treatment of multiple sclerosis.<sup>24,25</sup>



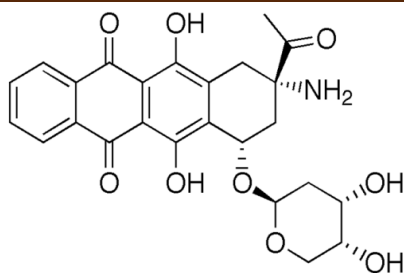
- ❖ **Valrubicin:** This molecule is used for the treatment of non-muscle invasive bladder cancer. Direct delivery of the drug to the bladder and its antineoplastic activity indicates that it is less toxic than adriamycin (doxorubicin)<sup>26</sup>



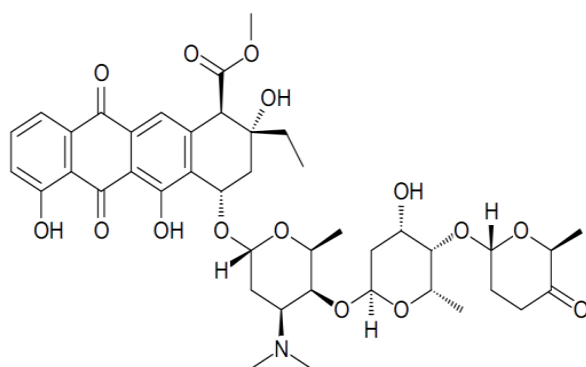
- ❖ **Esorubicin:** Esorubicin, an analogue of doxorubicin, is an active agent for metastatic breast cancer. Unlike doxorubicin it demonstrates no significant myocardial toxicity in an *in-vivo* model system.<sup>27</sup>



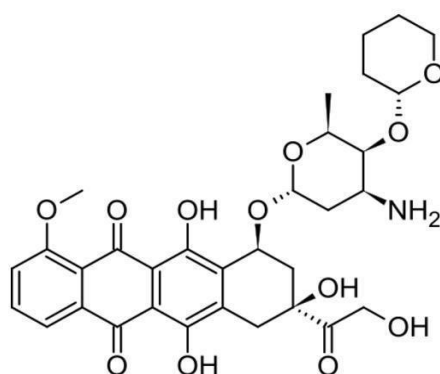
- ❖ **Amrubicin:** A synthetic anthracycline, having a structure similar to doxorubicin. It is used in the treatment of lung and breast cancers. Unlike other anthracycline derivatives amrubicin and amrubicinol have lower binding affinity towards DNA but is known to inhibit the action of topoisomerase II that relaxes supercoils of DNA during replication and therefore plays an important role in cancer chemotherapy.<sup>28,29,30</sup>



- ❖ **Aclarubicin:** Aclarubicin is considered less toxic than most anthracyclines and exhibits either comparable or in some cancers better antitumor activity.<sup>31</sup>



- ❖ **Pirarubicin:** Pirarubicin is an anthracycline antibiotic found to diminish the severe cardiotoxic side effects of doxorubicin. Comparing membrane transport and antitumor activity of pirarubicin against that reported for doxorubicin it was suggested pirarubicin is preferred in chemotherapy against M5076 ovarian sarcoma and certain breast cancers.<sup>32</sup>



### 2.3 Mode of action:

Anthracycline antibiotics are DNA targeting agents capable of intercalation into DNA strands. Drugs belonging to this family inhibit replication of DNA by interfering with the activity of DNA topoisomerase, known to relax DNA during replication. They are also active



in the free radical pathway where they are reported to initiate interaction through formation of radicals and reactive oxygen species (ROS) that may either target nucleobases or sugars present in DNA. In spite of a very high efficacy, aspects like myelo-suppression and cardiotoxicity are associated with their functioning owing to generation of reactive intermediates, that are both useful and harmful. Hence, this is a matter of serious concern.<sup>33</sup> Owing to anthracycline-induced adverse effects, a proper search for anticancer agents has become very important. In order to explain the complicated cytotoxic action of anthracyclines, multiple mechanisms have been proposed. Some of them are.

**i) Enzyme (topoisomerase) inhibition:**

DNA topoisomerases are enzymes that relax DNA during replication, transcription and recombination by catalyzing, breaking and re-joining the phosphodiester backbone of DNA strands. Human DNA topoisomerases are classified into two categories, the monomeric type I enzymes (topo 1) and dimeric type II enzymes (topo 2). Anthracycline drugs bind to topoisomerase forming a stable adduct that prevents the enzymes to regenerate the double helical structure again. Therefore, this results in a failure of older strands of DNA to have the proper three dimensional orientation essential for replication, which is pivotal in damaging of cells, leading to cell death.<sup>34,35</sup> Another highlighted fact in favour of anthracyclines regarding interference in the activity of DNA topoisomerases is that they produce persistent DNA cleavable species in comparison to other cytotoxic topoisomerase II inhibitors.<sup>36</sup>

**ii) DNA intercalation :**

Anthracycline drugs like doxorubicin being planar are readily taken up by cells and preferably intercalate between adjacent base pairs of DNA. The intercalation unwinds the DNA double helical structure producing DNA supercoils that result in increased torsional stress.<sup>37,38</sup> It is a good DNA intercalator and has high selectivity towards

guanine forming hydrogen-bonds with it. To form hydrogen bonds it selects intercalation as a mode, targeting adjacent GC base pairs.<sup>37,39</sup> The anthracycline-DNA adduct formed following intercalation causes substantial damage to DNA and therefore helps in promoting cell death, that is independent of their activity on topoisomerase II.

**iii) Generation of reactive oxygen species (ROS) :**

Antraquinone being the functional unit of anthracyclines, they are reduced enzymatically to a semiquinone by one electron-transfer reactions assisted by enzymes present in the biological system. This leads to a sequence of reactions culminating in the formation of reactive oxygen species (ROS) like the superoxide radical anion ( $O_2^{\bullet-}$ ). Superoxide dismutase (SOD) catalyzes dismutation of  $O_2^{\bullet-}$  to hydrogen peroxide ( $H_2O_2$ ) and molecular oxygen that in turn generate the extremely reactive hydroxyl radicals ( $\bullet OH$ ).<sup>40,41</sup> Although  $O_2^{\bullet-}$  or  $H_2O_2$  can be detoxified by enzymatic systems, the more dangerous  $\bullet OH$  cannot be eliminated by enzymes and results in oxidative stress leading to DNA damage and cell apoptosis.<sup>42</sup>

**2.4. Anthracycline-induced cardiotoxicity:**

Anthracyclines exhibit a range of toxic effects, among them cardiotoxicity could be permanent. Reactive oxygen species (ROS) like the superoxide radical anion ( $O_2^{\bullet-}$ ), hydrogen peroxide ( $H_2O_2$ ), peroxynitrite ( $ONOO^{\bullet-}$ ) and hydroxyl radicals ( $\bullet OH$ ) produced during oxidation-reduction cycles cause cell damage and are known to initiate lipid peroxidation.<sup>43,44</sup> Cardiac cells are more susceptible to free radical damage. High oxidative metabolism and a poor anti-oxidant defense due to absence of glutathione in cardiac cells<sup>45</sup> are factors that amplify their vulnerability to oxidative stress.<sup>46</sup> Peroxyl radicals generated from lipid peroxidation increase cell membrane permeability of the anthracyclines, facilitating localization of anthracyclines in the interior of cardiac cells. Anthracyclines like doxorubicin possess high affinity for cardiolipin, a phospholipid located in the inner mitochondrial

membrane resulting in good correlation between drug-cardiolipin binding constant and drug-induced cardiotoxicity.<sup>47,48</sup>

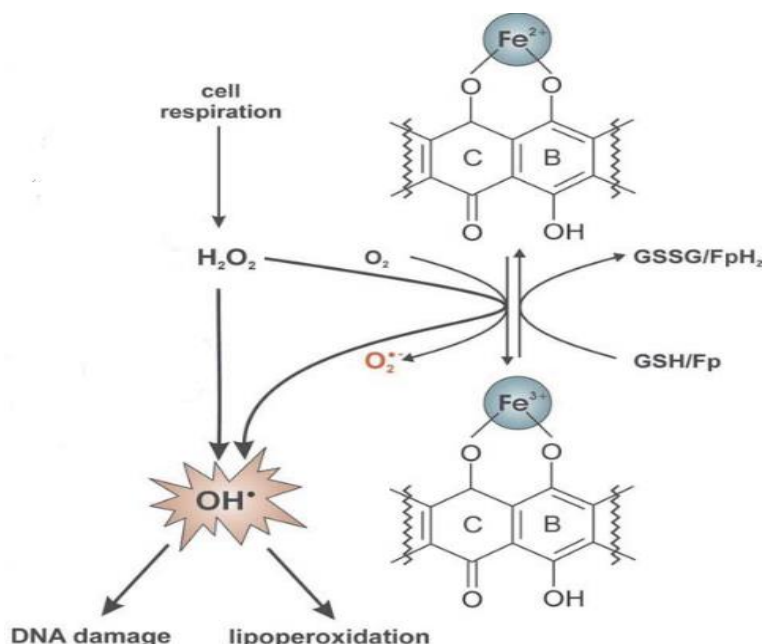
Three discrete types of anthracycline-induced cardiotoxicity have been reported so far, acute, sub-acute and chronic. Acute toxicity being most common. It is a reversible cardiovascular manifestation that occurs during or soon after administration of an anthracycline or within a week or after treatment that includes transient arrhythmias and acute left ventricular failure. The frequency of arrhythmia following doxorubicin treatment has been examined in two parts (1) the first hour following doxorubicin infusion and (2) remaining 23 hours following infusion. In the first hour, after infusion, occurrence of new arrhythmia is not seen during the control period and in the rest of the monitoring period there was no atrioventricular block or intraventricular conduction delay in a patient resulting in no difference in the mean heart rate from the control in both cases. Usually these abnormalities are impermanent, self-limiting and recover spontaneously with assistive therapy.<sup>49-51</sup> Modern methods of execution including lower doses and shielding methods (like sub-carinal blocking) have decreased the incidence from 20% to 2.5%.<sup>52</sup> Sub-acute cardiotoxicity could develop several days to several weeks after an administration, showing acute left heart failure, myocarditis, and pericarditis.<sup>53</sup> Chronic cardiotoxicity is categorized into type I (early onset) and type II (late onset).<sup>53</sup> Chronic anthracycline cardiotoxicity is a dilated heart disease (mimicking congestive cardiomyopathy) that increases exponentially with cumulative dose of anthracyclines.<sup>54</sup> Type I or early onset cardiotoxicity manifests as an irreversible cardiac cell injury within the first year of completion of chemotherapy resulting as occult ventricular dysfunction. Type II cardiotoxicity is detected after the first year and can be observed decades after the completion of chemotherapy. The type II cardiotoxicity is generally caused by novel biological-targeted antibodies and is associated with reversible myocardial dysfunction.<sup>50,55-59</sup>

Hence oncologists need to very closely follow the cardiac status of a patient receiving anthracyclines, both for their safe keeping and to cultivate a better plan for therapy in future.<sup>59</sup>

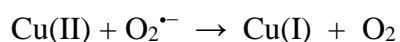
### **2.5. Future of Anthracyclines:**

Anthracyclines are mainstay anticancer drugs ever developed. Compounds like doxorubicin and daunorubicin enjoy an unexhausted range of activities in cancer cells. Despite extensive clinical utilization, toxic side effects like cardiomyopathy, congestive heart failure following their administration put up several controversies in anthracycline treatment.<sup>60</sup> In that background, researchers are now trying to either develop modified forms of existing anthracyclines or are searching for closely resembling analogues that either possess an almost similar or slightly less efficacy but enable a significant decrease in toxic side effects. Liposome-encapsulated anthracycline (doxil) formulations offer an active and well-tolerated alternative to conventional anthracyclines that seek to improve the therapeutic index and the spectrum of anticancer activity. However, Doxil treatment results in dose-dependent dilated cardiomyopathy with uncommon pharmacokinetic and toxicity profiles.<sup>16,61,62</sup> Hence, to modify anthracyclines to better anticancer agents, investigations have focused on the use of biologically active complexes formed by essential metal ions. When an anthracycline is complexed with a metal ion and if it is either Fe(III) or Cu(II), their efficacy is reported to increase several times while cardiotoxicity decreases.<sup>63-66</sup> Metal complexes easily undergo redox reactions generating ROS that allow them to interact with biological molecules causing apoptosis. Copper, iron are indispensable elements found in almost all living organisms. Anthracyclines eagerly bind iron, forming a 1:1, 2:1, or 3:1 complexes.<sup>67-69</sup> In the presence of a reducing system, like NADPH cytochrome P450 reductase, glutathione, cysteine, an anthracycline-Fe(III) complex is reduced to an anthracycline-Fe(II) complex. Subsequently, the anthracycline-Fe(II) complex is again re-oxidized to an anthracycline-Fe(III) complex by

transforming relatively safe species like  $O_2^{\bullet-}$  and  $H_2O_2$  into the more reactive and toxic hydroxyl radical ( $\bullet OH$ ).<sup>41,70</sup>



Copper forms a large variety of coordination complexes having oxidation states +2 and +1. Proposed mechanism to explain copper induced cellular toxicity comes from affinity of free copper ions to participate in ROS formation. In the presence of superoxide ( $O_2^{\bullet-}$ ) or other reducing agents like ascorbic acid or glutathione, Cu(II) is reduced to Cu(I), which is able to catalyze the formation of the more dangerous hydroxyl radicals ( $\bullet OH$ ) due to hydrogen peroxide ( $H_2O_2$ ).<sup>65,71</sup>



-----



Hence, besides DNA interaction and topo I / topo II inhibitory properties of organometallic complexes that allow a more effective anti-proliferative action on cancer cells<sup>72,73</sup>, formation of reactive oxygen species is an important pathway by which anthracyclines show activity.

## **2.6. Hydroxy 9, 10-anthraquinones as anticancer agents:**

Therapeutic efficacy and toxicity of anthracycline based anticancer drugs is controlled and regulated by a hydroxy-9,10-anthraquinone that is present at its core.<sup>74-77</sup> Anthracyclines, although effective are costly. Hence, there is an effort to consider simpler analogues i. e. hydroxy-9, 10-anthraquinones (the core) and see if it mimics the performance of anthracyclines; this would also make them economically viable. The search for simple molecules for use as drugs is an important aspect related to drug discovery, drug design and drug prospecting since simpler molecules can easily penetrate membranes and enter the cell.<sup>78-80</sup> In our laboratory, there has been an effort to consider relatively less costly, less toxic, simpler analogues that closely resemble anthracyclines in their action. Reports on anthracyclines as anticancer agents and on hydroxy-9, 10-anthraquinones from our laboratory and others indicate that the difference in efficacy may be attributed to presence of sugar in anthracyclines.<sup>45,81</sup> It known today that presence of sugar in several anticancer agents help them recognize cancer cells.<sup>82</sup> Besides, sugar units exercise a strong influence on the anthracycline-DNA interactions, assisted further by amino groups present on sugars.<sup>83</sup>

Location of hydroxyl groups on the anthraquinone in anthracyclines also influence their interactions within cells.<sup>83,84</sup> To realize this, attempts were made to study different types of hydroxy-9,10-anthraquinones in reference to anthracyclines, so that the role of –OH groups in anthracycline drugs is realized. Since absence of a sugar unit would reduce the cost of drugs substantially and since most of the chemistry in anthracyclines is centered around the quinone, it was thought hydroxy-9,10-anthraquinones might have a solution to some of the problems mentioned above.<sup>85,86</sup> Complex formation of simpler analogues using suitable metal ions was also attempted<sup>87-89</sup> resulting in modification of redox and biological properties and having a higher efficacy than the parent drug. Transition metal ions e. g., iron,<sup>90-93</sup> copper,<sup>90-93</sup> platinum, palladium<sup>94-96</sup>, manganese<sup>90,97</sup> have a capacity to coordinate anthracyclines as

ligands facilitating functional groups to approach molecular targets which then exhibit superb anti-proliferative properties.

Like anthracyclines, simpler molecules 1, 8-dihydroxy-9,10-anthraquinone (danthron) and 1, 4-dihydroxy-9,10-anthraquinone (quinizarin) exhibit high binding affinity towards calf thymus DNA. Their cell viability and cell proliferation activity decrease in a dose- and time-dependent manner.<sup>98</sup> Research revealed 1,2-dihydroxy-9,10-anthraquinone modifies the base-pair region of calf thymus DNA, catalyzes superoxide radical anion formation through an enzyme assisted pathway.<sup>99-101</sup> Complex formation increased DNA modification and decreased superoxide radical anion generation making the metal complexes of hydroxy-9,10-anthraquinones relatively safe anticancer agents.<sup>102,103</sup> Stability constants of metal complexes of hydroxy-9,10-anthraquinones were comparable to metal complexes formed by anthracyclines.<sup>103-109</sup> Performance of metal complexes of hydroxy-9,10-anthraquinones demonstrate a close resemblance with anthracyclines, that is considered a positive indication on coordination compound formation by hydroxy-9,10-anthraquinones.<sup>104-109</sup> As mentioned earlier, presence of a sugar unit alongside a hydroxy-9,10-anthraquinone is important since literature survey suggests that the sugar unit has a crucial role in drug action of several anticancer agents.<sup>45, 82</sup> For this reason, carminic acid an anthracycline analogue having a sugar unit linked directly to a hydroxy-9,10-anthraquinone, although not in the same manner in which sugars are present in anthracyclines, was selected for this study. Metal complex formation of carminic acid with Cu(II) has been reported earlier.<sup>109</sup> The complex unlike carminic acid was found to be a human DNA topoisomerase inhibitor and showed potent activity on ALL MOLT-4 cells.<sup>109</sup> Although the ability of the copper(II)-carminic acid to bind to calf thymus DNA was slightly lower than carminic acid, binding constant values for the complex remained constant over a wide range of pH, that has a high significance with regard to therapeutic efficacy.

## ***Chapter 2: A review of anthracycline..... anticancer agents***

---

All studies mentioned above reveal when we compare efficacy of hydroxy-9,10-anthraquinones with anthracyclines, most often the results are not very encouraging. However, modification of simpler analogues through complex formation with suitable metal ions, often achieve the efficacy of anthracyclines. Hence, complex formation of hydroxy-9,10-anthraquinones to look for attributes of anthracyclines is an interesting avenue of cancer research for it not only shows high antitumor activity but also minimal toxicity.<sup>106-111</sup>

### **References:**

- [1] S. Dilruba, G. V. Kalayda. 2016. Platinum-based drugs: past, present and future. *Cancer Chemother Pharmacol.* 77:1103-24. doi: 10.1007/s00280-016-2976-z. PMID: 26886018.
- [2] A. M. Florea, D. Büsselberg. 2011. Cisplatin as an anti-tumor drug: cellular mechanisms of activity, drug resistance and induced side effects. *Cancers (Basel).* 3 :1351-71.
- [3] C. J. Williams, J. M. Whitehouse. 1979. Cis-platinum: a new anticancer agent. *Br Med J.* 1:1689-91.
- [4] Y. P. Ho, S. C. Au-Yeung, K. K. To. 2003. Platinum-based anticancer agents: innovative design strategies and biological perspectives. *Med Res Rev.* 23:633-55.
- [5] J. Lokich, N. Anderson. 1998. Carboplatin versus cisplatin in solid tumors: an analysis of the literature. *Ann Oncol.* 9:13-21.
- [6] S. Kerpel-Fronius. 2006. Cisplatin and its analogues for cancer chemotherapy. *Analyse-based Drug Discovery.* <https://doi.org/10.1002/3527608001.ch19>.
- [7] A. M. Di Francesco, A. Ruggiero and R. Riccardi. 2002. Cellular and molecular aspects of drugs of the future: oxaliplatin. *Cell Mol Life Sci.* 59:1914–1927.



- [8] S. Faivre, D. Chan, R. Salinas, B. Woynarowska, J.M. Woynarowski. 2003. DNA strand breaks and apoptosis induced by oxaliplatin in cancer cells. *Biochem Pharmacol.* 66:225-37.
- [9] J. William Lown. 1993. Anthracycline and anthraquinone anticancer agents: current status and recent developments. *Pharmac. Ther.* 60:185-214.
- [10] J. William Lown. 1985. Molecular mechanisms of action of anticancer agents involving free radical intermediates. *Advances in Free Radical Biology & Medicine.* 1:225-264.
- [11] J. W. Lown. 1983. The mechanism of action of quinone antibiotics. *Mol Cell Biochem.* 55: 17-40.
- [12] E. Damiens. 2000. Molecular events that regulate cell proliferation: an approach for the development of new anticancer drugs. *Prog Cell Cycle Res.* 4:219-33.
- [13] A. Rabbani, R. M. Finn, J. Ausió. The anthracycline antibiotics: antitumor drugs that alter chromatin structure. *Bioessays.* 27:50-56.
- [14] J. W. Lown. 1993. Discovery and development of anthracycline antitumour antibiotics. *Chem. Soc. Rev.* 22:165-176.
- [15] F. Arcamone, G. Cassinelli. 1998. Biosynthetic anthracyclines. *Curr Med Chem.* 5:391-419.
- [16] H. Cortés-Funes, C. Coronado. 2007. Role of anthracyclines in the era of targeted therapy. *Cardiovasc Toxicol.* 7:56-60.
- [17] G. Laurent, J.P. Jaffrézou. 2001. Signaling pathways activated by daunorubicin. *Blood.* 98:913-924.
- [18] A. Di Marco, M. Gaetani and B. M. Scarpinato. 1969. Adriamycin (NSC-123,127): a new antibiotic with antitumoral activity. *Cancer Chemother. Rep.* 53:33-37.
- [19] K. Chatterjee, J. Zhang, N. Honbo, J. S. Karliner. 2010. Doxorubicin cardiomyopathy. 115:155–162

- [20] D. Mavroudis, A. Alexopoulos, N. Ziras, N. Malamos, C. Kouroussis, S. Kakolyris, S. Agelaki, K. Kalbakis, N. Tsavaris, A. Potamianou, G. Rigatos, V. Georgoulas. 2000. Front-line treatment of advanced breast cancer with docetaxel and epirubicin: A multicenter phase II study. *Annals of Oncology* 11: 1249-1254.
- [21] C. Pacilio, A. Morabito, F. Nuzzo, A. Gravina, V. Labonia, G. Landi, E. Rossi, E. De Maio, M. Di Maio, G. D'Aiuto, G. Botti, N. Normanno, P. Chiodini, C. Gallo, F. Perrone, A. de. 2006. Is epirubicin effective in first-line chemotherapy of metastatic breast cancer (MBC) after an epirubicin-containing adjuvant treatment? A single centre phase III trial. *Br J Cancer*. 94:1233 – 1236.
- [22] J. Wang, Y.G. Yang, M. Zhou, J. Y. Xu, Q. G. Zhang, R. F. Zhou, B. Chen, J. Ouyang. 2013. Meta-analysis of randomised clinical trials comparing idarubicin + cytarabine with daunorubicin + cytarabine as the induction chemotherapy in patients with newly diagnosed acute myeloid leukaemia. *PLoS One*. doi: 10.1371/journal.pone.0060699.
- [23] R. J. Cersosimo. 1992. Idarubicin: an anthracycline antineoplastic agent. *Clin Pharm*. 11:152-67.
- [24] B. S. Singhal, S. Geeta, S.G. Hundalani, S. Menon. 2009. Efficacy and safety of mitoxantrone, as an initial therapy, in multiple sclerosis: Experience in an Indian tertiary care setting. *Neurol India*. 57: 418-423
- [25] L. J. Scott, D.P. Figgitt. 2004. Mitoxantrone: A review of its use in multiple sclerosis. *CNS Drugs*. 18:379-396.
- [26] M. S. Cookson, S. S. Chang, C. Lihou, T. Li, S. Q. Harper, Z. Lang and R. F. Tutrone. 2014. Use of intravesical valrubicin in clinical practice for treatment of muscle invasive bladder cancer, including carcinoma *in situ* of the bladder. *Ther Adv Urol*. 6:181–191.

- [27] J. R. Rigas, M. G. Kris, R. J. Gralla, R. T. Heelan and L. D. Marks. 1991. Phase II trial of esorubicin (4'Deoxydoxorubicin, DxDx) in patients with small cell lung cancer. *Investigational New Drugs*. 9:187-190.
- [28] M. Hanada, S. Mizuno, A. Fukushima, Y. Saito, T. Noguchi, T. Yamaoka. 1998. A new antitumor agent amrubicin induces cell growth inhibition by stabilizing topoisomerase II-DNA Complex. *Jpn. J. Cancer Res*. 89:1229–1238.
- [29] Q. Ding, J. Zhan, 2013. Amrubicin: Potential in combination with cisplatin or carboplatin to treat small-cell lung cancer. *Drug Design, Development and Therapy*. 7:681–689.
- [30] V. Mamidipudi, T. Shi, H. Brady, S. Surapaneni, R. Chopra, S. L. Aukerman, C. Heise, V. Sung. 2012. Increased cellular accumulation and distribution of amrubicin contribute to its activity in anthracycline-resistant cancer cells. *Cancer Chemother Pharmacol*. 69:965-976.
- [31] W. Lu, J. Wan, Q. Zhang, Z. She, X. Jiang. 2006. Aclarubicin-loaded cationic albumin-conjugated pegylated nanoparticle for glioma chemotherapy in rats. *Int. J. Cancer*. 120:420–431.
- [32] T. Sugiyama, Y. Sadzuka, K. Nagasawa, N. Ohnishi, T. Yokoyama, T. Sonobe. 1999. Membrane transport and antitumor activity of pirarubicin, and comparison with those of doxorubicin. *Jpn. J. Cancer Res*. 90:775–780.
- [33] A. Szulawska, M. Czyz. 2006. Molecular mechanisms of anthracyclines action. *Postepy Hig Med Dosw (Online)*. 60:78-100.
- [34] J. Marinello, M. Delcuratolo, G. Capranico. 2018. Anthracyclines as topoisomerase II poisons: From early studies to new perspectives. *Int. J. Mol. Sci*. 19: 3480.
- [35] D. D. Ben, M. Palumbo, G. Zagotto, G. Capranico, S. Moro. 2007. DNA topoisomerase II structures and anthracycline activity: Insights into ternary complex formation. *Curr Pharm Des*. 13:2766-2780.

- [36] F. Zunino, G. Capranico, 1990. DNA topoisomerase II as the primary target of anti-tumor anthracyclines. *Anti-cancer Drug Design*. 5:307-317.
- [37] F. Yang, S. S. Teves, C. J. Kemp, S. Henikof. 2014. Doxorubicin, DNA torsion, and chromatin dynamics. *Biochim Biophys Acta*. 1845:84-89
- [38] D. A. Gewirtz.1999. A critical evaluation of the mechanisms of action proposed for the antitumor effects of the anthracycline antibiotics adriamycin and daunorubicin. *Biochem Pharmacol*. 57:727–741.
- [39] J. B. Chaires, K R. Fox, J E. Herrera, M. Britt, and M. J. Waring. 1987. Site and sequence specificity of the daunomycin-DNA interaction. *Biochemistry*. 26: 8227-8236.
- [40] I. Müller, D. Niethammer, G. Bruchelt. 1998. Anthracycline-derived chemotherapeutics in apoptosis and free radical cytotoxicity (Review). *Int J Mol Med*. 1:491-494.
- [41] T. Šimunek, M. Štirba, O. Popelová, M. Adamcová, R. Hrdina, V. Geršl. 2009. Anthracycline-induced cardiotoxicity: Overview of studies examining the roles of oxidative stress and free cellular iron. *Pharmacol Rep*. 61:154–171.
- [42] P. Angsutararux, S. Luanpitpong, and S. Issaragrisil. 2015. Chemotherapy-induced cardiotoxicity: Overview of the roles of oxidative stress. *Oxid Med Cell Longev*. 2015:795602. doi: 10.1155/2015/795602.
- [43] A. A. Markin, I. A. Popova, E.G. Vetrova, O.A. Zhuravleva, O.I. Balashov. 1997. Lipid peroxidation and activity of diagnostically significant enzymes in cosmonauts after flights of various durations. *Aviakosm Ekolog Med*. 31:14-18.
- [44] K. J. M. Schimmel, D. J. Richel, R. B. A. van den Brink, H. J. Guchelaar. 2004. Cardiotoxicity of cytotoxic drugs. *Cancer Treat Rev*. 30:181–191.
- [45] E. Goormaghtigh, J. M. Ruyschaert. 1984. Anthracycline glycoside-membrane interactions. *Biochim Biophys Acta*. 779:271-88.

- [46] A. L. A. Ferreira, L. S. Matsubara, B. B. Matsubara. 2008. Anthracycline-induced cardiotoxicity. *Cardiovasc Hematol Agents Med Chem.* 6:278-281.
- [47] M. S. Horenstein, R. S. Vander Heide and T. J. L'Ecuyer. 2000. Molecular basis of anthracycline-induced cardiotoxicity and its prevention. *Mol Genet Metab.* 71:436–444.
- [48] N. Ashley, J. Poulton. 2009. Mitochondrial DNA is a direct target of anti-cancer anthracycline drugs. *Biochem Biophys Res Commun.* 378:450–455.
- [49] J. S. Steinberg, A. J. Cohen, A. G. Wasserman, P. Cohen, A. M. Ross. 1987. Acute arrhythmogenicity of doxorubicin administration. *Cancer.* 60: 1213-1218.
- [50] D. Jain, R. R. Russell, R. G. Schwartz, G. S. Panjra, W. Aronow. 2017. Cardiac complications of cancer therapy: Pathophysiology, identification, prevention, treatment, and future directions. *Curr Cardiol Rep.* 19:36.
- [51] C. Jaworski, J. A. Mariani, G. Wheeler, D. M. Kaye. 2013. Cardiac complications of thoracic irradiation. *J Am Coll Cardiol.* 61:2319-28.
- [52] B. Robinson, J. Kingston, R. N. Costa, J S. Malpas, A. Barrett, T. J. McElwain. 1984. Chemotherapy and irradiation in childhood Hodgkin's disease. *Arch Dis Child.* 59:1162-1167.
- [53] F. Cai, M. A. F. Luis, X. Lin, M. Wang, L. Cai, C. Cen, E. Biskup. 2019. Anthracycline-induced cardiotoxicity in the chemotherapy treatment of breast cancer: Preventive strategies and treatment. *Mol Clin Oncol.* 11:15-23.
- [54] B. V. Jensen. 2006. Cardiotoxic consequences of anthracycline-containing therapy in patients with breast cancer. *Semin Oncol.* 33:15-21.
- [55] C. G. Tocchetti, C. Cadeddu, D. di Lisi, S. Femmino, R. Madonna, D. Mele, I. Monte, G. Novo, C. Penna, A. Pepe, P. Spallarossa, G. Varricchi, C. Zito, P. Pagliaro and G. Mercurio. 2017. From molecular mechanisms to clinical management of antineoplastic drug-

induced cardiovascular toxicity: A translational overview. *Antioxid Redox Signal*. 30:2110-2153.

[56] M. S. Ewer, S. M. Lippman. 2005. Type II chemotherapy-related cardiac dysfunction: Time to recognize a new entity. *J Clin Oncol*. 23:2900-2902.

[57] L. J. Steinherz, P. G. Steinherz, C. T. C. Tan, G. Heller, M. L. Murphy. 1991. Cardiac toxicity 4 to 20 years after completing anthracycline therapy. *JAMA*. 266:1672-1677.

[58] S. E. Lipshultz, S. D. Colan, R. D. Gelber, A. R. Perez-Atayde, S. E. Sallan, S.P. Sanders. 1991. Late cardiac effects of doxorubicin therapy for acute lymphoblastic leukemia in childhood. *N Engl J Med*. 324:808-815.

[59] S. A. Mortensen, H. S. Olsen, U. Baandrup. 1986. Chronic anthracycline cardiotoxicity: haemodynamic and histopathological manifestations suggesting a restrictive endomyocardial disease. *Br Heart J*. 55:274-282.

[60] G. Minotti, P. Menna, E. Salvatorelli E, G. Cairo, L. Gianni. 2004. Anthracyclines: molecular advances and pharmacologic developments in antitumor activity and cardiotoxicity. *Pharmacol Rev*. 56:185-229.

[61] O. Lyass, B. Uziely, R. Ben-Yosef, D. Tzemach N. I. Heshing, M. Lotem, G. Brufman, A. Gabizon. 2000. Correlation of toxicity with pharmacokinetics of pegylated liposomal doxorubicin (doxil) in metastatic breast carcinoma. *Cancer*. 89:1037-1047.

[62] R. E. Coleman, L. Biganzoli, P. Canney, L. Dirix, L. Mauriac, P. Chollet, V. Batter, E. Ngalula-Kabanga, C. Dittrich, M. Piccart. 2006. A randomised phase II study of two different schedules of pegylated liposomal doxorubicin in metastatic breast cancer (EORTC-10993). *European Journal of Cancer*. 42:882-887.

[63] J. R. F. Muindi, B. K. Sinha, L. Gianni, C. E. Myers. 1984. Hydroxyl radical production and DNA damage induced by anthracycline-iron complex. *FEBS Lett*. 172:226-30.

- [64] H. Beraldo, A. Garnier-Suillerot, L. Tosi, F. Lavelles. 1985. Iron(III)-adriamycin and iron(III)-daunorubicin complexes: Physicochemical characteristics, interaction with DNA, and antitumor activity. *Biochemistry*. 24: 284-289.
- [65] C. Santini, M. Pellei, V. Gandin, M. Porchia, F. Tisato, C. Marzano. 2014. Advances in copper complexes as anticancer agents, *Chem. Rev.* 114:815–862.
- [66] J. de Jong, B. C. P. Hijsken, B. Beekman, W. J. F. van der Vijgh, A. Bast. 1994. Radical formation by metal complexes of anthracyclines and their metabolites. Is there a relation with cardiotoxicity? *European Journal of Pharmaceutical Sciences*. 2:229-237.
- [67] X. Xu, H. L. Persson, D. R. Richardson. 2005. Molecular pharmacology of the interaction of anthracyclines with iron. *Mol Pharmacol*. 68:261–271.
- [68] M. M. L. Fiallo, H. Drechsel, A. G.-Suillerot, B. F. Matzanke, H. Kozłowski. 1999. Solution structure of iron(III)-anthracycline complexes, *J. Med. Chem.* 42:2844-2851.
- [69] K. Nawara, J. L. McCracken, P. Krysiński, and G. J. Blanchard. 2013. Structure-dependent complexation of Fe<sup>3+</sup> by anthracyclines. 1. The importance of pendent hydroxyl functionality. *J Phys Chem B*. 117:6859-6867.
- [70] E. Gammella, F. Maccarinelli, P. Buratti, S. Recalcati, G. Cairo. 2014. The role of iron in anthracycline cardiotoxicity. *Front Pharmacol*. 5:25. doi: 10.3389/fphar.2014.00025.
- [71] C. Marzano, M. Pellei, F. Tisato, C. Santini. 2009. Copper complexes as anticancer agents, *Anticancer Agents Med Chem*. 9:185-211.
- [72] S. M. V. de Almeidaa, A. G. Ribeiroc, G. C. de L. Silva, J. E. F. Alvesb, E. I. C. Beltrãob, J. F. de Oliveirac, L. B. de Carvalho Junior, M. do C. Alves de Limac. 2017. DNA binding and topoisomerase inhibition: How can these mechanisms be explored to design more specific anticancer agents? *Biomed Pharmacother*. 96:1538-1556.

- [73] X. Liang, Q. Wu, S. Luan, Z. Yin, C. He, L. Yin, Y. Zou, Z. Yuan, L. Li, X. Song, M. He, C. L. W. Zhang. 2019. A comprehensive review of topoisomerase inhibitors as anticancer agents in the past decade. *Eur J Med Chem.* 171:129-168.
- [74] F. Arcamone, 1984. Antitumor anthracyclines: Recent developments. *Med Res Rev.* 4: 153-188.
- [75] D. J. Booser, G. N. Hortobagyi. 1994. Anthracycline antibiotics in cancer therapy focus on drug resistance. *Drugs.* 47: 223-258.
- [76] S. Das, A. Saha, P. C. Mandal. 1996. Studies on the formation of Cu(II) and Ni(II) complexes of 1,2-dihydroxy-9, 10-anthraquinone and lack of stimulated superoxide formation by the complexes. *Talanta.* 43:95-102.
- [77] P. S. Guin, S. Das. 2016. Electrochemical reduction of Nickel(II)-dihydroxyanthraquinone sulfonate: How complex formation affects biochemical behavior. *Russian Journal of Physical Chemistry.* 90:876–881.
- [78] I. Muegge. 2003. Selection criteria for drug-like compounds. *Medicinal Research Reviews.* 23:302-321.
- [79] C. A. Lipinski. 2004. Lead- and drug-like compounds: the rule-of-five revolution. *Drug Discov Today Technol.* 1:337-341.
- [80] I. M. Sarah, L. Heald, D. Brittelli. 2001. Simple selection criteria for drug-like chemical matter. *J Med. Chem.* 44:1841-1846.
- [81] W. Priebe. 2000. Targeting DNA with anthracyclines: the importance of the sugar moiety. *Molecules.* 5:299–301.
- [82] M. B. Calvo, A. Figueroa, E. G. Pulido, R. G. Campelo, L. A. Aparicio. 2010. Potential role of sugar transporters in cancer and their relationship with anticancer therapy. *International journal of endocrinology.* <https://doi.org/10.1155/2010/205357>



- [83] T. Banerjee, R. Mukhopadhyay. 2008. Structural effects of nogalamycin, an antibiotic antitumour agent, on DNA. *Biochem. Biophys. Res. Comm.* 374:264-268.
- [84] A. Szulawska, M. Czyż. 2006. Molecular mechanisms of anthracyclines action. *Advances in Hygiene and Experimental Medicine.* 60:78–100.
- [85] P. S. Guin, S Das, P. C. Mandal. 2010. Sodium 1,4-dihydroxy–9,10-anthraquinone–2-sulphonate interacts with calf thymus DNA in a way that mimics anthracycline antibiotics: An electrochemical and spectroscopic study. *J. Phys. Org. Chem.* 23:477–482.
- [86] P. S. Guin, S. Das, P. C. Mandal. 2009. Studies on the formation of a complex of Cu(II) with sodium 1,4-dihydroxy–9,10-anthraquinone–2-sulphonate—An analogue of the core unit of anthracycline anticancer drugs and its interaction with calf thymus DNA. *J. Inorg. Biochem.* 103:1702–1710.
- [87] S. P. Fricker. 2007. Metal based drugs: from serendipity to design. *Dalton Trans.* 43:4903–4917.
- [88] E. Meggers. 2009. Targeting proteins with metal complexes. *Chem. Commun.* 7:1001–1010.
- [89] H. Drechsel. 2001. Spectroscopic studies on iron complexes of different anthracyclines in aprotic solvent systems. *Inorg. Chem.* 40: 5324-5333.
- [90] A. Jabłońska-Trypu, Grzegorz' Swiderski, Rafa Krętownski, and W. Lewandowski. 2017. Newly synthesized doxorubicin complexes with selected metals-synthesis, Structure and anti-breast cancer activity. *Molecules.* 22:1106.
- [91] M. Feng, Y. Yang, P. He, Y. Fang. 2000. Spectroscopic studies of copper(II) and iron(II) complexes of adriamycin. *Spectrochimica Acta Part A.* 56:581–587.
- [92] B. B. Hasinoff, J. P. Davey. 1988. Adriamycin and its iron(III) and copper(II) complexes. Glutathione-induced dissociation; cytochrome c oxidase inactivation and protection; binding to cardiolipin. *Biochem Pharmacol.* 37:3663-3669.

## ***Chapter 2: A review of anthracycline..... anticancer agents***

---

- [93] B. B. Hasinoff. 1990. The iron(III) and copper(II) complexes of adriamycin promote the hydrolysis of the cardioprotective agent ICRF-187((+)-1,2-bis(3,5-dioxopiperazinyl-1-yl)propane). *Agents Actions*. 29:374-381.
- [94] N. Nikolisa, C. Methenitisa, G. Pneumatikakisa, M. M.L. Fiallo. 2002. Interactions of the anticancer antibiotic altromycin B with copper(II), palladium(II) and platinum(II) ions and in vitro activity of the formed complexes. *J Inorg Biochem*. 89:131–141.
- [95] A. Pasini. 1987. A doxorubicin-Pt(II) complex. Chemistry and antitumor activity. *Inorganica Chimica Acta*, 137:123-124.
- [96] M. M. L. Fiallo, A. Garnier-Suillerot. 1986. Metal anthracycline complexes as a new class of anthracycline derivatives. Pd(II)-adriamycin and Pd(II)-daunorubicin complexes: Physicochemical characteristics and antitumor activity. *Biochemistry*. 25:924-930.
- [97] B. C. L. Cheung, T. H. T. Sun, J. M. Leenhouts, P. R. Cullis. 1998. Loading of doxorubicin into liposomes by forming Mn<sup>2+</sup>-drug complexes. *Biochimica et Biophysica Acta*. 1414:205-216.
- [98] M. B. Gholivanda, S. Kashaniana, H. Peyman. 2012. DNA-binding, DNA cleavage and cytotoxicity studies of two anthraquinone derivatives. *Spectrochimica Acta Part A*. 87:232–240.
- [99] X. Dong, J. Fu, X. Yin, C. Yang, X. Zhang, W. Wang, X. Du, Q. Wang, J. Ni. 2017. Cassiae semen: A review of its phytochemistry and pharmacology (Review). *Mol Med Rep*. 16: 2331-2346.
- [100] B. Pogjnsky, J. Westendorf, B. Blomeke, H. Marquardt, A. Hewer, P. L. Grover and D. H. Phillips. 1991. Evaluation of DNA-binding activity of hydroxyanthraquinones occurring in *Rubia tinctorum* L. *Carcinogenesis*. 12:1265-1271.

- [101] J. H. Lee, Y. G. Kim, S. Y. Ryu, J. Lee. 2016. Calcium-chelating alizarin and other anthraquinones inhibit biofilm formation and the hemolytic activity of *Staphylococcus aureus*. *Sci Rep.* 6: 19267
- [102] S. Das, A. Saha, P. C. Mandal. 1997. Radiation-induced double-strand modification in calf thymus DNA in the presence of 1,2-dihydroxy-9,10-anthraquinone and its Cu(II) complex. *Environ Health Perspect.* 105:1459-1462.
- [103] S. Das, A. Saha, P. C. Mandal. 1995. Radiosensitization of thymine by Fe (III)-1, 2 dihydroxyanthraquinone complex in dilute aqueous solution. *Journal of Radioanalytical and Nuclear Chemistry.* 196:57-63.
- [104] P. S. Guin, P. C. Mandal, S. Das. 2012. A comparative study on the interaction with calf thymus DNA of a Ni(II) complex of the anticancer drug adriamycin and a Ni(II) complex of sodium 1,4-dihydroxy-9,10-anthraquinone-2-sulphonate. *Journal of Coordination Chemistry.* 65:705–721.
- [105] C. A. Tsipis, E. G. Bakalbassis, V. P. Papageorgiou, M. N. Bakola-Christianopoulou. 1982. Structure and bonding of mononuclear and homobinuclear chelates of some divalent metal ions with the ligand 1,8-dihydroxyanthraquinone. *Canadian J. Chem.* 60:2477.
- [106] L. D. Pettit, J. Ueda, E. Morier-Teissier, N. Helbecque, J. L. Bernier, J. P. Henichart, H. Kozlowski. The coordination of copper (II) to 1-hydroxy-4-l glycyl-histidyl-lysine) - anthraquinone; a synthetic model of anthraquinone anti-cancer drugs. *Journal of Inorganic Biochemistry.* 45:203-210.
- [107] S. Mukherjee Chatterjee, C. K. Jain, S. Singha, P. Das, S. Roychoudhury, H K. Majumder, S. Das. 2018. Activity of Co<sup>II</sup>–quinalizarin: A novel analogue of anthracycline based anticancer agents targets human DNA topoisomerase, whereas quinalizarin itself acts via formation of semiquinone on acute lymphoblastic leukemia MOLT-4 and HCT 116 cells. *ACS Omega.* 3:10255–10266.

[108] B. Mandal, S. Singha, S. K. Dey, S. Mazumdar, T. K. Mondal, P. Karmakar, S. Kumar, S. Das. 2016. Synthesis, crystal structure from PXRD of a  $Mn^{II}(\text{purp})_2$  complex, interaction with DNA at different temperatures and pH and lack of stimulated ROS formation by the complex. *RSC Adv.* 6:51520–51532.

[109] P. Das, C. K. Jain, S. Roychoudhury, H. K. Majumder, S Das. 2016. Design, synthesis and in vitro anticancer activity of a Cu(II) complex of carminic acid: A novel small molecule inhibitor of human DNA topoisomerase I and topoisomerase II. *ChemistrySelect.* 1:6623 – 6631.

[110] E. V. Andreevaa, A. M. Vinogradova, A. N. Tevyashov, E. N. Olsufyeva, T. V. Burovac, N. V. Grinberg, V. Ya. Grinberg, S. G. Skuridin, M. N. Preobrazhenskay, A. A. Shtil, V. A. Kuzmin Studies of complex formation of olivomycin A, and its derivatives with DNA. *Biochemistry and Biophysics.* 435:334–338.

[111] S. Chakrabarti, M. A. Mir, D. Dasgupta. 2001. Differential interactions of antitumor antibiotics chromomycin A(3) and mithramycin with d(TATGCATA)(2) in presence of  $Mg^{2+}$ . *Biopolymers.* 62:131–140.

# CHAPTER 3

## Reactive Oxygen Species and their measurement



Free radicals are species having unpaired electrons in the valence shell of any atom that makes it highly reactive. They abstract electrons from other molecules turning them into free radicals. When oxygen molecules are cleaved they form unstable free radicals in the biological system which damage living cells. This process is known as oxidative stress. In 1956 Denham Harman's work, which suggests free radicals play a role in the ageing process unlocked the world of free radicals in biological systems.<sup>1</sup> The discovery of superoxide dismutase (SOD) by McCord and Fridovich in 1969 is considered yet another key milestone in the burgeoning research on radicals in biological systems, which provides convincing evidence of the importance of free radicals.<sup>2</sup> It is believed that there was no free oxygen on earth during the early stages.<sup>3</sup> The concentration of oxygen in the biosphere gradually rose as photosynthesis increased; therefore number of aerobic organisms increased. To accomplish cellular processes, aerobic organisms produce chemical energy in the form of adenosine 5'-triphosphate (ATP) in the presence of oxygen. The electronic configuration of dioxygen made it susceptible to radical generation due to the existence of two unpaired electrons in two distinct antibonding ( $\pi^*$ ) orbitals. When oxygen is reduced by one electron, it produces the superoxide radical anion ( $O_2^{\bullet-}$ ) which then spontaneously produces  $H_2O_2$  by dismutation.<sup>4,5</sup> Superoxide is the precursor of many radical and non-radical reactive oxygen species (ROS). By Fenton reactions  $H_2O_2$  can be fully converted to water or partially reduced to the hydroxyl radical ( $OH^\bullet$ ), involving the participation of some metal ions.<sup>5,6</sup>



Transition metal ions  $Fe^{3+}$  and  $Cu^{2+}$  with a stable lower oxidation state participate in the above-mentioned Fenton reactions, resulting in an increase in the formation of  $OH^\bullet$ , which is a source of damage to DNA or other cell organelles;  $OH^\bullet$  being one of the strongest radicals. Therefore complexes, particularly with such metal ions having the ability to switch from one

### *Chapter 3: Reactive oxygen species*

---

oxidation state to another involving  $O_2^{\bullet-}$  and  $H_2O_2$  propagating the process, exhibit better efficacy; a manifestation of complex formation.<sup>5-7</sup>

Reactive oxygen species (ROS) are primarily generated in two ways: endogenously or exogenously. Endogenously major producers of ROS are NADPH oxidase (NOX) complexes in the cell membrane, mitochondria, endoplasmic reticulum and peroxisomes.<sup>8,9</sup> If the proton concentration gradient in the inner membrane of the mitochondria is high (proton motive force) and the flow of electrons in the respiratory chain somewhat less favoured, particularly when availability of ADP is low, the likelihood of reduction of molecular oxygen to superoxide rather than to water increases i.e. the one-electron reduction with oxygen becomes higher.<sup>10</sup> The superoxide radical anion ( $O_2^{\bullet-}$ ) is not highly reactive on its own, but its protonated form, hydroperoxyl radical ( $HO_2^{\bullet}$ ) can inactivate specific enzymes or initiate lipid peroxidation.<sup>11</sup> Cellular superoxide is generated as a result of superoxide leakage into the cytoplasm via mitochondrial permeability transition pore (MPTP).<sup>12</sup>

Exogenous reactive oxygen species (ROS) are produced by pollutants, pharmaceuticals, cigarettes, xenobiotics, smoking and by radiation. When ionising radiation interacts with water it leads to radiolysis of water. This can produce harmful intermediates. Owing to the presence of an enormous amount of water in the human body, there is a high risk associated with radiolysis of water in the presence of ionising radiation. Water undergoes a three-step reaction pathway producing hydroxyl radicals ( $OH^{\bullet}$ ), hydrogen peroxide ( $H_2O_2$ ), superoxide radical anion ( $O_2^{\bullet-}$ ) and oxygen ( $O_2$ ). Hydroxyl radical is a highly reactive species capable of readily removing electrons from any molecule in its path and converting the target to a free radical; initiating a chain reaction.<sup>8,9,13-15</sup>

ROS such as hydrogen peroxide, hydroxyl radicals and superoxide anions that are produced under normal metabolic cellular processes such as aerobic metabolism or inflammation, are particularly reactive intermediates due to the presence of unpaired electrons. Depending on



their concentration, ROS can be beneficial or harmful. They appear to have a role in coordinating lymphoid cell recruitment to the wound site as well as in efficient tissue healing.<sup>16-18</sup> ROS can regulate formation of blood vessels (angiogenesis) at a wound site.<sup>16</sup> When ROS levels are high, they overwhelm the cell's antioxidant defence mechanism, causing redox equilibrium to be disrupted and oxidative stress to occur. Excess ROS can damage cellular lipids, proteins and DNA, disrupting normal function and hastening the ageing process.<sup>14</sup> Antioxidant scavengers like thioredoxin, glutathione and ascorbate as well as anti-oxidant enzymes like superoxide dismutase, catalase, thioredoxin reductase, and glutathione peroxidase protect cells by removing reactive oxygen species (ROS). Research has shown that cancer cells produce more ROS than normal cells.<sup>19</sup> In case of pancreatic cancer, low to moderately elevated levels of ROS promote carcinogenesis and cancer growth, but high levels of ROS cause considerable cell damage and death of cancer cells. ROS formation may be employed therapeutically to cure cancer and a cell's capacity to shield itself from ROS is linked to its resistance to chemotherapy. Although ROS generation is usually high in cancer patients, when external drugs enter the body it increases much more rapidly which could be damaging to the heart and can lead to heart attack. It is therefore important to maintain a delicate balance between beneficial and detrimental effects of ROS in a living organism; a process that is achieved in the cell through redox regulation. However, oxidative stress condition is found to assist cancer cells to survive in adverse conditions by activating an antioxidant programme.<sup>20</sup>

Various compounds having anticancer properties have been used as drugs. Various cytosolic drugs and antineoplastic agents are found to be effective in eliminating tumours by triggering programmed cell death or apoptosis. According to several research, formation of ROS is a crucial factor during treatment with drugs. Drug assisted excess production of ROS activates the redox sensitive c-Jun N-terminal kinases (JNKs) or stress activated protein kinase

(SAPK). Anthracyclines, like daunorubicin and doxorubicin, produce ROS, which activates the neutral sphingomyelinase enzyme and elevates intracellular ceramide.<sup>21</sup> In U937 human monoblastic leukaemia cells, cell permeant ceramides induce both an increase in ROS, JNK/SAPK activation that is responsible for apoptosis.<sup>22</sup> In case of breast cancer, diapirin is an effective anticancer drug that kills cancer cells by boosting ROS levels. However, too much ROS generation by drugs in cancer chemotherapy is dangerous since it has adverse effects on the biological system, the most serious being cardiotoxicity. Hence it is very much crucial to maintain a proper balance between efficacy and hazardous side effects associated with ROS formation while using different chemotherapeutic drugs. For anthracyclines, it is established that its metal complexes modulate ROS generation to an extent that diminishes cardiotoxic side effects. At the same time, since ROS is advantageous, having the potential to destroy cells, a compromise on drug action related to ROS formation might occur. However, in most cases, the complex comes out a winner because what it sacrifices in ROS generation pathways is compensated through other attributes of complex formation.<sup>21,23-33</sup>

Over the years, researchers have developed various methods for detecting ROS. Various fluorescent probes (for example, the DCFDA assay), ESR (electron spin resonance) are prominent among them. With progress in science and technology, more sophisticated methods for an exact measurement of ROS have become available. Some of them are detection of superoxide, cell-targeted hydroxylamine spin probes, fluorescent boronate containing probes, immune spin trapping etc.

❖ **Important techniques used for measurement of ROS:**

❖ **1. Spin trapping:**

Superoxide, one of the most important forms of ROS in the biological system, serves as the source to several other ROS that could include H<sub>2</sub>O<sub>2</sub>, ONOO<sup>-</sup> and lipid peroxides. Spin

trapping has been one of the early methods for measuring superoxide.<sup>34-36</sup> 5, 5-dimethyl-1-pyrroline-N-oxide (DMPO) is used in this experiment as the trapping material to lengthen the lifespan of radicals so that an ESR signal is detected accurately. This happens when a covalent bond is formed between the superoxide and DMPO, resulting in the formation of a DMPO-OOH adduct that is converted to DMPO-OH due to instability of DMPO-OOH.<sup>37</sup> This approach has several limitations due to the presence of superoxide dismutase (SOD) and ascorbate as rivals of DMPO in interacting with  $O_2^{\bullet-}$ .<sup>38</sup>

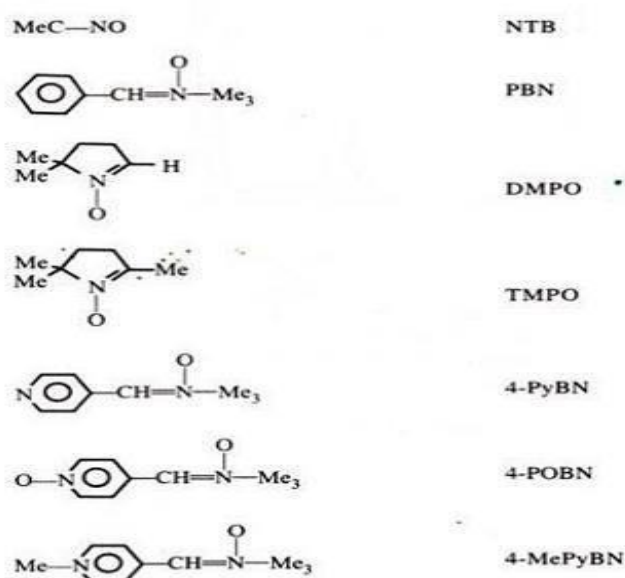


**Figure 1:** Various types of spin trapping agents.

## 2. Chemiluminescent technique:

Any free radical has the ability to emit low-level chemiluminescence.<sup>39</sup> The emitted energy is measured using a luminometer where radicals release energy in the form of light. The rate of reaction and intensity of chemiluminescence depend on the concentration of free radicals.<sup>40</sup> 2-methyl-6-(p-methoxyphenyl)-3,7-dihydroimidazole [1,2-a] pyrazin-3-one (MCLA), luminol, lucigenin, the luciferin analogue and coelenterazine are some chemiluminescent probes that are used as synthetic or natural luminating agents in biological systems to quantify luminescence.<sup>39</sup>

■ **Fluorescence probes:**

**3. Fluorescence of dihydroethidium:**

Dihydroethidium (DHE) is most often used as a “reactive oxygen species” probe for detecting intracellular superoxide. The combination of DHE and superoxide results in the formation of 2-hydroxyethidium, a red luminous molecule that is a specific adduct of the two. Simultaneously, a non-specific redox reaction yields another oxidised product (ethidium), which is also red in colour. Owing to the fact that the fluorescent spectra of ethidium and 2-hydroxyethidium overlap, determining the amount of 2-hydroxyethidium present from a simple fluorescence detection becomes exceedingly challenging. A tricky use of HPLC allows the separation of 2-hydroxyethidium and ethidium from a mixture by which it becomes possible to know the amount of the specific adduct of DHE and superoxide.<sup>34,41,42</sup>

**4. DCFDA Assay:**

The fluorogenic dye 2', 7'-dichlorofluorescein diacetate (DCFDA) is a cell permeant reagent that measures the activity of peroxy, hydroxyl and other reactive oxygen species (ROS).<sup>43-</sup><sup>46</sup> DCFDA is de-acetylated by cellular esterases to a non-fluorescent molecule after diffusion into the cell, which is then oxidised by ROS to 2', 7'-dichlorofluorescein (DCF).<sup>43-45</sup> DCF is a highly fluorescent chemical that fluoresces green. The LD<sub>50</sub> dose of the compounds under investigation is administered to cells, which are then left to stand for 30 minutes. By incubating the treated cells with the free radical generator H<sub>2</sub>O<sub>2</sub> (40 M) for further 30 minutes, ROS is induced. The cells are then rinsed with ice cold Hanks balanced salt solution (HBSS) and lysed with an alkaline solution and their fluorescence is recorded.

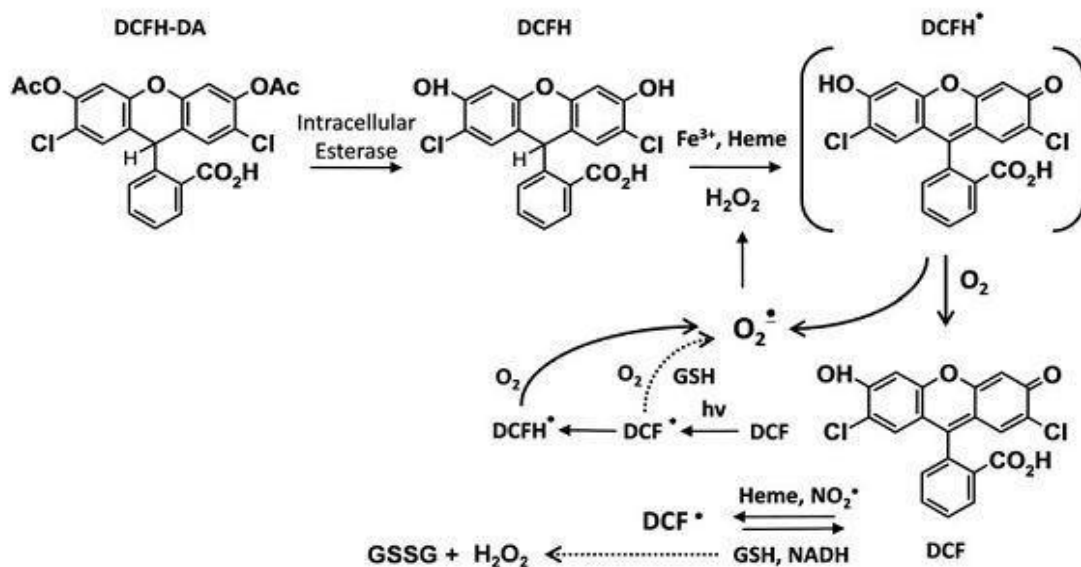


**Figure 2:** Intracellular reaction of dichlorodihydro-fluorescein diacetate (DCFH-DA) and redox cycling of 2, 7-di-chlorodihydrofluorescein.

### 5. Detection of extracellular H<sub>2</sub>O<sub>2</sub> by Amplex Red:

This method is used for detecting H<sub>2</sub>O<sub>2</sub> in the mitochondria.<sup>47,48</sup> There are some difficulties in using Amplex Red (N-acetyl-3,7-dihydroxy phenoxazine assay) due to its very high light sensitivity, inability to directly assess intracellular H<sub>2</sub>O<sub>2</sub> and instability.<sup>37</sup> Therefore, it cannot be used at high concentration due to production of O<sub>2</sub><sup>•-</sup> and H<sub>2</sub>O<sub>2</sub> by auto oxidation reactions.

### 6. Detection of superoxide by cytochrome c:

Another approach for detecting large amounts of O<sub>2</sub><sup>•-</sup> produced by cells into extracellular space by various chemical processes or separate enzymes is by the reduction of ferricytochrome c. This method is based on ferricytochrome c being reduced to ferrocycytochrome c by O<sub>2</sub><sup>•-</sup>. The reaction is followed by monitoring the absorbance at 550 nm. Ferricytochrome c can be reduced directly by electrons donated by enzymes or by other compounds.<sup>49-51</sup>

❖ **Modern methods for detection of ROS:**

**7. Cyclic hydroxylamine spin probes:**

To measure the total cellular and mitochondrial  $O_2^{\bullet-}$  in cultured cells, cyclic hydroxylamine can be used which is oxidised by  $O_2^{\bullet-}$  and other reactive oxygen species, resulting in the formation of an EPR detectable, stable, nitric oxide radical with a life time of many hours. The reaction is fast ( $10^3$  to  $10^4 M^{-1}s^{-1}$  at pH 7.4). As a result, it can detect superoxide radicals more precisely before they are converted to other forms by reacting with an anti-oxidant. Hydroxylamine can be used at low concentrations where there are low chances of having potential artifact due to its single step reaction with superoxide.<sup>52-54</sup>

**8. Boronate based fluorescence probes:**

Chang et al. recently developed cell permeable boronate-based probes peroxyresorufin-1, peroxyfluor-1, and peroxy xanthone-1 that fluoresces in the red, green and blue regions respectively when exposed to  $H_2O_2$ .<sup>55,56</sup> The probe can detect even trace amounts of  $H_2O_2$  in living cells. Researchers also developed a boronate-based peroxy-yellow 1 probe using triphenyl phosphonium that can detect  $H_2O_2$  in the mitochondria.<sup>57</sup> Researchers are now attempting to develop more precise methods for detecting ROS that are flawless. Immuno spin trapping and X- and L-band ESR spectroscopy for *in vivo* ROS detection are two techniques that have not yet been fully established but are under investigation.<sup>34</sup>

**References:**

- [1] D. Harman. 1956. Aging: a theory based on free radical and radiation chemistry. *J. Gerontol.* 11: 298-300.
- [2] J. M. McCords, I. Fridovich. 1969. Superoxide dismutase an enzymic function for erythrocyte cytochrome c (hemocyanin). *J. Biol. Chem.* 244:6049-6065.
- [3] D. L. Gilbert. 2011. Evolutionary aspects of atmospheric oxygen and organisms. *Comprehensive Physiology.* 1059–1094.
- [4] W. Droge. 2002. Free radicals in the physiological control of cell function. *Physiol. Rev.* 82: 47-95.
- [5] S. I. Liochev, I. Fridovich. 1999. Superoxide and iron: partners in crime. *IUBMB Life.* 48:157–161.
- [6] B. Lipinski. 2011. Hydroxyl radical and its scavengers in health and disease, *Oxidative Medicine and Cellular Longevity.* Article ID 809696, 9 pages.
- [7] J. F. Turrens. 2003. Mitochondrial formation of reactive oxygen species. *J. Physiol.* 552:335–344.
- [8] D. Han, E. Williams, E. Cadenas. 2001. Mitochondrial respiratory chain-dependent generation of superoxide anion and its release into the inter membrane space, *Biochem. J.* 353:411-416.
- [9] F. Muller. 2000. The nature and mechanism of superoxide production by the electron transport chain: its relevance to aging, *J. Amer. Aging Assoc.* 23:227-253.
- [10] G. Bartosz. 2009. Reactive oxygen species: destroyers or messengers? *Biochem. Pharmacol.* 77:1303–1315.

### **Chapter 3: Reactive oxygen species**

---

- [11] P. Storz. 2006. Reactive oxygen species–mediated mitochondria-to-nucleus signaling: a key to aging and radical-caused diseases. *Sci STKE*. 7 pages.
- [12] G. Y. Liou, P. Storz, 2010. Reactive oxygen species in cancer. *Free Radic Res*. 44:1-31.
- [13] J. Liu, E. Head, A. M. Gharib, W. Yuan, R. T Ingersoll, T. M. Hagen. 2002. Memory loss in old rats is associated with brain mitochondrial decay and RNA DNA oxidation: Partial reversal by feeding acetyl-L-carnitine and/or R- $\alpha$ -lipoic acid. *PNAS*. 99: 2356–2361.
- [14] E. R. Stadtman. 1992. Protein oxidation and aging. *Science*. 257: 1220-1224.
- [15] J. M. Carney, P. E. Starke-reed, C. N. Oliver, R. W. Landum, M. S. Cheng, J. F. Wu, R. A. Floyd. 1991. Reversal of age-related increase in brain protein oxidation, decrease in enzyme activity, and loss in temporal and spatial memory by chronic administration of the spin trapping compound N-tert-butyl-a-phenylnitron. *Neurobiology*. 88: 3633-3636.
- [16] T. Finkel. 1998. Oxygen radicals and signaling. *Current Opinion in Cell Biology*. 10: 248-253.
- [17] C. Dunnill, T. Patton, J. Brennan, J. Barrett, M. Dryden, J. Cooke, D. Leaper, N.T Georgopoulos. 2017. Reactive oxygen species (ROS) and wound healing: the functional role of ROS and emerging ROS-modulating technologies for augmentation of the healing process. *Int. Wound. J*. 14: 89-96.
- [18] N. J. Holbrook, S. Ikeyama. 2002. Age related decline in cellular response to oxidative stress: links to growth factor signaling pathways with common defects, *Biochemical Pharmacology*. 64: 999-1005.
- [19] D. Zhou, L. Shao, D. R. Spitz. 2014. Reactive oxygen species in normal and tumor stem cells, *Adv. Cancer Res*. 122: 1–67.



- [20] L. Zhang, J. Li, L. Zong X. Chen, K. Chen, Z. Jiang, L. Nan, X. Li, W. Li, T. Shan, Q. Ma, Z. Ma. 2016. Reactive oxygen species and targeted therapy for pancreatic cancer. *Oxid. Med. Cell Longev.* Article ID 1616781, 9 pages.
- [21] R. B. Martin. 1985. Metal ions in biological systems, H. Sigel, Ed., Dekker: New York, 19.
- [22] W. Davis, Z. Ronai, K. D. Tew. 2001. Cellular thiols and reactive oxygen species in drug-induced apoptosis. *J. Pharmacol. Exp. Ther.*, 296: 1-6.
- [23] F. T. Greenaway, J. C. Dabrowiak. 1982. The binding of copper ions to daunomycin and Adriamycin. *J. Inorg. Biochem.* 16: 91-107.
- [24] M. Tachibana, M. Iwaizumi, S. Tero-Kubota. 1987. EPR studies of copper (II) and cobalt (II) complexes of adriamycin. *J. Inorg. Biochem.* 30: 133-140.
- [25] B. F. Matzanke, E. Bill, C. Butzlaff, A. X. Trautwein, H. Winkler, C. Hermes, H.-F. Nolting, R. Barbieri,; U. Russo.1992. Evidence for polynuclear aggregates of ferric daunomycin. A Mössbauer, EPR, X-ray absorption spectroscopy and magnetic susceptibility study. *Eur.J. Biochem.* 207: 747-755.
- [26] S. S. Massoud, R. B. Jordan. 1991. Kinetic and equilibrium studies of the complexation of aqueous iron (III) by daunomycin, quinizarin, and quinizarin-2-sulfonate. *Inorg. Chem.* 30: 4851-4856.
- [27] D. Gelvan, E. Berg, P. Saltman, A. Samuni. 1990. Time-dependent modifications of ferricadriamycin. *Biochem. Pharmacol.* 39: 1289-1295.
- [28] H. Beraldo, A. Garnier-Suillerot, L. Tosi, F. Lavelle. 1985. Iron(III)-adriamycin and iron( III)-daunorubicin complexes: physicochemical characteristics, interaction with DNA, and antitumor activity. *Biochemistry.* 24: 284-289.

### **Chapter 3: Reactive oxygen species**

---

- [29] A. Moustatih, M. M. L. Fiallo. 1989. A. Garnier-Suillerot, Bifunctional antitumor compounds. Interaction of adriamycin with metallocene dichlorides. *J. Med. Chem.* 32: 336-342.
- [30] M. M. L. Fiallo, A. Garnier-Suillerot. 1986. Metal anthracycline complexes as a new class of anthracycline derivatives. Palladium (II)-adriamycin and palladium (II)-daunorubicin complexes: physicochemical characteristics and antitumor activity. *Biochemistry.* 25: 924-930.
- [31] A. Pasini, G. Pratesi, G. Savi, F. Zunino. 1987. A doxorubicin-Pt(II) complex. Chemistry and antitumor activity. *Inorg. Chim. Acta.* 137: 123-124.
- [32] T. Allman, R. E. Lenkinski. 1987. Adriamycin Complexes of Pd (II) and Pt(II), *J. Inorg. Biochem.* 30: 35-43.
- [33] V. Mansat-de Mas, C. Bezombes, A. Quillet-Mary, A. Bettaïeb, A. D. D'orgeix, G. Laurent, J. P. Jaffrézou. 1999. Implication of radical oxygen species in ceramide generation, c-Jun N-terminal kinase activation and apoptosis induced by daunorubicin, *Mol. Pharmacol.* 56: 867-874.
- [34] S. I. Dikalov, D. G. Harrison. 2014. Methods for detection of mitochondrial and cellular reactive oxygen species. *Antioxidants & Redox Signaling.* 20: 372-382.
- [35] G. R. Buettner, R. P. Mason. 1990. Chapter 2: Spin-trapping methods for detecting superoxide and hydroxyl free radicals in vitro and in vivo, *Methods Enzymol.* 186: 127-33.
- [36] S. Dikalov, K. K. Griendling, D. G. Harrison. 2007. Measurement of reactive oxygen species in cardiovascular studies. *Hypertension.* 49: 717-727.

- [37] E. Finkelstein, G. M. Rosen, E. J. Rauckman. 1980. Spin trapping of superoxide and hydroxyl radical: practical aspects. *Arch. Biochem. Biophys.* 200: 1-16.
- [38] H. Zhao, J. Joseph, H. M. Fales, E. A. Sokoloski, R. L. Levine, J. Vasquez-Vivar, B. Kalyanaraman. 2005. Detection and characterization of the product of hydroethidine and intracellular superoxide by HPLC and limitations of fluorescence. *PNAS.* 102: 5727–5732.
- [39] J. Stauf. 1965. Chemiluminescence of some reactions with molecular oxygen, *Photochemistry and photobiology.* 4: 1199-1205.
- [40] V. I. Bruskov, L. V. Malakhova, Z. K. Masalimov. 2002. Heat induced formation of Reactive oxygen species and 8-oxoguanine, a biomarker of damage to DNA. *Nucleic Acids Research.* 30: 1354-1363.
- [41] J. Zielonka, B. Kalyanaraman. 2010. Hydroethidine and mitosox-derived red fluorescence is not a reliable indicator of intracellular superoxide formation: Another inconvenient truth. *Free Radic. Biol. Med.* 48: 983–1001.
- [42] L. Benov, L. Sztejnberg, I. Fridovich. 1998. Critical evaluation of the use of hydroethidine as a measure of superoxide anion radical. *Free Radic. Biol. Med.* 25: 826– 831.
- [43] H. Wang, J. A. Joseph. 1999. Quantifying cellular oxidative stress by dichlorofluorescein assay using microplate reader. *Free Rad. Biol. Med.* 27: 612-616.
- [44] O. Myhre, J. M. Andersen, H. Aarnes, F. Fonnum. 2003. Evaluation of the probes 2',7'-dichlorofluorescein diacetate, luminol, and lucigenin as indicators of reactive species formation., *Biochem. Pharmacol.* 65: 1575–1582.
- [45] A. Gomes, E. Fernandes, J. L. Lima. 2005. Fluorescence probes used for detection of reactive oxygen species. *J. Biochem. Biophys. Methods.* 65: 45–80.

- [46] M. Zhou, Z. Diwu, N. Panchuk-Voloshina, R. P. Haugland. 1997. A stable nonfluorescent derivative of resorufin for the fluorometric determination of trace hydrogen peroxide: applications in detecting the activity of phagocyte NADPH oxidase and other oxidases. *Anal. Biochem.* 253:162–168.
- [47] A. Panov, S. Dikalov, N. Shalbuyeva, G. Taylor, T. Sherer, J. T. Greenamyre. 2005. Rotenone model of parkinson disease multiple brain mitochondria dysfunctions after short term systemic rotenone intoxication. *J. Biol. Chem.* 280: 42026–42035.
- [48] P. Das, C. K. Jain, S. K. Dey, R. Saha, A. Dutta Chowdhury, S. Roychoudhury, S. Kumar, H. K. Majumder, S. Das. 2014. Synthesis, crystal structure, DNA interaction and *in vitro* anticancer activity of a Cu(II) complex of purpurin: dual poison for human DNA topoisomerase I and II. *RSC Advances.* 4: 59344-59357.
- [49] S. Roy, P. Mondal, P. S. Sengupta, D. Dhak, R. C. Santra, S. Das, P. S. Guin. 2015. Spectroscopic, computational and electrochemical studies on the formation of the copper complex of 1-amino-4-hydroxy-9, 10-anthraquinone and effect of it on superoxide formation by NADH dehydrogenase. *Dalton Trans.* 44: 5428-5440.
- [50] S. Das, A. Saha, P. C. Mandal. 1996. Studies on the formation of Cu(II) and Ni(II) complexes of 1,2-dihydroxy-9,10-anthraquinone and lack of stimulated superoxide formation by the complexes. *Talanta.* 43: 95-102.
- [51] S. I. Dikalova, I. A. Kirilyukb, M. Voinovc, I. A. Grigor'ev. 2011. EPR detection of cellular and mitochondrial superoxide using cyclic hydroxylamines. *Free Radic. Res.* 45: 417–430.
- [52] D. C. Fernandes, J. Wosniak, L. A. Pescatore, M. A. Bertoline, M. Liberman, F. R. Laurindo, C. X. Santos. 2007. Analysis of DHE-derived oxidation products by HPLC in the

assessment of superoxide production and NADPH oxidase activity in vascular systems. *Am. J. Physiol. Cell Physiol.* 292: 413–422.

[53] E. Marchesi, C. Rota, Y. C. Fann, C. F. Chignell, R. P. Mason. 1999. Photoreduction of the fluorescent dye 2'-7'-dichlorofluorescein: a spin trapping and direct electron spin resonance study with implications for oxidative stress measurements, *Free Radic. Biol. Med.* 26: 148–161.

[54] M. C. Y. Chang, A. Pralle, E. Y. Isacoff, C. J. Chang. 1999. A selective, cell-permeable optical probe for hydrogen peroxide in living cells. *Free Radic. Biol. Med.* 26: 148–161.

[55] E. W. Miller, A. E. Albers, A. Pralle, E. Y. Isacoff, C. J. Chang. 2005. Boronate-based fluorescent probes for imaging cellular hydrogen peroxide. *J. Am. Chem. Soc.* 127: 16652-16659.

[56] B. C. Dickinson, C. J. Chang. 2008. A targetable fluorescent probe for imaging hydrogen peroxide in the mitochondria of living cells. *J. Am. Chem. Soc.* 130: 9638–9639.



# CHAPTER 4

## Chemical modification of nucleic acid bases and DNA





**Introduction:**

In 1869, a Swiss doctor Friedrich Miescher, while investigating on the chemical composition of leukocytes discovered what is today known as DNA. Some of the properties of DNA like its acidic nature, a large molecular weight and its presence in the nucleus were first determined by Miescher. He was also the first to link the role of DNA to cell proliferation. Analyzing pure DNA from salmon sperm he had stated DNA might have a key role in fertilization and in the transmission of hereditary traits.<sup>1,2</sup> After Miescher's initial explanation in the late 1870s, Albrecht Kossel discovered that DNA was composed of four bases and sugar molecules.<sup>3</sup> In late 1940s and early 1950s, Chargaff and coworkers determined the chemical composition of DNA to show it consists of purine [Adenine (A), Guanine (G)] and pyrimidine bases [Cytosine (C), Thymine (T)] called nucleotides and that the molar ratio of bases A/T and G/C were consistently nearly one. The relative distribution of bases in DNA i. e. in the DNA framework is the same in individuals of similar species but different between species.<sup>4</sup> Then the three dimensional structure of DNA was proposed by Watson and Crick in 1953 with substantial evidence obtained from the X-ray crystallography diffraction data generated by Rosalind Franklin and Maurice Wilkins establishing a double helical structure.<sup>5</sup> Each helix was shown to be a group of nucleotides held together by phosphodiester bonds between two adjoining sugar residues and that two helices are linked to each other by hydrogen bonds formed by pairs of bases. Chargaff's data showed T pairs only with A while C pairs only with G and that these two pairing combinations permit an efficient hydrogen bonding. Subsequently it was also identified that heating or exposure to various chemicals cause a disruption of hydrogen bonds that unwind the DNA strands resulting in a loss of its varied biological functions.<sup>6,7</sup> A change in the chemical structure of DNA that we commonly refer to as DNA modification or in more severe cases as DNA damage, is generated either following an exposure to radiation or to chemotherapeutic agents that initiate apoptosis

#### ***Chapter 4: Chemical modification of nucleic acid bases and DNA***

---

(programmed cell death). These, either directly interact with DNA or through formation of free radicals or several intermediates on them that in turn destroy the correct three dimensional structure. Damage occurs if the rate of DNA damage eclipses its repair capacity which then prevents cells from undergoing mutagenesis and progression to cancer.<sup>8,9</sup> Needless to say, a lot of effort is being made these days in terms of research to investigate various aspects of cancer although most approaches have serious side effects that adversely affect the health of a patient.

DNA is an intrinsically reactive molecule, highly prone to damage by endogenous and exogenous agents. Endogenous DNA damage arises from species that exist naturally within cells while exogenous DNA damage is mediated by cytotoxic drugs, alkylating or crosslinking DNA targeting agents, ultraviolet radiation,  $\gamma$ -radiation and various other forms of stimuli.<sup>10-12</sup> To get an idea as to how these stimuli cause a damage to DNA, researchers thought it essential to initially work with pyrimidine and purine bases using the same stimuli, so that damage caused to a pyrimidine or purine base is first identified. Then when experiments are performed on DNA, correlations with appropriate approximations on a scaled up system may easily be understood. It is also seen that damage caused to free pyrimidine and purine bases by the same techniques that are used for initiating DNA damage, lead to almost similar results as for DNA damage itself,<sup>13,14</sup> although mechanistic pathways for the degradation of free bases could be quite different from that of the same bases when present as a part of a macromolecule (say, DNA). Almost all forms of damage interferes with DNA replication and RNA transcription leading to alteration in protein function that reduces cell metabolism causing interphase death i.e. loss of reproductive capacity.<sup>11</sup> Chemical modification of nucleic acid bases are reported to have serious effects on cell viability and cell functioning.<sup>15,16</sup> Ionizing radiation can damage DNA either directly or via radiolysis of surrounding water molecules generating various forms of lesions, like single-strand breaks

(SSB), double-strand breaks (DSB) or base damage. Among these the most toxic is DSB and is responsible for cell death.<sup>17</sup> A large variety of damaged base products are formed upon irradiation of DNA that lead to strand breaks. Direct ionization of DNA results in qualitatively similar products to those formed in an indirect pathway during investigations using the pulse radiolysis technique.<sup>18</sup> Ionizing radiation passing through water molecules produce a cluster of radicals and molecular products that contain hydroxyl radicals ( $\bullet\text{OH}$ ), solvated electrons ( $e^-_{\text{aq}}$ ), hydrogen radicals ( $\bullet\text{H}$ ),  $\text{H}_2\text{O}_2$  and  $\text{H}_2$ . The highly reactive  $\bullet\text{OH}$  reacts with DNA i.e. with its constituent nucleic acid bases and sugar units at diffusion-controlled rates while solvated electrons react only with nucleic acid bases and not with sugar moieties. Reactions involving  $\bullet\text{H}$  are slow.  $\bullet\text{OH}$  is more reactive towards nucleobases than with the sugar-phosphate moiety.  $\bullet\text{OH}$  attacks the C5—C6 double bond of both cytosine and thymine generating cytosine glycol and thymine glycol respectively. Saturation of the 5, 6-double bond of cytosine as a consequence of radical reactions is extremely important in causing mutations.<sup>19-21</sup> Cytosine glycol converts to 5-hydroxycytosine by dehydration which is the major product after irradiation of DNA in dilute aerated solutions. Cytosine differs from uracil at the C4 position of the pyrimidine ring where there is  $-\text{NH}_2$  instead of  $-\text{OH}$  (if enol form of uracil is considered). It has been observed that with time most of the degraded products of cytosine undergo loss of the amino group at C4 in different pathways to become derivatives of uracil.<sup>22</sup> For thymine,  $\bullet\text{OH}$  abstracts hydrogen from the methyl group; this is followed by addition of  $\text{O}_2$  to result in the formation of a peroxo derivative. However, this is the minor pathway. Yield of such methyl oxidation products is significantly higher in cellular DNA than in free nucleoside.<sup>23</sup> Radiation chemistry of purines is relatively poorly understood in comparison to pyrimidines.<sup>24-26</sup>

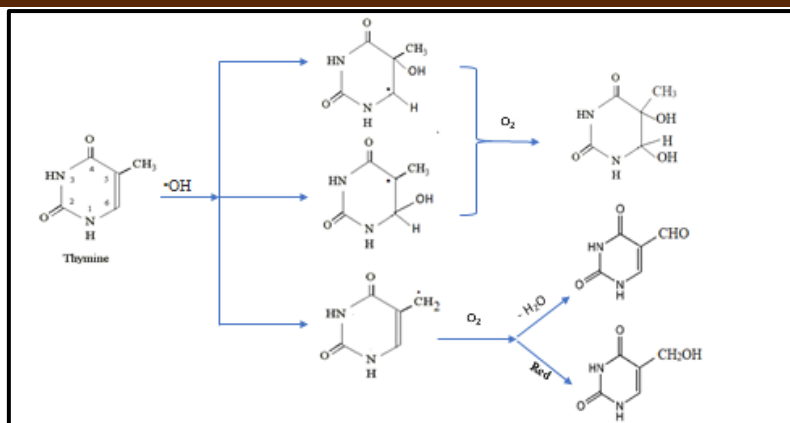


**Figure 1:** Three possible reactions between  $\bullet\text{OH}$  and thymine

Hydroxyl radical ( $\bullet\text{OH}$ ) being most responsive reactive oxygen species (ROS) instinctively react with neighbouring biomolecules. Hence, if their mode of reaction with nucleobases is known it would be helpful in interpreting their activity either with DNA or with any other molecule present in biological systems. Hence,  $\bullet\text{OH}$  induced oxidation or modification of nucleobases is a subject of active research.

Solvated electrons ( $e^-_{\text{aq}}$ ), produced due to radiolysis of water, reduce all forms of DNA bases.<sup>27</sup> The purine bases have extremely high intrinsic reactivity towards  $e^-_{\text{aq}}$ . Adenine reacts with  $e^-_{\text{aq}}$  at diffusion-controlled rates giving rise to the radical anion ( $\text{ade}^{\bullet-}$ ) that readily gets protonated at the heteroatom N upon reaction with water. This N-protonated radical converts to a C-protonated C<sub>8</sub>-H adduct radical involving a 1, 2-shift of hydrogen from nitrogen to an adjacent carbon.<sup>28</sup> The C<sub>8</sub>-H adduct radical is also produced following an attack by  $\text{H}\bullet$ , a free radical derived from the radiolysis of water at the C<sub>8</sub> position of adenine. The reaction between  $e^-_{\text{aq}}$  and guanine is almost similar to adenine. On the other hand, pyrimidine bases reacting both with  $e^-_{\text{aq}}$  and  $\text{H}\bullet$  form 5-H adduct radical yielding 5, 6-dihydro derivatives that undergo a further one electron reduction.<sup>29</sup>

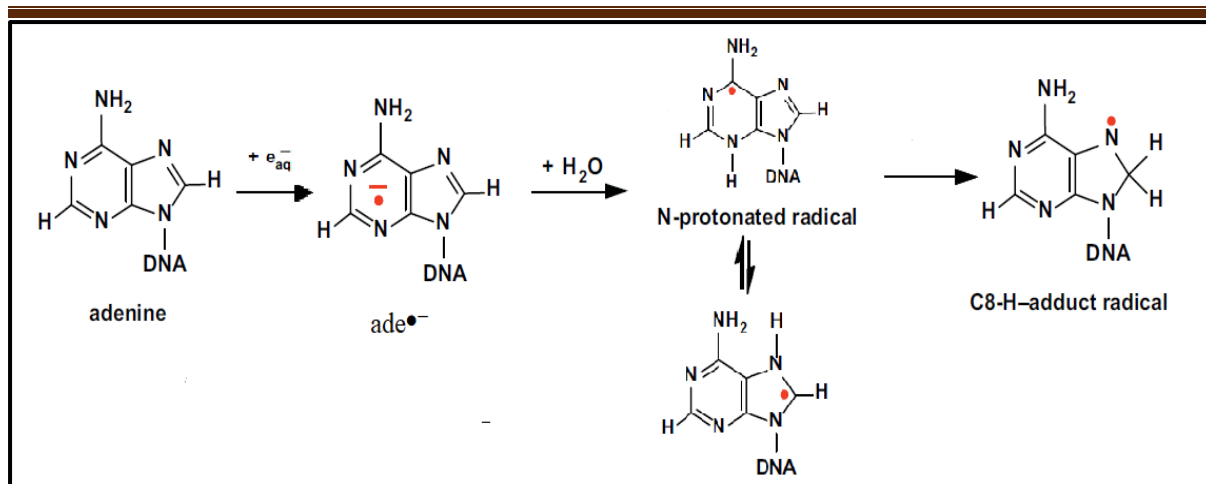


**Figure 2 :** Reaction of adenine with  $e_{aq}^-$

UV light is another powerful mutagenic and carcinogenic agent. Exposure of DNA to UV radiation modifies pyrimidine and purine bases producing an array of photoproducts that cause DNA protein crosslinks, DNA strand breaks etc. The wavelength and intensity of the radiation determines the distribution and yield of photoproducts. Upon absorbing UV photons directly, thymine undergoes intramolecular photochemical reactions through excited-state species that generate a thymine photo-dimer and their Dewar valence isomers. It was found that cytosine also experiences similar type of photodimerization either with adjacent cytosine or with thymine. Under physiological conditions, although the thymine moiety of these dimers is chemically stable, the cytosine moiety undergoes deamination producing either uracil or thymine-uracil photo-dimers. The resulting photo-adducts essentially contain a cyclobutane ring.<sup>30</sup> For a very long time, purine bases of DNA were considered to be extremely inert towards direct photochemical modification although a combined purine-pyrimidine photo-adduct (thymine-adenine) has been detected in UV-irradiated DNA.<sup>31,32</sup>

Oxidative DNA damage mediated by UV radiation brings about modification at the sugar moiety that initiates strand breaks. Several oxidation products of purine bases like 8-oxo-7, 8-dihydroguanyl (8-oxoGua), 2, 6-diamino-4-hydroxy-5-formamidoguanine (FapyGua), 8-oxo-Ade, FapyAde were reported to be produced upon exposure of DNA to UV radiation. These

#### ***Chapter 4: Chemical modification of nucleic acid bases and DNA***

---

are some of the most persistent lesions which if not repaired causes severe structural distortions affecting important cellular processes, compromising cellular viability, functional integrity, ultimately leading to mutagenesis and cell death.<sup>33-39</sup> If we compare the extent of nucleic acid base damage or DNA damage, a noticeable finding is that when a cell is exposed to  $\gamma$ -rays it shows much enhanced purine and pyrimidine base modification or DNA strand breaks than when exposed to UV light.<sup>23</sup>

Work on electrochemical stimuli induced (electrons delivered through solid phase interacting with matter in solution) damage of purine and pyrimidine based nucleobases although much fewer in number has also been performed.<sup>40</sup> The purine bases undergo two pH-dependent irreversible reduction at a dropping mercury electrode (DME) in acidic solution. One peak is due to a two-electron reduction of purine to 1, 6 dihydropurine while the other is due to a two-electron reduction of 1, 6 dihydropurine to 1, 2, 3, 6 tetrahydropurine. Each step involves addition of two electrons and two protons per N=C bond. If we consider the electrochemical behaviour of pyrimidines, it is seen cytosine exhibits redox behaviour that involves three successive steps. At first, the 3, 4 N=C bond undergoes a 2-electron reduction. The reduced product then converts to 2-hydroxypyrimidine by rapid deamination. This further reduces to a free radical that readily dimerizes before getting further reduced.<sup>40</sup> The study of DNA base modification by electrochemical methods is slightly problematic owing to very slow electron transfer kinetics, low sensitivity and overlapping oxidation peaks. Hence, to address such issues, development of electrochemical sensors by chemically modifying electrodes is considered beneficial.<sup>41</sup>

The above discussion provides an idea on DNA damage that occurs either through a direct interaction of ionizing radiation or through radiolysed products of water or due to interaction with UV light or by electrochemical stimuli. Another approach to the aspect of DNA damage is when the same techniques like ionizing radiation induced damage or UV light induced

damage or damage due to generation of electrochemical species is carried out in the presence of sensitizer molecules, making use of their electron affinic character. These enhance DNA damage. Several such exogenous damaging chemical agents cause a modification of cellular response as discussed below.

**Alkylating agents:**

Alkylating drugs are a primitive class of anticancer agents. Electrophilic alkylating agents attack the nucleophilic base ring nitrogens specifically at N<sub>7</sub> and exocyclic oxygen of guanine and at the N<sub>3</sub> position of adenine. Exocyclic N of the amino group of cytosine, adenine and guanine are poor nucleophiles to undergo methylation. *O*-alkylation of guanine is known to induce mutations as it readily mis-pairs with thymine followed by one round of replication of DNA containing O<sup>6</sup>-meG that result in DNA strand breaks whereas *N*-alkylations are cytotoxic and less mutagenic. Alkylating agents that are most commonly used in the laboratory include methylmethane sulphonate (MMS), ethylmethane sulphonate (EMS), *N*-methyl-*N'*-nitro-*N*-nitrosoguanidine (MNNG). For chemotherapy, cyclophosphamide is the most relevant alkylating agent clinically for treatment of various forms of leukaemia and solid tumor.<sup>42,43</sup>

**Crosslinking agents:**

Chemotherapy accompanied by radiotherapy has significantly enhanced tumor control and affected the chances of survival in patients. Several factors like enhanced DNA damage, prevention in DNA repair, perturbation of cell cycle can be achieved if the aspect of radiosensitization is incorporated into an otherwise traditional chemotherapeutic drug. Cisplatin, the first FDA approved platinum compound to be used as a chemotherapeutic agent has a square planar geometry, stable under normal temperature and pressure, that slowly converts to a *trans*-isomer. Literature survey shows irradiation of the oligonucleotide TTTTGTGTTT

#### ***Chapter 4: Chemical modification of nucleic acid bases and DNA***

---

with cisplatin in solution leads to a substantial amount of thymine base damage in comparison to that in the absence of cisplatin. Cisplatin binds to the N<sub>7</sub> reactive centre of the purine moiety that help to develop structural and chemical anomalies. Cisplatin, known to be a crosslinking agent, upon photo-activation by UV light, intercalates into DNA thereby causing both inter-strand crosslinks and formation of pyrimidine adducts. Crosslinking agents in combination with UV radiation are used for the treatment of various skin conditions like psoriasis, eczema and cutaneous T-cell lymphomas.<sup>12,44,45</sup> In cisplatin-resistant tumour cell lines multinuclear Pt compounds display greater cytotoxicity and better efficacy than cisplatin. Multinuclear Pt compounds demonstrate elevated affinity towards DNA bases leading to increased damage. Polycationic Pt(II) or Pd(II)-polyamine complexes are considered as efficient as polynuclear cisplatin on account of non-covalent interactions with DNA showing enhanced and extended cytotoxic activity.<sup>46,47</sup>

#### **Aromatic amines and polycyclic aromatic hydrocarbons:**

The influence of aromatic amines in the domain of human cancer treatment is certainly of growing interest. 2-aminofluorene and its acetylated derivative N-acetyl-2-aminofluorene are prominent examples of aromatic amines. They attack the C<sub>8</sub> position of guanine and the lesion thus formed is permanent that eventually provoke base substitutions. The polycyclic aromatic hydrocarbons are another group of relevant electrophiles that are known to damage DNA. The most intensively studied examples of polycyclic aromatic hydrocarbons are anthracene, naphthalene, pyrene, 1-hydroxypyrene, 1-nitropyrene, benzo(*a*)pyrene etc. Under normal physiological conditions, they are comparatively non-reactive towards biological macro-molecules. However, upon absorbing light, they become potent in undergoing electron or energy transfer to molecular oxygen or to biological molecules present in the cell to produce reactive oxygen species (ROS) or other reactive intermediates. Both ROS and other forms of reactive intermediates activate several proteins or enzymes that cause damage of



cellular constituents like the cell membrane, nucleic acid bases in healthy and cancer cells resulting in acute toxicity. Photoreactions of polycyclic aromatic hydrocarbons produce photo-products e.g., oxygenated derivatives, nitro-derivatives, halo-derivatives that are better photosensitizers than polycyclic aromatic hydrocarbons.<sup>48</sup> Halogenated polycyclic aromatic hydrocarbons are widespread in the environment and exhibit genotoxicity that include mutagenicity and carcinogenicity. Photochemical reactions of polycyclic aromatic hydrocarbons are efficient indicators for light induced DNA cleavage. The combination of polycyclic aromatic hydrocarbons and light energy forms covalent adducts with DNA, forms oxidative product 8-oxo-2'-deoxyguanosine (8-OxodG). 8-OxodG is a free radical-induced oxidative lesion. Studies reveal that formation of 8-oxodG is interceded by ROS.<sup>49,50</sup>

#### **Nitro-aromatic compounds:**

One of the major problems of treating cancer cells during radiotherapy is that such cells become radio-resistant, on being deprived of adequate oxygen, since the region around a cancer tumour becomes hypoxic.<sup>51</sup> Oxygen being a natural radio-sensitizer, decreased presence of oxygen close to a tumour adversely affects radiotherapy. Hence, to make up for the decreased presence of oxygen, there is a demand for suitable chemical agents that can amplify radiation-induced damage of hypoxic cells without affecting normal cells. Electron affinic nitro compounds are an important class of radiosensitizers since the nitro group is known to play a major role in this regard. Nitrofurans, nitrothiophenes, nitrothiazoles, nitropyrazoles and nitroimidazoles are some popular examples of heterocyclic aromatic nitro compounds that have been tried as radiosensitizers.<sup>52-54</sup> Aliphatic nitro compounds like nitroalkanes are however much less effective as radio-sensitizers. Two prominent derivatives of nitroimidazoles in this regard are misonidazole (2-nitroimidazole) and metronidazole (5-nitroimidazole). It is established that for human malignant melanoma, 2-nitro imidazole

#### ***Chapter 4: Chemical modification of nucleic acid bases and DNA***

---

derivatives are more powerful hypoxic cell radio-sensitizers than derivatives of 5-nitroimidazoles.<sup>55</sup>

Radio-sensitization of hypoxic cells using nitroaryl compounds in model studies containing nucleotides have been performed extensively.<sup>51</sup> Yield of phosphate was correlated to the performance of the nitro compound. The enhanced phosphate release being a measure of cell killing induced by nitro-benzenes.<sup>56</sup> Metal complexes of nitro compounds were prepared and their radio-sensitizing efficiencies were verified.<sup>57</sup> Most often the aim of complex formation was also to decrease the formation of the nitro-radical anion ( $-\text{NO}_2^{\bullet -}$ ) so that the immediate biological environment experiences less toxic side effects (neurotoxicity being a major concern). What is interesting is that inspite of decreased formation of  $-\text{NO}_2^{\bullet -}$ , reports indicate complexes showed better radio-sensitizing ability than the parent nitroimidazole. A point in case being that of the Cu(II) complex of tinidazole (a 5-nitroimidazole derivative) in whose presence if pyrimidine bases uracil and thymine are exposed to  $^{60}\text{Co}$   $\gamma$  rays, studies reveal enhanced radiation-induced base damage due to the complex. This implies better efficacy on the part of the complex than tinidazole present alone.<sup>58</sup> In another study, it was seen when electrochemically reduced products of Ornidazole and its Cu(II) complex were generated in solution in the immediate vicinity of different nucleic acid bases or calf thymus DNA, the nucleic acid bases were degraded to a greater extent due to products formed from the complex than from Ornidazole itself. Results showed electrochemically reduced products of both Ornidazole and its Cu(II) complex alter guanine and cytosine to a greater extent than adenine and thymine and that in all cases, the complex performed better than Ornidazole. Such findings indicate antibiotics having 5-nitroimidazole as a major component in a drug formulation was more effective on organisms with a high G C content in their DNA.<sup>59</sup>

**Quinones:**

This family of compounds are essentially an integral part of many biochemical processes and are used as antibiotics and antitumor agents. Research provides evidence that presence of a quinone group in the structure of a compound might result in considerable cell death by a process that seems to engage reactive oxygen species (ROS). Quinones upon reduction form the semiquinone radical anion, a reactive intermediate, either by one-electron reduction of the quinone or through comproportionation when the same quinone having undergone a two - electron reduction generates semiquinone radical anion.<sup>60</sup> ROS, in the form of superoxide radical anion, peroxide or hydroxyl radical may form during re-oxidization of semiquinone radical anion to quinone in the presence of molecular oxygen. All such radicals are damaging to biological systems and are known to affect DNA. Various studies have indicated compounds having a quinone moiety at their core, can initiate DNA strand breaks and induce cytotoxicity. This gets further increased when the species is able to bind to DNA.<sup>61</sup>

Photochemistry of quinones is controlled by electron transfer reactions because of the strong oxidizing properties of photochemically excited species. Photo-excited quinones would result in the formation of a hydroquinone by hydrogen abstraction and semiquinone radical anion by electron transfer all of which could lead to DNA damage.<sup>62</sup>

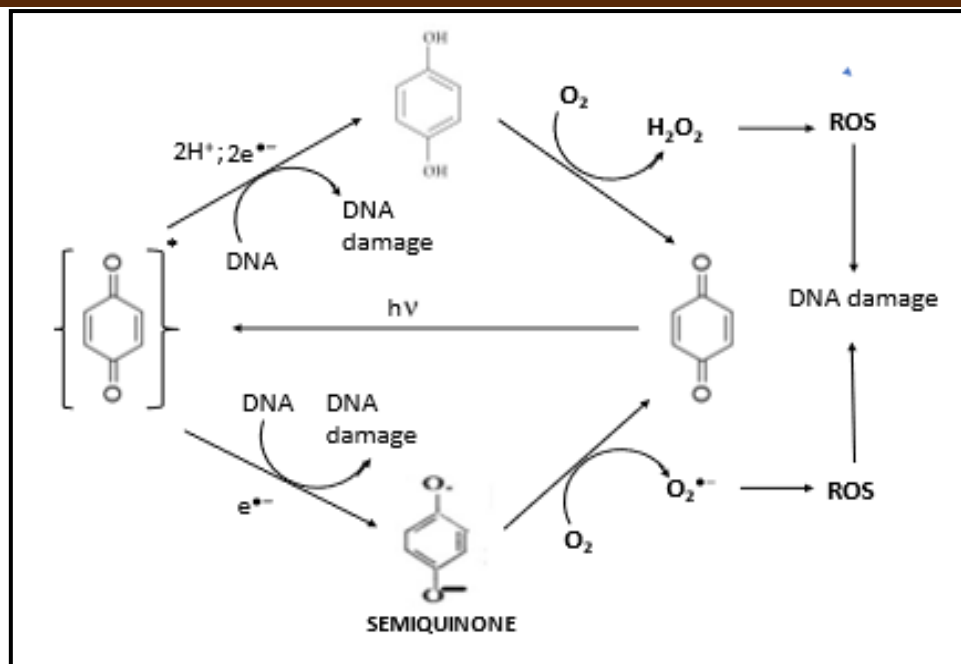
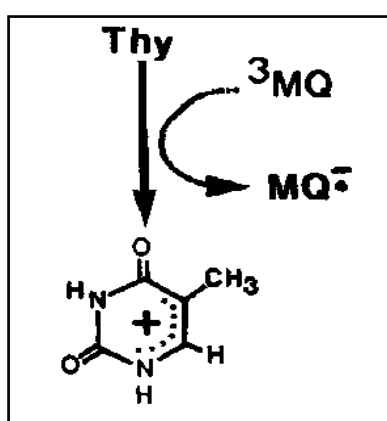


Figure 3: Oxidation-reduction cycle of Quinones

Anthraquinone derivatives are well known DNA photocleavage agents. A case in point of radical induced damage by quinones on different nucleic acid bases is the photosensitization of thymine by 2-methyl-1,4-naphthoquinone (MQ) in oxygenated aqueous solution that produces nine thymine-derived products. The first step of this photooxidation is proposed to be an electron transfer from the pyrimidine base to the excited quinone.



Irradiation of thymidine with near-UV light in the presence of adriamycin (an anthracycline antibiotic) results in almost similar product distribution as that obtained with 2-methyl-1,4-naphthoquinone which indicates both exhibit identical photochemical behaviour.<sup>63,64</sup>

In case of anthracyclines, the disproportion-comproportionation equilibria between quinone-dianion, free quinone and semiquinone appear to control most of the biological activity like producing base lesions, sugar lesions, single-strand breaks, double-strand breaks by different mechanisms.<sup>14,65</sup> In our laboratory, attempts were made to realize the role of the semiquinone radical anion and superoxide radical anion generated due to some simpler analogues of anthracyclines (Emodin and Quinalizarin) in causing DNA damage, to see if such damage were initiated through modification of nucleic acid bases or were a result of aspects like DNA binding or abstraction of hydrogen from sugar residues etc.<sup>66,67</sup> The radical environment determines the construction and yield of modified bases. To investigate the effect of electrochemically generated quinone di-anion or semiquinone radical anion on different nucleic acid bases and also on calf thymus DNA, biological targets were kept in the immediate vicinity of *in situ* electrochemically generated reduced species so that they got an opportunity to interact.<sup>68</sup> Difference in the extent of damage for each nucleobase implies there are differences in the generation of intermediates under similar electrochemical conditions.<sup>69</sup> Semiquinone radical anions also get intercalated in the  $\pi$ -stacking framework of DNA and oligonucleotides through delocalization of electrons leading to unwinding of DNA and also that modified nucleobases become sensitive to further damage that might permanently prevent them from regenerating the double strands.<sup>68,70</sup> One-electron reduction of quinone to semiquinone or two -electron reduction to quinone-dianion is crucial both for cytotoxicity and cardiotoxicity. The toxic side effect in case of quinones being cardiotoxicity, is a major concern in the use of drugs containing the quinone moiety. Generation of free radicals make anthracyclines cardiotoxic, hence, any change in the redox behaviour that addresses cardiotoxicity is welcome. One way to modify anthracyclines is to form inorganic complexes with bio-friendly metal ions. From previous studies, it is seen that complex formation of anthracycline leads to decreased semiquinone formation, a disadvantage in view

#### ***Chapter 4: Chemical modification of nucleic acid bases and DNA***

---

of efficacy that could be achieved in the free radical pathway when compared to anthracyclines and their analogues.<sup>71</sup> Therefore, damage caused to nucleic acid bases by complexes in the free radical pathway should be significantly less owing to decreased formation of semiquinone by the complexes.<sup>68</sup> However, greater damage to DNA was observed due to the Cu(II) complex of emodin than due to emodin itself. This could be because the complex binds DNA better and causes significant modification.<sup>67,72</sup>

In recent years, electrochemical investigation on the interaction between anticancer drugs and DNA is receiving increased attention. Such investigations help one to predict whether free radicals formed on chemical compounds that interact with DNA could lead to reactions that might initiate DNA damage. Such experiments could then mimic the phenomenon of electron transfer from species present in electron transport chains within the mitochondria of cells on to a drug candidate having a quinone in it.

#### **References:**

- [1] R. Dahm. 2010. From discovering to understanding Friedrich Miescher's attempts to uncover the function of DNA. *EMBO Rep.* 11:153-160.
- [2] Á. A. de Sojo, J. Ares, M. A. Martínez, J. Pazos, S. Rodríguez, J. G. Zato. 2014. Serendipity and the discovery of DNA. *Foundations of Science.* 19:387–401.
- [3] R. Dahm. 2005. Friedrich Miescher and the discovery of DNA. *Dev Biol.* 278:274-288
- [4] R. Dahm. 2008. Discovering DNA: Friedrich Miescher and the early years of nucleic acid research. *Hum Genet.* 122:565–581.

- [5] J. D. Watson, F. H. Crick. 1953. Molecular structure of nucleic acids; a structure for deoxyribose nucleic acid. *Nature*. 171:737-738.
- [6] A. J. F. Griffiths, J. H. Miller, D. T. Suzuki, R. C. Lewontin, W. M. Gelbart. 2000. An introduction to genetic analysis. 7th edition. New York: W. H. Freeman. ISBN-10 : 0716735202.
- [7] H. Lodish, A. Berk, S. L. Zipursky et al. 2000. Molecular Cell Biology. 4th edition. New York: W. H. Freeman. Section 4.1, Structure of nucleic acids.
- [8] C. Bernstein, H. Bernstein, M. C. Payne, H. Garewal. 2002. DNA repair/pro-apoptotic dual-role proteins in five major DNA repair pathways: fail-safe protection against carcinogenesis. *Mutat Res*. 511:145–178.
- [9] P. Fortini, E. Dogliotti. 2007. Base damage and single-strand break repair: Mechanisms and functional significance of short- and long-patch repair subpathways. *DNA Repair (Amst)*. 6:398-409.
- [10] S. Chakarov, R. Petkova, G. Ch Russev, N. Zhelev. 2014. DNA damage and mutation. Types of DNA damage. *BioDiscovery*. 11:1.
- [11] S. J. Whitaker. 1992. DNA Damage by Drugs and Radiation: What is important and How is it measured? *Eur J Cancer*. 28:273-276.
- [12] J. Hu, O. Adebali, S. Adar, A. Sancar. 2017. Dynamic maps of UV damage formation and repair for the human genome. *Proc Natl Acad Sci U S A*. 114:6758-6763.
- [13] S. Das, A. Saha, P. C. Mandal. 1997. Radiation-induced double-strand modification in calf thymus DNA in the presence of 1,2-dihydroxy-9,10-anthraquinone and its Cu(II) complex. *Environ Health Perspect*. 105:1459-462.

#### ***Chapter 4: Chemical modification of nucleic acid bases and DNA***

---

- [14] S. Das, A. Saha, P. C. Mandal. 1995. Radiosensitization of thymine by Fe(III)-1,2-dihydroxyanthraquinone complex in dilute aqueous solution. *Journal of Radioanalytical and Nuclear Chemistry*. 196:57-63.
- [15] Y. Fu, C. He. 2012. Nucleic acid modifications with epigenetic significance. *Curr Opin Chem Biol*. 16:516–524
- [16] K. Chen, B. S. Zhao, C. He. 2016. Nucleic acid modifications in regulation of gene expression. *Cell Chem Biol*. 23:74-85.
- [17] J. Vignard, G. Mirey, B. Salles. 2013. Ionizing-radiation induced DNA double-strand breaks: A direct and indirect lighting up. *Radiother Oncol*. 108:362-369.
- [18] J. F. Ward. 1988. DNA damage produced by ionizing radiation in mammalian cells: Identities, mechanisms of formation, and reparability. *Prog Nucleic Acid Res Mol Biol*. 35:95-125.
- [19] Y. Ji, Y. Xia, M. Zhao, F. Li, B. Huang. 2005. Reactions of OH with thymine studied using density functional theory. *International Journal of Quantum Chemistry*. 101:211-218.
- [20] S. V. Jovanovic, M. G. Simic. 1986. Mechanism of OH radical reactions with thymine and uracil derivatives. *J. Am. Chem. Soc*. 108:5969.
- [21] J-P. Pouget, S. Frelon, J-L. Ravanat, I. Testard, F. Odin, and J. Cadet. 2002. Formation of modified DNA bases in cells exposed either to gamma radiation or to high-LET particles. *Radiation Research*, 157:589-595.
- [22] J. R. Wagner, J. Cadet. 2010. Oxidation reactions of cytosine DNA components by hydroxyl radical and one-electron oxidants in aerated aqueous solutions. *Acc Chem Res*. 43:564-71.



- [23] J. Cadet, T. Douki, J-L Ravanat. 2010. Oxidatively generated base damage to cellular DNA. *Free Radic Biol Med.* 49:9–21
- [24] J. Cadet, T. Douki, J-L Ravanat. Oxidatively generated damage to the guanine moiety of DNA: Mechanistic aspects and formation in cells. *Acc Chem Res.* 41:1075-1083.
- [25] L. P. Candeias, S. Steenken. 2000. Reaction of HO• with guanine derivatives in aqueous solution: Formation of two different redox-active OH-adduct radicals and their unimolecular transformation reactions. properties of G(-H). *Chemistry.* 6:475- 484.
- [26] C. Chatgililoglu, M. D. \_Angelantonio, M. Guerra, P. Kaloudis, Q. G. Mulazzani. 2009. A re-evaluation of the ambident reactivity of the guanine moiety towards hydroxyl radicals. *Angew. Chem. Int. Ed.* 48:2214 –2217.
- [27] A. Kumar, A. Adhikary, L. Shamoun, M. D. Sevilla. 2016. Do solvated electrons (e(aq)<sup>-</sup>) reduce DNA bases? A G4 and DFT-MD study. *J Phys Chem B.* 120:2115–2123.
- [28] L. P. Camleias, P. Wolf, P. O'Neill, S. Steenken. 1992. Reaction of hydrated electrons with guanine nucleosides: Fast protonation on carbon of the electron adduct. *J. Phys. Chem.* 96:10302-10307.
- [29] M. Dizdaroglu, P. Jaruga. 2012. Mechanisms of free radical-induced damage to DNA *Free Radic Res.* 46:382–419
- [30] S. Mouret, C. Philippe, J. Gracia-Chantegrel, A. Banyasz, S. Karpati, D. Markovitsi, T. Douki. 2010. UVA-induced cyclobutane pyrimidine dimers in DNA: a direct photochemical mechanism? *Org. Biomol. Chem.* 8:1706–1711.
- [31] R. J. H. Davies. 1995. Ultraviolet Radiation Damage in DNA. *Biochem Soc Trans.* 23:407-418.

#### ***Chapter 4: Chemical modification of nucleic acid bases and DNA***

---

- [32] R. P. Rastogi, Richa, A. Kumar, M. B. Tyagi, R. P. Sinha. 2010. Molecular mechanisms of ultraviolet radiation-induced DNA damage and repair. *J Nucleic Acids*. doi: 10.4061/2010/592980.
- [33] J-L Ravanat, T. Douki, J. Cadet. 2001. Direct and indirect effects of UV radiation on DNA and its components. *J Photochem Photobiol B. Biology*. 63:88-102.
- [34] J. Cadet, T. Douki. 2018. Formation of UV-induced DNA damage contributing to skin cancer development. *Photochem. Photobiol. Sci*. 17:1816-1841.
- [35] S. Steenken, S. V. Jovanovic. 1997. How easily oxidizable is DNA? One-electron reduction potentials of adenosine and guanosine radicals in aqueous solution. *J. Am. Chem. Soc.* 119:617-618.
- [36] K. Kobayashi, R. Yamagami, S. Tagawa. 2008. Effect of base sequence and deprotonation of guanine cation radical in DNA. *J. Phys. Chem.* 112:10752–10757.
- [37] K. Kobayashi, S. Tagawa. 2003. Direct observation of guanine radical cation deprotonation in duplex DNA using pulse radiolysis. *J. Am. Chem. Soc.* 125:10213-10218
- [38] T. J. Merta, N. E. Geacintov, V. Shafirovich. 2019. Generation of 8-oxo-7,8-dihydroguanine in G-Quadruplexes models of human telomere sequences by one-electron oxidation. *Photochem Photobiol*. 95:244-251.
- [39] S. Steenken. 1989. Purine bases, nucleosides, and nucleotides: Aqueous solution redox chemistry and transformation reactions of their radical cations and e- and OH adducts. *Chem. Rev.* 89:503-520.
- [40] P. J. Elving, S. J. Pace, J. E. O'Reilly. 1973. Electrochemical reduction of purine, pyrimidine, and imidazole in aqueous media. Kinetics and mechanisms. *J. Am. Chem. Soc.* 95:647–658.

- [41] X. Qin, X. Liu, L. Hong-Bo, Y. Li-Na, H. Xiaoya. 2013. Electrochemical determination of purine and pyrimidine DNA bases based on the recognition properties of azocalix[4]arene. *Biosen Bioelectron.* 42:355–361
- [42] M. D. Wyatt, D. L. Pittman. 2006. Methylating agents and DNA repair responses: methylated bases and sources of strand breaks. *Chem Res Toxicol.* 19:1580–1594.
- [43] G. P. Margison, M. F. Santibañez Koref, A. C. Povey. 2002. Mechanisms of carcinogenicity/chemotherapy by O6-methylguanine. *Mutagenesis.* 17:483–487.
- [44] B. Behmand, J. R. Wagner, L. Sanche, D. J. Hunting. 2014. Cisplatin intrastrand adducts sensitize DNA to base damage by hydrated electrons. *J. Phys. Chem. B* 118:4803–4808
- [45] S. Dasari, P. B. Tchounwou. 2014. Cisplatin in cancer therapy: molecular mechanisms of action. *Eur J Pharmacol.* 740:364-78.
- [46] G. Cossa, L. Gatti, F. Zunino, P. Perego. 2009. Strategies to improve the efficacy of platinum compounds. *Curr Med Chem.* 16:2355-2365.
- [47] M. P. M. Marques. 2013. Platinum and palladium polyamine complexes as anticancer agents: The structural factor. *ISRN Spectroscopy.* Article ID 287353, 29 pages.
- [48] P. P. Fu, Q. Xia, X. Sun, H. Yu. 2012. Phototoxicity and Environmental Transformation of Polycyclic Aromatic Hydrocarbons (PAHs)—Light-Induced Reactive Oxygen Species, Lipid Peroxidation, and DNA Damage. *J Environ Sci Health C Environ Carcinog Ecotoxicol Rev.* 30:1–41.
- [49] G. J. Hammons, D. Milton, K. Stepps, F. P. Guengerich, R. H. Tukey, F. F. Kadlubar. 1997. Metabolism of carcinogenic heterocyclic and aromatic amines by recombinant human cytochrome P450 enzymes. *Carcinogenesis.* 18:851–854.

#### ***Chapter 4: Chemical modification of nucleic acid bases and DNA***

---

- [50] H. Yu. 2002. Environmental carcinogenic polycyclic aromatic hydrocarbons: photochemistry and phototoxicity. *J Environ Sci Health C Environ Carcinog Ecotoxicol Rev.* 20:149–183.
- [51] K. Graham, E. Unger. 2018. Overcoming tumor hypoxia as a barrier to radiotherapy, chemotherapy and immunotherapy in cancer treatment. *Int J Nanomedicine.* 13:6049–6058.
- [52] J. D. Champan, A. P. Reuvers, J. Borsa, A. Petkau, D. R. Mccalla. 1972. Nitrofurans as radiosensitizers of hypoxic mammalian cells. *Cancer Research*, 32, 2616-2624.
- [53] C. L. Greenstock, G. W. Ruddock, P. Neta. 1976. Pulse radiolysis and ESR studies of the electron-affinic properties of Nitroheterocyclic radiosensitizers. *radiat Res.* 66: 472–484.
- [54] G. W. Ruddock, C. L. Greenstock. 1977. Application of polarography to the study of chemical radiosensitization of DNA components. *Biochimica et Biophysica Acta (BBA) - General Subjects.* 496: 197-202
- [55] E. K. Rofstad. 1978. The radiosensitizing effect of metronidazole and misonidazole (Ro-07-0582) on a human malignant melanoma grown in the athymic mutant nude mouse. *Br J Radiol.* 51:381-386.
- [56] P. Wardman. 1984. Radiation chemistry in the clinic: Hypoxic cell radiosensitizers for radiotherapy. *Radiat. Phys. Chem.* 24:293-305.
- [57] R. C. Santra, D. Ganguly, J. Singh, K. Mukhopadhyay, S. Das. 2015. A study on the formation of the nitro radical anion by ornidazole and its significant decrease in a structurally characterized binuclear Cu(II)-complex: impact in biology. *Dalton Trans.* 44:1992-2000.
- [58] R. C. Santra, D. Ganguly, D. Bhattacharya, P. Karmakar, A. Saha, S. Das. 2017.  $\gamma$  radiation-induced damage of nucleic acid bases, calf thymus DNA and DNA within MCF-7 breast cancer cells by [Cu<sub>2</sub>(OAc)<sub>4</sub>(tnz)<sub>2</sub>]: A potential radiosensitizer. *New J. Chem.* 41:11679-11685.

- [59] P. Nandy, S. Das. 2020. In situ reactivity of electrochemically generated nitro radical anion on Ornidazole and its monomeric Cu(II) complex with nucleic acid bases and calf thymus DNA. *Inorganica Chimica Acta*. 501:119267.
- [60] M. Martínez-Cifuentes, R. Salazar, O. Ramírez-Rodríguez, B. Weiss-López, R. Araya-Maturana. 2017. Experimental and theoretical reduction potentials of some biologically active ortho-carbonyl para-quinones. *Molecules*. 22: 577.
- [61] A. Begleiter, 1985. Studies on the mechanism of action of quinone antitumor agents. *Biochemical Pharmacology*. 34: 2629-2636.
- [62] R. N. Alsulami. 2016. Oxidation of nucleic acids: Chemistry of pyrene quinone and development of dihydrodioxins as DNA photooxidizing agents.
- [63] J. R. Wanger, J. Cadet, G. J. Fisher. 1984. Photo-oxidation of thymine sensitized by 2-methyl-1,4-nathoquinone:analysis of products including three novel photo-dimers. *Phorochemistry and Photobiology*, 40:589 - 597.
- [64] J. R. Wagner, J. E. van Lier, L. J. Johnston. 1990. Quinone sensitized electron transfer photooxidation of nucleic acids: chemistry of thymine and thymidine radical cations in aqueous solution. *Photochem Photobiol*. 52:333-43.
- [65] N. Okumura, H. Mizutani, T. Ishihama, M. Ito, A. Hashibe, T. Nakayama, B. Unob. 2019. Study on redox properties and cytotoxicity of anthraquinone derivatives to understand antitumor active anthracycline substances. *Chem. Pharm. Bull*. 67:717–720.
- [66] S. Mukherjee-Chatterjee, C.K. Jain, S. Singha, P. Das, S. Roychoudhury, H.K.Majumder, S. Das. 2018. Activity of Co<sup>II</sup>-Quinalizarin: A novel analogue of anthracycline-based anticancer agents targets human DNA topoisomerase, whereas quinalizarin itself acts via formation of semiquinone on acute lymphoblastic leukemia MOLT-4 and HCT 116 Cells. *ACS Omega*. 3:10255-10266.

#### ***Chapter 4: Chemical modification of nucleic acid bases and DNA***

---

[67] B. Mandal, S. Singha, S. K. Dey, S. Mazumdar, S. Kumar, P. Karmakar, S. Das. 2017.

CuII complex of emodin with improved anticancer activity as demonstrated by its performance on HeLa and Hep G2 cells. *RSC Adv.* 7: 41403-41418.

[68] B. Mandal, H. K. Mondal, S. Das. 2019. *In situ* reactivity of electrochemically generated semiquinone on Emodin and its CuII/MnII complexes with pyrimidine based nucleic acid bases and calf thymus DNA: Insight into free radical induced cytotoxicity of anthracyclines.

*Biochemical and Biophysical Research Communications.* 515:505-509.

[69] E. J. Son, J. H. Kim, K. Kima, C. B. Park. 2016. Quinone and its derivatives for energy harvesting and storage materials. *J. Mater. Chem. A.* 4:11179–11202.

[70] G. B. Schuster. 2000. Long-Range Charge Transfer in DNA: Transient structural distortions control the distance dependence. *Acc. Chem. Res.* 33:253-260.

[71] S. Roy, P. Mondal, P. S. Sengupta, D. Dhak, R. C. Santra, S. Das, P. S. Guin. 2015. Spectroscopic, computational and electrochemical studies on the formation of the copper complex of 1-amino-4-hydroxy-9,10-anthraquinone and effect of it on superoxide formation by NADH dehydrogenase. *Dalton Trans.* 44:5428-5440.

[72] V. Adımcılar, M. Çesme , P. Senela, I. Danıs, D. Ünal, A. Gölcü. 2021. Comparative study of cytotoxic activities, DNA binding and molecular docking interactions of anticancer agent epirubicin and its novel copper complex. *Journal of Molecular Structure.* 1232:130072

# CHAPTER 5

## Genesis and Scope





Amongst the chemotherapeutic drugs, anthracyclines are one of the most effective and universally accepted anticancer agents<sup>1-3</sup> that impart cytotoxicity in multiple pathways. They are established DNA targeting agents capable of intercalation, thereby inhibiting macromolecule biosynthesis.<sup>4-9</sup> Anthracyclines inhibit the growth of cancer cells by targeting one or more enzymes useful in the life cycle of a cell.<sup>10,11</sup> Another mode of killing of cells is their ability to generate reactive oxygen species (ROS) that cause damage to cells in the free radical pathway. At the same time, ROS is responsible for toxic side effects.<sup>12-15</sup> Therefore, there is a need to have a correct balance in ROS generation such that it maintains anticancer activity as well as diminishes unwanted toxicity. Another major disadvantage on the use of anthracyclines is their high cost.<sup>16-18</sup> The presence of a sugar unit in anthracyclines is essential in determining drug efficacy since they help in recognition of cancer cells i.e. drugs containing them are drawn to a cancer cell.<sup>19,20</sup> However, its presence makes the drug very costly. Many studies bring forth the fact that hydroxy-9,10-anthraquinones, present at the core of anthracyclines, or some of their modified forms could be effective substitutes of anthracyclines.<sup>21-23</sup> However, since the anthraquinone is the potential functional unit for any form of chemical/electrochemical transformations for the anthracyclines or for their analogues (hydroxy-9,10-anthraquinones), it therefore appears that like anthracyclines, hydroxy-9,10-anthraquinones should also be cardiotoxic unless the generation of ROS is intelligently regulated.<sup>19,24</sup> Therefore, modification of anthracyclines or that of their analogues is an important aspect of research today. As already mentioned, anthracyclines (adriamycin and daunomycin) modified by forming metal complexes, show significant changes in therapeutic efficiency and controls cardiotoxic side effects.<sup>25-27</sup> These aspects have been discussed in **Chapter 2**.

While there is great resemblance in physicochemical and electrochemical behaviour of hydroxy-9,10-anthraquinones and anthracyclines, the anthracyclines appear to be far ahead in

terms of biophysical interactions and biological activity as has been realized from previous studies.<sup>21-23</sup> Therefore, hydroxy-9,10-anthraquinones would produce ROS like anthracyclines in enzyme-assisted electron transfer processes that could potentially kill cancer cells. The literature is rich in studies showing DNA damage at the site of nucleic acid bases, in organelles of living cells due to free radicals generated by anthracyclines.<sup>28,29</sup> Hence, redox properties of such molecules is a key factor in determining their chemotherapeutic efficacy and also with regard to aspects of toxicity. Aspects related to ROS formation and controlling them by preparing metal complexes and methods to detect and monitor them using various techniques has been discussed in **Chapter 3**.

Another important aspect is to understand how anthracyclines interact with DNA present within cells in any chemically induced damage that initiates apoptosis.<sup>30-32</sup> For this reason, it is important to know about damage caused to the constituents of DNA. Various stimuli that may be used for inducing damage to model nucleic acid bases and/or DNA in the presence of different chemical compounds are discussed in **Chapter 4**. Since electrochemical studies reveal that reactions of several compounds with model biomolecules depend essentially on their electron affinity this was reviewed extensively. Studies at the molecular level show that several electron affinic compounds can accept electrons from biological macromolecules. The compounds also bind to the transient radicals of biomolecules and such bound forms are able to destroy the double helical structure leading to inhibition of protein synthesis and cell death.<sup>33,34</sup> Therefore, a main reason for cytotoxicity of anthracyclines could be oxidative damage of intracellular DNA.

From an understanding of different aspects concerning the anthracyclines mentioned above, simpler molecules, having either a structural or functional similarity with anthracyclines, and a potency to be used as drugs were chosen.<sup>35-37</sup> Two such simple compounds considered for this study are alizarin (1, 2-dihydroxy-9,10-anthraquinone) and carminic acid (7- $\alpha$ -D-

glucopyranosyl-9,10-dihydro-3,5,6,8-tetrahydroxy-1-methyl-9,10-dioxoanthracenecarboxylic acid). While alizarin is a simple hydroxy-9, 10-anthraquinone, carminic acid has a glucopyranosyl unit directly linked to a hydroxy-9, 10-anthraquinone core. They were chosen to look at similarities and/or differences with the anthracyclines. Although carminic acid has a sugar present in its structure it is not present in the same manner in which sugars are found in anthracyclines. Complexes with biologically relevant metal ions  $Mn^{II}$  and  $Co^{II}$  were prepared and characterized (**Chapters 8, 9 & 10**). Their efficacy in relation to chosen compounds, particularly in the backdrop of standard anthracyclines was investigated.

When a compound exists in more than one form in solution, the overall binding constant with DNA is a consequence of the interaction of each individual form present in solution. Reasons for the existence of a compound in more than one form could be due to the fact that the compound has one or more easily dissociable protons whose  $pK_a$  lies in the physiological pH range. An important aspect is that  $pK_a$  of the compound could be different in the presence and absence of DNA; therefore contributions of different forms to the overall binding constant would be different in different cases. Hydroxy-9, 10-anthraquinones are compounds that has a number of protons that dissociate in physiological pH i.e., exist in more than one form in solution. Therefore, an attempt was made to understand the influence of  $pK_a$  of such simpler analogues through a study on DNA binding that could also find medicinal applications particularly if they interfere with cancer cells through interaction with DNA. This has been discussed in **Chapter 7**. Since extent of binding of DNA to drug molecules is tremendously influenced by factors like pH, temperature, ionic strength and polarity of the medium,<sup>38</sup> interaction of the prepared complexes with calf thymus DNA under varying conditions of pH and ionic strength were carried out to see i) if the complexes were able to address some of the limitations of hydroxy-9,10-anthraquinones in comparison to anthracyclines and ii) to what extent they perform better than hydroxy-9,10-anthraquinones from which they were prepared.

## *Chapter 5: Genesis and scope*

---

These are discussed in **Chapters 8, 9 & 10**. Anthracyclines or its metal complexes by virtue of possessing the desired redox potential, is reported to interact with components of the electron transport chain within cells and get reduced.<sup>39,40</sup> Such reduced species interact with cell organelles to show drug action.<sup>41,42</sup> This is therefore a major pathway by which cell damage is believed to occur. To realize how anthracycline analogues or their metal complexes mimic the activity of anthracyclines in human mitochondria, *in situ* reactivity of the electrochemically generated semiquinone on the chosen compounds and their metal complexes were studied. Electrochemical generation of species if done in presence of either nucleic acid bases or DNA could provide an idea what these species are capable of doing to biological targets and hence in this way some idea on the mechanism of the processes may be obtained. Results of such experiments are provided in **Chapter 11**. In a similar manner, reduced species could be generated on chosen compounds and their metal complexes in an enzyme assisted pathway to realize the phenomenon of electron transfer from a donor group present in a biological electron-transport chain on to a quinone system. In this regard the NADH dehydrogenase assay was performed from where generation of the superoxide radical anion due to compounds could be realized (provided in **Chapters 8 & 9**). Another very important aspect of realizing things pertaining to ROS is how external agents interact with ROS generated intrinsically i. e. due to metabolic activity within cells. We studied this by incubating our compounds in different carcinoma cell lines (HeLa, Hep G2, SIHA) and the normal WI 38 lung fibroblast cells, generating ROS initially using 70  $\mu\text{M}$   $\text{H}_2\text{O}_2$  and allowing it to remain for a specified time. ROS was subsequently measured with the help of  $\text{H}_2\text{DCFDA}$  assay (discussed in **Chapters 8 & 9**). The purpose of these experiments on ROS was to see the difference in behaviour when chosen compounds (being considered as analogues of anthracyclines) and their metal complexes interact with ROS, both with regard to cytotoxicity and cardiotoxic side effects. Eventually studies on cell killing were done using

the MTT assay to realize the efficacy of the complexes and of chosen compounds (alizarin and carminic acid) using which complexes were prepared.

Lastly wish to mention here that studies were performed with the intention of identifying whether alizarin and carminic acid, simpler analogues of anthracyclines and their modified forms (metal complexes) could be used as a relatively less costly, less cardiotoxic, yet effective alternatives to existing anthracycline anticancer drugs.

**Reference:**

- [1] F. Arcamone, S. Penco. 1988. In anthracycline and anthracenedione-based anticancer agents. (Ed. Lown, J. W.), Elsevier, Amsterdam.
- [2] T. Terasaki, T. Iga, Y. Sugiyama, Y. Sawada, M. Hanano.1984. Nuclear binding as a determinant of tissue distribution of adriamycin, daunomycin, adriamycinol, daunorubicinol and actinomycin D. *J. Pharmacobiodyn.* 7: 269-277.
- [3] D. A. Koster, A. Crut, S. Shuman, M. Bjornsti, N. H. Dekker. 2010. Cellular strategies for regulating DNA supercoiling: A single-molecule perspective. *Cell.* 142: 519-530.
- [4] S. Das, A. Saha, P. C. Mandal. 1996. Studies on the formation of Cu(II) and Ni(II) complexes of 1,2-dihydroxy-9,10-anthraquinone and lack of stimulated superoxide formation by the complexes. *Talanta.* 43: 95-102.
- [5] S. Das, A. Saha, P.C. Mandal.1995. Radiosensitization of thymine by Fe(III)-1,2-dihydroxyanthraquinone complex in dilute aqueous solution. *Journal of Radioanalytical and Nuclear Chemistry, Articles.* 196: 57-63.

## ***Chapter 5: Genesis and scope***

---

- [6] M. K. Goftar, N. M. Kor, Z. M. Kor. 2014. DNA intercalators and using them as anticancer drugs. *International journal of Advanced Biological and Biomedical Research*. 2: 811-822.
- [7] M. F. Braña, M. Cacho, A. Gradillas, B. de Pascual-Teresa and A. Ramos. 2001. Intercalators as anticancer drugs. *Current Pharmaceutical Design*. 7: 1745-1780.
- [8] F. Y. Sheila, S.T. Christopher, J.K. S. Henikof.2014. Doxorubicin, DNA torsion, and chromatin dynamics. *Biochimica et Biophysica Acta (BBA) - Reviews on Cancer*. 1845: 84-89.
- [9] D. A. Gewirtz. 1999. A Critical Evaluation of the Mechanisms of Action Proposed for the Antitumor Effects of the Anthracycline Antibiotics Adriamycin and Daunorubicin. *Biochem Pharmacol*. 57:727–741.
- [10] F. Guano , P. Pourquier , S. Tinelli , M. Binaschi , M. Bigioni , F. Animati , S. Manzini, F. Zunino, G. Kohlhagen, Y. Pommier, G. Capranico. 1999. Topoisomerase poisoning activity of novel disaccharide anthracyclines. *Mol. Pharmacol*. 56: 77-84
- [11] Y. Pommier. 2009. DNA topoisomerase I inhibitors, chemistry, biology and interfacial inhibition, *Chem. Rev*. 109: 2894-2902.
- [12] Y. Ichikawa, M. Ghanefar, M. Bayeva, R. Wu, A. Khechaduri, V. Sathyamangla, N. Prasad, R. K. Mutharasan, T. J. Naik, H. Ardehali. 2014. Cardiotoxicity of doxorubicin is mediated through mitochondrial iron accumulation. *J. Clin. Invest*. 124: 617–630.
- [13] R. M. Damiani, D. J. Moura, C.M. Viau, R.A. Caceres, J. A. P. Henriques, J. Saffi. 2016. Pathways of cardiac toxicity: comparison between chemotherapeutic drugs doxorubicin and mitoxantrone. *Arch Toxicol*. 90:2063-2076.

- [14] F. Cai, M. A. F. Luis, X. Lin, M. Wang, L. Cai, C. Cen and E. Biskup. 2019. Anthracycline- induced cardiotoxicity in the chemotherapy treatment of breast cancer: Preventive strategies and treatment (Review). *Molecular and clinical oncology*. 11: 15-23.
- [15] H. Beraldo, A. Garnier-Suillerot, L. Tosi, F. Lavelle. 1985. Iron(III)-adriamycin and Iron(III)-daunorubicin complexes: physicochemical characteristics, interaction with DNA, and antitumor activity. *Biochemistry*. 24: 284-289.
- [16] D. Platel, P. Pouna, S. Bonoron-Adele, J. Robert. 1999. Comparative cardiotoxicity of idarubicin and doxorubicin using the isolated perfused rat heart model. *Anticancer Drugs*. 10: 671-676.
- [17] J. Blasiak, E. Gloc, M. Warszawski. 2002. A comparison of the in vitro genotoxicity of anticancer drugs idarubicin and mitoxantrone. *Acta Biochim. Polonica*. 49: 145-155.
- [18] L. Zhu, X. Cao, W. Chen, G. Zhang, D. Sun, P. G. Wang. 2005. Syntheses and biological activities of daunorubicin analogs with uncommon sugars. *Bioorg. Med. Chem*. 13: 6381-6387.
- [19] W. Priebe. 2000. Targeting DNA with anthracyclines: the importance of the sugar moiety. *Molecules*. 5:299–301.
- [20] F. Zunino, G. Pratesi, P. Perego. 2001. Role of the sugar moiety in the pharmacological activity of anthracyclines: Development of a novel series of disaccharide analogs. *Biochemical Pharmacology*. 61: 933-938
- [21] P. S. Guin, S. Das, P. C. Mandal. 2010. Sodium 1, 4-dihydroxy-9,10-anthraquinone-2-sulphonate interacts with calf thymus DNA in a way that mimics anthracycline antibiotics: an electrochemical and spectroscopic study. *J. Phys. Org. Chem*. 23: 477-482.

## ***Chapter 5: Genesis and scope***

---

- [22] S. Mukherjee, P. Das, S. Das. 2012. Exploration of small hydroxy-9,10-anthraquinones as anthracycline analogues: physicochemical characteristics and DNA binding for comparison. *J. Phys. Org. Chem.* 25: 385-393.
- [23] P. S. Guin, S. Das, P.C. Mandal, 2012. A comparative study on the interaction with calf thymus DNA of a Ni(II) complex of the anticancer drug adriamycin and a Ni(II) complex of sodium 1,4-dihydroxy-9,10-anthraquinone-2-sulphonate. *J. Coord. Chem.* 65: 705-721.
- [24] A. J. Trypuc, G. Swiderski, R. Kretowski, W. Lewandowski. 2017. Newly Synthesized Doxorubicin Complexes with Selected Metals—Synthesis, Structure and Anti-Breast Cancer Activity. *Molecules.* 22:1106. doi: 10.3390/molecules22071106.
- [25] M. M. L. Fialo, A.G. Suillerot. 1985. Physicochemical studies of the iron(III)-carminomycin complex and evidence of the lack of stimulated superoxide production by NADH dehydrogenase. *Biochim. Biophys. Acta.* 840: 91-98.
- [26] H. Beraldo, A. Garnier-Suillerot, L.Tosi, F. Lavelle.1985. Iron(III)-adriamycin and iron(III) daunorubicin complexes: physicochemical characteristics, interaction with DNA, and antitumor activity. *Biochemistry.* 24: 284-289.
- [27] J. Jong, B.C.P. Hiisken, B. Beekman, W.J.F. van der Vijgh, A. Bast. 1994. Radical formation by metal complexes of anthracyclines and their metabolites. Is there a relation with cardiotoxicity? *European Journal of Pharmaceutical Sciences.* 2: 229-237.
- [28] T.J. Guzik, R. Korbut, T. Adamek-Guzik. 2003. Nitric oxide and superoxide in inflammation and immune regulation. *Journal of Physiology and Pharmacology.* 54:469-487.
- [29] P. Pignatelli, F. M. Pulcinelli, L. Lenti, P.P. Gazzaniga, F. Violi. 1998. Hydrogen peroxide is involved in collagen-induced platelet activation. *Blood.* 91: 484–490



- [30] R. Baskar, J. Dai, N. Wenlong, R. Yeo, K-W Yeoh. 2014. Biological response of cancer cells to radiation treatment. *Frontiers in Molecular Biosciences*. doi:10.3389/fmolb.2014.00024.
- [31] A. Munshi, J. F. Kurland, T. Nishikawa, T. Tanaka, M. L. Hobbs, S. L. Tucker, S. Ismail, C. Stevens, R. E. Meyn. 2005. Histone deacetylase inhibitors radiosensitize human melanoma cells by suppressing DNA repair activity. *Clin Cancer Res*. 11:4912-4922.
- [32] P. O. Neill, E. M. Fielden. 1986. Molecular aspects of DNA damage and its modification. *Radiation Carcinogenesis and DNA Alterations*. NATO ASI series, Series A, Life Sciences. 124:425-438.
- [33] B. Mandal, S. Singha, S.K. Dey, S. Mazumdar, S. Kumar, P. Karmakar, S. Das. 2017. CuII complex of emodin with improved anticancer activity as demonstrated by its performance on HeLa and Hep G2 cells. *RSC Adv*. 7: 41403-41418.
- [34] C. Fan, W. Zheng, X. Fu, X. Li, Y.S. Wong, T. Chen. 2014. Strategy to enhance the therapeutic effect of doxorubicin in human hepatocellular carcinoma by selenocystine, a synergistic agent that regulates the ROS-mediated signaling. *Oncotarget*. 5: 2853-2863.
- [35] I. D. Kuntz. 1992. Structure-based strategies for drug design and discovery. *Science*. 257: 1078-1082.
- [36] W. P. Walters, A. A. Murcko, M. A. Murcko. 1999. Recognizing molecules with drug-like properties. *Current Opinion in Chemical Biology*. 3: 384-387.
- [37] I. Muegge, S. L. Heald, D. Brittelli. 2001. Simple selection criteria for drug-like chemical matter. *J. Med. Chem*. 44: 1841-1846.
- [38] P. S. Guin, S. Das, P. C. Mandal. 2011. Electrochemical reduction of quinones in different media: a review, International Journal of Electrochemistry. *Int. J. Electrochem.*, Article ID 816202, DOI:10.4061/2011/816202.

[39] K. J. Davies, J. H. Doroshow. 1986. Redox cycling of anthracyclines by cardiac mitochondria. I. Anthracycline radical formation by NADH dehydrogenase. *J Biol Chem.* 261:3060-3067. PMID: 3456345.

[40] James H. Doroshow. 2019. Mechanisms of anthracycline-enhanced reactive oxygen metabolism in tumor cells. *Oxid Med Cell Longev.* <https://doi.org/10.1155/2019/9474823>

[41] C. Guven, Y. Sevgiler, E. Taskin. 2018. Mitochondrial dysfunction associated with doxorubicin. *Mitochondrial Diseases.* doi:10.5772/intechopen.80284.

[42] B. Perillo, M. Di Donato, A. Pezone. 2020. ROS in cancer therapy: the bright side of the moon. *Exp Mol Med.* 52:192–203.

# CHAPTER 6

## **Experimental: Materials and Methods**



**Introduction:**

This chapter mentions materials either purchased or prepared during the course of several experiments that were performed. It mentions different techniques employed either related to purification or characterization of different compounds prepared as part of the proposed research. Since the aim of the proposed study was to see if relatively simpler hydroxy-9,10-anthraquinones stand a chance at mimicking the core of anthracyclines, several experiments with model systems were performed that either relate to cell lines or to living organisms. Studies related to biological systems were designed to see if some of the attributes of anthracyclines, already established, as anticancer agents,<sup>1,2</sup> could be seen in the chosen compounds (hydroxy-9,10-anthraquinones) or in their metal complexes. An important aspect pertaining to research on anthracyclines being generation of reactive oxygen species (ROS) and their subsequent interaction with biological systems resulting in both positive (the ability to control the growth of unwanted cells) and negative (responsible for toxic side effects) aspects,<sup>3-5</sup> experiments on ROS generation and their subsequent controlled formation through preparation of a complex were studied by NADH dehydrogenase or H<sub>2</sub>DCFDA assays. Electrochemical behaviour of the compounds and subsequent interaction of intermediates with model targets enable one to understand the activity of anthracyclines in a free radical pathway.<sup>3</sup> Finally, studies were performed that identify cell viability due to interaction with the compounds. Various software were used for analysis and in fitting experimental data.

In the absence of single crystals of the prepared complexes, computational techniques were used to arrive at the structure of the complexes based on experimental evidences derived from UV-Vis spectroscopy, IR spectroscopy, fluorescence spectroscopy, mass spectrometry, magnetic susceptibility measurements and thermo-gravimetric analysis. Details of density functional theory (DFT) as a part of computations are mentioned elaborately.

**1. Materials:**

Alizarin (> 90% pure) purchased from TCI, Japan, purpurin (~ 96% pure) purchased from Sigma-Aldrich and carminic acid purchased from Sigma Chemical Company were purified by re-crystallization from ethanol-water mixtures. All compounds being photosensitive were stored in the dark. Stock solutions of each were either prepared in ethanol or in DMSO. NaNO<sub>3</sub> (AR) and NaCl (AR) purchased from Merck (India) were used to maintain ionic strengths of the medium. Phosphate buffer (pH ~ 7.4) was prepared in triple distilled water using appropriate amounts of sodium dihydrogen phosphate (AR) and disodium hydrogen phosphate (AR), that were procured from Merck (Germany). MnCl<sub>2</sub>.4H<sub>2</sub>O and CoCl<sub>2</sub>.6H<sub>2</sub>O were procured from Merck (India). NADH, cytochrome c, NADH dehydrogenase, superoxide dismutase (SOD) were obtained from Sigma-Aldrich. Calf thymus DNA was purchased from Sisco Research Laboratories, India. It was dissolved in triple distilled water containing 120 mM NaCl, 35 mM KCl and 5 mM CaCl<sub>2</sub>. The absorbance of a solution of calf thymus DNA was recorded at 260 nm and 280 nm respectively; A<sub>260</sub>/A<sub>280</sub> was noted. The ratio if found between 1.8 and 1.9 suggested the DNA was sufficiently free of protein and that it required no further purification. The DNA was also characterized by measuring its CD spectrum at 260 nm using a CD spectropolarimeter (J815, JASCO). Nucleic acid bases uracil, thymine and adenine were purchased from Sisco Research Laboratories, India, while cytosine was procured from Sigma-Aldrich. Tetrabutyl ammonium bromide (TBAB) obtained from Merck (India) was used as supporting electrolyte for electrochemical experiments performed in non-aqueous medium and KCl, also obtained from Merck (India) was used as supporting electrolyte for electrochemical experiments performed in aqueous solution. DMF (AR) and methanol (HPLC grade) were purchased from Merck India. They were used as solvents in several electrochemical experiments and in analysis involving HPLC. Ethidium Bromide

(EtBr) was purchased from Merck (India). Triple distilled water prepared in the laboratory was used in the preparation of all forms of either purely aqueous or semi aqueous solutions.

## **2. Experimental:**

### **2.1. Instruments used:**

Absorption spectra were recorded on a JASCO V-630 spectrophotometer, Japan. A digital pH meter (EQUIP-TRONICS, EQ-610, India) was used for pH measurements. FTIR of different compounds was recorded on a Perkin-Elmer RX-I spectrophotometer using KBr pellets while NIR spectra were recorded on Shimadzu 3600 UV-VIS-NIR spectrophotometer, Japan. Mass spectrum was recorded on Micromass Q-Tofmicro<sup>TM</sup>, Waters Corporation, USA. Elemental analysis was carried out on a Perkin Elmer 2400 Series-II CHN analyzer. Magnetic susceptibility measurements of powdered samples at room temperature (298 K) were done according to the Gouy method on a Magway MSB MK1, Sherwood Scientific Ltd., UK. Cyclic voltammetry experiments were carried out on Metrohm Autolab electrochemical analyzer. Fluorescence measurements were performed on a fluorescence spectrophotometer Horiba, Japan. HPLC (Shimadzu Corporation, Japan) was performed using a C-18 column and an appropriate mobile phase based on the requirement. Thermogravimetric analysis was done using METTLER TOLEDO TGA Sdta851 Thermogravimetric Analyzer.

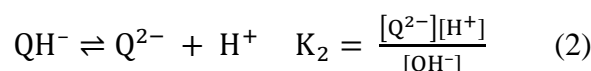
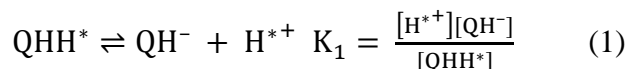
### **2.2. Determination of proton dissociation constants of chosen molecules:**

Proton dissociation constants for 1, 2-dihydroxy-9, 10-anthraquinone (alizarin), 1, 2, 4-trihydroxy-9, 10-anthraquinone (purpurin) and 7 $\beta$ -D-glucopyranosyl-3,5,6,8-tetrahydroxy-1-methyl-9,10-dioxo-9,10-dihydroanthracene-2-carboxylic acid (carminic acid) were determined using standard pH-metric titration techniques so that they could be used in different forms of analysis whenever required as a part of this work. In all such determinations, absorbance was measured at a particular wavelength determined by  $\lambda_{\max}$  of

## Chapter 6: Experimental: Materials and Methods

the concerned compound or compounds. These were then plotted against pH so that  $pK_a$  values could be evaluated.

Alizarin exists in two distinctly different forms,  $QHH^*$  and  $QH^-$ , depending on the pH and ionic strength of the medium;  $H^*$  represents the hydrogen on OH at  $C_2$  while H represents the hydrogen on OH at  $C_1$ .<sup>6</sup>



The absorbance of the solution at the monitoring wavelength was fitted either to Eq. 3a or Eq. 3b yielding  $pK_a$  values.<sup>6-9</sup>

$$A_{\text{obs}} = \frac{A_1}{(1 + 10^{\text{pH} - \text{p}K_{a1}} + 10^{\text{pH} - \text{p}K_{a2}})} + \frac{A_2}{(1 + 10^{\text{p}K_{a1} - \text{pH}} + 10^{\text{pH} - \text{p}K_{a2}})} + \frac{A_3}{(1 + 10^{\text{p}K_{a1} - \text{pH}} + 10^{\text{p}K_{a2} - \text{pH}})} \quad (3a)$$

$$A_{\text{obs}} = \frac{A_1}{(1 + 10^{\text{pH} - \text{p}K_{a1}} + 10^{\text{pH} - \text{p}K_{a2}} + 10^{\text{pH} - \text{p}K_{a3}})} + \frac{A_2}{(1 + 10^{\text{p}K_{a1} - \text{pH}} + 10^{\text{pH} - \text{p}K_{a2}} + 10^{\text{pH} - \text{p}K_{a3}})} + \frac{A_3}{(1 + 10^{\text{p}K_{a1} - \text{pH}} + 10^{\text{p}K_{a2} - \text{pH}} + 10^{\text{pH} - \text{p}K_{a3}})} + \frac{A_4}{(1 + 10^{\text{p}K_{a1} - \text{pH}} + 10^{\text{p}K_{a2} - \text{pH}} + 10^{\text{p}K_{a3} - \text{pH}})} \quad (3b)$$

Similarly, carminic acid exists in three distinctly different forms in solution in the pH range in which experiments were performed. The molecular form of carminic acid, later represented as CA has been denoted as  $QHH_1H_2$ . Presence of the anionic forms  $QHH_2^-$ ,  $QH^{2-}$  and  $Q^{3-}$  depend on pH and ionic strength of the medium;  $H_1$  represents the hydrogen at  $-\text{COOH}$  present on  $C_2$  while  $H_2$  represents the hydrogen on the phenolic  $-\text{OH}$  at  $C_3$ . H represents the hydrogen at  $C_6$ .



The absorbance of a CA solution at the monitoring wavelength was also fitted either to Eq. 3a or to Eq. 3b yielding  $pK_a$  values.<sup>6-9</sup>  $A_1$ ,  $A_2$ ,  $A_3$  and  $A_4$  refer to absorbances due to various forms of the chosen hydroxy-9,10-anthraquinone present in solution. For alizarin they are  $QHH^*$ ,  $QH^-$  and  $Q^{2-}$  respectively while for carminic acid they are  $QHH_1H_2$ ,  $QHH_2^-$ ,  $QH^{2-}$  and  $Q^{3-}$   $pK_{a1}$ ,  $pK_{a2}$  and  $pK_{a3}$  refer to respective  $pK_a$  values for the dissociation of protons on our chosen molecules (Eqs. 1 and 2)

### **2.3. Determination of proton dissociation constants of alizarin and purpurin in the presence of different concentrations of calf thymus DNA:**

Proton dissociation constants of the compounds used in this study were also determined in the presence of different concentrations of calf thymus DNA so that a correct value of  $pK_a$  of the compound could be used in equations that enable determination of the contributions of different forms of the compound present in solution to the overall binding constant. If a compound binds to DNA under a specified condition, then such contributions are significant and form an important part of the study undertaken related to binding of the compounds with calf thymus DNA that was chosen as a model target. During determination a 10% ethanol and 90% aqueous solution of the compounds were used. Ionic strength of the medium was maintained at 0.12 M, similar to what was maintained throughout the course of any DNA titration performed as a part of this work, leading to determination of overall binding constants, other than when the very determination of overall binding constant was followed as an outcome of the variation of ionic strength of the medium. In these determinations, the absorbance of alizarin was recorded at 525 nm while that of purpurin at 513 nm. These were then plotted against the pH of the medium. For these titrations also, Eq. 3a yields values for  $pK_{a1}$  and  $pK_{a2}$ , for dissociation of phenolic  $-OH$  protons present on the two compounds in the presence of different concentrations of calf thymus DNA.

**2.4. Determination of the stoichiometry of metal complexes of alizarin and carminic acid by mole ratio and Job's method of continuous variation:**

To be able to determine the composition of a complex formed in solution, equimolar solutions of either Mn(II) or Co(II) were used with compounds alizarin and carminic acid. In mole ratio method, either alizarin or carminic acid were kept constant while the metal ion was varied and vice-versa. The absorbance at 525 nm for Mn(II) interacting with alizarin, at 429 nm for Co(II) interacting with alizarin, were plotted against  $(T_M/T_L)T_L$  and  $(T_L/T_M)T_M$  respectively. Stoichiometry of interaction between carminic acid and Mn(II) was determined at two different pH to see if a variation in pH affects stoichiometry. Absorbance was monitored at 511 nm when the pH of the medium was 7.4 and 518 nm when the pH of the medium was 6.4. They were plotted against  $(T_M/T_L)T_L$ ; where  $T_M$  and  $T_L$  represent concentrations of Mn(II) and carminic acid respectively. Straight lines were obtained based on changes in absorbance, the intersection of which indicates the ratio in which either alizarin or carminic acid binds to a metal ion forming the complex. In Job's method of continuous variation complementary mixtures were prepared. In case of Mn(II) interacting with alizarin, a peak appeared at 525 nm, while for Co(II) interacting with alizarin, the peak appeared at 429 nm. For Mn(II) interacting with carminic acid, the peak appeared at 495 nm. Hence, job's plots for determination of stoichiometry of complex formation for Mn(II) with alizarin and with carminic acid or for Co(II) with alizarin could be obtained.

**2.5. Determination of proton dissociation constants of alizarin and carminic acid in the presence of metal ions and evaluation of stability constant of the complex in solution:**

In the presence of a metal ion, proton dissociation constants of each of the compounds trying to form a complex with the metal ion increases with the result that their  $pK_a$  value decreases. Spectrophotometric titrations were performed in the pH range 3.0 to 11.0 and  $pK_a$  values were determined.



$$\beta^* = \frac{[M(QH^*)_2][H^+]^2}{[M^{2+}][QHH^*]^2} \quad (5)$$



$$\beta = \frac{[M(QH^*)_2]}{[M^{2+}][QH^{*-}]^2} \quad (7)$$

$$\beta = \frac{\beta^*}{K_2^2} \quad (8)$$

Stability constants  $\beta^*$  and  $\beta$  were determined using Eqs. 4 – 8. To explain physico-chemical experiments precisely, hydrogens on the two OH groups (those at C<sub>1</sub> and C<sub>2</sub> of alizarin) are represented as H and H\* respectively. This was necessary as the trends in the dissociation of OH groups in the absence and presence of metal ions were known to be different.<sup>6</sup>

## 2.6. Synthesis of some 3d transition metal complexes of hydroxy-9,10-anthraquinones:

### 2.6.1 Synthesis of the Mn(II) complex of alizarin:

0.5 mmole MnCl<sub>2</sub>.4H<sub>2</sub>O was dissolved in a minimum volume of water. This was gradually added to a solution containing 1 mmole alizarin in 100 mL methanol. pH was adjusted to a value between 6.5 to 7.0. The mixture was warmed under reflux for approximately four hours. A violet coloured compound was recovered after proper work up. Anal. Calc. percentage for C<sub>28</sub>H<sub>14</sub>O<sub>8</sub>Mn.2H<sub>2</sub>O: C, 59.05; H, 3.16. Found: C, 59.12; H, 3.05. Molecular ion peak (m/z)<sub>calculated</sub> = 569.42; (m/z)<sub>observed</sub> = 569.86;  $\lambda_{\max}$  = 521 nm in DMSO.

### 2.6.2 Synthesis of the Co(II) complex of alizarin:

0.2 mmole of CoCl<sub>2</sub>.6H<sub>2</sub>O was dissolved in a minimum amount of distilled water. This was added drop wise to 0.6 mmole solution containing alizarin dissolved in a minimum amount of methanol. pH of the resulting solution was adjusted to 6.0. The mixture was warmed under reflux for approximately five hours. A dark violet coloured solid formed which was filtered.

## ***Chapter 6: Experimental: Materials and Methods***

---

Anal. Calc. percentage for  $C_{42}H_{21}O_{12}Co$ : C, 64.94; H, 2.73. Found: C, 64.37; H, 2.69.

Molecular ion peak  $(m/z)_{\text{calculated}} = 776.0869$ ;  $(m/z)_{\text{observed}} = 776.75$ ;  $\lambda_{\text{max}} = 535$  nm in DMSO.

### **2.6.3 Synthesis of Mn(II) complex of carminic acid:**

0.025 mmol  $MnCl_2 \cdot 4H_2O$  dissolved in minimum quantity of distilled water was added drop wise to a solution of 0.050 mmol CA in methanol. pH was adjusted to a value between 6.5 and 6.8 and warmed gently under reflux for approximately four hours. A violet amorphous compound was obtained. Anal. Calc. percentage for  $C_{44}H_{40}O_{28}MnNa_2$  is C, 47.26; H, 3.61. Found: C, 47.37; H, 3.69. Molecular ion peak  $(m/z)_{\text{calc}}$  for  $[Mn(CA)_2(H_2O)_2]^{2-} = 1071.23$ ;  $(m/z)_{\text{obs}} = 1070.667$ ;  $\lambda_{\text{max}} = 535$  nm in DMSO.

### **2.7. Computation for structure determination:**

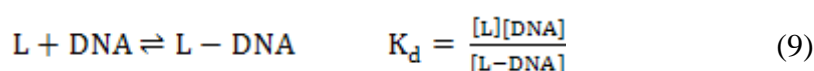
Theoretical calculations were performed using Gaussian 09W software<sup>10</sup> employing B3LYP.<sup>11</sup> Spin states of complexes were treated using the unrestricted formalism (“broken symmetry” treatment). For C, H and O atoms standard 6-31G basis set in conjunction with SDD effective core potential for the Mn atom was adopted.<sup>12</sup> Ground state geometries were fully optimized in gase and solution (solvent: DMSO) phases. Stability of optimized structures was established by vibrational analysis.

In case of electronic spectra, for transition energies between initial and final states of the complex, single point calculations were done using time dependent density functional theory (TDDFT)<sup>13</sup> on the basis of the ground state geometry optimized in DMSO using same function and basis set as simulated by conductor-like polarizable continuum model<sup>14</sup> using a non-equilibrium approach designed for the study of absorption processes. Orbital analysis was carried out with the help of Gauss View and MO composition using Gauss Sum program.<sup>15</sup> Spin contamination that usually arises while calculating with broken symmetry treatment in UDFT scheme for Mn, such spin contamination was investigated as the

difference between an expected value of  $S(S + 1)$  for an assigned spin state and the actual value of  $\langle S^2 \rangle$  from DFT calculations.

**2.8. Interaction of alizarin, purpurin, carminic acid and their complexes with calf thymus DNA followed by UV-Vis spectroscopy:**

Interaction of compounds with DNA resulted in a decrease in absorbance at wavelengths at which titrations were followed. The following equilibrium (Eq. 9) represents the interaction of calf thymus DNA with the compounds



L denotes compounds,  $K_d$  is the dissociation constant for interaction whose reciprocal provides a value for apparent binding constant ( $K_{app}$ ).<sup>7-9,16-20</sup> Eq. 10 obtained from Eq. 9 plots reciprocal of the change in absorbance against reciprocal of  $(C_D - C_0)$ .  $C_D$  refers to concentration of calf thymus DNA while  $C_0$  was the concentration of the compound. Using Eq. 10,  $\Delta A_{max}$  and  $K_{app}$  ( $1/K_d$ ) could be evaluated from the intercept and slope respectively.

$$\frac{1}{\Delta A} = \frac{1}{\Delta A_{max}} + \frac{K_d}{\Delta A_{max}(C_D - C_0)} \quad (10)$$

$\Delta A$  represents change in absorbance of compounds for each titration while  $\Delta A_{max}$  indicates the maximum change possible in terms of absorbance.

$$K_d = \frac{\left[ C_0 - \left( \frac{\Delta A}{\Delta A_{max}} \right) C_0 \right] \left[ C_D - \left( \frac{\Delta A}{\Delta A_{max}} \right) C_0 \right]}{\left( \frac{\Delta A}{\Delta A_{max}} \right) C_0} \quad (11)$$

$$C_0 \left( \frac{\Delta A}{\Delta A_{max}} \right)^2 - (C_0 + C_D + K_d) \left( \frac{\Delta A}{\Delta A_{max}} \right) + C_D = 0 \quad (12)$$

## Chapter 6: Experimental: Materials and Methods

---

$\Delta A/\Delta A_{\max}$  was plotted against  $C_D$ . Eq. 12 fits the data to a non-linear square fit analysis providing another set of values for apparent binding constant.<sup>7-9,16</sup> Titrations were also analyzed by a modified Scatchard equation [Eq. 13].<sup>21</sup> Overall binding constant ( $K^*$ ) and site size ( $n$ ) could be determined from Eq. 13.

$$r/C_f = K^* (n - r) \quad (13)$$

$r$  denotes the ratio of the concentration of a compound bound to DNA to that of the total concentration of DNA present in the reaction mixture at any point during the titration i. e.  $C_b/C_D$  where  $C_b$  represents concentration of the bound compound and  $C_f$  concentration of free compound. “ $n$ ” provides binding stoichiometry in terms of the compound under investigation bound per nucleotide while “ $n_b$ ” reciprocal of “ $n$ ” denotes binding site size in terms of the number of nucleotides bound to a compound. “ $n_b$ ” was obtained by plotting  $\Delta A/\Delta A_{\max}$  against  $C_D/[\text{compound}]$ .<sup>7-9,16</sup> Besides obtaining  $K^*$  from the modified Scatchard equation, it could also be obtained by multiplying  $K_{\text{app}}$  with “ $n_b$ ”, obtained from Eqs 10-12, and compared with values obtained from the modified Scatchard equation. Such titrations of compounds as mentioned above with calf thymus DNA were either performed at constant pH but different ionic strengths of the medium or at different pH, keeping the ionic strength of the medium constant.

### ●Variation of overall binding constant $K^*$ with pH:

Alizarin and purpurin, both exist in two different forms (neutral and anionic) under physiological conditions, pH range etc. in which DNA binding studies were performed. Contribution of the neutral and anionic forms of each compound towards overall binding constant determined through titrations with calf thymus DNA were obtained by considering  $pK_{a1}$  of each compound. Considering overall binding constant values for the two compounds at different pH and using Eqs. 14 and 15 respectively, contributions of the neutral ( $K^0$ ) and

anionic ( $K^-$ ) forms of each compound to overall binding constant with calf thymus DNA was evaluated.

$$K^* (1 + 10^{pH - pK}) = K^0 + K^- \times 10^{pH - pK} \quad (14)$$

$$\text{or} \quad K^* = (K^0 + K^- \times 10^{pH - pK}) / (1 + 10^{pH - pK}) \quad (15)$$

In Eq. 14 & 15,  $K^*$  is the overall binding constant for the interaction of a compound with calf thymus DNA and is an experimentally determined parameter.  $K^*$  obtained from the titration may be denoted as  $K^* = \frac{[C_b]}{[C_f][DNA]}$ <sup>22</sup> where terms have their usual meaning. Since experimentally determined overall binding constant ( $K^*$ ) is a consequence of individual interactions of the neutral and anionic forms, hence binding due to the neutral form may be denoted as  $K^0$  where ( $K^0 = \frac{[C_b^0]}{[C_f^0][DNA]}$ ) while that due to the anionic form may be denoted as  $K^-$  where  $K^- = \frac{[C_b^-]}{[C_f^-][DNA]}$ <sup>22,23</sup> The total concentration of each compound was considered as  $C_0$  where  $C_0 = C_b + C_f$ .  $C_b$  denotes the bound form and  $C_f$  the free form of the two compounds considered for interaction with calf thymus DNA. Again, of the bound form, a portion would bind to calf thymus DNA as neutral species while the other as an anionic species. Similarly, the total free form (that not bound to DNA) would also exist in the neutral form and the anionic form.

Hence,

$$[C_b] = [C_b^0] + [C_b^-] \quad (16)$$

$$\text{and} \quad [C_f] = [C_f^0] + [C_f^-] \quad (17)$$

A plot of  $K^*(1 + 10^{pH - pK})$  versus  $10^{pH - pK}$  as in Eq. 14, generates a straight line from where  $K^-$  may be determined as the slope and  $K^0$  as the intercept. The two parameters  $K^0$  and  $K^-$  may also be determined making use of Eq. 15. Here if  $K^*(1 + 10^{pH - pK})$  is plotted against  $(K^0 + K^- \times 10^{pH - pK})$  then a non-linear fit may determine values of  $K^0$  and  $K^-$  by the process of

iteration. Determination of  $K^0$  and  $K^-$  is crucial as it helps to predict reasons for observed changes in the interaction of different hydroxy-9,10-anthraquinones as they interact with calf thymus DNA under different conditions of the medium.

### **2.9. Electrochemical measurements:**

Electrochemical experiments on alizarin and its metal complexes were carried out in an air-tight 50 ml electrochemical cell. Voltammograms were recorded on a Metrohm–Autolab model PGSTAT 101 potentiostat. Analysis of data was done using the NOVA 1.10.1.9 program. A conventional three-electrode system, glassy carbon as the working electrode, a platinum wire as counter electrode and Ag/AgCl, satd. KCl as reference electrode were used. Before each electrochemical experiment, solutions were degassed for nearly 30 minutes using high purity argon. Reduction of the quinone moiety in these compounds was followed in aqueous, aqueous-dimethyl formamide (DMF) and in pure DMF solvents using cyclic voltammetry. As reported earlier with similar compounds, in DMF, a two step one-electron reduction (first to semiquinone, then to quinone dianion) was observed.<sup>24,25</sup> However, with increase in the percentage of water, two reduction peaks approach each other and eventually a single step two electron reduction occurs.<sup>26,27</sup> Quinone-dianion and free quinone upon comproportionation forms semiquinone radical anion that disproportionates.<sup>7,8,24,25,28-31</sup> All these were verified as a part of this study with the chosen compounds alizarin and carminic acid. Voltammograms were analyzed by Randles-Sevcik equation (Eq. 18) to check that the process was diffusion controlled which would be an important criterion for further experiments that would follow.<sup>32,33</sup>

$$i_{pc} = (2.69 \times 10^5).n^{3/2}. D_0^{1/2}.A.C.v^{1/2} \quad (18)$$

$i_{pc}$  refers to current in amperes at the cathodic peak potential,  $n$ , refers to total number of electrons involved,  $D_0$ , the diffusion coefficient of species,  $A$ , area of the electrode in  $cm^2$ ,  $C$ ,



concentration of the substance in moles/cm<sup>3</sup> and  $v$ , the scan rate in Vs<sup>-1</sup>. In aqueous solution the reduction potential of alizarin was obtained at -0.65V. Under exactly similar conditions, the reduction potential of the Mn(II) complex was ascertained to be at -0.75 V.

From a knowledge of the reduction potential of the quinone in each of these compounds and employing cyclic voltammetry in presence of DNA, it is possible to both reduce and oxidize them in an extremely small time interval in the vicinity of DNA, similar to what happens when such drugs interact with electrons from an electron transport chain in the mitochondria. Therefore by performing cyclic voltammetry in the presence of DNA it should become possible to predict whether the free radicals formed on chemical compounds like alizarin or its Mn(II) complex do actually interact with DNA and lead to reactions that might initiate DNA damage. Such experiments could then portray through model studies the aspect of electron transfer to drug candidates from electron transport chains within the mitochondria. However, in such cases damage inflicted on to DNA would be extremely small and hence difficult to quantify. Therefore, what was done is that with the help of cyclic voltammetry experiments the reduction potential or potentials (in case of more than one electron reduction) were first identified. Then the compound was maintained at that constant potential using a potentiostat so that electrons continuously reduce it at that potential for finite periods of time. A glassy carbon electrode was used during experiments. As a consequence the same radical or radical anions are now generated in greater amount and the damage they may cause on a target becomes quantifiable by a standard measuring technique. Experiments were performed under aerated/de-aerated (Ar saturated) conditions at constant pH (~ 7.4). Since biological targets were maintained in the immediate vicinity of *in situ* electrochemically generated quinone-dianion or semiquinone they got an opportunity to interact with reduced species. In aerated medium, there is the possibility of superoxide radical anion formation as well. The complexes show SOD activity.<sup>34</sup> The time for *in situ* electrochemical generation of species

## ***Chapter 6: Experimental: Materials and Methods***

---

was kept constant so that a similar charge was provided to each compound in all sets of experiments so that there is similar experimental error associated with the stimuli, here the potentiostat, that helps in the generation of reactive reduced species. Constancy of charge transferred to each compound under investigation was checked by chrono-amperometry. This enabled a proper comparison of the results obtained following interaction of species (radical anions or radicals) that were generated in solution with a target maintained in the immediate vicinity of such generation.<sup>35-37</sup> A semiquinone radical anion or protonated semiquinone under de-aerated condition or a superoxide radical-anion along with semiquinone radical anion (under aerated condition) interact with model biological targets maintained in an electrochemical cell. For control experiments, no compound was used but the respective potential of that compound for whom the control experiment was being performed was applied, using the same glassy carbon electrode having either a chosen nucleic acid base or calf thymus DNA in solution. Utmost care was taken to see all potentials were applied accurately since this formed the basis of these experiments involving generation of reactive intermediates since they in turn react with biological targets maintained in the immediate vicinity of their generation.<sup>35-37</sup> Concentrations of nucleic acid bases present in solution were approximately ten times that of the compounds used. pH was maintained at 7.4 with the help of phosphate buffer.

Aliquots were drawn from each experimental solution, following application of constant pre-determined potential for a definite period of time during which each nucleic acid base was subjected to interaction with *in situ* electrochemically generated species. Subsequently, HPLC was performed using a C-18 column as the stationary phase and 5% aqueous-methanol as the mobile phase. From the HPLC chromatograms, the amount of each nucleic acid base remaining unaltered was calculated.

In experiments where calf thymus DNA was the target, aliquots were drawn from the reaction vessel and saturated with EtBr. The DNA-EtBr adduct was excited at 510 nm and fluorescence was recorded at 602 nm.<sup>38-40</sup> From the loss in fluorescence of the DNA-EtBr adduct, the amount of calf thymus DNA that underwent modification following interaction with radicals generated under aerated and de-aerated (Ar saturated) conditions was ascertained.<sup>38</sup> For control experiments on DNA, the solution contained the same amount of calf thymus DNA as for other experimental solutions but no compound was added. Solutions were subjected to the same constant potential of that compound to serve as control, using the same glassy carbon electrode for similar times. Aliquots from these solutions were then treated with similar concentrations of EtBr and fluorescence was recorded at 602 nm.

## **2.10. ROS estimation:**

### **2.10.1. By NADH dehydrogenase assay:**

It is known that hydroxy-9,10-anthraquinones that form the core of anthracyclines, are reduced to semiquinone by electrons assisted by enzymes present in a biological system. This leads to a sequence of reactions culminating in the formation of reactive oxygen species (ROS) like the superoxide radical anion and other oxygen radical species. ROS produced in this manner have beneficial activity having a definite role in cell killing. At the same time, they are also responsible for toxic side effects; cardiotoxicity being a serious issue. We tested the ability of hydroxy-9,10-anthraquinones to be reduced by performing an assay at 298 K with cytochrome c as the electron acceptor<sup>41</sup> following the transfer of electrons from NADH to molecular oxygen in presence of NADH dehydrogenase. Alizarin,  $Mn^{II}(alz)_2(H_2O)_2$  and  $Co^{II}(alz)_3^-$  were tried in the NADH-cytochrome c reductase activity assay where reduction of cytochrome c at 550 nm was followed at pH 7.4 (100 mM Tris buffer)<sup>6,8,9,18,19,41</sup> to see whether complex formation is able to decrease generation of superoxide radical anion. Each test solution had 80  $\mu$ M cytochrome c, 160  $\mu$ M NADH and 5  $U l^{-1}$  NADH dehydrogenase and

## ***Chapter 6: Experimental: Materials and Methods***

---

the compounds. Compound concentration was varied from 0 to 60.0  $\mu\text{M}$ . Activity of NADH dehydrogenase has been expressed in units, where one unit of activity reduces 1.0  $\mu\text{mole}$  oxidized cytochrome c per minute at pH 7.4 and 300 K. Formation of superoxide radical anion catalyzed by the compounds was measured from reduction of cytochrome c inhibited by SOD in the presence of NADH and NADH dehydrogenase using the kinetics software of JASCO V-630 spectrophotometer, Japan.<sup>6,8,9,18,19,41</sup>

### **2.10.2. Making use of the H<sub>2</sub>DCFDA assay:**

The cell permeant reagent 2',7'-dichlorofluorescein diacetate (H<sub>2</sub>DCFDA) is a fluorogenic dye that measures the presence of reactive oxygen species (ROS) inside a cell.<sup>42-45</sup> Once inside the cell, H<sub>2</sub>DCFDA is de-acetylated by cellular esterases to a non-fluorescent compound. If ROS be present then this reduced compound is subsequently oxidized to 2',7'-dichlorofluorescein (DCF).<sup>42,44</sup> DCF is also highly fluorescent. Its excitation was done at 504 nm and emission measured at 529 nm using a fluorescence spectrophotometer (Hitachi, Japan). A stock solution of H<sub>2</sub>DCFDA (10 mM) was prepared in methanol and further diluted with culture medium to a concentration of 100  $\mu\text{M}$ . Two carcinoma cell lines (HeLa and HepG2) and the normal (WI-38 lung fibroblast) cell were chosen for the above mentioned assay. Cells were treated with IC<sub>50</sub> concentrations of compounds under investigation, determined by the MTT assay and allowed to stand for 30 minutes. ROS was induced by the free radical generator H<sub>2</sub>O<sub>2</sub> (70  $\mu\text{M}$ ) by incubating cells treated with compounds for a further 30 minutes. Cells were washed with ice cold Hanks balanced salt solution (HBSS) and incubated with 100  $\mu\text{M}$  H<sub>2</sub>DCFDA for 30 minutes at 37°C. Cells were then lysed with an alkaline solution and fluorescence was recorded. 10  $\mu\text{M}$  N-acetyl cysteine (NAC) was used as the control for these experiments.

## 2.11. Biological Experiments:

### 2.11.1. Cell culture:

Human cervical carcinoma cells (HeLa), human hepatocellular carcinoma cells (Hep G2), SiHa cervical carcinoma, PC3 Prostrate carcinoma, A549 lung carcinoma cells and the normal WI-38 lung fibroblast cells were cultured in DMEM medium (GIBCO, Invitrogen, Carlsbad, CA, US) supplemented with 10% fetal bovine serum (GIBCO), 100 IU/mL penicillin and 100 µg/mL streptomycin at 37°C in a humid atmosphere containing 5% CO<sub>2</sub> (Heraeus, Thermo Scientific, MA, USA). Cell lines were procured from the National Centre for Cell Science in Pune, India. Cells were seeded in 96 well plates for 24 hours prior to treatment with different compounds.<sup>45,46</sup>

### 2.11.2. Cell viability assay:

Each cell line was treated with compounds under investigation that were earlier dissolved in DMSO. Concentration of DMSO was less than 0.5 %. Cell viability was checked 48 hours after treatment with 3-(4,5-dimethylthiazol-2-yl)-2,5-diphenyltetrazolium bromide (MTT).<sup>19</sup> Briefly, cells were washed with 1 × PBS and treated with MTT for 4 hours at 37°C. Crystals were dissolved in DMSO and plates analyzed on a Thermo MULTISKAN EX plate reader at 595 nm.

## References:

- [1] J. William Lown. 1993. Discovery and development of anthracycline antitumour antibiotics. *Chem. Soc. Rev.* 22: 165-176
- [2] H. Corte's-Funes, C. Coronado. 2007. Role of anthracyclines in the era of targeted therapy. *Cardiovasc Toxicol.* 7: 56–60.

- [3] I. Muller, D. Niethammer and G. Bruchelt. 1998. Anthracycline-derived chemotherapeutics in apoptosis and free radical cytotoxicity (Review). *Int J mol med.* 1: 491-494.
- [4] T. Simůnek, M. Stérba, O. Popelová, M. Adamcová, R. Hrdina, V. Gersl. 2009. Anthracycline-induced cardiotoxicity: overview of studies examining the roles of oxidative stress and free cellular iron. *Pharmacol Rep.* 61 :154-71.
- [5] P. Angsutararux, S. Luanpitpong, S. Issaragrisil. 2015. Chemotherapy-induced cardiotoxicity: Overview of the roles of oxidative stress. *Oxid Med Cell Longev.* 2015: 795602. doi: 10.1155/2015/795602.
- [6] S.Das, A. Saha and P. C. Mandal. 1996. Studies on the formation of Cu(II) and Ni(II) complexes of 1,2-dihydroxy-9,10-anthraquinone and lack of stimulated superoxide formation by the complexes. *Talanta.* 43: 95-102.
- [7] P. Das, C. K. Jain, S. K. Dey, R. Saha, A. D. Chowdhury, S. Roychoudhury, S. Kumar, H.K. Majumder, S. Das. 2014. Synthesis, crystal structure, DNA interaction and *in vitro* anticancer activity of a Cu(II) complex of purpurin: dual poison for human DNA topoisomerase I and II. *RSC Adv.* 4: 59344-59357.
- [8] P. Das, C.K. Jain, S. Roychoudhury, H.K. Majumder, S. Das. 2016. Design, synthesis and *in vitro* anticancer activity of a Cu(II) complex of carminic acid: A novel small molecule inhibitor of human DNA topoisomerase I and topoisomerase II. *ChemistrySelect.* 1: 6623-6631.
- [9] S. Mukherjee-Chatterjee, C.K. Jain, S. Singha, P. Das, S. Roychoudhury, H.K. Majumder, S. Das. 2018. Activity of Co<sup>II</sup>-Quinalizarin: A novel analogue of anthracycline-based anticancer agents targets human DNA topoisomerase, whereas quinalizarin itself acts via

formation of semiquinone on acute lymphoblastic leukemia MOLT-4 and HCT 116 Cells. *ACS Omega*. 3:10255-10266.

[10] M. J. Frisch, G. W. Trucks, H. B. Schlegel, G. E. Scuseria, M. A. Robb, J. R. Cheeseman, G. Scalmani, V. Barone, G. A. Petersson, H. Nakatsuji, X. Li, M. Caricato, A. V. Marenich, J. Bloino, B.G. Janesko, R. Gomperts, B. Mennucci, H.P. Hratchian, J.V.Ortiz, A.F. Izmaylov, J.L. Sonnenberg, D. Williams-Young, F. Ding, F. Lipparini, F.Egidi, J. Goings, B. Peng, A. Petrone, T. Henderson, D. Ranasinghe, V.G.Zakrzewski, J. Gao, N. Rega, G. Zheng, W. Liang, M. Hada, M. Ehara, K.Toyota, R. Fukuda, J. Hasegawa, M. Ishida, T. Nakajima, Y. Honda, O. Kitao, H.Nakai, T. Vreven, K. Throssell, J.A. Montgomery Jr., J.E. Peralta, F. Ogliaro, M. J. Bearpark, J.J. Heyd, E.N. Brothers, K.N. Kudin, V.N. Staroverov, T.A. Keith, R.Kobayashi, J. Normand, K. Raghavachari, A.P. Rendell, J.C. Burant, S.S. Iyengar, J.Tomasi, M. Cossi, J.M. Millam, M. Klene, C. Adamo, R. Cammi, J.W. Ochterski, R.L. Martin, K. Morokuma, O. Farkas, J.B. Foresman, D.J. Fox, Gaussian 09,Revision A.02, Gaussian, Inc., Wallingford CT, 2016.

[11] (a) A. D. Becke. 1993. Density functional thermochemistry. III. The role of exact exchange. *J. Chem. Phys.* 98: 5648-5652. (b) C.T. Lee, W.T. Yang, R.G. Parr. 1988. Development of the Colle-Salvetti correlation-energy formula into a functional of the electron density. *Phys. Rev. B* 37: 785-789.

[12] X. Y. Cao, M. Dolg. 2002. Segmented contraction scheme for small-core lanthanide pseudopotential basis sets. *J. Mol. Struct.:THEOCHEM* 581: 139-147.

[13] E. K. U. Gross, W. Kohn. 1990. Time-dependent density-functional theory. *Quantum Chem.* 21: 255-291.

[14] M. Cossi, V. Barone. 2001. Time-dependent density functional theory for molecules in liquid solutions. *J. Chem. Phys.* 115: 4708-4717.

## ***Chapter 6: Experimental: Materials and Methods***

---

- [15] N. M. O'Boyle, A.L. Tenderholt, K.M. Langnerclib. 2008. cclib: a library for package-independent computational chemistry algorithms. *J. Comp. Chem.* 29:839-845.
- [16] S. Mukherjee, P.K. Gopal, S. Paul, S. Das. 2014. Acetylation of 1,2,5,8-tetrahydroxy-9,10-anthraquinone improves binding to DNA and shows enhanced superoxide formation that explains better cytotoxicity on JURKAT T lymphocyte cells. *J. Anal Oncol.* 3: 122-129.
- [17] P. Das, D. Bhattacharya, P. Karmakar, S. Das. 2015. Influence of ionic strength on the interaction of THA and its Cu(II) complex with DNA helps to explain studies on various breast cancer cells. *RSC Adv.* 5: 73099- 73111.
- [18] B. Mandal, S. Singha, S. K. Dey, S. Mazumdar, T. K. Mondal, P. Karmakar, S. Kumar and S. Das. 2016. Synthesis, crystal structure from PXRD of a Mn<sup>II</sup>(purp)<sub>2</sub> complex, interaction with DNA at different temperatures and pH and lack of stimulated ROS formation by the complex. *RSC Adv.* 6:51520-51532.
- [19] B. Mandal, S. Singha, S. K. Dey, S. Mazumdar, S. Kumar, P. Karmakar and S. Das. 2017. Cu<sup>II</sup> complex of emodin with improved anticancer activity as demonstrated by its performance on HeLa and Hep G2 cells. *RSC Adv.* 7: 41403-41418.
- [20] S. Roy, P. Mondal, P. S. Sengupta, D. Dhak, R. C. Santra, S. Das, P. S. Guin. 2015. Spectroscopic, computational and electrochemical studies on the formation of the copper complex of 1-amino-4-hydroxy-9,10-anthraquinone and effect of it on superoxide formation by NADH dehydrogenase. *Dalton Trans.* 44: 5428-5440.
- [21] G. Scatchard. 1949. The attractions of proteins for small molecules and ions. *Ann. NY Acad. Sci.* 51: 660-672.
- [22] R. Comanici, B. Gabel, T. Gustavsson, D. Markovitsi, C. Cornaggia, S. Pommeret, C. Rusu, C. Kryschi. 2006. Femtosecond spectroscopic study of carminic acid–DNA interactions. *ChemicalPhysics.* 325: 509-518.



- [23] F. Frezard, A. Garnier-Suillerot. 1990. Comparison of the binding of anthracycline derivatives to purified DNA and to cell nuclei. *Biochimica et Biophysica Acta*, 1036: 121-127.
- [24] P. S. Guin, S. Das, P. C. Mandal. 2010. Sodium 1, 4-dihydroxy-9, 10-anthraquinone-2-sulphonate interacts with calf thymus DNA in a way that mimics anthracycline antibiotics: an electrochemical and spectroscopic study. *J. Phy. Org. Chem.* 23: 477-482.
- [25] P. Das, P. S. Guin, P. C. Mandal, M. Paul, S. Paul, S. Das. 2011. Cyclic voltammetric studies of 1,2,4-trihydroxy-9,10-anthraquinone, its interaction with calf thymus DNA and anti-leukemic activity on MOLT-4 cell lines: a comparison with anthracycline anticancer drugs. *J. Phy. Org. Chem.* 24:774-785.
- [26] P. S. Guin, S. Das, P. C. Mandal. 2008. Electrochemical reduction of sodium 1, 4-dihydroxy-9, 10-anthraquinone-2-sulphonate in aqueous and aqueous dimethyl formamide mixed solvent: a cyclic voltammetric study. *Int. J. Electrochem. Sci.* 3: 1016-1028.
- [27] P. S. Guin, S. Das, P. C. Mandal. 2011. Electrochemical reduction of quinones in different media: A review. *Int. J. Electrochem.* Article ID 816202, 22 pages; doi:10.4061/2011/816202.
- [28] O. Wangpradit, A. Rahaman, S. V. S. Mariappan, G. R. Buettner, L. W. Robertson, G. Luthe. 2016. Breaking the dogma: PCB-derived semiquinone free radicals do not form covalent adducts with DNA, GSH, and amino acids. *Environ Sci Pollut Res Int.* 23: 2138-2147.
- [29] M. Quan, D. Sanchez, M. F. Wasylkiw, D. K. Smith. 2007. Voltammetry of quinones in unbuffered aqueous solution: reassessing the roles of proton transfer and hydrogen bonding in the aqueous electrochemistry of quinones. *J. Am. Chem. Soc.* 42: 12847-12856.

## ***Chapter 6: Experimental: Materials and Methods***

---

- [30] S. I. Bailey and I. M. Ritchie. 1985. A cyclic voltammetric study of the aqueous electrochemistry of some quinones. *Electrochim. Acta.* 30: 3-12.
- [31] E. Laviron. 1984. Electrochemical reactions with protonations at equilibrium: Part X. The kinetics of the p-benzoquinone/hydroquinone couple on a platinum electrode. *J. Electroanal. Chem.* 164: 213-227.
- [32] J. E. B. Randles. 1948. A cathode ray polarograph. Part II.—The current-voltage curves. *Trans. Faraday Soc.* 44: 327-338.
- [33] A. J. Bard, L. R. Faulkner. 2001. *Electrochemical methods fundamental and applications*, 2nd ed., (John Wiley & Sons, New York).
- [34] T. Saha, P. Kumar, N. Sepay, D. Ganguly, K. Tiwari, K. Mukhopadhyay, S. Das. 2020. Multitargeting antibacterial activity of a synthesized Mn<sup>2+</sup> complex of curcumin on Gram-positive and Gram-negative bacterial strains. *ACS Omega.* 5: 16342-16357.
- [35] P. Nandy, S. Das. 2018. Interaction of electrochemically generated reduction products of Ornidazole with nucleic acid bases and calf thymus DNA. *J. Indian Chem. Soc.* 95: 1009-1014.
- [36] B. Mandal, H. K. Mondal, S. Das. 2019. In situ reactivity of electrochemically generated semiquinone on Emodin and its Cu<sup>II</sup>/Mn<sup>II</sup> complexes with pyrimidine based nucleic acid bases and calf thymus DNA: Insight into free radical induced cytotoxicity of anthracyclines. *Biochem. Biophys. Res. Comm.* 515: 505-509.
- [37] P. Nandy, S. Das. 2020. In situ reactivity of electrochemically generated nitro radical anion on Ornidazole and its monomeric Cu(II) complex with nucleic acid bases and calf thymus DNA. *Inorg. Chim. Acta.* 501: 119267-119267;

- [38] H. C. Birnboim, J. J. Jevcak. 1981. Fluorometric method for rapid detection of DNA strand breaks in human white blood cells produced by low doses of radiation. *Cancer Research*. 41: 1889-1892.
- [39] S. Das, A. Saha, P. C. Mandal. 1997. Radiation-induced double-strand modification in calf thymus DNA in the presence of 1,2-dihydroxy-9,10-anthraquinone and its Cu(II) Complex. *Environ. Health Pers.* 105: 1459-1462
- [40] S. Das, P. C. Mandal. 2014. Anthracyclines as radiosensitizers: a Cu(II) complex of a simpler analogue modifies DNA in Chinese Hamster V79 cells under low-dose  $\gamma$  radiation. *J Radioanal Nucl Chem.* 299: 1665-1670.
- [41] H. R. Mahler. 1955. In: *Methods in enzymology* 11, Academic Press, New York, USA. pp. 668–672.
- [42] H. Wang, J. A. Joseph. 1999. Quantifying cellular oxidative stress by dichlorofluorescein assay using microplate reader. *Free Radical Biol. Med.* 27:612-616.
- [43] O. Myhre, J. M. Andersen, H. Aarnes, F. Fonnum. 2003. Evaluation of the probes 2',7'-dichlorofluorescein diacetate, luminol, and lucigenin as indicators of reactive species formation. *Biochem. Pharmacol.* 65: 1575-1582.
- [44] A. Gomes, E. Fernandes, J. L. Lima. 2005. Fluorescence probes used for detection of reactive oxygen species. *J. Biochem. Biophys. Methods.* 65: 45-80.
- [45] A. Pramanik, D. Laha, S. Chattopadhyay, S.K. Dash, S. Roy, P. Pramanik, P.Karmakar. 2015. Targeted delivery of “copper carbonate” nanoparticles to cancer cells in vivo. *Toxicol. Res.* 4: 1604-1612.
- [46] M. Dinda, U. Dasgupta, N. Singh, D. Bhattacharyya, P. Karmakar. 2015. PI3K-mediated proliferation of fibroblasts by *Calendula officinalis* tincture: implication in wound healing. *Phytother. Res.* 29: 607-616.



# CHAPTER 7

**Importance of pKa in an analysis of the interaction of compounds with DNA**



## 1. Introduction:

Studies on interaction of compounds with DNA are important because of their relevance and utility related to different aspects of chemical biology.<sup>1-13</sup> Many factors influence the interaction of compounds with DNA.<sup>6,10,12,14-16</sup> Things get slightly complicated when the compound exists in more than one form since each form interacts differently with DNA. Overall binding constant of the compound is therefore a consequence of the interaction of each form.<sup>15-22</sup> If a compound exhibits *cis-trans* isomerism or has one or more easily dissociable protons it has the possibility to exist in more than one form in that medium.<sup>17,19-21</sup> For proton dependent equilibria, such contributing forms change with changes in pH of the medium that affects binding parameters.<sup>19-22</sup> Compounds not having a second form at a particular pH, could well dissociate under the influence of nucleic acid bases in DNA as it tries to interact.<sup>23</sup> Most researchers report DNA binding not considering the existence of all possible forms under experimental conditions.<sup>19-25</sup>

For compounds where two or more forms exist in solution due to proton-dependent equilibria it is essential that a correct evaluation of the pKa of the compound is done as it would be extremely crucial for drug selection and optimization.<sup>26,27</sup> We usually determine pKa in aqueous solution at low ionic strength and then use it to realize different physicochemical parameters of physiological processes.<sup>28</sup> With regard to DNA binding for example, it is important to know the extent to which this is correct, i.e. to use the pKa of a compound that was determined at low ionic strength while evaluating DNA binding parameters for which the titration itself is performed at a certain high ionic strength.<sup>19,20,22</sup> When this is done, results concluded from such studies performed *in vitro* and *in vivo* have often differed in a big way from the standpoint of biological manifestations. It is known that pKa of a compound could be different in presence of DNA.<sup>23,29,30</sup> We performed an analysis of DNA binding data using our chosen compounds determining pKa values both in the absence and in the presence of

different concentrations of calf thymus DNA.<sup>20</sup> Since in our case different forms of the compound present in solution are a consequence of their proton dissociation equilibria, a proper determination of pKa is extremely essential. Change in pKa affects overall binding constant with DNA since the contributing forms differ and hence their interactions.<sup>31,32</sup> Another important factor responsible for changes in pKa is the ionic strength of the medium, but when ionic strength is constant it could also vary depending on the DNA present.<sup>8,10,23-25,32</sup> Moreover, when pH is different, it affects the three dimensional structures of DNA either exposing or holding back nucleic acid bases in different ways that influence the determination of pKa.<sup>23</sup> Ellipticine for example (pKa = 7.4), binds calf thymus DNA at pH 5 where its cationic form predominates while at pH 9 its neutral form is the major species.<sup>33</sup> This study did not consider the presence of the minor form at either pH. Hence, values reported for binding constants of the respective forms are not exclusively those due to the forms claimed in the report. The situation might not have been too serious for this report because the minor form's contribution at either pH would be extremely small and hence it could be neglected. However, when pKa of a compound lies in the physiological pH range as it was in the example above, only a slight variation in interaction could affect the calculations. Therefore, the influence of nucleic acid bases on compounds during determination of pKa and during binding requires proper investigation and analysis. This study made an attempt to understand fluctuations in pKa of alizarin and purpurin (hydroxy-9,10-anthraquinones) in the presence of varying concentrations of calf thymus DNA against that determined under normal physiological conditions (aqueous environment) to see manifestations due to changes in pKa.

## **2. Results & Discussion:**

Alizarin and purpurin were titrated using dilute NaOH in the presence of different concentrations of calf thymus DNA at a constant ionic strength of the medium. Figures 1 & 2



(A and B) show variation in absorbance of compounds with pH, recorded at different DNA concentrations.

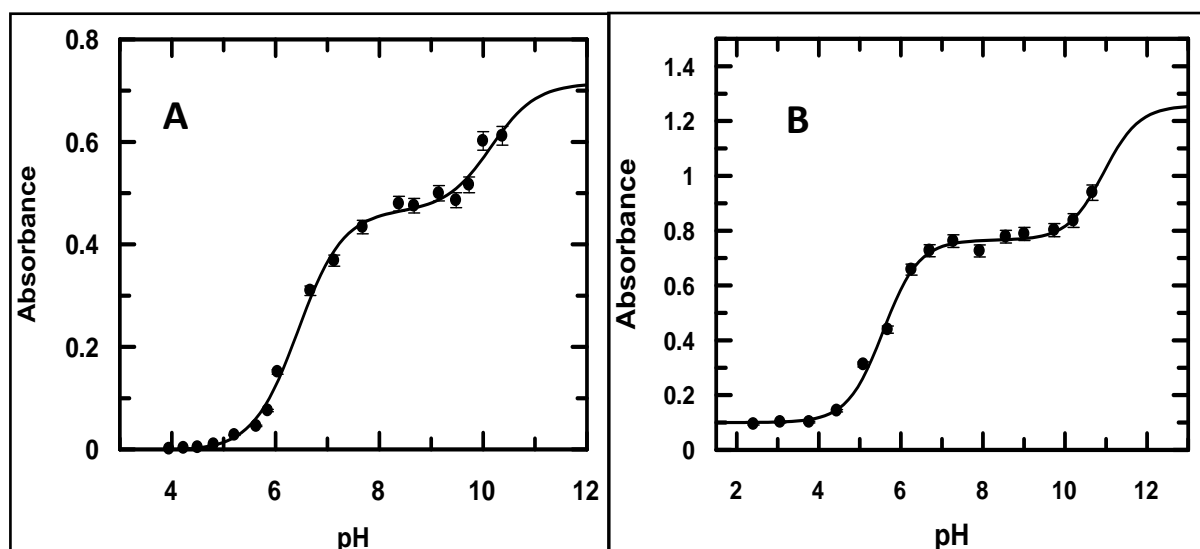


**Fig. 1:** pH-metric titration of alizarin shown by a variation in absorbance at 525 nm in presence of calf thymus DNA (A) 62.7  $\mu\text{M}$  and (B) 221.97 $\mu\text{M}$ . [alizarin] = 100  $\mu\text{M}$ ; T = 300 K.

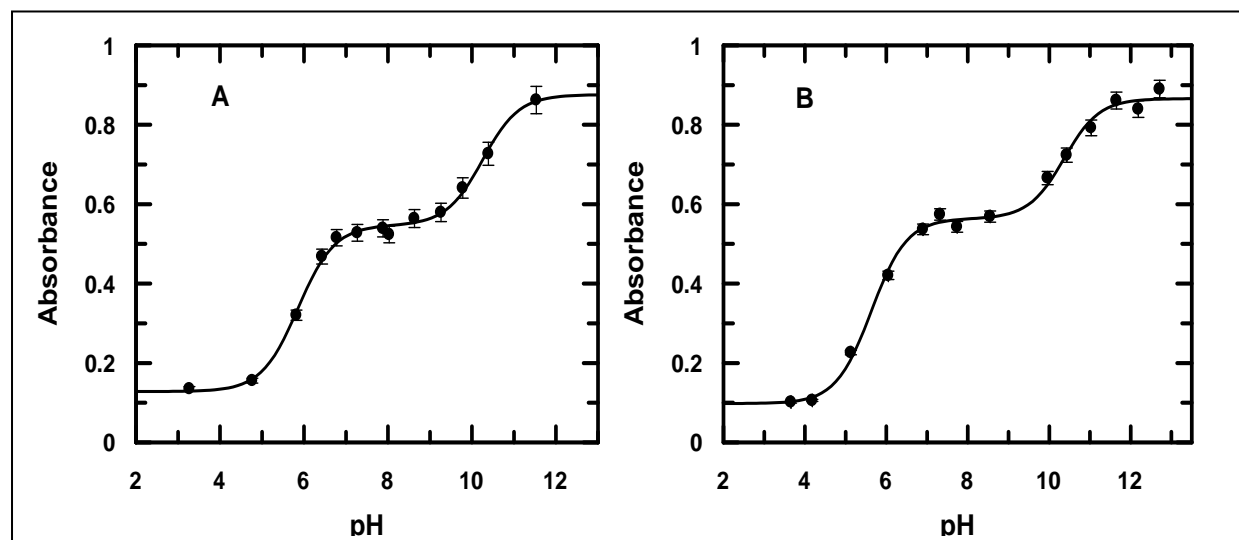


**Fig. 2:** pH-metric titration of purpurin shown by a variation in absorbance at 513 nm in presence of calf thymus DNA (A) 66.88  $\mu\text{M}$  and (B) 73.28  $\mu\text{M}$ . [purpurin] = 100  $\mu\text{M}$ ; T = 300 K.

### Chapter 7: The importance of pKa.... compounds with DNA

Fitting the experimental data according to Eq. 3a (*Chapter 6: Experimental*),  $pK_{a1}$  and  $pK_{a2}$  for alizarin and purpurin were determined. These were plotted against increased presence of calf thymus DNA for both compounds. It was observed that with an increase in the concentration of calf thymus DNA,  $pK_{a1}$  of alizarin and purpurin decreased [Figure 3] indicating that the constituent nucleic acid bases of DNA clearly affect the dissociation of phenolic –OH protons; gradient of the plots were however different for the two compounds, which is also expected. Since the second dissociation of alizarin,<sup>28</sup> second and third dissociations of purpurin<sup>34</sup> occur well beyond the physiological pH they are not included in the discussion. The second and third dissociation of purpurin occur almost together<sup>20</sup>; Figure 4 is a plot of  $pK_{a2}$  of purpurin with increased concentrations of calf thymus DNA.

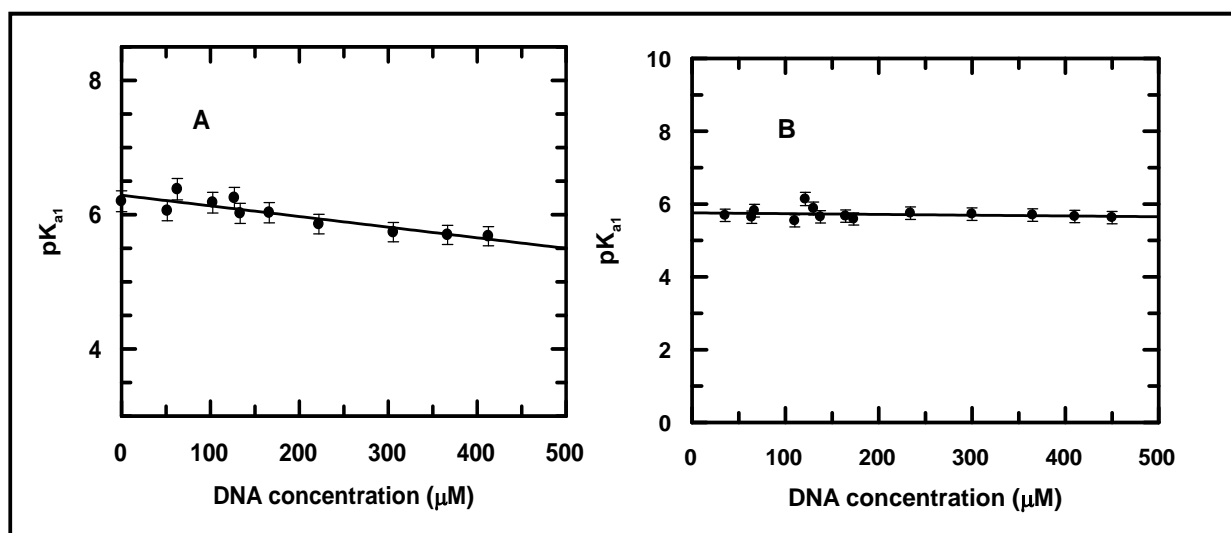


**Fig. 3:** A plot of  $pK_{a1}$  of (A) alizarin and (B) purpurin against increasing concentrations of calf thymus DNA. [Alizarin] = [Purpurin] = 100  $\mu\text{M}$ ; Temperature = 298 K.

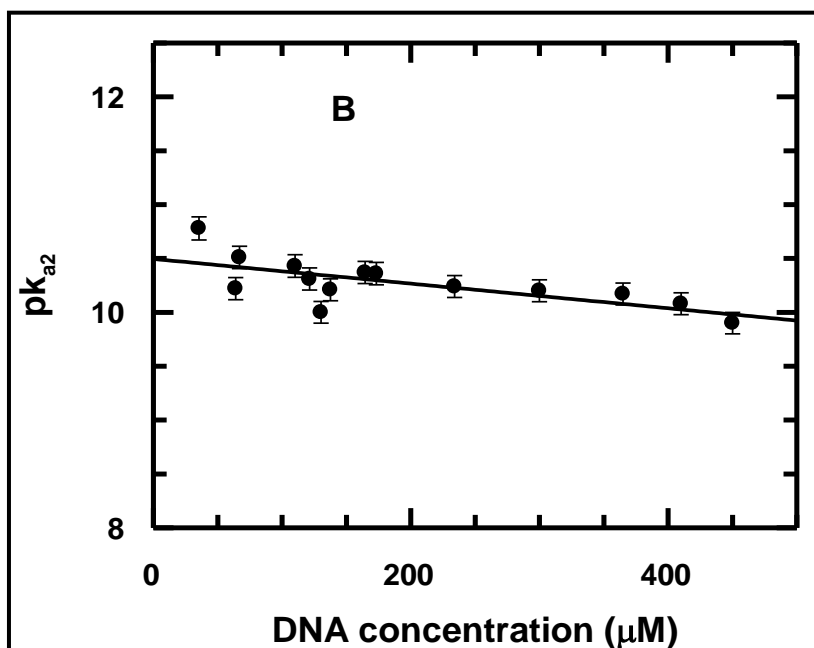


**Fig. 4:** Plot of pK<sub>a2</sub> of purpurin against increasing concentrations of calf thymus DNA.

[Purpurin] = 100 μM; Temperature = 298 K.

Interaction of purpurin with calf thymus DNA with regard to the evaluation of the contribution of its neutral and anionic forms to the evaluated overall binding constant determined earlier under physiological conditions was revisited.<sup>20</sup> For alizarin, interaction with calf thymus DNA was carried out with an emphasis on the contributions of its two forms. Contributions of neutral and anionic forms of compounds towards overall binding constant values with calf thymus DNA were determined by considering pK<sub>a1</sub> once evaluated in normal aqueous solution and again in the presence of a definite concentration of calf thymus DNA. For both compounds, pK<sub>a1</sub> used in the calculations and determined in presence of calf thymus DNA were chosen from Figures 3A and 3B respectively (from best fit lines) by selecting a value intermediate between the lowest and highest concentrations of calf thymus DNA used in the plots. Values chosen for pK<sub>a1</sub> were 5.94 for alizarin and 5.71 for

purpurin. The corresponding values determined in normal aqueous solution were 6.2 for alizarin and 5.57 for purpurin.

Table 1 provides the overall binding constant values ( $K^*$ ) of alizarin and purpurin determined at different pH at a constant ionic strength of the medium (120 mM NaCl).  $K^*$  values of purpurin were taken from an earlier study<sup>20</sup> while that for alizarin were determined as part of the present study (Fig. 5 – Fig. 9). Considering overall binding constant values for the two compounds at different pH and using Eq.14 & 15 (*Chapter 6: Experimental*), contributions of the neutral ( $K^0$ ) and anionic ( $K^-$ ) forms of each compound to its overall binding constant with calf thymus DNA were evaluated.<sup>17,20</sup> Since at any pH of the medium, during titration with calf thymus DNA, both bound and free forms of the compounds would be present simultaneously, the overall binding constant is actually due to bound forms of both species, neutral and anionic.

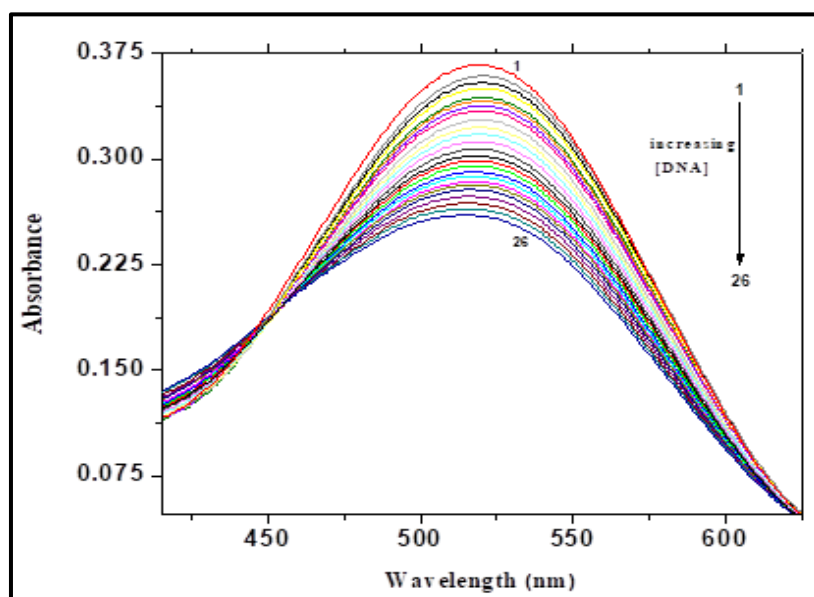


**Fig. 5:** Absorption spectra of alizarin in the absence (1) and presence of calf thymus DNA. Spectra recorded at pH 7.65 shows a gradual decrease in absorbance upon adding calf thymus DNA to an aqueous solution of alizarin. [alizarin] = 50  $\mu$ M, [NaCl] = 120 mM; [Tris buffer] = 30 mM, Temperature = 298 K.

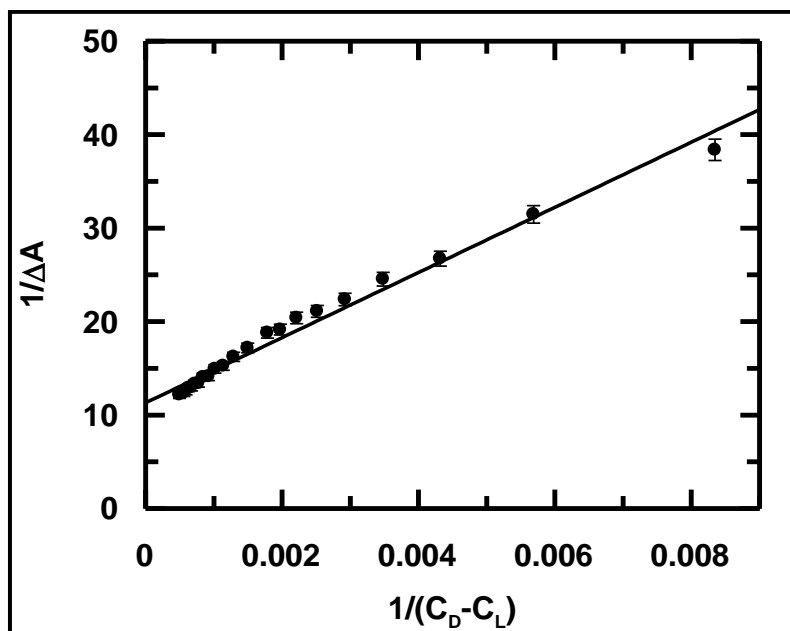


**Fig. 6:** A double reciprocal plot for the interaction of alizarin with calf thymus DNA leading to evaluation of apparent binding constant ( $K_{app}$ ) at pH 6.71 (30 mM Tris-HCl buffer) at an ionic strength 0.12 M. [alizarin] = 50  $\mu$ M; Temperature = 298 K.

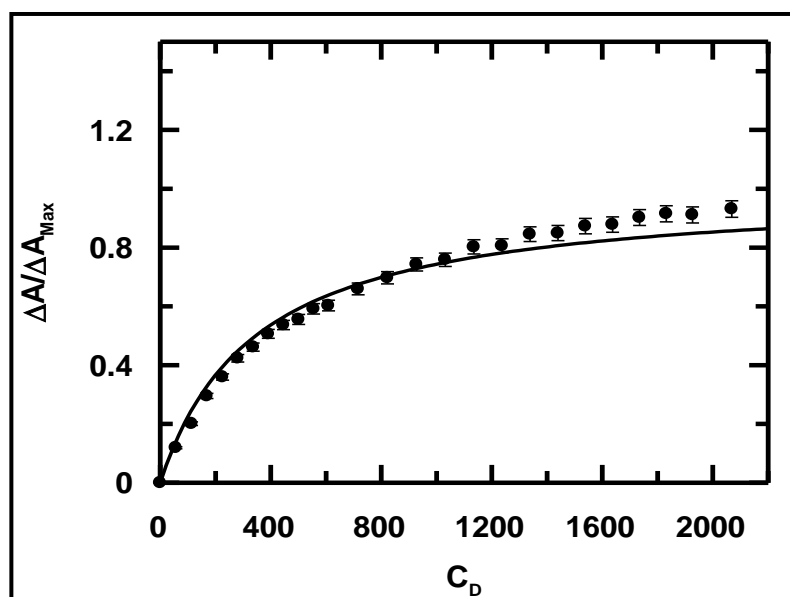


**Fig. 7:** A non-linear curve fit analysis showing plot of normalized increase in the change of absorbance against input concentration of DNA to evaluate dissociation constant for the association of alizarin with calf thymus DNA according to Eq. 12 (*Chapter 6: Experimental*). Inverse of dissociation constant ( $K_d$ ) provides apparent binding constant ( $K_{app}$ ) at pH 6.71 (30 mM Tris-HCl buffer) and ionic strength 0.12 M. [alizarin] = 50  $\mu$ M; Temperature = 298 K.

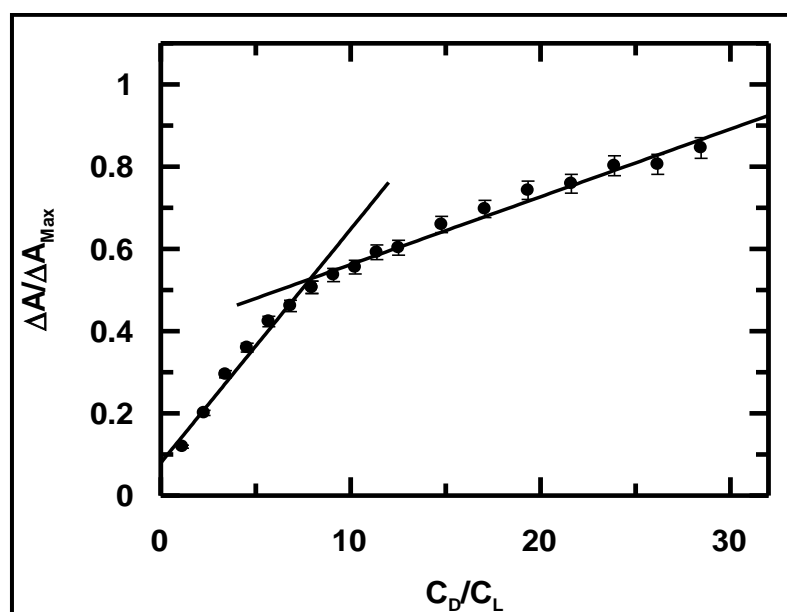


**Fig. 8:** Mole ratio plot for relative change in absorbance against ratio of concentration of DNA to that of alizarin at pH 6.71 (30 mM Tris-HCl buffer) and ionic strength 0.12 M. [alizarin] = 50  $\mu$ M; Temperature = 298 K.

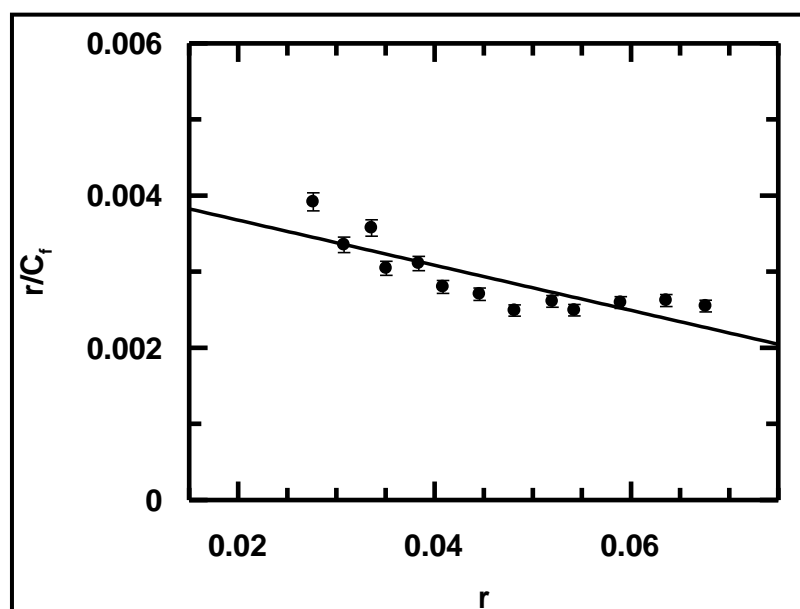


**Fig. 9:** A Scatchard plot for the interaction of alizarin with calf thymus DNA obeying Eq. 13 (Chapter 6: Experimental) at pH 6.71 (30 mM Tris-HCl buffer) and an ionic strength 0.12 M. [alizarin] = 50  $\mu$ M; Temperature = 298 K.

A plot of  $K^*(1 + 10^{pH - pK})$  versus  $10^{pH - pK}$  obeying Eq. 14 (*Chapter 6: Experimental*) considering different values of  $pK_{a1}$  for each compound (i.e., that determined in the absence and presence of calf thymus DNA) generates a straight line [Figures 10, B & D (for alizarin) and Figures 11, B & D (for purpurin)] from where  $K^-$  was determined as slope and  $K^0$  as intercept (Table 1). Overall binding constant ( $K^*$ ) was also plotted against different pH for both compounds. The data was fitted to Eq. 15 (*Chapter 6: Experimental*) [(Figures 10, A & C (for alizarin) and Figures 11, A & C (for purpurin))]. Values for binding constants of the neutral and anionic species,  $K^0$  and  $K^-$  were evaluated. Comparison of values obtained for  $K^0$  and  $K^-$  from Eq. 14 & 15 (*Chapter 6: Experimental*) for the two compounds suggest they are close to each other. What was observed as a consequence of these calculations (Table 1) is that  $K^0$ , the contribution of the neutral form to overall binding constant ( $K^*$ ) showed a good variation corresponding to a change in  $pK_{a1}$  (i.e. that determined in the absence and presence of DNA) while contribution of the anionic form ( $K^-$ ) remained practically constant. For alizarin,  $K^0$  was slightly higher when  $pK_{a1}$  was considered as 5.94 (determined in presence of calf thymus DNA) than when it was 6.2 (determined in normal aqueous solution). For purpurin, however,  $K^0$  was higher when  $pK_{a1}$  was 5.57 (determined in normal aqueous solution) than when it was 5.71 (determined in presence of calf thymus DNA).

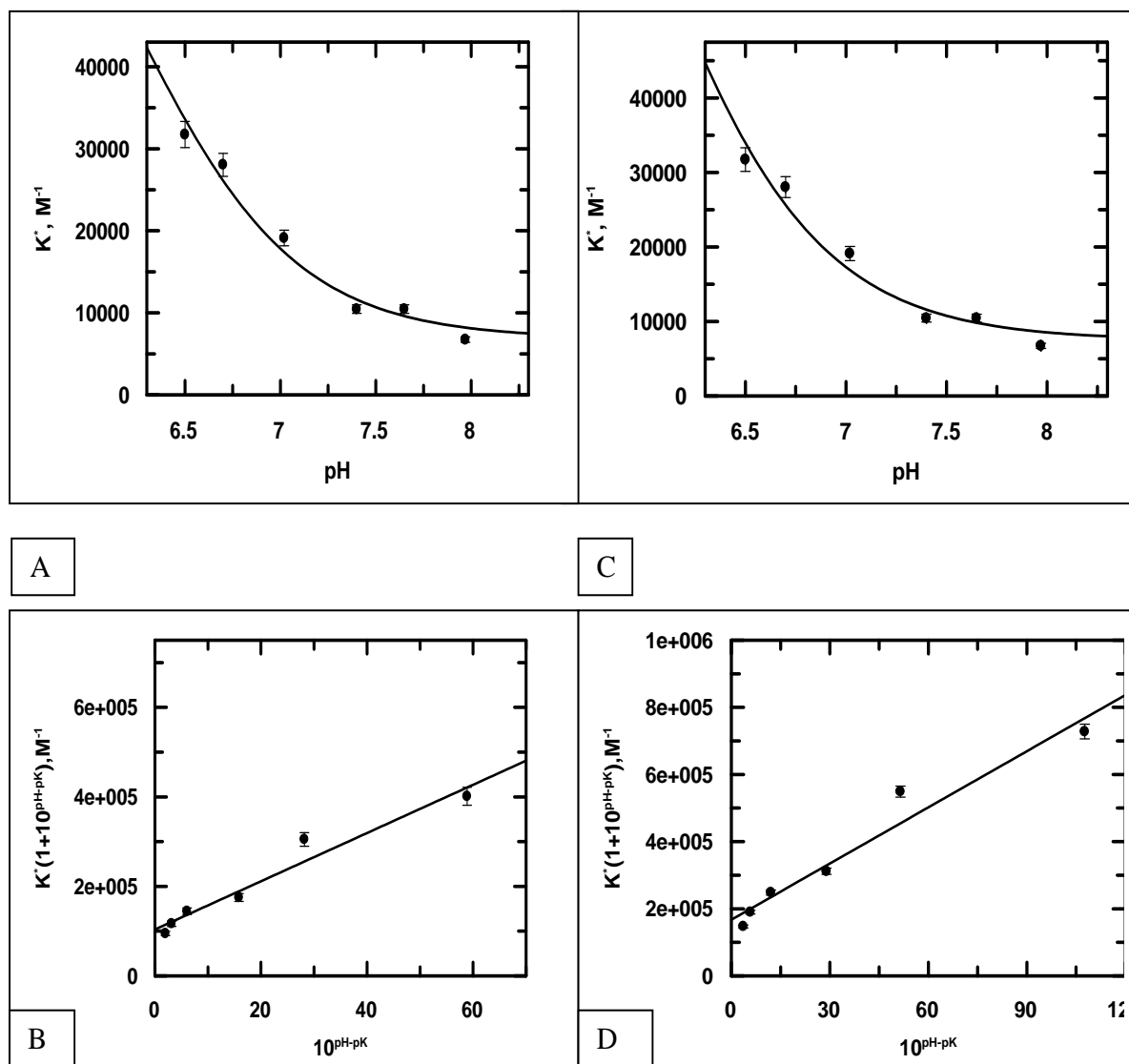


**Fig. 10:** (A) & (C) show overall binding constant ( $K^*$ ) for alizarin interacting with calf thymus DNA at different pH where the solid line is the fitted data obeying Equation 2 considering  $pK_{a1} = 6.2$  (A), determined in normal aqueous solution in absence of DNA and  $pK_{a1} = 5.94$  (C), determined in presence of calf thymus DNA. (B) and (D) are linear plots obtained by plotting  $K^*(1 + 10^{pH-pK})$  versus  $10^{pH-pK}$  where in (B)  $pK_{a1} = 6.2$  and in (D),  $pK_{a1} = 5.94$ . Each of the plots, provide  $K^0$  and  $K^-$ , i.e. binding constants of the neutral and anionic forms of alizarin from the intercept and slope respectively. [Alizarin] = 50  $\mu$ M; [NaCl] = 120 mM; [Tris buffer] = 30 mM; Temp. = 298 K.



**Table 1:** Overall binding constant values of alizarin and purpurin interacting with calf thymus DNA at different pH and contributions of the neutral ( $K^0$ ) and anionic ( $K^-$ ) forms of each compound to their respective overall binding constants.

Compound	pH	Overall binding constant with calf thymus DNA ( $K^* \times 10^{-4}$ )	$pK_{a1}$ in the absence of DNA	$pK_{a1}$ in the presence of DNA	$K^0$ from Eq. 1 ( $K^0 \times 10^{-5}$ )	$K^0$ from Eq. 2 ( $K^0 \times 10^{-5}$ )	$K^-$ from Eq. 1 ( $K^- \times 10^{-4}$ )	$K^-$ from Eq. 2 ( $K^- \times 10^{-4}$ )
Alizarin	6.50	3.17	6.2		1.04	0.87	0.54	0.69
	6.70	2.80						
	7.02	1.91						
	7.40	1.04	5.94		1.68	1.31	0.56	0.75
	7.65	1.05						
	7.97	0.67						
Purpurin	6.65	9.33	5.57		10.8	8.87	2.40	2.67
	6.88	6.45						
	7.16	4.84						
	7.40	4.51	5.71		8.0	6.68	2.39	2.65
	7.88	2.95						
	8.35	2.56						

It appears therefore that for alizarin the contribution coming from the neutral form was greater when  $pK_{a1}$  used was determined in the presence of calf thymus DNA while it was reverse in case of purpurin; the value of  $K^-$  remained more or less the same, not showing much variation corresponding to a change in the value of  $pK_{a1}$ .

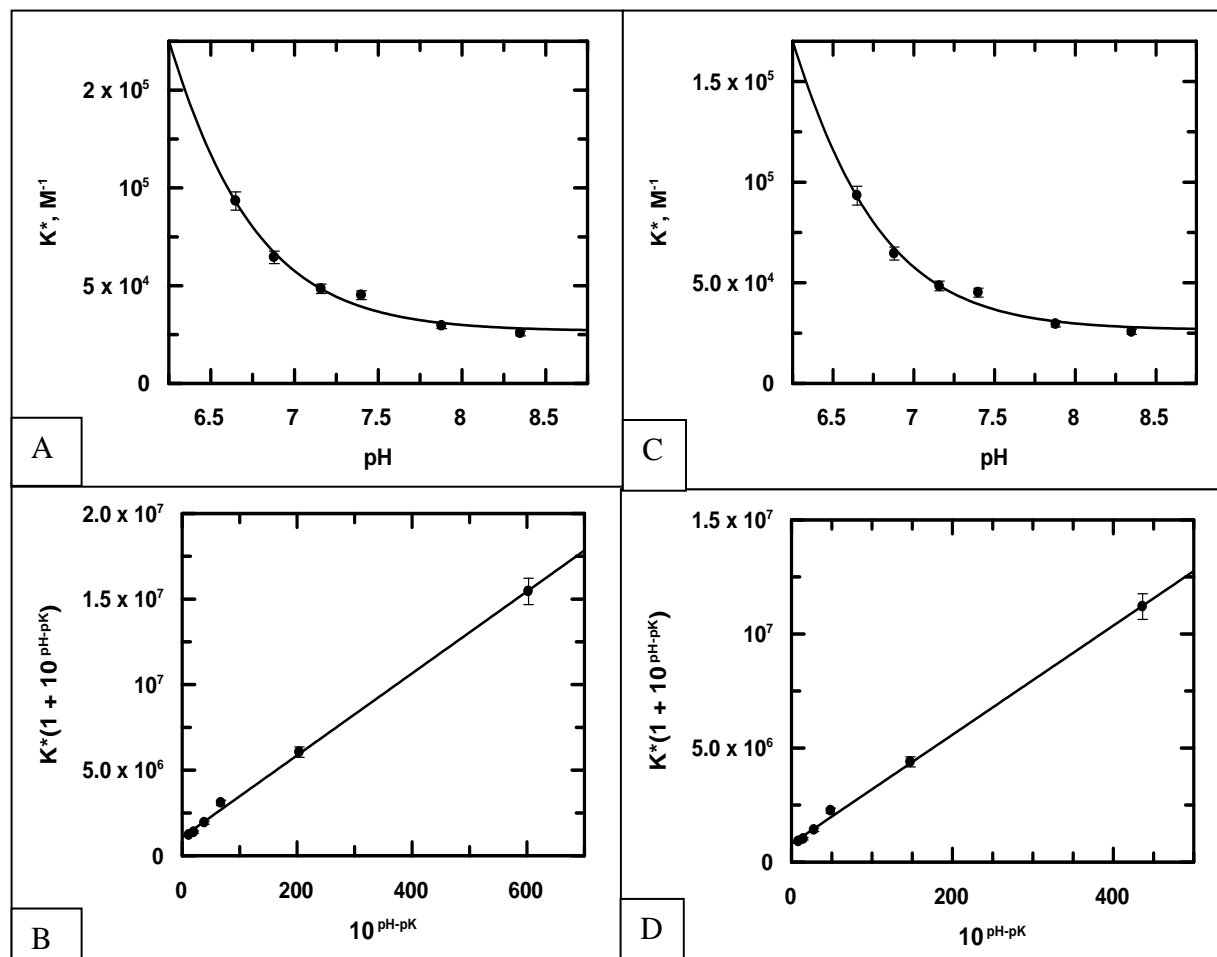


**Fig. 11:** (A) & (C) shows overall binding constant ( $K^*$ ) for purpurin interacting with calf thymus DNA at different pH where the solid line is the fitted data obeying Eq. 15 (*Chapter 6: Experimental*) considering  $pK_{a1} = 5.57$  (A), determined in normal aqueous solution in the absence of calf thymus DNA and  $pK_{a1} = 5.71$  (C), determined in presence of calf thymus DNA. (B) and (D) are linear plots obtained by plotting  $K^*(1 + 10^{pH-pK})$  versus  $10^{pH-pK}$  where in (B)  $pK_{a1} = 5.57$  and in (D)  $pK_{a1} = 5.71$ . They provide  $K^0$  and  $K^-$ , binding constants of the neutral and anionic forms of purpurin from the intercept and slope respectively. [Purpurin] =  $75\mu M$ ; [NaCl] = 120 mM; [Tris buffer] = 30 mM; Temp. = 298 K.

Results clearly indicate that both for alizarin and purpurin, dissociation of phenolic –OH is influenced by nucleic acid bases present in DNA. Therefore, for such molecules that exist in two distinctly different forms at physiological pH, in order to correctly determine their contributions to the overall binding constant ( $K^*$ ) of the compound interacting with DNA, it is absolutely essential that correct pKa values are used. A direct benefit of such a study is that from a knowledge of  $K^0$  and  $K^-$  it becomes possible to evaluate the overall binding constant of the molecule interacting with the same DNA at any pH without having to perform an experiment with the compound at that pH.

Since DNA titrations would form a substantial part of the intended study and would be required to explain the performance of chosen hydroxy-9,10-anthraquinones and their metal complexes on cancer and normal cell lines, a proper analysis using correct physico-chemical parameters like pKa etc., to know contributions of each form is essential. Correct and proper determination of pKa ensures a correct evaluation of the contribution of each form to overall binding constant of a compound at any pH or ionic strength of the medium. The study revealed contributions of different forms of alizarin and purpurin to overall binding constant are actually different when pKa are different. Hence, whenever molecules interact with DNA and are present in more than one form in solution, for a correct analysis of DNA interaction, correct values of pKa becomes crucial. This study also revealed that binding of purpurin to calf thymus DNA was higher than alizarin when the only difference between the two compounds is an –OH group, indicating role of –OH groups present in hydroxy-9,10-anthraquinones or in anthracyclines.

**3. References:**

- [1] G. Y. Park, J. J. Wilson, Y. Song, S. J. Lippard. 2012. Phenanthriplatin, a monofunctional DNA-binding platinum anticancer drug candidate with unusual potency and cellular activity profile. *PNAS*. 109: 11987-11992.
- [2] K. Cheung-Ong, G. Giaever, C. Nislow. 2013. DNA-damaging agents in cancer chemotherapy: serendipity and chemical biology. *Chemistry & Biology*. 20: 648-659.
- [3] S. S. David, E. Meggers. 2008. Inorganic chemical biology: from small metal complexes in biological systems to metalloproteins *Curr. Opin. Chem. Biol.* 12: 194-196.
- [4] A. Abibi, E. Protozanova, V. V. Demidov, M. D. Frank-Kamenetskii. 2004. Specific versus nonspecific binding of cationic PNAs to duplex DNA. *Biophys J*. 86: 3070-3078.
- [5] L. J. Boerner, J. M. Zaleski. 2005 Metal complex-DNA interactions: from transcription inhibition to photoactivated cleavage. *Curr. Opin. Chem. Biol.* 9: 135-144
- [6] T. Fessl, F. Adamec, T. Polívka, S. Foldynová-Trantírková, F. Vácha and L. Trantírek. 2012. Towards characterization of DNA structure under physiological conditions in vivo at the single-molecule level using single-pair FRET. *Nucleic Acids Res.* 40: e121.
- [7] K. R. Fox, M. J. Waring. 1984. Investigations into the sequence-selective binding of mithramycin and related ligands to DNA. *Eur. J. Biochem.* 145:579-586.
- [8] R. L. Jones, W. D. Wilson. 1981. Effect of ionic strength on the pKa of ligands bound to DNA. *Biopolymers*. 20: 141-154.
- [9] F. Barragán, P. López-Senín, L. Salassa, S. Betanzos-Lara, A. Habtemariam, V. Moreno, P. J. Sadler, V. Marchán. 2011. Photocontrolled DNA binding of a receptor-targeted organometallic ruthenium(II) complex. *J. Am. Chem. Soc.* 133: 14098-14108.

- [10] A. Paul, S. Bhattacharya. 2012. Chemistry and biology of DNA-binding small molecules. *Current Science*, 102: 212-231.
- [11] R. E. H. R. Drew, B. N. Conner, M. Wing, A. V. Fratini, M. L. Kopka. 1982. The anatomy of A-, B-, and Z-DNA. *Science*. 216, 475-485.
- [12] C. D. Mol, T. Izumi, S. Mitra, J. A. Tainer. 2000. DNA-bound structures and mutants reveal a basic DNA binding by APE1 DNA repair and coordination. *Nature*. 403: 451-456.
- [13] A. D. Miroshnikova, A. A., Kuznetsova, N. A. Kuznetsov, O. S. Fedorova. 2016. Thermodynamics of damaged DNA binding and catalysis by human AP endonuclease 1 *Acta Naturae*. 8: 103-110.
- [14] W. Engelen, B. M. G. Janssen, M. Merckx. 2016. DNA-based control of protein activity. *Chem. Commun.* 52: 3598-3610.
- [15] M. Egli 2002. DNA-Cation Interactions: Quo Vadis? *Chemistry & Biology*. 9: 277-286
- [16] B. J. Pages, D. L. Ang, E. P. Wright, J. R. Aldrich-Wright. 2015. Metal complex interactions with DNA. *Dalton Trans.* 44: 3505-3526.
- [17] F. Frezard, A. Garnier-Suillerot. 1990. Comparison of the binding of anthracycline derivatives to purified DNA and to cell nuclei. *Biochimica et Biophysica Acta*. 1036: 121-127.
- [18] R. Comanici, B. Gabel, T. Gustavsson, D. Markovitsi, C. Cornaggia, S. Pommeret, C. Rusu, C. Kryschi. 2006. Femtosecond spectroscopic study of carminic acid–DNA interactions. *ChemicalPhysics*. 325: 509-518.
- [19] S. Mukherjee, P. Das, S. Das. 2012. Exploration of small hydroxy-9,10-anthraquinones as anthracycline analogues: physicochemical characteristics and DNA binding for comparison. *J.Phy.Org. Chem.* 25: 385-393.

- [20] P. Das, C. K. Jain, S. K. Dey, R. Saha, A. D. Chowdhury, S. Roychoudhury, S. Kumar, H. K. Majumder, S. Das. 2014. Synthesis, crystal structure, DNA interaction and *in vitro* anticancer activity of a Cu(II) complex of purpurin: dual poison for human DNA topoisomerase I and II. *RSC Adv.* 4: 59344-59357.
- [21] S. Mukherjee, P. K. Gopal, S. Paul, S. Das. 2014. Acetylation of 1,2,5,8-tetrahydroxy-9,10-anthraquinone improves binding to DNA and shows enhanced superoxide formation that explains better cytotoxicity on JURKAT T lymphocyte cells. *J. Anal. Oncol.* 3: 122-129.
- [22] P. Das, C. K. Jain, S. Roychoudhury, H. K. Majumder, S. Das. 2016. Design, synthesis and *in vitro* anticancer activity of a Cu(II) complex of carminic acid: A novel small molecule inhibitor of human DNA topoisomerase I and topoisomerase II. *ChemistrySelect.* 1:6623-6631.
- [23] A. B. Pradhan, L. Haque, S. Bhuiya, A. Ganguly, S. Das. 2015. Deciphering the positional influence of the hydroxyl group in the cinnamoyl part of 3-hydroxy flavonoids for structural modification and their interaction with the protonated and B form of calf thymus DNA using spectroscopic and molecular modeling studies. *J. Phys. Chem. B.* 119: 6916-6929.
- [24] B. Mandal, S. Singha, S. K. Dey, S. Mazumdar, T. K. Mondal, P. Karmakar, S. Kumar, S. Das. 2016. Synthesis, crystal structure from PXRD of a Mn<sup>II</sup>(purp)<sub>2</sub> complex, interaction with DNA at different temperatures and pH and lack of stimulated ROS formation by the complex. *RSC Adv.* 6:51520-51532.
- [25] B. Mandal, S. Singha, S. K. Dey, S. Mazumdar, S. Kumar, P. Karmakar, S. Das. 2017. Cu<sup>II</sup> complex of emodin with improved anticancer activity as demonstrated by its performance on HeLa and Hep G2 cells. *RSC Adv.* 7: 41403-41418

- [26] L. Di, E. H. Kerns. 2005. Application of pharmaceutical profiling assays for optimization of drug-like properties. *Curr. Opin. Drug. Discov. Devel.*, 8: 495-504.
- [27] L. Di, E. H. Kerns. 2003. Profiling drug-like properties in discovery research. *Curr. Opin. Chem. Biol.* 7: 402-408.
- [28] S. Das, A. Saha, P. C. Mandal. 1996. Studies on the formation of Cu(II) and Ni(II) complexes of 1,2-dihydroxy-9,10-anthraquinone and lack of stimulated superoxide formation by the complexes. *Talanta.* 43: 95-102.
- [29] I. T. Suydam, S. D. Levandoski, S. A. Strobel. 2010. Catalytic importance of a protonated adenosine in the hairpin ribozyme active site. *Biochemistry.* 49: 3723–3732.
- [30] S. Das, G. S. Kuma, M. Maiti. 1999. Conversions of the left- handed form and the protonated form of DNA back to the bound right-handed form by sanguinarine and ethidium: A comparative study. *Biophys. Chem.* 76: 199–218.
- [31] J. Markovits, C. Garbay-Jaureguiberry, B. P. Roques, J. B. Le Pecq. 1989. Acridine dimers: influence of the intercalating ring and of the linking-chain nature on the equilibrium and kinetic DNA-binding parameters. *Eur. J. Biochem.* 180: 359-366.
- [32] P. Das, D. Bhattacharya, P. Karmakar, S. Das. 2015. Influence of ionic strength on the interaction of THA and its Cu(II) complex with DNA helps to explain studies on various breast cancer cells. *RSCAdv.* 5: 73099-73111.
- [33] G. Dodin, M-A.Schwaller, J. Aubard, C. Paoletti. 1988. Binding of ellipticine base and ellipticinium cation to calf-thymus DNA. *Eur. J. Biochem.* 176: 371-376.
- [34] P. Das, P. S. Guin, P. C. Mandal, M. Paul, S. Paul, S. Das. 2011. Cyclic voltammetric studies of 1, 2, 4-trihydroxy-9,10-anthraquinone, its interaction with calf thymus DNA and anti-leukemic activity on MOLT-4 cell lines: a comparison with anthracycline anticancer drugs. *J. Phy.Org. Chem.* 24: 774-785.





# CHAPTER 8

**Characterization of a Mn(II) complex of alizarin suggests attributes, that explain superior anticancer activity: A comparison with anthracycline antibiotics**



## **1. Introduction**

Hydroxy-9,10-anthraquinones, simpler analogues of anthracycline anticancer agents are at a disadvantage in terms of efficacy when compared with anthracyclines for a number of reasons.<sup>1-8</sup> Complex formation of hydroxy-9,10-anthraquinones is advantageous as it leads to decreased semiquinone formation, expected to decrease cardiotoxic side effects due to lesser superoxide formation;<sup>9-15</sup> simultaneously there is also the possibility of a compromise in cytotoxic action.<sup>1,5,8</sup> However, complexes have other attributes that make up loss in efficacy in the free radical pathway.<sup>1,5-8</sup> The mechanism of anticancer activity due to anthracyclines or hydroxy-9,10-anthraquinones and their metal complexes is different.<sup>1,5-10,16-21</sup> The complete mechanism of anthracycline functioning is still under investigation.<sup>1-10,14,15,20,21</sup> To probe into the fact, why a metal complex is often better than the parent anthracycline or a hydroxy-9,10-anthraquinone, a Mn<sup>II</sup> complex of 1,2-dihydroxy-9,10-anthraquinone (alizarin) was prepared and characterized. Mn<sup>II</sup> was chosen for its bio-friendly nature; but lacks a stable lower oxidation state like Cu<sup>II</sup> or Fe<sup>III</sup>.<sup>22-29</sup> Therefore, it is expected findings with a Mn<sup>II</sup> complex of a hydroxy-9,10-anthraquinone could be different from Cu<sup>II</sup> or Fe<sup>III</sup> complexes of similar ligands.<sup>1,3,5-8,16-19</sup>

Some of the major pathways by which anthracyclines or hydroxy-9,10-anthraquinones inflict damage to cells is either by the generation of semiquinone radical anion/quinone-dianion or through biophysical interaction with DNA or through inhibition of topoisomerase that affect processes like DNA replication and transcription.<sup>1-8,14,15,20,21,30-36,37</sup> Some of these pathways were investigated separately for alizarin and its Mn<sup>II</sup> complex to identify areas of resemblance or difference with established anthracyclines to realize modifications that might be required to bridge the gap in biological activity between the simpler analogues and anthracyclines that are already in use.<sup>1-8,12,16,30-36,37</sup>

## 2. Results and Discussion:

### 2.1. Determination of stoichiometry of interaction between Mn<sup>II</sup> and alizarin by mole ratio and Job's method of continuous variation

Composition of the complex in solution was determined by mixing different volumes of equimolar Mn<sup>II</sup> and alizarin. In the mole ratio method, alizarin was kept constant while Mn<sup>II</sup> was varied. Absorbance at 525 nm was plotted against  $(T_M/T_L)T_L$  (Fig. 1A);  $T_M$  and  $T_L$  being the concentrations of Mn<sup>II</sup> and alizarin respectively. Two lines were obtained, intersection of which indicates the ratio in which alizarin binds to Mn<sup>II</sup> in the complex. In Job's method of continuous variation (Fig. 1B), complementary mixtures were prepared. Absorbance was recorded at 525 nm. This was plotted against either the volume of alizarin or Mn<sup>II</sup>. Stoichiometry of Mn<sup>II</sup> to alizarin was found to be 1:2.

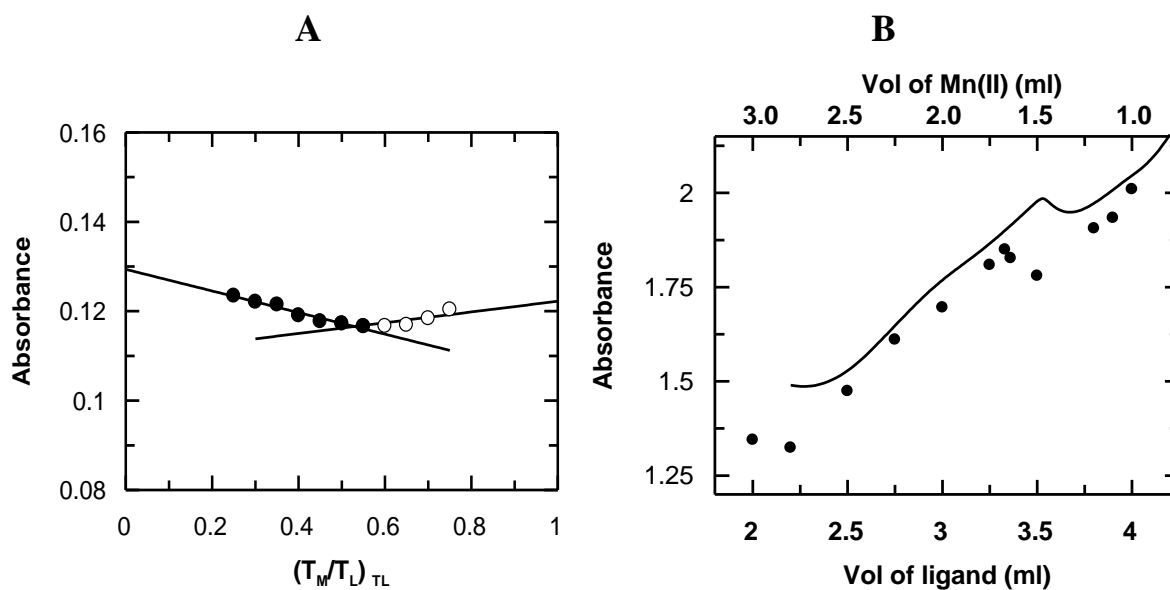


**Fig. 1:** Plots showing variation in absorbance at 525 nm for (A) a change in the ratio of [alz] to [Mn<sup>II</sup>] for a fixed concentration of alz (= 20  $\mu$ M) and (B) a continuous variation of [DHA] and [Mn<sup>II</sup>] at physiological pH (~7.4). In case of (B), the strength of the stock solutions of Mn<sup>II</sup> and DHA were 1000  $\mu$ M; [NaNO<sub>3</sub>] = 0.01 M, Temperature = 298 K.

## 2.2 Determination of $pK_a$ of alizarin at different ionic strengths of the medium:

Alizarin was titrated in solution at different ionic strengths. Figures 2A & 2B are plots that show a variation in absorbance with pH at different ionic strengths (0.12 M and 0.15 M) of the medium. Fitting the *experimental* data according to Eq. 3a (Chapter 6: Experimental),  $pK_{a1}$  and  $pK_{a2}$  were obtained.

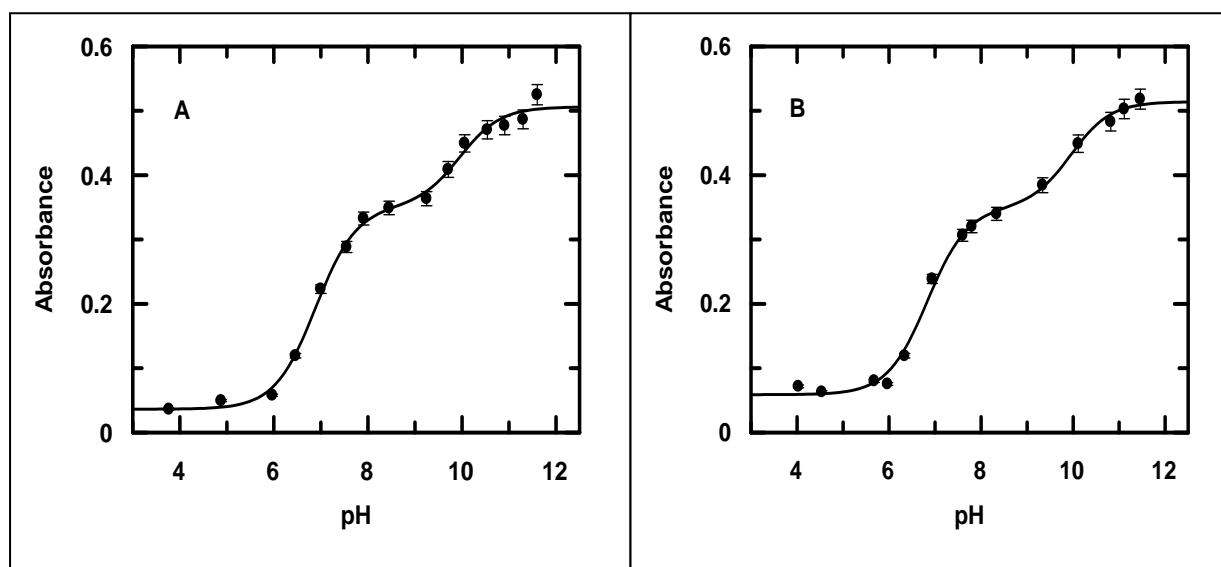


**Fig 2:** pH-metric titration of alizarin shown by a variation in absorbance at 530 nm at ionic strengths of (A) 0.12 M and (B) 0.15 M.

As the ionic strength of the medium increased, both  $pK_{a1}$  and  $pK_{a2}$  increased, showing that increase in ionic strength affects dissociation of OH groups.<sup>3</sup>  $pK_{a1}$  and  $pK_{a2}$  were separately plotted against the ionic strength of the medium (Fig. 3). For the same change in ionic strength, slope of the line obtained by plotting  $pK_{a1}$  was slightly steeper than  $pK_{a2}$ . Therefore, increase in ionic strength affects the first dissociation to a slightly greater extent than the second. Hence, from trends in  $pK_a$  values, it was realized dissociation of phenolic-OH decreased which is significant since dissociation of the first proton of alizarin generates anionic species at physiological pH that adversely affect its binding with DNA.<sup>1,3,8,38</sup>

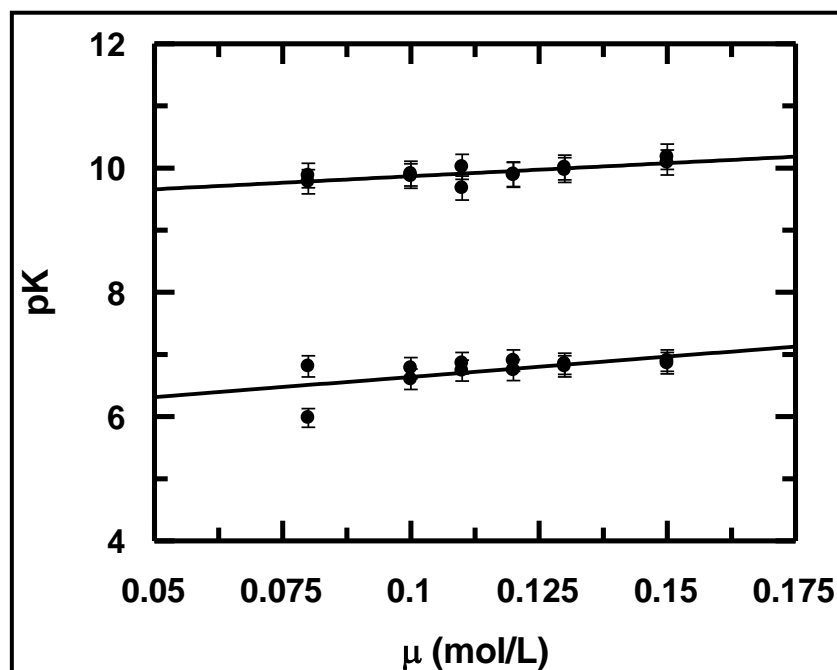


**Fig. 3:** Linear dependence of  $pK_a$  of alizarin with variation in ionic strength of the medium at 301 K; [alizarin] = 70  $\mu$ M; best fit lines were obtained using data points from two different sets of experiments. The line above shows variation of  $pK_{a2}$  while that below is for  $pK_{a1}$ .

### 2.3 Proton dissociation on Alizarin in presence of $Mn^{II}$ :

Alizarin and  $Mn^{II}$  were mixed in the ratio reported above. A spectrophotometric titration was performed in the pH range 3.0 to 11.0 (Fig. 4). The peak at 430 nm over the pH range 3.45 to 6.04 got shifted slightly to the right as pH increased to  $\sim$  6.84 showing an absorbance at 475 nm. A weak shoulder (not a peak) was seen which upon further increase in pH ( $\sim$ 7.33) developed into a peak at 530 nm that kept increasing in intensity as pH increased. This change suggests the formation of a new species which was followed at 534 nm (Fig. 5).

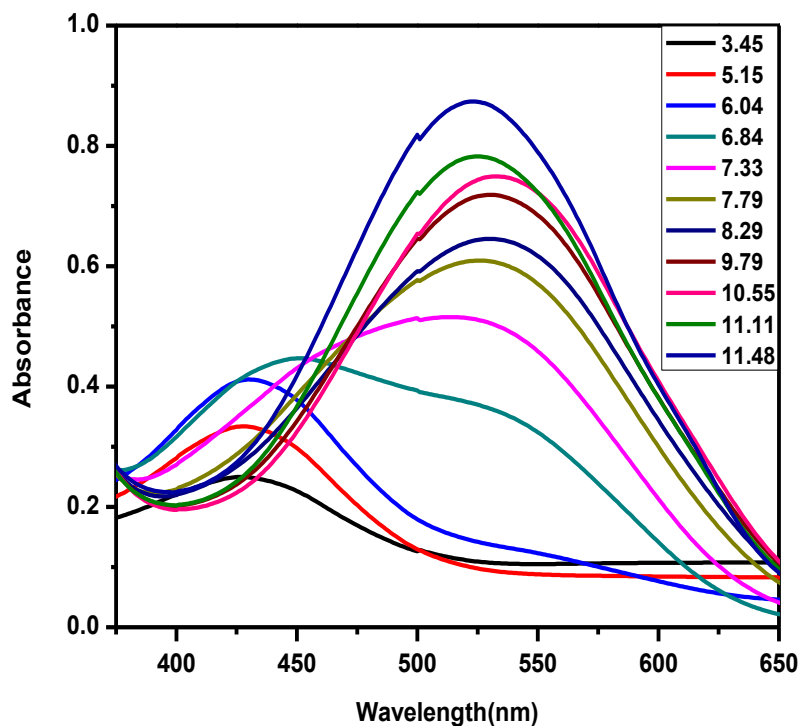


**Fig. 4:** Absorption spectra of Alizarin in presence of Mn<sup>II</sup> at different pH indicated with the help of different colors (pH mentioned alongside) in the inset of the plot. [Alizarin] = 200  $\mu$ M; [Mn<sup>II</sup>] = 100  $\mu$ M; [NaNO<sub>3</sub>] = 0.01 ; Temp. = 300 K.

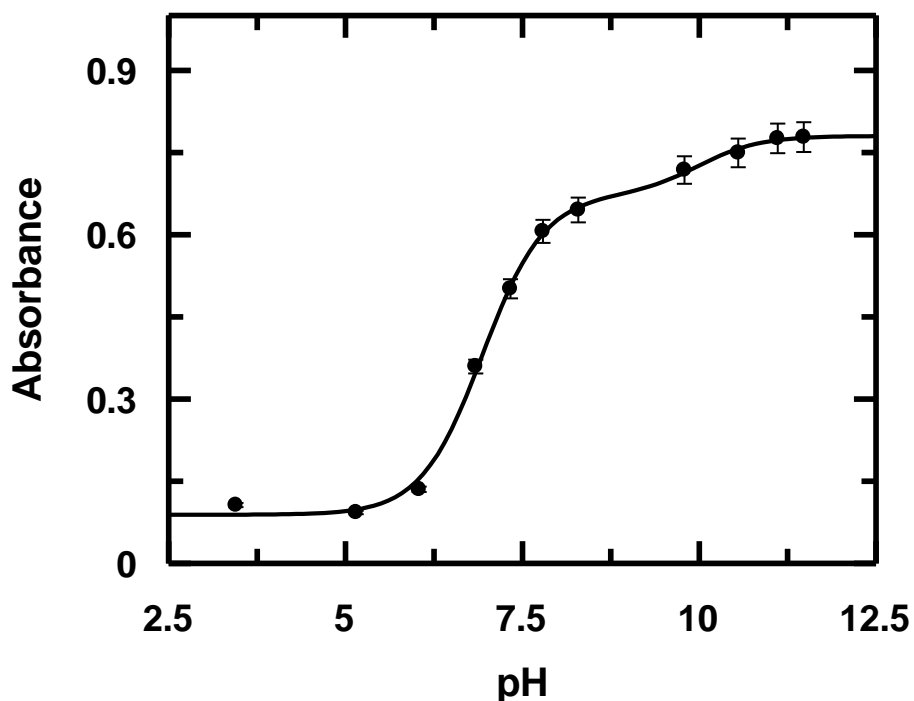


**Fig. 5:** Spectrophotometric titration of Alizarin in the presence of Mn<sup>II</sup> shown by a variation in absorbance at 534 nm; [Alizarin] = 200  $\mu$ M, [Mn<sup>II</sup>] = 100  $\mu$ M, [NaNO<sub>3</sub>] = 0.01 M, T=301K.

Using Eq. 3a (*Chapter 6: Experimental*),  $pK_{a1}$  and  $pK_{a2}$  of alizarin in presence of  $Mn^{II}$  were  $6.93 \pm 0.04$  and  $9.99 \pm 0.27$  respectively. Stability constants  $\beta^*$  and  $\beta$  were determined using Eqs. 4 – 8 (*Chapter 6: Experimental*).<sup>11,12</sup>  $\beta$  was found to be  $2.5 \times 10^{14}$  ( $\log \beta = 14.4$ ).

## **2.4 Characterization of the Mn(II) complex of alizarin:**

### **2.4.1 Comparison of the UV-Vis spectra of alizarin and its Mn(II) complex:**

Owing to poor solubility of the complex in water, its spectrum was recorded in aqueous-DMSO (Fig. 6). The recorded  $\lambda_{max}$  at 521 nm was close to the wavelength (525 nm) at which various physicochemical experiments for  $Mn^{II}$  and alizarin were performed to determine stoichiometry of complex formation (Fig. 1) indicating that the complex that was prepared was the same as that identified through physicochemical experiments.

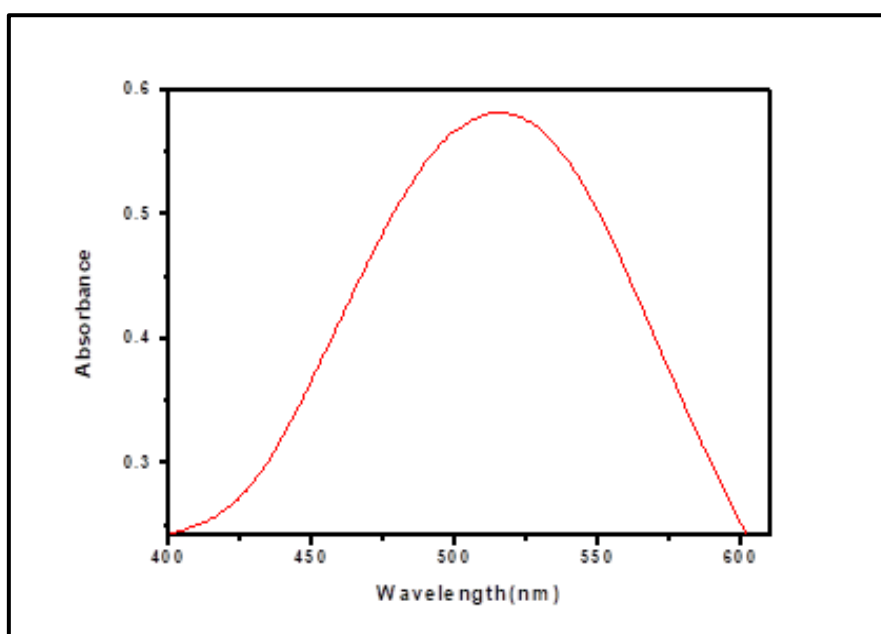


**Fig. 6:** UV-Vis spectrum of  $Mn^{II}(alz)_2$  recorded in aqueous-DMSO solution

### **2.4.2. IR of alizarin and its Mn(II) complex:**

IR spectrum of pure alizarin indicates a band at  $3375\text{ cm}^{-1}$  attributed to strong intra-molecular hydrogen bonding between the carbonyl at  $C_9$  and OH at  $C_1$  (Fig. 7).<sup>39</sup> Sharp bands at 1198



$\text{cm}^{-1}$  and  $1293 \text{ cm}^{-1}$  were due to O-H deformation and C-O stretching combinations due to phenolic -OH. The peak at  $1664 \text{ cm}^{-1}$  is characteristic of carbonyl stretching in quinones when both carbonyls are present in the same ring (Fig. 7).<sup>39</sup> In case of the complex, the band at  $3375 \text{ cm}^{-1}$  flattened due to absence of any interaction between phenolic-OH at  $\text{C}_1$  with the carbonyl at  $\text{C}_9$  (Fig. 8).<sup>39</sup> Appearance of a peak at  $\sim 469 \text{ cm}^{-1}$  indicates formation of an Mn-O bond.

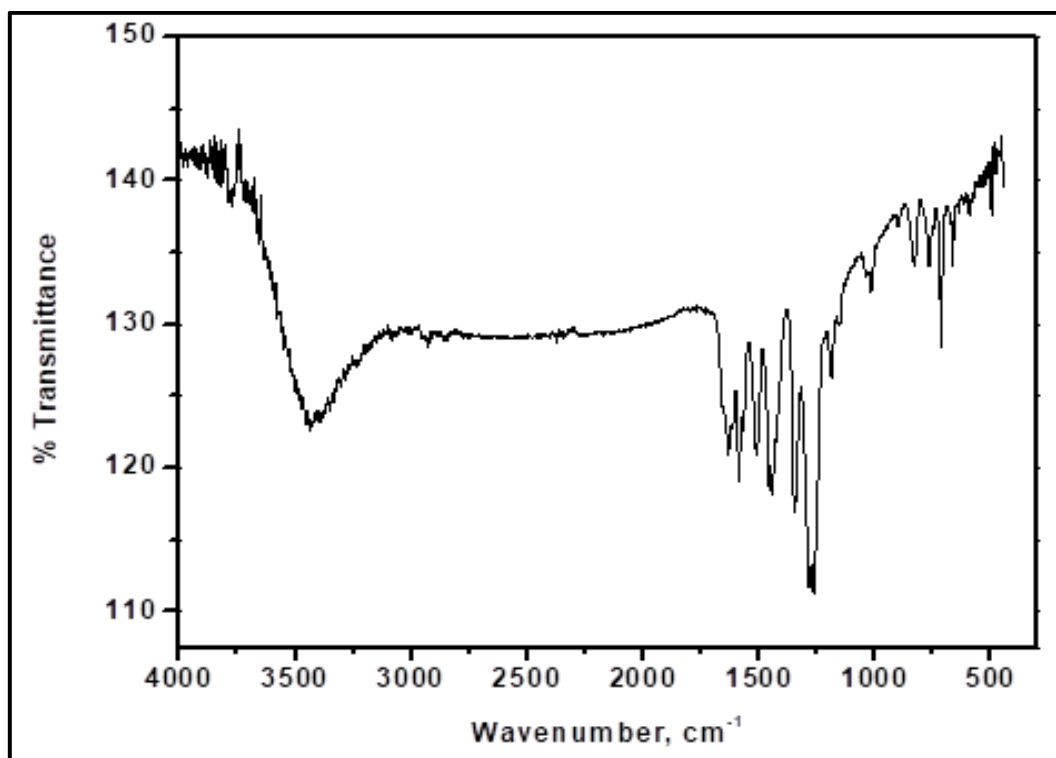


**Fig. 7:** IR spectrum of alizarin

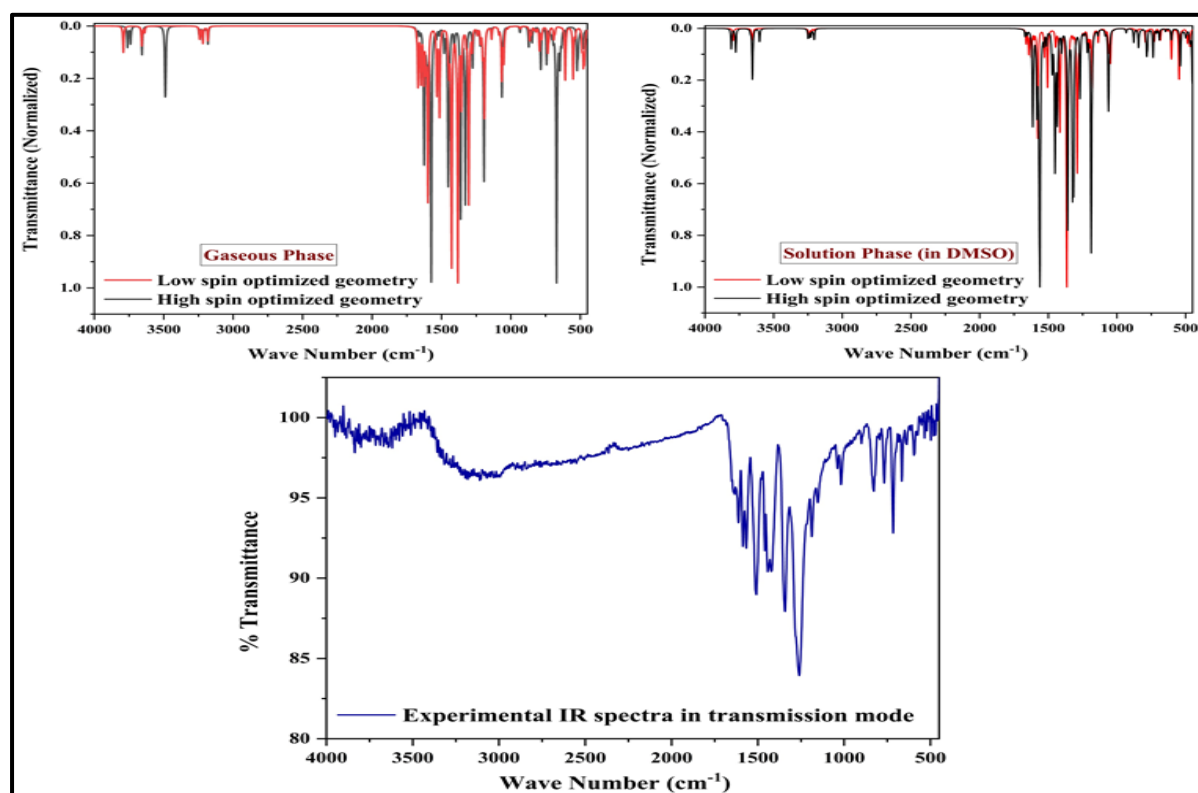


**Fig. 8:** Calculated IR spectra for different optimized geometries of the complex and also that of the experimentally obtained FT-IR spectrum for comparison.

### 2.4.3 CHN analysis:

Calculated percentage for  $C_{28}H_{14}O_8Mn \cdot 2H_2O$ : C, 59.05; H, 3.16.

Experimentally Found: C, 59.12; H, 3.05.

### 2.4.4 Analysis of the mass spectrum of the complex:

Mass spectrum was recorded in ESI+ mode (Fig. 9). The molecular ion peak expected at  $m/z = 569.42$  was detected as a cluster of peaks with  $m/z$  values 569.86, 570.86, 571.18 that match with two molecules of water bound to the fifth and sixth coordination sites of  $Mn^{II}$ . Therefore, considering the fact that the complex has two alizarin and two water molecules coordinated to  $Mn^{II}$ , peaks in the mass spectrum may be explained. Peaks having  $m/z$  values 317.08, 318.09, 319.08 indicate  $Mn^{II}$  bound to an alizarin molecule and an atom of sodium.

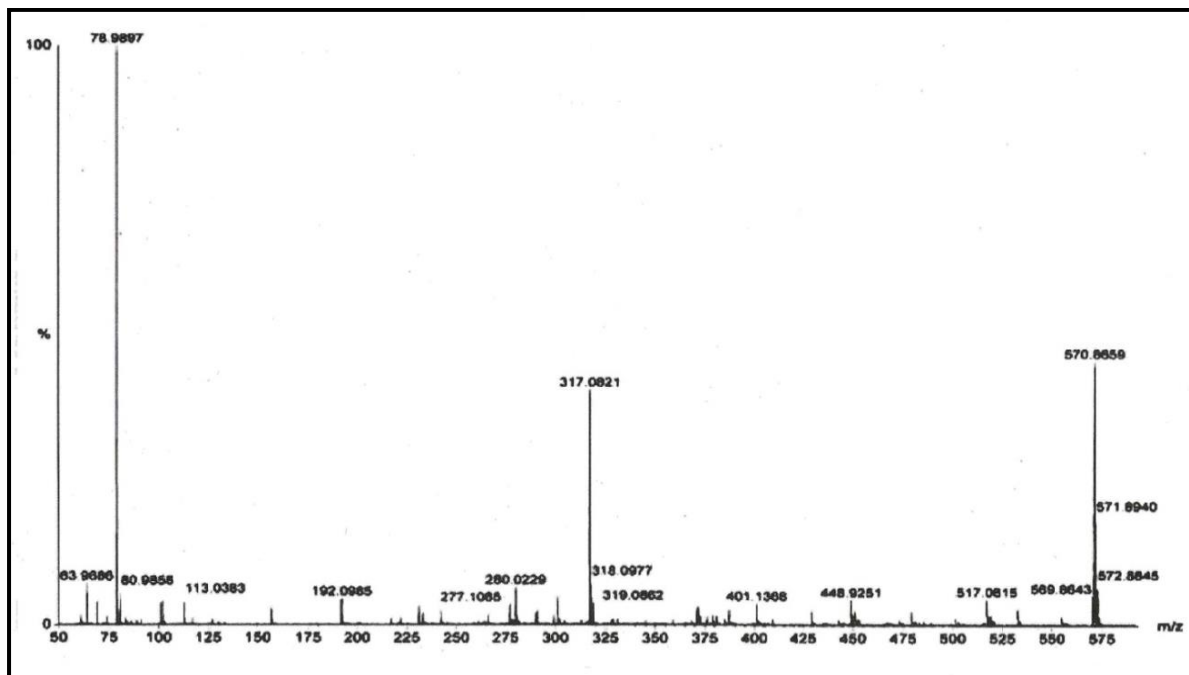


Fig. 9: Mass spectrum of  $\text{Mn}^{\text{II}}(\text{alz})_2$

#### 2.4.5. Magnetic moment of $\text{Mn}^{\text{II}}(\text{alz})_2$ :

Magnetic susceptibility was measured by the Gouy method and  $\mu_{\text{eff}}$  was found to be 5.81 BM suggesting the presence of five unpaired electrons.

#### 2.4.6. TGA of the complex:

Thermo-gravimetric analysis of the complex (Fig. 10) shows at 102°C there is an evidence for the loss of two molecules of water. Hence, there is evidence for the formation of a 1:2  $\text{Mn}^{\text{II}}$ : alizarin species having octahedral geometry where the fifth and sixth coordination sites are occupied by water molecules.

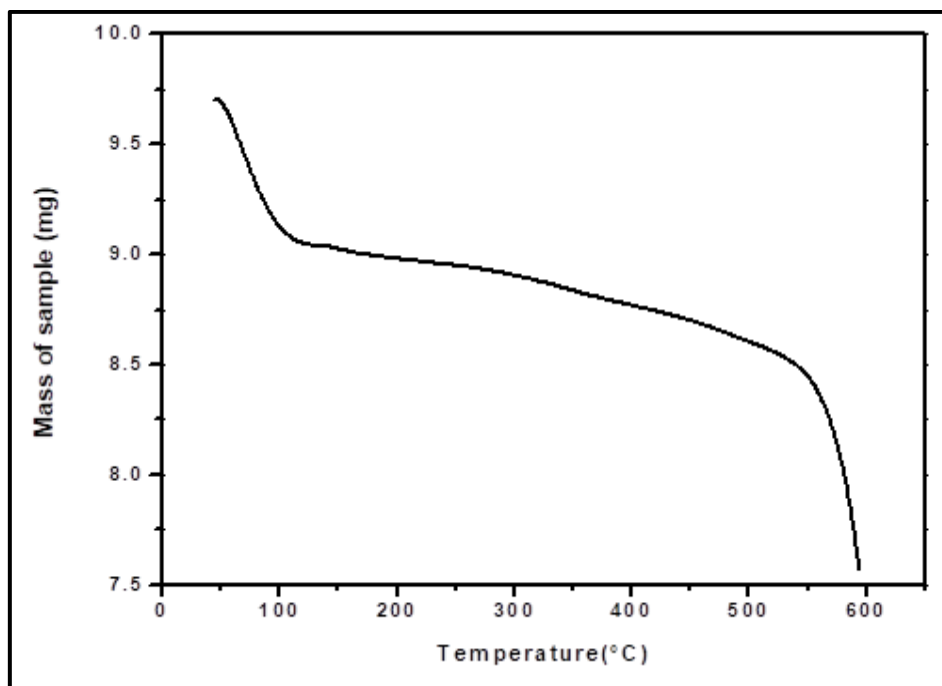


**Fig. 10:** TGA of Mn<sup>II</sup>(alz)<sub>2</sub>

#### 2.4.7 Structure of Mn<sup>II</sup>(alz)<sub>2</sub> by a computational technique:

Single crystals of complexes where only hydroxy-9,10-anthraquinones are present as ligands to a metal centre are rare. There are only two reports so far from single crystal data.<sup>40,41</sup> However, there are reports of structures of hydroxy-9,10-anthraquinone complexes of 3d transition metal ions using powder X-ray diffraction (PXRD) data and Rietveld analysis.<sup>1,6,7</sup> For this complex, single crystals suitable for X-ray diffraction could not be isolated. The PXRD data that was obtained for this complex could not be solved to generate a crystal structure as peaks did not suggest a crystalline nature of the material. So the only option left was to arrive at the structure by using computational techniques based on information obtained from spectroscopy, mass spectrometry and TGA. From the thermo-gravimetric data and mass spectrum it is evident that the complex has two alizarin and two water molecules coordinated to Mn<sup>II</sup> (Fig. 11).

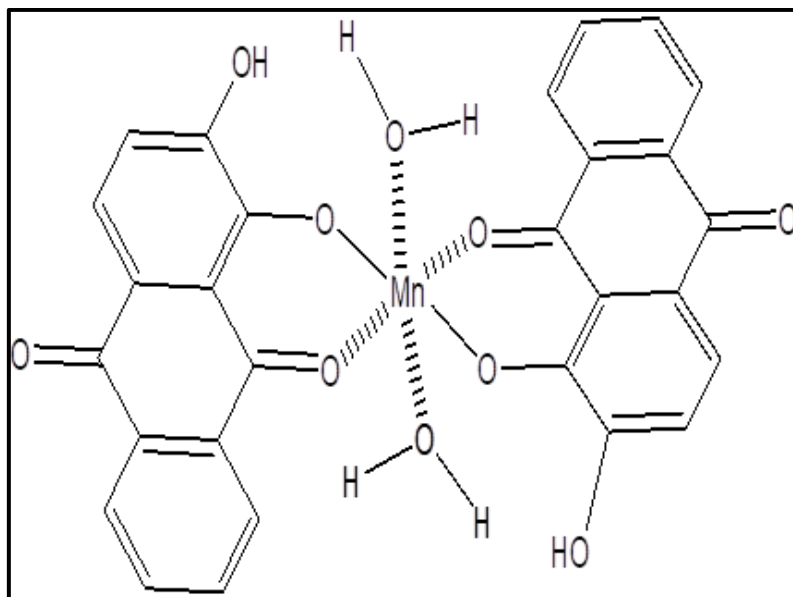


**Fig. 11:** A probable structure of the Mn<sup>II</sup> complex of alizarin

It is assumed that the Mn<sup>II</sup> complex has octahedral geometry (Fig. 11). Usually, octahedrally coordinated Mn<sup>II</sup> is high-spin although low spin Mn<sup>II</sup> complexes with strong field ligands exist.<sup>42</sup> Density functional theory (DFT) studies were carried out to predict the spin-state and structure of the complex. Two models were constructed for octahedral Mn<sup>II</sup> in which two alizarin moieties are present in trans-geometry (natural choice from symmetry considerations, Fig. 11), one with Mn<sup>II</sup> in low spin state ( $s = 1/2$ ), a doublet, and another in high spin state ( $s = 5/2$ ), a sextet. Geometry optimization was performed. Total energy calculations in gas phase and in solution (DMSO as solvent) along with single point TD-DFT calculations in DMSO were performed.<sup>43</sup> Experimentally obtained IR frequencies and those that were generated theoretically from frequency calculations for both optimized structures were compared. UV-Vis absorption spectrum recorded in DMSO was also compared with calculated ones.

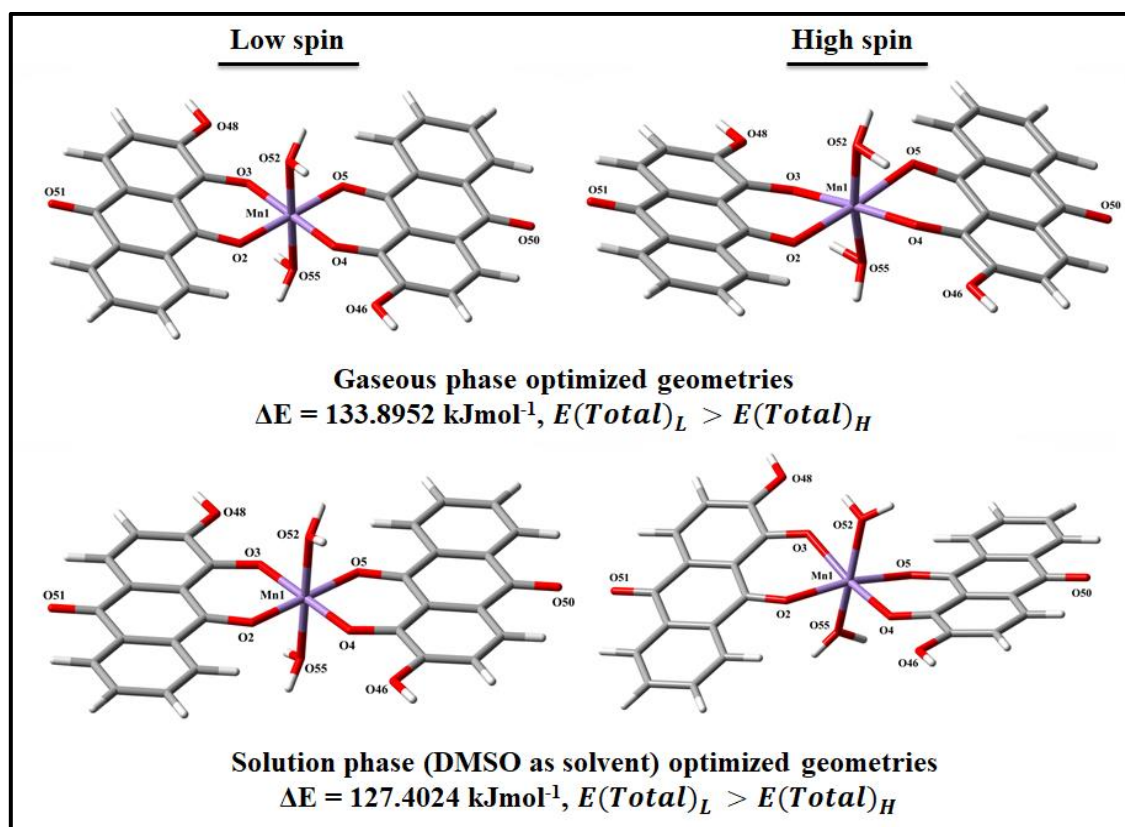


**Fig. 12:** Optimized geometries of the complex in two different spin states in gas phase and in DMSO medium.

The central objective of the attempted theoretical investigations was to determine the correct spin state of octahedral  $\text{Mn}^{\text{II}}$ . Any ambiguity was removed by comparing the total energy, IR frequencies between optimized structures of high and low spin complexes, their UV-Vis absorption spectrum in DMSO with corresponding experimental counterparts etc. For geometry optimization, negligible spin contamination occurred. The high spin geometry showed spin contamination in percentages of 0.10 and 0.06 for gas and solution phase optimizations respectively. All optimized geometries of the complex in the two spin states (in both phases) are shown in Fig. 12 with a numbering scheme showing the coordination environment. Optimized coordinates for the configurations are provided in Tables 1 & 2. Some important parameters of coordination geometries are provided in Tables 3 & 4. The low spin state forms a regular octahedron with two alizarin parallel to each other forming the basal plane;  $\text{Mn}^{\text{II}}$

and two water molecules are in a straight line with the latter forming the vertices of an octahedron. Although bond parameters change slightly upon changing the solvent, to do away with this effect, bonds within the basal plane or axial positions were considered almost equal to each other. The high spin state has a distorted octahedral geometry making bonds in the basal plane and axial unequal in length. Bond angles are twisted so that alizarin moieties are no longer parallel to each other (dihedral angle = 8.93° for the optimized structure in gas phase and 20.53° in solution phase). Axial water molecules are tilted to deform from an ideal octahedron vertices.

**Table 1.**

Optimized coordinates of the complex **Mn(II)-Alizarin** in high spin geometry.

<b>Gaseous phase</b>				<b>In DMSO solvent</b>			
<b>Atom</b>	<b>x</b>	<b>y</b>	<b>z</b>	<b>Atom</b>	<b>x</b>	<b>y</b>	<b>z</b>
Mn1	0.0083	-0.1078	-0.1118	Mn1	-0.0106	0.0946	-0.1391
O2	1.9117	-0.8685	0.4157	O2	1.8772	-0.7387	0.4800
O3	0.9769	1.6721	0.3918	O3	1.1097	1.8359	-0.0380
O4	-1.0637	-1.8649	-0.4579	O4	-1.1050	-1.6033	-0.7564
O5	-1.8598	0.7008	-0.7755	O5	-1.9684	0.9405	-0.2668
H6	4.8232	-4.6479	0.0694	H6	4.5765	-4.6303	1.1627
C7	5.0209	-3.5815	0.0504	C7	4.8399	-3.6033	0.9362
H8	2.9405	-3.0163	0.2690	H8	2.7919	-2.9132	0.8886
C9	3.9641	-2.6786	0.1637	C9	3.8357	-2.6464	0.7840
C10	6.5906	-1.7428	-0.1202	C10	6.5234	-1.9165	0.5028
C11	4.2124	-1.2968	0.1368	C11	4.1645	-1.3133	0.4896
C12	6.3364	-3.1141	-0.0904	C12	6.1876	-3.2387	0.7959
C13	5.5347	-0.8289	-0.0088	C13	5.5205	-0.9493	0.3480

**Chapter 8: Characterization of a Mn(II)....with anthracycline antibiotics**

---

C14	3.0786	-0.3564	0.2533	C14	3.0831	-0.3161	0.3289
H15	7.1563	-3.8190	-0.1781	H15	6.9669	-3.9829	0.9143
H16	7.5951	-1.3518	-0.2302	H16	7.5564	-1.6115	0.3887
C17	3.3237	1.0672	0.1915	C17	3.4175	1.0522	0.0158
C18	2.2452	2.0054	0.2855	C18	2.3982	2.0513	-0.1467
C19	4.6705	1.5461	0.0576	C19	4.8007	1.4246	-0.1245
H20	5.9595	3.2333	-0.0707	H20	6.1978	2.9856	-0.5130
C21	5.8161	0.6226	-0.0480	C21	5.8881	0.4456	0.0338
C22	2.5774	3.4061	0.2633	C22	2.8292	3.3979	-0.4502
C23	3.8845	3.8378	0.1370	C23	4.1646	3.7246	-0.5773
H24	4.1042	4.9023	0.1184	H24	4.4550	4.7452	-0.8055
C25	4.9317	2.9080	0.0304	C25	5.1492	2.7360	-0.4143
C26	-2.7365	-3.4528	0.0647	C26	-2.7268	-3.3179	-0.6917
C27	-2.333	-2.0954	-0.1937	C27	-2.3633	-1.9240	-0.5722
C28	-5.029	-2.7708	0.4191	C28	-5.0410	-2.8209	-0.2235
C29	-3.3453	-1.0825	-0.1422	C29	-3.4087	-0.9906	-0.2626
C30	-4.0485	-3.7743	0.3605	C30	-4.0284	-3.7474	-0.5233
C31	-4.6972	-1.4461	0.1755	C31	-4.7550	-1.4695	-0.0923
C32	-3.0295	0.2999	-0.4255	C32	-3.1386	0.4210	-0.1312
H33	-4.3227	-4.8086	0.5521	H33	-4.2710	-4.8009	-0.6198
H34	-6.0592	-3.0092	0.6526	H34	-6.0633	-3.1510	-0.0907
C35	-4.0892	1.3243	-0.3242	C35	-4.2478	1.3500	0.1782
C36	-3.7644	2.6724	-0.546	C36	-3.9821	2.7225	0.3115
C37	-5.4158	0.9712	-0.0021	C37	-5.5674	0.8800	0.3502
H38	-7.4112	1.6594	0.3337	H38	-7.6011	1.3969	0.7767
C39	-5.7744	-0.4412	0.2514	C39	-5.8686	-0.5595	0.2199

---



C40	-4.7505	3.6541	-0.4529	C40	-5.0129	3.6147	0.6093
H41	-2.7373	2.9224	-0.7815	H41	-2.9658	3.0707	0.1793
H42	-4.4934	4.6943	-0.6221	H42	-4.7981	4.6726	0.7102
C43	-6.071	63.3000	-0.1392	C43	-6.3241	3.1451	0.7784
H44	-6.8367	4.0658	-0.0688	H44	-7.1242	3.8391	1.0100
C45	-6.4011	1.9633	0.0860	C45	-6.5971	1.7829	0.6492
O46	-1.7275	-4.3937	-0.0039	O46	-1.6835	-4.1718	-0.9816
H47	-2.0697	-5.2895	0.1846	H47	-1.9817	-5.1010	-1.0444
O48	1.5048	4.2696	0.3771	O48	1.8137	4.3180	-0.6037
H49	1.7989	5.2008	0.3432	H49	2.1617	5.2085	-0.8096
O50	-6.959	-0.7615	0.5262	O50	-7.0482	-0.9831	0.3733
O51	6.9948	1.0435	-0.1677	O51	7.1008	0.7747	-0.0922
O52	0.3871	-0.5944	-2.2977	O52	0.5083	-0.2189	-2.2882
H53	-0.0816	0.0020	-2.9107	H53	1.3669	-0.1553	-2.7422
H54	-0.1358	-1.4215	-2.1635	H54	0.0664	-1.0784	-2.4460
O55	-0.6736	0.3959	1.9908	O55	-0.4354	-0.1826	2.0087
H56	-0.4248	-0.1397	2.7644	H56	0.3156	-0.4122	2.5846
H57	-0.1511	1.2324	1.9435	H57	-1.1806	0.1781	2.5202

**Table 2.**

Optimized coordinates of the complex **Mn(II)-Alizarin** in low spin geometry.

Gaseous phase				In DMSO solvent			
Atom	x	y	z	Atom	x	y	z
Mn1	0.0000	0.0000	0.0000	Mn1	0.0000	0.0000	0.0000
O2	1.6952	-0.8388	0.2216	O2	1.7166	0.8530	0.0107
O3	0.8158	1.7132	0.2054	O3	0.8212	-1.7270	0.0230
O4	-0.8158	-1.7132	-0.2054	O4	-0.8212	1.7271	-0.0229

**Chapter 8: Characterization of a Mn(II)....with anthracycline antibiotics**

---

O5	-1.6952	0.8388	-0.2216	O5	-1.7166	-0.8530	-0.0107
H6	4.5534	-4.6655	0.1758	H6	4.6114	4.6544	0.0220
C7	4.7703	-3.6036	0.1275	C7	4.8221	3.5907	0.0164
H8	2.6933	-3.0023	0.2267	H8	2.7422	3.0138	0.0222
C9	3.7263	-2.6830	0.1595	C9	3.7708	2.6770	0.0167
C10	6.3806	-1.8000	-0.0377	C10	6.4204	1.7714	0.0019
C11	3.9990	-1.3024	0.0967	C11	4.0292	1.2925	0.0100
C12	6.1017	-3.1635	0.0297	C12	6.1530	3.1389	0.0089
C13	5.3390	-0.8615	-0.0050	C13	5.3701	0.8401	0.0027
C14	2.8983	-0.3406	0.1218	C14	2.9168	0.3393	0.0082
H15	6.9112	-3.8852	0.0045	H15	6.9691	3.8527	0.0085
H16	7.3956	-1.4291	-0.1173	H16	7.4373	1.3979	-0.0040
C17	3.1645	1.0671	0.0515	C17	3.1775	-1.0717	0.0068
C18	2.1020	2.0244	0.1077	C18	2.1128	-2.0292	0.0152
C19	4.5230	1.5240	-0.0405	C19	4.5393	-1.5370	0.0018
H20	5.8359	3.1940	-0.1581	H20	5.8454	-3.2218	-0.0018
C21	5.6520	0.5790	-0.0814	C21	5.6720	-0.6018	-0.0037
C22	2.4445	3.4117	0.0727	C22	2.4544	-3.4213	0.0191
C23	3.7642	3.8262	-0.0285	C23	3.7749	-3.8428	0.0115
H24	3.9943	4.8879	-0.0639	H24	4.0046	-4.9035	0.0128
C25	4.8008	2.8844	-0.0842	C25	4.8116	-2.9007	0.0031
C26	-2.4445	-3.4117	-0.0727	C26	-2.4544	3.4213	-0.0192
C27	-2.1020	-2.0244	-0.1077	C27	-2.1128	2.0292	-0.0152
C28	-4.8008	-2.8844	0.0842	C28	-4.8116	2.9007	-0.0032
C29	-3.1645	-1.0671	-0.0515	C29	-3.1775	1.0717	-0.0068
C30	-3.7642	3.8262	0.0285	C30	-3.7749	3.8428	-0.0116
C31	-4.5230	1.5240	0.0405	C31	-4.5393	1.5370	-0.0018

---

*Chapter 8: Characterization of a Mn(II)...with anthracycline antibiotics*

---

C32	-2.8983	0.3406	-0.1218	C32	-2.9168	-0.3393	-0.0082
H33	-3.9943	-4.8879	0.0639	H33	-4.0046	4.9035	-0.0129
H34	-5.8359	-3.1940	0.1581	H34	-5.8454	3.2218	0.0017
C35	-3.9990	1.3024	-0.0967	C35	-4.0292	-1.2925	-0.0099
C36	-3.7263	2.6830	-0.1595	C36	-3.7708	-2.6770	-0.0166
C37	-5.3390	0.8615	0.0050	C37	-5.3701	-0.8401	-0.0027
H38	-7.3956	1.4291	0.1173	H38	-7.4373	-1.3979	0.0040
C39	-5.6520	-0.5790	0.0814	C39	-5.6720	0.6018	0.0037
C40	-4.7703	3.6036	-0.1275	C40	-4.8221	-3.5907	-0.0163
H41	-2.6933	3.0023	-0.2267	H41	-2.7422	-3.0138	-0.0221
H42	-4.5534	4.6655	-0.1758	H42	-4.6114	-4.6544	-0.0219
C43	-6.1017	3.1635	-0.0297	C43	-6.1530	-3.1389	-0.0088
H44	-6.9112	3.8852	-0.0045	H44	-6.9691	-3.8527	-0.0084
C45	-6.3806	1.8000	0.0377	C45	-6.4204	-1.7714	-0.0019
O46	-1.3839	-4.2979	-0.1390	O46	-1.3899	4.3000	-0.0287
H47	-1.7002	-5.2216	-0.1022	H47	-1.6903	5.2305	-0.0333
O48	1.3839	4.2979	0.1390	O48	1.3899	-4.3000	0.0286
H49	1.7002	5.2216	0.1022	H49	1.6903	-5.2305	0.0332
O50	-6.8444	-0.9775	0.1730	O50	-6.8706	1.0111	0.0122
O51	6.8444	0.9775	-0.1730	O51	6.8706	-1.0111	-0.0122
O52	0.3327	-0.0047	-2.0794	O52	-0.0555	0.0367	2.0917
H53	-0.1576	0.6809	-2.5678	H53	-0.5561	-0.6637	2.5479
H54	0.1462	-0.9037	-2.4112	H54	-0.1922	0.9052	2.5118
O55	-0.3327	0.0047	2.0794	O55	0.0555	-0.0367	-2.0917
H56	0.1576	-0.6809	2.5678	H56	0.5561	0.6636	-2.5479
H57	-0.1462	0.9037	2.4112	H57	0.1922	-0.9053	-2.5117

---

**Table 3.**

Coordinated bond distances (in Å) and bond angles (in °) of the complex Mn(II)-alizarin in the high spin state.

Bond	Gaseous phase	In DMSO	Angle	Gaseous phase	In DMSO
Mn1–O2	2.117	2.154	O2–Mn1–O3	80.16	80.64
Mn1–O3	2.088	2.073	O2–Mn1–O4	101.57	103.12
Mn1–O4	2.087	2.112	O3–Mn1–O5	99.07	99.53
Mn1–O5	2.141	2.137	O4–Mn1–O5	79.54	79.98
Mn1–O52	2.271	2.233	O52–Mn1–O2	90.74	91.07
Mn1–O55	2.267	2.207	O52–Mn1–O3	109.72	92.25
			O52–Mn1–O4	75.27	74.11
			O52–Mn1–O5	85.88	102.18
			O55–Mn1–O2	96.85	80.82
			O55–Mn1–O3	74.12	99.33
			O55–Mn1–O4	100.74	94.80
			O55–Mn1–O5	86.63	86.07
			O55–Mn1–O52	172.05	164.53

**Table 4.**

Coordinated bond distances (in Å) and bond angles (in °) of the complex Mn(II)-alizarin in the low spin state.

Bond	Gaseous phase	In DMSO	Angle	Gaseous phase	In DMSO
Mn1–O2	1.904	1.917	O2–Mn1–O3	90.14	90.99
Mn1–O3	1.909	1.912	O2–Mn1–O4	89.86	89.01
Mn1–O4	1.909	1.913	O3–Mn1–O5	89.86	89.01
Mn1–O5	1.904	1.917	O4–Mn1–O5	90.14	90.99
Mn1–O52	2.106	2.093	O52–Mn1–O2	88.47	90.59

Mn1-O55	2.106	2.093	O52-Mn1-O3	92.33	90.87
			O52-Mn1-O4	87.67	89.13
			O52-Mn1-O5	91.53	89.41
			O55-Mn1-O2	91.53	89.41
			O55-Mn1-O3	87.67	89.13
			O55-Mn1-O4	92.33	90.87
			O55-Mn1-O5	88.47	90.59
			O55-Mn1-O52	180.00	180.00

Fig. 12 depicts a difference in total energy ( $\Delta E$ ) between high and low spin geometries optimized in gas and solution phases. Calculations carried out at unrestricted DFT shows the high spin configuration has a lower energy which is expected given both alizarin and H<sub>2</sub>O are relatively weak field ligands. The value is 133.89 kJ/mol lower for the high spin geometry than it is for the low spin one in gas phase. Introducing the molecule to a dielectric medium (DMSO) reduces this difference to 127.40 kJ/mol. A close inspection of the IR spectra of computed geometries and that obtained experimentally (Fig. 8) reveal calculated frequencies obtained for high spin geometry are more comparable to the experimental ones, although there ought to be little difference in IR spectra if the only difference in structures is the spin of electrons on the central metal ion. Theoretical absorption spectrum in DMSO with oscillator strength and experimental UV-Vis spectrum are shown in Fig. 13. The calculated spectrum for high spin geometry shows better correlation for peak positions with the experimental spectrum than for the low spin geometry. These further allow one to conclude that the high spin state is more favourable. Subsequently, frontier MOs for the complex optimized in gas and solution (DMSO) phases were analyzed. Excitation in absorption spectrum in DMSO was analyzed using NTO analysis for high spin Mn<sup>II</sup>-alizarin.

At this stage, it is necessary to mention although we were not successful in obtaining single crystals for the complex and that the powder X ray diffraction data we obtained did not yield a structure either for reasons mentioned above, which is why we used DFT, we however compared parameters like Mn–O bond distances and O–Mn–O bond angles with previous reports, that evaluated them from single crystal X-ray diffraction data of Mn(II) in octahedral environment coordinated by six oxygen donor ligands like in our case.<sup>44-48</sup> Values obtained by us for Mn–O bond distances and O–Mn–O bond angles through computation in octahedral high spin geometry were in the same range as those obtained by several researchers in their studies with similar complexes, solved using single crystal X-ray diffraction.<sup>44-48</sup>

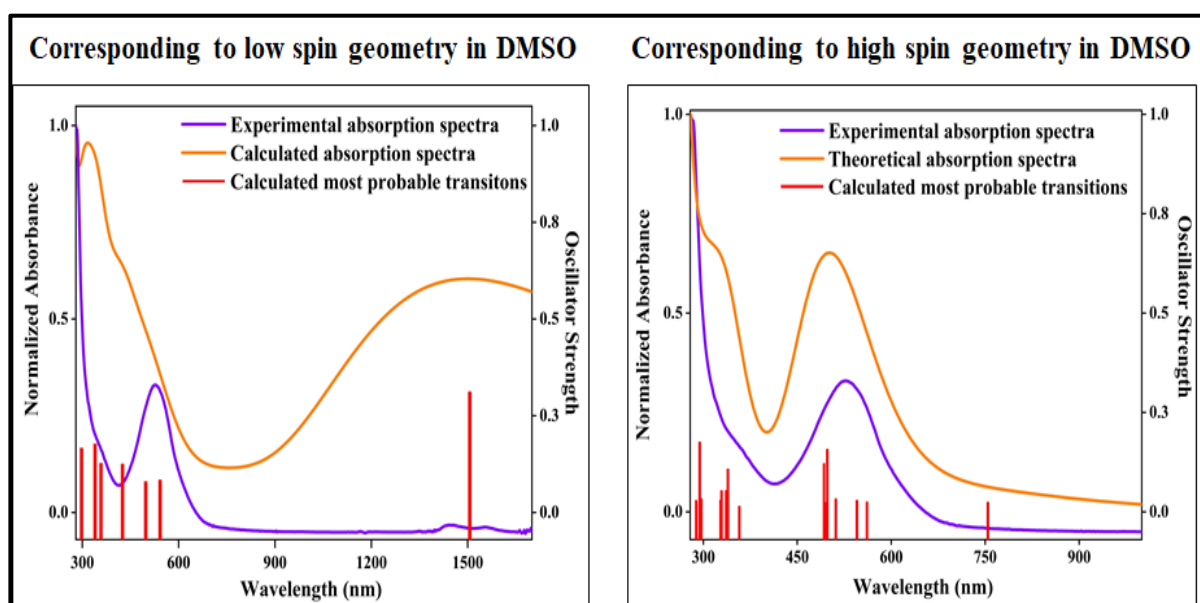


**Fig. 13:** Comparative descriptions of experimental absorption spectrum with the calculated spectra for low spin and high spin configurations at room temperature

#### **2.4.8 MO composition analysis:**

Molecules with odd number of electrons, calculated using U-DFT leads to a breakdown of symmetry. Each molecular orbital now has two components  $\alpha$  and  $\beta$  due to electron spin.  $\alpha$ -orbitals are more populated (five electrons) than  $\beta$  showing a typical sextet multiplicity. The HOMO–LUMO energy levels for both spin- $\alpha$  and spin- $\beta$  components of MOs, their energy

difference in gas and solution (DMSO) are shown in Fig. 14. Since spin- $\alpha$  and spin- $\beta$  components of an orbital is localized in different parts of the molecule, for MO composition analysis, contributions from five fragments viz., Mn, alizarin (L), alizarin (R), water (1) and water (2) were considered. Orbital energies, contribution of each fragment in terms of atomic orbitals to frontier molecular orbital (MO) for some frontier MOs are listed in Table 5.

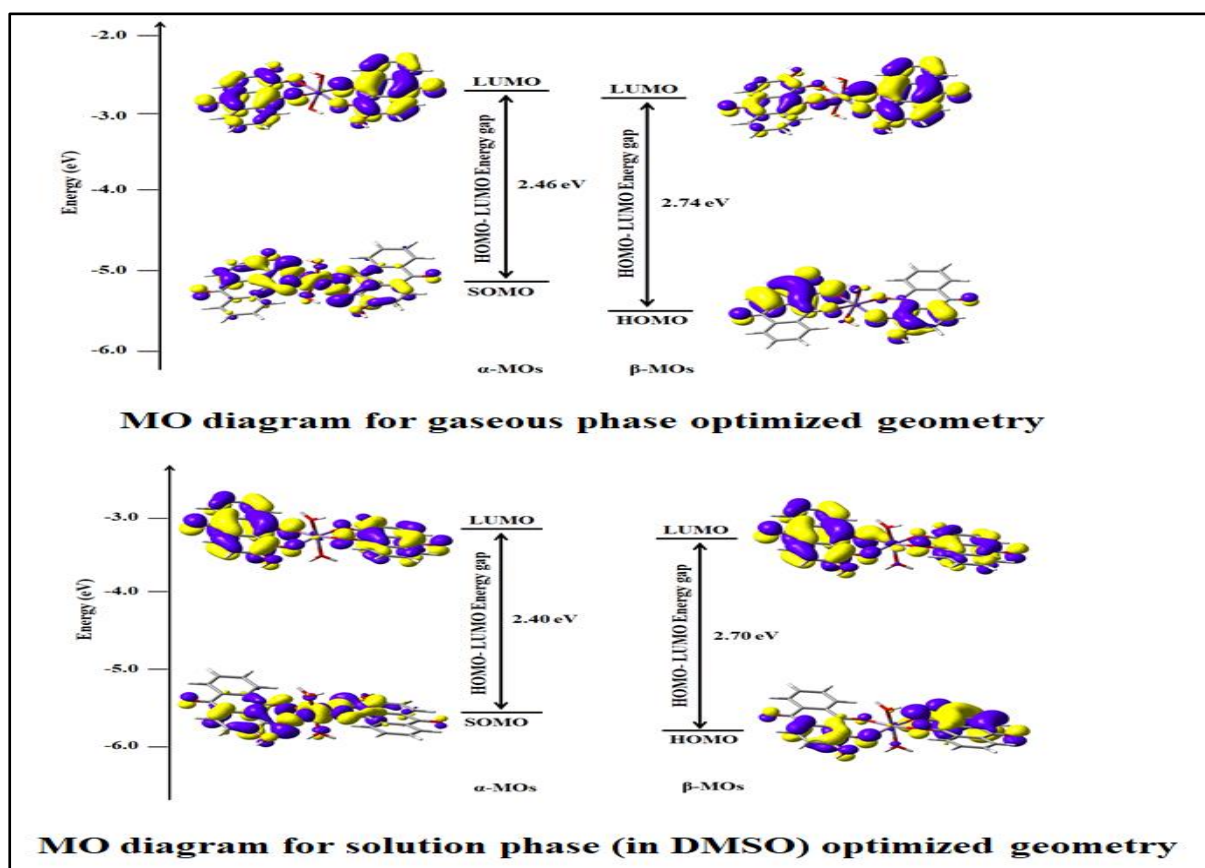


**Fig. 14:** HOMO and LUMO orbitals of the optimized complex (in high spin state) for  $\alpha$ - &  $\beta$ - spin states show the HOMO-LUMO energy gap.

For gas phase geometry, highest singly occupied spin- $\alpha$  orbital (SOMO) is delocalized over the whole framework (28% Mn and 61% alizarin) whereas the LUMO is delocalized over alizarin (i.e. the ligand, 99%). For spin- $\beta$  orbitals both HOMO and LUMO are ligand centred (i.e., 98% alizarin in each case) with practically negligible contribution from metal atomic orbitals. For geometry in solution phase, spin- $\alpha$  SOMO is distributed over the ligand with an

appreciable contribution from the metal ion (42% Mn and 57% alizarin). The LUMO is completely based on alizarin (ligand 100%) with no participation from metal atomic orbitals.

For spin- $\beta$  orbitals, both HOMO and LUMO are ligand centred (98% and 97% alizarin respectively). Introduction of the complex into a dielectric medium reduces the HOMO–LUMO energy gap for both spin- $\alpha$  and spin- $\beta$  orbitals (Fig. 14). These FMOs come handy in highlighting electronic structure and opto electronic properties of the complex.

**Table 5.**

Some of the selected MOs of the complex **Mn(II)-alizarin** in high spin state along with their energies and percentage compositions.

**Gas phase optimized structure:**

**For  $\alpha$ -electrons:**

Orbital	MO	Energy (eV)	% Composition				
			Mn	Alizarin(L)	Alizarin(R)	Water(1)	Water(2)
148	L+4	-0.51	80	2	2	7	10
147	L+3	-1.29	1	21	78	0	0
146	L+2	-1.34	1	78	21	0	0
145	L+1	-2.73	3	33	64	0	0
144	LUMO	-2.86	1	65	34	0	0
143	HOMO	-5.32	38	28	33	0	1
142	H-1	-5.57	14	27	59	1	0
141	H-2	-5.66	1	67	31	0	1
140	H-3	-6.21	58	12	14	8	7
139	H-4	-6.64	1	40	59	0	0



For  $\beta$ -electrons:

Orbital	MO	Energy (eV)	% Composition				
			Mn	Alizarin(L)	Alizarin(R)	Water(1)	Water(2)
143	L+4	-0.55	79	2	1	7	10
142	L+3	-1.31	1	21	78	0	0
141	L+2	-1.36	3	77	20	0	0
140	L+1	-2.81	1	21	78	0	0
139	LUMO	-2.88	3	78	20	0	0
138	HOMO	-5.62	1	23	75	1	0
137	H-1	-5.70	2	75	23	0	1
136	H-2	-6.59	1	22	77	0	0
135	H-3	-6.69	1	76	22	0	0
134	H-4	-6.81	0	3	97	0	0

Solution phase (DMSO) optimized structure:

For  $\alpha$ -electrons:

Orbital	MO	Energy (eV)	% Composition				
			Mn	Alizarin(L)	Alizarin(R)	Water(1)	Water(2)
148	L+4	-0.54	84	2	2	5	8
147	L+3	-1.49	1	81	18	0	0
146	L+2	-1.51	1	18	81	0	0
145	L+1	-2.98	2	63	35	0	0
144	LUMO	-3.04	0	36	64	0	0
143	HOMO	-5.44	42	23	34	1	0
142	H-1	-5.66	11	75	14	0	0
141	H-2	-5.81	5	22	72	0	0
140	H-3	-6.22	66	12	11	6	5
139	H-4	-6.83	13	43	44	0	0

For  $\beta$ -electrons:

Orbital	MO	Energy (eV)	% Composition				
			Mn	Alizarin(L)	Alizarin(R)	Water(1)	Water(2)
143	L+4	-0.56	83	2	1	6	8
142	L+3	-1.50	1	62	37	0	0
141	L+2	-1.54	2	36	62	0	0
140	L+1	-3.02	0	70	29	0	0
139	LUMO	-3.07	2	28	69	0	0
138	HOMO	-5.77	1	78	20	0	0
137	H-1	-5.82	2	20	78	0	0
136	H-2	-6.85	1	55	44	0	0
135	H-3	-6.94	1	72	27	0	0
134	H-4	-6.95	1	54	45	0	0

#### 2.4.9. Analysis of absorption spectra:

DMSO being the solvent, since there is a cut off wavelength (~ 268 nm) below which absorption of the compound may not be realized, hence absorption below 300 nm was not considered. Instead, the spectrum of the complex was recorded up to 1050 nm and compared with the calculated electronic spectrum of Mn(II)-alizarin in DMSO. Peaks in experimental spectrum were assigned by visual inspection.

Most pertinent transitions having moderate intensities ( $f \geq 0.02$ ) are close to the experimental absorption peaks, excitation wavelengths, energy, oscillator strengths ( $f$ ), character and CI coefficients and are listed in Table 6. Excitations were attributed to charge-transfer transitions among different moieties, viz. within alizarin, between water molecules and alizarin with varying amounts of metal to ligand contribution. First five computed transitions in DMSO are tabulated in Table 7. While performing TDDFT, excited states showed spin contamination with fractional values 0.212 to 0.019 (Tables 6 & 7); all states were considered to be sextets.

		Spin- $\alpha$		Spin- $\beta$	
		Hole NTO	Particle NTO	Hole NTO	Particle NTO
300 nm	Sext <sub>73</sub> 4.21 (0.1758) 294.26				
	Weight, $\lambda_i =$	0.46012		0.39694	
Character:		LLCT/MLCT & C=O lone pair $\rightarrow$ C=O anti bonding			
350 nm	Sext <sub>41</sub> 3.65 (0.1077) 339.27				
	Weight, $\lambda_i =$	0.55590		0.25557	
Character:		LLCT/MLCT			
526 nm	Sext <sub>14</sub> 2.52 (0.1213) 492.704				
	Weight, $\lambda_i =$	0.34414		0.46779	
Character:		LLCT/MLCT & C=O lone pair $\rightarrow$ C=O anti bonding			
526 nm	Sext <sub>12</sub> 2.49 (0.1574) 497.91				
	Weight, $\lambda_i =$	0.43709		0.28911	
Character:		LLCT/MLCT & C=O lone pair $\rightarrow$ C=O anti bonding			

**Fig. 15.** Natural transition orbitals (NTOs) for the complex elucidating the nature of excited states in the absorption spectra in comparison with experimentally obtained pattern in DMSO medium. For each state, the respective number of the state, transition energy (in eV) and oscillator strength (in parentheses) are listed.

Excited state computational results were interpreted by natural transition orbital (NTO) analyses based on the calculated transition density matrices.<sup>49</sup> Unoccupied and occupied NTOs are referred to as “electron” and “hole” transition orbitals respectively allowing us to identify them and visualize electronic transitions under consideration in terms of excitation from hole-NTO to electron-NTO for both  $\alpha$ - and  $\beta$ - spin components. NTOs for the most relevant peaks are depicted in Fig. 15. While analyzing NTOs lower energy transitions around 526 nm were found at 492.7 nm (2.52 eV,  $f = 0.1213$ ) and 497.9 nm (2.49 eV,  $f = 0.1574$ ). The first transition consists of  $d(\text{Mn}) + \pi(\text{alizarin}) \rightarrow \pi^*(\text{alizarin})$  LLCT with some MLCT character together with lone pair(O)  $\rightarrow$  antibonding (O) transition. Net electron transfer between metal to ligand fragments and within ligand fragments were 0.03681e and 0.13293e respectively.<sup>50</sup> The second one is ascribed to  $d(\text{Mn}) + \pi(\text{alizarin}) \rightarrow \pi^*(\text{alizarin})$  [MLCT transition] in association with LLCT character where net electron transfer between metal to ligand fragments and within ligand fragments are 0.0933e and 0.12326e respectively. Excitation near the experimentally observed peak at 350 nm was found by calculation to be at 339.27 nm (3.650 eV,  $f = 0.1077$ ) and ascribed to  $d(\text{Mn}) + \pi(\text{alizarin}) \rightarrow \pi^*(\text{alizarin})$  MLCT transition together with slight LLCT character where metal to ligand and ligand to ligand net electron transfers were 0.16419e and 0.03658e respectively. The UV transition around 300 nm was computed and found at 294.26 nm (4.21 eV,  $f = 0.1758$ ). This was attributed to  $d(\text{Mn}) + \pi(\text{alizarin}) \rightarrow \pi^*(\text{alizarin})$  LLCT transition in association with MLCT character together with lone pair (O)  $\rightarrow$  antibonding (O) transition. Net electron transfer between metal to ligand fragments and within ligand fragments were 0.08540e and 0.13293e respectively.

**Table 6:** A list of experimental UV-Vis transitions for the complex in the solvent DMSO with the corresponding theoretically calculated UV-Vis transitions with vertical excitation energies ( $E_{ex}$ ), oscillator strengths ( $f$ ) of the lowest few excitons obtained from TDDFT method in DMSO.

Experimental excitation values (nm)	Calculated excitation values (nm)	Excitation energy (eV)	CI expansion coefficient	Excited state involved	$\langle S^2 \rangle$ / Fractional diffrn. with ideal for the ext. state	Osc. strength ( $f$ )	Key transitions involved
300	294.262	4.2134	0.58222 -0.56265 -0.28947	Sext <sub>73</sub>	9.429/ 0.077	0.1758	H-13(A)→L+1(A) (34%) H-11(B)→L+1(B) (32%) H-14(A)→L+1(A) (8%)
	296.776	4.1777	-0.34343 0.32251 -0.43886 0.60004	Sext <sub>71</sub>	9.214/ 0.053	0.0330	HOMO(A)→L+4(A) (12%) H-11(B)→LUMO(B) (10%) H-11(B)→L+1(B) (19%) H-10(B)→L+1(B) (36%)
350	327.472	3.7861	-0.34459 0.32188 0.46288	Sext <sub>46</sub>	9.228/ 0.054	0.0292	H-12(A)→LUMO(A) (12%) H-12(A)→L+1(A) (10%) H-1(A)→L+2(A) (21%)
	329.028	3.7682	0.34273 0.28860 0.27387 -0.28600	Sext <sub>45</sub>	8.920/ 0.019	0.0535	H-11(A)→L+1(A) (12%) H-11(A)→LUMO(A) (8%) H-6(B)→LUMO(B) (8%) H-6(B)→L+1(B) (8%)
	336.356	3.6861	0.54346 -0.33398 -0.30241	Sext <sub>43</sub>	9.037/ 0.032	0.0539	H-1(A)→L+2(A) (30%) H-1(B)→L+2(B) (11%) HOMO(B)→L+2(B) (9%)
	339.274	3.6544	0.34671 0.51131 -0.31951	Sext <sub>41</sub>	9.020/ 0.030	0.1077	H-10(A)→LUMO(A) (12%) H-8(A)→LUMO(A) (26%) H-7(B)→LUMO(B) (10%)
526	492.704	2.5164	0.42040 0.39116 -0.33813	Sext <sub>14</sub>	10.084/ 0.152	0.1213	H-2(A)→L+1(A) (18%) H-2(B)→L+1(B) (15%) H-1(B)→L+1(B) (11%)
	497.908	2.4901	0.47983 -0.34893 -0.28693 -0.28752	Sext <sub>12</sub>	9.752/ 0.114	0.1574	H-2(A)→L+1(A) (23%) H-1(B)→L+1(B) (12%) H-3(A)→L+1(A) (8%) H-2(B)→L+1(B) (8%)
	511.570	2.4236	0.74445 0.31454 0.37190	Sext <sub>10</sub>	8.991/ 0.027	0.0327	H-3(A)→L+1(A) (55%) H-1(A)→L+1(A) (10%) HOMO(B)→L+1(B) (14%)
	545.249	2.2739	-0.40686 -0.42012 0.51862 -0.31356	Sext <sub>6</sub>	9.415/ 0.070	0.0291	H-2(A)→LUMO(A) (17%) H-2(A)→L+1(A) (18%) H-1(A)→L+1(A) (27%) HOMO(B)→LUMO(B) (10%)

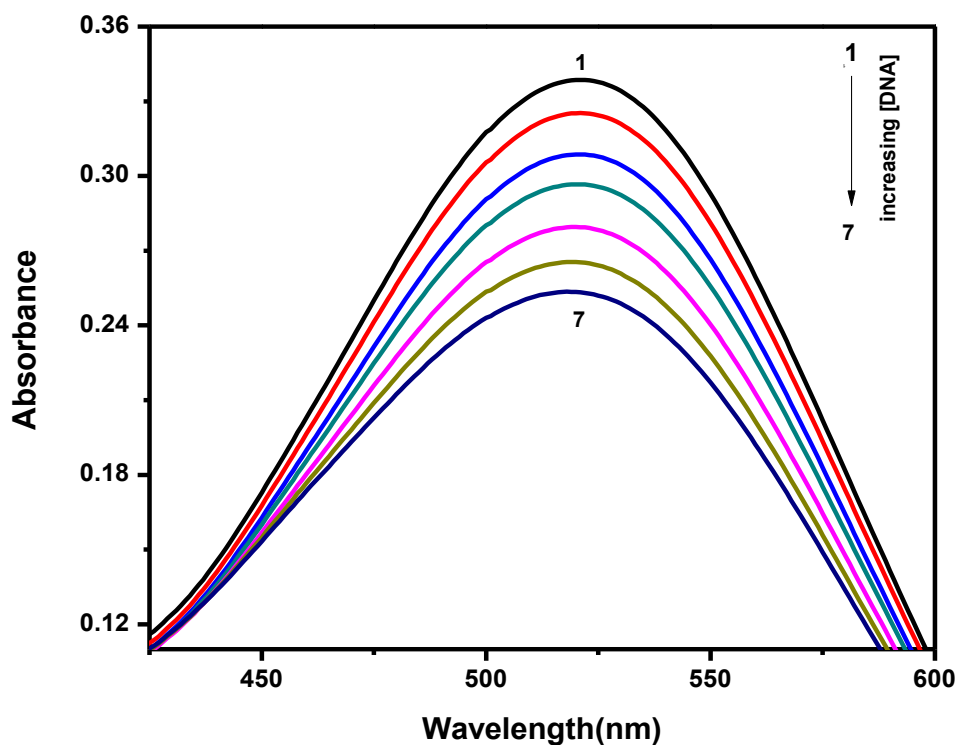
**Table 7:** The lowest first five calculated excitons obtained from TDDFT method in DMSO with the corresponding vertical excitation energies ( $E_{ex}$ ), oscillator strengths ( $f$ ) and key transitions involved.

Calculated excitation values (nm)	Excitation energy (eV)	CI expansion coefficient	Excited state involved	$\langle S^2 \rangle$ / Fractional diffrn. with ideal for the exct. state	Osc. strength (f)	Key transition involved
910.243	1.3621	0.35781 0.34813 0.45946 0.38092 0.40392	Sext <sub>1</sub>	10.534/ 0.204	0.0020	H-2(A)→L+1(A) (13%) H-1(A)→LUMO(A) (12%) HOMO(A)→LUMO(A) (21%) H-1(B)→L+1(B) (15%) HOMO(B)→LUMO(B) (16%)
905.456	1.3693	-0.37599 -0.46893 -0.31440 0.41975 0.50917	Sext <sub>2</sub>	10.608/ 0.212	0.0001	H-2(A)→LUMO(A) (14%) H-1(A)→L+1(A) (22%) HOMO(A)→L+1(A) (10%) H-1(B)→LUMO(B) (18%) HOMO(B)→L+1(B) (26%)
754.299	1.6437	-0.32120 0.76821 0.40440	Sext <sub>3</sub>	9.188/ 0.050	0.0245	H-1(A)→LUMO(A) (10%) HOMO(A)→LUMO(A) (59%) HOMO(A)→L+1(A) (16%)
728.034	1.703	-0.31563 0.77268	Sext <sub>4</sub>	9.219/ 0.054	0.0034	H-1(A)→L+1(A) (10%) HOMO(A)→L+1(A) (60%)
561.2684	2.209	0.73923 -0.45617	Sext <sub>5</sub>	9.610/ 0.111	0.0249	H-1(A)→LUMO(A) (55%) H-1(A)→L+1(A) (21%)

## 2.5 Analysis of the interaction of compounds with calf thymus DNA

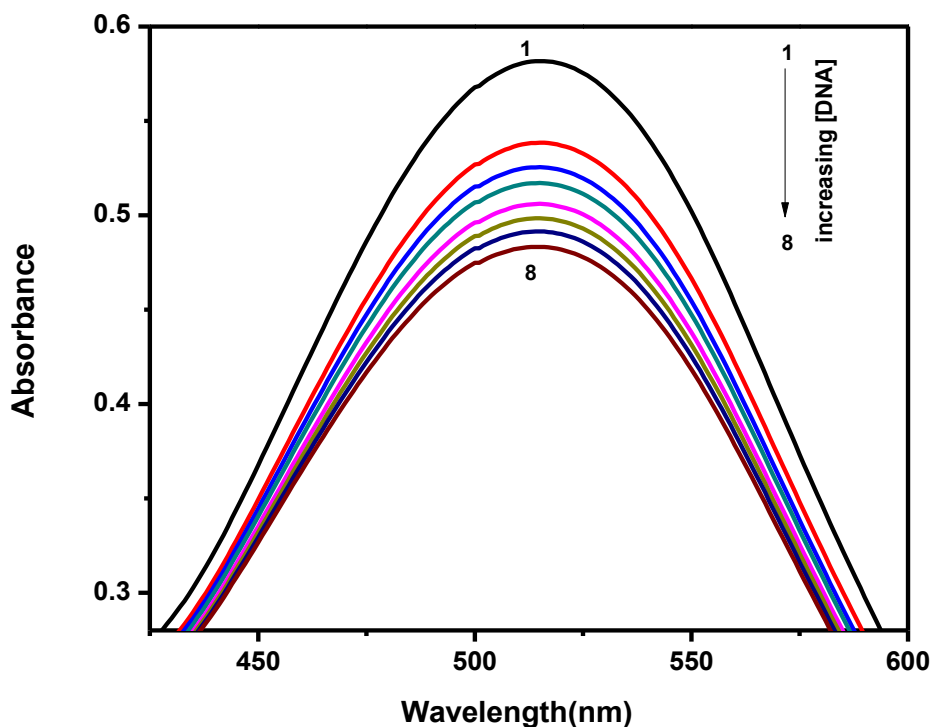
### 2.5.1 At different ionic strengths of the medium:

Ionic strength of the medium is an important parameter that influences the binding of several drugs to DNA; reasons for it are of course varied in nature.<sup>51,52</sup> Alizarin and its Mn(II) complex, were titrated with calf thymus DNA at different ionic strengths of the medium at a constant pH (~7.4). Titrations using alizarin were followed at 520 nm while for the complex it was followed at 515 nm (for ionic strength ~ 0.12M), at 510 nm (for ionic strength ~ 0.3M) and at 506 nm (for ionic strength ~ 0.5 M).



**Fig. 16:** Absorption spectra of 50 μM alizarin in aqueous solution in presence of 0.30 M NaCl, 30 mM Tris buffer (pH 7.4) in the absence (1) and presence of different concentrations of calf thymus DNA (2) 83.57 μM (3) 248.25 μM (4) 409.71 μM (5) 646.08 μM (6) 875.73 μM (7) 1098.93 μM; Temperature = 300 K.

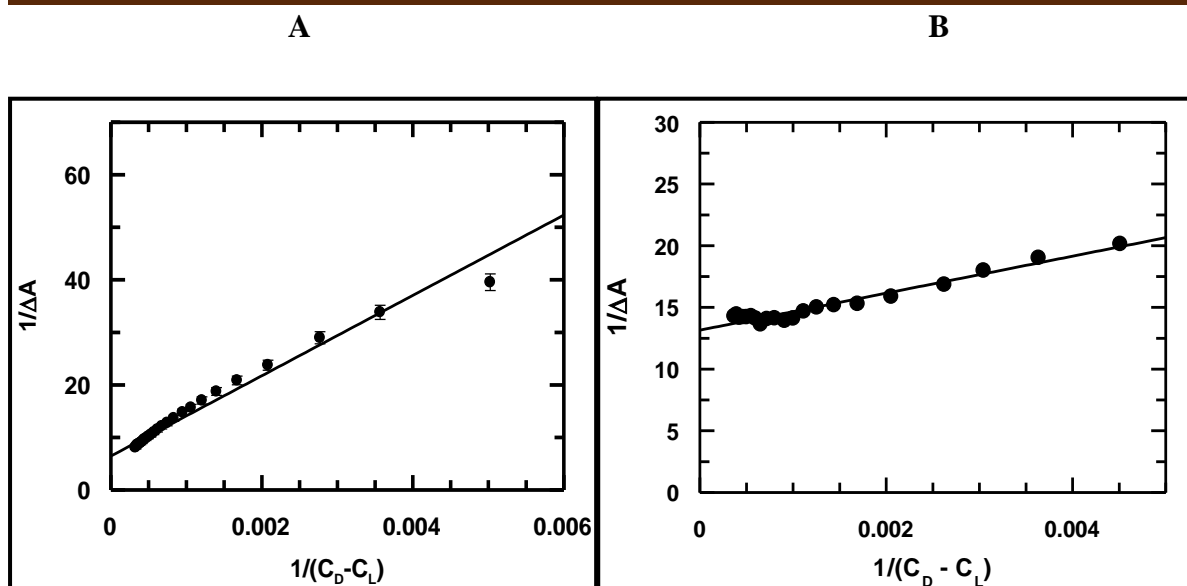
Figure 16 shows a gradual decrease in absorbance for a titration of alizarin with calf thymus DNA at an ionic strength 0.3M (using NaCl) while Figure 17 depicts a titration of the same complex at an ionic strength 0.12 M (using NaCl).



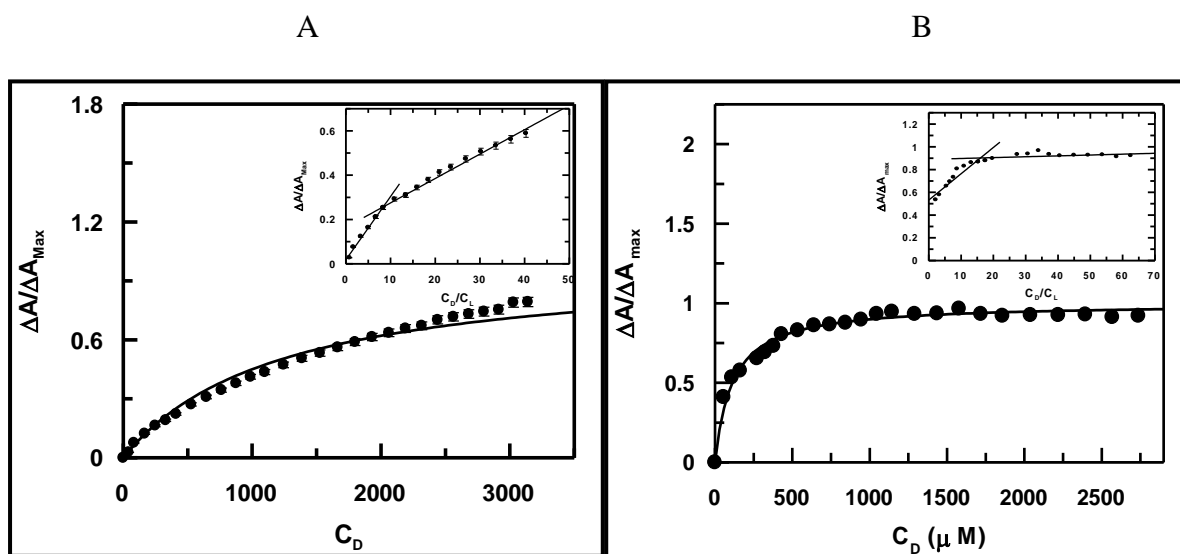
**Fig. 17:** Absorbance spectrum of 50  $\mu\text{M}$   $\text{Mn}^{\text{II}}(\text{alz})_2$  in 0.12 M NaCl and 30 mM tris buffer in aqueous solution, pH 7.4 in the absence (1) and presence of different concentrations of calf thymus DNA (2) 109.18  $\mu\text{M}$  (3) 217.28  $\mu\text{M}$  (4) 324.31  $\mu\text{M}$  (5) 535.24  $\mu\text{M}$  (6) 742.10  $\mu\text{M}$  (7) 945  $\mu\text{M}$  (8) 1144.05  $\mu\text{M}$ ; Temperature = 300 K.

Fig. 18A & 18B are representative plots of Eq. 10 (*Chapter 6: Experimental*) for titrations performed at ionic strengths of 0.3 M in case of alizarin and 0.12 M for the complex respectively. From such plots, apparent binding constants ( $K_{\text{app}}$ ) were evaluated (Table 8). Data in Figures 19A & 19B were fitted according to Eq. 12 (*Chapter 6: Experimental*) showing that saturation was achieved in the binding of the compounds to DNA;  $K_{\text{app}}$  was evaluated by a non-linear fit.





**Fig. 18:** Typical double reciprocal plots for interaction of (A) alizarin and (B)  $\text{Mn}^{\text{II}}(\text{alz})_2$  with calf thymus DNA that enables an evaluation of  $K_{\text{app}}$  at ionic strengths of 0.30 M for (A) and 0.12 M for (B).  $[\text{alizarin}] = [\text{Mn}^{\text{II}}(\text{alz})_2] = 50\mu\text{M}$ ,  $\text{pH} = 7.40$ , Temperature = 300 K.



**Fig. 19:** Binding isotherms of (A) alizarin and (B)  $[\text{Mn}^{\text{II}}(\text{alz})_2]$  with calf thymus DNA at ionic strengths 0.30 M and 0.12 M with respect to NaCl respectively. The corresponding non-linear fits are shown. Inset: Plot of normalized increase in absorbance as a function of the ratio of calf thymus DNA to (A) alizarin and (B)  $[\text{Mn}^{\text{II}}(\text{alz})_2]$ .  $[\text{alizarin}] = [\text{Mn}^{\text{II}}(\text{alz})_2] = 50\mu\text{M}$ ,  $\text{pH} = 7.40$ ,  $T = 301\text{K}$ .

Binding parameters at all ionic strengths are provided in Table 8. Inset of Fig. 19A & 19B provide  $n_b$ , the number of nucleotides bound to each compound (Table 8). It is interesting to note here that in case of the complex, the value of  $n_b$  obtained at each ionic strength was approximately double that obtained for alizarin binding to the same DNA at these ionic strengths of the medium. This also indicates that two molecules of alizarin are bound to  $Mn^{II}$  in the complex, realized from DNA binding experiments, besides being determined already from physicochemical studies (Table 8).<sup>1,8,12</sup>

Using  $K_{app}$  and  $n_b$  (Table 8) and the relation  $K_{app} \times n_b = K^*$ , overall binding constant was evaluated for alizarin and the Mn(II) complex at different ionic strengths of the medium. Overall binding constant was also obtained from a modified Scatchard equation (Eq. 13; Chapter 6: Experimental). Fig. 20A & 20B are plots that obey Eq. 13 (Chapter 6: Experimental). Values obtained for overall binding constant from the modified Scatchard equation was similar to that calculated using  $K_{app}$  and  $n_b$ .

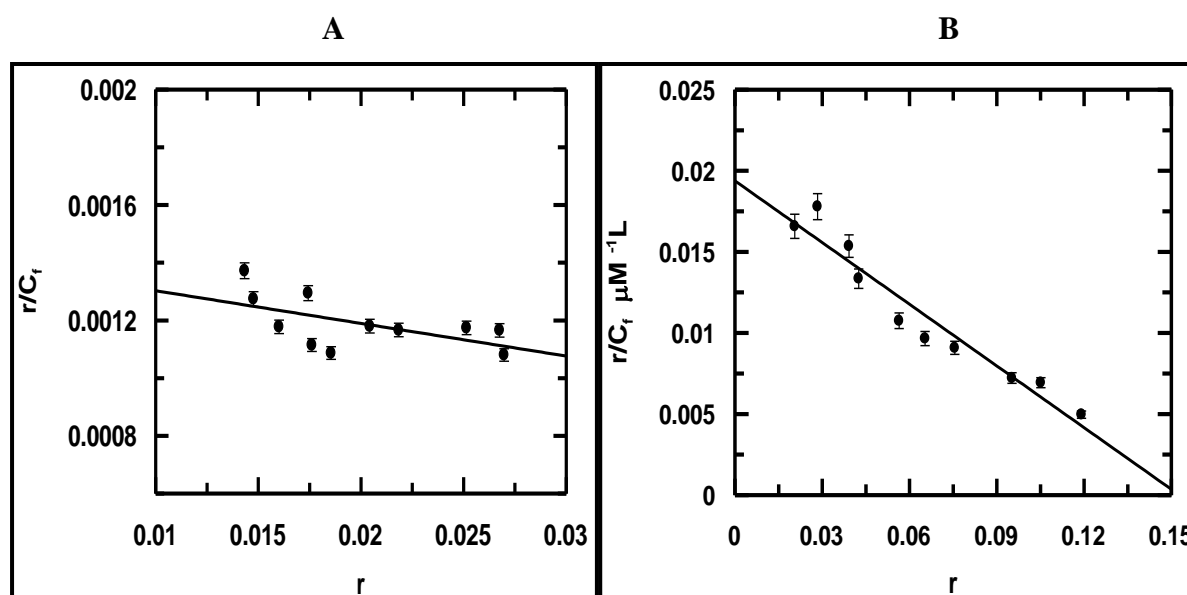


**Fig. 20:** Scatchard plots for interaction of (A) alizarin and (B)  $Mn(alz)_2$  with calf thymus DNA followed by UV-Vis spectroscopy at 521 nm for (A) and 515 nm for (B) respectively.  $[alizarin] = [Mn^{II}(alz)_2] = 50 \mu M$ ;  $[NaCl] = 0.24 M$  for (A) and  $0.12M$  for (B);  $pH = 7.40$ ,  $T = 301 K$ .

**Table 8:** Binding constant values obtained for the interaction of alizarin and  $[Mn^{II}(alz)_2]$  with calf thymus DNA at varying ionic strengths of the medium.

Compound	[NaCl] in M	$K_{app} (M^{-1})$			Site size	$K_{app} \times n_b =$ $K^* (M^{-1})$	$K^* (M^{-1})$ from Scatchard	$n_b$ calculated from Scatchard $n_b = (n^{-1})$
		From double- reciprocal plot(a)	From Non-linear plot (b)	Average $= (a+b)/2$				
Alizarin	0.12	$0.91 \times 10^3$	$0.69 \times 10^3$	$0.80 \times 10^3$	8	$0.64 \times 10^4$	$0.88 \times 10^4$	7
	0.18	$1.55 \times 10^3$	$1.15 \times 10^3$	$1.35 \times 10^3$	8	$1.01 \times 10^4$	$1.00 \times 10^4$	8
	0.24	$2.00 \times 10^3$	$1.37 \times 10^3$	$1.68 \times 10^3$	8	$1.34 \times 10^4$	$1.13 \times 10^4$	8
	0.30	$2.54 \times 10^3$	$2.58 \times 10^3$	$2.56 \times 10^3$	9	$2.30 \times 10^4$	$2.39 \times 10^4$	8
	0.36	$3.49 \times 10^3$	$3.09 \times 10^3$	$3.29 \times 10^3$	8	$2.63 \times 10^4$	$2.81 \times 10^4$	6
$Mn(alz)_2$	0.12	$0.87 \times 10^4$	$1.5 \times 10^4$	$1.19 \times 10^4$	16	$1.90 \times 10^5$	$1.38 \times 10^5$	10
	0.18	$1.67 \times 10^4$	$4.1 \times 10^4$	$2.89 \times 10^4$	16	$4.62 \times 10^5$	$4.86 \times 10^5$	12
	0.30	$1.11 \times 10^4$	$1.8 \times 10^4$	$1.46 \times 10^4$	14	$2.04 \times 10^5$	$5.05 \times 10^5$	11
	0.50	$1.64 \times 10^4$	$4.9 \times 10^4$	$3.27 \times 10^4$	16	$5.23 \times 10^5$	$5.58 \times 10^5$	14

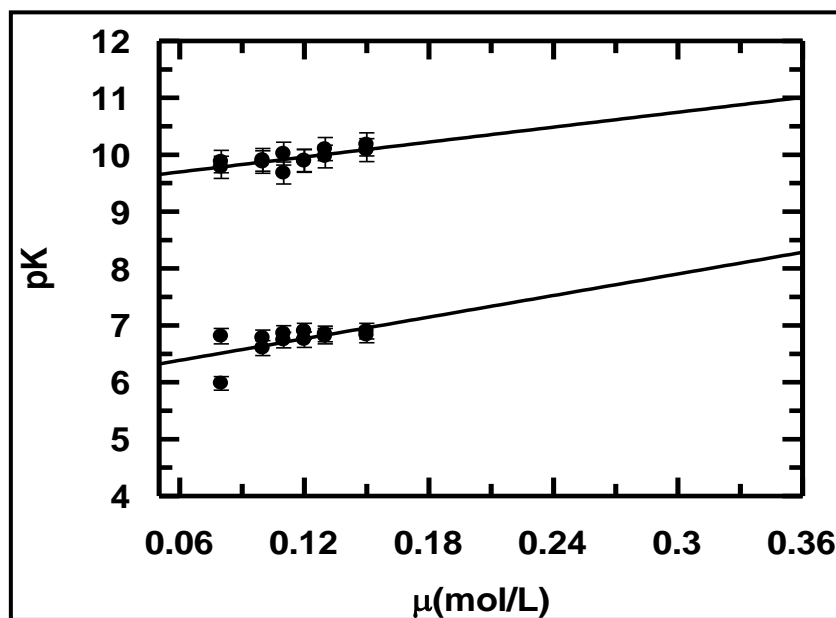


**Fig. 21:** Plot of linear dependence of  $pK_a$  values of alizarin with variation of ionic strength of the medium at 301 K; [alizarin] = 70  $\mu$ M.

## Chapter 8: Characterization of a Mn(II)...with anthracycline antibiotics

Since titrations were performed at pH 7.4 by varying the ionic strength of the medium, hence with gradual increase in ionic strength, ratio of the anionic form of alizarin to its neutral form changed continuously. This was evaluated by determining  $pK_a$  of alizarin at different ionic strengths of the medium (Fig. 21). From  $pK_{a1}$  of alizarin, ratio of its anionic to neutral forms were found to lie between 3.75 (at ionic strength = 0.12 M) to 0.14 (at ionic strength = 0.36 M). Hence, this makes it clearly evident that with increase in ionic strength of the medium, there is a gradual decrease in the anionic form of alizarin that manifests by its higher binding constant values with calf thymus DNA (Table 9).<sup>3</sup> On the other hand, for the complex since dissociation of OH present on alizarin bound to  $Mn^{II}$  is well beyond the physiological pH range, variation in ionic strength should hardly have any effect on the binding of the complex with DNA. However, an increase in binding constant values of  $Mn^{II}(alz)_2$  with calf thymus DNA was observed with an increase in the ionic strength of the medium (Tables 8 & 10).

**Table 9: Variation in overall binding constant of alizarin with calf thymus DNA at different ionic strength (pH~ 7.4).**

[NaCl] in M	$-\log[Na^+]$	$K^* (M^{-1}) = K_{app} \times n_b$	$\log K^*$	$K^* (M^{-1})$ from Scatchard plot	$\log K^*$
0.12	0.921	$0.64 \times 10^4$	3.81	$0.88 \times 10^4$	3.94
0.18	0.745	$1.01 \times 10^4$	4.00	$1.00 \times 10^4$	4.00
0.24	0.619	$1.34 \times 10^4$	4.13	$1.13 \times 10^4$	4.05
0.30	0.523	$2.30 \times 10^4$	4.36	$2.39 \times 10^4$	4.37
0.36	0.444	$2.63 \times 10^4$	4.42	$2.81 \times 10^4$	4.45

Fig. 22A & 22B indicate increasing nature of the binding of the complex and of alizarin with calf thymus DNA. In fact, at all ionic strengths, the complex was more effective in binding calf thymus DNA than alizarin (Tables 9 & 10). This has significance if the complex were to

be used as an anticancer agent. Patients with cancer, experience fluctuations in electrolyte concentration in body fluids during treatment for which most often electrolyte is added from outside. Under conditions of high ionic strength many drugs tend to be ineffective. From this study it may be said that this should not be the case for this complex as there is clear evidence that binding constant values are pretty high even at increased ionic strengths of the medium (Table 10, Fig. 22).

**Table 10: Variation of overall binding constant for interaction of Mn<sup>II</sup>(alz)<sub>2</sub> with calf thymus DNA at different concentrations of NaCl at physiological pH.**

[NaCl] in M	-log[Na <sup>+</sup> ]	$K^* = K_{app} \times n_b$	log K*	K*(10 <sup>5</sup> ) (from Scatchard plot)	log K*
0.12	0.921	$1.90 \times 10^5$	5.28	$1.38 \times 10^5$	5.13
0.18	0.745	$4.62 \times 10^5$	5.66	$4.86 \times 10^5$	5.68
0.30	0.523	$2.04 \times 10^5$	5.31	$5.05 \times 10^5$	5.70
0.50	0.301	$5.23 \times 10^5$	5.72	$5.58 \times 10^5$	5.75

Increase in pK<sub>a</sub> with ionic strength of the medium explains why there is a significant increase in the interaction of alizarin with calf thymus DNA. A slight change in pK<sub>a1</sub> is sufficient to cause a substantial difference to the presence of neutral and anionic forms in the medium and that affects its interactions with DNA. As mentioned earlier, increased presence of anions is a hindrance to interactions with DNA at physiological pH.<sup>2,38</sup>

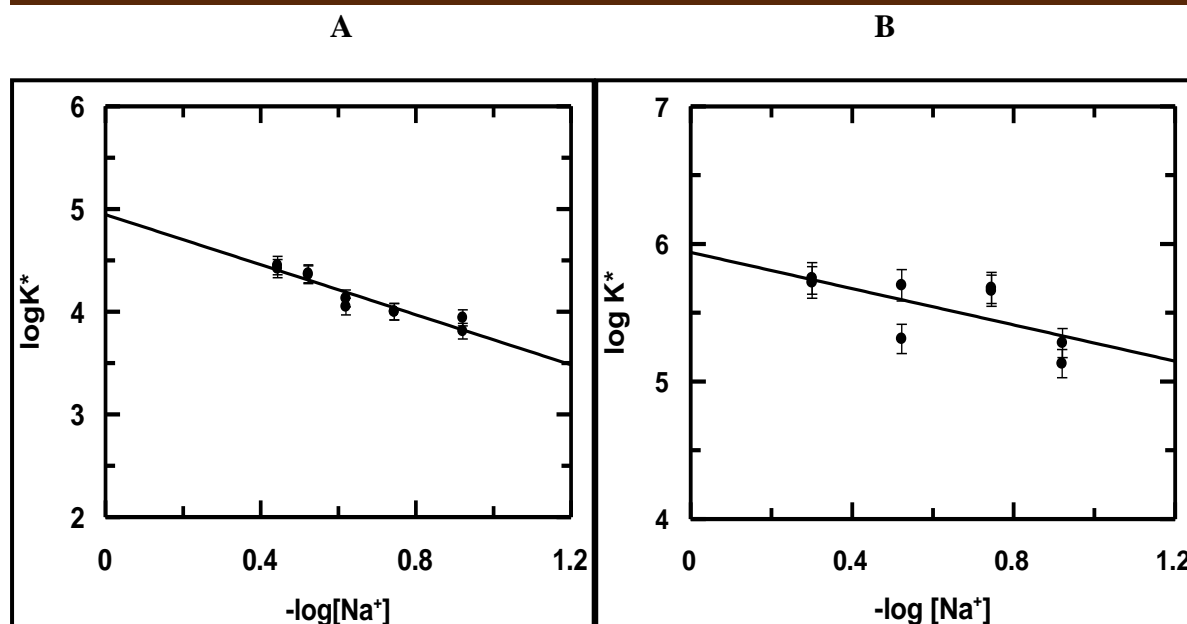


**Fig. 22:** Variation of overall binding constant of (A) alizarin and (B)  $\text{Mn}^{\text{II}}(\text{alz})_2$  with calf thymus DNA at different concentrations of NaCl at pH  $\sim 7.4$ ; Temperature = 298K.

Therefore, in a medium of high ionic strength hydroxy-9,10-anthraquinones (here alizarin) are likely to bind DNA much better as their anionic forms decrease; the compound being largely present as a neutral species in solution. Further to this, the presence of a metal ion in the complex makes DNA binding even better.

### 2.5.2 At different pH of the medium

Titration of  $\text{Mn}^{\text{II}}(\text{alz})_2$  with calf thymus DNA in the pH range 6.8 to 8.0 was followed at 520 nm. Figure 23 is a plot fitted to Eq. 10 (*Chapter 6: Experimental*) while Figure 24 is fitted by non-linear square fit analysis according to Eq. 12 (*Chapter 6: Experimental*) for a titration performed at pH 7.18. Both plots evaluate  $K_{\text{app}}$ . Inset of Figure 24 shows determination of  $n_b$ . Similar plots were obtained for titrations at other pH values also (Table 11). Data obtained were analyzed according to Eq. 13 as well (*Chapter 6: Experimental*) providing values for overall binding constant ( $K^*$ ) and site size of interaction “n” ( $n_b^{-1}$ ).<sup>53</sup> A modified Scatchard

plot for the complex interacting with calf thymus DNA at pH 7.18 is shown in Figure 23.

Results of Scatchard plots at all pH values are summarized in Table 11.

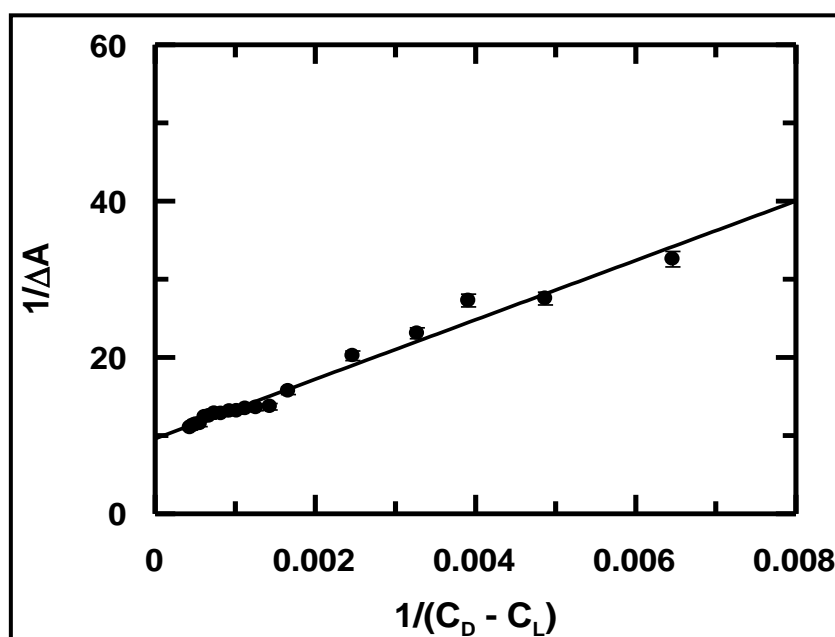


**Fig. 23:** Double reciprocal plot for  $[Mn^{II}(alz)_2]$  interacting with calf thymus DNA, followed by UV-Vis spectroscopy.  $[Mn^{II}(alz)_2] = 50 \mu M$ ,  $[NaCl] = 120 \mu M$ ,  $pH = 7.18$ ,  $T = 298 K$ .

**Table 11:** Variation of binding constants of the complex with calf thymus DNA at different pH

	pH	$K_{app}$			Site-size	$K_{app} \times n_b = K^*$	$K^*$ (from Scatchard)	Site-size
		From linear plot (a)	From Non-linear Plot(b)	Average $=(a+b)/2$				
[Mn <sup>II</sup> (LH) <sub>2</sub> ]	6.82	$0.10 \times 10^4$	$0.11 \times 10^4$	$0.11 \times 10^4$	16	$0.18 \times 10^5$	$0.15 \times 10^5$	13
	6.90	$0.84 \times 10^4$	$0.88 \times 10^4$	$0.86 \times 10^4$	15	$1.29 \times 10^5$	$0.60 \times 10^5$	6
	7.18	$0.26 \times 10^4$	$0.30 \times 10^4$	$0.28 \times 10^4$	16	$0.45 \times 10^5$	$0.44 \times 10^5$	10
	7.40	$0.87 \times 10^4$	$1.50 \times 10^4$	$1.19 \times 10^4$	16	$1.90 \times 10^5$	$1.38 \times 10^5$	8
	7.55	$1.39 \times 10^4$	$3.27 \times 10^4$	$2.33 \times 10^4$	14	$3.26 \times 10^5$	$1.53 \times 10^5$	7
	7.97	$0.91 \times 10^4$	$1.25 \times 10^4$	$1.08 \times 10^4$	14	$1.51 \times 10^5$	$0.65 \times 10^5$	10

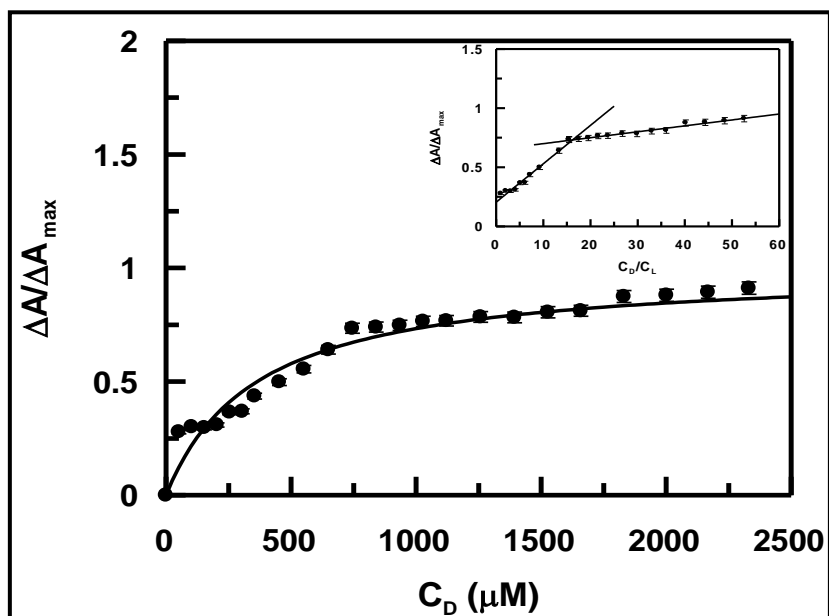


**Fig 24:** Binding isotherm of  $\text{Mn}(\text{alz})_2$  interacting with calf thymus DNA at pH 7.18. The corresponding non-linear fit is shown for a titration followed using UV-Vis spectroscopy. Inset: Plot of normalized increase in absorbance as a function of the ratio of calf thymus DNA to  $\text{Mn}^{\text{II}}(\text{alz})_2$ .  $[\text{Mn}(\text{alz})_2] = 50 \mu\text{M}$ ,  $[\text{NaCl}] = 120 \text{ mM}$ , Temperature = 298K.

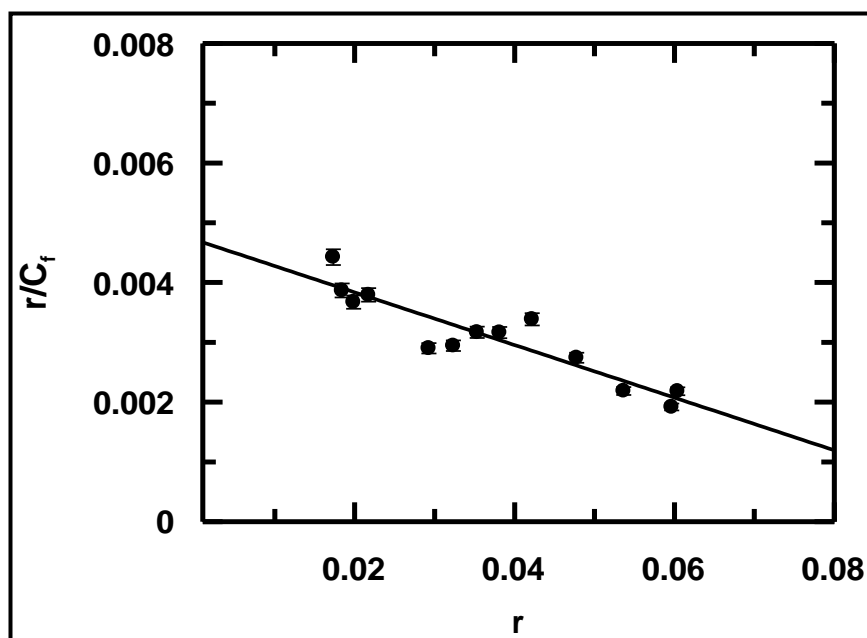


**Fig. 25:** Scatchard plot of interaction of  $\text{Mn}^{\text{II}}(\text{alz})_2$  with calf thymus DNA monitored at 520 nm;  $[\text{Mn}(\text{alz})_2] = 50\mu\text{M}$ ,  $[\text{NaCl}] = 120 \mu\text{M}$ , pH = 7.18, T = 298 K.



Unlike alizarin, binding constant values for the complex did not decrease with an increase in the pH of the medium (Fig. 26). In fact, values in Table 11 suggest they are higher than alizarin interacting with calf thymus DNA at each pH (Table 1 of *Chapter 7*). This is significant for it indicates complex formation prevents formation of anionic species on alizarin, that were earlier shown to be responsible for decreased binding with DNA.<sup>1,38</sup> The result is important from a biological point of view also because cancer patients experience fluctuation of pH in body fluids, a matter of concern on the application of several drugs.<sup>54,55</sup> Hence, if this complex is ever developed into a drug, at least its activity going by findings pertaining to DNA interaction may be said to be the same i.e. show similar activity over the physiological pH range.

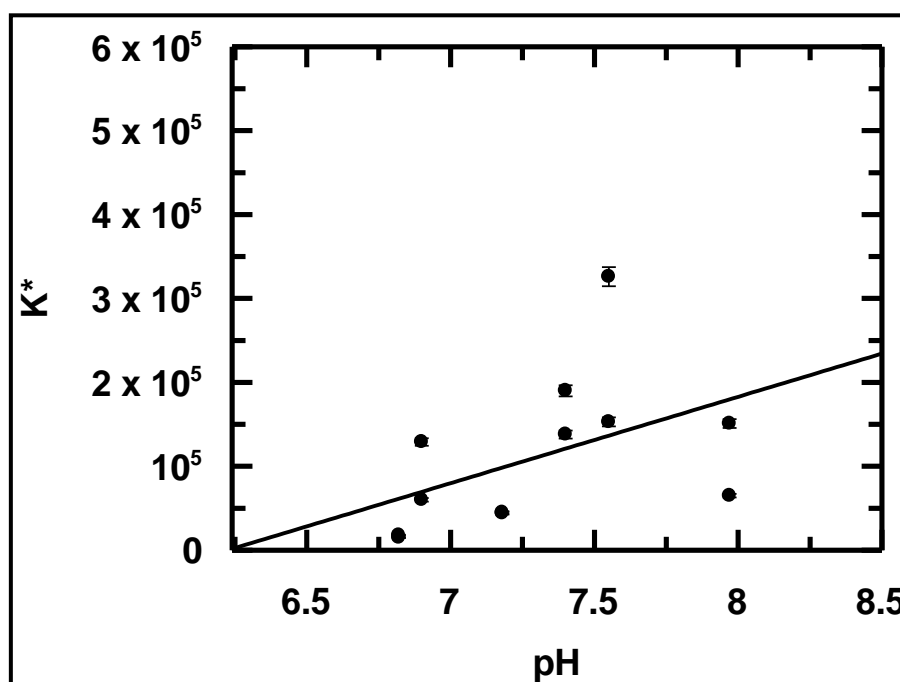


**Fig. 26:** Plot of variation of overall binding constant of  $Mn^{II}(alz)_2$  interacting with calf thymus DNA at different pH (maintained with tris buffer) at 298K and ionic strength of 0.12 M. [Results of two independent experiments is shown at each pH].

## 2.6. Detection of reactive oxygen species:

### 2.6.1 The NADH dehydrogenase assay:

The enzyme assay (discussed in *Chapter 6, Experimental*) was followed at 550 nm and involves the reduction of cytochrome c at 298 K. Concentration of alizarin or  $\text{Mn}^{\text{II}}(\text{alz})_2$  was varied from 0 to 50.0  $\mu\text{M}$ . Formation of superoxide radical anion catalyzed by alizarin or  $\text{Mn}^{\text{II}}(\text{alz})_2$  was measured from the reduction of cytochrome c inhibited by SOD in presence of NADH and NADH dehydrogenase (Fig. 27).<sup>1,5-13,56</sup>

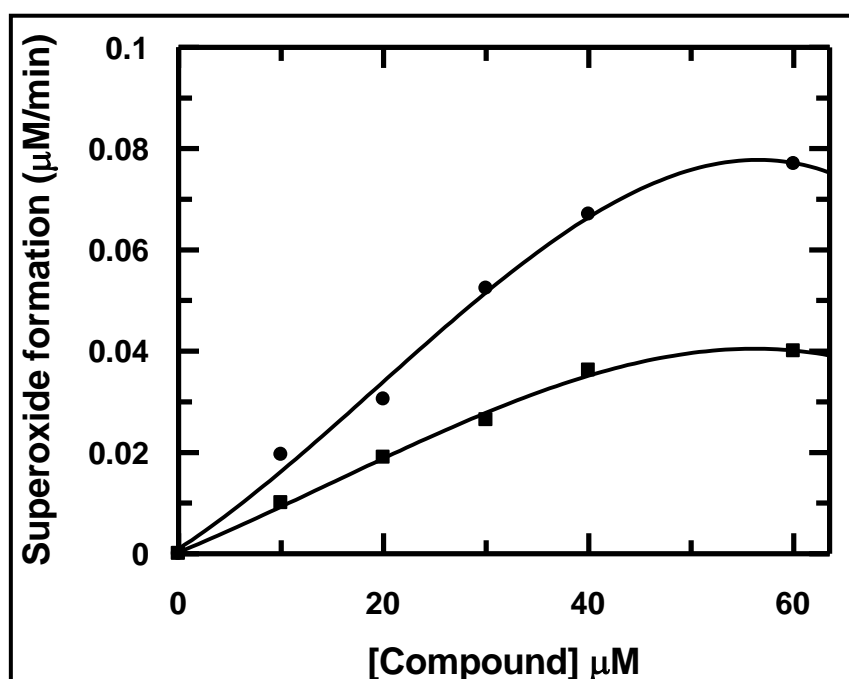


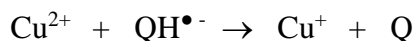
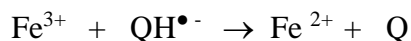
**Fig. 27:** Effect of alizarin and  $\text{Mn}^{\text{II}}(\text{alz})_2$  on superoxide formation by NADH dehydrogenase. Superoxide formation was determined from the rate of superoxide dismutase-inhibitable cytochrome c reduction using a spectrophotometer. The reaction mixture contained 100 mM Tris buffer (pH 7.4), 40.0  $\mu\text{g ml}^{-1}$  SOD, 160.0  $\mu\text{M}$  NADH, 80.0  $\mu\text{M}$  cytochrome c, 5  $\text{U l}^{-1}$  NADH dehydrogenase and the compounds being investigated; (●) alizarin; (■)  $\text{Mn}^{\text{II}}(\text{alz})_2$ .

Formation of superoxide radical anion in such enzyme assisted reactions occur when semiquinone formed on alizarin gets oxidized by molecular oxygen.<sup>1,5-13,56</sup> Following complex formation, this does not happen so easily on compounds like alizarin as it is now bound to a metal centre. Since one carbonyl of alizarin is involved in coordinating Mn(II) hence only the other carbonyl can form semiquinone when the complex is a participant in an electron transport chain of an enzyme assay. Hence, semiquinone formation decreases quite naturally in case of the complex leading to less formation of superoxide radical anion (Fig. 27).<sup>1,5-13,56</sup> Even if semiquinone is generated on the ligand (here alizarin), presence of a metal ion removes the electron from its site of formation by more than one mechanism.<sup>57</sup> This further decreases chances of semiquinone generation by complexes. As a direct consequence, the interaction of semiquinone formed on the complex with molecular oxygen also decreases considerably which is observed in Fig. 27. However, Mn<sup>II</sup>, like Co<sup>II</sup>, Ni<sup>II</sup> or Pd<sup>II</sup> lacking a stable lower oxidation state, unlike Fe<sup>III</sup> or Cu<sup>II</sup>, decrease in superoxide radical anion formation is comparatively less than Cu<sup>II</sup> or Fe<sup>III</sup> complexes of anthracyclines or their analogues.<sup>1,4-15,18</sup> Fig. 27 is comparable to that observed for a Co<sup>II</sup> complex of quinalizarin<sup>8</sup> but significantly different from Cu<sup>II</sup> or Fe<sup>III</sup> complexes of hydroxy-9,10-anthraquinones.<sup>1,9-13,18</sup> In case of metal ions having a stable lower oxidation state, electron transfer from semiquinone radical anion to the metal centre [say for Cu<sup>II</sup> or Fe<sup>III</sup>] results in the generation of their corresponding lower oxidation state [Cu<sup>I</sup> or Fe<sup>II</sup>]. Subsequently, hydrogen peroxide or other peroxy species present in the medium re-oxidize the lower oxidation state to its original state and in the process generate HO•. HO• is an established damaging agent for different cellular organelles and enhances cytotoxicity due to the compound towards target cells. This is over and above that achieved with a hydroxy-9,10-anthraquinone. Therefore, inspite of a decrease in semiquinone formation by Cu<sup>II</sup> or Fe<sup>III</sup> complexes (that decrease cardiotoxic side effects), there is also a simultaneous increase in HO• that enhances cytotoxic action. Hence,

## *Chapter 8: Characterization of a Mn(II)...with anthracycline antibiotics*

---

the compromise that complexes were expected to make with regard to efficacy following decrease in semiquinone formation is not really observed. In fact, such complexes where the metal ion has a stable lower oxidation state are seen to be more efficient, when actually a loss in cytotoxic activity was expected.<sup>1,9-13,17-19</sup>



However, in case of this complex (having  $\text{Mn}^{\text{II}}$  as the metal ion), since semiquinone or superoxide radical anion formation is not decreased to the extent observed for  $\text{Cu}^{\text{II}}$  or  $\text{Fe}^{\text{III}}$  complexes, cytotoxicity owing to free radical formation would not be totally compromised.<sup>1,4,5,7,9,11-13,17,18</sup> This is also an advantage. Hence,  $\text{Mn}^{\text{II}}(\text{alz})_2$  if promoted as an anticancer agent, it should be able to hold on to a substantial part of the cytotoxic activity due to alizarin in the free radical pathway and yet be less cardiotoxic i.e. dual advantage.<sup>1,2,4-13,18</sup> Besides, complexes have several other attributes that help them show better anticancer activity than hydroxy-9, 10-anthraquinones (here alizarin) taking the efficacy of metal-hydroxy-9,10-anthraquinones close to that of some of the established anticancer agents.<sup>1-19</sup>

### **2.6.2 The H<sub>2</sub>DCFDA assay:**

While the NADH dehydrogenase assay is a well-established technique for detecting ROS generation it is nevertheless a model study. A more realistic approach for detecting ROS is the H<sub>2</sub>DCFDA assay.<sup>58-61</sup> Here compounds were tried on cell lines. For this study, we used two cancer cell lines, HeLa and HepG2 and normal WI-38 lung fibroblast cells. As has been mentioned earlier (*Chapter 6, Experimental*) cells were previously treated with compounds at

their respective IC<sub>50</sub> concentrations determined by the MTT assay for 30 minutes. For such treated cells, ROS generation was followed after the addition of H<sub>2</sub>O<sub>2</sub> (~ 70 μM).

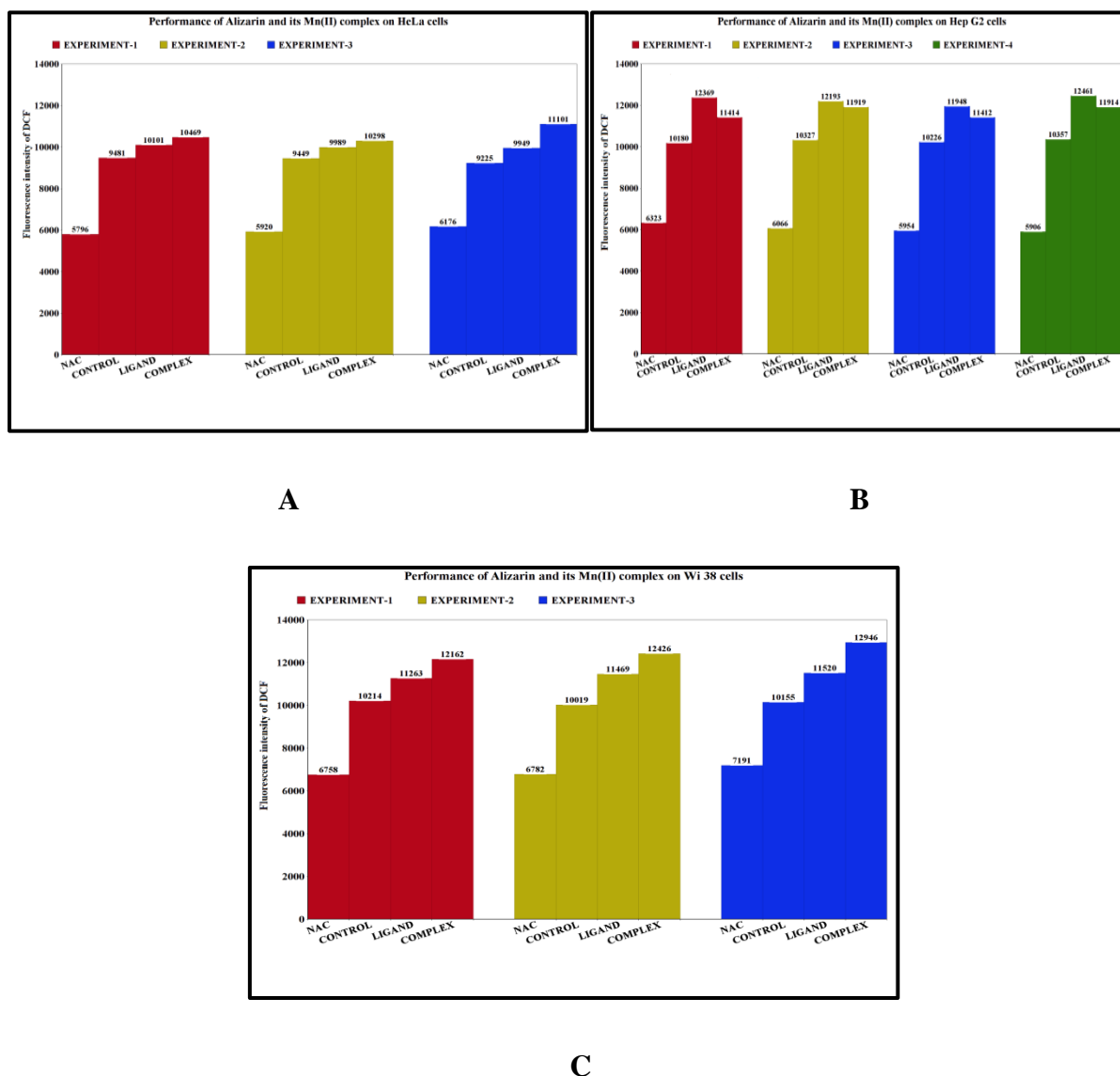


**Fig. 28:** Effect of alizarin and Mn(alz)<sub>2</sub> on the presence of ROS within (A) HeLa cells, (B) Hep G2 cells and (C) WI 38 lung fibroblast cells, detected by the H<sub>2</sub>DCFDA assay; ROS was generated using H<sub>2</sub>O<sub>2</sub>. In each diagram, NAC refers to cells treated with N-acetyl cysteine, CONTROL refers to cells not treated with any compound, LIGAND refers to cells treated with alizarin and COMPLEX refers to cells treated with Mn(alz)<sub>2</sub>. Different colors indicate separate experiments.

ROS formation in cells treated with a compound was substantially higher than when the same cells were treated with N-acetyl cysteine (NAC), a standard ROS quencher. It was even higher than experiments where cells were not treated with any compound i.e. treated only with H<sub>2</sub>O<sub>2</sub>. Experiments indicate, for all three cell lines, alizarin and its Mn(II) complex tend to amplify ROS introduced into the system using H<sub>2</sub>O<sub>2</sub>. For HeLa cells, a clear distinction could not be made between ROS amplification due to alizarin and Mn(alz)<sub>2</sub> (Fig. 28 A) while for HepG2 cells, a slight increase in ROS was observed for cells treated with alizarin than those that were treated with the complex (Fig. 28 B). In other words, in terms of ROS quenching although not substantial, there were less ROS in cells treated with the complex than those that were treated with alizarin. In case of WI 38 lung fibroblast (normal) cells, greater amount of ROS was detected in cells treated with Mn(alz)<sub>2</sub> than in cells treated with alizarin (Fig. 28 C).

### **2.7 Effect of alizarin and Mn<sup>II</sup>(alz)<sub>2</sub> on two different cancer cells and a normal cell**

MTT assay performed on cancer cells (HeLa and Hep G2) and on WI 38 lung fibroblast (normal) cells reveal (Fig. 29, A-F) compounds were more effective on carcinoma cells than on normal cells. Cell viability studies obtained for each cell line fitted to the ED<sub>50</sub> plus program provides IC<sub>50</sub> values for the compound on that cell line. From the data in Table 12 it appears that the performance of alizarin was slightly better on HeLa cells while Mn(alz)<sub>2</sub> performed better on HepG2 cells. On WI 38 lung fibroblast cells, IC<sub>50</sub> for alizarin was significantly higher indicating alizarin is less cytotoxic on normal cells. IC<sub>50</sub> of the complex on normal cells was comparable to that on HeLa cells but higher than Hep G2 cells. Hence, the MTT assay suggests Mn(alz)<sub>2</sub> is effective on Hep G2 cells.

Table 12: IC<sub>50</sub> values of compounds on three different cell lines

Compounds	Hep G2 cells IC <sub>50</sub> value (μM)		HeLa cells IC <sub>50</sub> value (μM)		WI 38 lung fibroblast cells IC <sub>50</sub> value (μM)	
	From the ED <sub>50</sub> plus program	From Graph	From the ED <sub>50</sub> plus program	From Graph	From the ED <sub>50</sub> plus program	From Graph
<b>Alizarin</b>	79.27	62.00	75.11	52.00	106.60	100.00
<b>Mn<sup>II</sup>(alz)<sub>2</sub></b>	65.36	50.00	90.51	60.00	89.10	72.00
<b>*cisplatin</b>	$(14.87 \pm 1.22)^{62}$		$(54.07 \pm 12.25)^{62}$			
<b>*Doxorubicin</b>	$(4.68 \pm 1.08)^{62}$		$(4.07 \pm 0.26)^{62}$			

\* The data for cisplatin and doxorubicin provided in the table was taken from literature to compare the performance of Mn(alz)<sub>2</sub> with some standard anticancer agents.

Cell viability results for alizarin and Mn(alz)<sub>2</sub> on three different cell lines

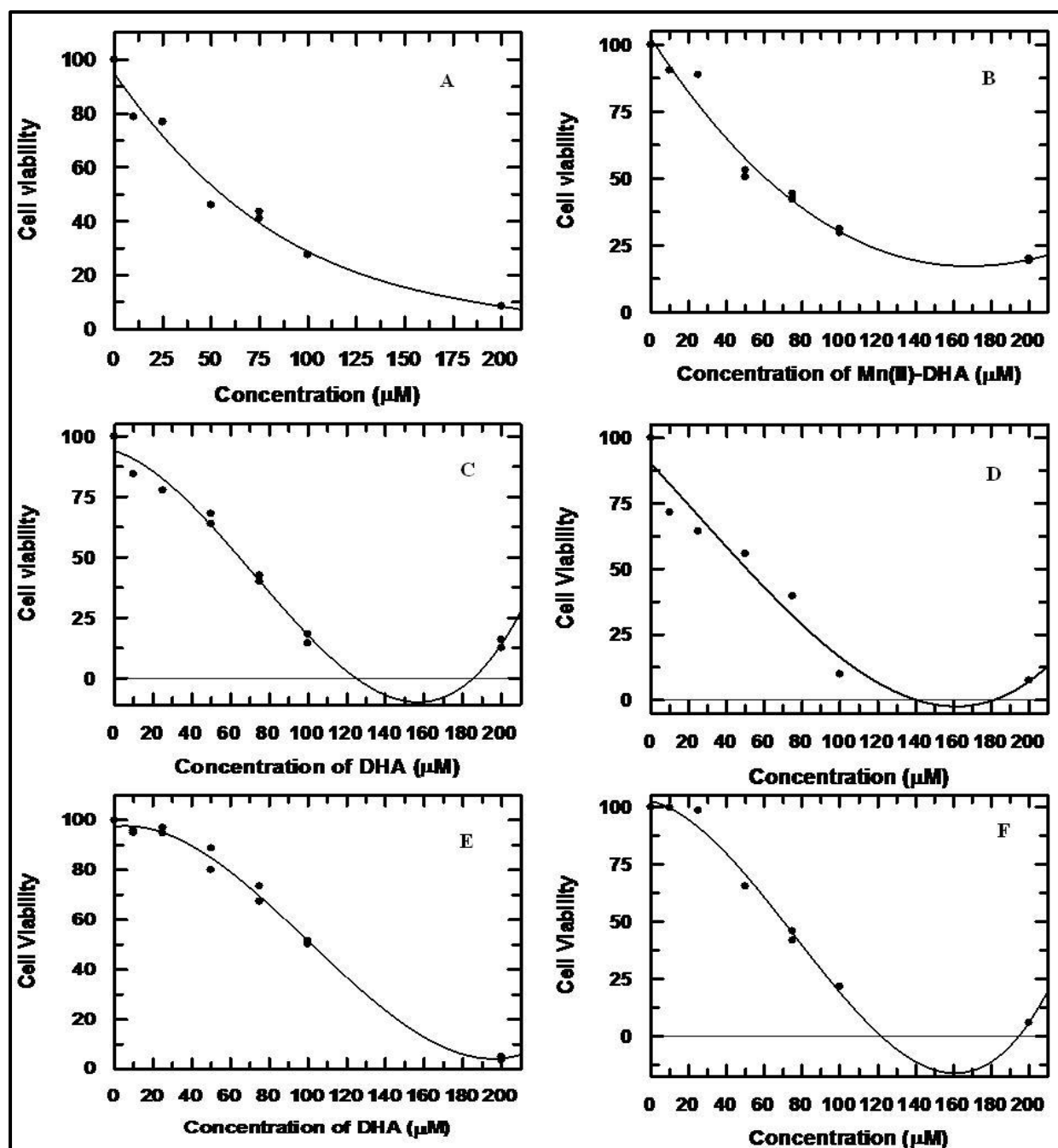


Fig. 29: Plots showing dose response curves for the effect of alizarin (A) and Mn(alz)<sub>2</sub> (B) on HeLa cells, alizarin (C) and Mn(alz)<sub>2</sub> (D) on Hep G2 cells and alizarin (E) and Mn(alz)<sub>2</sub> (F) on WI 38 lung fibroblast cells after the cells were treated with the respective compounds for 48 hours and MTT assay performed.



Therefore Mn(alz)<sub>2</sub> having a higher binding affinity for calf thymus DNA than alizarin, that follows an increasing trend under varying conditions of ionic strength and over a considerable pH range, may be used on cancer patients who experience fluctuation in electrolyte concentration in body fluids and in pH during treatment. The complex was found to amplify ROS present in cells that could come handy in promoting cytotoxic activity. With decreased superoxide formation, increased affinity towards DNA, Mn(alz)<sub>2</sub> could just be having the essential qualities of a potential anticancer agent.

#### **4. References:**

- [1] P. Das, C. K. Jain, S. K. Dey, R. Saha, A. D. Chowdhury, S. Roychoudhury, S. Kumar, H. K. Majumder, S. Das. 2014. Synthesis, crystal structure, DNA interaction and in vitro anticancer activity of a Cu(II) complex of purpurin: dual poison for human DNA topoisomerase I and II. *RSC Adv.* 4: 59344-59357.
- [2] S. Mukherjee, P.K. Gopal, S. Paul, S. Das. 2014. Acetylation of 1,2,5,8-tetrahydroxy-9,10-anthraquinone improves binding to DNA and shows enhanced superoxide formation that explains better cytotoxicity on JURKAT T lymphocyte Cells. *J. Anal Oncol.* 3: 122-129.
- [3] P. Das, D. Bhattacharya, P. Karmakar, S. Das. 2015. Influence of ionic strength on the interaction of THA and its Cu(II) complex with DNA helps to explain studies on various breast cancer cells. *RSC Adv.* 5: 73099-73111.
- [4] P. Mondal, S. Roy, G. Loganathan, B. Mandal, D. Dharumadurai, M. A. Akbarsha, P. S. Sengupta, S. Chattopadhyay, P. S. Guin. 2015. 1-Amino-4-hydroxy-9,10-anthraquinone – An analogue of anthracycline anticancer drugs, interacts with DNA and induces apoptosis in human MDA-MB-231 breast adenocarcinoma cells: Evaluation of structure–activity relationship using computational, spectroscopic and biochemical studies. *Biochem. Biophys. Rep.* 4: 312-323.

- [5] P. Das, C. K. Jain, S. Roychoudhury, H. K. Majumder, S. Das. 2016. Design, synthesis and in vitro anticancer activity of a Cu(II) complex of carminic acid: A novel small molecule inhibitor of human DNA topoisomerase I and topoisomerase II. *ChemistrySelect*. 1: 6623-6631.
- [6] B. Mandal, S. Singha, S. K. Dey, S. Mazumdar, T. K. Mondal, P. Karmakar, S. Kumar, S. Das. 2016. Synthesis, crystal structure from PXRD of a Mn<sup>II</sup>(purp)<sub>2</sub> complex, interaction with DNA at different temperatures and pH and lack of stimulated ROS formation by the complex. *RSC Adv*. 6: 51520-51532.
- [7] B. Mandal, S. Singha, S.K. Dey, S. Mazumdar, S. Kumar, P. Karmakar, S. Das. 2017. Cu<sup>II</sup> complex of emodin with improved anticancer activity as demonstrated by its performance on HeLa and Hep G2 cells. *RSC Adv*. 7: 41403-41418.
- [8] S. Mukherjee-Chatterjee, C. K. Jain, S. Singha, P. Das, S. Roychoudhury, H. K. Majumder, S. Das. 2018. Activity of Co<sup>II</sup>-Quinalizarin: A novel analogue of anthracycline-based anticancer agents targets human DNA topoisomerase, whereas quinalizarin itself acts via formation of semiquinone on acute lymphoblastic leukemia MOLT-4 and HCT 116 cells. *ACS Omega*. 3:10255-10266.
- [9] M. M. L. Fiallo, A. Garnier-Suillerot. 1985. Physicochemical studies of the iron(III)-carminomycin complex and evidence of the lack of stimulated superoxide production by NADH dehydrogenase. *Biochim. Biophys. Acta*. 840: 91-98.
- [10] M. M. L. Fiallo, A. Garnier-Suillerot. 1986. Metal anthracycline complexes as a new class of anthracycline derivatives. Palladium(II)-adriamycin and palladium(II)-daunorubicin complexes: physicochemical characteristics and antitumor activity. *Biochemistry*. 25: 924-930.

- [11] S. Das, A. Saha, P. C. Mandal. 1996. Studies on the formation of Cu(II) and Ni(II) complexes of 1,2-dihydroxy-9,10-anthraquinone and lack of stimulated superoxide formation by the complexes. *Talanta*. 43: 95-102.
- [12] P. S. Guin, S. Das, P. C. Mandal. 2009. Studies on the formation of a complex of Cu(II) with sodium 1,4-dihydroxy-9,10-anthraquinone-2-sulphonate – An analogue of the core unit of anthracycline anticancer drugs and its interaction with calf thymus DNA. *J. Inorg. Biochem.* 103: 1702-1710.
- [13] S. Roy, P. Mondal, P.S. Sengupta, D. Dhak, R.C. Santra, S. Das, P.S. Guin. 2015. Spectroscopic, computational and electrochemical studies on the formation of the copper complex of 1-amino-4-hydroxy-9,10-anthraquinone and effect of it on superoxide formation by NADH dehydrogenase. *Dalton Trans.* 44: 5428-5440.
- [14] S. E. Lipshultz, J. A. Alvarez, R. E. Scully. 2008. Anthracycline associated cardiotoxicity in survivors of childhood cancer. *Heart*. 4: 525-533.
- [15] C. Vergely, S. Delemasure, Y. Cottin, L. Rochette. 2007. Preventing the cardiotoxic effects of anthracyclines: From basic concepts to clinical data. *Heart and Metabolism* 35: 1-7.
- [16] M. M. L. Fiallo, A. Garnier-Suillerot, B. Matzanke, H. Kozlowski. 1999. How Fe<sup>3+</sup> binds anthracycline antitumour compounds: The myth and the reality of a chemical sphinx. *J. Inorg. Biochem.* 75: 105-115.
- [17] S. Das, A. Saha, P. C. Mandal. 1997. Radiation-Induced double-strand modification in calf thymus DNA in the presence of 1,2-dihydroxy-9,10-anthraquinone and its Cu(II) complex. *Environ. Health Pers.* 105: 1459-1462.
- [18] S. Das, A. Saha, P. C. Mandal. 1995. Radiosensitization of thymine by Fe(III)-1,2-dihydroxyanthraquinone complex in dilute aqueous solution. *J. Rad. Nucl. Chem.* 196: 57–63.

## ***Chapter 8: Characterization of a Mn(II)...with anthracycline antibiotics***

---

- [19] S. Das, P. C. Mandal. 2009. Influence of Ni(II) and Fe(III) complexes of 1,2 dihydroxy 9,10 anthraquinone on the modification in calf thymus DNA upon gamma irradiation. *Rad. Phys. Chem.* 78: 37-41.
- [20] J. Butler, B.M. Honey. 1987. Are reduced quinones necessarily involved in the antitumour activity of quinone drugs? *Br. J. Cancer Suppl.* 8: 53-59.
- [21] D. G. Sushkov, N. P. Gritsan, L. M. Weiner. 1987. Generation of OH radical during enzymatic reduction of 9,10-anthraquinone-2-sulphonate Can semiquinone decompose hydrogen peroxide? *FEBS Lett.* 225: 139-144.
- [22] T. C. Johnstone, E. M. Nolan. 2015. Beyond iron: non-classical biological functions of bacterial siderophores. *Dalton Trans.* 44: 6320-6339.
- [23] R. J. Debus. 2000. In: Metal ions in biological systems: Manganese and its role in biological processes. *Dekker Marcel, New York.* 657–711.
- [24] R. S. Magliozzo, J. A. Marcinkeviciene. 1997. The role of Mn(II)-peroxidase activity of mycobacterial catalase-peroxidase in activation of the antibiotic isoniazid. *J. Biol. Chem.* 272: 8867-8870.
- [25] D. G. Kehres, M. E. Maguire. 2003. Emerging themes in manganese transport, biochemistry and pathogenesis in bacteria. *FEMS Microbiol. Rev.* 27: 263-290.
- [26] A. Takeda. 2003. Manganese action in brain function. *Brain Res. Rev.* 41: 79-87.
- [27] R. Caspi, B.M. Tebo, M. G. Haygood. 1998. c-type cytochromes and Manganese oxidation in pseudomonas putida MnB1. *Appl. Environ. Microbiol.* 64: 3549-3555.
- [28] J. P. M. de Vrind, G. J. Brouwers, P. L. A. M. Corstjens, J. den Dulk, E. W. de Vrind-de Jong. 1998. The cytochrome c maturation operon is involved in manganese oxidation in pseudomonas putida GB-1. *Appl. Environ. Microbiol.* 64: 3556-3562.

- [29] G.-J. Brouwers, J. P. M. de Vrind, P. L. A. M. Corstjens, P. Cornelis, C. Baysse, E. W. de Vrind-de Jong. 1999. cumA, a gene encoding a multicopper oxidase, is involved in Mn<sup>2+</sup> oxidation in pseudomonas putida GB-1. *Appl. Environ. Microbiol.* 65: 1762-1768.
- [30] E. H. Rubin, W. N. Hait. 2000. Anthracyclines and DNA intercalators / epipodophyllotoxins / DNA topoisomerases. In *Holland-Frei Cancer Medicine*, B C Decker, Hamilton (ON), fifth ed. Chapter 49.
- [31] D. A. Gewirtz. 1999. A critical evaluation of the mechanisms of action proposed for the antitumor effects of the anthracycline antibiotics adriamycin and daunorubicin. *Biochem. Pharmacol.* 57: 727-741.
- [32] V. Kr̃en, T. R̃ezanka. 2008. Sweet antibiotics – the role of glycosidic residues in antibiotic and antitumor activity and their randomization. *FEMS Microbiol. Rev.* 32: 858-889.
- [33] Y. Pommier, E. Leo, H.L. Zhang, C. Marchand. 2010. DNA topoisomerases and their poisoning by anticancer and antibacterial drugs. *Chem. Biol.* 17: 421-433.
- [34] G. Lenglet, M. H. David-Cordonnier. 2010. DNA-destabilizing agents as an alternative approach for targeting DNA: Mechanisms of action and cellular consequences. *J. Nucl. Acids.* <https://doi.org/10.4061/2010/290935>, Article ID 290935, 17 pages.
- [35] T. Banerjee, S. Banerjee, S. Sett, S. Ghosh, T. Rakshit, R. Mukhopadhyay. 2016. Discriminating intercalative effects of threading intercalator nogalamycin, from classical intercalator daunomycin, using single molecule atomic force spectroscopy. *PLoS ONE.* 11(5), e0154666.
- [36] G. Cozza, M. Mazzorana, E. Papinutto, J. Bain, M. Elliott, G. di Maira, A. Gianoncelli, M. A. S. Sarno, M. Ruzzene, R. Battistutta, F. Meggio, S. Moro, G. Zagotto, L. A. Pinna. 2009. Quinalizarin as a potent, selective and cell-permeable inhibitor of protein kinase CK2. *Biochem J.* 421: 387-395.

- [37] B. Mandal, H. K. Mondal, S. Das. 2019. In situ reactivity of electrochemically generated semiquinone on emodin and its CuII/MnII complexes with pyrimidine based nucleic acid bases and calf thymus DNA: Insight into free radical induced cytotoxicity of anthracyclines. *Biochem. Biophys. Res. Comm.* 515: 505-509.
- [38] S. Mukherjee, P. Das, S. Das. 2012. Exploration of small hydroxy-9,10-anthraquinones as anthracycline analogues: physicochemical characteristics and DNA binding for comparison. *J. Phys. Org. Chem.* 25: 385-393.
- [39] K. Nakamoto. 1978. Infrared and Raman Spectra of Inorganic and Coordination Compounds, third ed. *Wiley-Interscience, New York, USA.*
- [40] M. Di Vaira, P. Orioli, F. Piccioli, B. Bruni, L. Messori. 2003. Structure of a Terbium(III)–quinizarine complex: The first crystallographic model for metalloanthracyclines. *Inorg. Chem.* 42:3157-3159.
- [41] S. Du, J. Feng, X. Lu, G. Wang. 2013. The syntheses and characterizations of vanadium complexes with 1,2-dihydroxyanthraquinone and the structure–effect relationship in their in vitro anticancer activities. *Dalton Trans.* 42: 9699-9705.
- [42] B. Trzaskowski, A. Les, L. Adamowicz. 2003. Modelling of octahedral manganese II complexes with inorganic ligands: A Problem with Spin-States. *Int. J. Mol. Sci.* 4: 503-511.
- [43] S. Pramanik, S. Roy, T. Ghorui, S. Ganguly and K. Pramanik. 2016. Iridium(III) mediated reductive transformation of closed-shell azo-oxime to open-shell azo-imine radical anion: Molecular and electronic structure, electron transfer, and optoelectronic properties. *Inorg. Chem.* 55: 1461-1468.
- [44] T. Lis. 1980. Structure of Mn(II) Glycolate dehydrate. *Acta Cryst B*36, 701-703.

- [45] Y. C. Chen, F. S. Guo, J. L. Liu, J. D. Leng, P. Vrbel, M. Orend, J. Prokleska, V. Sechovsky, M. L. Tong. 2014. Switching of the magnetocaloric effect of MnII glycolate by water molecules. *Chem. Eur. Jour.* 20: 3029 – 3035.
- [46] D. Esteves, C. D. Tedesco, S. S. Pedro, C. Cruz, M. S. Reis, P. Brandão. 2014. New manganese (II) structures derived from 2, 6-dichlorobenzoic acid: Syntheses, crystal structures and magnetism. *Mater. Chem. Phys.* 147: 611-616.
- [47] X. M. Zhang, X. B. Li, E. Q. Gao. 2011. Metal–organic supramolecular architectures derived from a new zwitterionic dicarboxylate ligand. *Jour. Coord. Chem.* 64: 244–255.
- [48] Y. F. Yue, W. Sun, E.Q. Gao, C. J. Fang, S Xu, C. H. Yan. 2007. Syntheses and crystal structures of three Mn(II) complexes with 2-hydroxynicotinate. *Inor. Chim. Acta.* 360: 1466–1473.
- [49] R. L. Martin. 2003. Natural transition orbitals. *J. Chem. Phys.* 118: 4775-4777.
- [50] (a) T. Lu, F. Chen. 2012. Quantitative analysis of molecular surface based on improved marching tetrahedra algorithm. *J. Mol. Graph. Model.* 38: 314-323. (b) T. Lu, F. Chen. 2012. Multiwfn: A multifunctional wavefunction analyzer. *J. Comput. Chem.* 33: 580-592.
- [51] K. L. Haas, K. J. Franz. 2009. Application of metal coordination chemistry to explore and manipulate cell biology. *Chem. Rev.* 109: 4921-4960.
- [52] R. A. G. Friedman, G. S. Manning. 1984. Polyelectrolyte effects on site-binding equilibria with application to the intercalation of drugs into DNA. *Biopolymers.* 23: 2671-2714.
- [53] G. Scatchard. 1949. The attractions of proteins for small molecules and ions. *Ann. NY Acad. Sci.* 51: 660-672.
- [54] G. K. Schwalfenberg. 2012. Incorporating Environmental Health in Clinical Medicine. *J. Environ. Pub Health.* 6: 727630, 7 pages.

- [55] B. P. Mahoney, N. Raghunand, B. Baggett, R. J. Gillies. 2003. Tumor acidity, ion trapping and chemotherapeutics. I. Acid pH affects the distribution of chemotherapeutic agents in vitro. *Biochem. Pharmacol.* 66: 1207-1218.
- [56] H. R. Mahler. 1955. In: *Methods in Enzymology* 11, Academic Press, New York, USA, pp. 668–672.
- [57] S. Das, A. Bhattacharya, P. C. Mandal, M. C. Rath, T. Mukherjee. 2002. One-electron reduction of 1,2-dihydroxy-9,10-anthraquinone and some of its transition metal complexes in aqueous solution and in aqueous isopropanol–acetone-mixed solvent: a steady-state and pulse radiolysis study. *Rad. Phys. Chem.* 65: 93-100.
- [58] H. Wang, J. A. Joseph. 1999. Quantifying cellular oxidative stress by dichlorofluorescein assay using microplate reader. *Free Radical Biol. Med.* 27: 612-616
- [59] O. Myhre, J. M. Andersen, H. Aarnes, F. Fonnum. 2003. Evaluation of the probes 2',7'-dichlorofluorescein diacetate, luminol, and lucigenin as indicators of reactive species formation. *Biochem. Pharmacol.* 65: 1575-1582.
- [60] A. Gomes, E. Fernandes, J. L. Lima. 2005. Fluorescence probes used for detection of reactive oxygen species. *J. Biochem. Biophys.* 65: 45-80.
- [61] A. Pramanik, D. Laha, S. Chattopadhyay, S. K. Dash, S. Roy, P. Pramanik, P. Karmakar. 2015. Targeted delivery of “copper carbonate” nanoparticles to cancer cells in vivo. *Toxicol. Res.* 4: 1604-1612.
- [62] A. D. Nurcahyanti, M. Wink. 2016. L-Canavanine potentiates the cytotoxicity of doxorubicin and cisplatin in arginine deprived human cancer cells. *Peer J.* 4:e1542  
<https://doi.org/10.7717/peerj.1542>



# CHAPTER 9

**A Cobalt<sup>II</sup>/Cobalt<sup>III</sup> complex of alizarin analyzed from the stand point of DNA binding, ROS generation and anticancer drug prospecting**



## **1. Introduction**

Studies on metal complex formation of anthracyclines reveal it leads to decreased semiquinone formation during electron transfer reactions and that the complexes usually have higher efficacy than the parent drugs.<sup>1-5</sup> Complex formation also decreases the tendency of anthracyclines to show cardiotoxic side effects.<sup>4-11</sup> Another relevant issue is the cost associated with anthracyclines, which is a major obstacle in patient care for economically challenged families.<sup>12-14</sup> The aspect of administration of drugs, important in chemotherapy, there is a search for molecules that address issues concerning anthracyclines. Again, these alternatives must have close resemblance to the established efficacy of anthracyclines.<sup>15-21</sup> Studies have shown, in spite of considerable similarity in structure and electronic properties, anthracyclines and hydroxy-9,10-anthraquinones differ significantly in aspects related to biophysical/biochemical interactions, with the latter trailing behind.<sup>15-23</sup> Apart from emodin and to some extent quinalizarin, not much is reported for the other hydroxy-9,10-anthraquinones in clinical trials or in advanced bio-medical research although good number of laboratory based data exist.<sup>22-28</sup> Going by the information available, efficacy of hydroxy-9,10-anthraquinones and its complexes in comparison to anthracyclines is far from being called satisfactory. What is encouraging is that hydroxy-9,10-anthraquinones show an almost similar ability to participate in electron transfer processes like anthracyclines.<sup>15-21,29,30</sup> Studies reveal anthracyclines have a distinct role due to the glycosyl group (sugar).<sup>15-21,29,30</sup> Therefore, in choosing to work with hydroxy-9,10-anthraquinones (the aglycones of anthracyclines), the role of the glycosyl unit is sacrificed which has to be made up in some other way. This is a major reason for the observed differences between anthracyclines and hydroxy-9,10-anthraquinones.<sup>15-21,29,30</sup> Although the representative aglycones are less costly, the purpose behind selecting them i.e. to replace anthracyclines requires proper

## ***Chapter 9: A Cobalt<sup>II</sup>/Cobalt<sup>III</sup> complex of alizarin..... a simpler anthracycline analogue***

investigation.<sup>15-21, 29, 30</sup> While simpler hydroxy-9,10-anthraquinone analogues are cheaper, their efficacy is also less.

Like in case of anthracyclines, complex formation of the simpler analogues (hydroxy-9,10-anthraquinones) control the generation of superoxide radical anion that help in decreasing toxic side effects.<sup>1, 2, 15-20</sup> Increasing efficacy of simpler analogues to compare with anthracyclines have met with limited success; a challenge that accompanies such drug simplification processes. What is however encouraging is that, complexes of several hydroxy-9,10-anthraquinones show attributes owing to a combined presence of a metal ion and quinone moiety that together make them better anticancer agents.<sup>1, 2, 4-6, 15-21</sup>

This study is able to show that complex formation of hydroxy-9,10-anthraquinones result in improved activities from a biological point of view in comparison to its parent hydroxy-9,10-anthraquinone. Although the possibility of decreased efficacy in the free radical pathway exist, complexes of hydroxy-9,10-anthraquinones are close in performance to anthracyclines; in some cases, even slightly better.<sup>15-21,29-31</sup> The mechanism of anticancer activity due to anthracyclines or hydroxy-9,10-anthraquinones and their metal complexes are different.<sup>4, 9, 17-21</sup> Although a complete mechanism of anthracycline functioning is still not very clear, several things are however known.<sup>3,7-11</sup> These may not be the same for the complexes. In fact, this study suggests that they are indeed different, depending considerably on the metal ion present. Metal ions used are bio-friendly, possessing a stable higher oxidation state. A Co<sup>II</sup> complex of a hydroxy-9,10-anthraquinone is different from Cu<sup>II</sup> or Fe<sup>III</sup> complexes in the sense that in the latter, the metal ions possess a stable lower oxidation state.<sup>1, 2, 4, 6, 15, 17-21</sup>

## 2. Results and Discussion:

### 2.1 Determination of stoichiometry of interaction between Co<sup>II</sup> and alizarin using mole ratio and Job's method of continuous variation:

Determination of composition of the complex was done in solution phase. For a determination by the mole ratio method, Co<sup>II</sup> was kept constant while alizarin was varied. Absorbance recorded at 429 nm was plotted against  $(T_L/T_M)_{TM}$  (Fig. 1A);  $T_M$  refers to fixed concentration of Co<sup>II</sup> while  $T_L$  indicates varying concentrations of alizarin. Data points were fitted to a linear equation yielding two straight lines. The intersection indicates stoichiometry of complex formation.

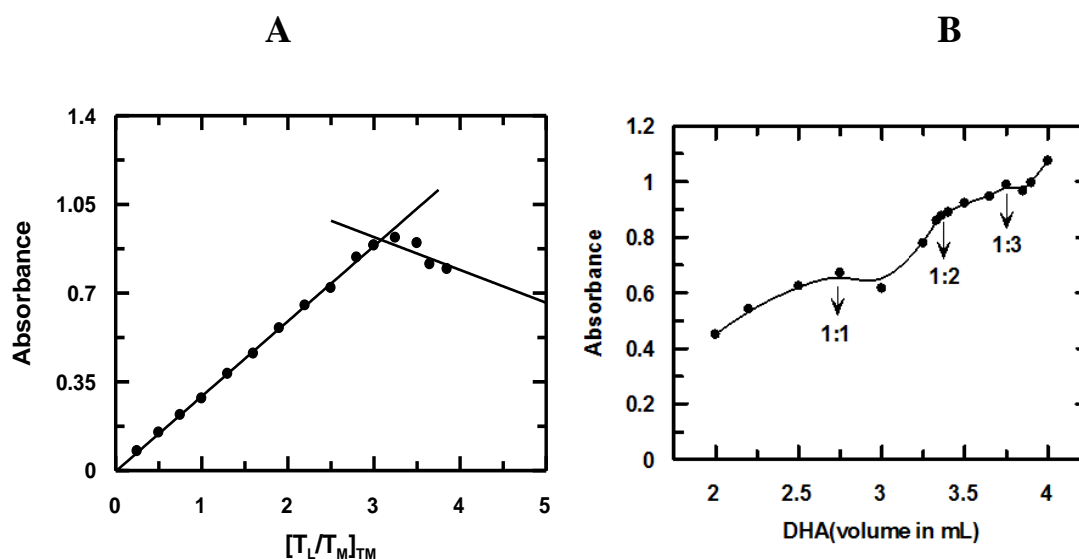


**Fig. 1:** Plots showing variation in absorbance at 429 nm for (A) change in ratio of alizarin to Co<sup>II</sup> for a fixed concentration of Co<sup>II</sup> (= 50  $\mu$ M) and (B) continuous variation of concentration of alizarin and Co<sup>II</sup> at physiological pH (~7.4). For (B), the strength of stock solutions of Co<sup>II</sup> and alizarin were 100  $\mu$ M; [NaNO<sub>3</sub>] = 0.01 M, Temperature = 298 K.

In Job's method of continuous variation (Fig. 1B), complementary mixtures were prepared. Absorbance was recorded at 429 nm and plotted against volume of alizarin. Stoichiometry of

Co<sup>II</sup> to alizarin from both methods was 1:3, although in case of Job's method, formation of a 1:1 metal alizarin species and a 1:2 metal alizarin species were also realized.

## 2.2 Dissociation of proton per alizarin in presence of Co<sup>II</sup>:

Alizarin and Co<sup>II</sup> were mixed in the ratio reported above and a spectrophotometric titration was performed in the pH range 3.0 - 12.0. pH was measured using a digital pH meter (LMPH-10, LABMAN). The change in absorbance of alizarin with pH in the presence of Co<sup>II</sup> was recorded at 540 nm and the data was fitted to Eq. 3a (*Chapter 6: Experimental*). Fitting the experimental data (Fig. 2), pK<sub>1</sub>, i. e. dissociation of alizarin in presence of Co<sup>II</sup> was 6.75 ± 0.30 at 25°C.

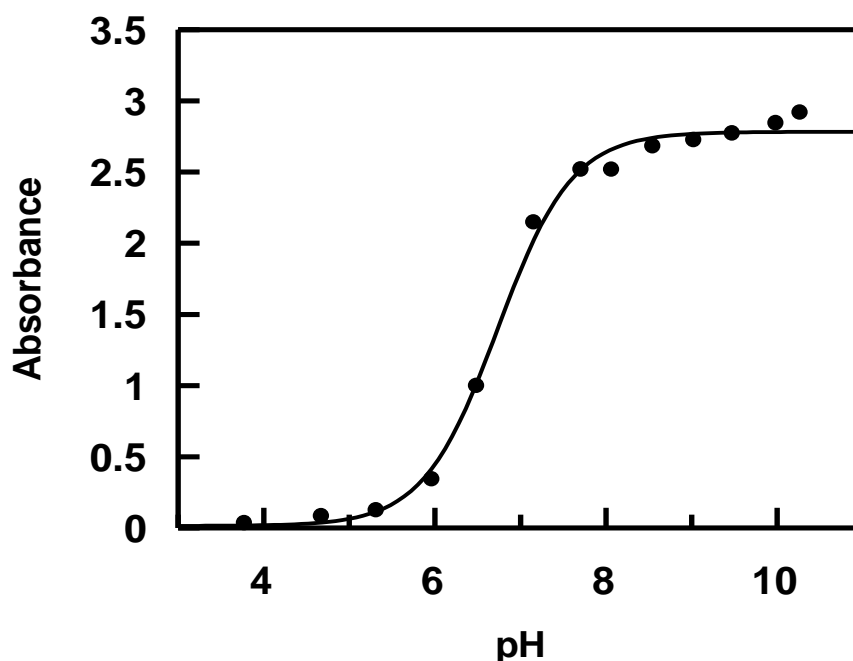


**Fig. 2:** Spectrophotometric titration of alizarin in presence of Co<sup>II</sup>, shown by a variation in absorbance at 540 nm; [alizarin] = 60 μM, [Co<sup>II</sup>] = 20 μM, [NaNO<sub>3</sub>] = 0.01 M, T = 301 K.

Formation constants β and β\* were evaluated using Eqs. 4 – 8 (*Chapter 6: Experimental*).<sup>31</sup> pK for the dissociation of phenolic OH at C<sub>1</sub> of alizarin in presence of Co<sup>II</sup>

was used to calculate stability constant of  $[\text{Co}(\text{alz})_3]^-$  in solution. Value for formation constant  $\beta$  for  $[\text{Co}(\text{alz})_3]^-$  was  $9.09 \times 10^{19}$  ( $\log \beta = 19.96$ ).

### 2.3 Characterization of $\text{Na}[\text{Co}(\text{alz})_3]$

#### 2.3.1 Comparison of the UV-Vis spectra of alizarin and $\text{Na}[\text{Co}^{\text{II}}(\text{alz})_3]$ :

The absorption spectrum of alizarin was recorded in methanol showing a  $\lambda_{\text{max}}$  at 521 nm (Fig. 3). Owing to poor solubility in water, the spectrum of the complex was recorded in aqueous-DMSO showing  $\lambda_{\text{max}}$  at 536 nm.

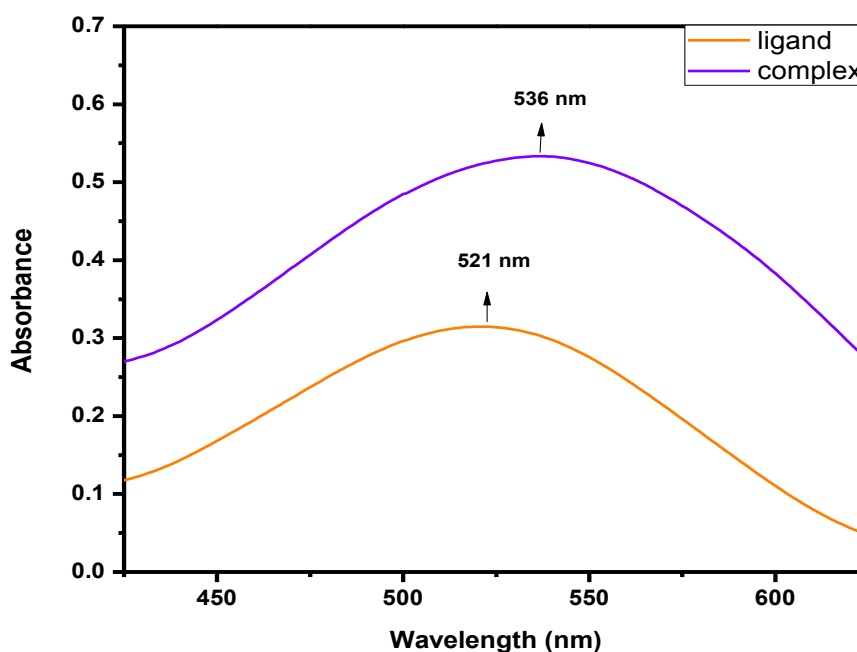


**Fig. 3:** Absorption spectra of alizarin in methanol and  $\text{Co}^{\text{II}}$  complex in aqueous-DMSO

#### 2.3.2 IR spectra of alizarin and $\text{Na}[\text{Co}(\text{alz})_3]$ :

Analysis of FTIR data of alizarin and  $\text{Na}[\text{Co}(\text{alz})_3]$  [Fig. 4(A) and 4(B) respectively] were procured on a spectrophotometer (Perkin Elmer) using KBr pellets. Studies reveal that the sharp peak obtained for phenolic-OH at  $3357 \text{ cm}^{-1}$  for alizarin was detected as a broad band in the complex ( $3413 \text{ cm}^{-1}$ ). Carbonyl stretching peaks at  $1665 \text{ cm}^{-1}$  to  $1586 \text{ cm}^{-1}$  for alizarin

[Fig. 4(A)] were obtained at  $1580\text{ cm}^{-1}$  for the complex [Fig. 4(B)].<sup>32</sup> Response for carbonyl stretching did not disappear completely in the complex since of the two carbonyls present in alizarin, only one got involved in complex formation. Peaks obtained in the region  $1452\text{ cm}^{-1}$  to  $775\text{ cm}^{-1}$  [Fig. 4(A)] for alizarin and between  $1341\text{ cm}^{-1}$  to  $718\text{ cm}^{-1}$  [Fig. 4(B)] for the complex (due to -OH and -CH bending vibrations) were slightly different. Response for Co-O stretching expected between  $450\text{ cm}^{-1}$  to  $390\text{ cm}^{-1}$ ,<sup>15, 32, 33</sup> could not be detected for a limitation in the instrument used to detect responses in that region accurately.

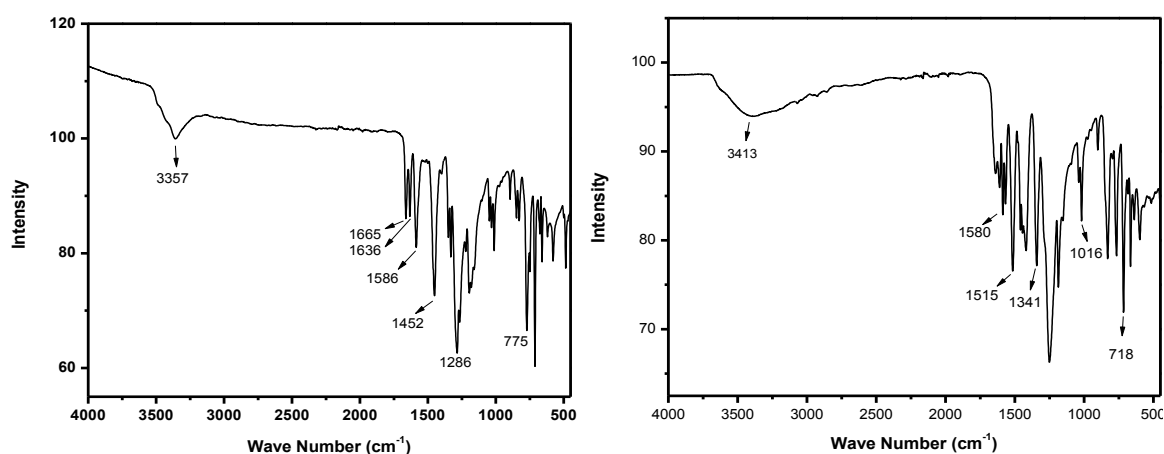


**Fig. 4:** (A) IR spectrum of alizarin and (B) IR spectrum of Na[Co(alz)<sub>3</sub>]

### 2.3.3 CHN analysis:

Calculated percentage for C<sub>42</sub>H<sub>21</sub>O<sub>12</sub>CoNa is C, 63.03; H, 2.65.

Experimentally found: C, 63.37; H, 2.69.

### 2.3.4 Analysis of the mass spectrum of Na[Co(alz)<sub>3</sub>]:

Evidence from physico-chemical experiments and elemental analysis suggests formation of a 1:3 Co<sup>II</sup>-alizarin complex [Co<sup>II</sup>(alz)<sub>3</sub>]<sup>-</sup> whose mass is 776.63. Hence, the peak in the mass spectrum at  $m/z = 776.76$  (Fig. 5), recorded on a Micromass Q-Tofmicro<sup>TM</sup>, Waters Corporation is the molecular ion of the complex. From the molecular ion, if one ligand and an -OH group from another ligand departs followed by entry of DMSO (used in analysis) in the



coordination sphere, a species having  $m/z = 599.03$  is expected. The peak at  $m/z = 601.08$  (+2H) could be this species. From the molecular ion, since loss of one alizarin vacates two coordination sites, if they are subsequently occupied by two molecules of water (either present as an impurity in the solvent or from moisture) then this fragment should show up at  $m/z = 573.03$  (theoretical); an experimental peak at  $m/z = 574.28$  (+ H) could be this species. Mass spectrum of the oxidized form of the complex  $[\text{Co}^{\text{III}}(\text{alz})_3]$  was pretty much the same.

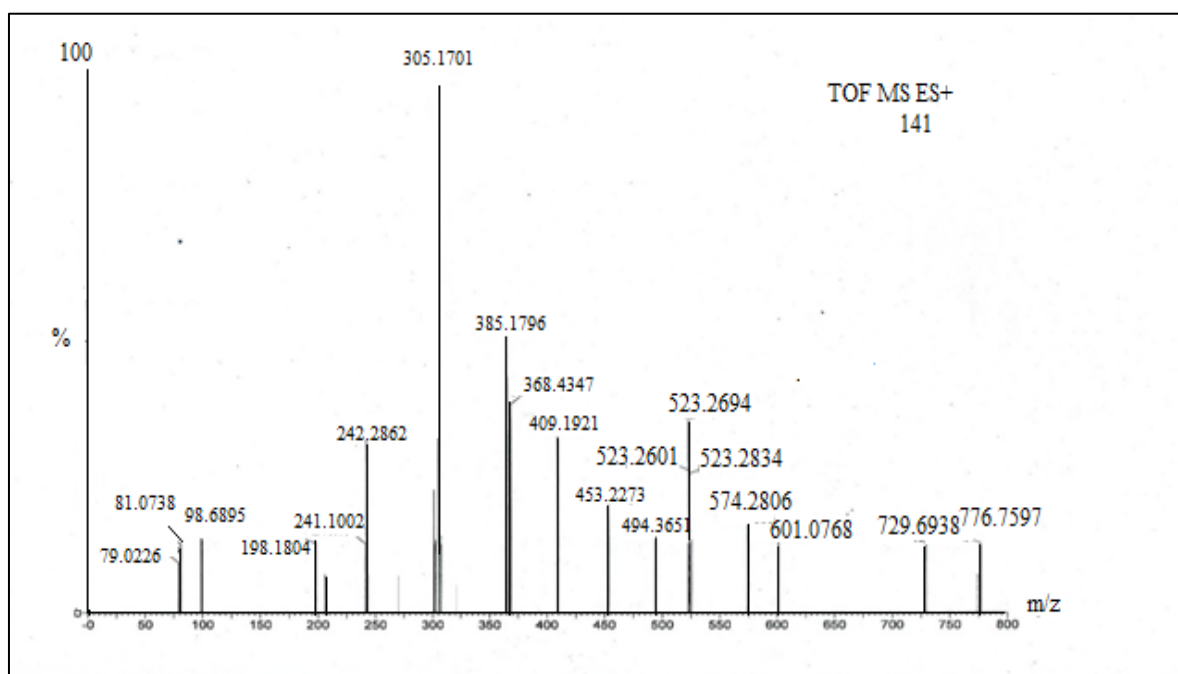


**Fig. 5:** Mass spectrum of  $\text{Na}[\text{Co}(\text{alz})_3]$

### 2.3.5 Thermo-gravimetric analysis:

Fig. 6 suggests, by  $100^\circ\text{C}$ , there is a decrease in weight by 4.3%. By  $\sim 140^\circ\text{C}$ , the decrease is about 15.63%. While that at  $100^\circ\text{C}$  could be due to loss of absorbed water molecules, by  $140^\circ\text{C}$ , it could be due to further loss of three unbound OH groups. Otherwise, the complex is stable.

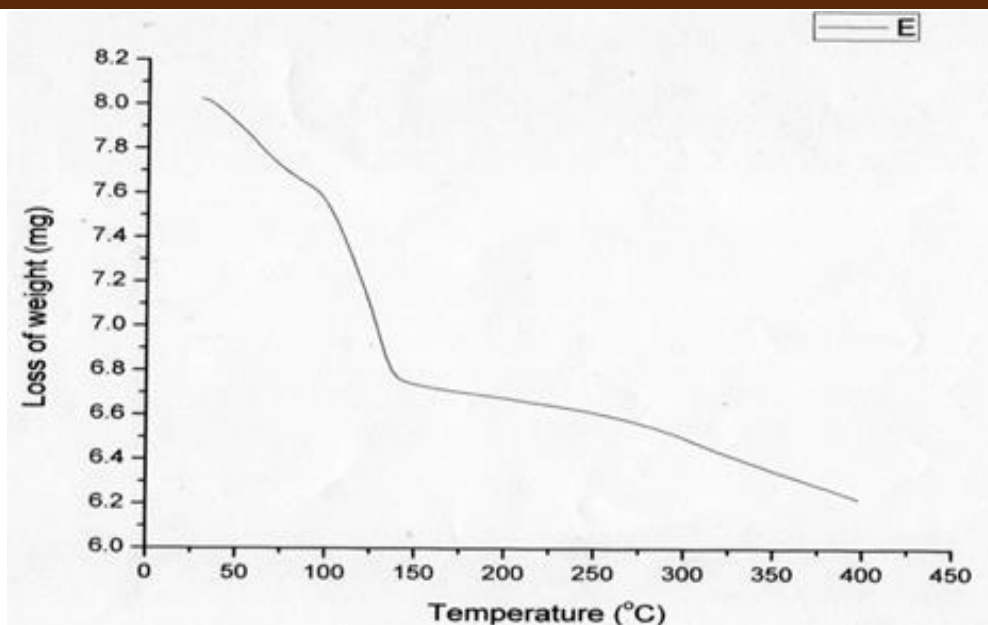


**Fig. 6:** Thermo-gravimetric analysis of Na[Co<sup>II</sup>(alz)<sub>3</sub>]

### 2.3.6 Magnetic moment of Na[Co<sup>II</sup>(alz)<sub>3</sub>] and [Co<sup>III</sup>(alz)<sub>3</sub>]:

Magnetic susceptibility was measured by Gouy method and  $\mu_{\text{eff}}$  was found to be 3.67 BM for Na[Co<sup>II</sup>(alz)<sub>3</sub>] suggesting the presence of three unpaired electrons. [Co<sup>III</sup>(alz)<sub>3</sub>] was diamagnetic.

### 2.3.7 Electrochemical studies

To examine electrochemical properties of the mono-anionic complex, cyclic voltammetry was performed over the potential range 0 to -1500 mV (Fig. 7). A single cathodic quasi-reversible wave was obtained at customary scan rates. Keeping in mind that some of our experiments would expose the mono-anionic complex to reactive oxygen species, we needed to know how it might behave following such an exposure. Hence, an understanding of electrochemical processes was necessary to be sure on issues related to performance of the complex in experiments pertaining to ROS and cell viability studies to be able to look for a correlation between them. Since Co<sup>II</sup> complexes are prone to oxidation in presence of oxidizing agents like H<sub>2</sub>O<sub>2</sub>, we thought it necessary to have some prior knowledge on what

might happen if Na[Co<sup>II</sup>(alz)<sub>3</sub>] is exposed to H<sub>2</sub>O<sub>2</sub>. In every likelihood, a Co<sup>III</sup>(alz)<sub>3</sub> species would form that was verified electrochemically (Fig. 8A).

Under exactly similar conditions as that employed for Fig 7, we found the quasi reversible nature of Na[Co<sup>II</sup>(alz)<sub>3</sub>] had changed completely when subjected to ~ 1% H<sub>2</sub>O<sub>2</sub> (Fig. 8A).

Fig. 8B is the CV trace of a previously prepared Co<sup>III</sup> complex [Co<sup>III</sup>(alz)<sub>3</sub>] (*Section 2.9: Experimental*).

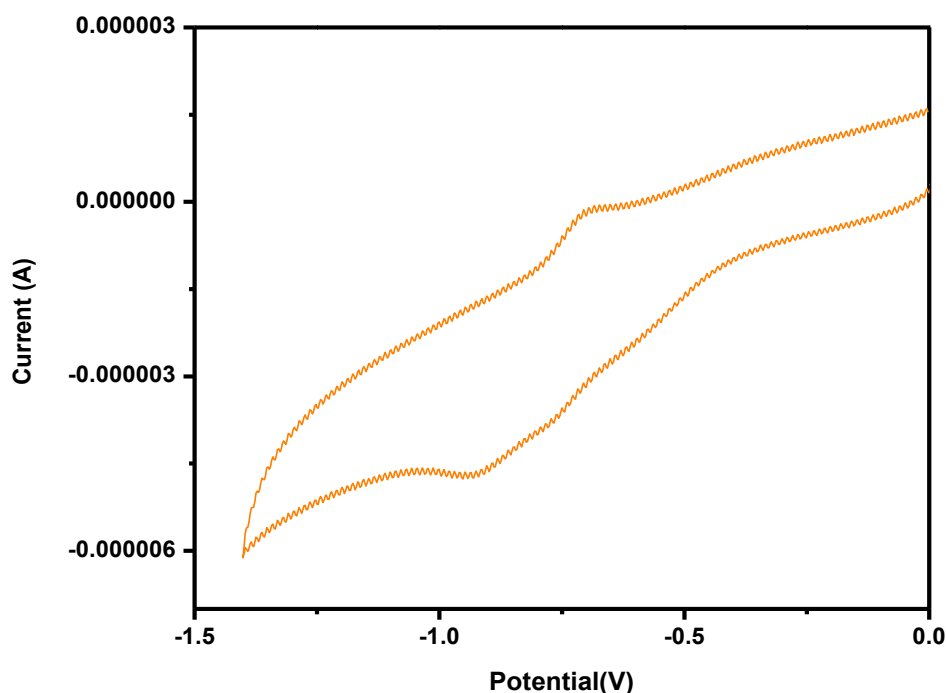


**Fig. 7:** Cyclic voltammogram of a 0.01 mM Na[Co<sup>II</sup>(alz)<sub>3</sub>] at pH ~ 7.4 showing a single step one electron reduction of quinone in aqueous solution containing 0.12 M KCl using a glassy carbon electrode (surface area 0.1256 cm<sup>2</sup>); Scan rate 100 mV/sec.

Fig. 8A and Fig. 8B clearly indicate that the species formed in solution upon addition of ~1% H<sub>2</sub>O<sub>2</sub> to a solution of Na[Co<sup>II</sup>(alz)<sub>3</sub>] is the same as that characterized as Co<sup>III</sup>(alz)<sub>3</sub>. Hence, it may be said that in presence of H<sub>2</sub>O<sub>2</sub> the predominant species present in solution is Co<sup>III</sup>(alz)<sub>3</sub>. This is important in realizing the form in which the complex is most likely to exist in a medium where H<sub>2</sub>O<sub>2</sub> or other forms of ROS are present since that would be useful in

interpreting the results of ROS based experiments performed on different cell lines. As expected, following treatment of Na[Co<sup>II</sup>(alz)<sub>3</sub>] with H<sub>2</sub>O<sub>2</sub> or on previously prepared Co<sup>III</sup>(alz)<sub>3</sub>, the single reduction peak for the complex moved to more positive potential.

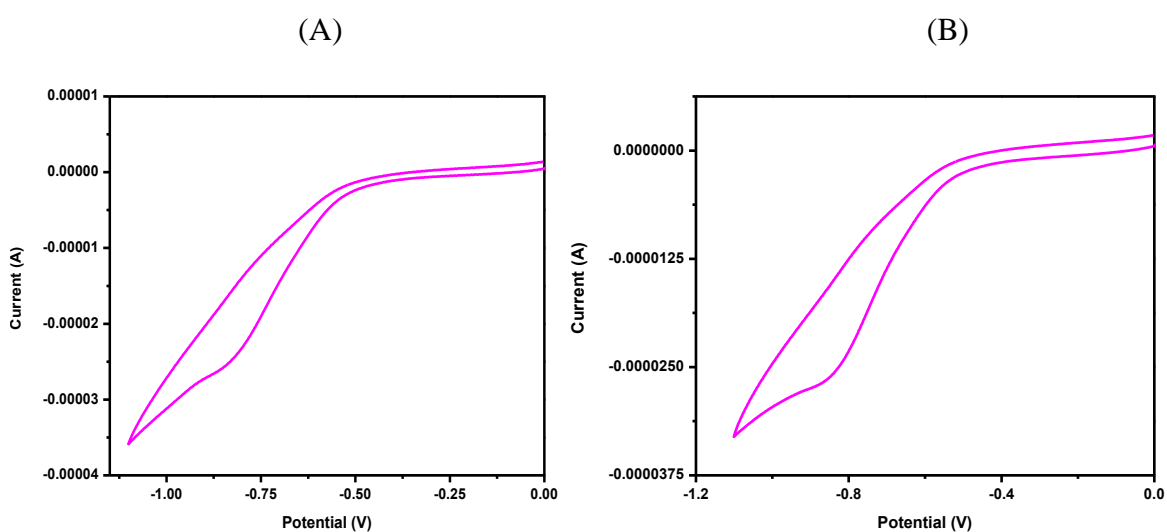


**Fig. 8:**(A) Cyclic voltammogram of a 0.01 mM Na[Co<sup>II</sup>(alz)<sub>3</sub>] at pH ~ 7.4 taken approximately 20 minutes after being treated with ~1% H<sub>2</sub>O<sub>2</sub> under gently warm conditions, showing a single step one-electron irreversible reduction; (B) Cyclic voltammogram of a 0.01 mM previously prepared and characterized [Co<sup>II</sup>(alz)<sub>3</sub>] at pH ~ 7.4; shows a single step one-electron irreversible reduction. In both cases, the solution was aqueous-DMF (50:50) containing 0.12 M KCl; Temperature: 301 K. A glassy carbon electrode (surface area 0.1256 cm<sup>2</sup>) was used. Scan rate: 100 mV/sec.

### 2.3.8 Structure of Co(alz)<sub>3</sub> by computation

#### 2.3.8.1 DFT calculations based on spectroscopy and other evidence:

Molecular geometry of octahedral Co<sup>III</sup>(alz)<sub>3</sub> was optimized at its electronic ground state (S<sub>0</sub>) in gaseous and DMSO medium with appropriately labelled coordination environments as depicted in Fig. 9. Some selected bond lengths and bond angles are listed in Table 1 while coordinates of optimized structures are provided in Table 2. Final optimized structures of the

ground state configuration show an octahedral coordination environment both for gas and solution (in DMSO) phase calculations. Two oxygen atoms of each alizarin are connected to Co<sup>III</sup> (Fig. 9).

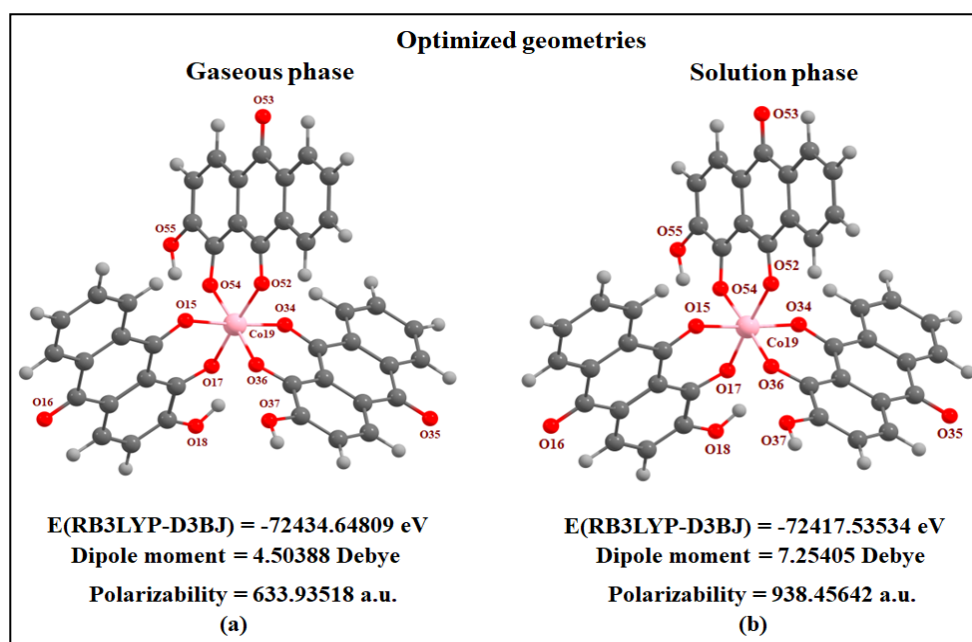


Fig. 9: Ground state optimized geometries of the complex

Table 1: Coordinated bond distances (in Å) and bond angles (in °) of Co(alz)<sub>3</sub>.

Bond	Gaseous phase	In DMSO	Angle	Gaseous phase	In DMSO
Co19–O15	1.897	1.898	O15–Co19–O17	94.35	98.77
Co19–O17	1.877	1.877	O15–Co19–O36	87.79	88.37
Co19–O34	1.892	1.887	O15–Co19–O52	88.05	88.59
Co19–O36	1.875	1.879	O15–Co19–O54	89.42	88.92
Co19–O52	1.912	1.910	O17–Co19–O36	89.50	89.27
Co19–O54	1.894	1.894	O17–Co19–O34	88.69	88.80
			O17–Co19–O54	88.67	89.11
			O36–Co19–O34	94.14	93.37
			O36–Co19–O52	88.58	88.96
			O34–Co19–O54	88.74	89.41
			O52–Co19–O54	93.37	92.77

**Table 2: Coordinates of Optimized Structure:**

Atom	Gaseous phase			Solution phase (DMSO)		
	x	y	z	x	y	z
C1	-2.9536	-0.2710	0.0801	2.9592	0.4642	0.1603
C2	-4.1508	0.3693	0.6715	4.1830	-0.1194	0.7357
C3	-5.4124	-0.2536	0.5881	5.4249	0.5470	0.6000
C4	-5.5765	-1.5676	-0.1016	5.5155	1.8368	-0.1256
C5	-4.3686	-2.1679	-0.7094	4.2807	2.3935	-0.7046
C6	-3.0853	-1.5285	-0.6083	3.0237	1.7091	-0.5572
C7	-4.4984	-3.3655	-1.3947	4.3425	3.5942	-1.4054
C8	-3.3899	-3.9745	-2.0095	3.1906	4.162	-1.9836
C9	-2.1486	-3.3767	-1.9315	1.9785	3.5151	-1.8534
C10	-1.9583	-2.1376	-1.2211	1.86	2.2763	-1.1377
C11	-4.0267	1.6031	1.3305	4.1199	-1.3414	1.4289
C12	-5.1464	2.2106	1.8938	5.2766	-1.8982	1.9805
C13	-6.4003	1.5911	1.8091	6.5082	-1.2381	1.8461
C14	-6.5304	0.3639	1.1608	6.5788	-0.0218	1.1594
O15	-1.8646	0.3604	0.2161	1.8681	-0.2027	0.3388
O16	-6.6803	-2.1112	-0.1572	6.6249	2.431	-0.2396
O17	-0.7284	-1.7032	-1.2364	0.6245	1.7845	-1.1097
O18	-1.0635	-3.9314	-2.5145	0.8316	4.0402	-2.407
Co19	-0.1232	-0.2119	-0.2712	0.099	0.2329	-0.1939
C20	3.7511	-1.6599	-0.8246	-3.8459	1.4457	-0.8984
C21	4.7085	-2.5384	-0.2792	-4.8713	2.2908	-0.4119
C22	5.9494	-2.6941	-0.9085	-6.0907	2.3695	-1.1015
C23	6.2407	-1.9834	-2.0715	-6.2977	1.6178	-2.2621
C24	5.2897	-1.1102	-2.616	-5.2806	0.7791	-2.745

*Chapter 9: A Cobalt<sup>II</sup>/Cobalt<sup>III</sup> complex of alizarin..... a simpler anthracycline analogue*

---

C25	4.0517	-0.9487	-1.9981	-4.0613	0.6944	-2.068
C26	2.4296	-1.4802	-0.177	-2.5545	1.3534	-0.1923
C27	2.1166	-2.2034	1.0254	-2.332	2.1021	1.0131
C28	3.0868	-3.1042	1.5878	-3.3732	2.9592	1.5171
C29	4.4154	-3.3085	0.962	-4.664	3.0893	0.817
C30	0.8502	-2.0267	1.6697	-1.0984	1.9951	1.7267
C31	0.6031	-2.7886	2.8769	-0.9524	2.7554	2.9424
C32	1.5553	-3.6477	3.3848	-1.9653	3.5757	3.4021
C33	2.7978	-3.8058	2.7425	-3.1745	3.6771	2.6884
O34	1.6468	-0.669	-0.7592	-1.6792	0.5665	-0.7299
O35	5.251	-4.077	1.4385	-5.574	3.8532	1.2477
O36	-0.1062	-1.2499	1.2903	-0.0677	1.247	1.3796
O37	-0.613	-2.5886	3.4463	0.2559	2.6048	3.5930
C38	1.3182	3.3549	1.4149	-1.1632	-3.476	1.3731
C39	1.5104	2.8832	2.7238	-1.4632	-3.0376	2.6753
C40	2.0005	3.7372	3.7091	-1.9447	-3.9392	3.6281
C41	2.3037	5.0696	3.3986	-2.1314	-5.2884	3.2887
C42	2.1133	5.5452	2.1021	-1.835	-5.7321	1.9960
C43	1.6206	4.6961	1.1041	-1.3506	-4.8369	1.0305
C44	1.4207	5.2292	-0.2766	-1.0389	-5.3224	-0.3353
C45	0.8907	4.2933	-1.2919	-0.5296	-4.349	-1.3162
C46	0.586	2.9265	-0.9618	-0.3454	-2.9678	-0.9566
C47	0.7977	2.4375	0.3742	-0.6557	-2.5197	0.3738
C48	0.6926	4.7587	-2.5819	-0.2270	-4.7802	-2.6043
C49	0.1943	3.9154	-3.5924	0.2603	-3.8865	-3.5782
C50	-0.1058	2.6009	-3.3010	0.4404	-2.559	-3.2480

---

*Chapter 9: A Cobalt<sup>II</sup>/Cobalt<sup>III</sup> complex of alizarin..... a simpler anthracycline analogue*

---

C51	0.0791	2.0656	-1.9734	0.1443	-2.0618	-1.9332
O52	0.5714	1.2485	0.7489	-0.5171	-1.2977	0.7685
O53	1.69	6.4024	-0.5384	-1.2088	-6.5380	-0.6371
O54	-0.2518	0.8129	-1.8592	0.3708	-0.7612	-1.7824
O55	-0.5821	1.7598	-4.2427	0.9127	-1.6535	-4.1722
H56	-5.4804	-3.8219	-1.4512	5.2987	4.0930	-1.5042
H57	-3.4913	-4.9110	-2.5488	3.2432	5.0974	-2.5284
H58	-3.0501	2.0684	1.3937	3.1655	-1.8430	1.5288
H59	-5.044	3.1660	2.3999	5.2201	-2.8414	2.5129
H60	-7.2721	2.0664	2.2493	7.4062	-1.6700	2.2745
H61	-7.4889	-0.1383	1.0829	7.5227	0.4988	1.0487
H62	-0.3153	-3.3339	-2.3271	0.0745	3.4401	-2.2093
H63	6.6664	-3.3779	-0.4663	-6.8659	3.0217	-0.7169
H64	7.2049	-2.1076	-2.5557	-7.2440	1.6837	-2.7881
H65	5.515	-0.5566	-3.5227	-5.4387	0.1953	-3.6452
H66	3.3074	-0.2780	-2.4112	-3.2715	0.0514	-2.4355
H67	1.3412	-4.2096	4.2920	-1.8300	4.1442	4.3170
H68	3.5473	-4.4791	3.1431	-3.9666	4.3187	3.0540
H69	-0.7006	-3.1446	4.2327	0.3110	3.1305	4.4160
H70	1.2688	1.8508	2.9495	-1.3159	-1.9950	2.9279
H71	2.1470	3.3669	4.7195	-2.1735	-3.5936	4.6304
H72	2.6866	5.7334	4.1683	-2.5053	-5.9884	4.0281
H73	2.3387	6.5724	1.8353	-1.974	-6.7709	1.7206
H74	0.9331	5.7941	-2.7972	-0.3727	-5.8242	-2.8534
H75	0.0403	4.2810	-4.6027	0.4941	-4.2270	-4.5802
H76	-0.7135	0.8993	-3.7995	0.9690	-0.7649	-3.7468

---



### **2.3.8.2 Frontier Molecular Orbital analysis:**

Frontier orbitals of the Co complex with orbital energies, optimized in gas and solution phases, are shown in Fig. 10. Assignment of both occupied and virtual MOs were made on the basis of their composition in terms of atomic contribution and visual inspection of their three-dimensional representation. The complex was assumed to be made of four constituents, Co, alizarin (L1), alizarin (L2), alizarin (L3). Composition from fragments is shown in Table 3. Both for gas and solution phase optimized geometries, we observed that HOMO and subsequent occupied orbitals up to HOMO-4 has major contributions from different alizarin moieties with varying ratios while contribution from metal atom/ion was negligible. Similar observations were found for LUMO upto LUMO +2. However, LUMO +3 and LUMO +4 orbitals had contributions from “Co d orbitals” along with some contribution from each alizarin but in different proportion. In both cases, the calculated HOMO-LUMO energy gap was found to be 2.69 eV. Some selected MOs of Co<sup>III</sup>(alz)<sub>3</sub> along with their energies and percentage composition are provided in Table 3.

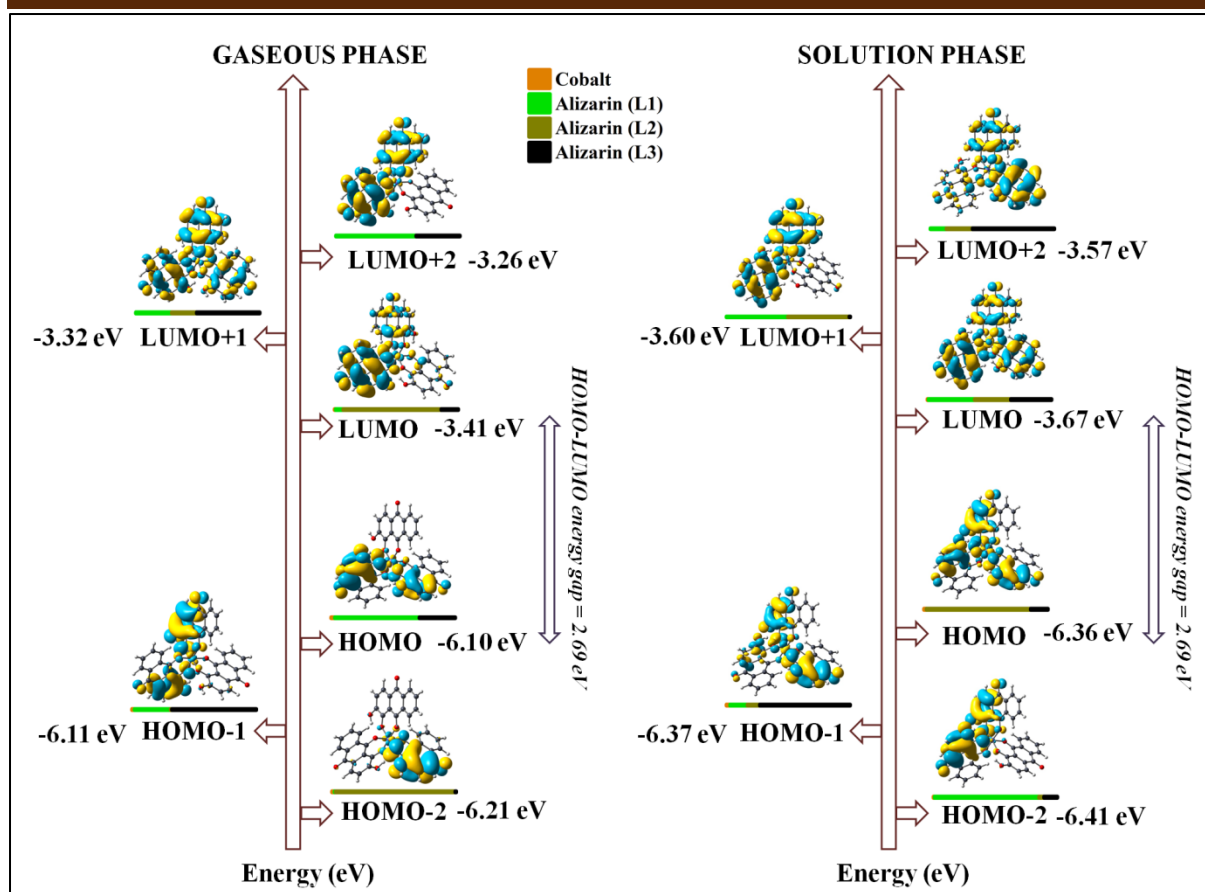


**Fig.10:** Frontier molecular orbitals (FMOs) of optimized geometries of Co(II)-(alizarin)<sub>3</sub> and the graphical contribution from the four fragments to FMOs.

**Table 3:** Some of selected MOs of the complex **Co(II)-(Alizarin)<sub>3</sub>** in high spin state along with their energies and percentage compositions from four fragments in both gaseous phase and DMSO medium.

Sl. No.	MO	Energy (eV)		% Composition							
		Gas	DMSO	Co		Alizarin (L1)		Alizarin (L2)		Alizarin (L3)	
				Gas	DMSO	Gas	DMSO	Gas	DMSO	Gas	DMSO
198	L+4	-2.42	-2.54	68	68	5	5	13	13	13	13
197	L+3	-2.57	-2.68	69	70	17	16	9	9	6	6
196	L+2	-3.26	-3.57	0	0	64	13	0	21	35	66
195	L+1	-3.32	-3.60	0	0	29	49	20	49	51	1
194	LUMO	-3.41	-3.67	1	1	6	37	79	29	14	33
193	HOMO	-6.10	-6.36	3	2	68	0	0	83	29	14
192	H-1	-6.11	-6.37	2	3	29	14	1	10	68	73
191	H-2	-6.21	-6.41	2	1	1	84	96	4	1	11
190	H-3	-7.19	-7.39	1	1	94	7	1	1	4	91
189	H-4	-7.23	-7.41	1	1	3	60	0	36	95	3

### 2.3.8.3 MEP Surface Analysis:

Molecular electrostatic potential surfaces calculated over optimized geometries both for gas and solvent phases are presented in Fig. 11 using the reverse rainbow color scheme and chosen iso-value of 0.02 a.u. for the envelope. The red color indicates regions of negative potential while blue represents those having positive potential. It is understood that hydrogen atoms of O–H bonds are the most positive region while hydrogen atoms of C–H bonds are only slightly positive. The most negative potential regions are located around oxygen atoms of carbonyls (C=O). Oxygen atoms of O–H bonds also depict negative potential energy whereas  $\pi$  rings of anthraquinone moieties were found to have higher MEP values than carbonyl oxygens. Thus it can be inferred there is a high possibility of molecules to form

hydrogen bonding interactions between hydroxyl-H and carbonyl O that subsequently stabilize such systems.

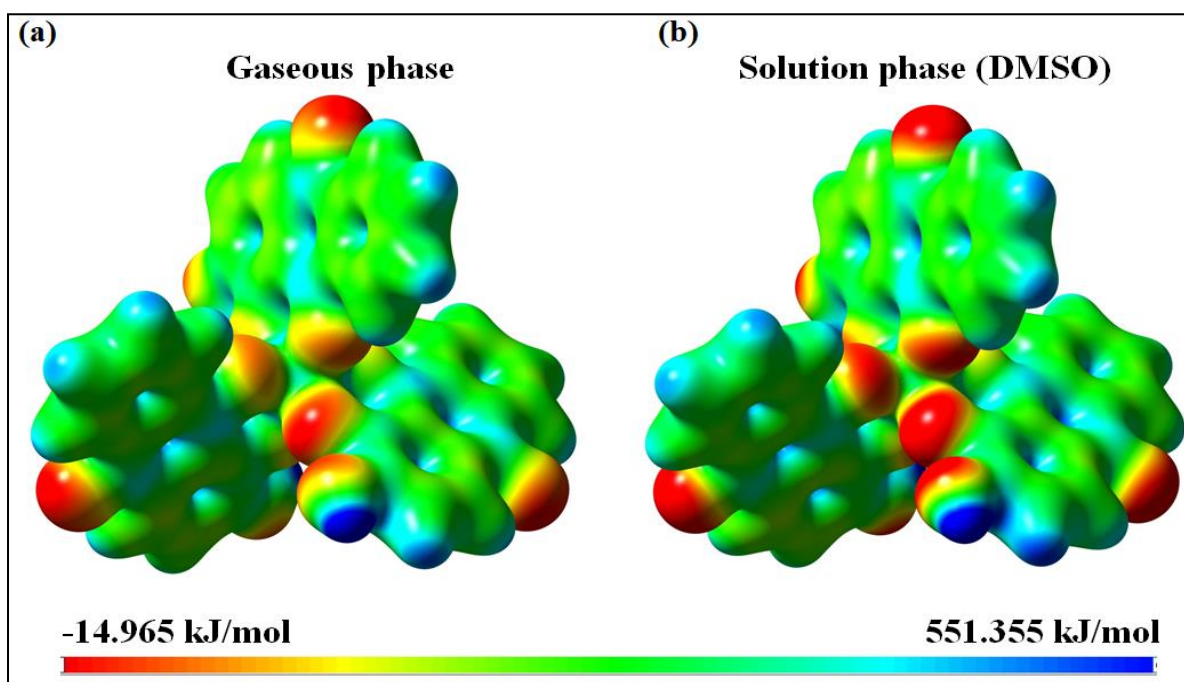
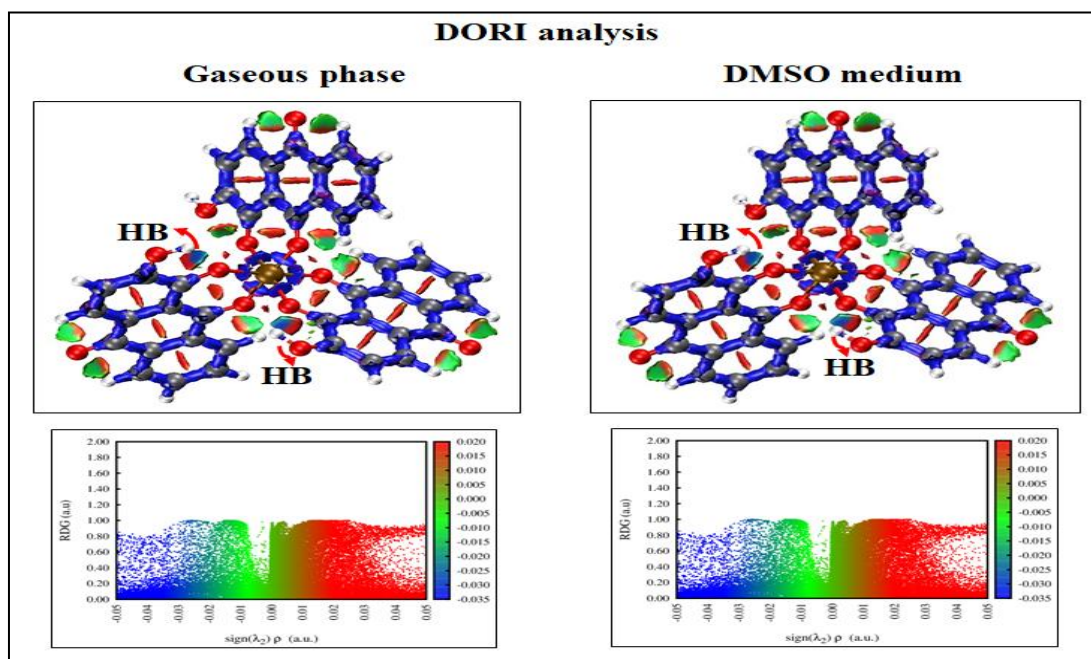


Fig 11: Molecular electrostatic potential surface of  $\text{Co}^{\text{III}}(\text{alz})_3$ (a) gas phase (b) solution phase

#### 2.3.8.4 DORI analysis:

To distinguish between attractive and repulsive interactions with molecular systems “Density Overlap Regions Indicator” (DORI) analysis was performed that enabled one to visualize covalent and non-covalent interactions simultaneously by mapping them as iso-surfaces over the molecular system (Fig 12). The plot of reduced density gradient versus sign of the second Hessian eigenvalue times the electron density [ $\text{sign}(\lambda_2) \rho$  in a.u.] enables one to differentiate between attractive/stabilizing (thus favourable) and repulsive (thus unfavourable) interactions. Strength of interactions are portrayed with the help of the red-green-blue colour scheme where blue iso-surface represents strong attractive interactions; a red iso-surface, strong repulsive interactions and a green iso-surface, weak attractive interactions. As expected, coordination as well as covalent bonds are represented as blue iso-surfaces. Intra-

molecular weak hydrogen bonding interactions between carbonyl-O and C–H hydrogens are presented as green iso-surfaces while for alizarin (L1) and alizarin (L3) presence of strong O–H···O intra-molecular hydrogen bonding interactions between hydroxyl-H and carbonyl-O are visualized by blue iso-surfaces.



**Fig. 12:** Density Overlap Regions Indicator (DORI) analysis of Co(alz)<sub>3</sub>

## 2.4 Analysis of the interaction of the complexes with calf thymus DNA

### 2.4.1 At different ionic strengths of the medium

Performance of several anticancer drugs is affected owing to fluctuation in ionic strength or pH.<sup>34-36</sup> Hence, it is important to investigate interactions of drugs or “molecules” that could be potential drugs with a biological target, under varying conditions of ionic strength and pH. An essential criterion for good performance is that molecules should be able to hold onto their efficacy over a large range of pH and ionic strength of the medium. Both forms of the Cobalt complex, Na[Co<sup>II</sup>(alz)<sub>3</sub>] and Co<sup>III</sup>(alz)<sub>3</sub>] were considered for interaction with calf thymus DNA.

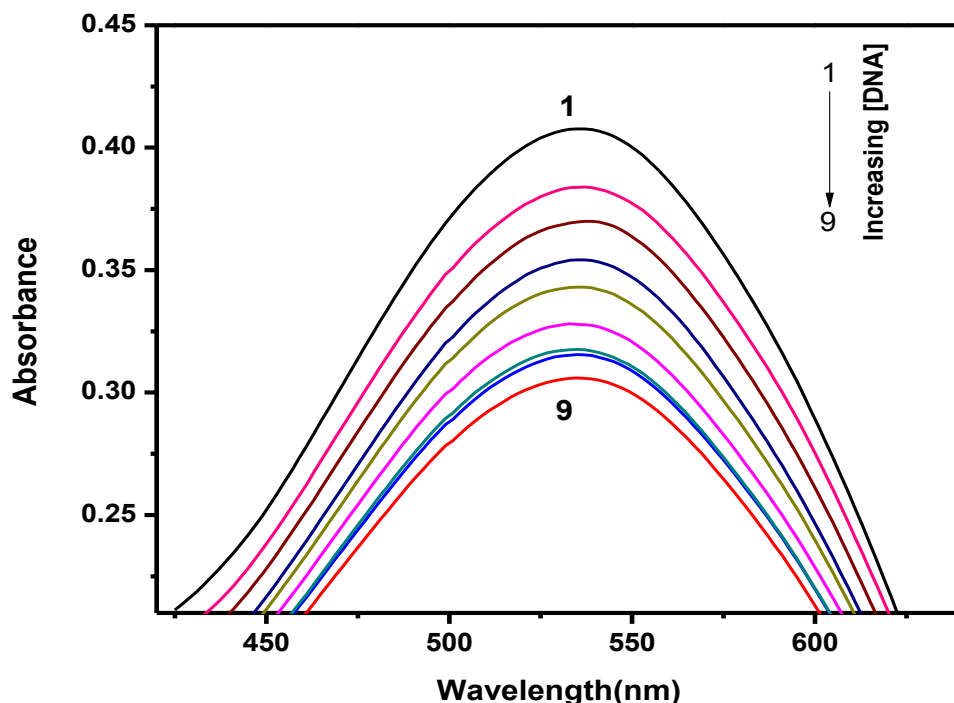


**Fig. 13:** Absorption spectra of 50  $\mu\text{M}$   $\text{Na}[\text{Co}^{\text{II}}(\text{alz})_3]$  in 0.12 M NaCl and 30 mM tris buffer in aqueous solution of pH 7.4 ; (1) in absence and in presence of different concentrations of calf thymus DNA (2) 103.30  $\mu\text{M}$  (3) 205.58  $\mu\text{M}$  (4) 306.86  $\mu\text{M}$  (5) 506.44  $\mu\text{M}$  (6) 702.16  $\mu\text{M}$  (7) 988.76  $\mu\text{M}$  (8) 1448  $\mu\text{M}$ ; Temperature = 301 K.

Titration were performed at pH 7.4, at varying ionic strengths. For  $\text{Na}[\text{Co}^{\text{II}}(\text{alz})_3]$ , since dissociation of free phenolic -OH on each alizarin (the one not bound to  $\text{Co}^{\text{II}}$ ) was beyond physiological pH, hence at pH  $\sim 7.4$ , the complex was largely mono-anionic. Titrations were followed at 536 nm. Fig. 13 depicts a titration of  $\text{Na}[\text{Co}^{\text{II}}(\text{alz})_3]$  followed at ionic strength due to 0.12 M NaCl. Fig. 14 is a plot obeying Eq. 10 (*Chapter 6: Experimental*) for titrations performed at an ionic strength due to 0.3 M NaCl. The apparent binding constants ( $K_{\text{app}}$ ) were evaluated (Table 4) from such plots.

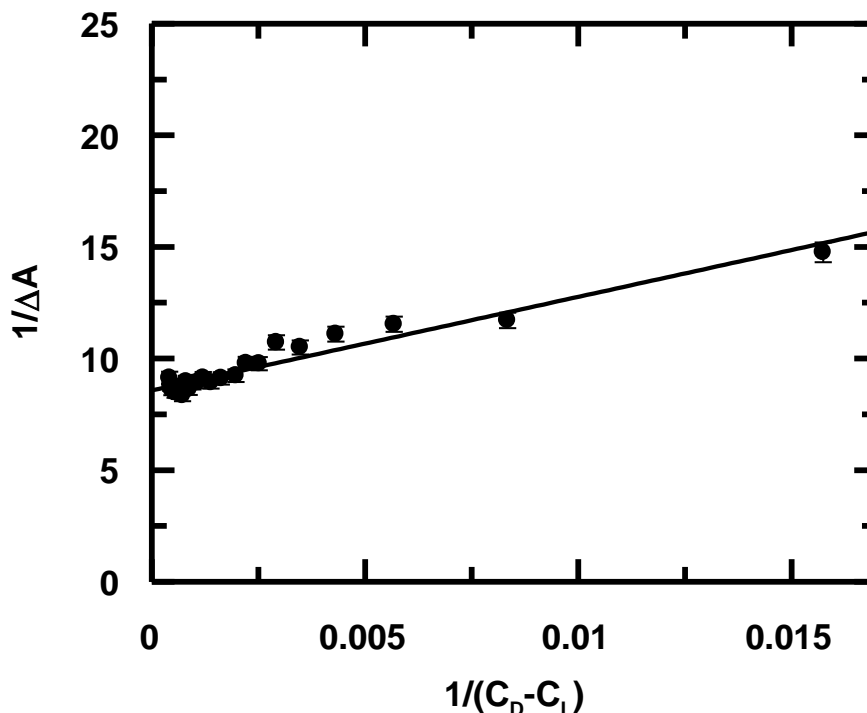


**Fig. 14:** A typical double reciprocal plots for the interaction of Na[Co(alz)<sub>3</sub>] with calf thymus DNA that enables evaluation of  $K_{app}$  at ionic strengths of 0.30 M. of Na[Co(alz)<sub>3</sub>] = 50 μM, pH = 7.40, Temp. = 300 K.

**Table 4:** Binding constant values obtained for the interaction of Na[Co(alz)<sub>3</sub>] with calf thymus DNA at varying ionic strengths of the medium.

Compound	[NaCl] in M	$K_{app}(M^{-1})$			Site size	$K_{app} \times n_b =$ $K^*(M^{-1})$	$K^*$ from Scatchard	$n_b$ calculated from Scatchard $n_b = (n^{-1})$
		From double- reciprocal plot (a)	From Non-linear plot (b)	Average $= (a+b)/2$				
Na[Co <sup>II</sup> (alz) <sub>3</sub> ]	0.12	$1.06 \times 10^4$	$1.35 \times 10^4$	$1.20 \times 10^4$	12	$1.44 \times 10^5$	$1.09 \times 10^5$	8
	0.20	$1.88 \times 10^4$	$3.58 \times 10^4$	$2.73 \times 10^4$	13	$3.54 \times 10^5$	$2.30 \times 10^5$	9
	0.30	$2.15 \times 10^4$	$3.89 \times 10^4$	$3.02 \times 10^4$	14	$4.26 \times 10^5$	$4.37 \times 10^5$	10
	0.36	$1.72 \times 10^4$	$6.18 \times 10^4$	$3.95 \times 10^4$	15	$5.92 \times 10^5$	$5.77 \times 10^5$	10

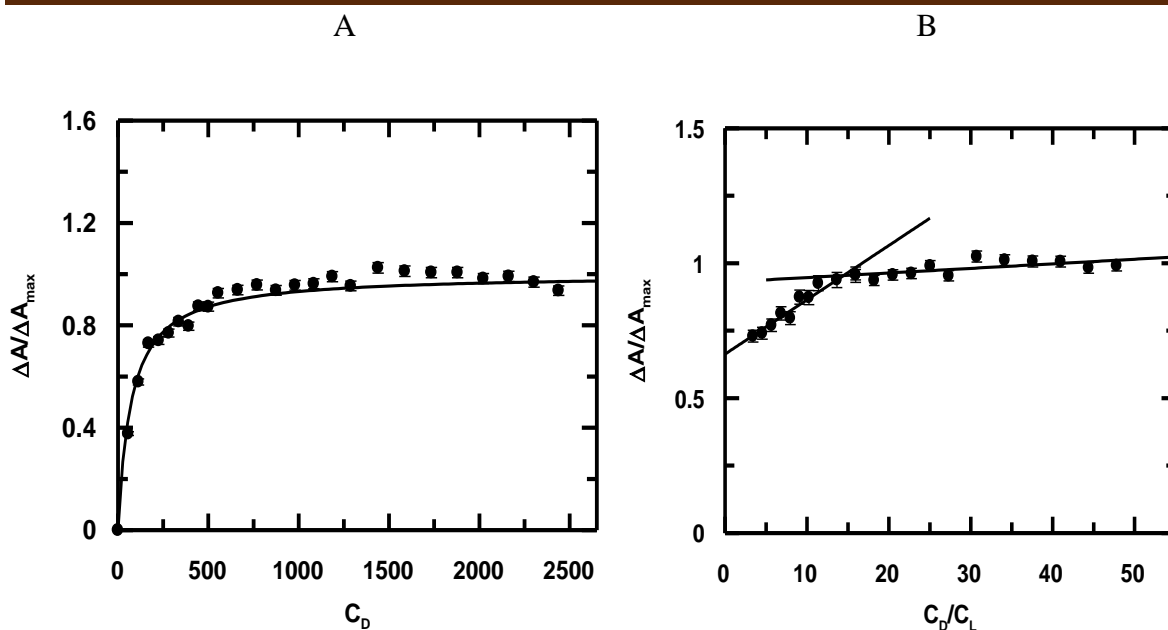


**Fig. 15:**(A) Binding isotherm of Na[Co(alz)<sub>3</sub>] with calf thymus DNA at an ionic strength of 0.30 M with respect to NaCl. The corresponding non-linear fit (Eq. 11) (B) Plot of normalized increase in absorbance as a function of the ratio of calf thymus DNA to Na[Co(alz)<sub>3</sub>]. Na[Co(alz)<sub>3</sub>] = 50 μM, pH = 7.40, T = 301K.

Fig. 15 (A) is a plot fitted to Eq. 11 (*Chapter 6: Experimental*) from where the apparent binding constant ( $K_{app}$ ) was evaluated following an interaction of the complex with calf thymus DNA.

Table 5 provides values for binding parameters at different ionic strengths at which titrations were carried out. Fig.15 (B) provides  $n_b$ , number of nucleotides bound to the complex (Table 4). If a comparison of site size of interaction ( $n_b$ ) for alizarin and Na[Co<sup>II</sup>(alz)<sub>3</sub>] is made, it is seen that the value of  $n_b$  for the complex at each ionic strength is approximately double that of alizarin at an almost similar ionic strength (*Chapter 8*). Considering evaluated values for  $K_{app}$  and  $n_b$  (Table 4), overall binding constant ( $K^*$ ) was obtained using the relation  $K_{app} \times n_b = K^*$ . Overall binding constant was also determined using a modified Scatchard equation (Eq. 13, *Chapter 6: Experimental*) (Fig. 16). The values obtained for overall binding constant from Scatchard plots were close to those obtained by multiplying  $K_{app}$  and  $n_b$  (Table 4).



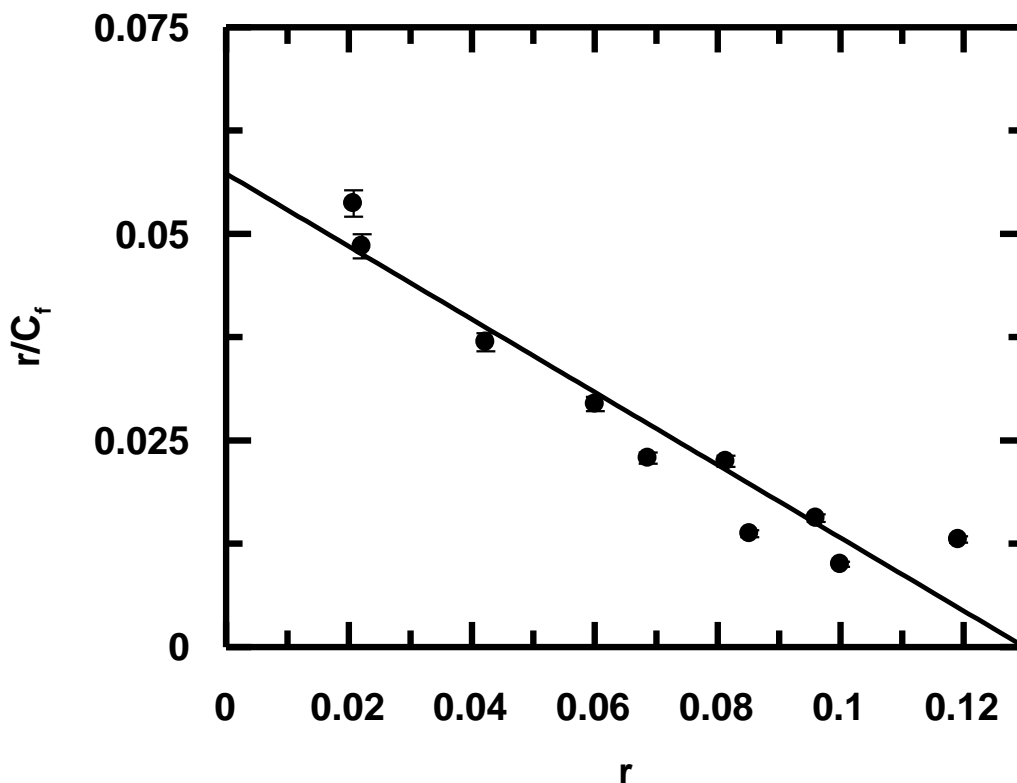


**Fig.16:** A typical Scatchard plot (modified form of the original equation) showing interaction of Na[Co<sup>II</sup>(alz)<sub>3</sub>] with calf thymus DNA that was followed by UV-Vis spectroscopy at 537 nm. Na[Co<sup>II</sup>(alz)<sub>3</sub>] = 50 μM; [NaCl] =0.30M, pH = 7.40, Temperature = 301 K.

In general, binding constant values increased for the complex. In fact, they were higher than we expected, i.e. if one considers only the suppression of dissociation of the unbound phenolic –OH on each alizarin at physiological pH due to increased ionic strength of the medium (Tables 4 & 5). Fig. 17 shows an increasing trend for binding constant values for Na[Co<sup>II</sup>(alz)<sub>3</sub>] with calf thymus DNA, that is significantly higher than alizarin under similar conditions; a consequence of the presence of the metal ion showing its contribution towards interaction with nucleic acid bases, enabling a better targeting of DNA. The values obtained for the complex are in close agreement with those obtained earlier for several anthracyclines that are either being used as drugs in cancer chemotherapy or are in clinical trials.

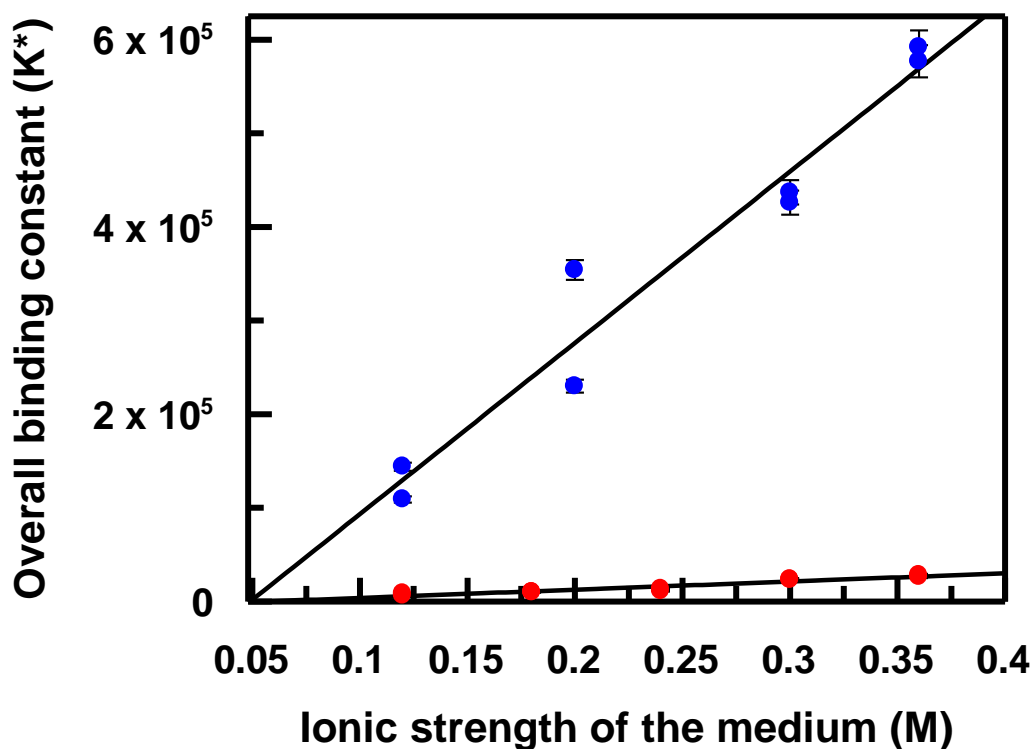


**Fig. 17:** Variation of overall binding constant of alizarin (•) and Na[Co<sup>II</sup>(alz)<sub>3</sub>] (•) with calf thymus DNA at different ionic strength of the medium at pH ~7.4; Temperature = 301K.

Both findings mentioned above i. e. (i) number of nucleotides bound to the complex being almost double that found bound to alizarin and (ii) that there is an increase in the tendency of the complex to bind to DNA, particularly at high ionic strength of the medium, suggests that as the complex approaches DNA, probably one of the three ligands break away resulting in a change in geometry from octahedral to square planar, allowing for better interaction with DNA as reported earlier for several complexes of similar molecules that are either square planar or have water molecules on the third (z) axis.<sup>17, 19, 20, 29</sup> Such re-organization on the part of the complex could be driven by an affinity of the nucleic acid bases located on DNA, trying to coordinate with the metal centre at its fifth and sixth coordination sites, somewhat

similar to that reported for dimeric rhodium (II) acetates, enabling them to act as effective DNA destabilizing agents.<sup>37, 38</sup>

Titration performed with Co<sup>III</sup>(alz)<sub>3</sub> at similar ionic strengths provide binding constant values that are close to those obtained for Na[Co<sup>II</sup>(alz)<sub>3</sub>], but slightly higher at each ionic strength of the medium. However, at the highest ionic strength of 0.36 M with respect to NaCl, binding of neutral Co<sup>III</sup>(alz)<sub>3</sub> to calf thymus DNA was substantially high compared to Na[Co<sup>II</sup>(alz)<sub>3</sub>]. This is attributed to Co<sup>III</sup>(alz)<sub>3</sub> being neutral and that Co is in a higher oxidation state (Fig. 18).

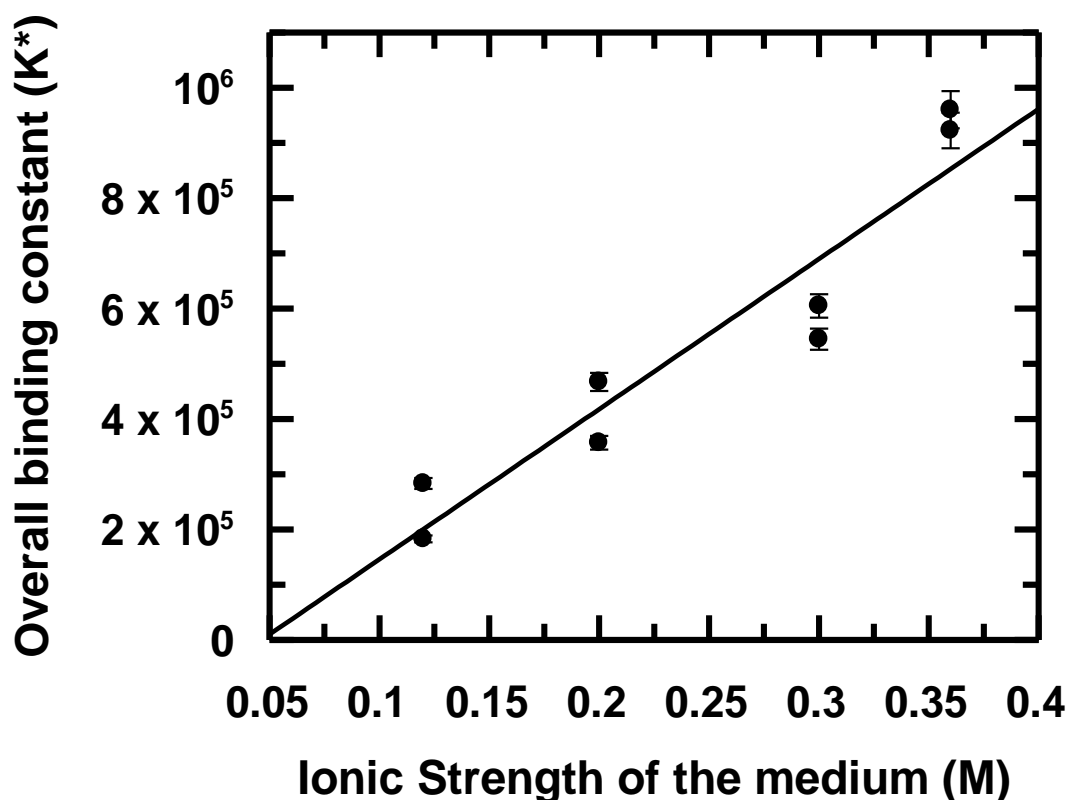


**Fig. 18:** Variation of overall binding constant for Co<sup>III</sup>(alz)<sub>3</sub> interacting with calf thymus DNA at different ionic strengths of the medium at pH ~7.4; Temperature = 301K.

**Table 5: Variation in overall binding constant of Na[Co(alz)<sub>3</sub>]with calf thymus DNA at different ionic strength of the medium (pH~ 7.4).**

[NaCl] in M	-log[Na <sup>+</sup> ]	K* = K <sub>app</sub> × n <sub>b</sub> (M <sup>-1</sup> )	log K*	K*(M <sup>-1</sup> ) from Scatchard plot	log K*
0.12	0.921	1.44 × 10 <sup>5</sup>	5.15	1.09 × 10 <sup>5</sup>	5.04
0.20	0.699	3.54 × 10 <sup>5</sup>	5.55	2.30 × 10 <sup>5</sup>	5.36
0.30	0.523	4.26 × 10 <sup>5</sup>	5.63	4.37 × 10 <sup>5</sup>	5.64
0.36	0.444	5.92 × 10 <sup>5</sup>	5.77	5.77 × 10 <sup>5</sup>	5.76

#### 2.4.2 At different pH of the medium

Titration of Na[Co<sup>II</sup>(alz)<sub>3</sub>] with calf thymus DNA was also followed at different pH (from 6.8 to 8.0). Fig. 19 is a plot obtained by fitting the data to Eq. 10 (*Chapter 6: Experimental*) while Fig. 20 was obtained using Eq. 12 (*Chapter 6: Experimental*) for a titration performed at pH 7.50. From the plots K<sub>app</sub> was evaluated.

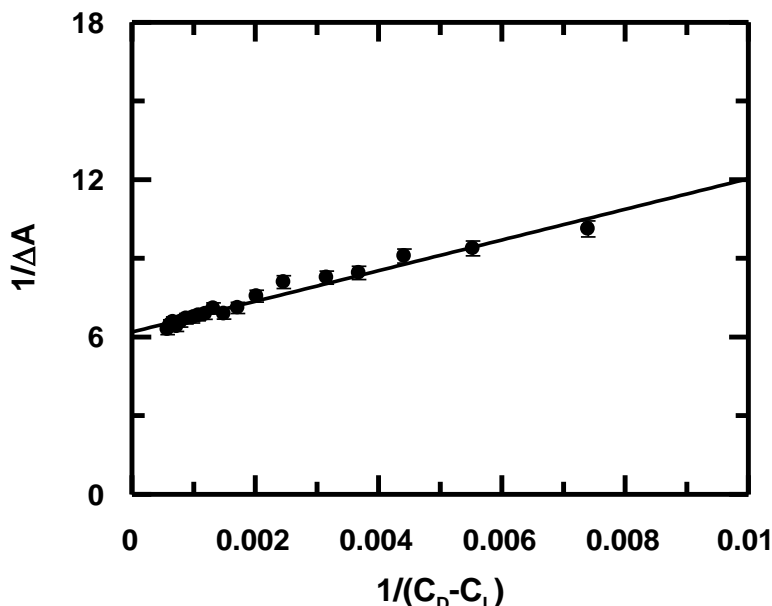


**Fig. 19:** Double reciprocal plot of Na[Co<sup>II</sup>(alz)<sub>3</sub>] interacting with calf thymus DNA, followed by UV-Vis spectroscopy. Na[Co<sup>II</sup>(alz)<sub>3</sub>] = 50 μM, [NaCl] = 0.12 M, pH = 7.50, T = 301 K

Inset of Fig. 20 indicates the site size of interaction ( $n_b$ ) for  $\text{Na}[\text{Co}^{\text{II}}(\text{alz})_3]$  interacting with calf thymus DNA. The titrimetric data was analyzed using Eq. 13 (*Chapter 6: Experimental*) that provide values for overall binding constant ( $K^*$ ) and site size of interaction “n” ( $n_b^{-1}$ ) using the modified Scatchard equation (Table 6). Fig.21 is a modified Scatchard plot for  $\text{Na}[\text{Co}^{\text{II}}(\text{alz})_3]$  interacting with calf thymus DNA at pH 7.50. Similar titrations were performed at other pH and the results are shown in Table 6. Titrations were also performed with  $\text{Co}^{\text{III}}(\text{alz})_3$ . However, interaction of calf thymus DNA with it at different pH did not yield binding constant values that were any different from those of  $\text{Na}[\text{Co}^{\text{III}}(\text{alz})_3]$ .

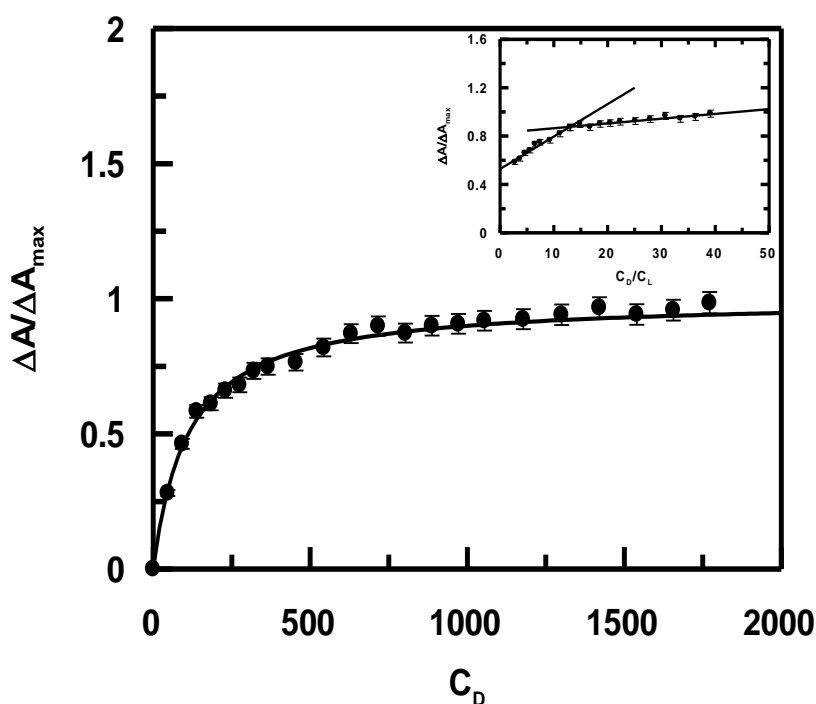


**Fig 20:** Binding isotherm of  $\text{Na}[\text{Co}^{\text{II}}(\text{alz})_3]$  interacting with calf thymus DNA at pH 7.50. The corresponding non-linear fit is shown for the titration followed by UV-Vis spectroscopy. Inset: Plot of normalized increase in absorbance as a function of the ratio of calf thymus DNA to  $\text{Na}[\text{Co}^{\text{II}}(\text{alz})_3]$ .  $\text{Na}[\text{Co}^{\text{II}}(\text{alz})_3] = 50 \mu\text{M}$ ,  $[\text{NaCl}] = 120 \text{ mM}$ , Temperature = 301 K.

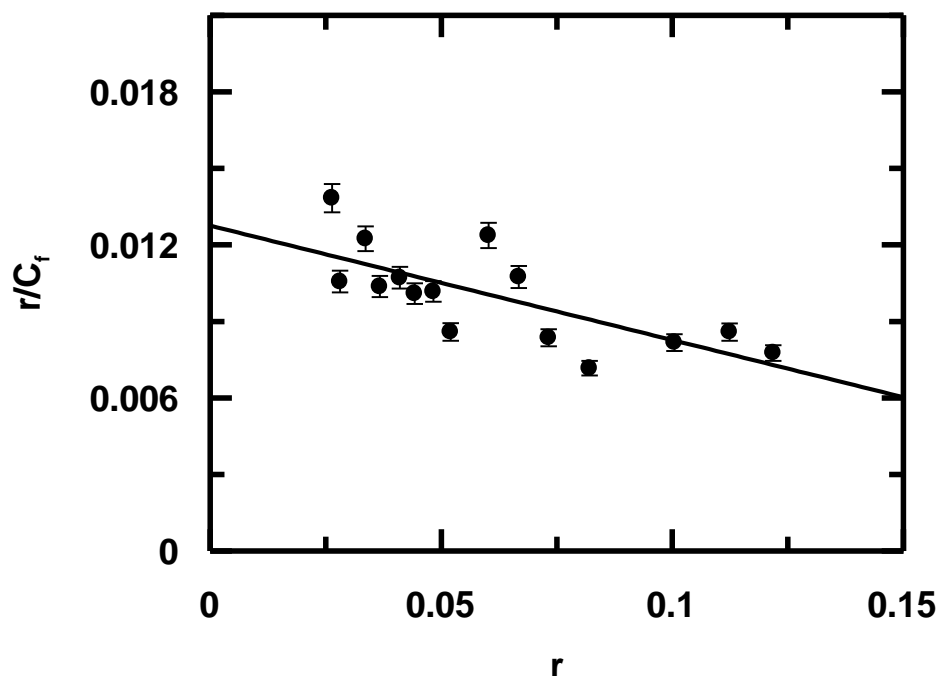


**Fig. 21:** Scatchard plot of interaction of Na[Co(alz)<sub>3</sub>] with calf thymus DNA monitored at 538 nm; Na[Co(alz)<sub>3</sub>] = 50μM, [NaCl] = 0.12 M, pH = 7.50, T = 301 K.

**Table 6: Variation in binding constant values of Na[Co<sup>II</sup>(alz)<sub>3</sub>]with calf thymus DNA at different pH**

Compound	pH	K <sub>app</sub> (M <sup>-1</sup> )			Site size	K <sub>app</sub> × n <sub>b</sub> = K* (M <sup>-1</sup> )	K* from Scatchard	n <sub>b</sub> calculated from Scatchard n <sub>b</sub> = (n <sup>-1</sup> )
		From double-reciprocal plot(a)	From Non-linear plot (b)	Average = (a+b)/2				
Na[Co <sup>II</sup> (alz) <sub>3</sub> ]	6.80	0.98 × 10 <sup>4</sup>	1.18 × 10 <sup>4</sup>	1.08 × 10 <sup>4</sup>	10	1.08 × 10 <sup>5</sup>	0.84 × 10 <sup>5</sup>	08
	7.11	0.80 × 10 <sup>4</sup>	1.17 × 10 <sup>4</sup>	0.98 × 10 <sup>4</sup>	12	1.18 × 10 <sup>5</sup>	1.19 × 10 <sup>5</sup>	12
	7.50	0.87 × 10 <sup>4</sup>	1.16 × 10 <sup>4</sup>	1.02 × 10 <sup>4</sup>	13	1.33 × 10 <sup>5</sup>	1.12 × 10 <sup>5</sup>	11
	7.81	0.95 × 10 <sup>4</sup>	1.00 × 10 <sup>4</sup>	0.98 × 10 <sup>4</sup>	10	0.98 × 10 <sup>5</sup>	1.28 × 10 <sup>5</sup>	14

Evaluation of binding constant values for alizarin with calf thymus DNA had earlier indicated a decreasing trend with increase in pH of the medium (Table 1 in chapter 7). In case of

alizarin, an increase in pH leads to greater generation of anionic species. DNA being a negative polymer, binding of alizarin to calf thymus DNA was affected. The same is true for other hydroxy-9,10-anthraquinones as well.<sup>16, 17, 39</sup> For Na[Co<sup>II</sup>(alz)<sub>3</sub>] however, binding constant values were higher than alizarin in the same pH range and more importantly they remained constant over the entire range of pH over which titrations were performed (Table 6 & Fig. 22). This is significant because complex formation is able to arrest the decreasing trend observed in binding constant values for alizarin for an increase in the pH of the medium (mentioned earlier in chapter 8 as well for the Mn<sup>II</sup> complex). This is therefore an attribute of complex formation and important from a biological point of view since in some forms of cancer, patients experience a fluctuation in pH in body fluids.<sup>40,41</sup>

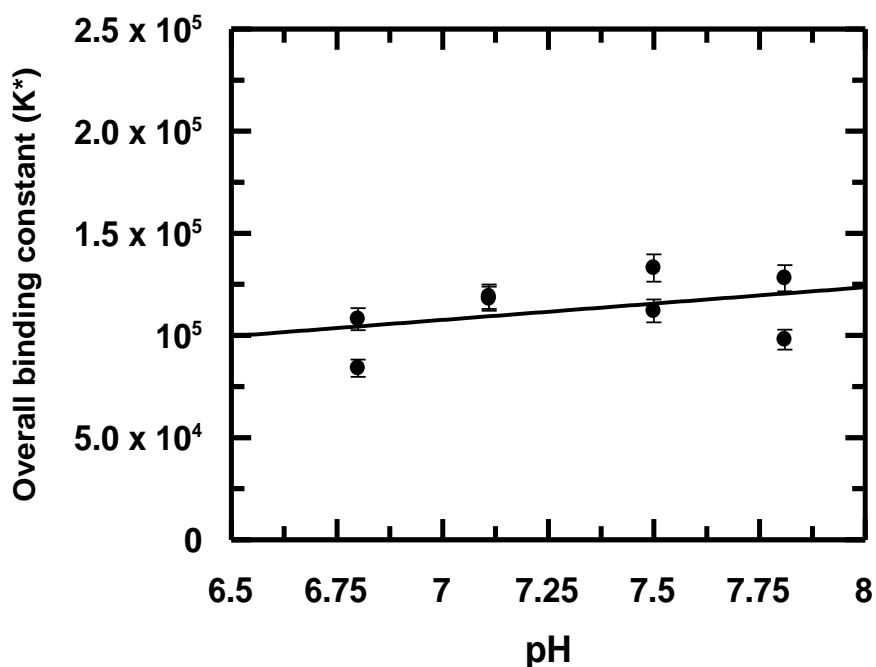


**Fig. 22:** Plot of variation of overall binding constant of Na[Co<sup>II</sup>(alz)<sub>3</sub>] interacting with calf thymus DNA at different pH (maintained using tris buffer) at 301 K and an ionic strength of 0.12 M with respect to NaCl. [Results of two independent experiments at each pH is shown].

Thus complexes are able to overcome some of the problems reported for alizarin pertaining to its binding with DNA. Since binding constant values for the complexes are close to those known for standard anthracyclines, this improves the chances of such complexes for consideration as potential anticancer agents that would also be less costly than anthracyclines.

### **2.5 Alizarin and Na[Co(alz)<sub>3</sub>] in NADH dehydrogenase assay to detect the generation of semiquinone**

A serious drawback of the hydroxy-9,10-anthraquinone based anthracycline anticancer agents is the generation of semiquinone radical anion, capable of forming superoxide radical anion, that are cardiotoxic and affects cancer patients adversely. At the same time, both semiquinone and superoxide radical anions are necessary for cytotoxic activity having a role in mechanism of drug action.<sup>1, 2, 7-11, 15-21</sup> Hence, owing to both positive and negative aspects associated with the formation of reduced oxygen species there is a need to have a correct balance in the generation of such intermediates so that efficacy and toxic side effects are such that it goes in favor of drug action benefitting the patient, i.e. minimizes adverse effects.<sup>1, 2, 7-11, 15-21, 23</sup> This is a major reason why complexes of hydroxy-9,10-anthraquinones (here alizarin) was studied; to be able to modulate the generation of semiquinone in a manner that their cardiotoxicity is checked.<sup>23</sup> The compromise a complex makes regarding efficacy in the free radical pathway is made up by some of its other attributes; facts that compelled researchers to prepare metal complexes of hydroxy-9,10-anthraquinones and try them in enzyme assays. Monitoring the generation of superoxide radical anion inhibited by superoxide dismutase (SOD) is important to realize how much is achieved through complex formation. In our case, generation of superoxide radical anion in presence of alizarin and its Co<sup>II</sup> complex were followed by measuring the reduction of cytochrome c inhibited by SOD.<sup>1, 2, 17, 18, 20, 29, 30, 31, 42</sup> As concentration of compounds increased, yield of O<sub>2</sub><sup>-</sup> due to alizarin increased (Fig. 23) suggesting that it catalyzes the flow of electrons from NADH to molecular oxygen in the



presence of NADH dehydrogenase. For the complex, however, formation of  $O_2^{\cdot -}$  was a lot less at similar concentrations. At the same time, it should be mentioned here that the decrease was not as much as that obtained with complexes of metal ions having a stable lower oxidation state, like that of Cu(II) or Fe(III).<sup>1, 2, 17-19</sup>

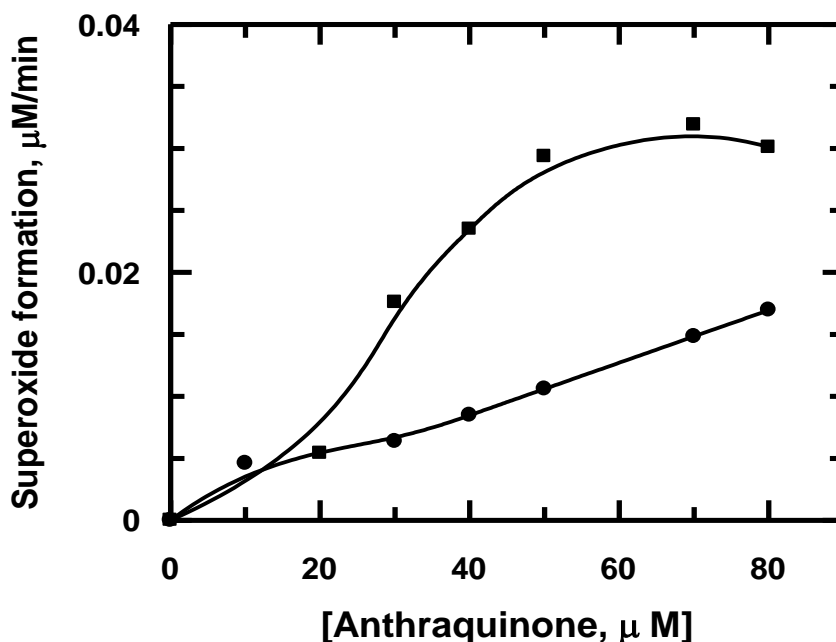


**Fig. 23:** A plot showing lack of stimulated superoxide formation by  $Na[Co(alz)_3]$  in comparison to alizarin in NADH dehydrogenase catalyzed reduction of cytochrome c by NADH.

$Co^{II}$ , lacking a stable lower oxidation state, the decrease was like that observed for  $Mn^{II}$  complexes of hydroxy-9,10-anthraquinones reported earlier.<sup>1, 2, 17-19</sup> For  $Na[Co(alz)_3]$ , the carbonyl at  $C_9$  of alizarin is involved in coordinating  $Co^{II}$ . The carbonyl not coordinated to the metal centre can still form semiquinone (Fig. 23). However, immediately after its formation, the electron gets transferred to a metal centre located on an adjacent complex leading to its decrease.<sup>43</sup> As a result, semiquinone formation for the complex decreases which is eventually successful in preventing them from being cardiotoxic (however, this couldn't be verified through experiments on cardiac muscle cells).

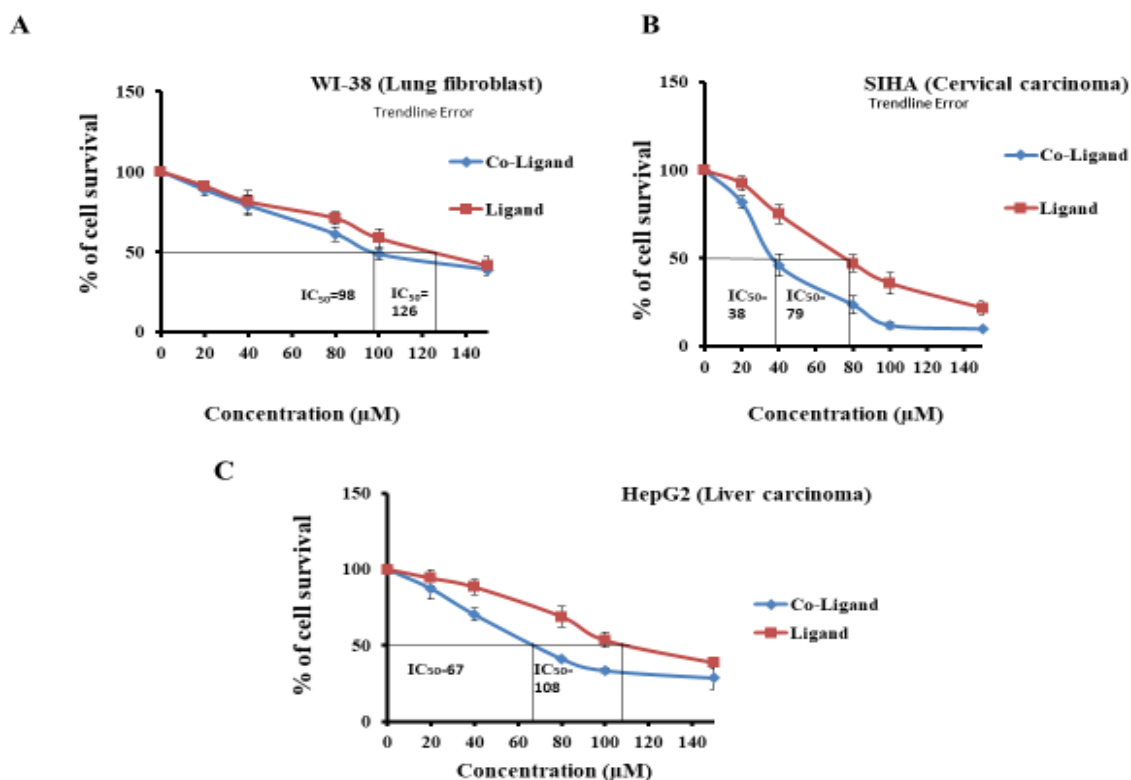


Fig. 24: Cell viability results of alizarin and Na[Co<sup>II</sup>(alz)<sub>3</sub>] on three different cell lines

## 2.6 Effect of alizarin and the complex on different cell lines

Cell viability assay performed with the compounds on normal human lung fibroblast (WI 38) cells and different cancer cell lines (SIHA and Hep G2) (Fig. 24 A-C) indicate that the complex is more effective on all three cell lines. From the data in Table 7, it is clear that the performance of the complex on cancer cells was significantly better than that on normal cells which is encouraging from the point of view of considering it as an anticancer agent. MTT assay indicates the complex is more effective on cervical cancer (SIHA) cells than on Hep G2 cells and that although significantly weaker in performance in comparison to doxorubicin or cisplatin, it is comparable to the reported activity of carboplatin and significantly better than Gemcitabine, some of the established drugs used in the treatment of cervical cancer.<sup>44-46</sup> Hence, the findings suggest that Co complexes of alizarin might have the potential to be an anticancer agent.

Table 7: IC<sub>50</sub> values of compounds on three different cell lines

Compounds	Normal human lung fibroblasts (WI 38) IC <sub>50</sub> value (μM)	SIHA cells IC <sub>50</sub> value(μM)	Hep G2 cells IC <sub>50</sub> value (μM)
Alizarin	126.0	79.0	108.0
Na[Co(alz) <sub>3</sub> ] or Co <sup>III</sup> (alz) <sub>3</sub>	98.0	38.0	67.0
*cisplatin <sup>46</sup>	30 ± 0.3	24.10 ± 0.15	(14.87 ± 1.22)
*Doxorubicin <sup>45, 47</sup>	0.01	0.02	(4.68 ± 1.08)

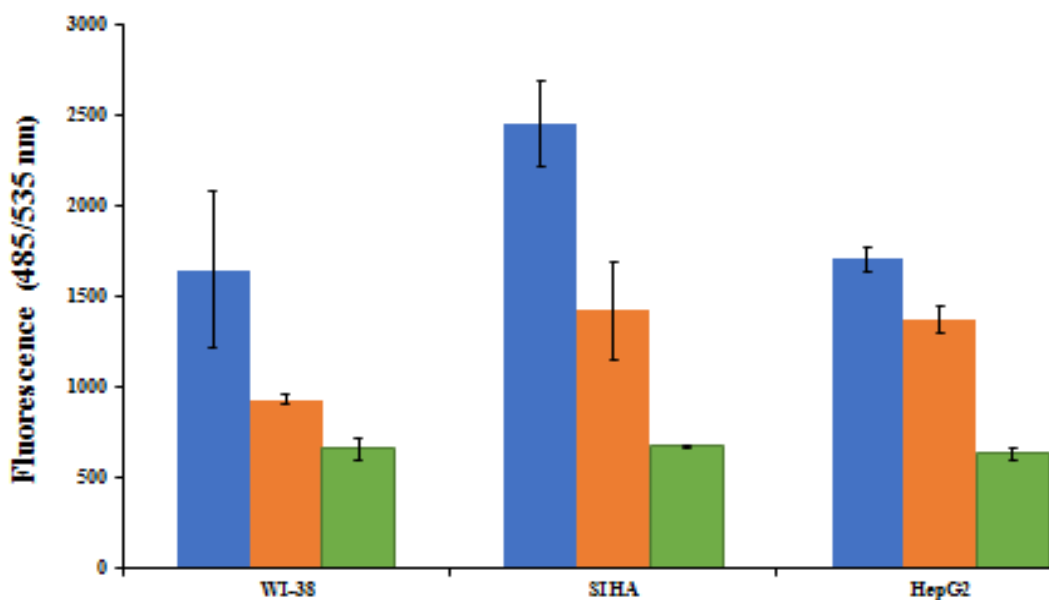


Fig. 25: Modulation of ROS generated by H<sub>2</sub>O<sub>2</sub> (~ 70 μM) in presence of alizarin (■) and Na[Co<sup>II</sup>(alz)<sub>3</sub>] (■). Presence of ROS in the absence of any compound is shown by (■). Difference in height for bars in blue is because the three cell lines are different and ROS due to a cell's own contribution gets added to ROS introduced from outside; Temperature = 301 K.

## **2.7 Detection of reactive oxygen species by the H<sub>2</sub>DCFDA assay**

An elegant approach to realizing the formation of ROS and its scavenging activity due to the complex was used by detecting them within cells by the H<sub>2</sub>DCFDA assay.<sup>47-50</sup> The complex and alizarin were investigated on cancer cell lines SIHA and HepG2 and on normal human lung fibroblast (WI-38) cells. As mentioned earlier, cells were previously treated with compounds at their respective IC<sub>50</sub> dose determined by the MTT assay. For such treatment of cells, ROS was generated by adding H<sub>2</sub>O<sub>2</sub> (~ 70 μM).

In ROS related experiments, where cells were not treated with any compound but only with H<sub>2</sub>O<sub>2</sub>, served as the control. In all three cell lines, depletion of ROS was greater for alizarin than for the complex. A result like this one on the presence of ROS, has a role related to the activity of the compounds, on a chosen cell line i.e. if we consider the free radical pathway to play a major role in the mode of action of the compounds. The experiment on ROS clearly demonstrates why the complex performs better than alizarin on all three cell lines although extent of damage was different. Although on all chosen cell lines, ROS was found to be quenched to a maximum extent by alizarin, the difference in the presence of ROS due to compounds was larger and in favor of the complex on the two cancer cell lines. Hence, Fig. 25 provides evidence why the complex performs better on cancer cells than on normal human lung fibroblast (WI-38) cells. Besides, biophysical interactions quite clearly suggest why the results on MTT assay are in favor of the complex. Going by the findings shown in Fig. 25, a prediction for the activity of the complex and of alizarin on normal human lung fibroblast (WI-38) cells, it can be said that they should be the same if one only considers the free radical pathway since the difference in the presence of ROS is extremely small. There is thus good correlation between sustenance (presence) of ROS on carcinoma (SIHA and HepG2) cells due to alizarin and the complex (Fig. 25) and that such trends were maintained in the results obtained from the MTT assay (Table 8). This further suggests that free radical induced

damage of cells is an important pathway showing cytotoxic activity. Although not investigated as a part of this study, it has been reported earlier that a good number of metal complexes of hydroxy-9,10-anthraquinones are effective inhibitors of human DNA topoisomerase I and human DNA topoisomerase II.<sup>17, 18, 20</sup>

Therefore, this complex that is structurally similar to such previously reported metal-hydroxy-9,10-anthraquinone complexes, could well be a human DNA topoisomerase I and human DNA topoisomerase II inhibitor and that might also serve as further reason for its superior anticancer activity.

### **3. References:**

- [1] M. M. L. Fiallo, A. Garnier-Suillerot. 1985. Physicochemical studies of the iron(III)-carminomycin complex and evidence of the lack of stimulated superoxide production by NADH dehydrogenase. *Biochim. Biophys. Acta.-Gen. Subj.* 840:91-98. [https://doi.org/10.1016/0304-4165\(85\)90165-5](https://doi.org/10.1016/0304-4165(85)90165-5)
- [2] M. M. L. Fiallo, A. Garnier-Suillerot. 1986. Metal anthracycline complexes as a new class of anthracycline derivatives. Palladium(II)-adriamycin and palladium(II)-daunorubicin complexes: physicochemical characteristics and antitumor activity. *Biochemistry*. 25:924–930.
- [3] M. Volkova and R. Russell. 2011. Anthracycline cardiotoxicity: Prevalence, pathogenesis and treatment. *Curr Cardiol Rev.* 7:214–220; doi: 10.2174/157340311799960645.
- [4] A. Jabłońska-Trypuć, G. Swiderski, R. Kręćkowski, W. Lewandowski. 2017. Newly synthesized doxorubicin complexes with selected metals—Synthesis, structure and anti-breast cancer activity. *Molecules*. 22:1106; doi:10.3390/molecules22071106.

**Chapter 9: A Cobalt<sup>II</sup>/Cobalt<sup>III</sup> complex of alizarin..... a simpler anthracycline analogue**

---

- [5] M. Kozsup, O. Domotor, S. Nagy, E. Farkas, E. A. Enyedy, P. Buglyo. 2020. Synthesis, characterization and albumin binding capabilities of quinizarin containing ternary cobalt(III) complexes. *J. Inorg. Biochem.* 204:110963.
- [6] M. M. L. Fiallo, A. Garnier-Suillerot, B. Matzanke, H. Kozlowski. 1999. How Fe<sup>3+</sup> binds anthracycline antitumour compounds. *J. Inorg. Biochem.* 75:105–115; 10.1016/s0162-0134(99)00040-9.
- [7] C. Vergely, S. Delemasure, Y. Cottin, L. Rochette. 2007. Preventing the cardiotoxic effects of anthracyclines: From basic concepts to clinical data. *Heart Metab.* 35:1-7.
- [8] S. E. Lipshultz, J. A. Alvarez, R. E. Scully. 2008. Anthracycline associated cardiotoxicity in survivors of childhood cancer. *Heart.* 4:525–533. 10.1136/hrt.2007.136093..
- [9] M. Štěřba, O. Popelová, A. Vávřová, E. Jirkovský, P. Kovaříková, V. Geršl, T. Šimůnek. 2013. Oxidative stress, redox signaling, and metal chelation in anthracycline cardiotoxicity and pharmacological cardioprotection. *Antioxid Redox Signal.* 18:899–929.
- [10] A. A. Lohade, R. R. Jain, K. Iyer, S. K. Roy, H. H. Shimpi, Y. Pawar, M. G. R. Rajan, M. D. Menon. 2016. A novel folate-targeted nanoliposomal system of doxorubicin for cancer targeting. *AAPS PharmSciTech.* 17:1298–1311. <https://doi.org/10.1208/s12249-015-0462-2>.
- [11] D. Cardinale, F. Iacopo, C. M. Cipolla. 2020. Cardiotoxicity of anthracyclines. *Front. Cardiovasc. Med.* 7:26. doi: 10.3389/fcvm.2020.00026.
- [12] K. Shee, A. T. Kono, S. P. D' Anna, M. A. Seltzer, X. Lu, T. W. Miller, Mary D. 2016. Chamberlin, Maximizing the benefit-cost ratio of anthracyclines in metastatic breast cancer: case report of a patient with a complete response to high-dose doxorubicin. *Case Rep Oncol.* 9:840–846.
- [13] M. Braun, V. R. Jacobs, S. Wagenpfeil, D. Sattler, N. Harbeck, U. Nitz, R. Bernard, W. Kuhn, A. Ihbe-Heffinger. 2009. Cost analysis comparing an anthracycline/docetaxel regimen

to CMF in patients with early stage breast cancer. *Onkologie*. 32:473-81. doi: 10.1159/000226211

[14] S. Y. van der Zanden, X Qiao, J. Neefjes. 2020. New insights into the activities and toxicities of the old anticancer drug doxorubicin. *FEBS J*. <https://doi.org/10.1111/febs.15583>.

[15] P. S. Guin, P. C. Mandal, S. Das. 2012. A comparative study on the interaction with calf thymus DNA of a Ni(II) complex of the anticancer drug adriamycin and a Ni(II) complex of sodium 1,4-dihydroxy-9,10-anthraquinone-2-sulphonate. *J. Coord. Chem.* 65:705-721.

[16] S. Mukherjee, P. K. Gopal, S. Paul, S. Das. 2014. Acetylation of 1,2,5,8-tetrahydroxy-9,10-anthraquinone improves binding to DNA and shows enhanced superoxide formation that explains better cytotoxicity on JURKAT T lymphocyte cells. *J. Anal. Oncol.* 3:122–129. <https://doi.org/10.6000/1927-7229.2014.03.03.2>

[17] P. Das, C. K. Jain, S. K. Dey, R. Saha, A. D. Chowdhury, S. Roychoudhury, S. Kumar, H. K. Majumder, S. Das. 2014. Synthesis, crystal structure, DNA interaction and in vitro anticancer activity of a Cu(II) complex of purpurin: dual poison for human DNA topoisomerase I and II. *RSC Adv.* 4:59344-59357.

[18] P. Das, C. K. Jain, S. Roychoudhury, H. K. Majumder, S. Das. 2016. Design, synthesis and in vitro anticancer activity of a Cu(II) complex of carminic acid: A novel small molecule inhibitor of human DNA topoisomerase I and topoisomerase II. *ChemistrySelect*.1:6623-6631.

[19] B. Mandal, S. Singha, S. K. Dey, S. Mazumdar, S. Kumar, P. Karmakar, S. Das. 2017. CuII complex of emodin with improved anticancer activity as demonstrated by its performance on HeLa and Hep G2 cells. *RSC Adv.* 7:41403-41418.

[20] S. Mukherjee-Chatterjee, C. K. Jain, S. Singha, P. Das, S. Roychoudhury, H. K. Majumder, S. Das. 2018. Activity of CoII–Quinalizarin: A novel analogue of anthracycline-

### ***Chapter 9: A Cobalt<sup>II</sup>/Cobalt<sup>III</sup> complex of alizarin..... a simpler anthracycline analogue***

based anticancer agents targets human DNA topoisomerase, whereas quinalizarin itself acts via formation of semiquinone on acute lymphoblastic leukemia MOLT-4 and HCT 116 cells. *ACS Omega*. 3:10255-10266.

[21] P. Das, D. Bhattacharya, P. Karmakar, S. Das. 2015. Influence of ionic strength on the interaction of THA and its Cu (II) complex with DNA helps to explain studies on various breast cancer cells. *RSC Adv*. 5:73099-73111.

[22] N. Ozenver, M. Saeed, L. O. Demirezer, T. Efferth. 2018. Aloe-emodin as drug candidate for cancer therapy. *Oncotarget*. 9: 17770-17796. doi: 10.18632/oncotarget.24880.

[23] E. K. Akkol, I. I. Tatlı, G. S. Karatoprak, O.T. Aşgar, Ç. Yücel, E. Sobarzo-Sánchez, R. Capasso. 2021. Is emodin with anticancer effects completely innocent? Two sides of the coin. *Cancers*. 13:2733. <https://doi.org/10.3390/cancers13112733>.

[24] Activity of emodin in different types of cancer (Review), *Oncology Reports*, **30**, 2555-2562 (2013). <https://doi.org/10.3892/or.2013.2741>.

[25] G. Cozza, A. Venerando, S. Sarno, L. A. Pinna. 2015. The selectivity of CK2 inhibitor quinalizarin: A re-evaluation, *Biomed Res. Int.* 734127. <https://doi.org/10.1155/2015/734127>.

[26] X. Li, H. Wang, J. Wang, Y. Chen, X. Yin, G. Shi, H. Li, Z. Hu, X. Liang. 2016. Emodin enhances cisplatin-induced cytotoxicity in human bladder cancer cells through ROS elevation and MRP1 down regulation. *BMC Cancer* 16:578. <https://doi.org/10.1186/s12885-016-2640-3>.

[27] Y. Q. Zang, Y. Y. Feng, Y. H. Luo, Y. Q. Zhai, X. Y. Ju, Y. C. Feng, Y. N. Sheng, J. R. Wang, C. Q. Yu, C. H. Jin. 2019. Quinalizarin induces ROS-mediated apoptosis via the MAPK, STAT3 and NF-κB signaling pathways in human breast cancer cells, *Mol. Med. Rep.* 20:4576-4586.



- [28] Y. Zhou, K.Li, S.Zhang, Q.Li, Z.Li, F.Zhou, X.Dong, L.Liu, G.Wu, R.Meng. 2015. Quinalizarin, a specific CK2 inhibitor, reduces cell viability and suppresses migration and accelerates apoptosis in different human lung cancer cell lines, *Ind. Jour. Cancer.* 52:119-124.
- [29] P. S. Guin, S. Das, P. C. Mandal. 2009. Studies on the formation of a complex of Cu(II) with sodium 1,4-dihydroxy-9,10-anthraquinone-2-sulphonate – An analogue of the core unit of anthracycline anticancer drugs and its interaction with calf thymus DNA. *J. Inorg. Biochem.* 103:1702-1710.
- [30] S. Roy, P. Mondal, P. S. Sengupta, D. Dhak, R. C. Santra, S. Das, P. S. Guin. 2015. Spectroscopic, computational and electrochemical studies on the formation of the copper complex of 1-amino-4-hydroxy-9,10-anthraquinone and effect of it on superoxide formation by NADH dehydrogenase. *Dalton Trans.* 44:5428-5440.
- [31] F. Perveen, N. Arshad, R. Qureshi, J. Nowsherwan, A. Sultan, B. Nosheen. 2018. Electrochemical, spectroscopic and theoretical monitoring of anthracyclines' interactions with DNA and ascorbic acid by adopting two routes: Cancer cell line studies. *PLoS ONE.* 13, e0205764. <https://doi.org/10.1371/journal.pone.0205764>
- [32] K. Nakamoto. 1978. *Infrared and Raman spectra of inorganic and coordination compounds.* 3<sup>rd</sup> edn. Wiley-Interscience: New York, USA.
- [33] O. L. Alves, Y.Hase. 1982. The infrared spectra of cobalt(II) halide complexes with trimethylphosphine oxide (TMPO), *Spec. Lett.* 15: 423-433.
- [34] F. Andrade, M. M. Roca-Melendres, E. F. Durán-Lara, D. Rafael, S. Schwartz Jr. 2021. Stimuli-responsive hydrogels for cancer treatment: The role of pH, light, ionic strength and magnetic field. *Cancers.* 13:1164; <https://doi.org/10.3390/cancers13051164>.

***Chapter 9: A Cobalt<sup>II</sup>/Cobalt<sup>III</sup> complex of alizarin..... a simpler anthracycline analogue***

---

[35] S. Senapati, A. K. Mahanta, S. Kumar, P. Maiti. 2018. Controlled drug delivery vehicles for cancer treatment and their performance. *Sig Transduct Target Ther.* <https://doi.org/10.1038/s41392-017-0004-3>.

[36] B. Manocha, A. Margaritis. 2010. Controlled release of doxorubicin from doxorubicin/-polyglutamic acid ionic complex. *J. Nanomaterials*. Article ID 780171, 9 pages; <https://doi.org/10.1155/2010/780171>.

[37] J. M. Asara, J. S. Hess, E. Lozada, K. R. Dunbar, J. Allison. 2000. Evidence for Binding of Dirhodium Bis-Acetate Units to Adjacent GG and AA Sites on Single-Stranded DNA. *J. Am. Chem. Soc.* 1: 8–13.

[38] H. T. Chifotides, J. M. Koomen, M. Kang, S. E. Tichy, K. R. Dunbar, D. H. Russell. 2004. Binding of DNA purine sites to dirhodium compounds probed by mass spectrometry. *Inorg. Chem.* 20: 6177–6187.

[39] S. Mukherjee, P. Das, S. Das. 2012. Exploration of small hydroxy-9,10-anthraquinones as anthracycline analogues: Physicochemical characteristics and DNA binding for comparison. *J. Phys. Org. Chem.* 25:385-393.

[40] S. M. Noh. 2003. Measurement of peritoneal fluid pH in patients with non-serosal invasive gastric cancer. *Yonsei Med J.* 44:45-48; 10.3349/ymj.2003.44.1.45.

[41] G. Hao, Z. P. Xu, L. Li. 2018. Manipulating extracellular tumour pH: an effective target for cancer therapy. *RSC Adv.* 8: 22182-22192; DOI:10.1039/C8RA02095G.

[42] H. R. Mahler. 1955. In: *Methods in Enzymology* 11 (S. P. Colowick and N. O. Kaplan, eds.) New York, USA: Academic Press. 668-672.

[43] S. Das, A. Bhattacharya, P. C. Mandal, M. C. Rath, T. Mukherjee. 2002. One-electron reduction of 1,2-dihydroxy-9,10-anthraquinone and some of its transition metal complexes in

aqueous solution and in aqueous isopropanol–acetone-mixed solvent: a steady-state and pulse radiolysis study. *Rad. Phys. Chem.* 65:93-100.

[44] R. Koivusalo, S. Hietanen. 2004. The cytotoxicity of chemotherapy drugs varies in cervical cancer cells depending on the p53 status. *Cancer Biol. Ther.* 3:1177-1183; DOI: 10.4161/cbt.3.11.1340.

[45] C. W. Lewis, R. M. Golsteyn. 2016. Cancer cells that survive checkpoint adaptation contain micronuclei that harbor damaged DNA. *Cell Cycle.* 15:3131–3145.

[46] L. A. Lambert, N. Qiao, K. K. Hunt, D. H. Lambert, G. B. Mills, L. Meijer, K. Keyomarsi. 2008. Autophagy: a novel mechanism of synergistic cytotoxicity between doxorubicin and roscovitine in a sarcoma model, *Cancer Res.* 68: 7966-7974.

[47] A. Pramanik, D. Laha, S. Chattopadhyay, S. K. Dash, S. Roy, P. Pramanik, P. Karmakar. 2015. Targeted delivery of “copper carbonate” nanoparticles to cancer cells in vivo. *Toxicol. Res.* 4:1604–1612.

[48] H. Wang, J. A. Joseph. 1999. Quantifying cellular oxidative stress by dichlorofluorescein assay using microplate reader. *Free Radical Biol. Med.* 27:612–616.

[49] O. Myhre, J. M. Andersen, H. Aarnes, F. Fonnum. 2003. Evaluation of the probes 2',7'-dichlorofluorescein diacetate, luminol, and lucigenin as indicators of reactive species formation. *Biochem. Pharmacol.* 65:1575-1582.

[50] A. Gomes, E. Fernandes, J. L. Lima. 2005. Fluorescence probes used for detection of reactive oxygen species. *J. Biochem. Biophys. Methods.* 65:45–80.



# CHAPTER 10

**Comparing chemical, biophysical  
and biochemical attributes of  
anthracyclines as anticancer  
agents using carminic acid and  
its  $Mn^{II}$  complex**

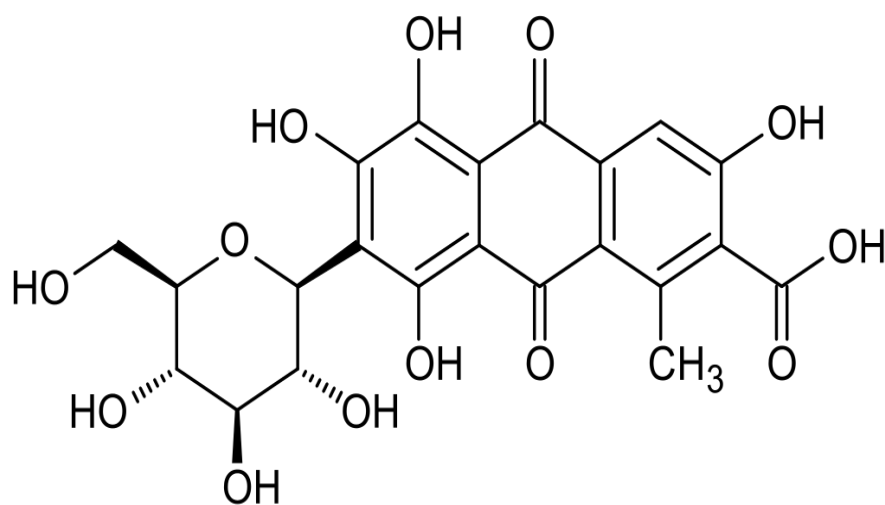


## 1. Introduction:

Anthracyclines derived from soil bacterium *streptomyses* constitute an important group of molecules being tried in numerous forms of cancer.<sup>1,2</sup> They are reported to be active by different mechanisms that inhibit replication and transcription of DNA interfering with topoisomerase activity, and leading to cell death.<sup>3,4</sup> Some of the already established pathways for its action are i) intercalation into DNA causing a distortion of the correct three dimensional structure required for DNA to function under nature's direction, ii) forming semiquinone (and in oxic medium, superoxide radical anion), they damage various biomolecules in a free radical pathway inflicting damage either to sugar residues or to nucleic acid bases, iii) by forming an adduct with topoisomerase and DNA, they prevent the latter to return to the desired double helical form during replication and/or transcription. Any or all of these and many more initiates a cascade of reactions responsible for cell death.<sup>3-7</sup>

As mentioned previously also, a major limitation is their toxic side effects; of particular concern is cardiotoxicity, seen as a major hurdle in utilizing them to maximum potential.<sup>8,9</sup> The anthraquinone unit in anthracyclines upon reduction form semiquinone and quinone dianion.<sup>7</sup> Although important for drug action, these form species that affect cardiac muscles adversely. Reports indicate patients treated with anthracyclines either succumb to heart problems or live their lives with an ailing heart.<sup>8-10</sup> Research has revealed metal ion complexes of anthracyclines control generation of semiquinone and that such complexes are less cardiotoxic.<sup>11-14</sup> However, in an attempt to check cardiotoxicity i.e. in trying to decrease generation of semiquinone, a compromise on efficacy in the free radical pathway is expected. Usually, this does not affect overall activity of a complex in reference to parent anthraquinone. Another major limitation of anthracyclines is their high cost. Hence, there is an effort to see if simpler analogues that are less costly could be promoted as substitutes. Work on hydroxy-9,10-anthraquinones indicate, while there is undoubtedly an economic advantage in using

simpler analogues, biological efficacy of analogues are almost three order less. Several types of research identified the fact that efficacy of anthracyclines may be attributed to sugar units present that the simpler hydroxy-9,10-anthraquinone analogues lack.<sup>15,16</sup> Hence, another simple analogue, carminic acid, but having a sugar unit bound to hydroxy-9, 10-anthraquinone was selected and its Mn(II) complex was prepared to see if they show comparable efficacy as known for anthracyclines.<sup>17-23</sup>



CARMINIC ACID

## 2. Results and Discussion:

### 2.1 Determination of stoichiometry of interaction between Mn<sup>II</sup> and carminic acid using mole ratio and Job's method of continuous variation:

To determine the composition of the complex in solution, equimolar solutions of Mn(II) and CA were used. Stoichiometry of complex formation was ascertained by the mole ratio and Job's method of continuous variation. In the mole ratio method, concentration of CA was kept constant, while Mn<sup>II</sup> was varied. Absorbance of solutions were plotted against ratio of concentration of Mn(II) to CA at a fixed concentration of CA at two different pH. T<sub>M</sub> and T<sub>L</sub> indicate concentrations of Mn<sup>II</sup> and CA respectively. Fig. 1A & 1B represent mole ratio plots of experiments performed at pH 7.4 and 6.4 respectively.



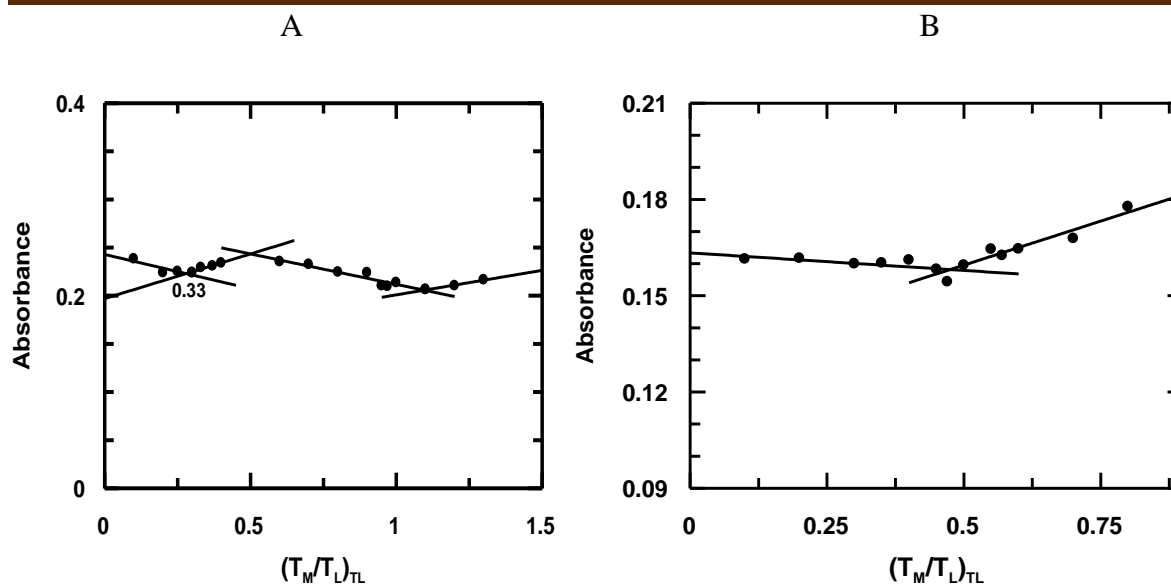


**Fig. 1:** Mole ratio plot of absorbance at 511 nm for [Mn(II)]/[CA] at a fixed concentration of CA at (A) pH 7.4 and (B) pH 6.4. [CA] =  $10^{-3}$  M, [NaNO<sub>3</sub>] = 0.1 M, T = 297 K.

The mole ratio plots indicate at pH 7.4, all three species, 1:1, 1:2 and 1:3 may clearly be identified in solution from the intersection of lines shown (Fig. 1 A). However, on decreasing pH to ~6.4, only 1:2 species was obtained. Hence, stoichiometric determination by mole ratio method at different pH, provide a clue to preparing the 1:2 complex. In fact, variation of pH for stoichiometry determination was done for many more values; results obtained at two such values are presented here.

In Job's method of continuous variation, complementary mixtures were prepared. Absorbance of solutions were measured at 495 nm and plotted against changing metal ion and ligand concentrations (Fig. 2). Stoichiometry was ascertained from the maxima in the curve occurring at a ratio of 1:2 for Mn<sup>II</sup> : CA. Therefore we see that both from mole ratio and Job's method of continuous variation, in the pH range 6.4 to 6.8 stoichiometry of complex formation between Mn(II) and CA is 1:2.

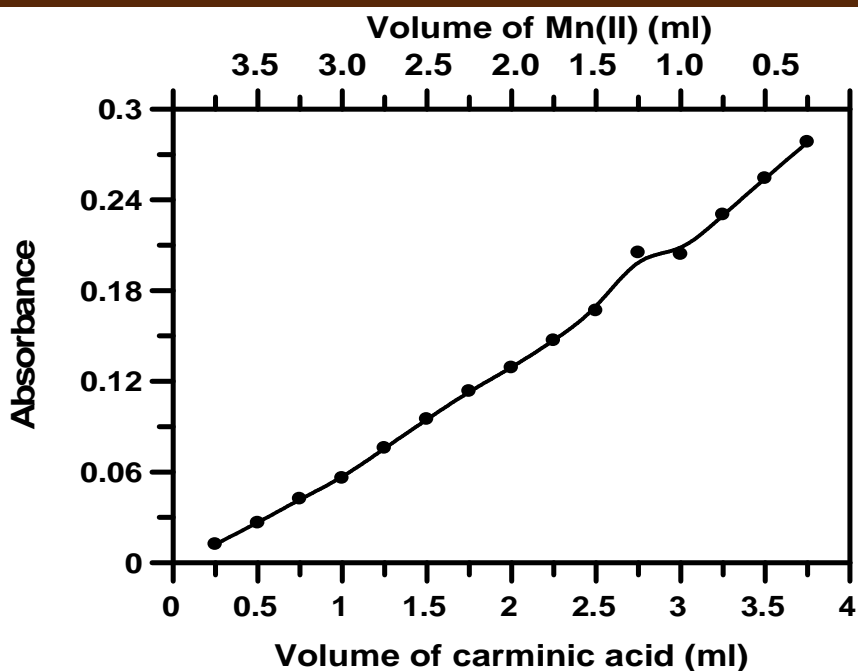


**Fig. 2:** Job's plot showing variation in absorbance for varying concentrations of CA and  $Mn(II)$  at  $pH = 6.8$ ;  $[NaNO_3] = 0.1 M$ ,  $T = 298 K$ .

## 2.2. Proton dissociations in CA in the absence and presence of $Mn^{II}$ :

An aqueous solution of CA was titrated in the  $pH$  range 3.0 to 11.0 and its absorbance followed at 529 nm. Fitting the experimental data according to Eq. 3b (*Chapter 6: Experimental*), as shown in Fig. 3,  $pK_1$ ,  $pK_2$  and  $pK_3$  were found to be  $5.30 \pm 0.24$ ,  $7.20 \pm 0.25$  and  $10.30 \pm 0.15$  respectively.

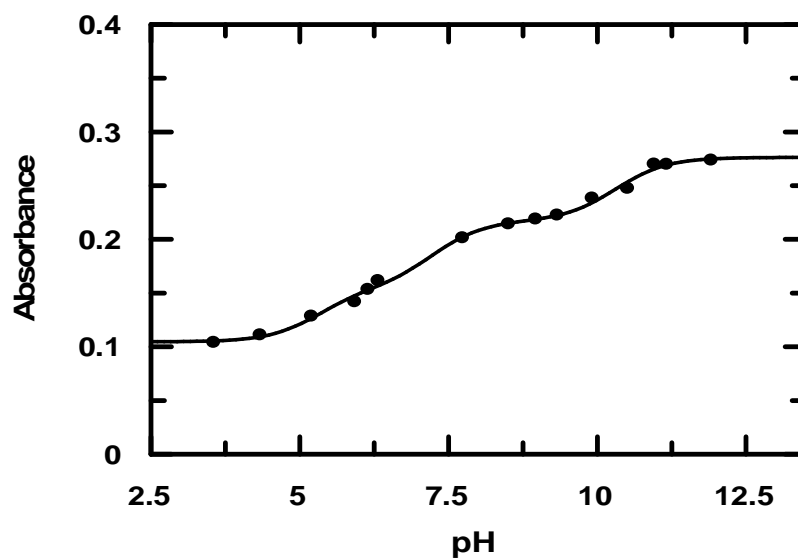


**Fig. 3:** Spectrophotometric titration of CA as shown by a variation in absorbance at 529 nm;  $[CA] = 10^{-3} M$ ,  $[NaNO_3] = 0.1 M$ ,  $T = 297 K$ .

Subsequently, CA and Mn<sup>II</sup> were mixed in the ratio 2:1 and a spectrophotometric titration was performed in the pH range 3.0 to 11.0. The change in absorbance of CA in the presence of Mn(II) was followed at 493 nm.

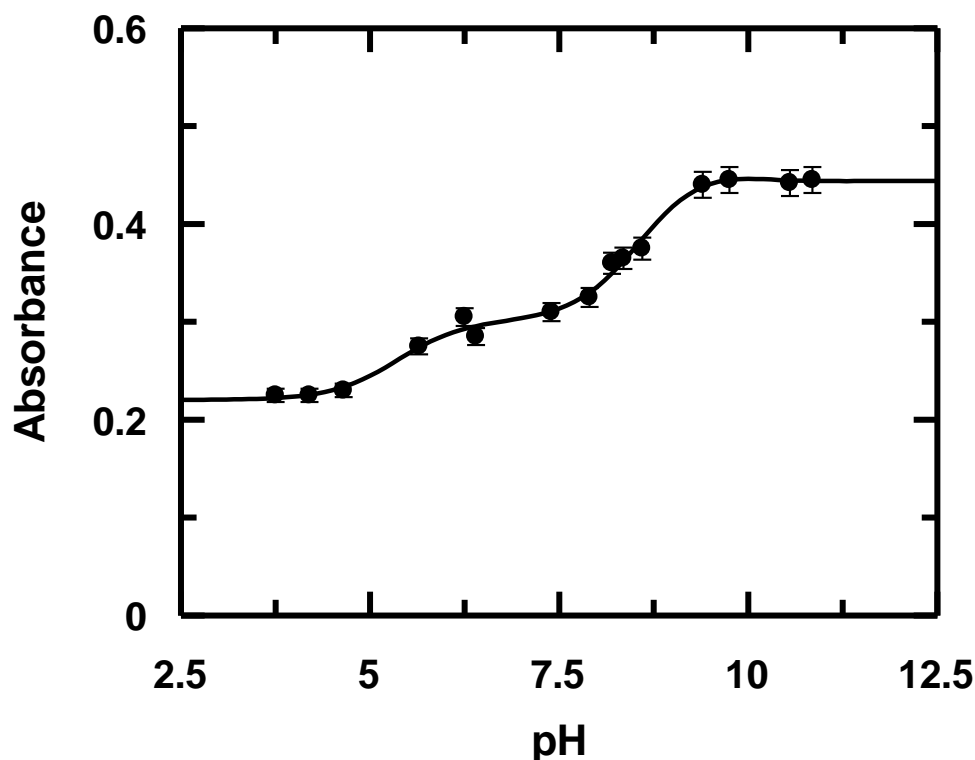


**Fig. 4:** Spectrophotometric titration of CA in the presence of Mn(II) as shown by a variation in absorbance at 493 nm; [CA] =  $10^{-3}$  M, [NaNO<sub>3</sub>] = 0.1 M, T = 297 K.

Fitting the experimental data according to Eq. 3b (*Chapter 6: Experimental*), three pK values,  $pK_1 = 5.35 \pm 0.23$ ,  $pK_2 = 8.52 \pm 0.10$  and  $pK_3 = 10.24 \pm 1.76$  were obtained. While  $pK_1$  corresponds to dissociation of the carboxyl proton,  $pK_2$  and  $pK_3$  are due to phenolic -OH.  $pK_2$  corresponds to the dissociation of phenolic -OH proton at C<sub>3</sub> carbon atom while  $pK_3$  denotes dissociation of phenolic-OH proton at C<sub>6</sub> carbon atom. The pK values of CA determined in the presence of Mn(II) helps in preparing the complex in the sense that, if complex formation is attempted around pH 6.5, while -COOH would be substantially dissociated, dissociation of the proton on phenolic -OH at C<sub>3</sub> would be slightly less than 50%

( $pK_2 = 8.52 \pm 0.08$ ) dissociated and dissociation of phenolic –OH at C<sub>6</sub> would be negligible.

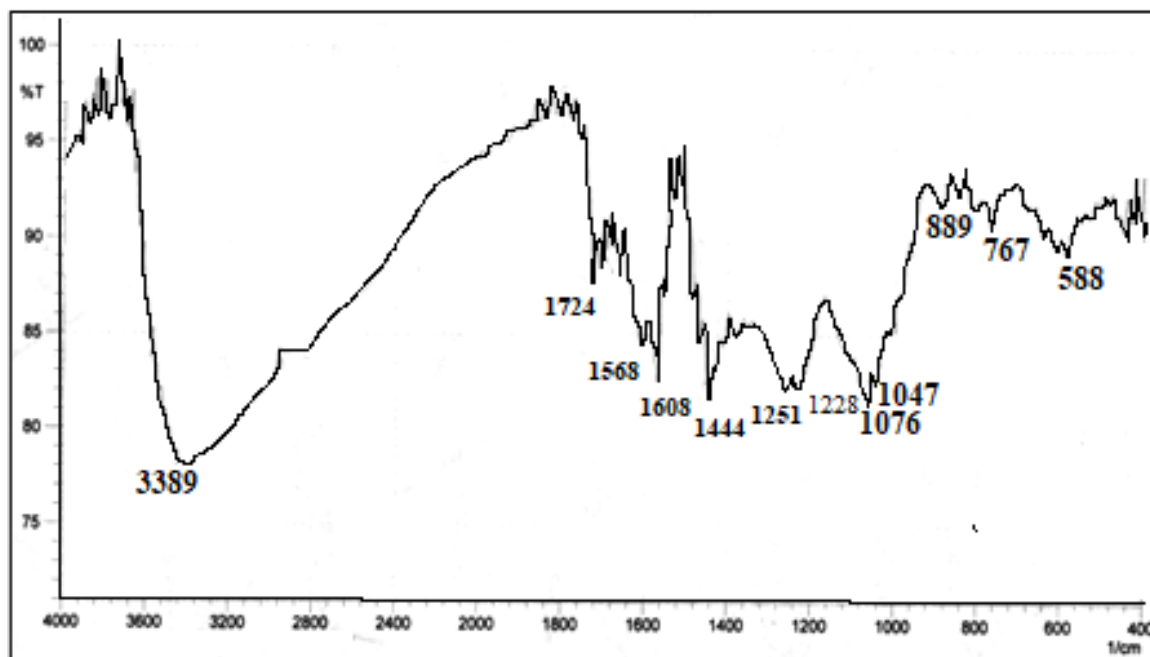
Hence, going by the above mentioned dissociations of CA in presence of Mn(II) at pH ~6.5, it may be said that the likelihood of coordination of Mn(II) in the 1:2 complex species identified during stoichiometry determination (Figs. 1 & 2) are –COO<sup>-</sup> and phenolate (–O<sup>-</sup>) anion at C<sub>3</sub>. Hence, the complex would be anionic with a charge of -2.

### **2.3 Characterization of [Mn(CA)<sub>2</sub>]<sup>2-</sup>**

#### **2.3.1 Comparison IR of CA and [Mn(CA)<sub>2</sub>]<sup>2-</sup>:**

IR spectrum of pure CA indicates a band in the region 3535 cm<sup>-1</sup> to 3270 cm<sup>-1</sup> attributed to strong intramolecular H- bonding between quinone carbonyls and phenolic–OH (Fig. 5A). This is almost unchanged in the complex with a reasonably strong response at 3334 cm<sup>-1</sup> (Fig. 5B) suggesting that the region around the carbonyl and adjoining phenolic –OH do not undergo much of a change following complex formation and that intramolecular H-bonding found in CA is maintained in the complex. Further support is obtained from stretching of quinone carbonyls obtained at 1608 cm<sup>-1</sup> in CA and 1598 cm<sup>-1</sup> in the complex, suggesting that quinone carbonyls in CA are not involved in complex formation. Appearance of a strong peak at 603 cm<sup>-1</sup> indicates the formation of Mn–O bonds. Hence, from IR spectroscopy it becomes apparent CA binds Mn(II) via the –COO<sup>-</sup> phenolate anion at C<sub>3</sub>.<sup>24</sup>

A



B

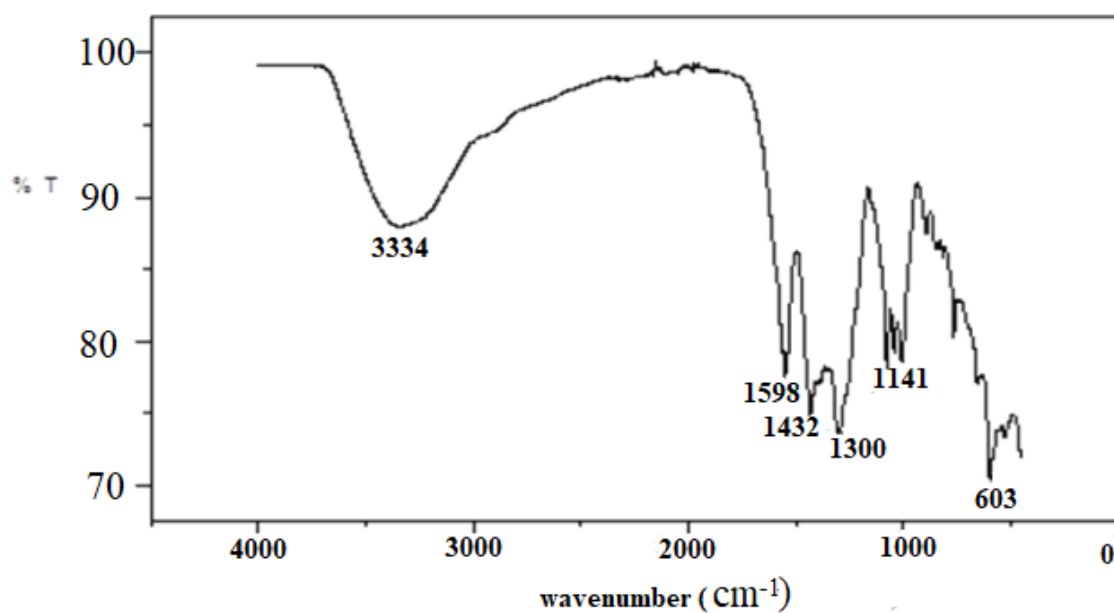
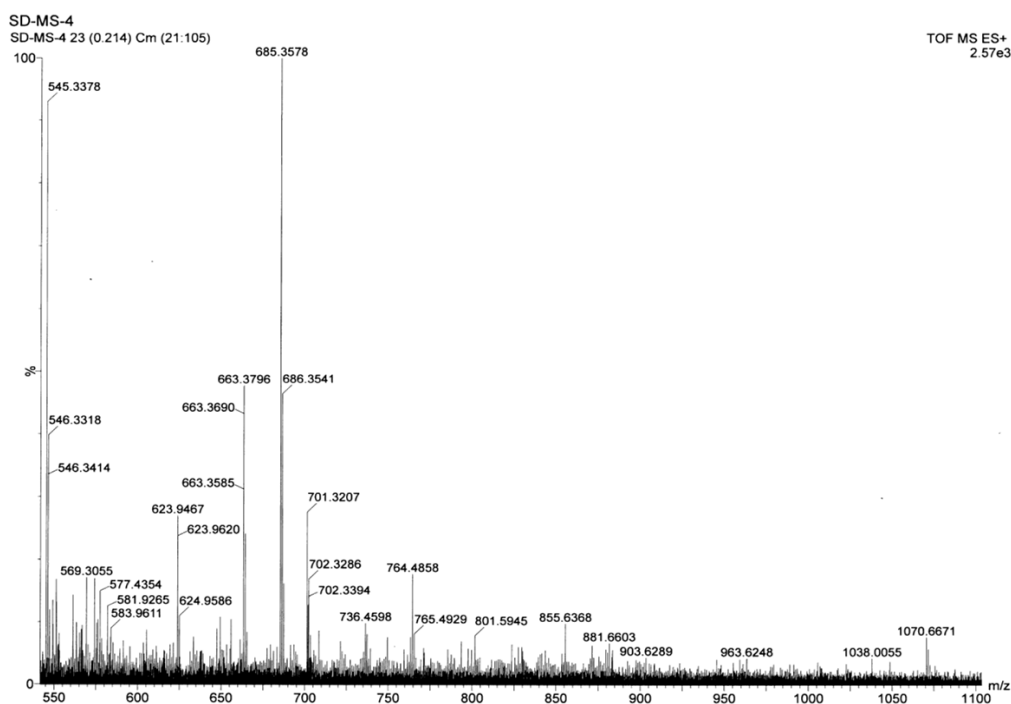


Fig. 5: (A) IR spectrum of carminic acid and (B) Na<sub>2</sub>[Mn(CA)<sub>2</sub>]



**Fig. 6:** Mass spectrum of [Mn(CA)<sub>2</sub>]

### 2.3.2 Analysis of the mass spectrum of Na[Co<sup>II</sup>(alz)<sub>3</sub>]:

Evidence from physico-chemical experiments and elemental analysis suggest formation of a 1:2 Mn<sup>II</sup>-CA complex. The molecular ion peak was obtained at  $m/z = 1070.6671$  (Fig. 6). This corresponds to the formula  $[\text{Mn}^{\text{II}}(\text{CA})_2(\text{H}_2\text{O})_2]^{2-}$ . From the molecular ion peak, loss of two molecules of water results in  $[\text{Mn}^{\text{II}}(\text{CA})_2]^{2-}$  having  $m/z = 1038.0055$  (theoretically expected value is 1035.76). From the fragment with  $m/z = 1038.0055$ , if two sugar units depart we should get a species having  $m/z = 714.0055$  that upon further loss of a methyl group should result in a species with  $m/z = 700.0055$  (experimental peaks were found at  $m/z = 701.3207, 702.3286$  and  $702.3394$ ). Loss of another methyl group should result in a species having  $m/z = 686$ . Two very intense peaks at  $m/z = 686.3541$  and  $685.3578$  support the generation of such a species. Hence, the mass spectrum of the complex suggests that Mn(II) forms an octahedral complex with CA whose formula is  $\text{Na}_2[\text{Mn}^{\text{II}}(\text{CA})_2(\text{H}_2\text{O})_2]$ . However, as

we have been mentioning, henceforth also, the complex is being represented as [Mn<sup>II</sup>(CA)<sub>2</sub>]<sup>2-</sup>.

### 2.3.3 Magnetic moment of [Mn(CA)<sub>2</sub>]:

Magnetic susceptibility was measured by Gouy method and  $\mu_{\text{eff}}$  was found to be 6.3 BM. Such a high value for magnetic moment indicates the compound possesses 5 unpaired electrons and hence Mn in the complex has an oxidation state +2.

### 2.3.4 Electrochemical studies

Cyclic voltammetry was used to study electrochemical behaviour of CA in DMF using Ag/AgCl, KCl (saturated) electrode as reference and TBAB as supporting electrolyte. Potential was varied from 0.0 V to -1.9 V using different scan rates. Variation of cathodic peak current with square root of potential sweep rate provides a straight line passing through the origin indicating reduction of CA is diffusion controlled (Fig. 7).

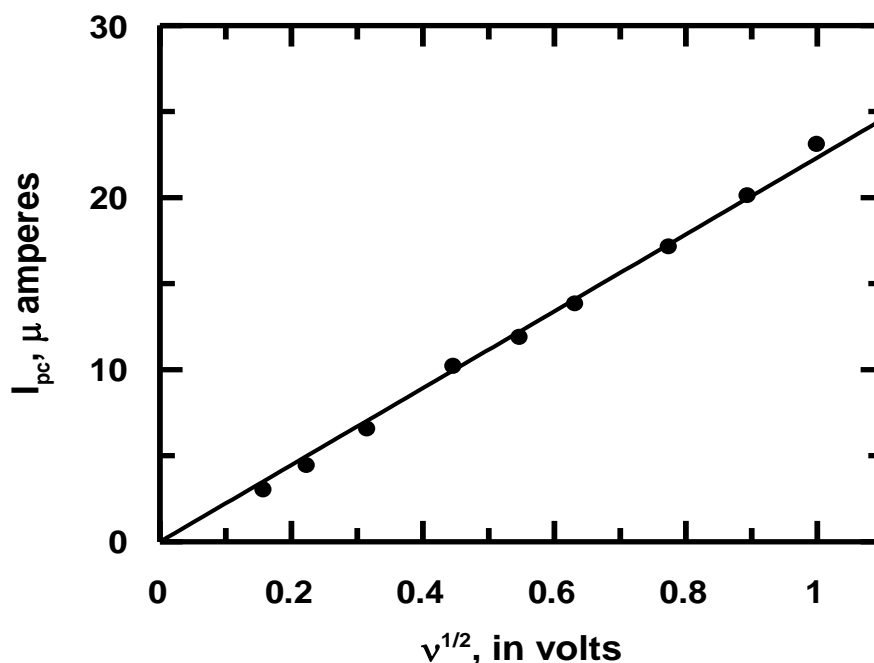
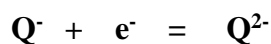
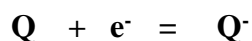


**Fig. 7:** Linear dependence of cathodic peak current on square root of potential sweep rate in pure DMF.

The study showed CA in DMF undergoes two successive one-electron reductions, first forming a semiquinone ( $Q^{\bullet-}$ ) and then quinone dianion ( $Q^{2-}$ ) (Scheme 1). In the reverse scan, quinone dianion is oxidised to semiquinone and thereafter to the neutral quinone (Fig. 8). When the scan was reversed immediately after the first reduction, shown by a red (—) line in Fig. 8 voltammograms revealed that anodic peak current for the oxidation of semiquinone to quinone was much smaller than when the scan was reversed after the second reduction shown by a black (—) line. This is suggestive that there is a greater presence of semiquinone in solution when the scan is reversed after the second reduction than when it is reversed after the first reduction, attributed to comproportionation between a quinone dianion and a neutral quinone, that occurs immediately after formation of the dianion (Scheme 2).

**Scheme 1: The redox reactions**



**Scheme 2: Homogeneous Chemical Reactions**



Therefore, using cyclic voltammetry, it could be shown that in case of CA, semiquinone is easily formed in solution be it directly due to one-electron reduction of CA or through the process of comproportionation between a quinone dianion and a neutral quinone. Similar results were obtained at other scan rates as well (Fig. 8)



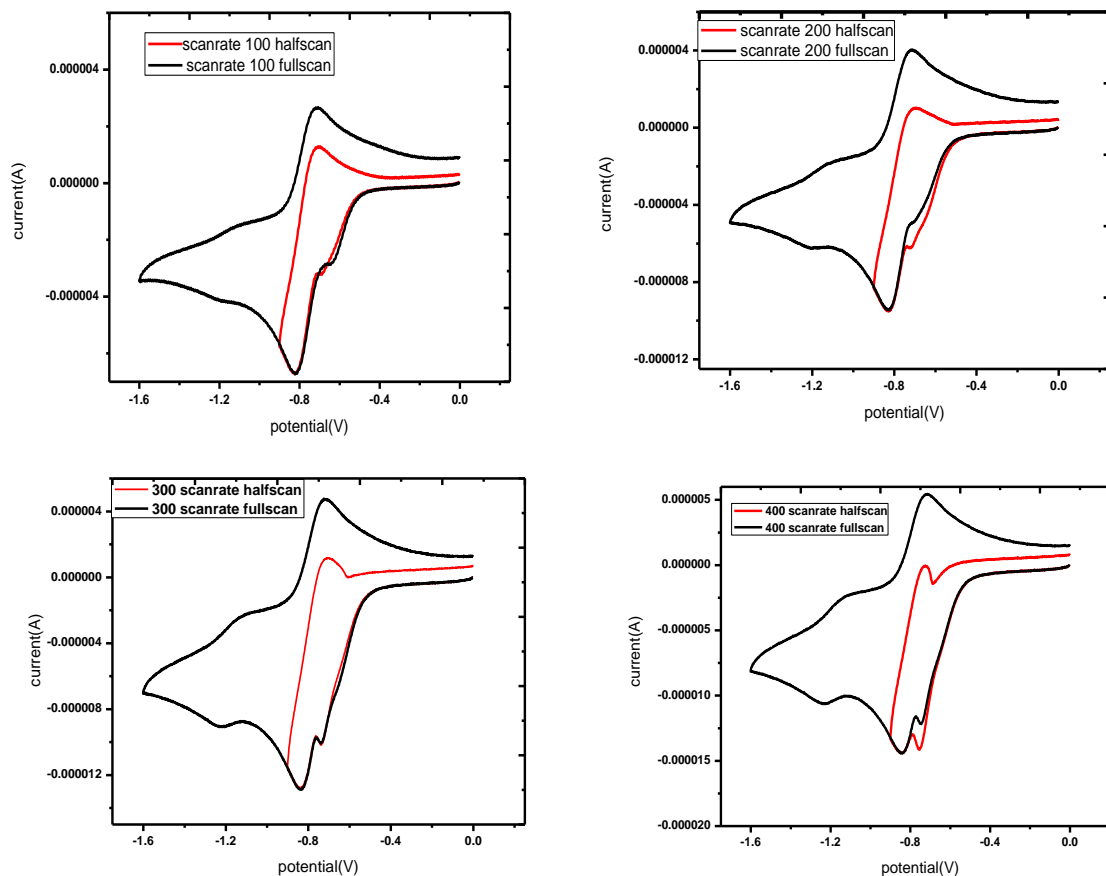


**Fig. 8:** Cyclic voltammetry of CA at 0.05 V/s, 0.10 V/s, 0.20 V/s, 0.3 V/s, 0.4 V/s potential sweep rates in 0.1 M TBAB (as supporting electrolyte) in DMF using a glassy carbon electrode of surface area 0.1256 cm<sup>2</sup> at 298K; (—) shows voltammogram when the scan was reversed immediately after the first reduction.

CA and [Mn(CA)<sub>2</sub>]<sup>2-</sup> were subjected to cyclic voltammetry in DMF (Fig. 9). Experiments reveal under identical conditions, reduction due to one electron both for CA and its Mn(II) complex produce almost identical voltammograms. Only a very slight difference in the nature of the two voltammograms was observed attributed to the fact that once CA is on its own and in another bound to Mn(II). Otherwise, the two voltammograms indicate that the nature of reduction at a quinone centre, whether it is on CA itself, or on CA bound to Mn(II) is not much different. Hence, for [Mn(CA)<sub>2</sub>]<sup>2-</sup> it may be said that there is probably not much of a change in semiquinone formation as is generally expected for such complexes.

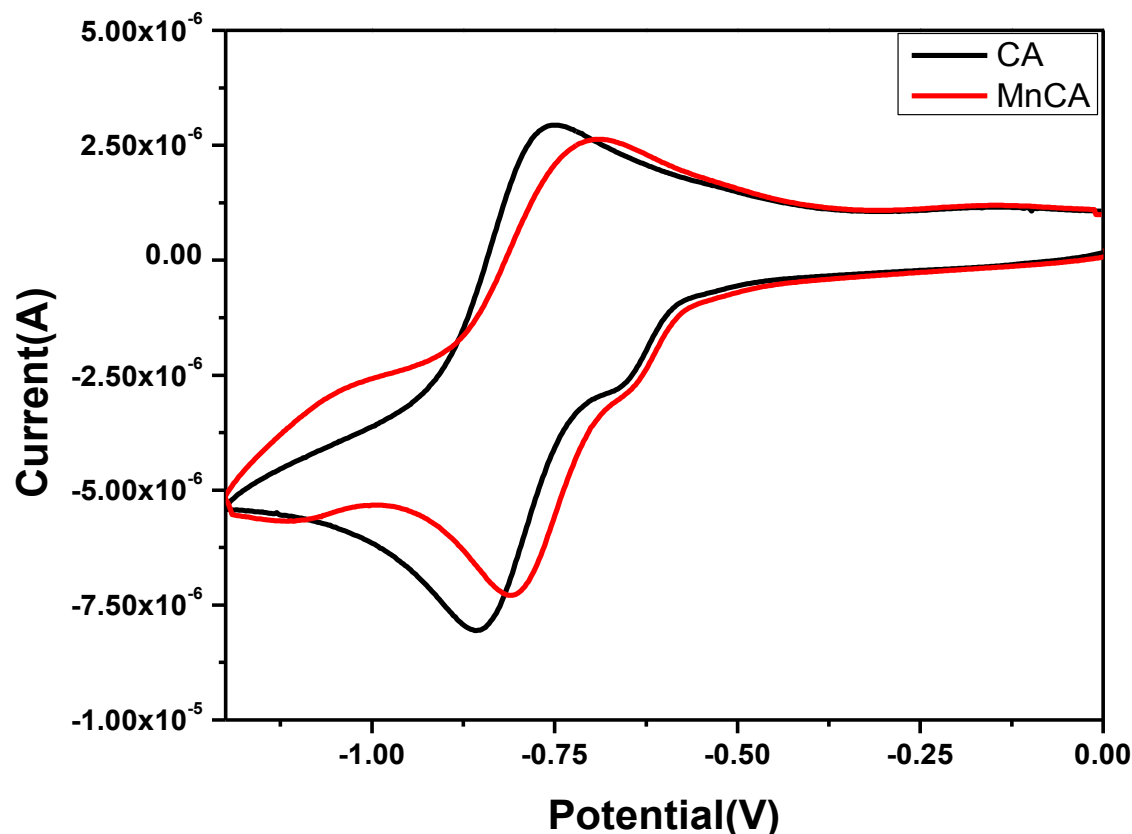


**Fig. 9:** Cyclic voltammograms of 100  $\mu\text{M}$  CA &  $[\text{Mn}(\text{CA})_2]^{2-}$  in DMF containing 0.12 M KCl using a glassy carbon electrode (surface area 0.1256  $\text{cm}^2$ ); Scan rate 25 mV/sec.

### 2.3.5 Structure of $[\text{Mn}(\text{CA})_2(\text{H}_2\text{O})_2]^{2-}$ through DFT calculations based on spectroscopy and other evidence

Molecular geometry of  $[\text{Mn}(\text{CA})_2(\text{H}_2\text{O})_2]^{2-}$  was optimized at its electronic ground state ( $S_0$ ) in gaseous phase with appropriately labelled coordination environments as depicted in Fig. 10. Energy optimization indicates Mn(II) forms an octahedral complex with the two water molecules present mutually *cis* to each other in the coordination environment. Calculations for an octahedral form where two water molecules are mutually *trans* to each other was also drawn. However, when this was uploaded to the Gaussian software it got converted to *cis* and proceeded with the calculations clearly indicating the *trans* form is unstable. Calculation for a tetrahedral structure

was also considered in gas phase. However, the energy of a tetrahedral form was found to be much higher than *cis* octahedral.

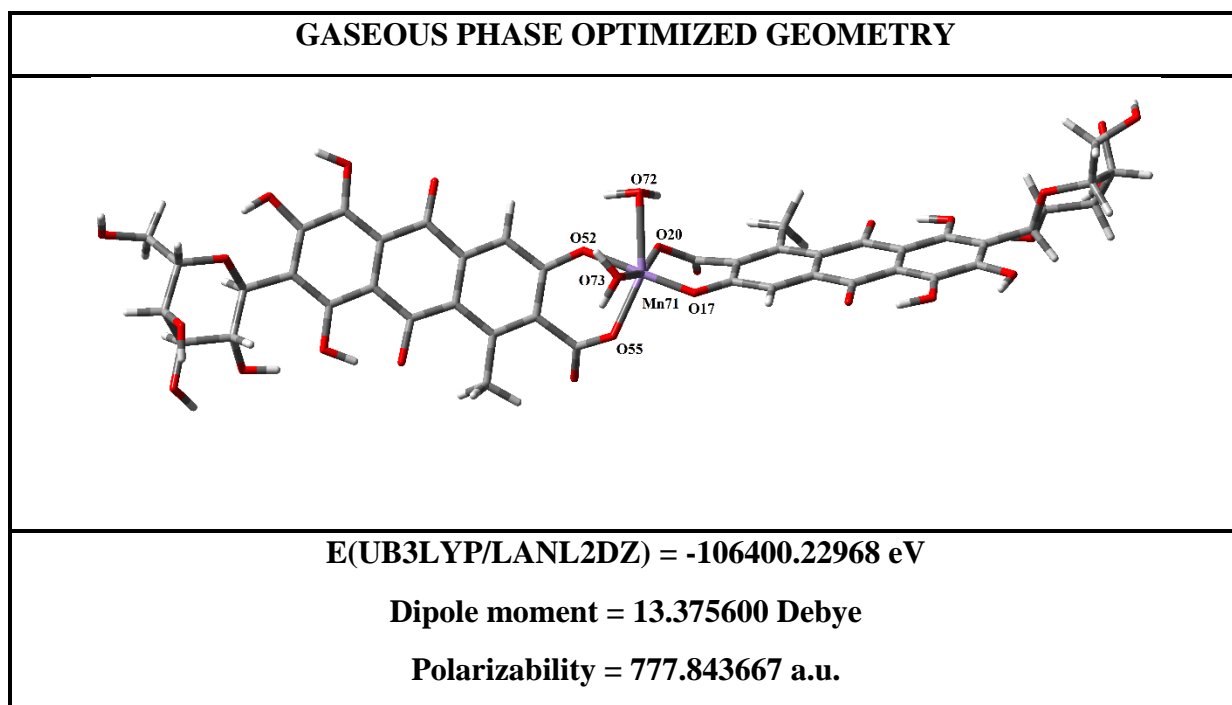


**Fig. 10:** Ground state optimized geometries of  $[\text{Mn}(\text{CA})_2(\text{H}_2\text{O})_2]^{2-}$

#### 2.4 Interaction of $[\text{Mn}(\text{CA})_2]^{2-}$ with calf thymus DNA at different pH of the medium:

Titration of the complex with calf thymus DNA was followed at 536 nm in the range of pH from 7.3 to 8.0. Fig. 11 depicts a titration of  $[\text{Mn}(\text{CA})_2]^{2-}$  at pH 7.4. Fig. 12 is a plot obtained by fitting the data to Eq. 10 (*Chapter 6: Experimental*) while Fig. 13 was obtained using Eq. 11 (*Chapter 6: Experimental*).  $K_{\text{app}}$  was evaluated from Figures 12 and 13 (shown in Table 1). Fig. 14 indicates site size of interaction ( $n_b$ ) for  $[\text{Mn}(\text{CA})_2]^{2-}$  interacting with calf thymus DNA.

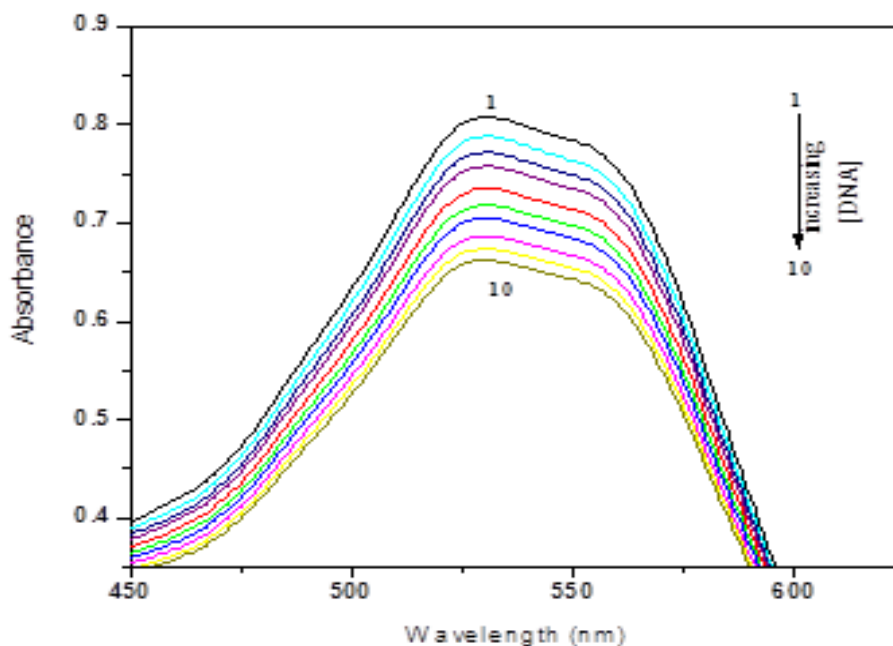


**Fig. 11:** Absorption spectra of  $80 \mu M [Mn(CA)_2]^{2-}$  in 120 mM NaCl and 15 mM Tris-buffer at pH 7.4 (1) in the absence and (2-10) presence of different concentrations of calf thymus DNA; (2) 20  $\mu M$  (3) 30  $\mu M$  (4) 40  $\mu M$  (5) 60  $\mu M$  (6) 100  $\mu M$  (7) 130  $\mu M$  (8) 160  $\mu M$  (9) 205  $\mu M$  (10) 235  $\mu M$ .

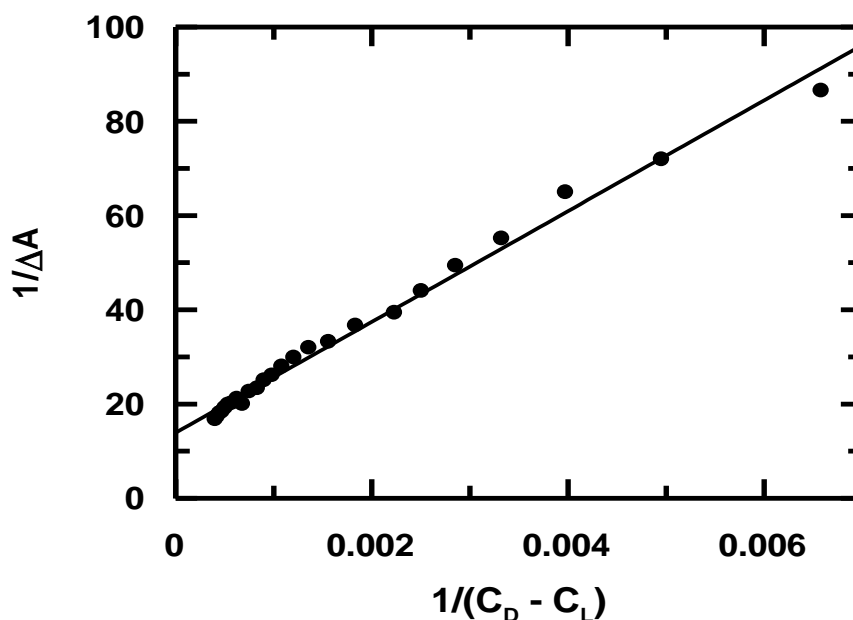


**Fig. 12:** Double reciprocal plot for the interaction of  $[Mn(CA)_2]^{2-}$  with calf thymus DNA followed by UV-Vis spectroscopy.  $[Mn(CA)_2]^{2-} = 80 \mu M$ ,  $[NaCl] = 120 \text{ mM}$ ;  $T = 300 \text{ K}$ .

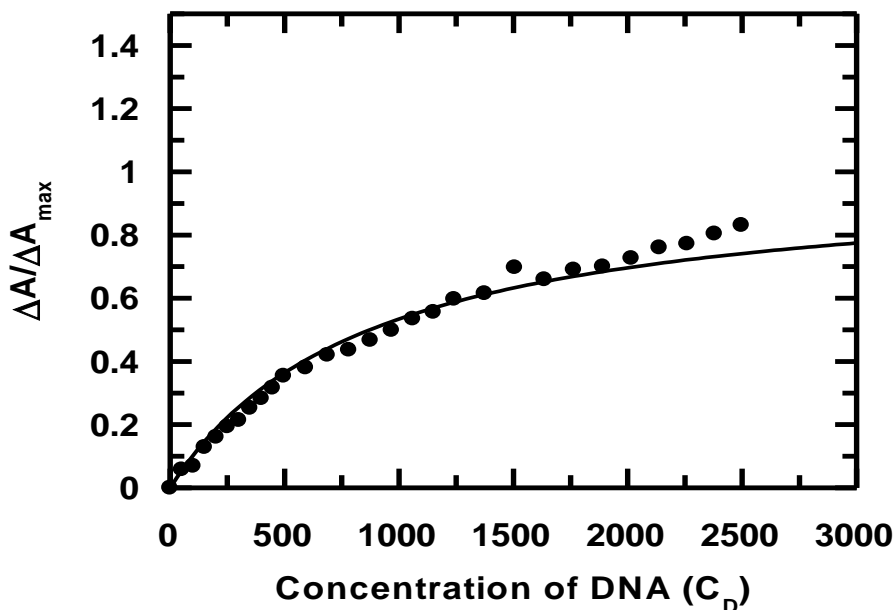


**Fig. 13:** Binding isotherm for the interaction of  $[\text{Mn}(\text{CA})_2]^{2-}$  with calf thymus DNA. The corresponding non-linear fit was obtained for the titration followed by UV-Vis spectroscopy.  $[\text{Mn}(\text{CA})_2]^{2-} = 80 \mu\text{M}$ ,  $[\text{NaCl}] = 120 \text{ mM}$ ,  $T = 298\text{K}$ .

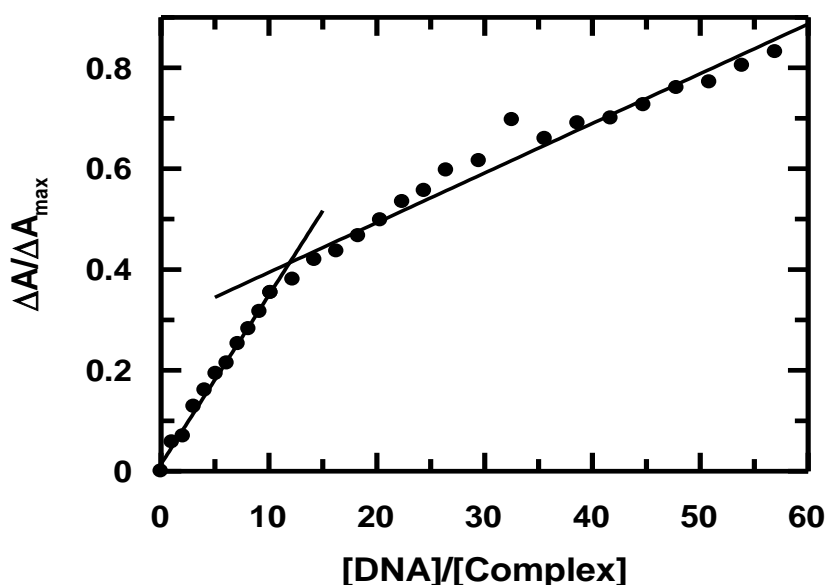


**Fig. 14:** A plot of normalized increase in absorbance as a function of the ratio calf thymus DNA to  $[\text{Mn}(\text{CA})_2]^{2-}$  at 533 nm.

The titrimetric data was also analyzed using Eq. 13 (*Chapter 6: Experimental*) that provide values for the overall binding constant ( $K^*$ ) and site size of interaction “n” ( $n_b^{-1}$ ) using a modified Scatchard equation (Table 1). Fig. 15 is a modified Scatchard plot for  $[\text{Mn}(\text{CA})_2]^{2-}$

interacting with calf thymus DNA at pH 7.40. Similar titrations were performed at other pH as well and the results are shown in Table 1.

**Table 1: Binding constants for [Mn(CA)<sub>2</sub>]<sup>2-</sup> with calf thymus DNA at different pH**

pH	K <sub>app</sub> (M <sup>-1</sup> )			Site size	K <sub>app</sub> × n <sub>b</sub> = K* (M <sup>-1</sup> )	K* from Scatchard	n <sub>b</sub> from Scatchard n <sub>b</sub> = (n <sup>-1</sup> )
	From double-reciprocal plot(a)	From Non-linear plot (b)	Average = (a+b)/2				
7.31	1.37 × 10 <sup>3</sup>	1.44 × 10 <sup>3</sup>	1.41 × 10 <sup>3</sup>	10	1.41 × 10 <sup>4</sup>	1.18 × 10 <sup>4</sup>	8.95
7.40	1.13 × 10 <sup>3</sup>	1.06 × 10 <sup>3</sup>	1.10 × 10 <sup>3</sup>	13	1.43 × 10 <sup>4</sup>	1.19 × 10 <sup>4</sup>	8.47
7.68	0.64 × 10 <sup>3</sup>	0.67 × 10 <sup>3</sup>	0.66 × 10 <sup>3</sup>	12	0.79 × 10 <sup>4</sup>	2.21 × 10 <sup>4</sup>	8.87
7.81	1.90 × 10 <sup>3</sup>	1.94 × 10 <sup>3</sup>	1.92 × 10 <sup>3</sup>	10	1.92 × 10 <sup>4</sup>	3.64 × 10 <sup>4</sup>	9.66

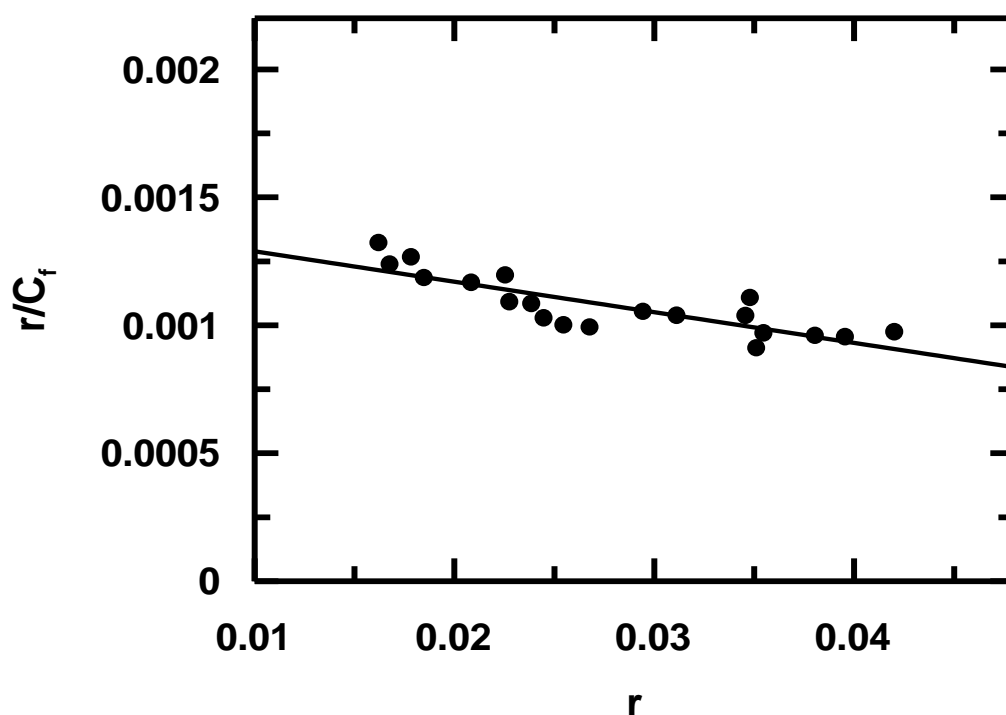


**Fig. 15:** Modified Scatchard plot of the interaction of [Mn(CA)<sub>2</sub>]<sup>2-</sup> with calf thymus DNA monitored at 518 nm; . [Mn(CA)<sub>2</sub>]<sup>2-</sup> = 80μM, [NaCl] = 120 mM, T = 298K.

It was reported earlier that in case of CA there is a gradual decrease in binding constant values for its interaction with calf thymus DNA if there is an increase in the pH of the medium.<sup>21</sup> The reason for this was attributed to the fact that as pH increases dissociable protons present in CA (either on the carboxyl group or on several phenolic –OH) gradually begin to dissociate and progressively convert CA into either a monovalent or divalent or trivalent or even a tetravalent anion (pK<sub>a</sub> values of 5.3, 7.2, and 10.3 respectively).

As a consequence, increase in the pH of the medium increases the intensity of negative charge on CA making interaction between CA and calf thymus DNA extremely difficult (DNA being a negative polymer). This study was able to show that this above mentioned trend (decreasing) for binding constant values of CA interacting with calf thymus DNA could be arrested to a considerable extent through complex formation.<sup>17,25</sup> As can be seen from Table 1, overall binding constant values (K<sup>\*</sup>) for [Mn(CA)<sub>2</sub>]<sup>2-</sup> were found to be more or less constant in the pH range from 7.3 to 7.8, rather it increased slightly, even when the complex [Mn(CA)<sub>2</sub>]<sup>2-</sup> has two units of negative charge [Fig. 16]. This is definitely a positive attribute of complex formation that might help in better targeting of DNA.<sup>26,27</sup>

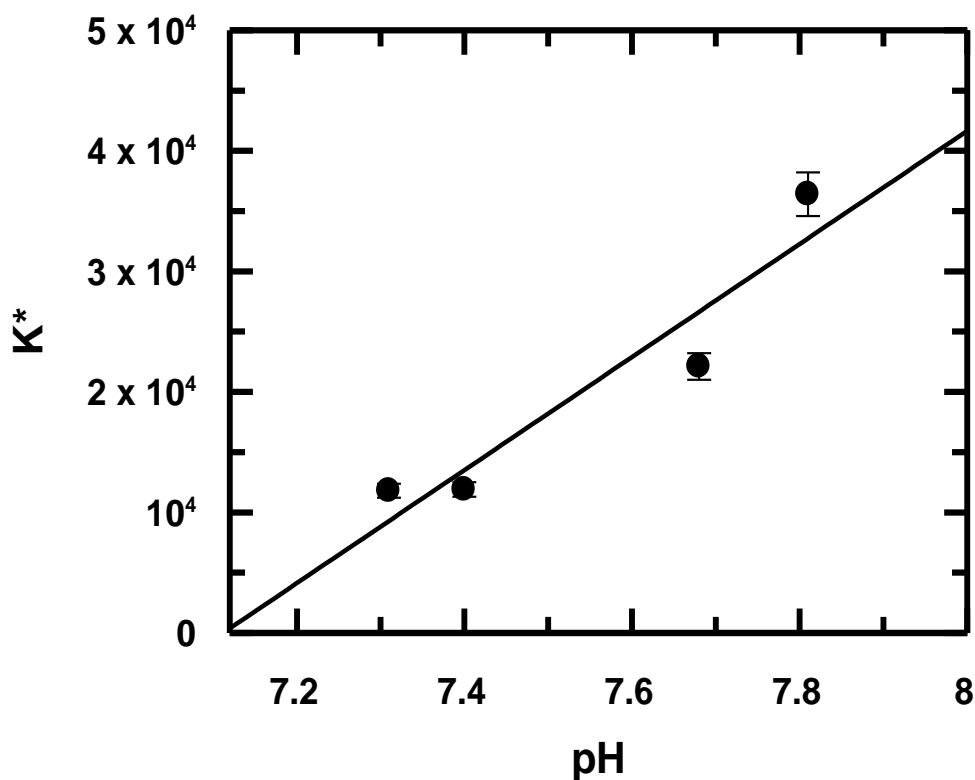


**Fig. 16:** Plot of a variation in overall binding constant of  $[\text{Mn}^{\text{II}}(\text{CA})_2]^{2-}$  interacting with calf thymus DNA at different pH (maintained with tris buffer) at 298 K and an ionic strength of 120 mM.

### 2.5 Effect of CA and $[\text{Mn}^{\text{II}}(\text{CA})_2]^{2-}$ on two different cancer cells

Efficacy of CA and its Mn(II) complex was ascertained on two carcinoma cell lines namely, PC3 (prostrate carcinoma cells) and A549 (lung carcinoma cells). Going by their  $\text{IC}_{50}$  values, it may be said that for both carcinoma cell lines, the complex was much more effective than CA. Results from each such studies are shown in Fig. 17.



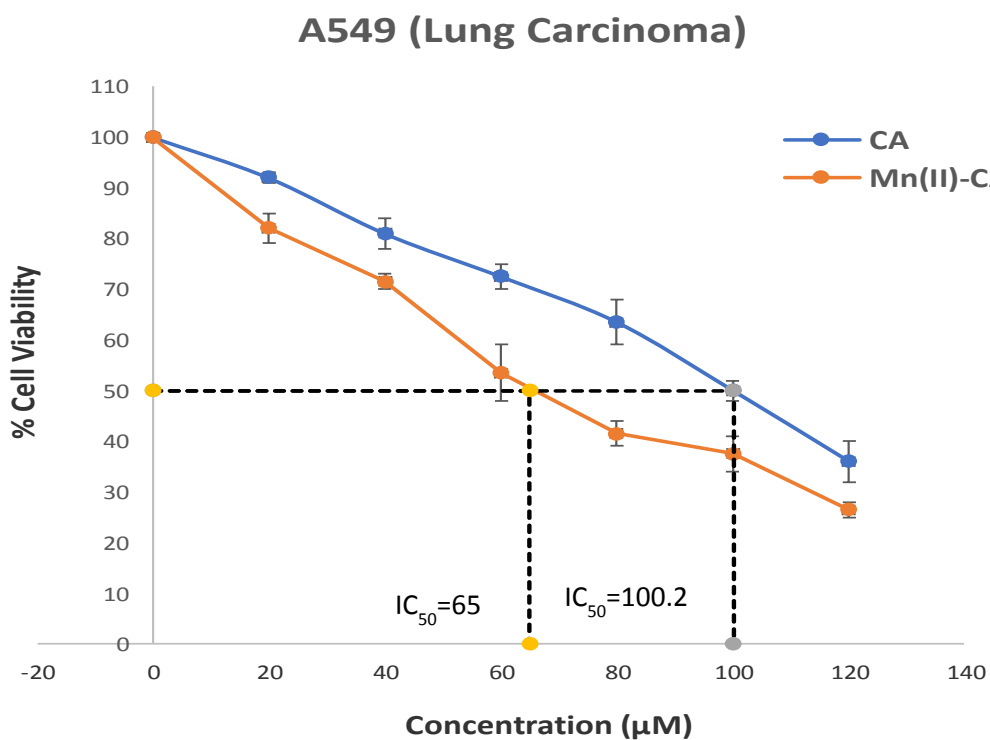
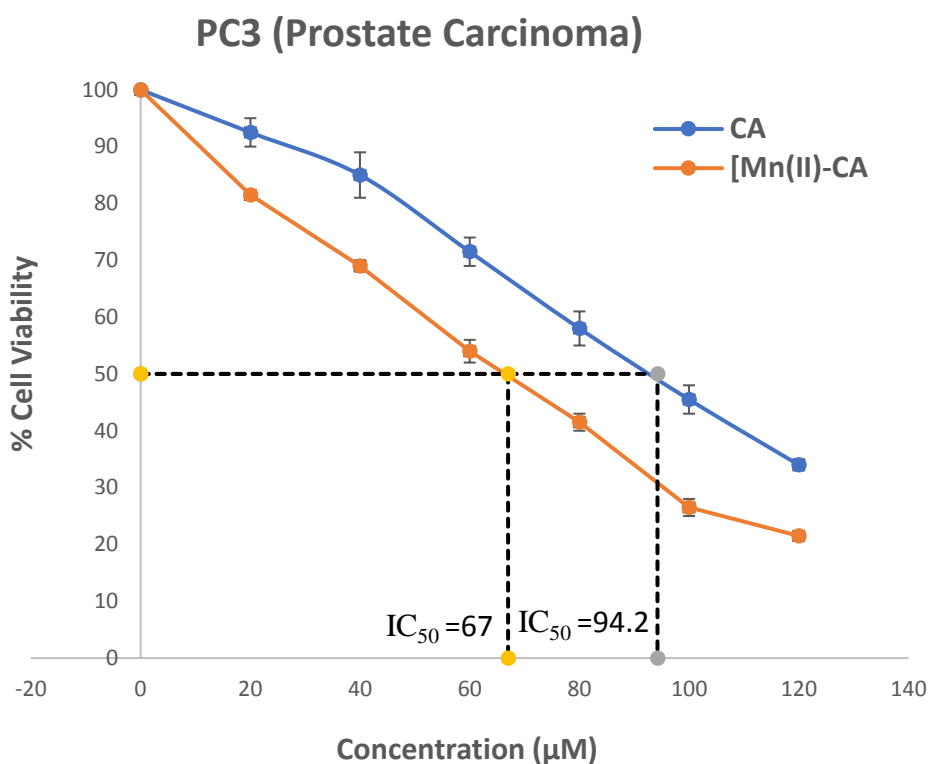


**Fig. 17:** Cell viability results of CA and  $Na_2[Mn^{II}(CA)_2]^{2-}$  on three different cell lines

### ***Chapter 10: Comparing chemical, biophysical and.....its Mn<sup>II</sup> complex***

---

A complex of Mn<sup>II</sup> with CA was synthesized and characterized with an intention of realizing its performance on model biological targets. Biophysical studies related to interaction of the complex with DNA revealed binding of the complex to DNA was better than that of CA. What is more important is that the complex was able to arrest the decreasing trend observed in binding constant values for CA interactin with calf thymus DNA for an increase in the pH of the medium. This happened inspite of the fact that the complex was anionic and also much larger in size than CA, therefore highlighting the influence a metal ion might have on the DNA binding process. This could manifest as an application for cancer patients who experience fluctuation of pH in body fluids during the course of treatment that often adversely affects drug action.

### **3. References:**

- [1] J. W. Lown. 1993. Discovery and development of anthracycline antitumour antibiotics. *Chem. Soc. Rev.* 22:165-176.
- [2] J. W. Lown. 1983. The mechanism of action of quinone antibiotics. *Mol Cell Biochem.* 55: 17-40.
- [3] F. Zunino, G. Capranico, 1990. DNA topoisomerase II as the primary target of anti-tumor anthracyclines. *Anti-cancer Drug Design.* 5:307-317.
- [4] D. A. Gewirtz.1999. A critical evaluation of the mechanisms of action proposed for the antitumor effects of the anthracycline antibiotics adriamycin and daunorubicin. *Biochem Pharmacol.* 57:727–741, **1999**
- [5] F. Yang, S. S. Teves, C. J. Kemp, S. Henikof. 2014. Doxorubicin, DNA torsion, and chromatin dynamics. *Biochim Biophys Acta.* 1845:84-89

- [6] J. B. Chaires, K R. Fox, J E. Herrera, M. Britt, and M. J. Waring. 1987. Site and sequence specificity of the daunomycin-DNA interaction. *Biochemistry*. 26: 8227-8236.
- [7] I. Müller, D. Niethammer, G. Bruchelt. 1998. Anthracycline-derived chemotherapeutics in apoptosis and free radical cytotoxicity (Review). *Int J Mol Med*. 1:491-494.
- [8] T. Šimunek, M. Štirba, O. Popelová, M. Adamcová, R. Hrdina, V. Geršl. 2009. Anthracycline-induced cardiotoxicity: Overview of studies examining the roles of oxidative stress and free cellular iron. *Pharmacol Rep*. 61:154–171.
- [9] A.L.A. Ferreira, L.S. Matsubara and B.B. Matsubara. 2008. Anthracycline-induced cardiotoxicity. *Cardiovascular & Hematological Agents in Medicinal Chemistry*. 6: 278-281
- [10] P. Angsutararux, S. Luanpitpong, and S. Issaragrisil. 2015. Chemotherapy-induced cardiotoxicity: Overview of the roles of oxidative stress. *Oxid Med Cell Longev*. 2015:795602. doi: 10.1155/2015/795602.
- [11] J. R. F. Muindi, B. K. Sinha, L. Gianni, C. E. Myers. 1984. Hydroxyl radical production and DNA damage induced by anthracycline-iron complex. *FEBS Lett*. 172:226-30.
- [12] H. Beraldo, A. Garnier-Suillerot, L. Tosi , F. Lavelles. 1985. Iron(III)-adriamycin and iron(III)-daunorubicin complexes: Physicochemical characteristics, interaction with DNA, and antitumor activity. *Biochemistry*. 24: 284-289.
- [13] C. Santini, M. Pellei, V. Gandin, M. Porchia, F. Tisato, C. Marzano.2014. Advances in copper complexes as anticancer agents, *Chem. Rev*. 114:815–862.
- [14] J. de Jong, B. C. P. Hiisken, B. Beekman, W. J. F. van der Vijgh, A. Bast. 1994. Radical formation by metal complexes of anthracyclines and their metabolites. Is there a relation with cardiotoxicity? *European Journal of Pharmaceutical Sciences*. 2:229-237.

[15] W. Priebe. 2000. Targeting DNA with anthracyclines: the importance of the sugar moiety. *Molecules*. 5:299–301

[16] T. Banerjee, R. Mukhopadhyay. 2008. Structural effects of nogalamycin, an antibiotic antitumour agent, on DNA. *Biochem. Biophys. Res. Comm.* 374:264-268.

[17] P. Das, C. K. Jain, S. K. Dey, R. Saha, A. D. Chowdhury, S. Roychoudhury, S. Kumar, H. K. Majumder, S. Das. 2014. Synthesis, crystal structure, DNA interaction and in vitro anticancer activity of a Cu(II) complex of purpurin: dual poison for human DNA topoisomerase I and II. *RSC Adv.* 4: 59344-59357.

[18] S. Mukherjee, P.K. Gopal, S. Paul, S. Das. 2014. Acetylation of 1,2,5,8-tetrahydroxy-9,10-anthraquinone improves binding to DNA and shows enhanced superoxide formation that explains better cytotoxicity on JURKAT T lymphocyte Cells. *J. Anal Oncol.* 3: 122-129.

[19] P. Das, D. Bhattacharya, P. Karmakar, S. Das. 2015. Influence of ionic strength on the interaction of THA and its Cu(II) complex with DNA helps to explain studies on various breast cancer cells. *RSC Adv.* 5: 73099-73111.

[20] P. Mondal, S. Roy, G. Loganathan, B. Mandal, D. Dharumadurai, M. A. Akbarsha, P. S. Sengupta, S. Chattopadhyay, P. S. Guin. 2015. 1-Amino-4-hydroxy-9,10-anthraquinone – An analogue of anthracycline anticancer drugs, interacts with DNA and induces apoptosis in human MDA-MB-231 breast adenocarcinoma cells: Evaluation of structure–activity relationship using computational, spectroscopic and biochemical studies. *Biochem. Biophys. Rep.* 4: 312-323.

[21] P. Das, C. K. Jain, S. Roychoudhury, H. K. Majumder, S. Das. 2016. Design, synthesis and in vitro anticancer activity of a Cu(II) complex of carminic acid: A novel small molecule inhibitor of human DNA topoisomerase I and topoisomerase II. *ChemistrySelect.* 1: 6623-6631.

- [22] B. Mandal, S. Singha, S. K. Dey, S. Mazumdar, T. K. Mondal, P. Karmakar, S. Kumar, S. Das. 2016. Synthesis, crystal structure from PXRD of a Mn<sup>II</sup>(purp)<sub>2</sub> complex, interaction with DNA at different temperatures and pH and lack of stimulated ROS formation by the complex. *RSC Adv.* 6: 51520-51532.
- [23] B. Mandal, S. Singha, S.K. Dey, S. Mazumdar, S. Kumar, P. Karmakar, S. Das. 2017. Cu<sup>II</sup> complex of emodin with improved anticancer activity as demonstrated by its performance on HeLa and Hep G2 cells. *RSC Adv.* 7: 41403-41418.
- [24] K. Nakamoto. 1978. Infrared and Raman Spectra of Inorganic and Coordination Compounds, third ed. *Wiley-Interscience, New York, USA.*
- [25] S. Mukherjee, P. Das, S. Das. 2012. Exploration of small hydroxy-9,10-anthraquinones as anthracycline analogues: physicochemical characteristics and DNA binding for comparison. *J. Phys. Org. Chem.* 25: 385-393.
- [26] G. K. Schwalfenberg. 2012. Incorporating Environmental Health in Clinical Medicine. *J. Environ. Pub Health.* 6: 727630, 7 pages.
- [27] B. P. Mahoney, N. Raghunand, B. Baggett, R. J. Gillies. 2003. Tumor acidity, ion trapping and chemotherapeutics. I. Acid pH affects the distribution of chemotherapeutic agents in vitro. *Biochem. Pharmacol.* 66: 1207-1218.



# CHAPTER 11

Free radical induced activity of alizarin and its  $Mn^{II}$  complex on biological targets through *in situ* electrochemical generation of semiquinone





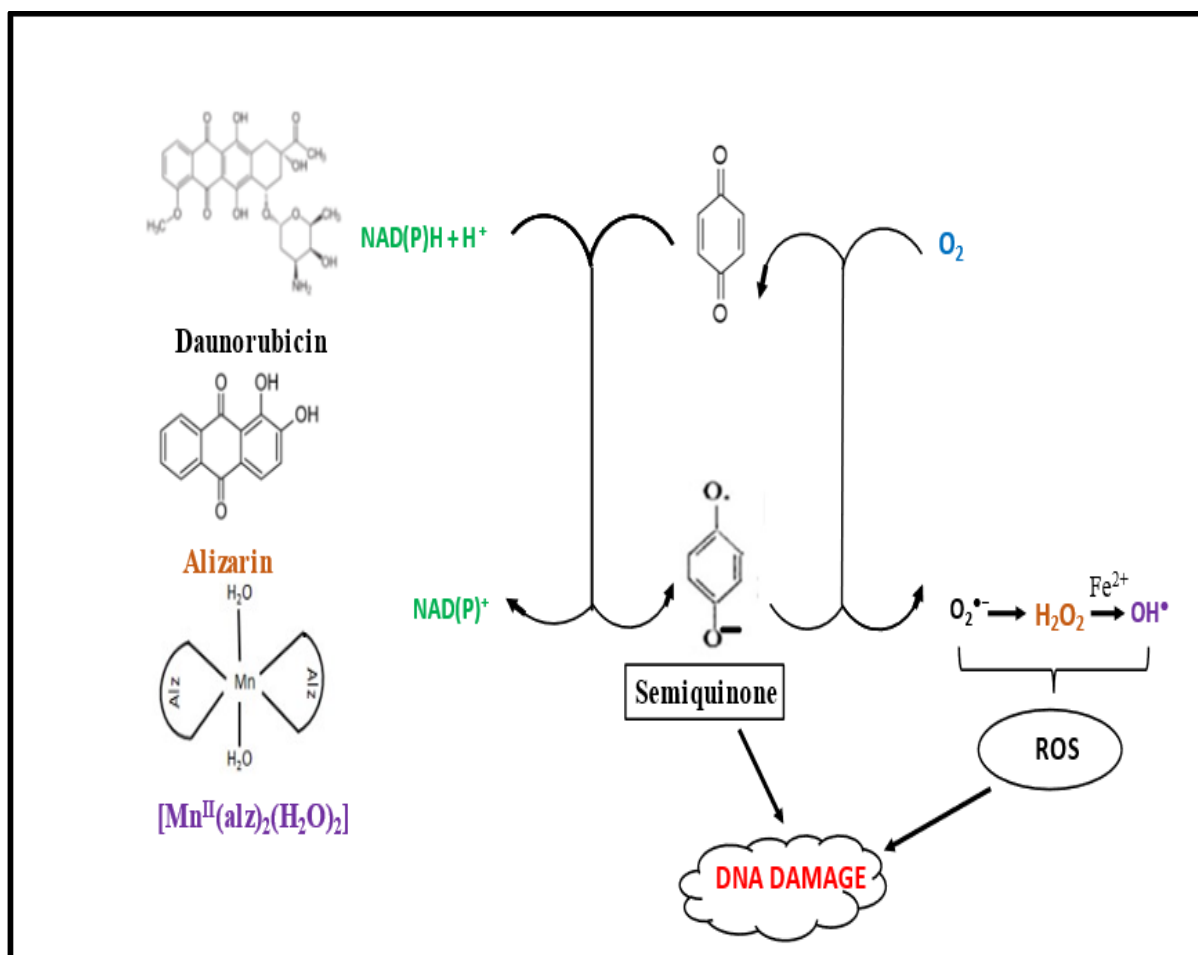
## 1. Introduction:

Anthracyclines, although extremely effective anticancer agents, one disturbing aspect is their associated toxic side effects, an almost inseparable phenomenon affecting drug efficacy.<sup>4-12</sup> Therefore, an effort is now underway to modify anthracyclines in a manner that toxic side effects are addressed without compromising efficacy.<sup>13-21</sup> However, in trying to achieve this, a compromise is often made with regard to drug action, which is becoming an area of concern.<sup>10,11,18,20,21</sup> One approach to modifying anthracyclines is by forming inorganic complexes using bio-friendly metal ions.<sup>22-24</sup> Whether it be anthracyclines or hydroxy-9,10-anthraquinones, studies reveal, intermediates like semiquinone radical anion<sup>25,26</sup> an important component of drug action, are either moderately or significantly decreased following complex formation.<sup>22-24,27-34</sup> In majority of cases, it is seen complexes are more effective (*in vitro*) than the parent molecule.<sup>23,27,29,31-34</sup> This means that the loss in efficacy in the free radical pathway is compensated by attributes of complex formation.<sup>22,23,27-34,35-37</sup>

For anthracyclines, accumulating evidence suggest there is *in vivo* formation of semiquinone either by one-electron reduction of anthracyclines and its analogues or by comproportionation when they undergo two-electron reduction to form quinone-dianion.<sup>27,32,38-40</sup> The reactive intermediates formed damage DNA causing cell death.<sup>41-44</sup> Redox reactions of drugs affect the response of damaged DNA since reactive oxygen species (ROS) either activate or inhibit cellular proteins/enzymes related to response in healthy or cancer cells.<sup>45,46</sup> This chapter tries to identify the contribution of the free radical pathway in causing cellular damage using an anthracycline analogue, alizarin and its  $Mn^{II}$  complex analyzing interactions with DNA. The *in situ* reactivity of electrochemically generated quinone di-anion or semiquinone formed on alizarin and its  $Mn^{II}$  complex with different nucleic acid bases and calf thymus DNA maintained in the immediate vicinity of their generation is discussed. The study helps one to

**Chapter 11: Free radical induced activity.... generation of semiquinone**

realize the role of semiquinones or superoxide radical anions generated by anthracyclines or similar compounds<sup>47</sup> in causing DNA damage and suggest reasons for efficacy.<sup>28-32</sup> Since  $Mn^{II}$  complexes show significant SOD like activity and because  $Mn^{II}$  can acquire higher oxidation states in presence of peroxides generated as part of ROS, attempts were made to see if an  $Mn^{II}$  complex would be beneficial for cell killing.<sup>48,49</sup> It is reported almost all mitochondria contain a form of manganese (Mn-SOD) where Mn could be in +2 or +3 oxidation states.<sup>50</sup> Our prepared complex could be a mimic of such Mn-SOD found in human mitochondria since anthracyclines, its analogues or their metal complexes upon entering the cells eventually interact with mitochondrial electron transport system to show drug action.<sup>50</sup>



**A scheme showing the basis for the study**

## 2. Results and Discussion:

### Interaction of electrochemically generated species with nucleic acid bases

Following an interaction of the semiquinone radical anion and/or protonated semiquinone under de-aerated condition or the superoxide radical anion and semiquinone radical anion in aerated medium (at pH ~7.4), aliquots that were collected from experimental solutions were subjected to HPLC to ascertain the amount of nucleobases that remained (Fig 1).

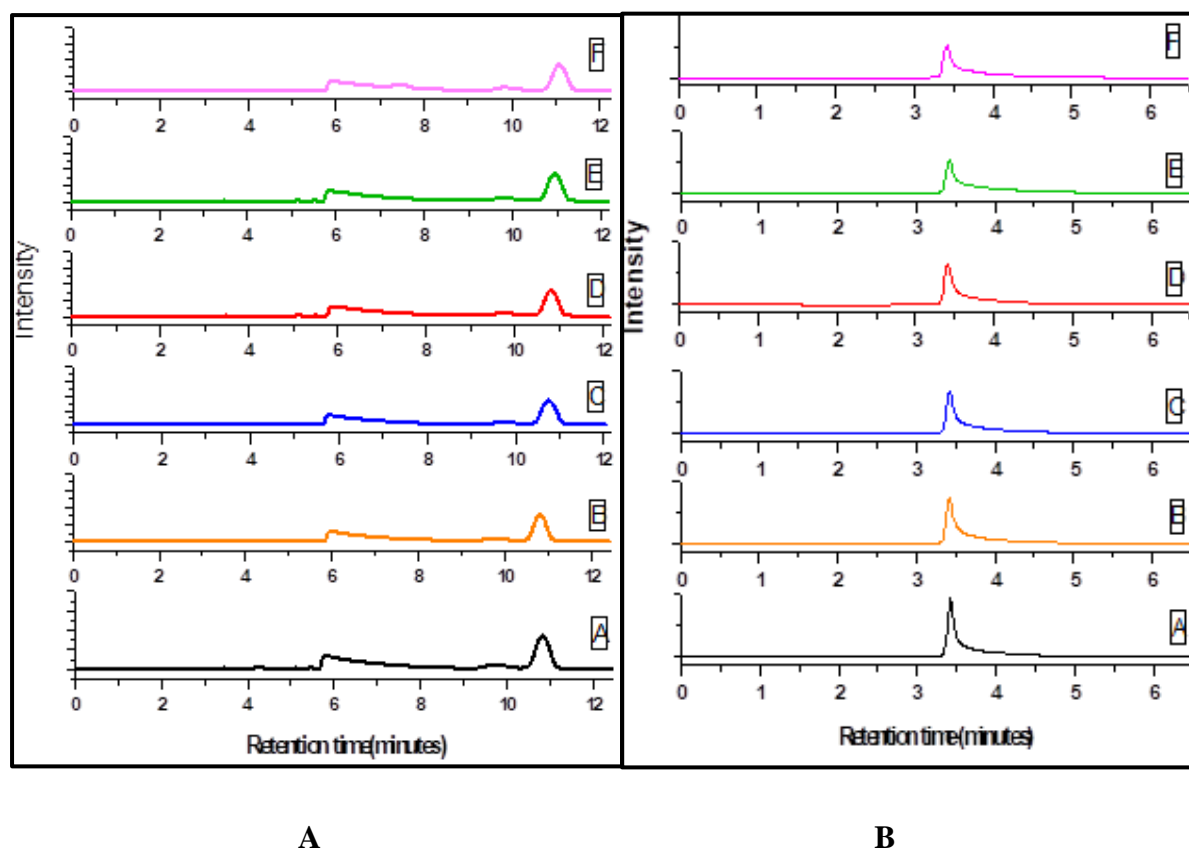


**Fig 1:** HPLC chromatograms obtained at 254 nm for  $1 \times 10^{-3} \text{ mol dm}^{-3}$  of (A) thymine, (B) cytosine solutions that were subjected to a constant potential of  $-0.65 \text{ V}$  in the presence of  $1 \times 10^{-5} \text{ mol dm}^{-3}$  alizarin under de-aerated (Ar saturated) conditions. A to F indicates time in minutes for which such constant potential was applied to the solution; A: 0 minutes, B: 2 minutes, C: 4 minutes, D: 6 minutes, E: 8 minutes, F: 10 minutes.

Voltammograms were analyzed by Randles-Sevcik equation Eq. 18 (chapter 6: Experimental) to check that the process was under diffusion control which would be essential for experiments to follow (Fig. 2A & 2B).

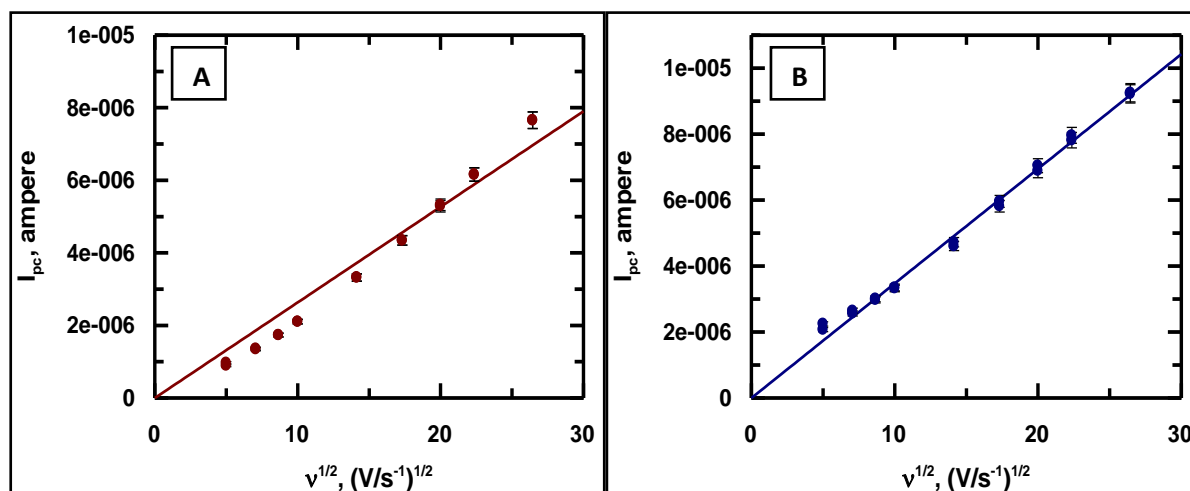


**Fig. 2:** Plot of the cathodic peak current ( $I_{pc}$ ) vs. square root of scan rate ( $v$ ) for a two-electron reduction of (A) alizarin and (B) Mn(II) complex of alizarin in aqueous solution at a potential of -0.65 V and 0.75 V respectively, pH ~ 7.4.

The damage caused to a nucleobase was plotted against time for which the electrochemical generation of species was attempted. Fig. 3 (A), 3 (B), 3 (C) and 3 (D) are plots that show the degradation of uracil, thymine, cytosine and adenine respectively in the presence and absence of the compounds under similar experimental conditions. Slopes of the degradation plots are an estimate of the amount of damage caused to each nucleobase under different conditions. Different extents of base damage were observed under different conditions indicating selectivity owing to the type and amount of radicals that were generated. Extent of damage depends on the ability of species formed in solution to interact with the target. (Fig. 3, Table 1).

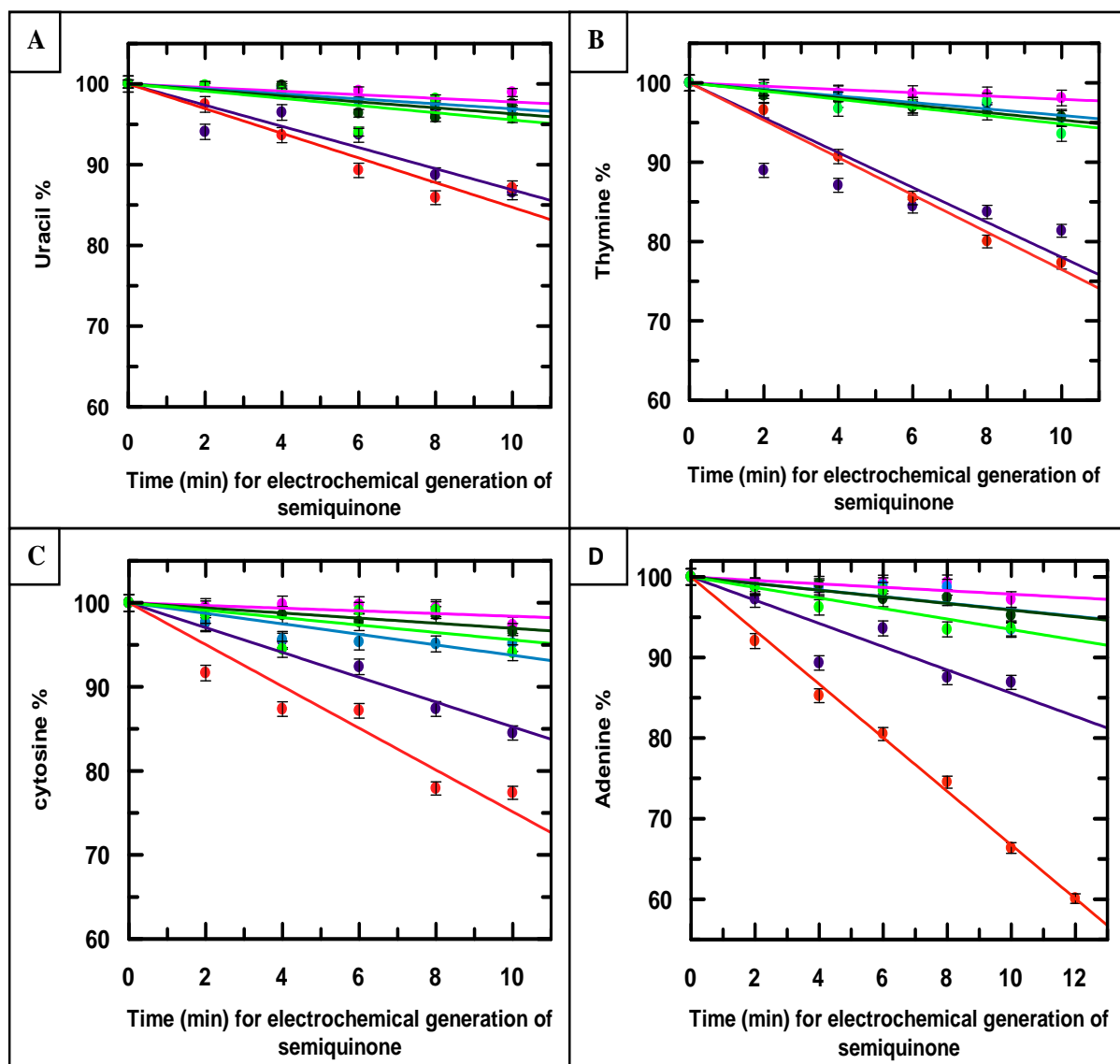


**Fig. 3:** Plots shown in (A), (B), (C) and (D) indicate percentage of uracil, thymine, cytosine and adenine remaining following interaction of *in situ* electrochemically generated species on alizarin and its  $\text{Mn}^{\text{II}}$  complex. Different experimental conditions were (●) nucleobase alone in absence of  $\text{O}_2$ ; (●) nucleobase alone in presence of  $\text{O}_2$ ; (●) nucleobase in presence of alizarin but absence of  $\text{O}_2$ ; (●) nucleobase in presence of alizarin and presence of  $\text{O}_2$ ; (●) nucleobase in presence of  $\text{Mn}^{\text{II}}(\text{alz})_2(\text{H}_2\text{O})_2$  but absence of  $\text{O}_2$ ; (●) nucleobase in presence of  $\text{Mn}^{\text{II}}(\text{alz})_2(\text{H}_2\text{O})_2$  and presence of  $\text{O}_2$ .

Under exactly similar conditions, the reduction potential of the  $\text{Mn}^{\text{II}}$  complex (-0.75 V) was ascertained. Table 1 shows in the absence of alizarin or its  $\text{Mn}^{\text{II}}$  complex, if glassy carbon electrode was held at a constant potential of -0.65 V and -0.75 V respectively, there was no

significant damage on any nucleobase. However, when a compound was present, application of the same constant potential of -0.65 V for alizarin (Fig. 4) or -0.75 V for its  $\text{Mn}^{\text{II}}$  complex, caused a damage to nucleobases suggesting free radicals formed on the compounds react with the target kept in the immediate vicinity of such generation. The extent of base damage was different for different targets and for different conditions suggesting some selectivity of radicals during the process of interaction. Base damage in Table 1 is expressed as EER, where EER denotes electrochemical enhancement ratio, calculated by dividing the slope of any degradation plot achieved for a certain nucleobase in the presence of a compound under a specified condition by the slope obtained for the damage of the same nucleobase in the absence of that compound under aerated condition. Value of the slope for the plot obtained under aerated condition in the absence of a compound was considered the fundamental since for these experiments when the potential was held constant either at -0.65 V or -0.75 V there would be reduction of molecular oxygen to different species that might interact with the nucleobases; hence the damage that was achieved over and above that value was considered.

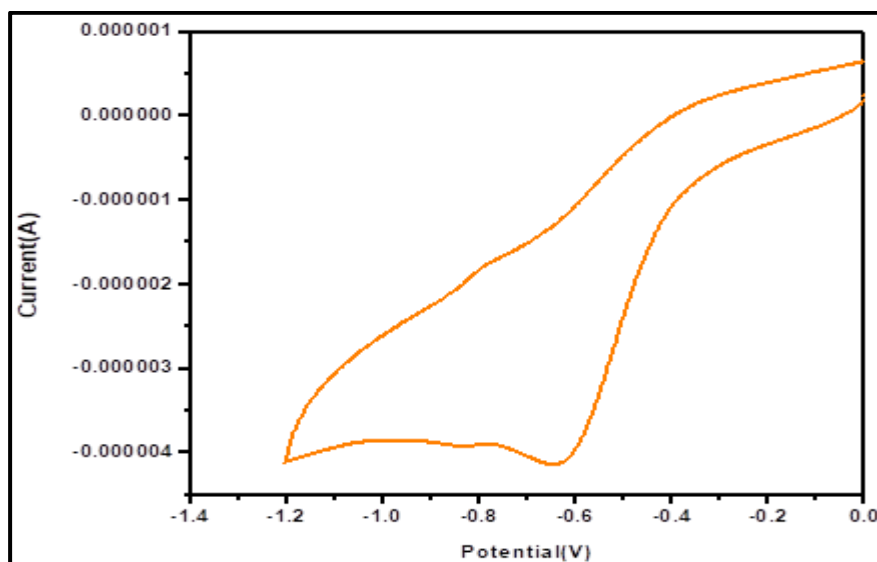


**Fig. 4:** Cyclic voltammogram of 0.01 mM alizarin at pH ~ 7.4 showing a single step two electron reduction of the quinone in aqueous solution containing 0.12 M KCl on a glassy carbon electrode (surface area 0.1256  $\text{cm}^2$ ); Scan rate 100 mV/sec.

In the presence of alizarin, damage on cytosine in the absence of O<sub>2</sub> (de-aerated condition) was maximum, significantly higher than on any other nucleobase used. In an earlier study also it was found cytosine was more prone to electron transfer damage whereas adenine and other purine/pyrimidine bases were less susceptible.<sup>51,52</sup> Incidentally, we got a similar result working with nucleobases in the presence of sensitizer molecules. For the complex however, damage caused to thymine under de-aerated condition was the highest. Baring the result on thymine in presence of alizarin (EER = 1.61), in aerated medium, no other nucleobase showed such significant damage under these conditions.

**Table 1: Degradation of nucleic acid bases due to electrochemically generated species (semiquinone or quinone dianion or various oxygen radicals) followed by HPLC.**

Compound	T A R G E T																	
	Uracil				Thymine				Cytosine				Adenine				Calf thymus DNA	
	Slope of plot in aerated Medium	EER	Slope of plot in de-aerated medium	EER	Slope of plot in aerated medium	EER	Slope of plot in de-aerated Medium	EER	Slope of plot in aerated medium	EER	Slope of plot in de-aerated medium	EER	Slope of plot in aerated medium	EER	Slope of plot in de-aerated medium	EER	Slope of plot in de-aerated medium	EER
-	-0.46	-	-0.37	-	-0.52	-	-0.48	-	-0.41	-	-0.30	-	-0.78	-	-0.42	-	-0.045	-
Alizarin	-0.36	-	-1.61	<b>3.50</b>	-0.41	-	-2.37	<b>4.56</b>	-0.66	<b>1.61</b>	-2.35	<b>5.73</b>	-0.46	-	-3.15	<b>4.03</b>	-0.16	<b>3.55</b>
Mn(II) complex of Alizarin	-0.28	-	-1.31	<b>2.85</b>	-0.22	-	-2.23	<b>4.29</b>	-0.24	-	-1.49	<b>3.63</b>	-0.31	-	-1.48	<b>1.90</b>	-0.10	<b>2.22</b>

An interesting aspect is that the  $Mn^{II}$  complex was less effective in the free radical pathway, a fact discussed in previous reports with regard to efficacy of complexes prepared using anthracyclines, or with hydroxy-9,10-anthraquinones, owing to decreased semiquinone formation<sup>27,33,34</sup> It has been mentioned earlier on different occasions that complexes of anthracyclines or of their analogues are at a disadvantage with regard to activity in the free radical pathway<sup>27,33,34</sup> but very few studies have shown it by working on this aspect exclusively. Decrease in activity observed for the  $Mn^{II}$  complex in the free radical pathway in comparison to alizarin is expected, since reports on anthracyclines and on its analogues indicate decreased generation of semiquinone by the complexes.<sup>27,30-34</sup> In this study, using alizarin, and its  $Mn^{II}$  complex, this got manifested by way of a maximum difference in damage observed for adenine and minimum for thymine suggesting under conditions of similar electrochemical generation of intermediates, there is either a difference in the generation of intermediates on each compound or in their tendency to interact in the free radical pathway. If this isn't true, then the nucleobase damage should have been similar. Table 1 indicates a difference in reactivity of the two compounds on different targets under identical conditions suggesting compounds might affect different types of DNA differently. Therefore, the general apprehension, that a complex prepared with anthracyclines or with its analogues compromise on aspects related to cytotoxicity in the free radical pathway, is true to a considerable extent. Yet, complexes of anthracyclines or of its analogues are prepared because they modulate the generation of semiquinone helping to decrease cardiotoxicity<sup>27,30-</sup>

<sup>34</sup> In a previous study, performance of  $Cu^{II}$  and  $Mn^{II}$  complexes of emodin against that of emodin itself, under similar experimental conditions found that the  $Mn^{II}$ -emodin complex was almost similar in activity to that of emodin.<sup>36</sup> The  $Cu^{II}$  complex was reported to perform much better, attributed to the presence of a stable lower oxidation state ( $Cu^I$ ) enabling  $Cu^{II}$  complexes to participate in Fenton reactions generating  $\cdot OH$  which in turn enhanced the



modification of nucleobases.<sup>25,26,36,37,53,54</sup> That particular study reported base damage due to Cu<sup>II</sup>-emodin was higher in aerated medium than in de-aerated medium.<sup>36</sup>

From EER values in Table 1, on the performance of a compound on nucleobases it might become possible to predict the damage that a compound might cause on a particular DNA whose base composition is known. In fact, this aspect could have been an important outcome of the study. However, the difficulty in correlating nucleobase damage to that observed in calf thymus DNA lay in the fact we could not generate the data where guanine was a possible target. This was because preparing an aqueous solution of guanine having similar concentration as that of the others was difficult owing to its poor solubility in buffer.

Using information from a previous study performed in our laboratory with a dimeric Cu<sup>II</sup> complex of tinidazole, where base degradation was followed using  $\gamma$  radiation, products formed in this study were identified.<sup>55</sup> Products were characterized following the degradation of thymine, cytosine and uracil.<sup>55</sup> Since HPLC profiles for degraded products of thymine were saved as method files in our system as part of an earlier study, they were utilized for this work to identify products related to the degradation of thymine, cytosine and uracil in the absence and presence of alizarin and its Mn<sup>II</sup> complex. Results indicate in presence of alizarin and its Mn<sup>II</sup> complex, 5,6-dihydroxy-5,6-dihydrothymine (thymine glycol) and 5-hydroxymethyl uracil were formed when thymine was the target. The amounts of which were extremely small as the charge provided at constant potential was not very high. The peak for 5,6-dihydrothymine was not detected even when thymine was subjected to electrochemical generation of intermediates using compounds (alizarin and Mn<sup>II</sup> complex) at longer times. Products were identified based on retention times using authentic samples.<sup>55</sup>

Cytosine differs from uracil at the fourth position (carbon) of the pyrimidine ring where there is an -NH<sub>2</sub> instead of -OH (if the enol form of uracil is considered). Since 5,6-dihydroxy-5,6-dihydrocytosine (cytosine glycol) is unstable and converts to 5,6-dihydroxy-5,6-dihydrouracil

(uracil glycol) by deamination,<sup>56</sup> existing HPLC method files on uracil to identify degraded products when either cytosine or uracil were maintained as targets during experiments were used;<sup>56</sup> the peaks for degraded products were very small. Observations suggest pyrimidine based nucleobases experience an initial free-radical attack by species generated as a consequence of the application of current at a constant potential on C<sub>5</sub>—C<sub>6</sub> double bond.<sup>55,56</sup> For the nucleobase adenine, HPLC chromatograms did not show any new peak in the time frame of the application of constant potential.

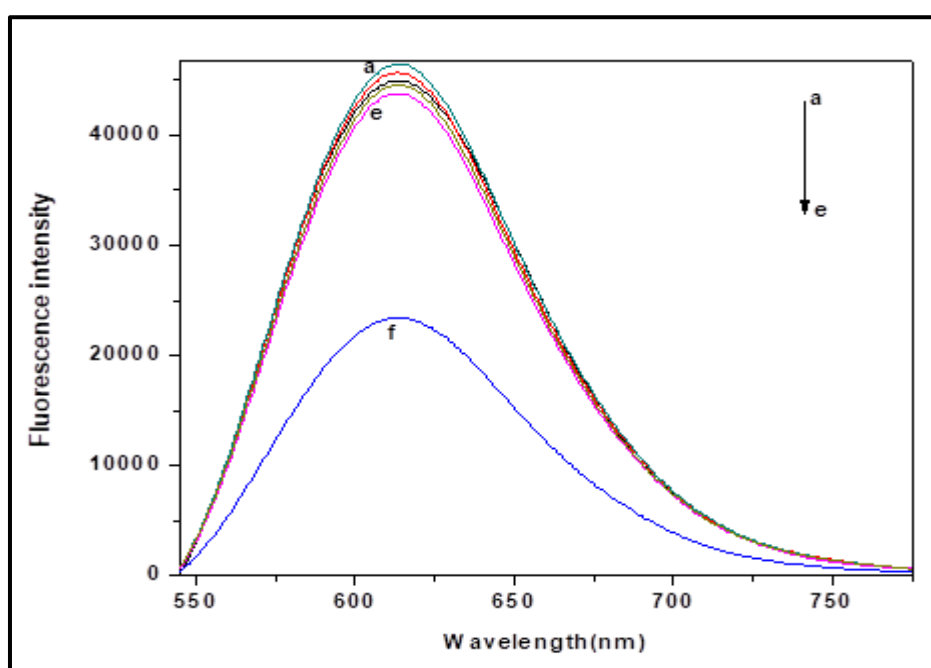


**Fig. 5:** Fluorescence spectra of  $1 \times 10^{-3}$  mol dm<sup>-3</sup> calf thymus DNA after treatment with EtBr following interaction with the products generated on the Mn(II) complex of alizarin that was subjected to reduction at constant potential (-0.75 V) in de-aerated (Argon saturated) conditions.  $[\text{Mn}^{\text{II}}(\text{alz})_2] = 3 \times 10^{-5}$  mol dm<sup>-3</sup>. “a” to “e” indicates time in minutes for which potential was applied to the solution; a: 0 minutes, b: 15 minutes, c: 30 minutes, d: 45 minutes, e: 60 minutes. “f” denotes the spectrum of EtBr when it was excited alone i.e. in absence of DNA at 510 nm.

**Interaction of electrochemically generated species with calf thymus DNA:**

In experiments with calf thymus DNA, samples had similar concentrations as that for studies with nucleobases, subjected to interaction with *in situ* electrochemically generated species and other products formed thereof at different time intervals. Double strand modification was ascertained by the change in fluorescence of the DNA-EtBr adduct, considered a measure of the extent of modification caused to DNA by free radicals (Fig. 5).<sup>53,54,57</sup>

Fig. 6 shows the amount of DNA remaining intact following interaction with intermediates (semiquinone/protonated semiquinone, superoxide radical anion/its protonated form, quinone dianion and its corresponding protonated form etc.) at pH 7.4. Using Fig. 6, it may be said double strand modification of DNA was higher for alizarin than for  $[\text{Mn}^{\text{II}}(\text{alz})_2(\text{H}_2\text{O})_2]$ . Interestingly, the data shown in Figure 6 has the same trend as that of the interaction of species (generated electrochemically) with the four nucleobases. It was reported earlier that DNA and oligonucleotides tend to stabilize semiquinone radical anions through delocalization of electrons in a  $\pi$ -stacking framework, that result in a radical intercalated situation rather than forming covalent bonds.<sup>40</sup> This was further supported by some semi-empirical calculations showing there is a gain in energy by  $\sim 9.8 \text{ kcal mol}^{-1}$ .<sup>40</sup>

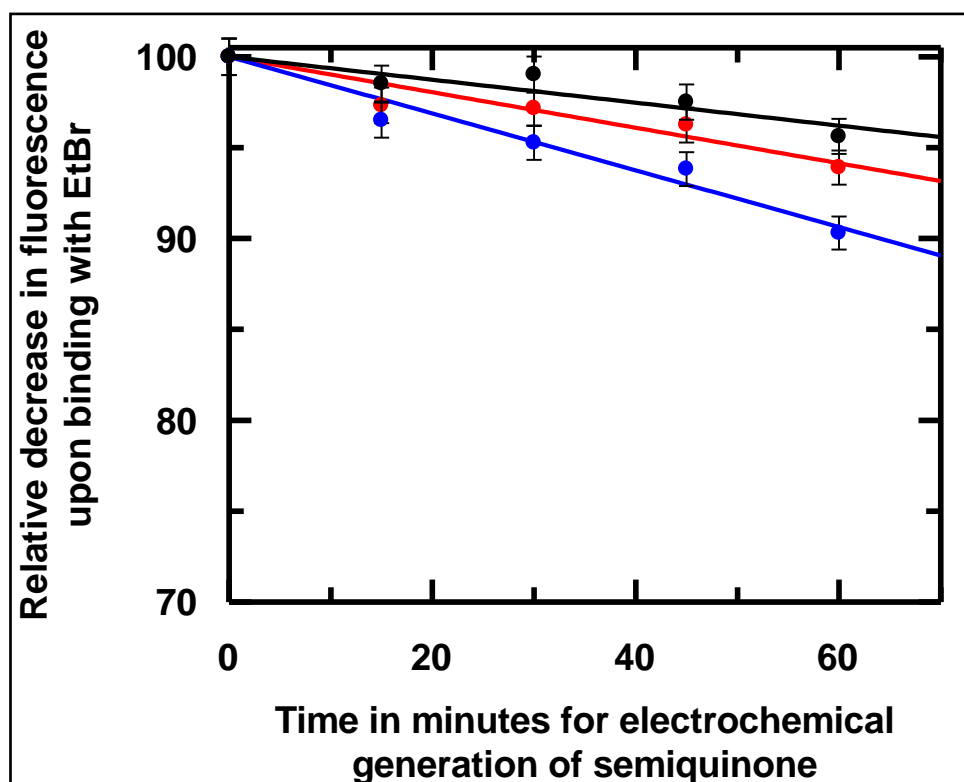


**Fig. 6:** Plots obtained for semiquinone radical anion induced modification of calf thymus DNA in the absence and presence of alizarin and its Mn<sup>II</sup> complex in an argon saturated medium at pH 7.4; absence of any compound (●); presence of alizarin (●) and [Mn<sup>II</sup>(alz)<sub>2</sub>](●).

Insertion of semiquinone radical anions into a DNA strand was reported and believed to result in DNA strand breaks leading to disruption in DNA replication or activate radical mediated reactions. pH as expected, was reported to shift the equilibrium of dianions of hydroquinones, thereby having an influence on the formation of semiquinone radical anion which in turn influences interactions with DNA.<sup>40,50</sup> The fact that our results show modification of nucleobases only adds to previous information following intercalation leading to unwinding of DNA, the exposed nucleobases become vulnerable to further damage that might permanently prevent them from regenerating the double strands again, should a favourable situation arise.

Another interesting aspect of the study is that the difference between damage caused to DNA by species generated on alizarin and on  $[\text{Mn}^{\text{II}}(\text{alz})_2(\text{H}_2\text{O})_2]$  was not as large as that observed for nucleobases. This suggests that in case of DNA, some attribute of complex formation comes into play causing substantial modification to DNA by other pathways that are also detected by a loss of fluorescence due to formation of the DNA-EtBr adduct. Therefore, excess modification due to a greater amount of free radicals formed on alizarin over that formed on the complex (the gap) is somewhat realized. Besides,  $\text{Mn}^{\text{II}}$  having stable higher oxidation states might get oxidized by ROS, by substances like  $\text{H}_2\text{O}_2$  (if formed in the medium) to generate transient  $\text{Mn}^{\text{III}}$  that could then show its oxidative role,<sup>48,49</sup> leading to damage of DNA that would also be detected by the EtBr-DNA fluorescence technique. Therefore, although formation of semiquinone on alizarin is greater than that formed on the complex as realized from damage caused to nucleobases (Table 1), other aspects related to complex formation might bridge the gap between the performance of alizarin and its  $\text{Mn}^{\text{II}}$  complex on calf thymus DNA. Although binding of the complex to calf thymus DNA is better than alizarin, here it was not a major contributor towards damage to DNA as one would have expected because in this study the concentration of compounds were 0.03 mM (i. e. almost 100 times less than the concentration of DNA used).<sup>54</sup> Therefore, although  $\text{Mn}^{\text{II}}$ -alizarin has a strong affinity for DNA, in case of this study, there should not be much of an influence based on its better binding to DNA since concentration of compounds used were too small compared to the substrate used. Since the technique of decreasing fluorescence of a DNA-EtBr adduct detects double strand modification in general (i.e. however it may be caused), all modifications are actually detected.<sup>57,53,54</sup> Thus this technique provides an overall double strand modification i.e. caused by the action of free radicals as well as by other pathways.<sup>57,53,54</sup> Hence, for the study with calf thymus DNA, a “leveling effect” might have been observed in case of interaction of compounds, following an *in situ* electrochemical

generation of reactive species under the conditions of the experiment (Fig. 6, Table 1). Even then, alizarin was better than the complex indicating the extent of compromise complexes of this class of compounds make in the free radical pathway.

The study clearly demonstrates each compound's ability to initiate radical induced damage on different nucleic acid bases, considered a significant pathway by which anthracyclines, its analogues and their metal complexes show cytotoxic activity on cancer cells.<sup>14-17,32</sup> The study provides evidence why complex formation of anthracyclines or its analogues, although beneficial with regard to decrease in cardiotoxic side effects, compromise with cytotoxicity in the free radical pathway.

### **3. References:**

- [1] G. N. Hortobágyi. 1997. Anthracyclines in the treatment of cancer. An overview. *Drugs*. 54: 1-7.
- [2] A. J. M. Ferreri, E. Campo, A. Ambrosetti, F. Ilariucci, J. F. Seymour, R. Willemze, G. Arrigoni, G. Rossi, A. Lopez-Guillermo, E. Berti, M. Eriksson, M. Federico, S. Cortelazzo, S. Govi, N. Frungillo, S. Dell'Oro, M. Lestani, S. Asioli, E. Pedrinis, M. Ungari, T. Motta, R. Rossi, T. Artusi, P. Iuzzolino, E. Zucca, F. Cavalli and M. Ponzoni. 2004. Anthracycline-based chemotherapy as primary treatment for intravascular lymphoma. *Ann. Oncol.* 15: 1215-1221.
- [3] D. Robson and S. Verma. 2009. Anthracyclines in early-stage breast cancer: Is it the end of an era? *The Oncologist*. 14: 950-958.

- [4] L. A. Smith, V. R. Cornelius and C. J. Plummer. 2010. Cardiotoxicity of anthracycline agents for the treatment of cancer: Systematic review and meta-analysis of randomised controlled trials. *BMC Cancer*. 10: 337. doi:10.1186/1471-2407-10-337.
- [5] M. Xing, F. Yan, S. Yu and P. Shen. 2015. Efficacy and Cardiotoxicity of Liposomal Doxorubicin-Based Chemotherapy in Advanced Breast Cancer: A Meta-Analysis of Ten Randomized Controlled Trials. *PLoS ONE*, 10, e0133569; <https://doi.org/10.1371/journal.pone.0133569>.
- [6] F. Marano, R. Frairia, L. Rinella, M. Argenziano, B. Bussolati, C. Grange, R. Mastrocola, I. Castellano, L. Berta, R. Cavalli and M. G. Catalano. 2017. Combining doxorubicin-nanobubbles and shockwaves for anaplastic thyroid cancer treatment: preclinical study in a xenograft mouse model. *Endocrine-Related Cancer*. 24: 275-286.
- [7] E. V. Barry, S. E. Lipshultz, S. E. Sallan. 2008. Anthracycline-induced cardiotoxicity: natural history, risk factors, and prevention. *American Society of Clinical Oncology, Alexandria*, p. 448-453.
- [8] G. Curigliano, D. Cardinale, T. Suter, G. Plataniotis, E. de Azambuja, M. T. Sandri, C. Criscitiello, A. Goldhirsch, C. Cipolla, F. Roila. 2012. Cardiovascular toxicity induced by chemotherapy, targeted agents and radiotherapy: ESMO Clinical Practice Guidelines. On behalf of the ESMO Guidelines Working Group. *Annals of Oncology*. 23: vii155–vii166. <https://doi.org/10.1093/annonc/mds293>
- [9] J. V. McGowan, R. Chung, A. Maulik, I. Piotrowska, J. M. Walker, D. M. Yellon. 2017. Anthracycline Chemotherapy and Cardiotoxicity. *Cardiovasc Drugs Ther*. 31: 63-75.
- [10] E. Gammella, F. Maccarinelli, P. Buratti, S. Recalcati, G. Cairo. 2014. The role of iron in anthracycline cardiotoxicity. *Front. Pharmacol*. 25; doi: 10.3389/fphar.2014.00025

- [11] D. W. Edwardson, R. Narendrula, S. Chewchuk, K. Mispel-Beyer, J. P. J. Mapletoft, A. M. Parissenti. 2015. Role of drug metabolism in the cytotoxicity and clinical efficacy of anthracyclines. *Curr Drug Metab.* 16: 412-426.
- [12] C. G. Nebigil, L. Désaubry. 2018. Updates in Anthracycline-Mediated Cardiotoxicity. *Front. Pharmacol.* 9, 1262; doi: 0.3389/fphar.2018.01262. eCollection.
- [13] J. M. Nabholtz, A. Riva. 2001. Taxane/anthracycline combinations: setting a new standard in breast cancer? *The Oncologist.* 6: 5-12.
- [14] Y. Sun. 2008. Chemosensitization by emodin, a plant-derived anti-cancer agent: mechanism of action. *Cancer Biology & Therapy.* 7: 476-478.
- [15] X. Huang, J. Wang, C. Huang, Y. Chen, G. Shi, Q. Hu, J. Yi. 2008. Emodin enhances cytotoxicity of chemotherapeutic drugs in prostate cancer cells: The mechanisms involve ROS-mediated suppression of multidrug resistance and hypoxia inducible factor-1. *Cancer Biology & Therapy.* 7: 468-475.
- [16] S. C. Hsu, J. G. Chung. 2012. Anticancer potential of emodin. *BioMedicine.* 2: 108-116.
- [17] W. T. Wei, S. Z. Lin, D. L. Liu, Z. H Wang. 2013. The distinct mechanisms of the antitumor activity of emodin in different types of cancer (Review). *Oncology Reports.* 30: 2555-2562.
- [18] K. Rygiel. 2016. Benefits of antihypertensive medications for anthracycline- and trastuzumab-induced cardiotoxicity in patients with breast cancer: Insights from recent clinical trials. *Ind. J. Pharmacol.* 48: 490-497.
- [19] Y. Kwon. 2016. Mechanism-based management for mucositis: option for treating side effects without compromising the efficacy of cancer therapy. *Onco Targets and Therapy.* 9: 2007-2016.



- [20] C. Henninger, G. Fritz. 2018. Statins in anthracycline-induced cardiotoxicity: Rac and Rho, and the heartbreakers. *Cell Death Dis.* 8, e2564; doi:10.1038/cddis.2016.418.
- [21] R. S. Cvetković, L. J. Scott. 2005. Dexrazoxane: a review of its use for cardioprotection during anthracycline chemotherapy. *Drugs.* 65: 1005-1024.
- [22] A. Jabłonska-Trypuc, G. Swiderski, R. Kretowski, W. Lewandowski. 2017. Newly synthesized doxorubicin complexes with selected metals—synthesis, structure and anti-breast cancer activity. *Molecules.* 22, 1106; doi:10.3390/molecules22071106.
- [23] H. Mizutani, A. Nishimoto, S. Hotta, K. Ikemura, M. Imai, D. Miyazawa, K. Ohta, Y. Ikeda, T. Maeda, M. Yoshikawa, Y. Hiraku, S. Kawanishi. 2018. Oxidative DNA damage induced by Pirarubicin, an anthracycline anticancer agent, in the Presence of Copper (II). *Anticancer Research.* 38: 2643-2648.
- [24] K. D. Mjos, J. F. Cawthray, G. Jamieson, J. A. Fox, C. Orvig. 2015. Iron(iii)-binding of the anticancer agents doxorubicin and vosaroxin. *Dalton Trans.* 44: 2348-2358.
- [25] J. Butler, B. M. Hoey, A. J. Swallow. 1985. Reactions of the semiquinone free radicals of anti-tumour agents with oxygen and iron complexes. *FEBS Lett.* 182: 95-98.
- [26] E. J. Land, T. Mukherjee, A. J. Swallow, J. M. Bruce. 1985. Possible intermediates in the action of adriamycin—A pulse radiolysis study. *Br. J. Cancer.* 51: 515-523.
- [27] P. Das, C. K. Jain, S. K. Dey, R. Saha, A. D. Chowdhury, S. Roychoudhury, S. Kumar, H. K. Majumder, S. Das. 2014. Synthesis, crystal structure, DNA interaction and in vitro anticancer activity of a Cu(II) complex of purpurin: dual poison for human DNA topoisomerase I and II. *RSC Adv.* 4:59344-59357.
- [28] S. Mukherjee, P. K. Gopal, S. Paul, S. Das. 2014. Acetylation of 1,2,5,8-tetrahydroxy-9,10-anthraquinone improves binding to DNA and shows enhanced superoxide formation that explains better cytotoxicity on JURKAT T Lymphocyte Cells. *J. Anal. Oncol.* 3: 122-129.

[29] P. Das, D. Bhattacharya, P. Karmakar, S. Das. 2015. Influence of ionic strength on the interaction of THA and its Cu(II) complex with DNA helps to explain studies on various breast cancer cells. *RSC Adv.* 5: 73099-73111.

[30] S. Roy, P. Mondal, P. S. Sengupta, D. Dhak, R. C. Santra, S. Das, P. S. Guin. 2015. Spectroscopic, computational and electrochemical studies on the formation of the copper complex of 1-amino-4-hydroxy-9,10-anthraquinone and effect of it on superoxide formation by NADH dehydrogenase. *Dalton Trans.* 44: 5428-5440.

[31] B. Mandal, S. Singha, S. K. Dey, S. Mazumdar, T. K. Mondal, P. Karmakar, S. Kumar, S. Das. 2016. Synthesis, crystal structure from PXRD of a MnII(purp)<sub>2</sub> complex, interaction with DNA at different temperatures and pH and lack of stimulated ROS formation by the complex. *RSC Adv.* 6: 51520-51532.

[32] P. Das, C. K. Jain, S. Roychoudhury, H. K. Majumder, S. Das. 2016. Design, Synthesis and in vitro Anticancer Activity of a Cu(II) Complex of Carminic Acid: A Novel Small Molecule Inhibitor of Human DNA Topoisomerase I and Topoisomerase II. *ChemistrySelect.* 1: 6623-6631.

[33] B. Mandal, S. Singha, S. K. Dey, S. Mazumdar, S. Kumar, P. Karmakar, S. Das. 2017. CuII complex of emodin with improved anticancer activity as demonstrated by its performance on HeLa and Hep G2 cells. *RSC Adv.* 7: 41403-41418.

[34] S. Mukherjee-Chatterjee, C. K. Jain, S. Singha, P. Das, S. Roychoudhury, H. K. Majumder, S. Das. 2018. Activity of CoII–Quinalizarin: A novel analogue of anthracycline-based anticancer agents targets human DNA topoisomerase, whereas Quinalizarin itself acts via formation of semiquinone on acute lymphoblastic leukemia MOLT-4 and HCT 116 cells. *ACS Omega.* 3, 10255-10266.

- [35] P. Nandy, S. Das. 2018. Interaction of electrochemically generated reduction products of Ornidazole with nucleic acid bases and calf thymus DNA. *J. Indian Chem. Soc.* 95: 1009-1014.
- [36] B. Mandal, H. K. Mondal, S. Das. 2019. In situ reactivity of electrochemically generated semiquinone on Emodin and its Cu II/Mn II complexes with pyrimidine based nucleic acid bases and calf thymus DNA: Insight into free radical induced cytotoxicity of anthracyclines. *Biochem. Biophys. Res. Comm.* 515: 505-509.
- [37] P. Nandy, S. Das. 2020. In situ reactivity of electrochemically generated nitro radical anion on Ornidazole and its monomeric Cu(II) complex with nucleic acid bases and calf thymus DNA. *Inorg. Chim. Acta.* 501: 119267-119267;
- [38] P. S. Guin, S. Das, P. C. Mandal. 2010. Sodium 1,4- dihydroxy-9,10-anthraquinone-2-sulphonate interacts with calf thymus DNA in a way that mimics anthracycline antibiotics: an electrochemical and spectroscopic study. *J. Phy. Org. Chem.* 23: 477-482.
- [39] P. Das, P. S. Guin, P. C. Mandal, M. Paul, S. Paul, S. Das. 2011. Cyclic voltammetric studies of 1,2,4-trihydroxy-9,10- anthraquinone, its interaction with calf thymus DNA and anti-leukemic activity on MOLT-4 cell lines: a comparison with anthracycline anticancer drugs. *J. Phy. Org. Chem.* 24: 774-785.
- [40] O. Wangpradit, A. Rahaman, S. V. S. Mariappan, G. R. Buettner, L. W. Robertson, G. Luthe. 2016. Breaking the dogma: PCB-derived semiquinone free radicals do not form covalent adducts with DNA, GSH, and amino acids. *Environ Sci Pollut Res Int.* 23: 2138-2147. doi: 10.1007/s11356-015-5007-4.
- [41] A. Tubbs, A. Nussenzweig. 2017. Endogenous DNA Damage as a Source of Genomic Instability in Cancer. *Cell.* 168, 644-656.

- [42] W. P. Roos, A. D. Thomas, B. Kaina. 2016. DNA damage and the balance between survival and death in cancer biology. *Nat Rev Cance*. 16: 20-33.
- [43] S. P. Jackson, J. Bartek. 2009. The DNA-damage response in human biology and disease. *Nature*. 461: 1071-1078.
- [44] P. Strzyz. 2016. Cell thriving despite DNA damage. *Nature Reviews Molecular Cell Biology*. 17, 396; <https://doi.org/10.1038/nrm.2016.86>.
- [45] J. M. Floberg, L. Wang, N. Bandara, R. Rashmi, C. Mpoy, J. R. Garbow, B. E. Rogers, G. J. Patti, J. K. Schwarz. 2020. Alteration of Cellular Reduction Potential Will Change 64 Cu-ATSM Signal With or Without Hypoxia. *J Nucl Med*. 61: 427-432.
- [46] M. Goldstein, M. B. Kastan. 2015. The DNA damage response: implications for tumor responses to radiation and chemotherapy. *Annu Rev Med*. 66: 129-143.
- [47] M. Hayyan, M. A. Hashim, I. M. AlNashef. 2016. Superoxide Ion: Generation and Chemical Implications. *Chem. Rev*. 116: 3029-3085; DOI: 10.1021/acs.chemrev.5b00407
- [48] J. K. Glenn, L. Akileswaran, M. H. Gold. 1986. Mn(II) oxidation is the principal function of the extracellular Mn-peroxidase from *Phanerochaete chrysosporium*. *Arch Biochem Biophys*. 251: 688-696.
- [49] T. Saha, P. Kumar, N. Sepay, D. Ganguly, K. Tiwari, K. Mukhopadhyay, S. Das. 2020. Multitargeting antibacterial activity of a synthesized Mn<sup>2+</sup> complex of curcumin on gram-positive and gram-negative bacterial strains. *ACS Omega*. 5: 16342-16357.
- [50] G. E. Borgstahl, H. E. Parge, M. J. Hickey, W. F. Beyer, R. A. Hallewell, J. A. Tainer. 1992. The structure of human mitochondrial manganese superoxide dismutase reveals a novel tetrameric interface of two 4-helix bundles. *Cell*. 71: 107-118.

- [51] P. J. Elving, S. J. Pace, J. E. O'Reilly. 1973. Electrochemical reduction of purine, pyrimidine, and imidazole in aqueous media. Kinetics and Mechanisms. *J. Am. Chem. Soc.* 95:647–658.
- [52] G. Dryhurst, P. J. Elving. 1969. Electrochemical oxidation-reduction paths for pyrimidine, cytosine, purine and adenine Correlation and application. *Talanta.* 16:855-874.
- [53] S. Das, A. Saha, P. C. Mandal. 1997. Radiation-induced double-strand modification in calf thymus DNA in the presence of 1,2-dihydroxy-9,10-anthraquinone and its Cu(II) complex. *Environ Health Pers.* 105: 1459-1462.
- [54] S. Das, P. C. Mandal. 2014. Anthracyclines as radiosensitizers: A Cu (II) complex of a simpler analogue modifies DNA in Chinese Hamster V79 cells under low-dose  $\gamma$  radiation. *J Radioanal Nucl Chem.* 299: 1665-1670.
- [55] R. C. Santra, D. Ganguly, D. Bhattacharya, P. Karmakar, A. Saha, S. Das. 2017.  $\gamma$  radiation-induced damage of nucleic acid bases, calf thymus DNA and DNA within MCF-7 breast cancer cells by [Cu<sub>2</sub>(OAc)<sub>4</sub>(tnz)<sub>2</sub>]: a potential radiosensitizer. *New J. Chem.* 41: 11679-11685.
- [56] S. Tremblay, J. R. Wagner. 2008. Dehydration, deamination and enzymatic repair of cytosine glycols from oxidized poly (dG-dC) and poly (dI-dC). *Nucleic Acids Res.* 36: 284-293; doi:10.1093/nar/gkm1013.
- [57] H. C. Birnboim, J. J. Jevcak. 1981. Fluorometric Method for Rapid Detection of DNA Strand Breaks in Human White Blood Cells Produced by Low Doses of Radiation. *Cancer Research.* 41: 1889-1892.



# CHAPTER 12

## Conclusion





The research reported in this dissertation aimed to identify if simpler analogues of established anthracyclines used as chemotherapeutic agents in treating cancer could be effectively used as less costly substitutes. For this purpose, hydroxy-9,10-anthraquinones alizarin, purpurin and carminic acid that closely resemble the core of anthracyclines, responsible for most of its chemical action were chosen. While alizarin and purpurin are simple hydroxy-9,10-anthraquinones, carminic acid has an  $\alpha$ -D-glucopyranosyl unit directly attached to an otherwise hydroxy-9,10-anthraquinone. Earlier studies reveal although simple and cost effective, simple analogues like alizarin and purpurin resemble anthracyclines to the maximum extent only with regard to chemical behaviour while a considerable gap with regard to biophysical interactions and biochemical action for exist making such molecules trail behind on grounds of efficacy. The cause for the difference among other things was attributed to the presence of sugar units in anthracyclines and an absence of it in simpler analogues making them less effective biologically. For this reason, another simple analogue carminic acid, having a sugar moiety bound to a hydroxy-9,10-anthraquinone was tried as a part of this study, since a significant amount of difference in biophysical and biochemical activity is of hydroxy-9,10-anthraquinones and anthracyclines are reported to be bridged owing to inclusion of a sugar moiety.<sup>1-3</sup>

Studies on the interaction of chosen compounds with DNA were attempted since they help to realize the action of the compounds on cells and their relevance in different aspects of chemical biology. Hydroxy-9, 10-anthraquinones dissociate at physiological pH i. e. exist in more than one form in solution. Hence, the  $pK_a$  of such compounds have a decisive role in evaluating the contributions of different forms present in solution to the overall binding; that would obviously be different. Hence depending on the pH of the medium, binding constant values of such compounds vary since the composition of the solution changes continuously with pH. Hence for a proper evaluation of binding constants and the relative contribution of

## ***Chapter 12: Conclusion***

---

each species, it is extremely essential that correct i. e. properly determined  $pK_a$  values are used. This study was able to show that indeed there is a difference in the evaluation of the contributions of each species, if there is a difference in evaluation of  $pK_a$ . For this reason,  $pK_a$  were determined in normal aqueous solution and also in the presence of DNA. They were found to differ significantly.

***This study emphasizes on the fact that a correct determination of  $pK_a$  is extremely essential in realizing a molecule's ability to interact with DNA and to have a clear idea on the extent to which a certain species in solution contributes towards binding.***

Since extent of binding with DNA is highly influenced by factors like pH, temperature, ionic strength and polarity of the medium, interaction of chosen hydroxy-9,10-anthraquinones with DNA were performed under varying conditions of pH and ionic strength of the medium. Studies reveal binding constant values decreased with an increase in the pH of the medium. It also revealed binding of purpurin to calf thymus DNA was higher than alizarin when the only difference in their structures is an  $-OH$  group. This signifies that location of  $-OH$  groups in case of such compounds have a profound influence on their DNA targeting ability that has already been identified for anthracyclines.

***Therefore, the above findings reaffirm certain known facts regarding anthracyclines through studies performed on its simpler analogues.***

It is now well known that metal complexes of anthracyclines are able to decrease formation of semiquinone, modulate ROS generation and are less cardiotoxic. Since a basic intention of this work was to see the extent to which hydroxy-9,10-anthraquinones resemble anthracyclines, it was important to compare the properties of metal complexes of the chosen simpler analogues with those of metal complexes of anthracyclines.  $Mn^{II}$ ,  $Co^{II}/Co^{III}$  complexes of alizarin and  $Mn^{II}$  complex of carminic acid were synthesized and characterised

both from experimental and theoretical approaches. Since the complexes would be tried in biological experiments, it was essential to know their stability in biological solvents. For this reason the stability constants of the prepared complexes were determined in solution. Log  $\beta$  values were,  $[\text{Mn}(\text{alz})_2(\text{H}_2\text{O})_2] = 14.39$ ,  $\text{Na}[\text{Co}(\text{alz})_3] = 19.96$ ,  $\text{Na}_2[\text{Mn}^{\text{II}}(\text{CA})_2(\text{H}_2\text{O})_2] = 11.60$ . In the absence of single crystals of the prepared complexes (single crystals being rare for such systems<sup>4,5</sup>), density functional theory (DFT) studies were done to predict structures of complexes based experimental data like their UV-Vis spectrum, IR spectrum, mass spectrum, magnetic susceptibility measurements, thermo-gravimetric data etc.

*DFT studies indicate octahedral geometry for the Mn<sup>II</sup> complex of alizarin having high spin configuration, an octahedral geometry for [Co<sup>III</sup>(alz)<sub>3</sub>] and octahedral geometry for Na<sub>2</sub>[Mn<sup>II</sup>(CA)<sub>2</sub>(H<sub>2</sub>O)<sub>2</sub>] with two water molecules mutually cis to each other.*

Since a major reason for performing this study was to look at the biological efficacy of the prepared complexes both with respect to hydroxy-9,10-anthraquinones and anthracyclines in clinical use, interaction with DNA at different ionic strengths and pH were done. Complexes showed increased affinity towards DNA. Experiments also revealed that binding constant values did not decrease either with an increase in pH or decrease in ionic strength of the medium. This was considered a positive attribute of complex formation of the chosen hydroxy-9,10-anthraquinones. Since hydroxy-9,10-anthraquinones themselves suffer from decreasing trend in binding constant values for an increase in pH of the medium, this is considered a set back in the use of hydroxy-9,10-anthraquinones as anticancer agents in reference to anthracyclines. Therefore, complexes address the shortcomings of hydroxy-9,10-anthraquinones with regard to DNA binding. Values obtained for the complexes approach those reported for anthracyclines. In fact, for  $[\text{Mn}(\text{alz})_2(\text{H}_2\text{O})_2]$ , binding constant with calf thymus DNA is as high as that reported for anthracyclines (of the order  $\sim 10^5$ ). This is

## ***Chapter 12: Conclusion***

---

particularly significant because cancer patients often experience fluctuation in pH and ionic strength in body fluids during treatment that affects efficacy of many drugs.

***Therefore, if such complexes are tried on cancer patients then for a wide range of pH and varying electrolyte concentration, such model studies suggest that the likelihood of the compounds being active would be much greater than hydroxy-9,10-anthraquinones themselves.***

A serious drawback of hydroxy-9,10-anthraquinone based anthracyclines is the generation of semiquinone radical anion that forms superoxide radical anion in aerated medium and is cardiotoxic. Although useful for cytotoxic activity, their uncontrolled generation take away the merit of the drugs. Literature reports indicate metal complexes of anthracyclines are less cardiotoxic. To explore this further, the two complexes of alizarin were subjected to enzyme assay where generation of superoxide radical anion was followed. Both complexes of alizarin form significantly less superoxide radical anion in comparison to alizarin itself under similar assay conditions. Therefore, going by previous reports and the general perception, it may be said, complexes would be less cardiotoxic. Similarly, it is logically expected that complexes would be less effective in free radical pathways responsible for cytotoxicity i. e. as anticancer agents. To investigate further the consequences of the generation of semiquinone radical anion, alizarin and its Mn(II) complex were subjected to reduction at respective reduction potentials keeping either pyrimidine based nucleic acid bases or DNA in its immediate vicinity. The study revealed alizarin was more effective on nucleobases and calf thymus DNA than the complex.

***Hence, again, the general expectation that following complex formation there is some compromise made in the free radical pathway owing to decreased semiquinone formation, could be established.***

Radical formation and consequently their scavenging by compounds present in cellular medium form an important aspect of drug action pertaining to cellular damage. This has been established by several studies. Our compounds were tried on cancer cell lines (HeLa, SIHA, HepG2) and also on normal WI-38 human lung fibroblast cells. ROS was generated by H<sub>2</sub>O<sub>2</sub> and assessed by the DCFDA assay in presence of alizarin and its Mn<sup>II</sup> and Co<sup>II</sup> complexes. The Mn<sup>II</sup> complex was way ahead in Hep G2 cells in ROS amplification over alizarin while for HeLa cells no clear distinction could be made between ROS identified due to alizarin and Mn<sup>II</sup> complex. The Co<sup>II</sup> complex was found ahead in SIHA cells over alizarin. For normal WI 38 human lung fibroblast cells, Mn<sup>II</sup> complex generated ROS to a greater extent than alizarin.

*This study identified a pathway by which compounds are responsible for cytotoxic activity.*

*It revealed better ROS amplification was achieved due to the complexes suggesting why they were found to be better in cell killing.*

*MTT assay carried out on different cell lines indicate complexes were better in killing cells than the corresponding hydroxy-9,10-anthraquinones.*

Hence, considering all forms of findings pertaining to this study it may be said complexes of hydroxy-9,10-anthraquinones have several attributes like increased affinity for DNA, effective cellular uptake, capability to amplify ROS present in cells that together equip them to interfere with one or more cellular mechanisms enabling them to be more effective on cellular systems than hydroxy-9,10-anthraquinones, even if they fall behind in semiquinone generation during their involvement in electron transport chains.

**References:**

[1] W. Priebe. 2000. Targeting DNA with anthracyclines: the importance of the sugar moiety. *Molecules*. 5:299–301

[2] T. Banerjee, R. Mukhopadhyay. 2008. Structural effects of nogalamycin, an antibiotic antitumour agent, on DNA. *Biochem. Biophys. Res. Comm.* 374:264-268.

[3] P. Das, C. K. Jain, S. Roychoudhury, H. K. Majumder, S. Das. 2016. Design, synthesis and in vitro anticancer activity of a Cu(II) complex of carminic acid: A novel small molecule inhibitor of human DNA topoisomerase I and topoisomerase II. *ChemistrySelect*. 1: 6623-6631.

[4] M. Di Vaira, P. Orioli, F. Piccioli, B. Bruni, L. Messori. 2003. Structure of a Terbium(III)–quinizarine complex: The first crystallographic model for metalloanthracyclines. *Inorg. Chem.* 42:3157-3159.

[5] S. Du, J. Feng, X. Lu, G. Wang. 2013. The syntheses and characterizations of vanadium complexes with 1,2-dihydroxyanthraquinone and the structure–effect relationship in their in vitro anticancer activities. *Dalton Trans.* 42: 9699-9705.

# APPENDIX-1





## List of publications

1. **Mouli Saha**, Promita Nandy, Mousumi Chakraborty, Piyal Das, Saurabh Das. 2018. The importance of  $pK_a$  in an analysis of the interaction of compounds with DNA. *Biophysical Chemistry*. 236: 15-21
2. **Mouli Saha**, Soumen Singha, Mousumi Chakraborty, Swagata Mazumdar, Sanjay Kumar, Parimal Karmakar, Saurabh Das. 2019. Characterization of a  $Mn^{II}$  complex of Alizarin suggests attributes explaining a superior anticancer activity: A comparison with anthracycline drugs. *Polyhedron*. 173: 114104
3. **Mouli Saha**, Saurabh Das. 2021. Free radical induced activity of an anthracycline analogue and its  $Mn^{II}$  complex on biological targets through *in situ* electrochemical generation of semiquinone. *Heliyon*. 7: e07746
4. **Mouli Saha**, Soumen Singha, Deblina Ghosh, Sanjay Kumar, Parimal Karmakar, Saurabh Das. 2022. A Cobalt<sup>II</sup>/Cobalt<sup>III</sup> complex of alizarin that was analyzed from the stand point of binding with DNA, for ROS generation and anticancer drug prospecting was identified as an analogue of anthracyclines. *Journal of Molecular Structure*. 1262: 133011

### **Probable publications from the work reported in the thesis**

1. **Mouli Saha**, Tanmoy Saha, Swarupa Sarkar, Parimal Karmakar, Saurabh Das, Comparing chemical, biophysical and biochemical attributes of anthracyclines as anticancer agents using carminic acid and its Mn<sup>II</sup> complex. *Manuscript under preparation.*

# APPENDIX-II

## List of Conference proceedings



## **PUBLICATION OF ABSTRACT IN CONFERENCE PROCEEDINGS:**

**2016 Poster: Mouli Saha, Promita Nandy, Saurabh Das.** “Influence of the pK values of purpurin on its interaction with calf thymus DNA helps to realize the contributions of the various forms of the molecule towards overall binding” at the **Chemistry of Functional Materials of Current Interest, on March 16, 2016**, organized by Department of Chemistry, Jadavpur University, Kolkata 700032.

**2016 Poster: Mouli Saha, Swagata Mazumdar, Bitapi Mandal, Parimal Karmakar, Saurabh Das.** Influence of ionic strength on the interaction of alizarin and its Mn<sup>II</sup> complex with DNA that helps to explain the trend observed in binding with variation in the ionic strength of the medium” at **19<sup>th</sup> CRSI NATIONAL SYMPOSIUM IN CHEMISTRY, 14<sup>th</sup> – 16<sup>th</sup> July 2016**, organized by Department of Chemistry, University of North Bengal.

**2017 Poster: Mouli Saha, Sayantani Mukherjee, Chetan Kumar Jain, Moushumi Chakraborty, Hemanta Kumar Majumder, Saurabh Das.** “Tuning the generation of semiquinones through complex formation of hydroxy-9,10-anthraquinones with Co<sup>II</sup>: balance between efficacy and toxic side effects of anthracyclines” in the **5<sup>th</sup> Symposium on Advanced Biological Inorganic Chemistry**, organized by Tata Institute of Fundamental Research, Mumbai and Indian Association for the Cultivation of Science, Kolkata in Kolkata, **January 7-11, 2017.**

**2020 Poster: Mouli Saha, Soumen Singha, Deblina Ghosh, Sanjay Kumar, Parimal Karmakar, Saurabh Das..** “Characterization of a Cobalt<sup>II</sup>/Cobalt<sup>III</sup> complex of alizarin suggests attributes, that explain anticancer activity: A comparison with anthracycline antibiotics” at **RECENT TRENDS IN INORGANIC CHEMISTRY**, organized by Inorganic Chemistry Section, Department of Chemistry, Jadavpur University, Kolkata 700 032 on **March 06, 2020.**



# **APPENDIX-III**

**Reprint of publications  
included in the thesis**







## The importance of $pK_a$ in an analysis of the interaction of compounds with DNA



Mouli Saha<sup>1</sup>, Promita Nandy<sup>1</sup>, Mousumi Chakraborty, Piyal Das, Saurabh Das\*

Department of Chemistry, Jadavpur University, Kolkata 700 032, India

### HIGHLIGHTS

- Most of the compounds interacting with DNA exist in more than one form in solution.
- Most often this is a consequence of one or more proton dissociation equilibrium.
- The amount of the contributing forms present in solution keeps changing with pH.
- To know the correct amount of a form present appropriate  $pK_a$  must be used.
- Overall binding of a compound with DNA is a consequence of the contributions of different forms of it.

### GRAPHICAL ABSTRACT

Anthracycline analogues alizarin and purpurin were used to find how DNA influences determination of  $pK_a$ .  $pK_{a1}$  and  $pK_{a2}$  were different when evaluated in presence of DNA.  $pK_{a1}$  determined in presence of DNA was used to evaluate contributions of two forms of the molecules towards overall binding with calf thymus DNA. Revised calculations show contribution of the neutral form was different while that of the anionic form was same.

### ARTICLE INFO

#### Keywords:

$pK_a$   
Alizarin  
Purpurin  
Contribution of species  
 $K^0$   
 $K^-$   
pH

### ABSTRACT

$pK_a$  of a compound is crucial for determining the contributions of different forms of it towards overall binding with DNA. Hence it is important to use correct  $pK_a$  values in DNA interaction studies. This study takes a look at the importance of  $pK_a$  values to realize binding of compounds with DNA. Since  $pK_a$  of a compound determined in the presence of DNA is quite different from that determined in its absence hence, presence of different forms of a compound during interaction with DNA is different from that realized if the determination of  $pK_a$  is done in normal aqueous solution in absence of DNA. Hence, calculations determining contributions of different forms of a compound interacting with DNA are affected accordingly. Two simple analogues of anthracyclines, alizarin and purpurin, were used to investigate the influence DNA has on  $pK_a$  values. Indeed, they were different in presence of DNA than when determined in normal aqueous solution.  $pK_{a1}$  for alizarin and purpurin determined in the absence and presence of calf thymus DNA were used in equations that determine contributions of two forms (neutral and anionic) towards overall binding with DNA. The study concludes that correct  $pK_a$  values, determined correctly i.e. under appropriate conditions, must be used for DNA binding experiments to evaluate contributions of individual forms.

### 1. Introduction

Studies on interaction of compounds with DNA are important for many reasons and there are lots of information in the literature as well [1–9]. They help us realize the utility of these interactions and their

relevance in different aspects of chemical biology [10–13]. Although lot is known on interaction of different compounds with DNA, it is still too early, even for experiments in vitro, to say that all interactions are characterized correctly. This is because there are too many factors involved in an interaction of a compound with DNA than we can possibly

\* Corresponding author.

E-mail address: [sdas@chemistry.jdvu.ac.in](mailto:sdas@chemistry.jdvu.ac.in) (S. Das).

<sup>1</sup> MS and PN have equal contribution.

imagine [6,10,12,14,16,17]. Things get even more complicated when the compound exists in more than one form in solution [18–23]. When that is the case, experimental values determined for overall binding constant are actually a consequence of the interaction of each individual form of the compound in solution [18–23]; each form interacting with DNA differently depending on its characteristic properties [16–18]. The amount of each form present during interaction with DNA is also crucial for a correct determination of binding parameters [18,20–23]. Since interaction of each form with DNA is different, it gets manifested in the overall binding constant, an experimentally determined parameter [18,20]. Hence, the contribution of different forms of a compound towards overall binding constant is important in understanding DNA interactions.

Reasons for the existence of a compound in more than one form are varied. It could be the consequence of a racemic mixture, or of *cis-trans* isomerism, or that the compound has one or more easily dissociable protons [18,20–22]. For a proton dependent equilibrium for example, the contributing forms of the compound change with changes in pH of the medium affecting binding parameters with DNA [20–23]. Most studies somehow fail to realize this. In fact, very few compounds exist exclusively in one form in solution; there is almost always another form present (however small it may be) that influences binding with DNA and hence determination of binding parameters.

DNA being a negative polymer, as a general rule, tendency of cationic species interacting with it is greater than species that are neutral which in turn is greater than species negatively charged [10,16–18]. A good deal of approximation has allowed most researchers to either knowingly or unknowingly report DNA binding data as if the compound exists in one form; not considering the fact there could be at least another form in solution under different experimental conditions like pH, ionic strength or temperature and that different structural forms interact differently with DNA [20–25]. In fact, some of the variations observed experimentally in the determination of overall binding constant of a compound with DNA under different conditions have sometimes been reported as “within experimental error” when these small differences were actually because different forms of the molecule were present in different amounts; their contribution to overall binding constant being different. For example, the titration of a compound at pH 6.8 and 7.5 would not be the same if it has a group present in it whose  $pK_a$  is 7.2. Species present in solution at the two pH would be completely different, having a huge impact on binding parameters. This is the case in cell biology processes which can therefore be explained [9–12]. Hence, there is a need to incorporate the aspect of contribution of different forms while considering data generated on DNA interaction to arrive at a realistic picture. As mentioned earlier, a vast majority of compounds studied for DNA binding exists in two or more forms in solution. The ones which do not apparently have a second form at a particular pH could dissociate under the influence of nucleic acids present in DNA as the compound tries to interact with it [26]. While some researchers have been careful to take a note of this, many neglected the fact there could be more than one form in solution whose interaction with DNA is different from the main species they were reporting [18–20,22,27].

Apart from the aspect mentioned above another reason for concern is the very determination of  $pK_a$  of a compound which is crucial for drug selection and optimization [28,29]. We usually determine  $pK_a$  in an aqueous solution at a low ionic strength of the medium and utilize it to understand its implications in different physicochemical experiments to realize its importance in physiological processes [30]. The question here is to what extent is this correct i.e. to use a  $pK_a$  determined in normal aqueous solution not containing DNA and to use it in a DNA binding analysis, the very experiment for which is performed at a reasonably high ionic strength [20,21,23]. Needless, to say this is one of many reasons why results for most compounds studied *in vitro* and *in vivo* differ in a big way. It is now known  $pK_a$  of a compound could be different in presence of DNA or more specifically in presence of nucleic

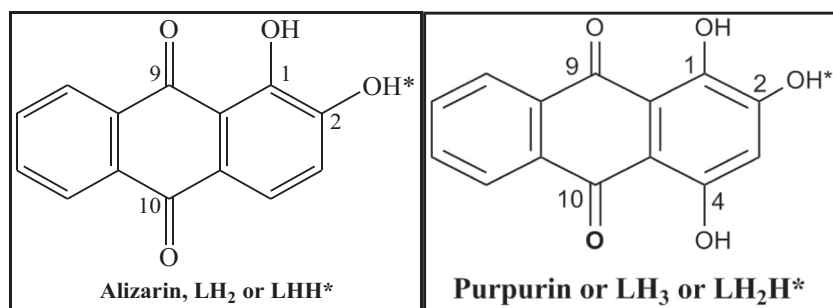
acid bases that make DNA [26]. In fact, DNA itself (i.e. nucleic acid bases that make it) undergoes significant changes owing to changes in the pH of the medium [26]. Protonation causes change in DNA conformation depending on the composition of nucleic acid bases present and the ionic strength of the medium [31,32]. For this reason, we decided to re-investigate some of our own DNA binding data where  $pK_a$  used to evaluate contributions of different forms of a compound binding with DNA was determined in normal aqueous solution [21].  $pK_a$  for the same dissociation was re-determined, this time in presence of different concentrations of calf thymus DNA and that was done in an ionic strength of the medium that is normally maintained for DNA titrations. Since different forms of the compound present in solution are a consequence of their proton dissociation equilibria, proper determination of  $pK_a$  becomes very essential.

When the  $pK_a$  of a compound falls in the physiological pH range in which most of our DNA titrations are performed its importance is even more. Any change in  $pK_a$  obviously affects the overall binding constant value since the contributing forms differ and hence their interaction with DNA [27,33]. Therefore, it is important to find out the reasons responsible for changes in  $pK_a$ . One important factor is the ionic strength of the medium but when ionic strength is kept constant it could vary depending on the amount of DNA present, with which it interacts [8,10,24–26,33]. Nucleic acid bases present in DNA influence proton-dissociation equilibria [26]. Moreover, when the pH of the medium is different it affects the three dimensional structure of DNA which in turn either exposes or withholds nucleic acid bases present in it in different ways that affect the manner in which they influence  $pK_a$  of the compound [26]. Only when  $pK_a$  value is either well below or well beyond the physiological pH range, a single form of a compound would exist or predominate [27]. As early as 1988, a report showed the base ellipticine ( $pK_a = 7.4$ ) binds calf thymus DNA at pH 5 when its cationic form, the ellipticinium cation predominates, while at pH 9 the neutral form is the principal species responsible for binding [34]. However, there are no reports to show what happens between pH 5 and pH 9 when both forms are simultaneously present in solution. Although an excellent piece of work, it does not consider the fact that at pH 5.0, apart from the cation there is ~0.40% of a neutral form and at pH 9.0, apart from ellipticine free base there would be ~2.45% of the cation in solution. This requires consideration for it affects overall binding constant values; hence values reported for the binding constant of the respective forms are not exclusively those claimed in the report. Although the situation is not that serious for the study mentioned above [34] because the presence of the minor form at any pH is really very small it could however altogether change binding constant values for many other compounds reported in the literature. In the example above, had titrations been done at four or five other pH values between pH 5.0 and pH 9.0 then with the help of appropriate equations and a proper use of  $pK_a$  contributions of the two forms could be obtained [18]. Using them, overall binding constant of ellipticine could then be known at any pH without having to perform a titration at that pH [18]. When  $pK_a$  of a compound lies in the physiological pH range as in the example above, a slight change due to interaction of the compound with nucleic acid bases could affect calculations. Therefore, the influence nucleic acid bases might have on a molecule chosen for DNA interaction needs proper investigation. In fact, if this is done, DNA binding parameters may be claimed to have been more rigorously determined. The present study makes an attempt to understand fluctuations in  $pK_a$  of alizarin and purpurin, simpler analogues of anthracycline anticancer agents, evaluated with the help of pH-metric titrations in presence of varying concentrations of calf thymus DNA against those determined in normal aqueous solution. When  $pK_a$  values determined in the presence of DNA were used in Eqs. (4) & (5) to determine contributions of each form to overall binding constant at physiological pH they gave different results from those determined earlier i.e. when  $pK_a$  values were determined in normal aqueous solution. The work allowed us to see manifestations small changes in  $pK_a$  has on contributions of different forms of a

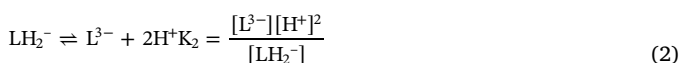
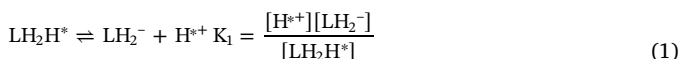
compound to its overall binding with DNA.

## 2. Experimental

Alizarin and purpurin (~96% pure) were purchased from Sigma-Aldrich and re-crystallized from an ethanol-water mixture. Since hydroxy-9,10-anthraquinones are photosensitive, compounds were carefully stored in the dark. Stock solutions in ethanol were  $\sim 10^{-4}$  M. HEPES buffer [4-(hydroxyethyl)-1-piperazine ethane sulphonic acid] was used. Sodium nitrate (AR) and sodium chloride (AR) were used to maintain ionic strength of the medium. Calf thymus DNA purchased from Sisco Research Laboratories, India was dissolved in triple distilled water using 120 mM NaCl, 35 mM KCl and 5 mM MgCl<sub>2</sub>. Concentration of DNA was determined from its absorbance at 260 and 280 nm respectively.  $A_{260}/A_{280}$  was calculated. The ratio obtained being in the range  $1.8 < A_{260}/A_{280} > 1.9$  indicate no further purification was required. The DNA was also characterized with the help of CD spectroscopy at 260 nm using a CD spectropolarimeter J815, JASCO. Concentration of DNA was determined in terms of nucleotide considering its molar extinction coefficient at 260 nm to be  $6600 \text{ M}^{-1} \text{ cm}^{-1}$ .



Proton dissociation constants of the compounds were determined with the help of pH-metric titrations in the presence of different concentrations of calf thymus DNA. 10% ethanol-90% aqueous solutions of compounds were used. The ionic strength of the medium was maintained at 0.12 M. pH was recorded with the help of a pH meter [Equiptronics, EQ-610, India]. Absorbance of alizarin recorded at 525 nm and purpurin at 513 nm were plotted against pH of the medium. Equilibrium showing dissociation of purpurin is provided in Eqs. (1) and (2) respectively. In case of alizarin,  $\text{LH}_2\text{H}^*$  would be  $\text{LHH}^*$  [20,30].



Eq. (3) yields values for  $\text{pK}_{a1}$  and  $\text{pK}_{a2}$  respectively [20,21,30,35]

$$A_{\text{obs}} = \frac{A_1}{(1 + 10^{\text{pH}-\text{pK}_{a1}} + 10^{\text{pH}-\text{pK}_{a2}})} + \frac{A_2}{(1 + 10^{\text{pK}_{a1}-\text{pH}} + 10^{\text{pH}-\text{pK}_{a2}})} + \frac{A_3}{(1 + 10^{\text{pK}_{a1}-\text{pH}} + 10^{\text{pK}_{a2}-\text{pH}})} \quad (3)$$

$A_1$ ,  $A_2$  and  $A_3$  refer to absorbance of the forms  $\text{LH}_2\text{H}^*$ ,  $\text{LH}_2^-$ ,  $\text{L}^{3-}$  respectively for purpurin and  $\text{LHH}^*$ ,  $\text{LH}^-$ ,  $\text{L}^{2-}$  respectively for alizarin [20,21,30].  $\text{pK}_{a1}$  and  $\text{pK}_{a2}$  are  $\text{pK}_a$  values for the dissociation of the two compounds in the presence of different concentrations of calf thymus DNA.

## 3. Results & discussion

The compounds were titrated very slowly using very dilute NaOH in the presence of different concentrations of calf thymus DNA at a constant ionic strength of the medium. Figs. 1 & 2(A and B) are typical plots for variation of absorbance of alizarin and purpurin with pH, recorded

at different concentrations of calf thymus DNA. Fitting the experimental data according to Eq. (3),  $\text{pK}_{a1}$  and  $\text{pK}_{a2}$  for alizarin and purpurin were determined. These were individually plotted against increased presence of calf thymus DNA for both compounds. It was observed that with an increase in concentration of calf thymus DNA,  $\text{pK}_{a1}$  of alizarin and purpurin decreased [Fig. 3] indicating constituent nucleic acid bases of DNA clearly affect the dissociation of phenolic  $-\text{OH}$  protons; the gradient of the plots were however different for the two compounds, which is expected. Since the second dissociation of alizarin [30], second and third dissociations of purpurin [36] occur well beyond physiological pH these were not included in the main text. The second and third dissociation of purpurin occur almost at the same time [21]; Fig. 1S [SI] is a plot of  $\text{pK}_{a2}$  of purpurin with increased concentrations of calf thymus DNA.

The interaction of purpurin with calf thymus DNA with regard to evaluation of the contribution of its neutral and anionic forms to overall binding constant under physiological conditions was revisited [21]. For alizarin, its interaction with calf thymus DNA with an emphasis on the contribution of its two forms was evaluated. Contributions of the neutral and anionic forms of the compounds towards their overall binding

constant with calf thymus DNA was determined by considering  $\text{pK}_{a1}$  once evaluated in normal aqueous solution and again in presence of a definite concentration of calf thymus DNA. For both compounds,  $\text{pK}_{a1}$  that was used in the calculations and determined in the presence of calf thymus DNA was chosen from Fig. 3A and B respectively (from best fit lines) by selecting a value intermediate between lowest and highest concentrations of DNA used in the plots. Values chosen for  $\text{pK}_{a1}$  were 5.94 for alizarin and 5.71 for purpurin. The corresponding values determined in normal aqueous solution was 6.2 for alizarin and 5.57 for purpurin.

Table 1 provides overall binding constant values of alizarin and purpurin determined at different pH at a constant ionic strength (with respect to 120 mM NaCl) of the medium. Considering overall binding constant values for the two compounds at different pH and using Eqs. (4) and (5), contributions of neutral ( $K^0$ ) and anionic ( $K^-$ ) forms of each compound to the overall binding constant with calf thymus DNA was evaluated.

$$K^*(1 + 10^{\text{pH}-\text{pK}}) = K^0 + K^- \times 10^{\text{pH}-\text{pK}} \quad (4)$$

$$\text{or } K^* = (K^0 + K^- \times 10^{\text{pH}-\text{pK}})/(1 + 10^{\text{pH}-\text{pK}}) \quad (5)$$

In Eqs. (4) & (5),  $K^*$  is the overall binding constant (determined experimentally) for the interaction of either alizarin or purpurin with calf thymus DNA.  $K^*$  is equal to  $\frac{[C_b]}{[C_f][\text{DNA}]}$ .  $K^*$  values of purpurin were taken from an earlier study [21] while that of alizarin was determined as a part of this study [Fig. 2S–Fig. 6S].  $K^0$  denotes the binding constant of the neutral form [ $K^0 = \frac{[C_b^0]}{[C_f^0][\text{DNA}]}$ ] and  $K^-$  that of the anionic form [ $K^- = \frac{[C_b^-]}{[C_f^-][\text{DNA}]}$ ] [18,21]. The total concentration of each compound was considered as  $C_0$  where  $C_0 = C_b + C_f$ .  $C_b$  denotes bound form and  $C_f$ , the free form of the two compounds interacting with calf thymus DNA.

Therefore, at any pH of the medium, during titration with calf

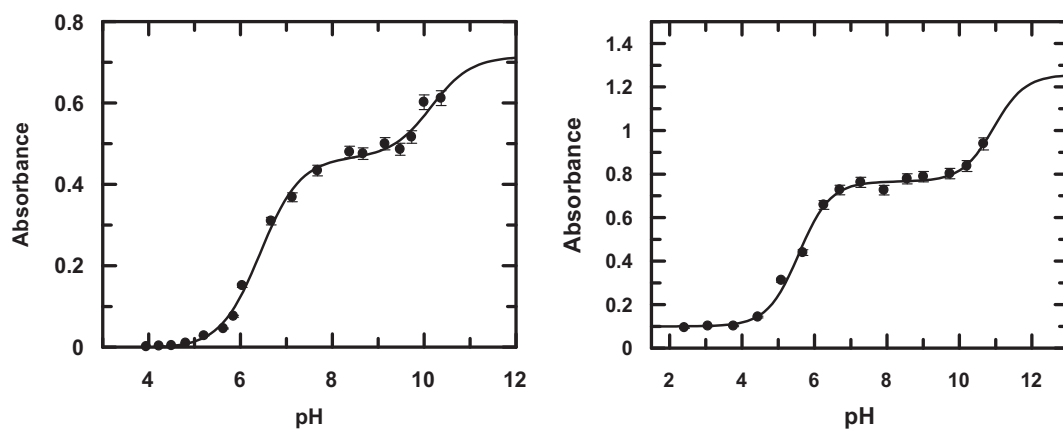


Fig. 1. pH-metric titration of alizarin as shown by a variation in absorbance at 525 nm in the presence of calf thymus DNA of concentrations (A) 62.7  $\mu\text{M}$  and (B) 221.97  $\mu\text{M}$ . [alizarin] = 100  $\mu\text{M}$ ; Temperature = 300 K.

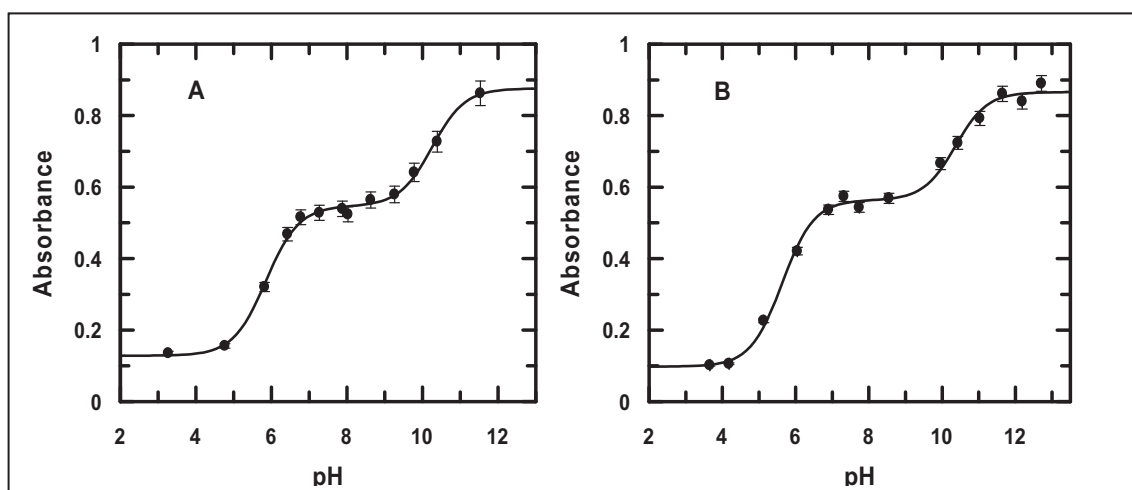


Fig. 2. pH-metric titration of purpurin as shown by a variation of absorbance at 513 nm in the presence of calf thymus DNA of concentrations (A) 66.88  $\mu\text{M}$  and (B) 173.28  $\mu\text{M}$ . [purpurin] = 100  $\mu\text{M}$ ; Temperature = 300 K.

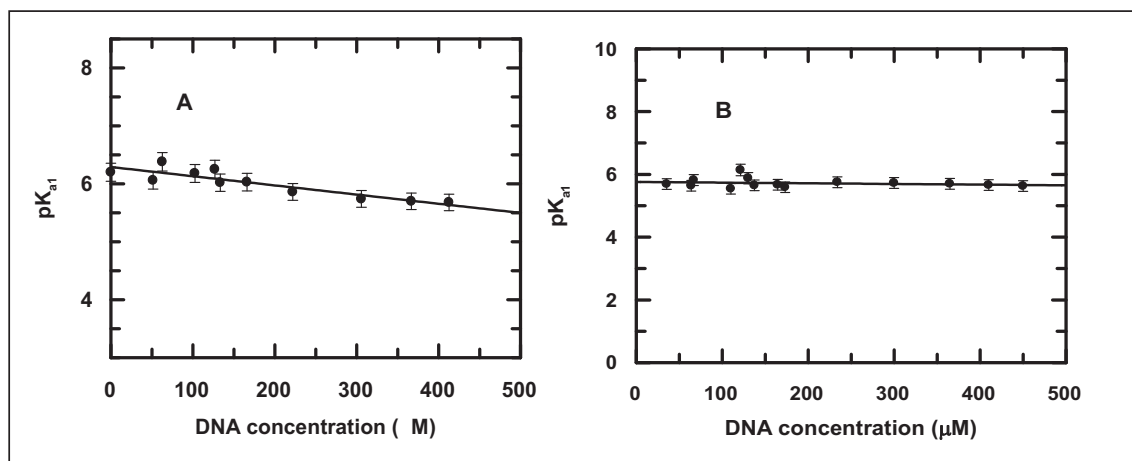


Fig. 3. A plot of  $\text{pK}_{a1}$  of (A) alizarin and (B) purpurin against increasing concentrations of calf thymus DNA. [Alizarin] = [Purpurin] = 100  $\mu\text{M}$ ; Temperature = 298 K.

thymus DNA both bound and free forms of the compounds would be present in solution. Of the bound form, a portion would bind to calf thymus DNA as neutral species while another portion would bind to it as anionic species. Similarly, the free form (not bound to DNA) would exist as neutral and anionic species. Hence, we may write

$$[\text{C}_b] = [\text{C}_b^0] + [\text{C}_b^-] \quad (6)$$

$$\text{and } [\text{C}_f] = [\text{C}_f^0] + [\text{C}_f^-] \quad (7)$$

A plot of  $K^*(1 + 10^{\text{pH}-\text{pK}})$  versus  $10^{\text{pH}-\text{pK}}$  (Eq. (4)) considering

**Table 1**

Overall binding constant values of alizarin and purpurin interacting with calf thymus DNA at different pH. Contributions of the neutral ( $K^0$ ) and anionic ( $K^-$ ) forms of each compound to their respective overall binding constants.

Compound	pH	Overall binding constant with calf thymus DNA ( $K^* \times 10^{-4}$ )	$pK_{a1}$ in the absence of DNA	$pK_{a1}$ in the presence of DNA	$K^0$ from Eq. (4) ( $K^0 \times 10^{-5}$ )	$K^0$ from Eq. (5) ( $K^0 \times 10^{-5}$ )	$K^-$ from Eq. (4) ( $K^- \times 10^{-4}$ )	$K^-$ from Eq. (5) ( $K^- \times 10^{-4}$ )
Alizarin	6.50	3.17	6.2		1.04	0.87	0.54	0.69
	6.70	2.80						
	7.02	1.91						
	7.40	1.04	5.94	1.68	1.31	0.56	0.75	
	7.65	1.05						
	7.97	0.67						
Purpurin	6.65	9.33	5.57		10.8	8.87	2.40	2.67
	6.88	6.45						
	7.16	4.84						
	7.40	4.51	5.71	8.0	6.68	2.39	2.65	
	7.88	2.95						
	8.35	2.56						

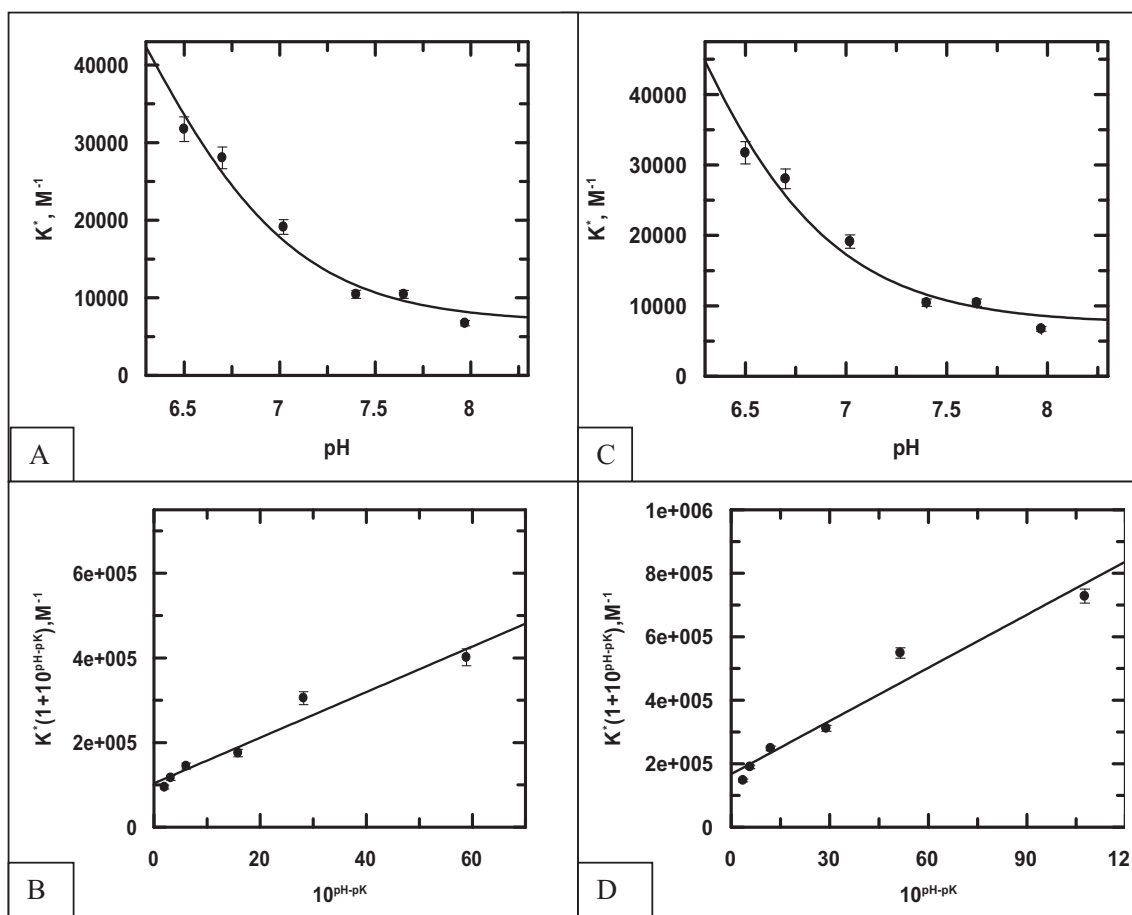


Fig. 4. (A) & (C) show overall binding constant ( $K^*$ ) for alizarin interacting with calf thymus DNA at different pH where the solid line is the fitted data obeying Eq. (5) considering  $pK_{a1} = 6.2$  (A) determined in normal aqueous solution in absence of DNA and  $pK_{a1} = 5.94$  (C) determined in presence of DNA. (B) and (D) are linear plots obtained by plotting  $K^*(1 + 10^{pH-pK})$  versus  $10^{pH-pK}$  where (B) uses  $pK_{a1}$  as 6.2 and (D) uses  $pK_{a1}$  as 5.94. They provide  $K^0$  and  $K^-$ , binding constants of neutral and anionic forms of alizarin from the intercept and slope respectively. [Alizarin] = 50  $\mu$ M; [NaCl] = 120 mM; [Tris buffer] = 30 mM; Temp. = 298 K.

different values of  $pK_{a1}$  for each compound (i.e. determined in the absence and presence of calf thymus DNA) generates a straight line (Fig. 4B & D, alizarin and Fig. 5B & D, purpurin) from where  $K^-$  was determined as the slope and  $K^0$  as the intercept (Table 1). Overall binding constant ( $K^*$ ) was also plotted against different pH for the two compounds. The data was fitted to Eq. (5) (Fig. 4A & C, alizarin and Fig. 5A & C, purpurin) and values for binding constants of the neutral and anionic species,  $K^0$  and  $K^-$  were evaluated. A comparison of the values obtained for  $K^0$  and  $K^-$  from Eqs. (4) & (5) for the two

compounds suggest they are close to each other. What was observed as a consequence of these calculations (Table 1) is that  $K^0$ , contribution of the neutral form to the overall binding constant ( $K^*$ ) showed a good variation corresponding to a change in  $pK_{a1}$  (i.e. determined in the absence and presence of DNA) while contribution of the anionic form ( $K^-$ ) remained practically the same.

In case of alizarin,  $K^0$  was slightly higher when  $pK_{a1}$  was considered to be 5.94 (determined in presence of DNA) than when it was 6.2 (determined in normal aqueous solution). In case of purpurin however,

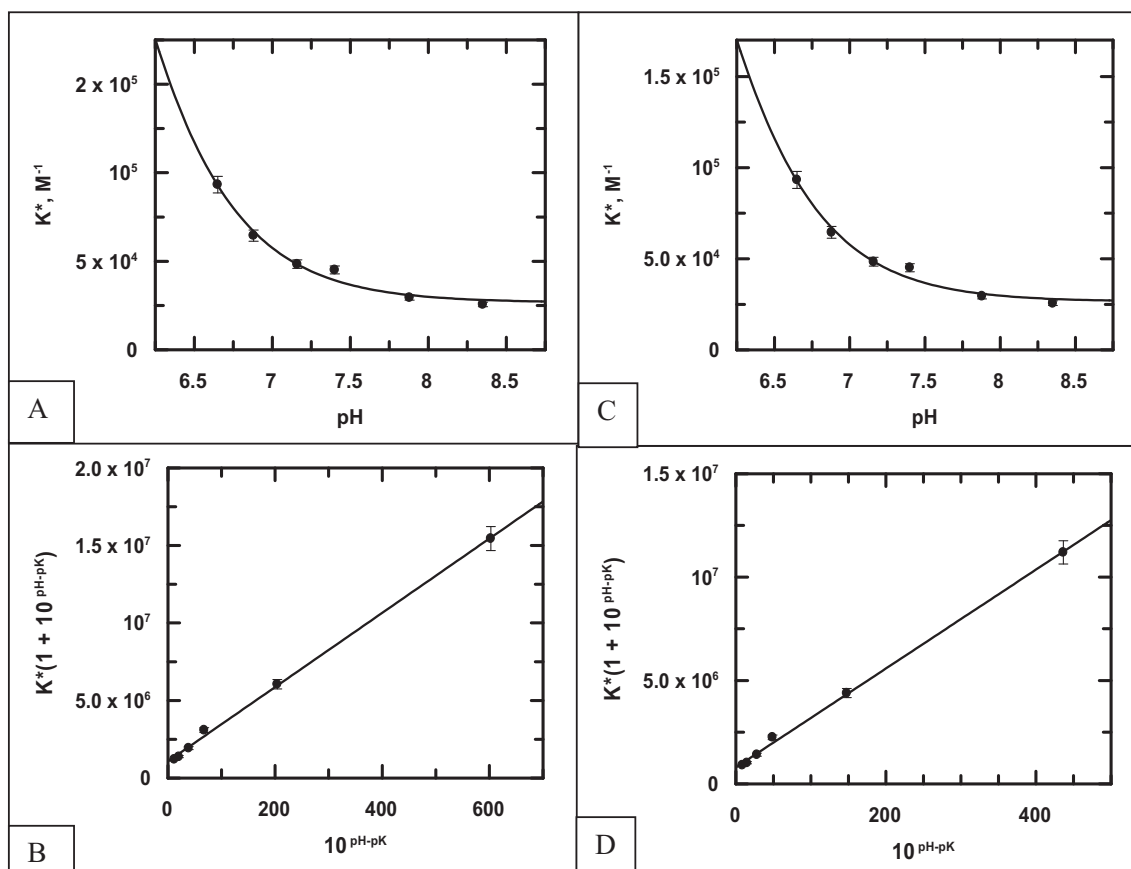


Fig. 5. (A) & (C) show overall binding constant ( $K^*$ ) for purpurin interacting with calf thymus DNA at different pH where the solid line is the fitted data obeying Eq. (5) considering  $pK_{a1} = 5.57$  (A) determined in normal aqueous solution in absence of DNA and  $pK_{a1} = 5.71$  (C) determined in presence of DNA. (B) and (D) are linear plots obtained by plotting  $K^*(1 + 10^{pH-pK_a})$  versus  $10^{pH-pK_a}$  where (B) uses  $pK_{a1}$  as 5.57 and (D) uses  $pK_{a1}$  as 5.71. They provide  $K^0$  and  $K^-$ , binding constants of the neutral and anionic forms of purpurin from the intercept and slope respectively. [Purpurin] = 75  $\mu M$ ; [NaCl] = 120 mM; [Tris buffer] = 30 mM; Temp. = 298 K.

$K^0$  was higher when  $pK_{a1}$  was 5.57 (determined in normal aqueous solution) than when it was 5.71 (determined in presence of DNA). It appears therefore that for alizarin contribution coming from the neutral form was greater when  $pK_{a1}$  used was determined in the presence of DNA while it was the reverse for purpurin; the value of  $K^-$  remained more or less the same, i.e. not showing much variation corresponding to a change in  $pK_{a1}$ .

Results clearly indicate that for both alizarin and purpurin, dissociation of phenolic  $-OH$  is influenced by the nucleic acid bases present in DNA. Therefore, such molecules that exist in two distinctly different forms at physiological pH, to correctly determine their contributions to the overall binding constant ( $K^*$ ) with DNA, it is essential that correct values of  $pK_a$  are used. A direct benefit of the study is that from a knowledge of  $K^0$  and  $K^-$  it would be possible to evaluate the overall binding constant of a molecule interacting with DNA at any pH without having to perform the experiment at that pH.

#### 4. Conclusion

The study helps us to realize that a proper determination of  $pK_a$  is essential for use in physicochemical experiments for determination of biophysical parameters. This was understood through this study using two hydroxy-9,10-anthraquinones, alizarin and purpurin. Evaluation of the contributions of the neutral and anionic forms of the molecules with the help of suitable equations, where  $pK_{a1}$  of the compounds have a decisive role, reveal contributions of different forms to the overall binding constants are actually different when the  $pK_a$  are different.

Therefore, if appropriate values of  $pK_a$  are not used, like that realized from this study, there is every possibility of either over emphasizing or under emphasizing the contribution of a certain form. The study emphasizes on the fact that there is a need to realize that most molecules interacting with DNA have more than one form in solution and that it must be considered for a correct analysis of any DNA interaction. This is also the reason why overall binding constants of a molecule change with a change in experimental (environmental) conditions having very high physiological significance. The study further revealed binding of purpurin to calf thymus DNA was higher than alizarin when the only difference between the two is an  $-OH$  group.

#### Acknowledgements

SD gratefully acknowledges financial support received from Department of Science & Technology, Govt. of West Bengal, India for the research project [794(Sanc.)1(10) ST/P/S&T/9G-23/2013]. MS expresses her gratitude to UGC, New Delhi for a Rajiv Gandhi National Fellowship. PN wish to thank the Department of Science & Technology, New Delhi for a DST-INSPIRE fellowship. SD is grateful to UGC, New Delhi for funds received as part of the research program on "Advanced Materials", as part of UPE II, under operation at Jadavpur University. He is grateful to DST-PURSE and UGC-CAS programs of the Government of India, operating at the Department of Chemistry, Jadavpur University for financial support. It needs mentioning here that the work was performed following a question by Dr. Sukanya Chakrabarti made at a seminar SD delivered at the Lady Brabourne College, Kolkata,

sometime in 2016, where he was asked whether it was correct to use  $pK_a$  values determined under normal conditions in aqueous solution for use in DNA binding analysis for evaluation of contribution of different forms of a compound binding to DNA. SD acknowledges the question once again.

## Appendix A. Supplementary data

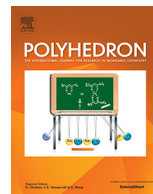
Supplementary data to this article can be found online at <https://doi.org/10.1016/j.bpc.2018.02.001>.

## References

- [1] G.Y. Park, J.J. Wilson, Y. Song, S.J. Lippard, Phenanthriplatin, a monofunctional DNA-binding platinum anticancer drug candidate with unusual potency and cellular activity profile, *PNAS* 109 (2012) 11987–11992.
- [2] K. Cheung-Ong, G. Giaever, C. Nislow, DNA-damaging agents in cancer chemotherapy: serendipity and chemical biology, *Chem. Biol.* 20 (2013) 648–659.
- [3] S.S. David, E. Meggers, Inorganic chemical biology: from small metal complexes in biological systems to metalloproteins, *Curr. Opin. Chem. Biol.* 12 (2008) 194–196.
- [4] A. Abibi, E. Protozanova, V.V. Demidov, M.D. Frank-Kamenetskii, Specific versus nonspecific binding of cationic PNAs to duplex DNA, *Biophys. J.* 86 (2004) 3070–3078.
- [5] L.J. Boerner, J.M. Zaleski, Metal complex-DNA interactions: from transcription inhibition to photoactivated cleavage, *Curr. Opin. Chem. Biol.* 9 (2005) 135–144.
- [6] T. Fessl, F. Adamec, T. Polívka, S. Foldynová-Trantírková, F. Vácha, L. Trantírek, Towards characterization of DNA structure under physiological conditions in vivo at the single-molecule level using single-pair FRET, *Nucleic Acids Res.* 40 (2012) e121.
- [7] K.R. Fox, M.J. Waring, Investigations into the sequence-selective binding of mitramycin and related ligands to DNA, *Eur. J. Biochem.* 145 (1984) 579–586.
- [8] R.L. Jones, W.D. Wilson, Effect of ionic strength on the  $pK_a$  of ligands bound to DNA, *Biopolymers* 20 (1981) 141–154.
- [9] F. Barragán, P. López-Senín, L. Salassa, S. Betanzos-Lara, A. Habtemariam, V. Moreno, P.J. Sadler, V. Marchán, Photocontrolled DNA binding of a receptor-targeted organometallic ruthenium(II) complex, *J. Am. Chem. Soc.* 133 (2011) 14098–14108.
- [10] A. Paul, S. Bhattacharya, Chemistry and biology of DNA-binding small molecules, *Curr. Sci.* 102 (2012) 212–231.
- [11] R.E. Dickerson, H.R. Drew, B.N. Conner, M. Wing, A.V. Fratini, M.L. Kopka, The anatomy of A-, B-, and Z-DNA, *Science* 216 (1982) 475–485.
- [12] C.D. Mol, T. Izumi, S. Mitra, J.A. Tainer, DNA-bound structures and mutants reveal abasic DNA binding by APE1 DNA repair and coordination, *Nature* 403 (2000) 451–456.
- [13] A.D. Miroshnikova, A.A. Kuznetsova, N.A. Kuznetsov, O.S. Fedorova, Thermodynamics of damaged DNA binding and catalysis by human AP endonuclease 1, *Acta Nat.* 8 (2016) 103–110.
- [14] W. Engelen, B.M.G. Janssen, M. Merkkx, DNA-based control of protein activity, *Chem. Commun.* 52 (2016) 3598–3610.
- [15] M. Egli, DNA-cation interactions: quo vadis? *Chem. Biol.* 9 (2002) 277–286.
- [16] B.J. Pages, D.L. Ang, E.P. Wright, J.R. Aldrich-Wright, Metal complex interactions with DNA, *Dalton Trans.* 44 (2015) 3505–3526.
- [17] F. Frezard, A. Garnier-Suillerot, Comparison of the binding of anthracycline derivatives to purified DNA and to cell nuclei, *Biochim. Biophys. Acta* 1036 (1990) 121–127.
- [18] R. Comanici, B. Gabel, T. Gustavsson, D. Markovitsi, C. Cornaggia, S. Pommeret, C. Rusu, C. Kryschi, Femtosecond spectroscopic study of carminic acid–DNA interactions, *Chem. Phys.* 325 (2006) 509–518.
- [19] S. Mukherjee, P. Das, S. Das, Exploration of small hydroxy-9,10-anthraquinones as anthracycline analogues: physicochemical characteristics and DNA binding for comparison, *J. Phys. Org. Chem.* 25 (2012) 385–393.
- [20] P. Das, C.K. Jain, S.K. Dey, R. Saha, A.D. Chowdhury, S. Roychoudhury, S. Kumar, H.K. Majumder, S. Das, Synthesis, crystal structure, DNA interaction and in vitro anticancer activity of a Cu(II) complex of purpurin: dual poison for human DNA topoisomerase I and II, *RSC Adv.* 4 (2014) 59344–59357.
- [21] S. Mukherjee, P.K. Gopal, S. Paul, S. Das, Acetylation of 1,2,5,8-tetrahydroxy-9,10-anthraquinone improves binding to DNA and shows enhanced superoxide formation that explains better cytotoxicity on JURKAT T lymphocyte cells, *J. Anal. Oncol.* 3 (2014) 122–129.
- [22] P. Das, C.K. Jain, S. Roychoudhury, H.K. Majumder, S. Das, Design, synthesis and in vitro anticancer activity of a Cu(II) complex of carminic acid: a novel small molecule inhibitor of human DNA topoisomerase I and topoisomerase II, *ChemistrySelect* 1 (2016) 6623–6631.
- [23] B. Mandal, S. Singha, S.K. Dey, S. Mazumdar, T.K. Mondal, P. Karmakar, S. Kumar, S. Das, Synthesis, crystal structure from PXRD of a  $Mn^{II}$ (purp)<sub>2</sub> complex, interaction with DNA at different temperatures and pH and lack of stimulated ROS formation by the complex, *RSC Adv.* 6 (2016) 51520–51532.
- [24] B. Mandal, S. Singha, S.K. Dey, S. Mazumdar, S. Kumar, P. Karmakar, S. Das, Cu<sup>II</sup> complex of emodin with improved anticancer activity as demonstrated by its performance on HeLa and Hep G2 cells, *RSC Adv.* 7 (2017) 41403–41418.
- [25] A.B. Pradhan, L. Haque, S. Bhuiya, A. Ganguly, S. Das, Deciphering the positional influence of the hydroxyl group in the cinnamoyl part of 3-hydroxy flavonoids for structural modification and their interaction with the protonated and B form of calf thymus DNA using spectroscopic and molecular modeling studies, *J. Phys. Chem. B* 119 (2015) 6916–6929.
- [26] J. Markovits, C. Garbay-Jaureguiberry, B.P. Roques, J.B. Le Pecq, Acridine dimers: influence of the intercalating ring and of the linking-chain nature on the equilibrium and kinetic DNA-binding parameters, *Eur. J. Biochem.* 180 (1989) 359–366.
- [27] L. Di, E.H. Kerns, Application of pharmaceutical profiling assays for optimization of drug-like properties, *Curr. Opin. Discov. Devel.* 8 (2005) 495–504.
- [28] L. Di, E.H. Kerns, Profiling drug-like properties in discovery research, *Curr. Opin. Chem. Biol.* 7 (2003) 402–408.
- [29] S. Das, A. Saha, P.C. Mandal, Studies on the formation of Cu(II) and Ni(II) complexes of 1, 2-dihydroxy-9,10-anthraquinone and lack of stimulated superoxide formation by the complexes, *Talanta* 43 (1996) 95–102.
- [30] I.T. Suydam, S.D. Levandoski, S.A. Strobel, Catalytic importance of a protonated adenosine in the hairpin ribozyme active site, *Biochemistry* 49 (2010) 3723–3732.
- [31] S. Das, G.S. Kumar, M. Maiti, Conversions of the left-handed form and the protonated form of DNA back to the bound right-handed form by sanguinarine and ethidium: a comparative study, *Biophys. Chem.* 76 (1999) 199–218.
- [32] P. Das, D. Bhattacharya, P. Karmakar, S. Das, Influence of ionic strength on the interaction of THA and its Cu(II) complex with DNA helps to explain studies on various breast cancer cells, *RSC Adv.* 5 (2015) 73099–73111.
- [33] G. Dodin, M.-A. Schwaller, J. Aubard, C. Paoletti, Binding of ellipticine base and ellipticinium cation to calf-thymus DNA, *Eur. J. Biochem.* 176 (1988) 371–376.
- [34] P.S. Guin, S. Das, P.C. Mandal, Studies on the formation of a complex of Cu(II) with sodium 1,4-dihydroxy-9,10-anthraquinone-2-sulphonate – an analogue of the core unit of anthracycline anticancer drugs and its interaction with calf thymus DNA, *J. Inorg. Biochem.* 103 (2009) 1702–1710.
- [35] P. Das, P.S. Guin, P.C. Mandal, M. Paul, S. Paul, S. Das, Cyclic voltammetric studies of 1, 2, 4-trihydroxy-9,10-anthraquinone, its interaction with calf thymus DNA and anti-leukemic activity on MOLT-4 cell lines: a comparison with anthracycline anticancer drugs, *J. Phys. Org. Chem.* 24 (2011) 774–785.







# Characterization of a Mn<sup>II</sup> complex of Alizarin suggests attributes explaining a superior anticancer activity: A comparison with anthracycline drugs



Mouli Saha<sup>a</sup>, Soumen Singha<sup>b</sup>, Mousumi Chakraborty<sup>a</sup>, Swagata Mazumdar<sup>c</sup>, Sanjay Kumar<sup>b</sup>, Parimal Karmakar<sup>c</sup>, Saurabh Das<sup>a,\*</sup>

<sup>a</sup> Department of Chemistry (Inorganic Section), Jadavpur University, Kolkata 700032, India

<sup>b</sup> Department of Physics, Jadavpur University, Kolkata 700032, India

<sup>c</sup> Department of Life Science & Biotechnology, Jadavpur University, Kolkata 700032, India

## ARTICLE INFO

### Article history:

Received 12 June 2019

Accepted 7 August 2019

Available online 13 August 2019

### Keywords:

Alizarin

Mn<sup>II</sup>(QH)<sub>2</sub>

Semiquinone

HeLa

HepG2

## ABSTRACT

Alizarin (DHA), a simple analogue of the anthracycline core was used to form a complex with Mn<sup>II</sup> to see if the complex matches the efficacy of anthracyclines. It was characterized by spectroscopic techniques, mass spectrometry and TGA. In the absence of a single crystal, the structure was obtained by computational techniques. Interaction of the complex with DNA at different ionic strength and pH was compared with anthracyclines to see if it addresses some of the shortcomings of hydroxy-9,10-anthraquinones in general and DHA in particular when compared to anthracyclines. Increased affinity of the complex towards DNA and that its binding constant values do not decrease with increase in pH or decrease in ionic strength of the medium are positive attributes of complex formation. This is significant since cancer patients often experience fluctuation of pH and ionic strength in body fluids during treatment that affect efficacy of drugs. The complex decreases the flow of electrons from NADH to molecular oxygen owing to decreased semiquinone formation; a fact important for controlling cardiotoxicity. Experiments on ROS depletion in HeLa, Hep G2 and WI 38 lung fibroblast cells by the H<sub>2</sub>DCFDA assay suggests a shift in mechanism for the complex from that of DHA. Loss in efficacy due to decrease in semiquinone formation by the complex is made up by other attributes of complex formation that eventually promote cytotoxicity. Compounds were tried on HeLa, Hep G2 and WI 38 lung fibroblast cells. An effort was made to correlate aspects of semiquinone formation, ROS generation and interaction with DNA with results obtained on two cancer cell lines and a normal cell line.

© 2019 Elsevier Ltd. All rights reserved.

## 1. Introduction

Hydroxy-9,10-anthraquinones, simpler analogues of anthracycline anticancer agents are at a disadvantage on a number of counts regarding efficacy when compared with anthracyclines [1–8]. Complex formation of anthracyclines or hydroxy-9,10-anthraquinones has several advantages [9–13]. By decreasing semiquinone formation, complexes are expected to decrease cardiotoxic side effects owing to less superoxide formation [9–15]. There is however a simultaneous decrease in efficacy in the free radical pathway which is a matter of concern [1,5,8]. However,

an interesting aspect is that in spite of a decrease in efficacy in the free radical pathway, overall performance of complexes in most cases is usually better than anthracyclines or hydroxy-9,10-anthraquinones. This is due to certain attributes of complex formation [1,5–8]. In fact the mechanism of anticancer activity due to anthracyclines or hydroxy-9,10-anthraquinones and their metal complexes is often different, that is, pathways responsible for cell damage differ considerably [1,5–10,16–21]. Although, the complete mechanism for anthracycline functioning is still under investigation, several aspects are known [1–10,14,15,20,21]. However, the fact that a metal complex is most often better than a parent molecule does not guarantee all complexes would be effective; a lot depends on the metal ion involved [1,3–8]. Hence, to realize the involvement of a metal ion, Mn<sup>II</sup> was chosen on the one hand for its bio-friendly nature and on the other because it lacks a stable

Abbreviations: DHA, Alizarin.

\* Corresponding author.

E-mail address: [sdas@chemistry.jdvu.ac.in](mailto:sdas@chemistry.jdvu.ac.in) (S. Das).

lower oxidation state unlike  $\text{Cu}^{\text{II}}$  or  $\text{Fe}^{\text{III}}$  [22–29]. Therefore, it is expected that findings with a  $\text{Mn}^{\text{II}}$  complex of a hydroxy-9,10-anthraquinone could be different from  $\text{Cu}^{\text{II}}$  or  $\text{Fe}^{\text{III}}$  complexes of similar ligands [1,3,5–8,16–19]. Keeping this in mind, a  $\text{Mn}^{\text{II}}$  complex of 1,2-dihydroxy-9,10-anthraquinone (DHA) was prepared and characterized.

Some of the major pathways by which anthracyclines or hydroxy-9,10-anthraquinones inflict damage on cells are by generation of a semiquinone radical anion/quinone-dianion, or through biophysical interaction with DNA where owing to a planar structure they are able to easily intercalate and modify DNA, or through inhibition of topoisomerase that affect processes like DNA replication [1–8,14,15,20,21,30–36,37]. Some molecules can even recognize specific regions of DNA, showing selectivity, specificity, interrupting the biochemistry of the cell at elementary levels of DNA replication and transcription [38,39]. Some of these pathways were investigated separately for DHA and its  $\text{Mn}^{\text{II}}$  complex to identify areas of resemblance or difference with established anthracyclines like doxorubicin, daunorubicin, epirubicin in order to realize modifications that might be required to bridge the gap in biological activity between some of the simpler analogues and anthracyclines already in use [1–8,12,16,30–36,37]. DHA and the complex were studied on two cancer cell lines for a comparison with anthracyclines and their complexes. If modification of simple analogues are able to take efficacy close to that of established anthracyclines, then issues like making available an “anthracycline-like” drug at a competitive price, the biological advantages of using a simple molecule, assistance in drug targeting and bio-availability following complex formation, aspects pertaining to drug resistance could be addressed [40,41].

## 2. Experimental

### 2.1. Materials

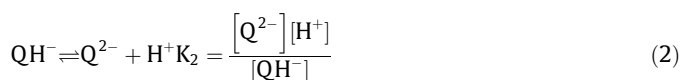
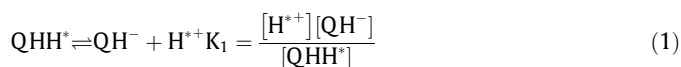
Alizarin (>90% pure) was purchased from TCI, Japan and purified by re-crystallization from ethanol-water mixtures. The compound being photosensitive was stored in the dark. Solutions were prepared in ethanol ( $\sim 10^{-4}$  M) and stored with care. Phosphate buffer was prepared using  $\text{NaH}_2\text{PO}_4$  and  $\text{Na}_2\text{HPO}_4$  using triple distilled water.  $\text{NaNO}_3$  (AR) and  $\text{NaCl}$  (AR) were used to maintain the ionic strength of the medium. Calf thymus DNA, purchased from Sisco Research Laboratories, India was dissolved in triple distilled water containing 120 mM  $\text{NaCl}$ , 35 mM  $\text{KCl}$  and 5 mM  $\text{CaCl}_2$ . Absorbance

was recorded at 260 and 280 nm respectively;  $A_{260}/A_{280}$  was noted. The ratio found between 1.8 and 1.9 suggests the DNA to be sufficiently free of protein. DNA was also characterized by measuring its CD spectrum at 260 nm with the help of a CD spectropolarimeter (J815, JASCO). Concentration was determined in terms of nucleotide considering molar extinction coefficient at 260 nm to be  $6600 \text{ M}^{-1} \text{ cm}^{-1}$ .

### 2.2. Methods

#### 2.2.1. $pK_a$ of DHA at different ionic strengths of the medium

Proton dissociation constants for DHA were determined at different ionic strengths with the help of pH-metric titrations. A pH meter, Equip-Tronics EQ-610 (India) was used. Absorbance at 530 nm was plotted against pH at different ionic strengths. DHA exists in two distinctly different forms,  $\text{QHH}^*$  and  $\text{QH}^-$  respectively depending on pH and ionic strength;  $\text{H}^*$  represents the hydrogen on OH at  $\text{C}_2$  while H denotes the hydrogen on OH at  $\text{C}_1$  [11,42].



Absorbance at 530 nm was fitted to Eq. (3) yielding  $pK_{a1}$  and  $pK_{a2}$  respectively [1,5,8,11,12,42].

$$A_{\text{obs}} = \frac{A_1}{(1 + 10^{\text{pH}-pK_{a1}} + 10^{\text{pH}-pK_{a2}})} + \frac{A_2}{(1 + 10^{pK_{a1}-\text{pH}} + 10^{\text{pH}-pK_{a2}})} + \frac{A_3}{(1 + 10^{pK_{a1}-\text{pH}} + 10^{pK_{a2}-\text{pH}})} \quad (3)$$

$A_1$ ,  $A_2$  and  $A_3$  are absorbances due to  $\text{QHH}^*$ ,  $\text{QH}^-$ ,  $\text{Q}^{2-}$  respectively while  $pK_{a1}$ ,  $pK_{a2}$  are the  $pK_a$  values for the dissociation of the two protons (Eqs. (1) and (2)) [11,42].

#### 2.2.2. Determination of stoichiometry of interaction between $\text{Mn}^{\text{II}}$ and DHA by mole ratio and Job's method of continuous variation

Complex composition in solution was determined by mixing different volumes of equimolar  $\text{Mn}^{\text{II}}$  and DHA. In the mole ratio

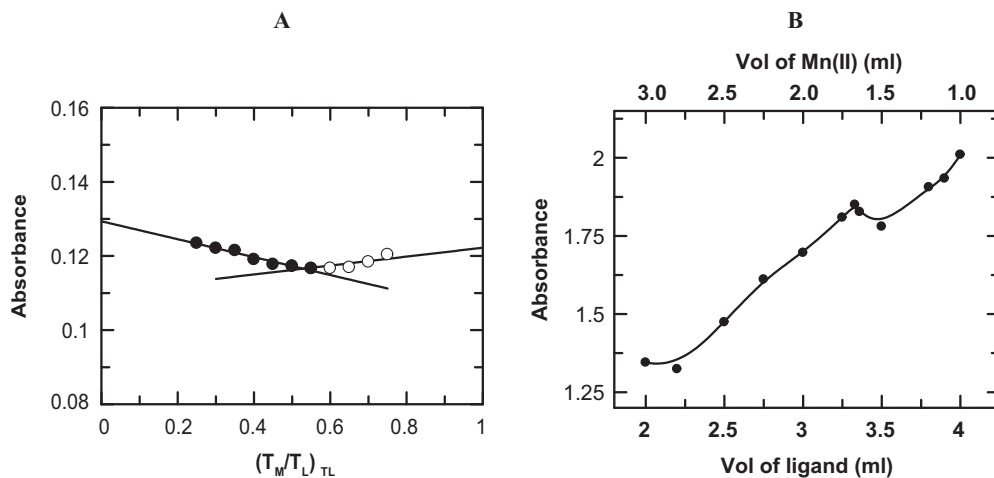


**Fig. 1.** Plots showing variation in absorbance at 525 nm for (A) a change in the ratio of [DHA] to  $[\text{Mn}^{\text{II}}]$  for a fixed concentration of DHA (=20  $\mu\text{M}$ ) and (B) a continuous variation of [DHA] and  $[\text{Mn}^{\text{II}}]$  at physiological pH ( $\sim 7.4$ ). In case of (B), the strength of the stock solutions of  $\text{Mn}^{\text{II}}$  and DHA were 1000  $\mu\text{M}$ ;  $[\text{NaNO}_3] = 0.01 \text{ M}$ , Temperature = 298 K.

method, DHA was kept constant while  $Mn^{II}$  was varied. Absorbance at 525 nm was plotted against  $(T_M/T_L)_{TL}$  (Fig. 1A);  $T_M$  and  $T_L$  being concentrations of  $Mn^{II}$  and DHA respectively. Two lines were obtained, the intersection of which indicates the ratio in which DHA binds to  $Mn^{II}$  in the complex. In Job's method of continuous variation (Fig. 1B), complementary mixtures were prepared. Absorbance was recorded at 525 nm. This was plotted against either volume of DHA or  $Mn^{II}$ . Stoichiometry of  $Mn^{II}$  to DHA was 1:2.

### 2.2.3. Proton dissociation on DHA in presence of $Mn^{II}$

DHA and  $Mn^{II}$  were mixed in the ratio determined in Section 2.2.2. A spectrophotometric titration was performed in the pH range 3.0–11.0 (Fig. S1, SI). The peak at 430 nm over the pH range 3.45–6.04 got shifted slightly to the right as pH increased to ~6.84 showing an absorbance at 475 nm. A weak shoulder (not a peak) was seen which upon further increase in pH (~7.33) developed into a peak at 530 nm that kept increasing in intensity as pH was increased. The change suggests formation of a new species which was followed at 534 nm (Fig. 2).

Using Eq. (3),  $pK_{a1}$  and  $pK_{a2}$  of DHA in the presence of  $Mn^{II}$  were  $6.93 \pm 0.04$  and  $9.99 \pm 0.27$  respectively. Stability constants  $\beta^*$  and  $\beta$  were determined using Eqs. S1–S5, SI where  $QH^*$  represents DHA [11,12,42].  $\beta$  was found to be  $2.5 \times 10^{14}$  ( $\log \beta = 14.4$ ).

To be able to explain physico-chemical experiments precisely, hydrogens on the two OH groups ( $C_1$  and  $C_2$  of DHA) were represented as H and  $H^*$  respectively. This was necessary since the trends in dissociation of OH groups in the absence and presence of metal ions are different [11]. However, with that now explained, for the rest of the manuscript, the complex is referred to as  $Mn^{II}(QH)_2$  instead of  $Mn^{II}(QH^*)_2$  i.e. not considering hydrogens on the two -OH groups different anymore.

### 2.2.4. Preparation of $Mn^{II}(QH)_2$

0.5 mmole  $MnCl_2 \cdot 4H_2O$  was dissolved in a minimum volume of water. This was gradually added to a solution containing 1 mmole DHA in 100 mL methanol. pH was adjusted to a value between 6.5 and 7.0. The mixture was warmed under reflux for approximately four hours. A violet coloured compound was recovered after proper work up. Anal. Calc.: (%) for  $C_{28}H_{14}O_8Mn \cdot 2H_2O$ : C, 59.05; H, 3.16. Found: C, 59.12; H, 3.05. Molecular ion peak  $(m/z)_{calculated} = 569.42$ ;  $(m/z)_{observed} = 569.86$ ;  $\lambda_{max} = 521$  nm in DMSO.

### 2.2.5. Computation for structure determination

Theoretical calculations were performed using the Gaussian 09W software [43] employing B3LYP [44]. Spin states of complexes were treated using the unrestricted formalism ("broken symme-

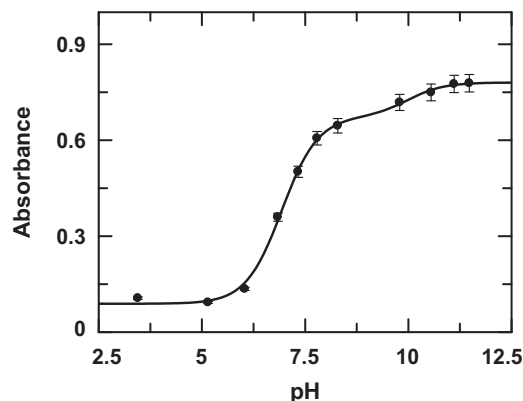


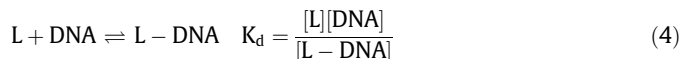
Fig. 2. Spectrophotometric titration of DHA in the presence of  $Mn^{II}$  shown by a variation in absorbance at 534 nm;  $[DHA] = 200 \mu M$ ,  $[Mn^{II}] = 100 \mu M$ ,  $[NaNO_3] = 0.01$  M,  $T = 301$  K.

try" treatment). For C, H and O atoms standard 6-31G basis set in conjunction with SDD effective core potential for the Mn atom was adopted [45]. Ground state geometries were fully optimized in gaseous and solution phase (solvent: DMSO). Stability of optimized structures was established by vibrational analysis.

In case of electronic spectra, for transition energies between initial and final states of the complex, single point calculations were done using time dependent density functional theory (TDDFT) [46] on the basis of the ground state geometry optimized in DMSO using the same function and basis set as simulated by conductor-like polarizable continuum model [47] using a non-equilibrium approach designed for the study of an absorption process. Orbital analysis was carried out with the help of Gauss View and MO composition using the Gauss Sum program [48]. Spin contamination usually arises while calculating with broken symmetry treatment in UDFT scheme for Mn. Such spin contamination was investigated as the difference between the expected value of  $S(S+1)$  for an assigned spin state and the actual value of  $\langle S^2 \rangle$  from DFT calculations.

### 2.2.6. Interaction of the complex with calf thymus DNA followed by UV-Vis spectroscopy

50  $\mu M$  DHA or  $Mn^{II}(QH)_2$  was titrated with calf thymus DNA at constant pH but at different ionic strengths of the medium. Titrations were also performed for  $Mn^{II}(QH)_2$  at different pH when ionic strength of the medium was kept constant. Interaction of the compounds with DNA resulted in a decrease in absorbance at the wavelengths at which titrations were followed. Interaction obeys Eq. (4).



L represents compounds,  $K_d$  is the dissociation constant for the interaction whose reciprocal provides apparent binding constant values ( $K_{app}$ ) [1,2,3,5–8,13]. Eq. (5) obtained from Eq. (4) plots reciprocal of the change in absorbance against reciprocal of  $(C_D - C_0)$ .  $C_D$  and  $C_0$  refer to concentration of calf thymus DNA and compound respectively. Using Eq. (5)  $\Delta A_{max}$  and  $K_{app}$  ( $1/K_d$ ) were evaluated from intercept and slope respectively.

$$\frac{1}{\Delta A} = \frac{1}{\Delta A_{max}} + \frac{K_d}{\Delta A_{max}(C_D - C_0)} \quad (5)$$

$\Delta A$  represents the change in absorbance of compounds for each titration while  $\Delta A_{max}$  indicates the maximum change possible in absorbance.

$$K_d = \frac{[C_0 - (\frac{\Delta A}{\Delta A_{max}})C_0][C_D - (\frac{\Delta A}{\Delta A_{max}})C_0]}{(\frac{\Delta A}{\Delta A_{max}})C_0} \quad (6)$$

$$C_0 \left( \frac{\Delta A}{\Delta A_{max}} \right)^2 - (C_0 + C_D + K_d) \left( \frac{\Delta A}{\Delta A_{max}} \right) + C_D = 0 \quad (7)$$

$\Delta A/\Delta A_{max}$  was plotted against  $C_D$ . Eq. (7) fits the data to a non-linear square fit analysis providing new values for apparent binding constant [1,2,5,8]. Titrations were also analyzed by a modified Scatchard equation [Eq. (8)] [49]. Overall binding constant ( $K'$ ) and site size ( $n$ ) were determined.

$$\frac{r}{C_f} = K'(n - r) \quad (8)$$

$r$  denotes ratio of the concentration of a compound bound to DNA to total concentration of DNA present in the reaction mixture at any point during the titration ( $C_b/C_D$ );  $C_b$  is the concentration of bound compound and  $C_f$  the free compound. "n" provides binding stoichiometry in terms of bound compound per nucleotide while

" $n_b$ " reciprocal of " $n$ " denotes binding site size in terms of number of nucleotides bound to a compound. " $n_b$ " was obtained by plotting  $\Delta A/\Delta A_{max}$  against  $C_D/[compound]$  [1,2,5,8].  $K'$  can also be obtained by multiplying  $K_{app}$  with " $n_b$ " and compared with values obtained from the modified Scatchard equation (Table 1).

### 2.2.7. ROS estimation

**2.2.7.1. Making use of NADH-NADH dehydrogenase assay.** An assay was performed at 298 K with cytochrome c as electron acceptor [50]. DHA and  $Mn^{II}(QH)_2$  were both tried in NADH-cytochrome c reductase activity assay where reduction of cytochrome c at 550 nm was followed at pH 7.4 (100 mM Tris buffer) [5–8,11,50]. Each test solution had 80  $\mu M$  cytochrome c, 160  $\mu M$  NADH and 5  $U l^{-1}$  NADH dehydrogenase and compounds. Compound concentration was varied from 0 to 60.0  $\mu M$ . Activity of NADH dehydrogenase is expressed in units where one unit of activity reduces 1.0  $\mu mole$  oxidized cytochrome c per minute at pH 7.4 and 300 K. Formation of superoxide radical anion catalyzed by DHA and  $Mn^{II}(QH)_2$  was measured from the reduction of cytochrome c inhibited by SOD in presence of NADH and NADH dehydrogenase using the kinetics software of JASCO V-630 spectrophotometer, Japan [5–8,11,50].

**2.2.7.2. Making use of the  $H_2DCFDA$  assay.** The cell permeant reagent 2,7-dichlorofluorescein diacetate ( $H_2DCFDA$ ) is a fluorogenic dye that measures the presence of reactive oxygen species (ROS) inside a cell [51–54]. Once inside the cell,  $H_2DCFDA$  is de-acetylated by cellular esterases to a non-fluorescent compound to be subsequently oxidized if ROS is present to 2/7-dichlorofluorescein (DCF) [51,53]. DCF is also highly fluorescent. Excitation was done at 504 nm and emission measured at 529 nm using a fluorescence spectrophotometer (Hitachi, Japan). A stock solution of  $H_2DCFDA$  (10 mM) was prepared in methanol and further diluted with culture medium to a concentration of 100  $\mu M$ . Two carcinoma cell lines (HeLa and HepG2) and normal (WI-38 lung fibroblast) cells were treated with  $IC_{50}$  concentration of DHA and  $Mn^{II}(QH)_2$  (determined by the MTT assay) and allowed to stand for 30 min. ROS was induced by the free radical generator  $H_2O_2$  (70  $\mu M$ ) by incubating cells treated with compounds for a further 30 min. Cells were washed with ice cold Hanks balanced salt solution (HBSS) and incubated with 100  $\mu M$   $H_2DCFDA$  for 30 min at 37 °C. Cells were lysed with an alkaline solution and fluorescence was recorded. 10  $\mu M$  N-acetyl cysteine (NAC) was used as the control for the experiment.

### 2.2.8. Biological experiments

**2.2.8.1. Cell culture.** Human cervical carcinoma cells (HeLa), human hepatocellular carcinoma cells (Hep G2) and normal WI-38 lung fibroblast cells were cultured in DMEM medium (GIBCO, Invitro-

gen, Carlsbad, CA, US) supplemented with 10% fetal bovine serum (GIBCO), 100 IU/mL penicillin and 100  $\mu g/mL$  streptomycin at 37 °C in a humid atmosphere containing 5%  $CO_2$  (Heraeus, Thermo Scientific, MA, USA). Cell lines were procured from the National Centre for Cell Science in Pune, India. Cells were seeded in 96 well plates for 24 h prior to treatment with the compounds [54,55].

**2.2.8.2. Cell viability assay.** After 24 h, each cell line was treated with DHA and  $[Mn^{II}(QH)_2]$  that were earlier dissolved in DMSO. Concentration of DMSO was less than 0.5%. Cell viability was checked 48 h after treatment with 3-(4,5-dimethylthiazol-2-yl)-2,5-diphenyltetrazolium bromide (MTT) [7]. Briefly, cells were washed with  $1 \times$  PBS and treated with MTT for 4 h at 37 °C. Crystals were dissolved in DMSO and plates analyzed on Thermo MULTISKAN EX plate reader at 595 nm.

### 2.3. Instruments used

Absorption spectra were recorded on JASCO V-630 spectrophotometer. A digital pH meter (EQUIP-TRONICS, EQ-610) was used for pH measurement. FTIR of the complex was recorded on Perkin-Elmer RX-I spectrophotometer using KBr pellets while NIR spectrum of its solution in DMSO was recorded on Shimadzu 3600 UV-Vis-NIR spectrophotometer. Mass spectrum was recorded on Micromass Q-Tofmicro™, Waters Corporation. Elemental analysis was done on Perkin Elmer 2400 Series-II CHN analyzer. Magnetic susceptibility measurements of powdered samples at room temperature (298 K) were done by Gouy method on Magway MSB MK1, Sherwood Scientific Ltd.

## 3. Results and discussion

### 3.1. Determination of $pK_a$ of DHA at different ionic strengths of the medium

DHA was titrated in solution at different ionic strengths. Fig. 3A & B are plots showing variation in absorbance with pH at different ionic strengths (0.12 M and 0.15 M). Fitting the experimental data according to Eq. (3),  $pK_{a1}$  and  $pK_{a2}$  were obtained.

As ionic strength increased, both  $pK_{a1}$  and  $pK_{a2}$  increased, showing that increase in ionic strength of the medium affects dissociation of OH groups [3].  $pK_{a1}$  and  $pK_{a2}$  were separately plotted against the ionic strength of the medium (Fig. 4). For the same change in ionic strength, slope of the line obtained by plotting  $pK_{a1}$  was slightly steeper than  $pK_{a2}$ . Therefore, increase in ionic strength affects the first dissociation to a slightly greater extent than the second. From trends in  $pK_a$  values, it was realized that dissociation of phenolic-OH decreased which is significant since dissociation of the first proton of DHA generates anionic species at

**Table 1**  
Binding constant values obtained for the interaction of DHA and  $Mn^{II}(QH)_2$  with calf thymus DNA at varying ionic strengths of the medium.

Compound	[NaCl] in M	$K_{app}$			Site size	$K_{app} \times n_b = K^*$	$K^*$ from Scatchard	$n_b$ calculated from Scatchard $n_b = (n^{-1})$
		From double-reciprocal plot(a)	From non-linear plot (b)	Average = (a + b)/2				
DHA	0.12	$0.91 \times 10^3$	$0.69 \times 10^3$	$0.80 \times 10^3$	8	$0.64 \times 10^4$	$0.88 \times 10^4$	7
	0.18	$1.55 \times 10^3$	$1.15 \times 10^3$	$1.35 \times 10^3$	8	$1.01 \times 10^4$	$1.00 \times 10^4$	8
	0.24	$2.00 \times 10^3$	$1.37 \times 10^3$	$1.68 \times 10^3$	8	$1.34 \times 10^4$	$1.13 \times 10^4$	8
	0.30	$2.54 \times 10^3$	$2.58 \times 10^3$	$2.56 \times 10^3$	9	$2.30 \times 10^4$	$2.39 \times 10^4$	8
	0.36	$3.49 \times 10^3$	$3.09 \times 10^3$	$3.29 \times 10^3$	8	$2.63 \times 10^4$	$2.81 \times 10^4$	6
$Mn(LH)_2$	0.12	$0.87 \times 10^4$	$1.5 \times 10^4$	$1.19 \times 10^4$	16	$1.90 \times 10^5$	$1.38 \times 10^5$	10
	0.18	$1.67 \times 10^4$	$4.1 \times 10^4$	$2.89 \times 10^4$	16	$4.62 \times 10^5$	$4.86 \times 10^5$	12
	0.30	$1.11 \times 10^4$	$1.8 \times 10^4$	$1.46 \times 10^4$	14	$2.04 \times 10^5$	$5.05 \times 10^5$	11
	0.50	$1.64 \times 10^4$	$4.9 \times 10^4$	$3.27 \times 10^4$	16	$5.23 \times 10^5$	$5.58 \times 10^5$	14

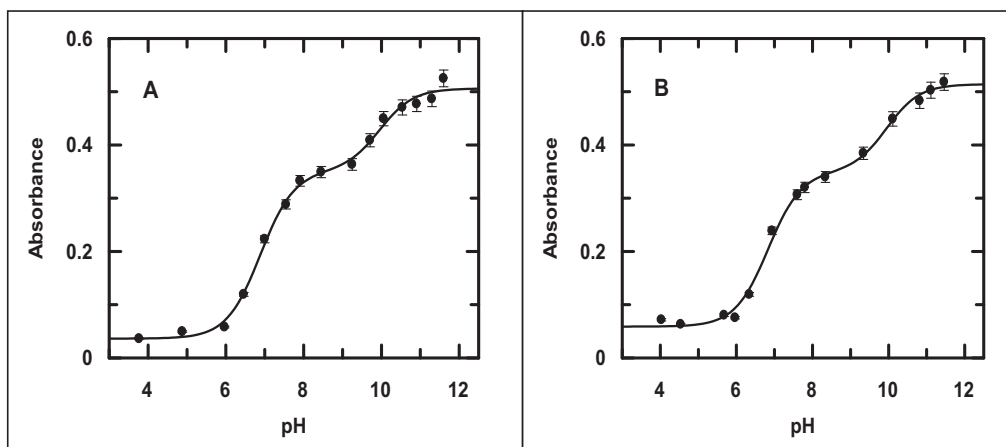


Fig. 3. pH-metric titration of DHA shown by a variation in absorbance at 530 nm at ionic strengths of (A) 0.12 M and (B) 0.15 M.

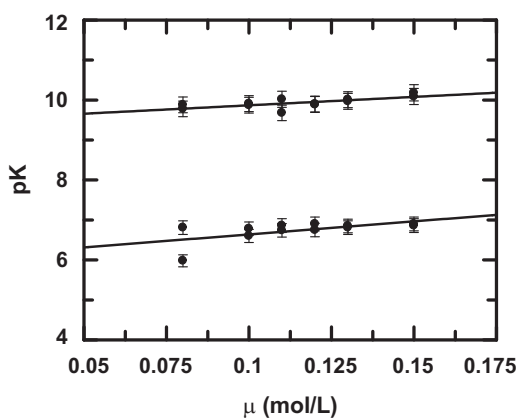


Fig. 4. Linear dependence of  $pK_a$  of DHA with variation in ionic strength of the medium at 301 K; [DHA] = 70  $\mu\text{M}$ ; best fit lines are obtained using data points from two different sets of experiments. The line above shows variation of  $pK_{a2}$  while that below is for  $pK_{a1}$ .

physiological pH that adversely affects binding with DNA [1,3,8,56].

### 3.2. Characterization of $\text{Mn}^{\text{II}}(\text{QH})_2$

#### 3.2.1. Comparison of the UV-Vis spectra of DHA and $\text{Mn}^{\text{II}}(\text{QH})_2$

Owing to poor solubility of the complex in water, its spectrum was recorded in aqueous-DMSO (Fig. S2, SI). The recorded  $\lambda_{\text{max}}$  at 521 nm was close to the wavelength (525 nm) at which physico-chemical experiments for  $\text{Mn}^{\text{II}}$  and DHA were performed to determine stoichiometry of complex formation (Fig. 1) indicating that the complex prepared is the same as that identified through physicochemical experiments.

#### 3.2.2. IR of DHA and $\text{Mn}^{\text{II}}(\text{QH})_2$

IR spectrum of pure DHA indicates a band at  $3375\text{ cm}^{-1}$  attributed to strong intra-molecular hydrogen bonding between the carbonyl at  $\text{C}_9$  and OH at  $\text{C}_1$  (Fig. S3, SI) [57]. Sharp bands at  $1198\text{ cm}^{-1}$  and  $1293\text{ cm}^{-1}$  are due to O–H deformation and C–O stretching combinations due to phenolic –OH. Peak at  $1664\text{ cm}^{-1}$  is characteristic of carbonyl stretching in quinones when both carbonyls are present in the same ring (Fig. S3, SI) [57]. In  $\text{Mn}^{\text{II}}(\text{QH})_2$ , band at  $3375\text{ cm}^{-1}$  flattened due to absence of any interaction between

phenolic–OH at  $\text{C}_1$  with carbonyl at  $\text{C}_9$  (Fig. S4, SI) [57]. Appearance of a peak at  $\sim 469\text{ cm}^{-1}$  indicates the formation of an Mn–O bond.

#### 3.2.3. Analysis of mass spectrum

Mass spectrum was recorded in the ESI+ mode (Fig. 5). The molecular ion peak expected at  $m/z = 569.42$  was detected in a cluster of peaks with  $m/z$  values 569.86, 570.86, 571.18 considering two molecules of water bound to the fifth and sixth coordination sites of  $\text{Mn}^{\text{II}}$ . Considering the complex to have two DHA and two water molecules coordinated to  $\text{Mn}^{\text{II}}$  the peaks in the mass spectrum could be explained. Peak shaving  $m/z$  values 317.08, 318.09, 319.08 indicate  $\text{Mn}^{\text{II}}$  bound to a single DHA molecule and an atom of sodium.

#### 3.2.4. TGA of the complex

Thermo-gravimetric analysis of the complex (Fig. S5, SI) shows that at  $102\text{ }^\circ\text{C}$  there is an evidence for the loss of two water molecules. Hence, there is an evidence for the formation of a 1:2  $\text{Mn}^{\text{II}}$ :DHA species having octahedral geometry where the fifth and sixth coordination sites are occupied by water.

#### 3.2.5. Magnetic moment of $\text{Mn}^{\text{II}}(\text{QH})_2(\text{H}_2\text{O})_2$

Magnetic susceptibility was measured by Gouy method and  $\mu_{\text{eff}}$  was found to be 5.81 BM suggesting the presence of five unpaired electrons.

#### 3.2.6. Structure of $\text{Mn}^{\text{II}}(\text{QH})_2(\text{H}_2\text{O})_2$ by computational technique

Single crystals of complexes where only hydroxy-9,10-anthraquinones are present as ligands bound to a metal centre are rare. There are only two reports so far from single crystal data [58,59]. We reported structures of hydroxy-9, 10-anthraquinone complexes of 3d transition metal ions from X-ray powder diffraction data [1,6,7]. In the present study, single crystals of the complex suitable for X-ray diffraction could not be isolated. The powder X-ray diffraction (PXRD) data we obtained could not be solved to generate a crystal structure as peaks obtained did not suggest a crystalline nature of the material. So we were left to arrive at the structure from information we had from various spectroscopic techniques, mass spectrometry and TGA. From thermo-gravimetric data and the mass spectrum it is evident  $\text{Mn}^{\text{II}}$ -DHA has two water molecules and two DHA coordinated to  $\text{Mn}^{\text{II}}$  (Fig. S6, SI). We assume that the  $\text{Mn}^{\text{II}}$  complex has an octahedral geometry (Fig. S6, SI). Usually, octahedrally coordinated  $\text{Mn}^{\text{II}}$  is high-spin, although low spin  $\text{Mn}^{\text{II}}$  complexes with strong field ligands exist [60]. We carried out density functional theorem (DFT) studies to predict the spin-state and structure of the complex. Two models

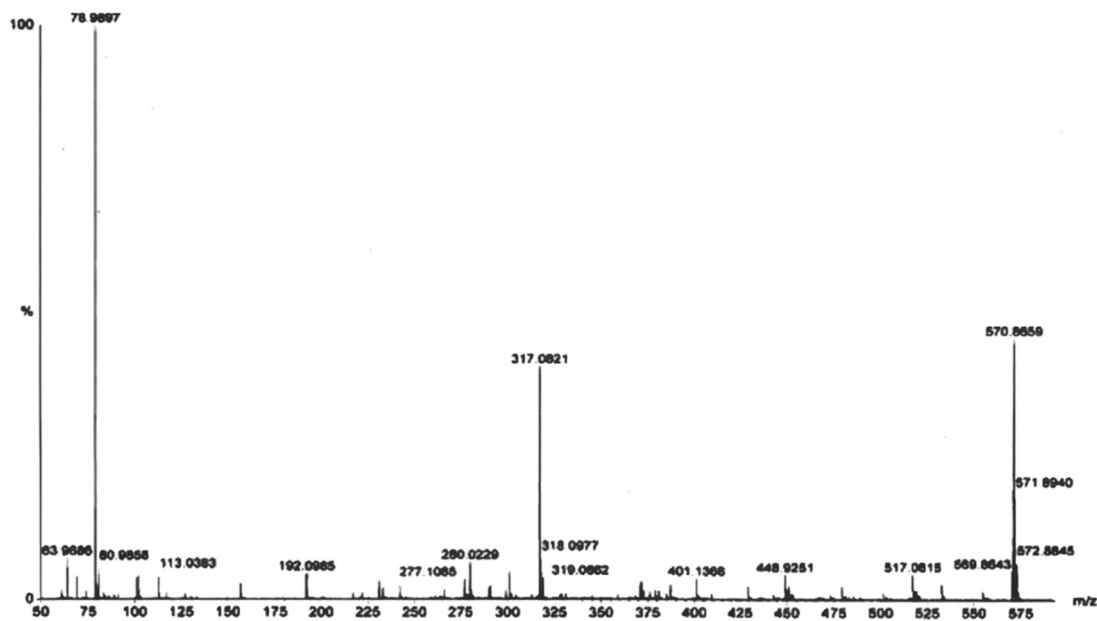


Fig. 5. Mass spectrum of  $\text{Mn}^{\text{II}}(\text{QH})_2(\text{H}_2\text{O})_2$ .

were constructed for octahedral  $\text{Mn}^{\text{II}}$  in which two DHA moieties are present in trans-geometry (a natural choice from symmetry considerations, Fig. S6, SI), one with  $\text{Mn}^{\text{II}}$  in low spin state ( $s = 1/2$ ), a doublet, and another in high spin state ( $s = 5/2$ ), a sextet. Geometry optimization was performed. Total energy calculations in gas phase and in solution (DMSO as solvent) along with single point TD-DFT calculations in DMSO were performed [61]. Experimentally obtained IR frequencies and theoretically gener-

ated ones from frequency calculations for both the optimized structures were compared. UV-Vis absorption spectrum recorded in DMSO was compared with calculated ones.

The central objective of the attempted theoretical investigation was to determine the correct spin state of an octahedral  $\text{Mn}^{\text{II}}$ . We removed any ambiguity by comparing the total energy, IR frequencies between optimized structures of high and low spin complexes, their UV-Vis absorption spectrum in DMSO with their correspond-

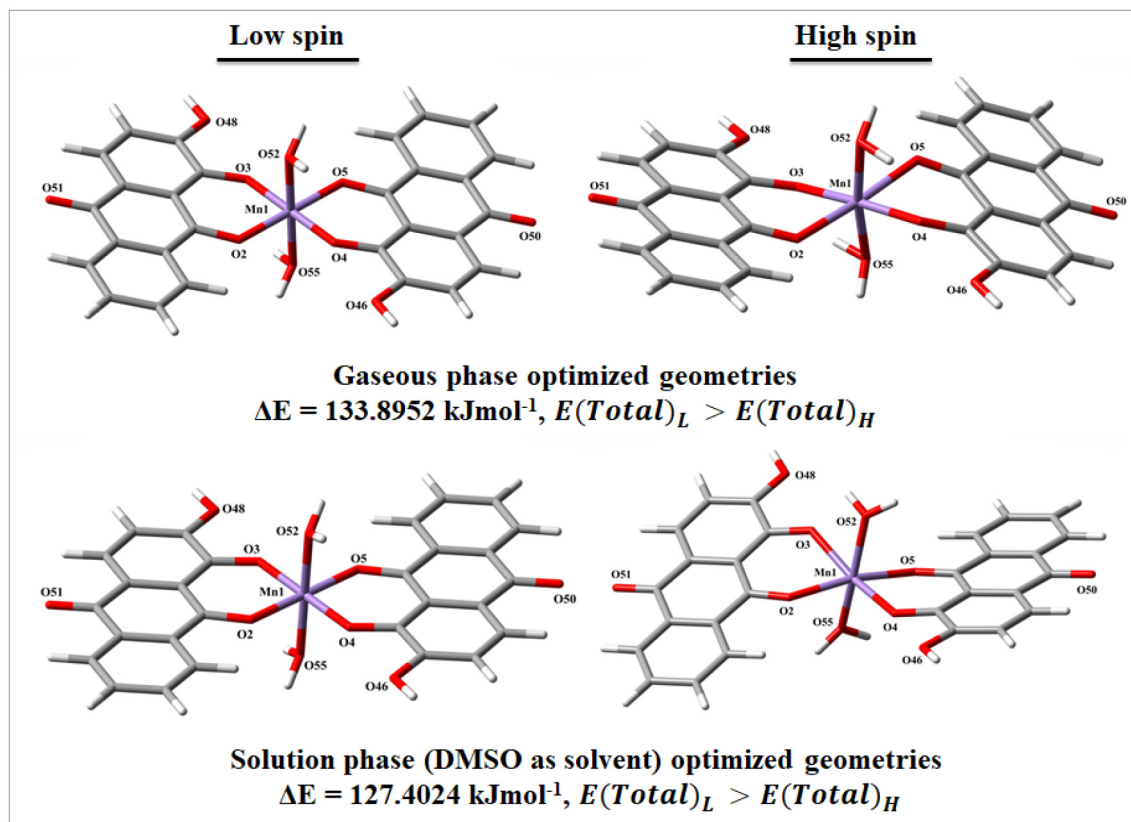


Fig. 6. Optimized geometries of the complex in two different spin states in gas phase and in DMSO medium.

ing experimental counterparts. For geometry optimization, negligible spin contamination occurred. The high spin geometry showed spin contamination in percentage of 0.10 and 0.06 for the gas phase and solution phase optimizations respectively.

All optimized geometries of the complex in the two spin states (in both phases) are shown in Fig. 6 with a numbering scheme showing coordination environment. Optimized coordinates for the configurations are provided in Tables S1 & S2, SI. Some important parameters of coordination geometries are provided in Tables S3 & S4, SI. The low spin state forms a regular octahedron with two DHA parallel to each other forming the basal plane; Mn<sup>II</sup> and two water molecules are in a straight line with the latter forming the vertices of the octahedron. Although bond parameters change slightly upon changing solvent, to do away with this effect, bonds within the basal plane or axial positions were considered almost equal to each other. The high spin state has a distorted octahedral geometry making bonds in the basal plane and axial unequal in length. Bond angles are twisted so that DHA moieties are no longer parallel to each other (dihedral angle = 8.93° for the optimized structure in the gas phase and 20.53° in solution phase). Axial water molecules are tilted to deform from ideal octahedron vertices.

Fig. 6 depicts a difference in total energy ( $\Delta E$ ) between high and low spin geometries optimized in gas and solution phases. Calculations carried out at Unrestricted DFT shows that the high spin configuration has a lower energy which is expected given both DHA and H<sub>2</sub>O are relatively weak field ligands. The value is 133.89 kJ/mol lower for the high spin geometry than the low spin geometry in gas phase. Introducing the molecule to a dielectric medium (DMSO) reduces this difference to 127.40 kJ/mol. A close inspection of IR spectra of the computed geometries and that obtained experimentally (Fig. S4, SI) reveal calculated frequencies obtained for high spin geometry are more comparable to experimental ones, although there ought to be little difference in IR spectra if the only difference in structures is due to spin of electrons on the central metal ion.

Theoretical absorption spectrum in DMSO with oscillator strength and experimental UV-Vis spectrum are shown in Fig. S7, SI. Calculated spectrum for high spin geometry shows better correlation for peak positions with the experimental spectrum than for low spin geometry. These further allow us to conclude that high spin state is more favorable. Subsequently, we analyzed frontier MOs for the complex optimized in gas phase and in solution (DMSO). Excitation in the absorption spectrum in DMSO was analyzed using NTO analysis for high spin Mn<sup>II</sup>-DHA.

**3.2.6.1. MO composition analysis.** For molecules having odd number of electrons, calculated using U-DFT leads to breakdown of symmetry. Each molecular orbital now has two components  $\alpha$  and  $\beta$  due to electron spin.  $\alpha$ -orbitals are more populated (five electrons) than  $\beta$ -orbitals showing a typical sextet multiplicity. The HOMO-LUMO energy levels for both spin- $\alpha$  and spin- $\beta$  components of MOs, their energy difference in gas phase and in solution (DMSO) are shown in Fig. 7. As spin- $\alpha$  and spin- $\beta$  components of each orbital is localized in different parts of the molecule, for MO composition analysis, contributions from five fragments viz., Mn, DHA(L), DHA(R), Water(1) and Water(2) were considered. Orbital energies, contribution of each fragment in terms of atomic orbitals to the frontier molecular orbital (MO) for some of the frontier MOs are listed in Table S5, SI.

For gas phase geometry, the highest singly occupied spin- $\alpha$  orbital (SOMO) is delocalized over the whole framework (28% Mn and 61% DHA) whereas LUMO is delocalized over DHA (ligand, 99%). For spin- $\beta$  orbitals both HOMO and LUMO are ligand centred (i.e. 98% DHA in each case) with practically negligible contribution from metal atomic orbitals. For geometry in solution phase, spin- $\alpha$

SOMO is distributed over the ligand with an appreciable contribution from the metal ion (42% Mn and 57% DHA). The LUMO is completely based on DHA (ligand 100%) with no participation from metal atomic orbitals. For spin- $\beta$  orbitals, both HOMO and LUMO are ligand centred (98% and 97% DHA respectively). Introduction of the complex into a dielectric medium reduces the HOMO-LUMO energy gap for both spin- $\alpha$  and spin- $\beta$  orbitals (Fig. 7). These FMOs come handy in highlighting electronic structure and opto electronic properties of the complex.

**3.2.6.2. Analysis of absorption spectra.** DMSO being the solvent, there is a cut off wavelength ( $\sim 268$  nm) below which the absorption of the compound may not be realized. Hence, absorption below 300 nm was not considered. Instead, the spectrum of the complex was recorded up to 1050 nm and compared with the calculated electronic spectrum of Mn<sup>II</sup>-DHA in DMSO.

Peaks in the experimental spectrum were assigned by visual inspection. The most pertinent transitions having moderate intensities ( $f \geq 0.02$ ) are close to the experimental absorption peaks, excitation wavelengths, energy, oscillator strengths ( $f$ ), character and CI coefficients are listed in Table S6, SI. Excitations were attributed to charge-transfer transitions among different moieties, viz. within DHA, between water molecules and DHA with varying amounts of metal to ligand contribution. We tabulated the first five computed transitions in DMSO (Table S7, SI). While performing TDDFT, excited states showed spin contamination with fractional values 0.212–0.019 (Table S6 & S7, SI); all states were considered to be sextets.

Excited state computational results were interpreted by natural transition orbital (NTO) analyses based on calculated transition density matrices [62]. Unoccupied and occupied NTOs were referred to as “electron” and “hole” transition orbitals respectively allowing us to identify them and visualize electronic transitions under consideration, in terms of excitation from hole-NTO to electron-NTO for both  $\alpha$ - and  $\beta$ -spin components. The NTOs for the most relevant peaks are depicted in Fig. S8, SI. While analyzing NTOs lower energy transitions around 526 nm were found at 492.7 nm (2.52 eV,  $f = 0.1213$ ) and 497.9 nm (2.49 eV,  $f = 0.1574$ ). The first transition consists of  $d(\text{Mn}) + \pi(\text{DHA}) \rightarrow \pi^*(\text{DHA})$  LLCT with some MLCT character together with lone pair(O)  $\rightarrow$  antibonding (O) transition. Net electron transfer between metal to ligand fragments and within ligand fragments were 0.03681e and 0.13293e respectively [63]. The second one is ascribed  $\text{tod}(\text{Mn}) + \pi(\text{DHA}) \rightarrow \pi^*(\text{DHA})$  [MLCT transition] in association with LLCT character where the net electron transfer between metal to ligand fragments and within ligand fragments are 0.0933e and 0.12326e respectively. Excitation near the experimentally observed peak at 350 nm was found by calculation to be at 339.27 nm (3.650 eV,  $f = 0.1077$ ) and ascribed to  $d(\text{Mn}) + \pi(\text{DHA}) \rightarrow \pi^*(\text{DHA})$  MLCT transition together with slight LLCT character where metal to ligand and ligand to ligand net electron transfers were 0.16419e and 0.03658e respectively. UV transition around 300 nm was computed and found at 294.26 nm (4.21 eV,  $f = 0.1758$ ). This was attributed to  $d(\text{Mn}) + \pi(\text{DHA}) \rightarrow \pi^*(\text{DHA})$  LLCT transition in association with MLCT character together with lone pair (O)  $\rightarrow$  antibonding (O) transition. Net electron transfer between metal to ligand fragments and within ligand fragments were 0.08540e and 0.13293e respectively.

### 3.3. Interaction of compounds with calf thymus DNA at different ionic strengths

Ionic strength of the medium is an important parameter influencing the binding of several drugs with DNA; the reasons being varied in nature [41,64]. Compounds were titrated with calf

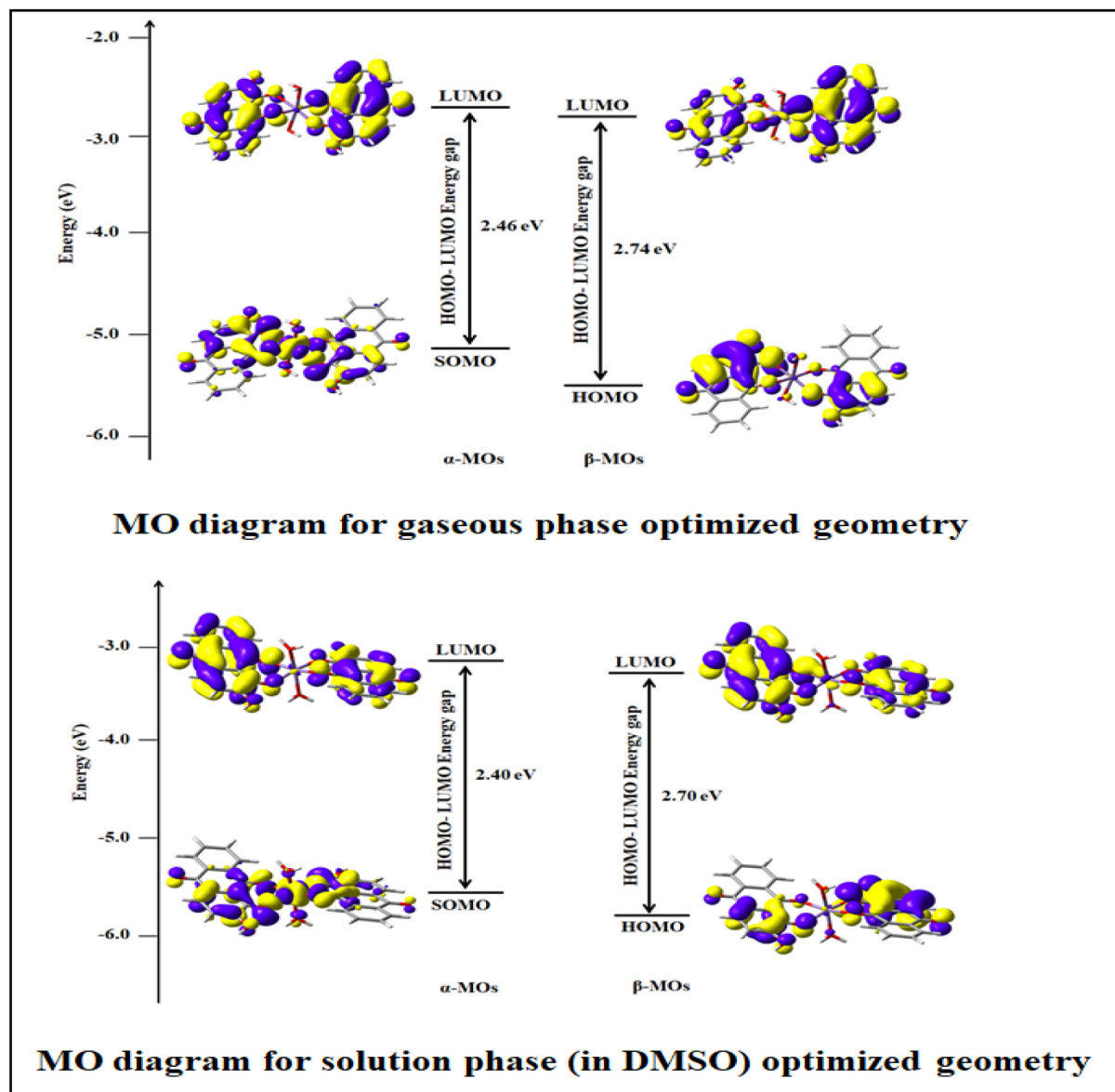


Fig. 7. HOMO and LUMO orbitals of the optimized complex (in high spin state) for  $\alpha$ - &  $\beta$ -spin states show the HOMO–LUMO energy gap.

thymus DNA at different ionic strengths at constant pH ( $\sim 7.4$ ). Titration of DHA with calf thymus DNA at different ionic strengths were followed at 520 nm while for the complex it was followed at 515 nm (for ionic strength =  $\sim 0.12$  M), at 510 nm (for ionic strength =  $\sim 0.3$  M) and at 506 nm (for ionic strength =  $\sim 0.5$  M).

Fig. S9, SI shows a gradual decrease in absorbance for a titration of DHA with calf thymus DNA at an ionic strength of 0.3 M (using NaCl) while Fig. S10, SI is for a titration of the complex at an ionic strength 0.12 M (using NaCl). Fig. 8A & B are representative plots of Eq. (5) for titrations performed at ionic strengths of 0.3 M in case of DHA and 0.12 M for the complex respectively. From such plots, apparent binding constant ( $K_{app}$ ) was evaluated (Table 1). Data in Fig. 9A & B were fitted according to Eq. (7) showing saturation achieved in binding of the compounds to DNA;  $K_{app}$  was evaluated by a non-linear fit.

Binding parameters at all ionic strengths are provided in Table 1. Inset of Fig. 9A & B provide  $n_b$ , number of nucleotides bound to compounds (Table 1). It is interesting to note that in case of the complex, the value of  $n_b$  obtained at each ionic strength was approximately double that obtained for DHA binding to the same

DNA at these ionic strengths. This indicates two molecules of DHA are bound to  $Mn^{II}$  in the complex, a fact realized from DNA binding experiments (Table 1) [1,8,12].

Using  $K_{app}$  and  $n_b$  (Table 1) and the fact that  $K_{app} \times n_b = K'$ , overall binding constant was evaluated for DHA and the complex at different ionic strengths of the medium. Overall binding constant was also obtained from the modified Scatchard equation (Eq. (8)). Fig. 10A & B are plots that obey Eq. (8). Values obtained for overall binding constant from the modified Scatchard equation was similar to that calculated using  $K_{app}$  and  $n_b$ .

Since titrations were performed at pH 7.4 by varying the ionic strength of the medium, hence with gradual increase in ionic strength ratio of the anionic form of DHA to its neutral form changed continuously. This was evaluated by determining the  $pK_a$  of DHA at different ionic strengths of the medium (Fig. S11, SI).

From  $pK_{a1}$  of DHA, ratio of anionic to neutral form of DHA was found to lie between 3.75 (at ionic strength = 0.12 M) to 0.14 (at ionic strength = 0.36 M). Hence, it is clearly evident that with increase in ionic strength there is a gradual decrease in the anionic form of DHA that manifests by a higher binding constant value



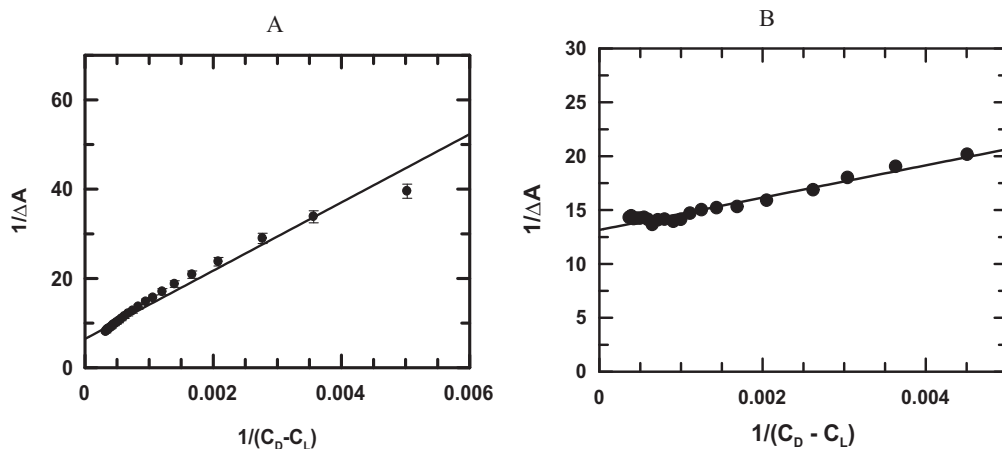


**Fig. 8.** Typical double reciprocal plots for the interaction of (A) DHA and (B)  $\text{Mn}^{\text{II}}(\text{QH})_2$  with calf thymus DNA that enables evaluation of  $K_{\text{app}}$  at ionic strengths of 0.30 M for (A) and 0.12 M for (B).  $[\text{DHA}] = [\text{Mn}^{\text{II}}(\text{QH})_2] = 50 \mu\text{M}$ ,  $\text{pH} = 7.40$ , Temperature = 300 K.

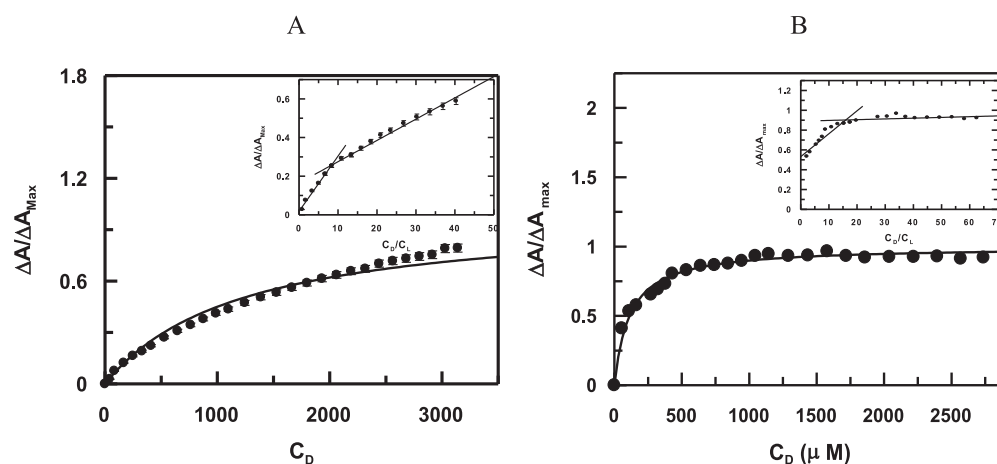


**Fig. 9.** Binding isotherms of (A) DHA and (B)  $[\text{Mn}^{\text{II}}(\text{QH})_2]$  with calf thymus DNA at ionic strengths of 0.30 M and 0.12 M with respect to NaCl respectively. The corresponding non-linear fits are shown. Inset: Plot of normalized increase in absorbance as a function of the ratio of calf thymus DNA to (A) DHA and (B)  $[\text{Mn}^{\text{II}}(\text{QH})_2]$ .  $[\text{DHA}] = [\text{Mn}^{\text{II}}(\text{QH})_2] = 50 \mu\text{M}$ ,  $\text{pH} = 7.40$ ,  $T = 301 \text{ K}$ .

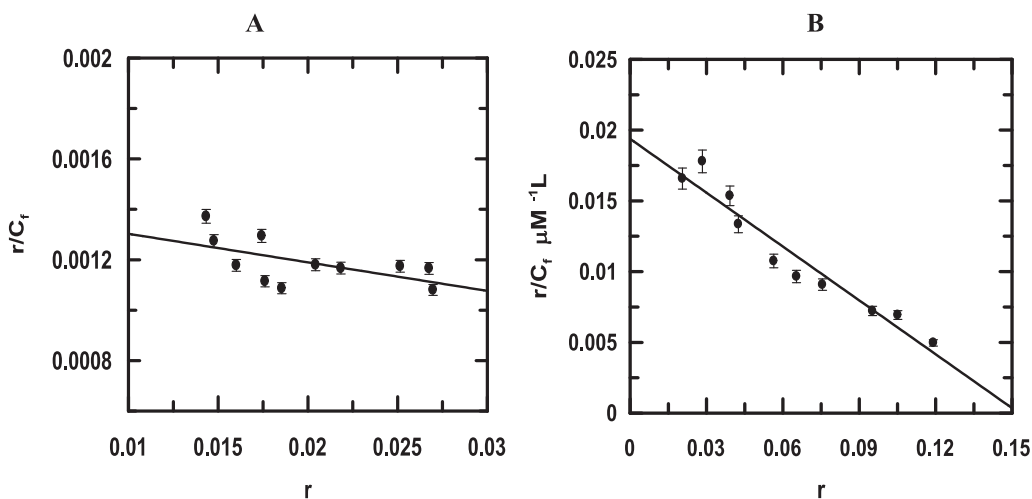


**Fig. 10.** Scatchard plots for the interaction of (A) DHA and (B)  $\text{Mn}(\text{QH})_2$  with calf thymus DNA that was followed by UV-Vis spectroscopy at 521 nm for (A) and 515 nm for (B) respectively.  $[\text{DHA}] = [\text{Mn}^{\text{II}}(\text{QH})_2] = 50 \mu\text{M}$ ;  $[\text{NaCl}] = 0.24 \text{ M}$  for (A) and 0.12M for (B);  $\text{pH} = 7.40$ ,  $T = 301 \text{ K}$ .

**Table 2**  
Variation in overall binding constant of DHA with calf thymus DNA at different ionic strength (pH ~ 7.4).

[NaCl] in M	$-\log[\text{Na}^+]$	$K^* = K_{\text{app}} \times n_b$	$\log K^*$	$K^*$ from Scatchard plot	$\log K^*$
0.12	0.921	$0.64 \times 10^4$	3.81	$0.88 \times 10^4$	3.94
0.18	0.745	$1.01 \times 10^4$	4.00	$1.00 \times 10^4$	4.00
0.24	0.619	$1.34 \times 10^4$	4.13	$1.13 \times 10^4$	4.05
0.30	0.523	$2.30 \times 10^4$	4.36	$2.39 \times 10^4$	4.37
0.36	0.444	$2.63 \times 10^4$	4.42	$2.81 \times 10^4$	4.45

**Table 3**  
Variation of overall binding constant for interaction of  $\text{Mn}(\text{QH})_2$  with calf thymus DNA at different concentrations of NaCl at physiological pH.

[NaCl] in M	$-\log[\text{Na}^+]$	$K^* = K_{\text{app}} \times n_b$	$\log K^*$	$K^*(10^5)$ (from Scatchard plot	$\log K^*$
0.12	0.921	$1.90 \times 10^5$	5.28	$1.38 \times 10^5$	5.13
0.18	0.745	$4.62 \times 10^5$	5.66	$4.86 \times 10^5$	5.68
0.30	0.523	$2.04 \times 10^5$	5.31	$5.05 \times 10^5$	5.70
0.50	0.301	$5.23 \times 10^5$	5.72	$5.58 \times 10^5$	5.75

(Table 2) [3,42]. On the other hand, for the complex since dissociation of OH present on DHA bound to  $\text{Mn}^{\text{II}}$  is well beyond the physiological pH range, variation in ionic strength should not have much effect on binding with DNA. However, an increase in binding constant value of  $\text{Mn}(\text{QH})_2$  with calf thymus DNA was observed with increase in the ionic strength of the medium (Tables 1 & 3).

Fig. 11A & B indicate this increasing nature for binding of the complex and DHA with calf thymus DNA. In fact, at all ionic strengths, the complex was more effective in binding calf thymus DNA than DHA (Tables 2 & 3). This has significance if the complex is to be used as an anticancer agent. Patients having cancer experience fluctuation in electrolyte concentration in their body fluids during the course of treatment for which most often electrolyte is added from outside. Under conditions of high ionic strength many drugs tend to be ineffective. Going by our results, this should not be the case for this complex as there is clear evidence that binding constant values are high even at increased ionic strengths of the medium (Table 3, Fig. 11).

Increase in  $\text{pK}_a$  with the ionic strength of the medium explains why there is a significant increase in interaction of DHA with calf thymus DNA [42]. A slight change in  $\text{pK}_{a1}$  is sufficient to cause a substantial difference to the presence of neutral and anionic forms of DHA in the medium that affects interactions with DNA [42]. As mentioned earlier, increased presence of anions is a hindrance to interactions with DNA at physiological pH [2,42,56]. Therefore, in a medium of high ionic strength hydroxy-9,10-anthraquinones (here DHA) are likely to bind DNA better as their anionic forms decrease; the compound is largely present as neutral species. Fur-

ther to this, the presence of a metal ion in a complex of DHA makes binding even better.

#### 3.4. Interaction of $\text{Mn}^{\text{II}}(\text{QH})_2$ with calf thymus DNA at different pH

Titrations of  $\text{Mn}^{\text{II}}(\text{QH})_2$  with calf thymus DNA in the pH range 6.8–8.0 was followed at 520 nm. Fig. S12, SI is a plot fitted to Eq. (5) while Fig. 12 is fitted by non-linear square fit analysis according to Eq. (7) for a titration that was performed at pH 7.18. Both plots evaluate  $K_{\text{app}}$ . Inset of Fig. 12 shows determination of  $n_b$ . Similar plots were also obtained for titrations at other pH values (Table 4). Data obtained were analyzed according to Eq. (8) providing new values for overall binding constant ( $K^*$ ) and site size of interaction " $n$ " ( $n_b^{-1}$ ) [49]. A modified Scatchard plot for the complex interacting with calf thymus DNA at pH 7.18 is shown in Fig. S13, SI. Results of Scatchard plots at all pH values are summarized in Table 4.

Unlike DHA, binding constant values for the complex did not decrease with increase in the pH of the medium (Fig. 13). In fact, values in Table 4 suggest they are higher than DHA interacting with calf thymus DNA at each pH (determined earlier) [42]. This is significant for it indicates complex formation prevents formation of anionic species on DHA, that were earlier shown to be responsible for decreased binding with DNA [1,42,56]. The result is important from a biological point of view as cancer patients experience fluctuation of pH in body fluids, a matter of concern on the application of several drugs [65,66]. Hence, if this complex is ever

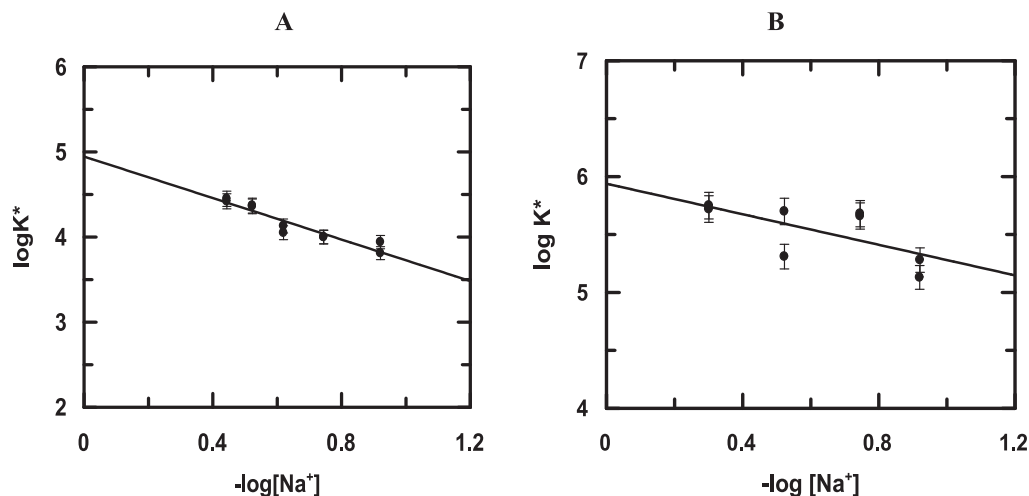


**Fig. 11.** Variation of overall binding constant of (A) DHA and (B)  $\text{Mn}(\text{QH})_2$  with calf thymus DNA at different NaCl concentrations at pH ~ 7.4; Temperature = 298 K.

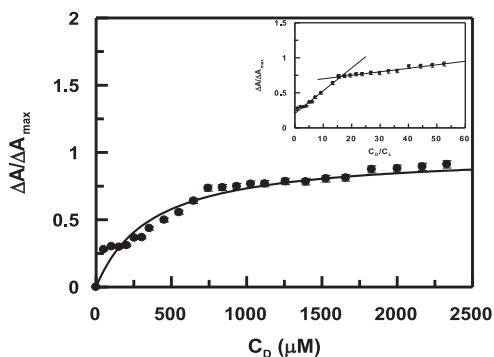


**Fig. 12.** Binding isotherm of  $\text{Mn}(\text{QH})_2$  interacting with calf thymus DNA at pH 7.18. The corresponding non-linear fit is shown for a titration that was followed by UV–Vis spectroscopy. Inset: Plot of normalized increase in absorbance as a function of the ratio of calf thymus DNA to  $\text{Mn}(\text{QH})_2$ .  $[\text{Mn}(\text{QH})_2] = 50 \mu\text{M}$ ,  $[\text{NaCl}] = 120 \text{ mM}$ , Temperature = 298 K.

developed into a drug, at least its activity based on DNA interaction would remain same over the physiological pH range.

### 3.5. The detection of reactive oxygen species

#### 3.5.1. The NADH dehydrogenase assay

The enzyme assay was followed at 550 nm and involves reduction of cytochrome c at 298 K. Concentration of DHA or  $\text{Mn}(\text{QH})_2$  was varied from 0 to 50.0  $\mu\text{M}$ . Formation of superoxide radical anion catalyzed by DHA or  $\text{Mn}(\text{QH})_2$  was measured from the reduction of cytochrome c inhibited by SOD in presence of NADH and NADH dehydrogenase (Fig. 14) [1,5–13,50].

Formation of superoxide radical anion in such enzyme assisted reactions occurs when semiquinone formed on DHA gets oxidized by molecular oxygen [1,5–13,50]. Following complex formation, this does not happen so easily on compounds like DHA as it is now bound to a metal ion. Since one carbonyl of DHA is involved in coordinating  $\text{Mn}^{\text{II}}$  hence only the other carbonyl can form semiquinone when the complex is a participant of the electron transport chain. Hence, semiquinone formation decreases quite naturally in case of the complex leading to less superoxide radical anion (Fig. 14) [1,5–13,50]. Even if semiquinone is generated on the ligand (here DHA), the presence of a metal ion removes an electron from its site of formation by more than one mechanism [67]. This further decreases the possibility of semiquinone generation on complexes. Automatically, the chances of an interaction of a semiquinone formed on the complex with molecular oxygen decreases considerably which explains Fig. 14. However,  $\text{Mn}^{\text{II}}$ , like  $\text{Co}^{\text{II}}$ ,  $\text{Ni}^{\text{II}}$  or  $\text{Pd}^{\text{II}}$  lacking a stable lower oxidation state, unlike  $\text{Fe}^{\text{III}}$  or  $\text{Cu}^{\text{II}}$ , decrease in superoxide radical anion formation is comparatively less than that observed for  $\text{Cu}^{\text{II}}$  or  $\text{Fe}^{\text{III}}$  complexes of anthracyclines or their analogues [1,4–15,18]. Fig. 14 is comparable to that observed for a  $\text{Co}^{\text{II}}$  complex of quinalizarin [8] but significantly different from that of  $\text{Cu}^{\text{II}}$  or  $\text{Fe}^{\text{III}}$  complexes of hydroxy-9,10-anthraquinones [1,9–13,18]. Metal ions having a stable lower oxidation

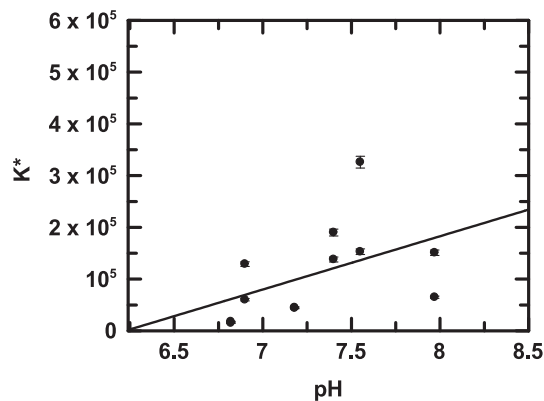


**Fig. 13.** Plot of variation of overall binding constant of  $\text{Mn}(\text{QH})_2$  interacting with calf thymus DNA at different pH (maintained with tris buffer) at 298 K and ionic strength of 0.12 M. [Results of two independent experiments at each pH is shown.]

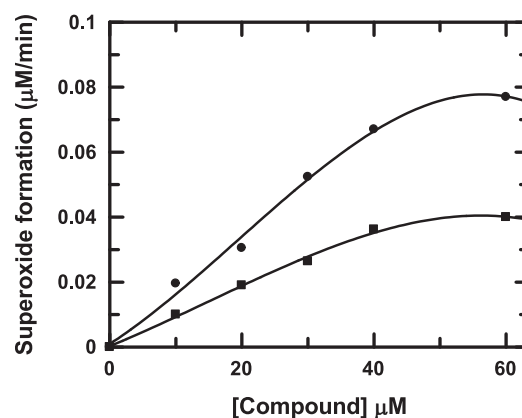


**Fig. 14.** Effect of DHA and  $\text{Mn}(\text{QH})_2$  on superoxide formation by NADH dehydrogenase. Superoxide formation was determined from the rate of superoxide dismutase-inhibitable cytochrome c reduction using a spectrophotometer. The reaction mixture contained 100 mM Tris buffer (pH 7.4), 40.0  $\mu\text{g ml}^{-1}$  SOD, 160.0  $\mu\text{M}$  NADH, 80.0  $\mu\text{M}$  cytochrome c, 5  $\text{UI}^{-1}$  NADH dehydrogenase and the compounds being investigated; (●) DHA; (■)  $\text{Mn}(\text{QH})_2$ .

state has an advantage if they form a complex with anthracyclines or hydroxy-9,10-anthraquinones (shown in SI) [1,9–13,17–19]. This should not happen for this complex. However, in case of this complex (with  $\text{Mn}^{\text{II}}$  as the metal ion), since semiquinone or superoxide radical anion formation is not decreased to the extent observed for  $\text{Cu}^{\text{II}}$  or  $\text{Fe}^{\text{III}}$  complexes, cytotoxicity owing to free radical formation would not be totally compromised [1,4,5,7,9,11–13,17,18]. This becomes an advantage. Hence,  $\text{Mn}(\text{QH})_2$  if promoted as an anticancer agent, it should be able to hold on to a substantial part of the cytotoxic activity of DHA by the free radical pathway and yet be less cardiotoxic i.e. a dual advantage [1,2,4–13,18]. Besides, complexes have several other attributes that help

**Table 4**  
Variation of binding constants of the complex with calf thymus DNA at different pH.

	pH	$K_{\text{app}}$			Site-size	$K_{\text{app}} \times n_b = K^*$	$K^*$ (from Scatchard)	Site-size
		From linear plot (a)	From non-linear plot (b)	Average = (a + b)/2				
[Mn(LH) <sub>2</sub> ]	6.82	$0.10 \times 10^4$	$0.11 \times 10^4$	$0.11 \times 10^4$	16	$0.18 \times 10^5$	$0.15 \times 10^5$	13
	6.90	$0.84 \times 10^4$	$0.88 \times 10^4$	$0.86 \times 10^4$	15	$1.29 \times 10^5$	$0.60 \times 10^5$	6
	7.18	$0.26 \times 10^4$	$0.30 \times 10^4$	$0.28 \times 10^4$	16	$0.45 \times 10^5$	$0.44 \times 10^5$	10
	7.40	$0.87 \times 10^4$	$1.50 \times 10^4$	$1.19 \times 10^4$	16	$1.90 \times 10^5$	$1.38 \times 10^5$	8
	7.55	$1.39 \times 10^4$	$3.27 \times 10^4$	$2.33 \times 10^4$	14	$3.26 \times 10^5$	$1.53 \times 10^5$	7
	7.97	$0.91 \times 10^4$	$1.25 \times 10^4$	$1.08 \times 10^4$	14	$1.51 \times 10^5$	$0.65 \times 10^5$	10

them show better anticancer activity than hydroxy-9, 10-antraquinones taking the efficacy of metal-hydroxy-9,10-antraquinones close to that of some of the established anticancer agents [1–19].

### 3.5.2. The $H_2DCFDA$ assay

While the NADH dehydrogenase assay is a well-established technique for detecting ROS generation it is nevertheless a model study. A more realistic approach for detecting ROS is the  $H_2DCFDA$  assay [51–54]. Here compounds are tried on cell lines. In this study, we attempted it on two cancer cells, HeLa and HepG2 as well as on normal WI-38 lung fibroblast cells. As mentioned earlier, cells were previously treated with compounds at their respective  $IC_{50}$  concentrations, determined by the MTT assay for 30 min. For such treated cells, ROS generation was followed after addition of  $H_2O_2$  ( $\sim 70 \mu M$ ).

ROS formation for cells treated with a compound was substantially higher than when the same cells were treated with N-acetyl cysteine (NAC), a standard ROS quencher used as control. In fact, it was even higher than experiments where cells were not treated with any compound i.e. only treated with  $H_2O_2$ . Experiments indicate for all three cell lines compounds tend to amplify the ROS introduced into the system using  $H_2O_2$ . For HeLa cells, a clear distinction cannot be made between ROS amplification due to DHA and  $Mn^{II}(QH)_2$  (Fig. 15A) while for Hep G2 cells, slight increase in ROS was observed for cells treated with the complex against cells treated with DHA (Fig. 15B). In case of WI 38 lung fibroblast (normal) cells also,  $Mn^{II}(QH)_2$  increased ROS formation to a greater extent than that observed with DHA (Fig. 15C).

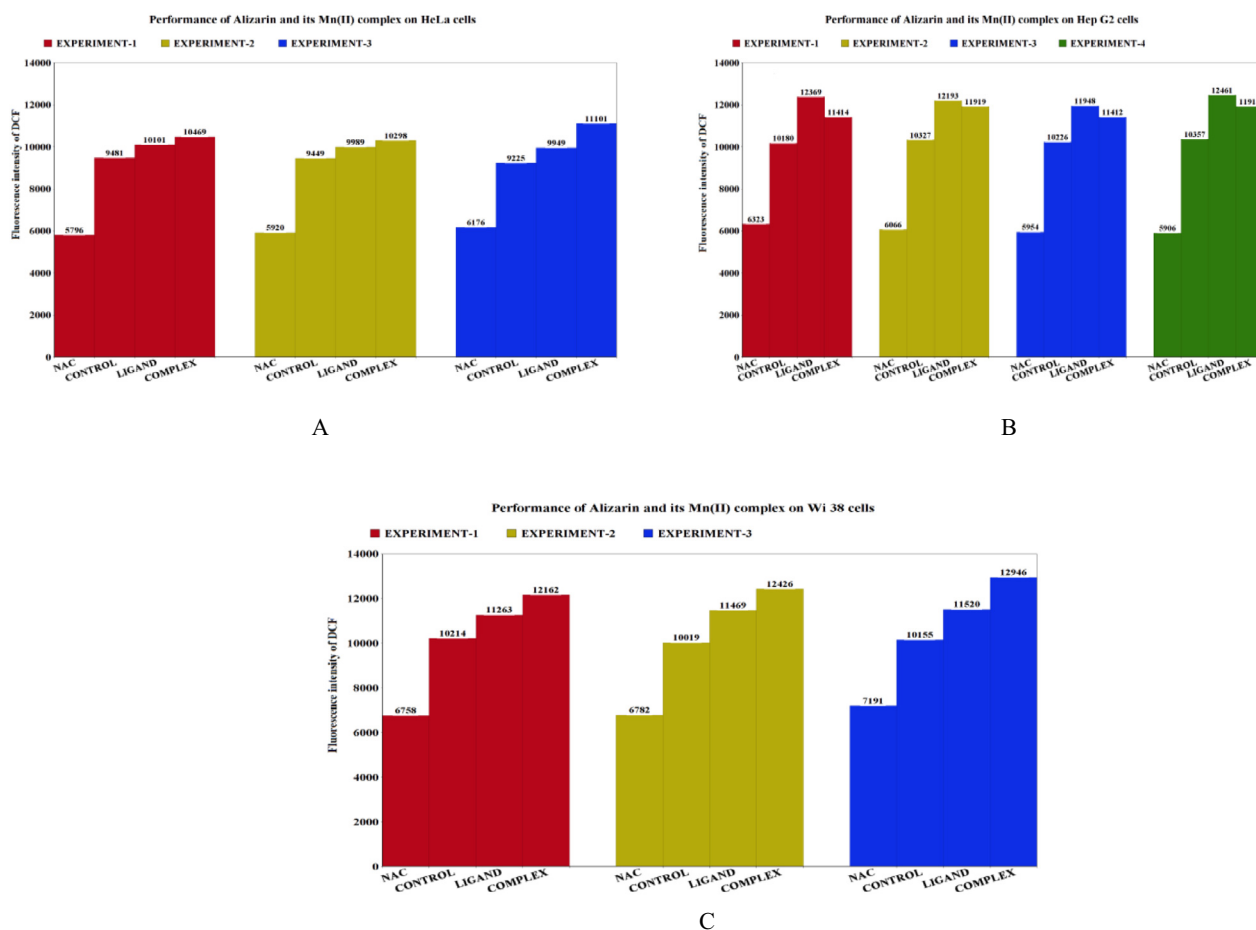


**Fig. 15.** Effect of DHA and  $Mn^{II}(QH)_2$  on the presence of ROS within (A) HeLa cells, (B) Hep G2 cells and (C) WI 38 lung fibroblast cells as detected by the  $H_2DCFDA$  assay; ROS was generated using  $H_2O_2$ . In each diagram, the term NAC refers to cells treated with N-acetyl cysteine, CONTROL refers to cells not treated with any compound, LIGAND refers to cells treated with DHA and COMPLEX refers to cells treated with  $Mn^{II}(QH)_2$ . Different colors indicate separate experiments. (Color online.)

**Table 5**  
 $IC_{50}$  values of compounds on three different cell lines.

Compounds	Hep G2 cells $IC_{50}$ value ( $\mu M$ )		HeLa cells $IC_{50}$ value ( $\mu M$ )		WI 38 lung fibroblast cells $IC_{50}$ value ( $\mu M$ )	
	From the ED <sub>50</sub> plus program	From Graph	From the ED <sub>50</sub> plus program	From Graph	From the ED <sub>50</sub> plus program	From Graph
DHA	79.27	62.00	75.11	52.00	106.60	100.00
$Mn^{II}(QH)_2$	65.36	50.00	90.51	60.00	89.10	72.00
*cisplatin	(14.87 ± 1.22) <sup>68</sup>		(54.07 ± 12.25) <sup>68</sup>			
*Doxorubicin	(4.68 ± 1.08) <sup>68</sup>		(4.07 ± 0.26) <sup>68</sup>			

\*The data for cisplatin and doxorubicin provided in the table was taken from literature to compare the performance of  $Mn^{II}(QH)_2$  with some standard anticancer agents.

### 3.6. Effect of DHA and $Mn^{II}(QH)_2$ on two different cancer cells and a normal cell

MTT assay performed on cancer cells (HeLa and Hep G2) and WI 38 lung fibroblast (normal) cells reveal (Fig. S11, A–F, SI) compounds were more effective on carcinoma cells than on normal cells. Cell viability studies obtained for each cell line fitted to the ED<sub>50</sub> plus program provides IC<sub>50</sub> values for a compound on that cell line. From the data (Table 5) it appears that performance of DHA was slightly better on HeLa cells while  $Mn^{II}(QH)_2$  performed better on Hep G2 cells. On WI 38 lung fibroblast cells, IC<sub>50</sub> for DHA was significantly higher indicating DHA is less cytotoxic on normal cells. IC<sub>50</sub> of the complex on normal cells was comparable to HeLa cells but higher than Hep G2 cells. Hence, the MTT assay suggests  $Mn^{II}(QH)_2$  is effective on Hep G2 cells that correlates with its ROS generating ability in these cells indicating that generation of ROS is responsible for the enhanced cytotoxic activity of the complex on this cell line.

## 4. Conclusion

A complex of  $Mn^{II}$  with DHA was synthesized and characterized with the intention of realizing the performance of complexes of simpler analogues of anthracyclines with bio-friendly 3d transition metal ions not possessing a stable lower oxidation state. Biophysical studies on the complex with DNA as well as ROS generation studies help to realize the probable mode of action of the complex on cancer cells in comparison to DHA. The complex was found to be clearly ahead in human hepatocellular carcinoma (Hep G2) cells that may be attributed to an increased steady binding ability with DNA under varying conditions of ionic strength and pH as well as its ability to amplify ROS present in cells that could come handy in promoting cytotoxic activity [68]. Biophysical studies help to identify complex formation prevents generation of anionic species under physiological conditions that make DNA binding more effective than that observed with DHA. This would be important for an application on cancer patients who experience fluctuation in pH and electrolyte concentration in body fluids during treatment. With cancer cells surviving at low pH and feeling uncomfortable in basic media, increasing pH of body fluids is an important form of treatment [69,70]. This complex could be useful in that perspective. With decreased superoxide formation, increased affinity towards DNA,  $Mn^{II}(QH)_2$  could just be having the essential qualities of a potential anticancer agent.

## Declaration of Competing Interest

The authors declare that they have no known competing financial interests or personal relationships that could have appeared to influence the work reported in this paper.

## Acknowledgements

SD is grateful to the Department of Science & Technology, Govt. of West Bengal for financial support vide an R & D Project [794 (Sanc.)1(10) ST/P/S&T/9G-23/2013]. He is grateful to the DST-PURSE program of the Government of India for financial support to Jadavpur University from which funds were utilized for this work. Authors wish to acknowledge Govt. of India for grants to the Department of Chemistry, Jadavpur University with which the mass spectrometer (Micromass-Q-ToF micro™, Waters Corporation) used as a part of the investigations in this work was purchased. MS wish to acknowledge UGC for a “Rajiv Gandhi National” fellowship (JRF). SD is grateful to Dr. Shouvik Chattopadhyay of the Department of Chemistry, Jadavpur University for

kindly providing the IR data of the compounds and also for useful discussions. He expresses his gratitude to Prof. Sujoy Baitalik of the same department for kindly providing the near-infrared spectrum of the complex. Authors are grateful to Dr. Chetan Kumar Jain for fitting the MTT assay data to the ED<sub>50</sub> plus program to evaluate IC<sub>50</sub> values.

## Appendix A. Supplementary data

Supplementary data to this article can be found online at <https://doi.org/10.1016/j.poly.2019.08.007>.

## References

- [1] P. Das, C.K. Jain, S.K. Dey, R. Saha, A.D. Chowdhury, S. Roychoudhury, S. Kumar, H.K. Majumder, S. Das, RSC Adv. 4 (2014) 59344.
- [2] S. Mukherjee, P.K. Gopal, S. Paul, S. Das, J. Anal. Oncol. 3 (2014) 122.
- [3] P. Das, D. Bhattacharya, P. Karmakar, S. Das, RSC Adv. 5 (2015) 73099.
- [4] P. Mondal, S. Roy, G. Loganathan, B. Mandal, D. Dharumadurai, M.A. Akbarsha, P.S. Sengupta, S. Chattopadhyay, P.S. Guin, Biochem. Biophys. Rep. 4 (2015) 312.
- [5] P. Das, C.K. Jain, S. Roychoudhury, H.K. Majumder, S. Das, ChemistrySelect 1 (2016) 6623.
- [6] B. Mandal, S. Singha, S.K. Dey, S. Mazumdar, T.K. Mondal, P. Karmakar, S. Kumar, S. Das, RSC Adv. 6 (2016) 51520.
- [7] B. Mandal, S. Singha, S.K. Dey, S. Mazumdar, S. Kumar, P. Karmakar, S. Das, RSC Adv. 7 (2017) 41403.
- [8] S. Mukherjee-Chatterjee, C.K. Jain, S. Singha, P. Das, S. Roychoudhury, H.K. Majumder, S. Das, ACS Omega 3 (2018) 10255.
- [9] M.M.L. Fiallo, A. Garnier-Suillerot, Biochim. Biophys. Acta.-Gen. Subj. 840 (1985) 91.
- [10] M.M.L. Fiallo, A. Garnier-Suillerot, Biochemistry 25 (1986) 924.
- [11] S. Das, A. Saha, P.C. Mandal, Talanta 43 (1990) 95.
- [12] P.S. Guin, S. Das, P.C. Mandal, J. Inorg. Biochem. 103 (2009) 1702.
- [13] S. Roy, P. Mondal, P.S. Sengupta, D. Dhak, R.C. Santra, S. Das, P.S. Guin, Dalton Trans. 44 (2015) 5428.
- [14] S.E. Lipshultz, J.A. Alvarez, R.E. Scully, Heart 4 (2008) 525.
- [15] C. Vergely, S. Delemasure, Y. Cottin, L. Rochette, Heart Metab. 35 (2007) 1.
- [16] M.M.L. Fiallo, A. Garnier-Suillerot, B. Matzkanke, H. Kozlowski, J. Inorg. Biochem. 75 (1999) 105.
- [17] S. Das, A. Saha, P.C. Mandal, Environ. Health Pers. 105 (1997) 1459.
- [18] S. Das, A. Saha, P.C. Mandal, J. Rad. Nucl. Chem. 196 (1995) 57–63.
- [19] S. Das, P.C. Mandal, Rad. Phys. Chem. 78 (2009) 37.
- [20] J. Butler, B.M. Hoey, Br. J. Cancer Suppl. 8 (1987) 53.
- [21] D.G. Sushkov, N.P. Gritsan, L.M. Weiner, FEBS Lett. 225 (1987) 139.
- [22] T.C. Johnstone, E.M. Nolan, Dalton Trans. 44 (2015) 6320.
- [23] R.J. Debus, in: Metal Ions in Biological Systems: Manganese and its Role in Biological Processes, Dekker Marcel, New York, 2000, pp. 657–711.
- [24] R.S. Magliozzo, J.A. Marcinkiewicz, J. Biol. Chem. 272 (1997) 8867.
- [25] D.G. Kehres, M.E. Maguire, FEMS Microbiol. Rev. 27 (2003) 263.
- [26] A. Takeda, Brain Res. Rev. 41 (2003) 79.
- [27] R. Caspi, B.M. Tebo, M.G. Haygood, Appl. Environ. Microbiol. 64 (1998) 3549.
- [28] J.P.M. de Vrind, G.J. Brouwers, P.L.A.M. Corstjens, J. den Dulk, E.W. de Vrind-de Jong, Appl. Environ. Microbiol. 64 (1998) 3556.
- [29] G.-J. Brouwers, J.P.M. de Vrind, P.L.A.M. Corstjens, P. Cornelis, C. Baysse, E.W. de Vrind-de Jong, Appl. Environ. Microbiol. 65 (1999) 1762.
- [30] E.H. Rubin, W.N. Haitln, Holland-Frei Cancer Medicine, B C Decker, Hamilton (ON), 2000, fifth ed. Chapter 49.
- [31] D.A. Gewirtz, Biochem. Pharmacol. 57 (1999) 727.
- [32] V. Křen, T. Řezanka, FEMS Microbiol. Rev. 32 (2008) 858.
- [33] Y. Pommier, E. Leo, H.L. Zhang, C. Marchand, Chem. Biol. 17 (2010) 421.
- [34] G. Lenglet, M.H. David-Cordonnier, J. Nucl. Acids (2010), <https://doi.org/10.4061/2010/290935>, Article ID 290935, 17 pages.
- [35] T. Banerjee, S. Banerjee, S. Sett, S. Ghosh, T. Rakshit, R. Mukhopadhyay, PLoS ONE 11 (2016) e0154666.
- [36] G. Cozza, M. Mazzorana, E. Papinutto, J. Bain, M. Elliott, G. di Maira, A. Gianoncelli, M.A.S. Sarno, M. Ruzzene, R. Battistutta, F. Meggio, S. Moro, G. Zagotto, L.A. Pinna, Biochem. J. 421 (2009) 387.
- [37] B. Mandal, H.K. Mondal, S. Das, Biochem. Biophys. Res. Comm. 515 (2019) 505.
- [38] K.A. Jones, J.T. Kadonaga, P.J. Rosenfeld, T.J. Kelly, R. Tijian, Cell 48 (1987) 79.
- [39] P. Romanowski, M.A. Madine, A. Rowles, J.J. Blow, R.A. Laskey, Curr. Biol. 6 (1996) 1416.
- [40] T. Deb, P.K. Gopal, D. Ganguly, P. Das, M. Paul, M.B. Saha, S. Paul, S. Das, RSC Adv. 4 (2014) 18419.
- [41] K.L. Haas, K.J. Franz, Chem. Rev. 109 (2009) 4921.
- [42] M. Saha, P. Nandy, M. Chakraborty, P. Das, S. Das, Biophys. Chem. 236 (2018) 15.
- [43] M.J. Frisch, G.W. Trucks, H.B. Schlegel, G.E. Scuseria, M.A. Robb, J.R. Cheeseman, G. Scalmani, V. Barone, G.A. Petersson, H. Nakatsuji, X. Li, M. Caricato, A.V. Marenich, J. Bloino, B.G. Janesko, R. Gomperts, B. Mennucci, H.P. Hratchian, J.V. Ortiz, A.F. Izmaylov, J.L. Sonnenberg, D. Williams-Young, F. Ding, F. Lipparini, F.

- Egidi, J. Goings, B. Peng, A. Petrone, T. Henderson, D. Ranasinghe, V.G. Zakrzewski, J. Gao, N. Rega, G. Zheng, W. Liang, M. Hada, M. Ehara, K. Toyota, R. Fukuda, J. Hasegawa, M. Ishida, T. Nakajima, Y. Honda, O. Kitao, H. Nakai, T. Vreven, K. Throssell, J.A. Montgomery Jr., J.E. Peralta, F. Ogliaro, M.J. Bearpark, J.J. Heyd, E.N. Brothers, K.N. Kudin, V.N. Staroverov, T.A. Keith, R. Kobayashi, J. Normand, K. Raghavachari, A.P. Rendell, J.C. Burant, S.S. Iyengar, J. Tomasi, M. Cossi, J.M. Millam, M. Klene, C. Adamo, R. Cammi, J.W. Ochterski, R. L. Martin, K. Morokuma, O. Farkas, J.B. Foresman, D.J. Fox, Gaussian 09, Revision A.02, Gaussian, Inc., Wallingford CT, 2016.
- [44] (a) A.D. Becke, *Chem. Phys.* 98 (1993) 5648;  
(b) C.T. Lee, W.T. Yang, R.G. Parr, *Phys. Rev. B* 37 (1988) 785.
- [45] X.Y. Cao, M. Dolg, *J. Mol. Struct.:THEOCHEM* 581 (2002) 139.
- [46] E.K.U. Gross, W. Kohn, *Quantum Chem.* 21 (1990) 255.
- [47] M. Cossi, V. Barone, *J. Chem. Phys.* 115 (2001) 4708.
- [48] N.M. O'Boyle, A.L. Tenderholt, K.M. Langnerclib, *J. Comp. Chem.* 29 (2008) 839.
- [49] G. Scatchard, *Ann. NY Acad. Sci.* 51 (1949) 660.
- [50] H.R. Mahler, in: *Methods in Enzymology* 11, Academic Press, New York, USA, 1955, pp. 668–672.
- [51] H. Wang, J.A. Joseph, *Free Radical Biol. Med.* 27 (1999) 612.
- [52] O. Myhre, J.M. Andersen, H. Aarnes, F. Fonnum, *Biochem. Pharmacol.* 65 (2003) 1575.
- [53] A. Gomes, E. Fernandes, J.L. Lima, *J. Biochem. Biophys. Methods* 65 (2005) 45.
- [54] A. Pramanik, D. Laha, S. Chattopadhyay, S.K. Dash, S. Roy, P. Pramanik, P. Karmakar, *Toxicol. Res.* 4 (2015) 1604.
- [55] M. Dinda, U. Dasgupta, N. Singh, D. Bhattacharyya, P. Karmakar, *Phytother. Res.* 29 (2015) 607.
- [56] S. Mukherjee, P. Das, S. Das, *J. Phys. Org. Chem.* 25 (2012) 385.
- [57] K. Nakamoto, *Infrared and Raman Spectra of Inorganic and Coordination Compounds*, third ed., Wiley-Interscience, New York, USA, 1978.
- [58] M. Di Vaira, P. Orioli, F. Piccioli, B. Bruni, L. Messori, *Inorg. Chem.* 42 (2003) 3157.
- [59] S. Du, J. Feng, X. Lu, G. Wang, *Dalton Trans.* 42 (2013) 9699.
- [60] B. Trzaskowski, A. Les, L. Adamowicz, *Int. J. Mol. Sci.* 4 (2003) 503.
- [61] S. Pramanik, S. Roy, T. Ghorui, S. Ganguly, K. Pramanik, *Inorg. Chem.* 55 (2016) 1461.
- [62] R.L. Martin, *J. Chem. Phys.* 118 (2003) 4775.
- [63] (a) T. Lu, F. Chen, *J. Mol. Graph. Model.* 38 (2012) 314;  
(b) T. Lu, F. Chen, *J. Comput. Chem.* 33 (2012) 580.
- [64] R.A.G. Friedman, G.S. Manning, *Biopolymers* 23 (1984) 2671.
- [65] G.K. Schwalfenberg, *J. Environ. Pub Health* (2012), 7 pages 727630.
- [66] B.P. Mahoney, N. Raghunand, B. Baggett, R.J. Gillies, *Biochem. Pharmacol.* 66 (2003) 1207.
- [67] S. Das, A. Bhattacharya, P.C. Mandal, M.C. Rath, T. Mukherjee, *Rad. Phys. Chem.* 65 (2002) 93.
- [68] A.D.R. Nurcahyanti, M. Wink, *Peer J.* (2016), <https://doi.org/10.7717/peerj.1542>.
- [69] S.M. Noh Yonsei, *Med. J.* 44 (2003) 45.
- [70] M. Damaghi, J.W. Wojtkowiak, R.J. Gillies, *Front. Physiol.* 4 (2013) 370.



## Research article

Free radical induced activity of an anthracycline analogue and its Mn<sup>II</sup> complex on biological targets through *in situ* electrochemical generation of semiquinone

Mouli Saha, Saurabh Das\*

Department of Chemistry (Inorganic Section), Jadavpur University, Kolkata, 700032, India

## ARTICLE INFO

## Keywords:

Alizarin  
Semiquinone-radical anion  
Superoxide-radical anion  
Mn<sup>II</sup>-alizarin  
Glassy carbon electrode  
Nucleobases

## ABSTRACT

Cytotoxicity by anthracycline antibiotics is attributed to several pathways. Important among them are formation of free-radical intermediates. However, their generation makes anthracyclines cardiotoxic which is a concern on their use as anticancer agents. Hence, any change in redox behavior that address cardiotoxicity is welcome. Modulation of redox behavior raises the fear that cytotoxicity could be compromised. Regarding the generation of free radical intermediates on anthracyclines, a lot depends on the surrounding environment (oxic or anoxic), polarity and pH of the medium. In case of anthracyclines, one-electron reduction to semiquinone or two-electron reduction to quinone-dianion are crucial both for cytotoxicity and for cardiotoxic side effects. The disproportionation-comproportionation equilibria at play between quinone-dianion, free quinone and semiquinone control biological activity. Whatever is the form of reduction, semiquinones are generated as a consequence of the presence of anthracyclines and these interact with a biological target. Alizarin, a simpler anthracycline analogue and its Mn<sup>II</sup> complex were subjected to electrochemical reduction to realize what happens when anthracyclines are reduced by compounds present in cells as members of the electron transport chain. Glassy carbon electrode maintained at the pre-determined reduction potential of a compound was used for reduction of the compounds. Nucleobases and calf thymus DNA that were maintained in immediate vicinity of such radical generation were used as biological targets. Changes due to the generated species under aerated/de-aerated conditions on nucleobases and on DNA helps one to realize the process by which alizarin and its Mn<sup>II</sup> complex might affect DNA. The study reveals alizarin was more effective on nucleobases than the complex in the free radical pathway. Difference in damage caused by alizarin and the Mn<sup>II</sup> complex on DNA is comparatively less than that observed on nucleobases; the complex makes up for any inefficacy in the free radical pathway by its other attributes.

## 1. Introduction

In the present day context of cancer chemotherapy, anthracyclines are an important class of molecules used as effective anticancer agents in different forms of the disease [1, 2, 3, 4, 5, 6]. However, a disturbing aspect related to anthracyclines is their associated toxic side effects, an almost inseparable phenomenon affecting drug efficacy [4, 5, 6, 7, 8, 9, 10]. What is realized till now is that, both efficacy and toxic side effects (cardiotoxicity) involves a common intermediate [5, 7, 8, 9, 10, 11, 12]. Hence, while using anthracyclines, extreme care is necessary during drug administration, particularly in case of children, who even if cured of cancer, run the risk of living the rest of their lives with different forms of cardiac problems [7, 13, 14, 15]. In fact, during administration of most

anthracyclines, functioning of the heart of the patient is monitored continuously and if complications arise treatment is discontinued. Dose-related heart problems have been reported to occur as late as 7–10 years after treatment [4, 5, 6, 7, 8, 9, 10, 13, 14, 15].

Hence, effort is now underway to modify anthracyclines in a manner that address such toxic side effects or search for analogues having less toxicity or administer drugs in presence of compounds that help to reduce toxic side effects or bring about changes in methodology of drug administration so that some improvement is achieved. Needless to say, they are to be done without compromising efficacy [16, 17, 18, 19, 20, 21, 22, 23, 24]. However, often, in trying to achieve that, a compromise is made with drug action, which is another area of concern [10, 11, 21, 23, 24].

\* Corresponding author.

E-mail addresses: [dasrsv@yahoo.in](mailto:dasrsv@yahoo.in), [saurabh.das@jadavpuruniversity.in](mailto:saurabh.das@jadavpuruniversity.in) (S. Das).

One approach to modifying anthracyclines is through complex formation using bio-friendly metal ions [25, 26, 27]. Simpler analogues seeking to decrease the cost of such drugs have also been tried [17, 18, 19, 20, 28, 29, 30, 31, 32, 33, 34, 35]. While results vary, there are several issues before such simpler analogues could become drugs [17, 18, 19, 20, 28, 29, 30, 33, 34, 35]. Whether it be anthracyclines or its hydroxy-9,10-anthraquinone analogues, studies reveal intermediates like semiquinone radical anion [36, 37] are an important component of drug action that are either moderately or significantly decreased following complex formation [25, 26, 27, 28, 29, 30, 31, 32, 33, 34, 35]. Therefore, while complex formation could address cardiotoxic side effects, efficacy could be affected as well [28, 29, 30, 31, 32, 33, 34, 35]. In majority of cases however, it is seen that complexes are more effective (*in vitro*) than the parent molecule [26, 28, 30, 32, 33, 34, 35]. This means in case of complexes, loss in efficacy owing to decreased formation of semiquinone is compensated by other attributes of complex formation [25, 26, 28, 29, 30, 31, 32, 33, 34, 35]. Although this is widely accepted as a logical explanation on the performance of metal complexes of anthracyclines or their analogues, there are only a few studies that show a comparative investigation of anthracyclines, its analogues and their respective complexes that involve the free radical pathway. We made attempts to explore aspects related to free radical pathways of some drugs or their analogues when they are either on their own or complexed with metal ions [38, 39, 40]. For anthracyclines, accumulating evidence suggest there is *in vivo* formation of semiquinone either due to one-electron reduction or by comproportionation when they undergo two-electron reduction to form quinone-dianion [28, 33, 41, 42, 43]. The reactive intermediates that are formed, damage DNA, serving as important signal-transduction networks either promoting cell cycle arrest or causing cell death in order to repair DNA lesions [44, 45, 46, 47]. DNA damage response leads to initiation of tumor growth and a somewhat defective damage response generates genomic instability [48]. An up-regulated response of DNA damage is known to cause resistance to treatment [44, 45, 46, 47]. Redox reactions of drugs also affect response of damaged DNA since reactive oxygen species (ROS) either activate or inhibit cellular proteins/enzymes related to response in healthy or cancer cells [49]. Hence, changes in response of damaged DNA by proper modulation of ROS is of interest and has an impact on several parameters [49]. ROS affects DNA in cancer patients differently either during

progress of cancer or during treatment [50]. Through this study, we tried to identify the contribution of the free radical pathway to cell damage by an anthracycline analogue and its  $Mn^{II}$  complex.

To realize how anthracyclines or its analogues interact with DNA in the free radical pathway it is important to analyze the interactions between them [7, 8, 9, 10, 11, 12, 13, 14, 15]. Herein, investigation of such pathways is reported. The study was performed using a potentiostat as the source of electrons. *In situ* reactivity of electrochemically generated quinone di-anion or semiquinone formed either on alizarin or its  $Mn^{II}$  complex with different nucleobases and calf thymus DNA that were maintained in the immediate vicinity of their generation is discussed. The study could help to realize the role of semiquinone or superoxide radical anion [51] in causing DNA damage and to see if damage is initiated through modification of nucleobases or is a consequence of aspects like DNA binding or the abstraction of hydrogen from sugar units. The study helps to realize interactions of anthracyclines or similar compounds with a biological target suggesting reasons for their efficacy [29, 30, 31, 32, 33]. As is known from previous studies, complex formation of anthracyclines lead to decreased semiquinone formation [28, 31, 32, 33, 34, 35] and hence the risk of cardiotoxicity decreases, but complexes could be at a loss regarding efficacy in the free radical pathway when compared with anthracyclines or their analogues [15, 16, 18, 20, 21, 22, 23, 34, 35, 36].

Since  $Mn^{II}$  complexes show significant SOD like activity and because  $Mn^{II}$  is able to acquire higher oxidation states in presence of peroxides that are generated as part of ROS, we wanted to see if the  $Mn^{II}$  complex would be beneficial for cell killing [52, 53]. It is reported that almost all mitochondria contain a form of Mn-SOD where Mn could be in +2 or +3 oxidation states [54]. Our complex could then be a mimic of Mn-SOD found in human mitochondria since anthracyclines, its analogues or metal ion complexes on entering cells eventually interact with the mitochondrial electron transport system to show drug action [54].

## 2. Experimental

### 2.1. Materials and methods

Alizarin was procured from Sigma and purified by re-crystallization using ethanol. The  $Mn^{II}$  complex of alizarin [ $Mn^{II}(alz)_2(H_2O)_2$ ]

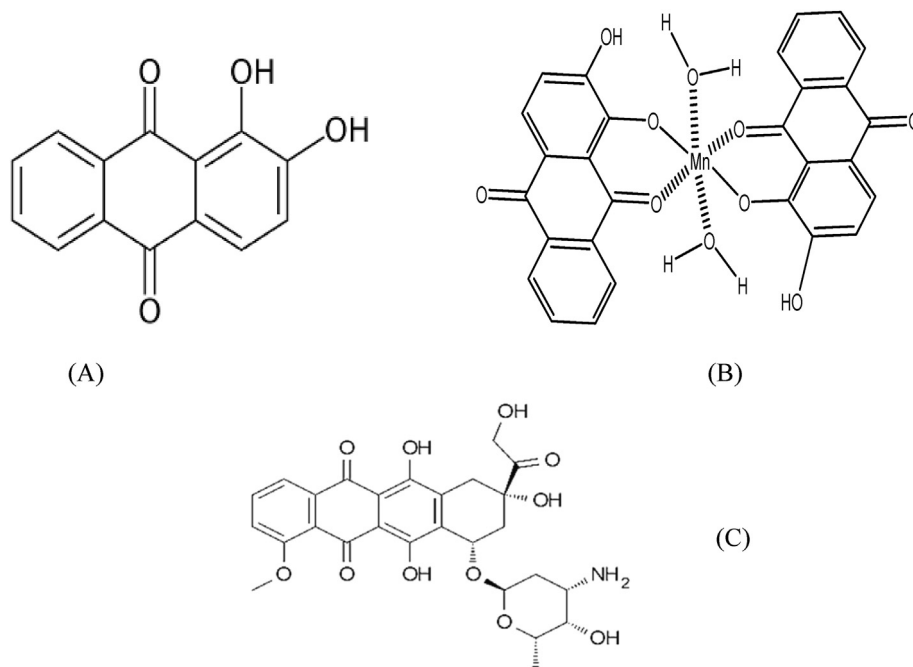


Figure 1. Structure of (A) Alizarin, (B)  $[Mn^{II}(alz)_2(H_2O)_2]$  and (C) an anthracycline anticancer drug.



(Figure 1) was prepared and characterized earlier [55]. KCl (AR), purchased from Merck India, was used as an electrolyte for electrochemical experiments in aqueous medium. Nucleobases uracil, thymine and adenine were obtained from Sisco Research Laboratories, India; cytosine was obtained from Sigma. Calf thymus DNA was obtained from Sisco Research Laboratories, India. Tetrabutyl ammonium bromide (TBAB) (AR) and Ethidium bromide (EtBr) were purchased from Merck, India. Triple distilled water was used for preparing solutions. Phosphate buffer (pH ~ 7.4) was prepared in triple distilled water using sodium dihydrogen phosphate (AR) and disodium hydrogen phosphate (AR) procured from Merck, Germany.

## 2.2. Electrochemical measurements

Electrochemical experiments on alizarin and its  $Mn^{II}$  complex were carried out in an air-tight 50 ml electrochemical cell. Voltammograms were obtained on a Metrohm–Autolab model PGSTAT 101 potentiostat. Analysis of data was done using NOVA 1.10.1.9 program. A conventional three-electrode system, glassy carbon as the working electrode, platinum wire as the counter electrode and Ag/AgCl, satd. KCl as the reference electrode were used.

Before each electrochemical experiment, solutions were degassed for ~30 min using high purity argon. Reduction of the quinone moiety in compounds was followed in aqueous, aqueous-dimethyl formamide (DMF) and in pure DMF using cyclic voltammetry. In DMF, a two step one-electron reduction (first to semiquinone and then to quinone dianion) was observed [41, 42]. With increase in percentage of water, two reduction peaks approach each other and a single step two electron reduction occurs [56, 57]. Quinone-dianion and free quinone upon comproportionation form semiquinone radical anion that undergoes disproportionation as well [28, 33, 41, 42, 43, 58, 59, 60]. This was again verified as a part of this study. Voltammograms were analyzed by the Randles-Sevcik equation [Eq. 1, Figure 2A and B] to check that the process was diffusion controlled, which was extremely essential for experiments related to this study [61, 62].

$$i_{pc} = (2.69 \times 10^5) \cdot n^{3/2} \cdot D_0^{1/2} \cdot A \cdot C \cdot \nu^{1/2} \quad (1)$$

$i_{pc}$  refers to current in amperes at the cathodic peak potential,  $n$ , the total number of electrons,  $D_0$ , diffusion coefficient of species,  $A$ , area of the electrode in  $cm^2$ ,  $C$ , concentration of compounds in moles/ $cm^3$  and  $\nu$ , scan rate in  $Vs^{-1}$ . Figure 3 is a typical voltammogram of alizarin in aqueous solution from where its reduction potential (-0.65V) was obtained. Under exactly similar conditions, reduction potential of  $Mn^{II}$  complex (-0.75 V) was ascertained.

These reduction potentials were subsequently used for reducing the compounds using the same glassy carbon electrode, by maintaining

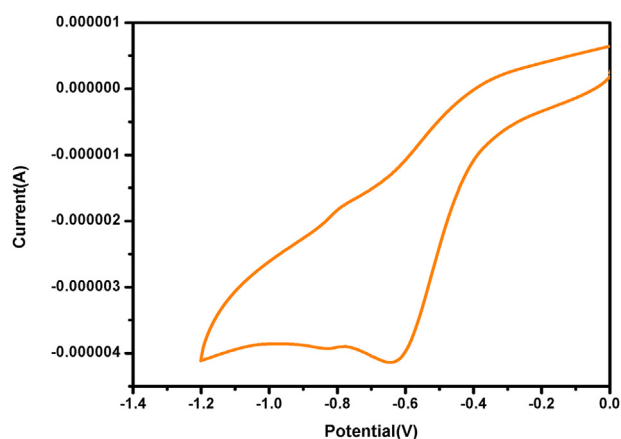


**Figure 3.** Cyclic voltammogram of 0.01 mM alizarin at pH ~ 7.4 showing single step two electron reduction of the quinone in aqueous solution containing 0.12 M KCl on a glassy carbon electrode (surface area 0.1256  $cm^2$ ); Scan rate 100 mV/s.

either a nucleobase (one at a time) or double stranded calf thymus DNA in the vicinity of the reduced products, under aerated/de-aerated (Ar saturated) conditions at constant pH (~7.4). Since biological targets were present in the immediate vicinity of *in situ* electrochemically generated quinone-dianion or semiquinone they get an opportunity to interact with reduced species. In aerated medium, there is a possibility for the formation of superoxide radical anion and that here the  $Mn^{II}$  complex could show SOD activity [53]. The time for *in situ* electrochemical generation of species was kept a constant so that similar charge was made available to each compound in all the sets of the experiment and that there is similar experimental error associated with the stimuli (here, the potentiostat) that helps to generate the reactive species. Constancy of charge transferred to compounds was checked by chrono-amperometry. This enabled a proper comparison of results obtained the following interaction of species (radical anions or radicals) generated in solution with a target maintained in the vicinity of such generation [38, 39, 40]. A semiquinone radical anion or protonated semiquinone under de-aerated condition or superoxide radical-anion alongwith the semiquinone radical anion (under aerated condition) interact with nucleobases or DNA, that was maintained in the electrochemical cell (Figure 4). In case of control experiments, no compound was used but respective potentials (i.e. -0.65 V for alizarin and -0.75 V for the complex) were applied using the same glassy carbon electrode with either a chosen nucleobase or calf thymus DNA in solution. Needless to say, all potentials were maintained and applied accurately since this

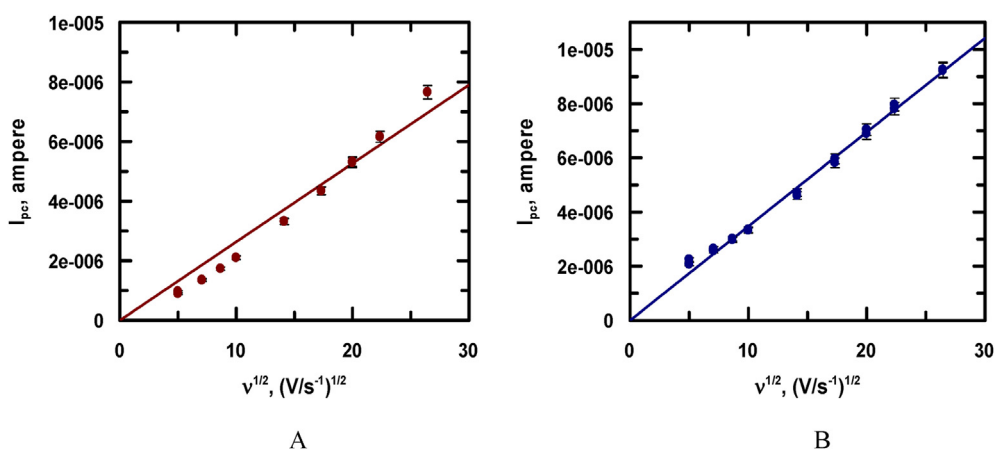


**Figure 2.** Plot of cathodic peak current ( $I_{pc}$ ) vs. square root of scan rate ( $\nu$ ) for two-electron reduction of alizarin (A) and  $Mn(II)$ -alizarin complex (B) in aqueous solution at a potential of -0.65 V and -0.75 V respectively at pH ~ 7.4.

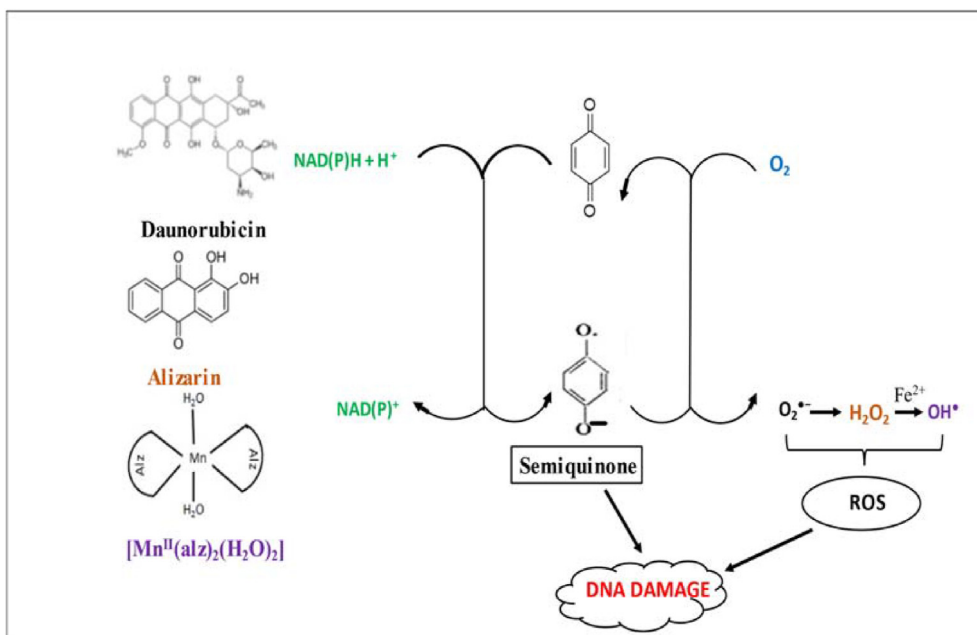


Figure 4. A scheme showing the basis for this study.

formed the basis of our experiments [38, 39, 40]. Concentration of nucleobases present in solution was approximately ten times that of the compounds used. pH was maintained at 7.4 with the help of phosphate buffer.

Aliquots were taken from an experimental solution, following the application of a constant pre-determined potential for a definite period of time, during which each nucleobase was subjected to interaction with *in situ* electrochemically generated species in solution. Then, HPLC was performed using a C-18 column as the stationary phase and 5 % aqueous-methanol as the mobile phase. From HPLC chromatograms, amount of each nucleobase remaining unaltered, was calculated. Control experiments were performed for each set (aerated or de-aerated) and for all targets using the same glassy carbon electrode maintained for the same time in solutions containing same amount of nucleobases but in the absence of a compound.

In experiments, where calf thymus DNA was the target, aliquots were taken from the reaction vessel and treated with EtBr. The DNA-EtBr adduct was excited at 510 nm and fluorescence was recorded at 602 nm [63, 64, 65]. From the loss in fluorescence of the DNA-EtBr adduct, amount of calf thymus DNA that underwent modification following interaction with the radicals generated under aerated and de-aerated (Ar saturated) conditions was ascertained [63]. For control experiments with DNA, the solution contained the same amount of calf thymus DNA but no compound. Solutions were subjected to a constant potential of -0.65 V to serve as the control for alizarin and at -0.75 V to serve as control for the complex using the same glassy carbon electrode for similar times. Aliquots from these solutions were subsequently treated with similar concentrations of EtBr and fluorescence was recorded at 602 nm.

### 3. Results and discussion

#### 3.1. Interaction of electrochemically generated species with nucleobases

After interaction of semiquinone radical anions and/or protonated semiquinones under de-aerated condition or superoxide radical anions or semiquinone radical anions in aerated medium (pH ~7.4), aliquots collected from experimental solutions were subjected to HPLC to ascertain the amount of nucleobases remaining (Figure 5).

Damage caused to each nucleobase was plotted against time for which the electrochemical generation of species was attempted. Figures 6 (A), 4 (B), 4 (C) and 4 (D) are plots showing degradation of uracil, thymine, cytosine and adenine respectively in the absence and presence of compounds under similar experimental conditions. Slopes of degradation plots are an estimate of the amount of damage caused to each nucleobase under different conditions. Different extents of base damage were observed under different conditions that indicate selectivity owing to the type and the amount of radicals generated. Extent of damage depends on the ability of species formed in solution to interact with a target (Figure 6, Table 1).

Table 1 shows in the absence of alizarin or its Mn<sup>II</sup> complex, if glassy carbon electrode was held at constant potentials of -0.65 V and -0.75 V respectively, there was no significant damage on any nucleobase. However, when a compound was present, application of a constant potential (-0.65 V for alizarin or -0.75 V for Mn<sup>II</sup> complex) caused damage to nucleobases suggesting free radicals formed on a compound react with a target maintained in the vicinity of their generation. Extent of base damage was different for different targets and for different conditions suggesting selectivity of radicals during interaction. Base damage in Table 1 is expressed as EER, where EER denotes the electrochemical enhancement ratio, calculated by dividing the slope of any degradation plot achieved for a certain nucleobase in the presence of a compound under a specified condition by the slope obtained for the damage of the same nucleobase in the absence of that compound under aerated condition. The value of the slope for the plot obtained under aerated condition in the absence of a compound was considered fundamental since for these experiments when potential was held constant either at -0.65 V or -0.75 V there would be reduction of molecular oxygen to different species that might also interact with nucleobases; hence damage achieved over and above that value was considered.

In the presence of alizarin, damage on cytosine in the absence of O<sub>2</sub> (de-aerated condition) was maximum, significantly higher than on any other nucleobase used. For the complex however, damage caused to thymine under de-aerated condition was the highest. Barring the result on thymine in presence of alizarin (EER = 1.61), in aerated medium, no other nucleobase showed such significant damage under these conditions. An interesting aspect is that the Mn<sup>II</sup> complex was less effective in

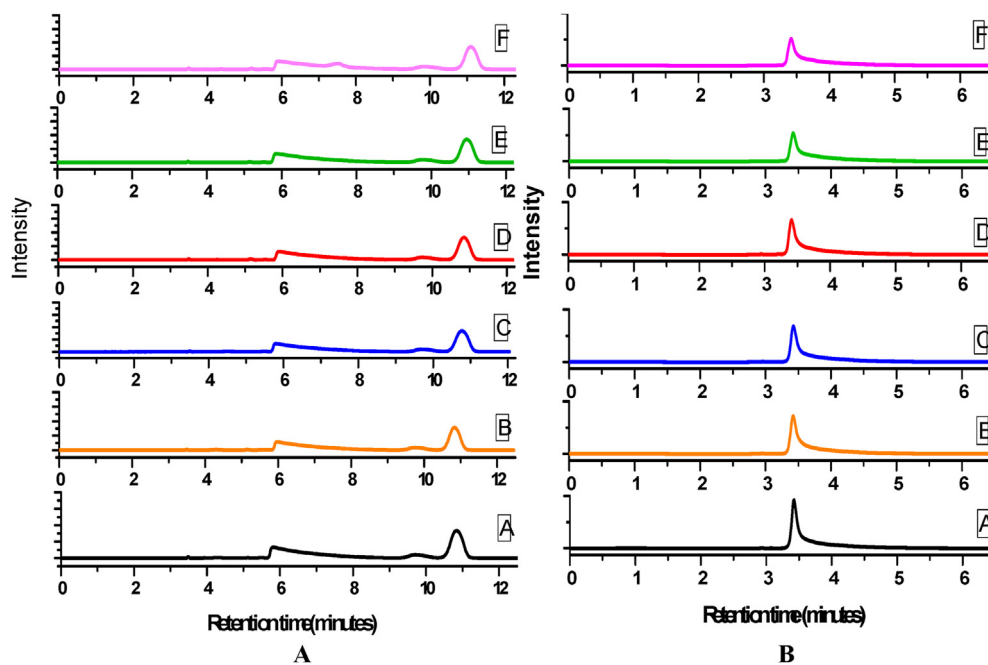


**Figure 5.** HPLC chromatograms obtained at 254 nm for  $1 \times 10^{-3}$  mol dm $^{-3}$  of (A) thymine, (B) cytosine solutions that were subjected to a constant potential of -0.65 V in the presence of  $1 \times 10^{-5}$  mol dm $^{-3}$  alizarin under de-aerated (Ar saturated) conditions. A to F indicates time in minutes for which such constant potential was applied to the solution; A: 0 min, B: 2 min, C: 4 min, D: 6 min, E: 8 min, F: 10 min.

the free radical pathway, a fact discussed in previous reports with regard to efficacy of complexes prepared, using anthracyclines, or with hydroxy-9,10-anthraquinones, owing to decrease in semiquinone formation [28, 34, 35]. It has been mentioned earlier on different occasions that complexes of anthracyclines or of their analogues are at a disadvantage with regard to activity in the free radical pathway [28, 34, 35] but very few studies have shown it by working on this aspect exclusively. Decrease in activity observed for the Mn<sup>II</sup> complex in the free radical pathway in comparison to alizarin is expected, since reports on anthracyclines and on its analogues indicate decreased generation of semiquinone by the complexes [28, 31, 32, 33, 34, 35].

In this study, using alizarin, and its Mn<sup>II</sup> complex, this got manifested by way of a maximum difference in damage observed for adenine and minimum for thymine suggesting under conditions of similar electrochemical generation of intermediates, there is either a difference in generation of intermediates on each compound or in their tendency to interact in the free radical pathway. If this isn't true, then base damage should have been similar. Table 1 indicates a difference in reactivity of the two compounds on different targets under identical conditions suggesting compounds might affect different types of DNA differently. Therefore, the general apprehension, that a complex prepared with anthracyclines, or with its analogues, compromise on aspects related to cytotoxicity in the free radical pathway, is true to a considerable extent. Yet, complexes of anthracyclines or of its analogues are prepared because they modulate the generation of semiquinone helping to decrease cardiotoxicity [28, 31, 32, 33, 34, 35]. In a previous study, we compared the performance of a Cu<sup>II</sup> and a Mn<sup>II</sup> complex of emodin against that of emodin itself, under similar experimental conditions and found that the emodin-Mn<sup>II</sup> complex was almost similar in activity to emodin [39]. The Cu<sup>II</sup> complex, performed much better, attributed to the presence of a stable lower oxidation state (Cu<sup>I</sup>) enabling Cu<sup>II</sup> complexes to participate in Fenton reactions generating ·OH, that in turn enhance modification of nucleobases [36, 37, 39, 40, 64, 65]. In that study, base damage due to Cu<sup>II</sup>-emodin was higher in aerated medium than in de-aerated medium [39].

From the EER values in Table 1, on the performance of a compound on nucleobases it might become possible to predict the damage that a compound might cause on a particular DNA whose base composition is

known. In fact, this aspect could have been an important outcome of this study itself. However, the difficulty in correlating nucleobase damage to that observed in case of calf thymus DNA lay in the fact we could not generate the data where guanine was a possible target. This was because preparing an aqueous solution of guanine having similar concentration as that of the others was difficult owing to its poor solubility in buffer.

Using the information from a previous study that was performed by our group with a dimeric Cu(II) complex of tinidazole, where base degradation was followed using  $\gamma$  radiation, products formed in this study were identified [66]. Products were characterized following the degradation of thymine, cytosine and uracil [66]. Since HPLC profiles of degraded products of thymine were saved as method files in our system as a part of that study [66], they were utilised for this one to identify products related to degradation of thymine, cytosine and uracil in the absence and presence of alizarin and its Mn<sup>II</sup> complex. Results indicate in presence of alizarin and its Mn<sup>II</sup> complex, 5,6-dihydroxy-5,6-dihydrothymine (thymine glycol) and 5-hydroxymethyl uracil were formed when thymine was the target, although amounts were extremely small as the charge provided at constant potential was not very high. The peak for 5,6-dihydrothymine was not detected even when thymine was subjected to an electrochemical generation of intermediates using compounds (alizarin and Mn<sup>II</sup> complex) at longer times. Products were identified based on retention times using authentic samples [66].

Cytosine differs from uracil at the fourth position (carbon) of the pyrimidine ring where there is an -NH<sub>2</sub> instead of -OH (if enol form of uracil be considered). Since 5,6-dihydroxy-5,6-dihydrocytosine (cytosine glycol) is unstable and converts to 5,6-dihydroxy-5,6-dihydrouracil (uracil glycol) by deamination [67], we used our existing HPLC method files on uracil to identify degraded products when cytosine or uracil were maintained as targets during experiments performed as a part of this study [67]; however peaks for the degraded products were very small. Observations suggest pyrimidine based nucleobases experience an initial free-radical attack by species generated as a consequence of the application of current at a constant potential on the C<sub>5</sub>-C<sub>6</sub> double bond [66, 67]. For the nucleobase adenine, HPLC chromatograms did not show any new peak in the time frame of the application of constant potential.

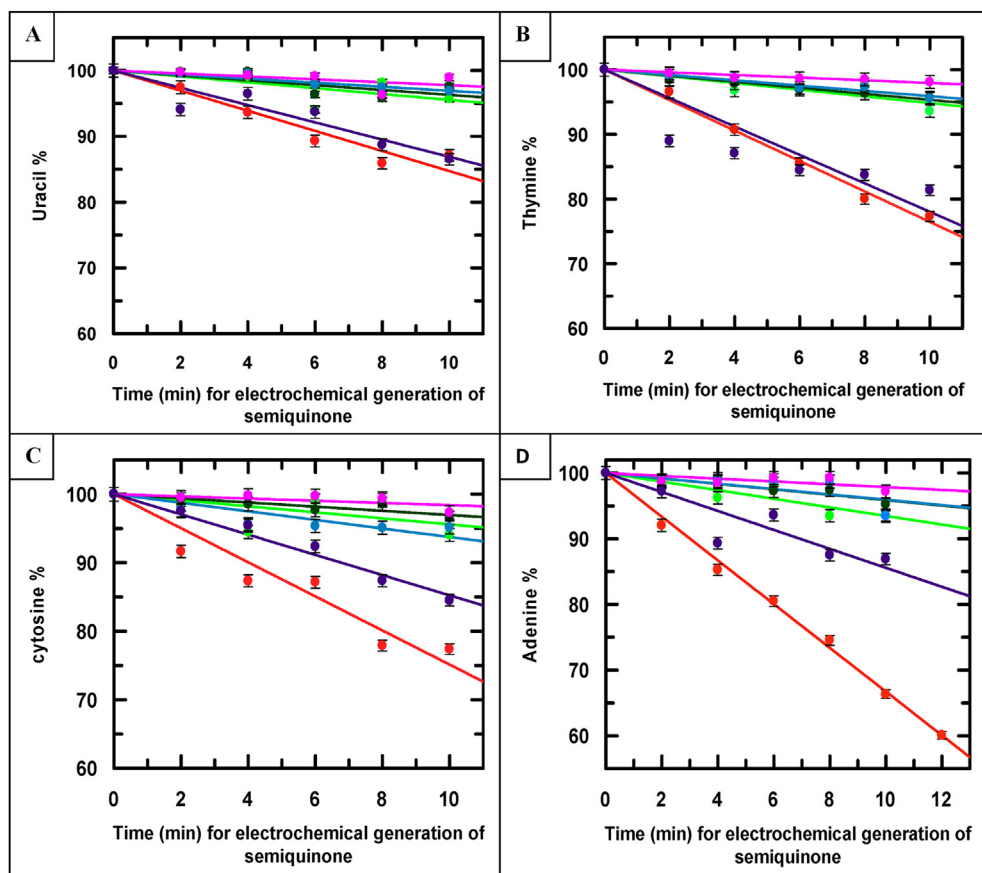


**Figure 6.** Plots shown in (A), (B), (C) and (D) indicate percentage of uracil, thymine, cytosine and adenine remaining following interaction of *in situ* electrochemically generated species on alizarin and its  $Mn^{II}$  complex. Different experimental conditions were: nucleobase alone in absence of  $O_2$  (black circles); nucleobase alone in presence of  $O_2$  (green circles); nucleobase in presence of alizarin but absence of  $O_2$  (red circles); nucleobase in presence of alizarin and presence of  $O_2$  (blue circles); nucleobase in presence of  $Mn^{II}(alz)_2(H_2O)_2$  but absence of  $O_2$  (magenta circles); nucleobase in presence of  $Mn^{II}(alz)_2(H_2O)_2$  and presence of  $O_2$  (pink circles).

**Table 1.** Degradation of nucleobases due to electrochemically generated species (semiquinone or quinone dianion or oxygen based radicals) followed by HPLC.

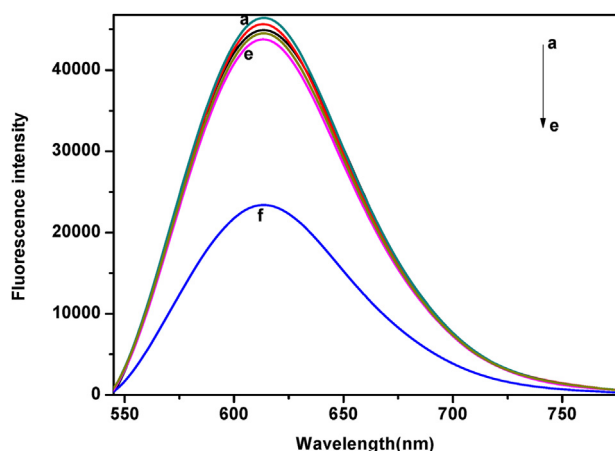
Compound	Target																	
	Uracil		Thymine		Cytosine		Adenine		Calf thymus DNA									
	Slope of plot in aerated Medium	EER	Slope of plot in de-aerated medium	EER	Slope of plot in aerated medium	EER	Slope of plot in de-aerated medium	EER	Slope of plot in aerated medium	EER	Slope of plot in de-aerated medium	EER	Slope of plot in aerated medium	EER	Slope of plot in de-aerated medium	EER		
–	-0.46	–	-0.37	–	-0.52	–	-0.48	–	-0.41	–	-0.30	–	-0.78	–	-0.42	–	-0.045	–
Alizarin	-0.36	–	-1.61	3.50	-0.41	–	-2.37	4.56	-0.66	1.61	-2.35	5.73	-0.46	–	-3.15	4.03	-0.16	3.55
$Mn^{II}$ complex of Alizarin	-0.28	–	-1.31	2.85	-0.22	–	-2.23	4.29	-0.24	–	-1.49	3.63	-0.31	–	-1.48	1.90	-0.10	2.22

### 3.2. Interaction of electrochemically generated species with calf thymus DNA

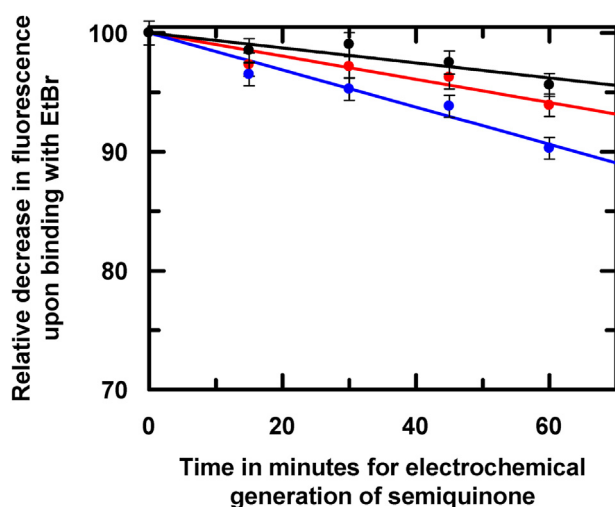
In experiments with calf thymus DNA, samples had similar concentrations as that for studies with nucleobases, subjected to interaction with *in situ* electrochemically generated species and other products formed thereof at different time intervals. Double strand modification was ascertained by the change in fluorescence of the DNA-EtBr adduct, considered a measure of the extent of modification caused to DNA by free radicals (Figure 7) [63–65].

Figure 8 shows the amount of DNA remaining intact following interaction with intermediates (semiquinone/protonated semiquinone, superoxide radical anion/its protonated form, quinone dianion and its corresponding protonated forms etc.) at pH 7.4. Using Figure 8, it may be said double strand modification of DNA was higher for alizarin than for

$[Mn^{II}(alz)_2(H_2O)_2]$ . Interestingly, the data shown in Figure 8 has the same trend as that of interaction of species (generated electrochemically) with the four nucleobases. It was reported earlier DNA and oligonucleotides tend to stabilize semiquinone radical anions through delocalization of electrons in a  $\pi$ -stacking framework, that result in a radical intercalated situation rather than forming covalent bonds [43]. This was further supported by some semi-empirical calculations showing there is a gain in energy by  $\sim 9.8 \text{ kcal mol}^{-1}$  [43]. Insertion of semiquinone radical anions into a DNA strand was reported and believed to result in DNA strand breaks leading to disruption in DNA replication or activate radical mediated reactions. pH as expected, was reported to shift the equilibrium of dianions of hydroquinones, thereby having an influence on the formation of semiquinone radical anion which in turn influences interactions with DNA [43, 54]. The fact that our results show modification of nucleobases only adds to previous information following intercalation



**Figure 7.** Fluorescence spectra of  $1 \times 10^{-3}$  mol  $\text{dm}^{-3}$  calf thymus DNA after treatment with EtBr following interaction with the products generated on the Mn(II) complex of alizarin that was subjected to reduction at constant potential (-0.75 V) in de-aerated (Argon saturated) conditions.  $[\text{Mn}^{\text{II}}(\text{alz})_2(\text{H}_2\text{O})_2] = 3 \times 10^{-5}$  mol  $\text{dm}^{-3}$ . "a" to "e" indicates time in minutes for which the potential was applied to the solution; a: 0 min, b: 15 min, c: 30 min, d: 45 min, e: 60 min "f" denotes the spectrum of EtBr when it was excited alone i.e. in the absence of DNA at 510 nm.



**Figure 8.** Plots obtained for semiquinone radical anion induced modification of calf thymus DNA in the absence and presence of alizarin and the Mn<sup>II</sup> complex in an argon saturated medium at pH 7.4; in absence of a compound (black circles); in the presence of alizarin (blue circles) and  $[\text{Mn}^{\text{II}}(\text{alz})_2(\text{H}_2\text{O})_2]$  (red circles).

leading to unwinding of DNA, the exposed nucleobases become vulnerable to further damage that might permanently prevent them from regenerating the double strands again, should a favourable situation arise.

Another interesting aspect of the study is that the difference between damage caused to DNA by species generated on alizarin and on  $[\text{Mn}^{\text{II}}(\text{alz})_2(\text{H}_2\text{O})_2]$  was not as large as that observed for nucleobases. This suggests in case of DNA, some attribute of complex formation comes into play causing substantial modification to DNA by other pathways that are also detected by the loss of fluorescence due to the formation of the DNA-EtBr adduct. Therefore, excess modification due to a greater amount of free radicals formed on alizarin over that formed on the complex (the gap) is somewhat realized. Besides, Mn<sup>II</sup> having stable higher oxidation states might get oxidized by ROS, by substances like  $\text{H}_2\text{O}_2$  (if formed in the medium) to generate transient Mn<sup>III</sup> that could then show its oxidative role [52, 53], leading to a damage of DNA that

would also be detected by the EtBr-DNA fluorescence technique that we used. Therefore, although formation of semiquinone on alizarin is greater than that formed on the complex as realized from damage caused to nucleobases (Table 1), other aspects related to complex formation might bridge the gap between the performance of alizarin and its Mn<sup>II</sup> complex on calf thymus DNA. Although binding of the complex to calf thymus DNA is better than alizarin [55], here it was probably not a major contributor towards any significant damage to DNA as one would have expected because in this study the concentration of the compounds were 0.03 mM (i. e. almost 100 times less than the concentration of DNA used) [65]. Therefore, although Mn<sup>II</sup>-alizarin has a strong affinity for DNA, in case of this study there should not be much of an influence due to its binding to DNA [55] since the concentration of compounds used were too small compared to the substrate. Since the technique of decreasing fluorescence of a DNA-EtBr adduct detects double strand modification in general (i.e. however it may be caused), all modifications are actually detected [63, 64, 65]. Thus this technique provides overall double strand modification i.e. caused by the action of free radicals as well as by other pathways [63, 64, 65]. Hence, for the study with calf thymus DNA, a "leveling effect" might have been observed in case of the interaction of the compounds, following an *in situ* electrochemical generation of reactive species under the conditions of the experiment (Figure 8, Table 1). Even then, alizarin was better than the complex indicating the extent of compromise complexes of this class of compounds make in the free radical pathway.

#### 4. Conclusion

The study demonstrates the manner in which nucleobases that constitute DNA might be affected by semiquinone-radical anion and other species generated in solution following the reduction of alizarin (an anthracycline analogue) and its Mn<sup>II</sup> complex. It clearly demonstrates each compound's ability to initiate radical induced damage on different nucleobases, considered a significant pathway by which anthracyclines and its analogues (emodin or carminic acid) show cytotoxic activity on cancer cells [17, 18, 19, 20, 33]. The study provides evidence why complex formation of anthracyclines or its analogues, although beneficial with regard to decrease in cardiotoxic side effects, compromise with cytotoxicity in the free radical pathway. The study shows electrochemically generated species on alizarin are able to cause greater damage to nucleobases than those that are generated on the complex. In case of calf thymus DNA, results indicate a better performance by alizarin than by the complex, however the difference in performance is not as large as that observed for the nucleobases. This indicates the complex is able to make up lost ground substantially owing to several attributes of complex formation like being able to derive the benefits of the redox behavior of Mn<sup>II</sup>. The study is also able to explain the performance of various hydroxy-9,10-anthraquinones and their metal complexes on different cancer cells and on normal cells [28, 29, 30, 31, 32, 33, 34, 35].

#### Declarations

##### Author contribution statement

Mouli Saha: Performed the experiments; Analyzed and interpreted the data.

Saurabh Das: Conceived and designed the experiments; Analyzed and interpreted the data; Contributed reagents, materials, analysis tools or data; Wrote the paper.

##### Funding statement

Mouli Saha was supported by Rajiv Gandhi National Fellowship from UGC, New Delhi; Saurabh Das was supported by UGC-DAE-CSR

Collaborative Research Scheme (UGC-DAE-CSR-KC/CRS/1 9/RC11/0985), RUSA 2.0 program of the Government of India operating at Jadavpur University "Research in Sustainable Development" (Sanction Ref. no. R-11/438/19 dated 30.05.2019), UGC, New Delhi 'Advanced Materials' as part of UPE II to Jadavpur University, "DST-PURSE" program of the Government of India, Department of Chemistry, Jadavpur University, "UGC-CAS II" program at the Department of Chemistry, Jadavpur University.

#### Data availability statement

Data included in article/supplementary material/referenced in article.

#### Declaration of interests statement

The authors declare no conflict of interest.

#### Additional information

No additional information is available for this paper.

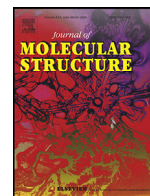
#### References

- G.N. Hortobágyi, Anthracyclines in the treatment of cancer an overview, *Drugs* 54 (1997) 1–7.
- A.J.M. Ferreri, E. Campo, A. Ambrosetti, F. Ilariucci, J.F. Seymour, R. Willemze, G. Arrighi, G. Rossi, A. Lopez–Guillermo, E. Berti, M. Eriksson, M. Federico, S. Cortelazzo, S. Govi, N. Frungillo, S. Dell’Oro, M. Lestani, S. Asioli, E. Pedrinis, M. Ungari, T. Motta, R. Rossi, T. Artusi, P. Iuzzolino, E. Zucca, F. Cavalli, M. Ponzoni, Anthracycline-based chemotherapy as primary treatment for intravascular lymphoma, *Ann. Oncol.* 15 (2004) 1215–1221.
- D. Robson, S. Verma, Anthracyclines in early-stage breast cancer: is it the end of an era? *Oncol.* 14 (2009) 950–958.
- L.A. Smith, V.R. Cornelius, C.J. Plummer, Cardiotoxicity of anthracycline agents for the treatment of cancer: systematic review and meta-analysis of randomised controlled trials, *BMC Canc.* 10 (2010) 337.
- M. Xing, F. Yan, S. Yu, P. Shen, Efficacy and cardiotoxicity of liposomal doxorubicin-based chemotherapy in advanced breast cancer: a meta-analysis of ten randomized controlled trials, *PLoS One* 10 (2015), e0133569.
- F. Marano, R. Frairia, L. Rinella, M. Argenziano, B. Bussolati, C. Grange, R. Mastrocola, I. Castellano, L. Berta, R. Cavalli, M.G. Catalano, Combining doxorubicin-nanobubbles and shockwaves for anaplastic thyroid cancer treatment: preclinical study in a xenograft mouse model, *Endocr. Relat. Canc.* 24 (2017) 275–286.
- E.V. Barry, S.E. Lipshultz, S.E. Sallan, Anthracycline-induced cardiotoxicity: natural history, risk factors, and prevention, in: R. Govindan By (Ed.), *American Society of Clinical Oncology 2008 Educational Book*, American Society of Clinical Oncology, Alexandria, 2008, p. 448.
- G. Curigliano, D. Cardinale, T. Suter, G. Plataniotis, E. deAzambuja, M.T. Sandri, C. Cristicciello, A. Goldhirsch, C. Cipolla, F. Roila, On behalf of the ESMO guidelines working group, *Ann. Oncol.* 23 (2012) vii155–vii166.
- J.V. McGowan, R. Chung, A. Maulik, I. Piotrowska, J.M. Walker, D.M. Yellon, Anthracycline chemotherapy and cardiotoxicity, *Cardiovasc. Drugs Ther.* 31 (2017) 63–75.
- E. Gammella, F. Maccarinelli, P. Buratti, S. Recalcati, G. Cairo, The role of iron in anthracycline cardiotoxicity, *Front. Pharmacol.* 5 (2014) 25.
- D.W. Edwardson, R. Narendrula, S. Chewchuk, K. Mispel-Beyer, J.P.J. Mapletoft, A.M. Parissenti, Role of drug metabolism in the cytotoxicity and clinical efficacy of anthracyclines, *Curr. Drug Metabol.* 16 (2015) 412–426.
- C.G. Nebigil, L. Désaubry, Updates in anthracycline-mediated cardiotoxicity, *Front. Pharmacol.* 9 (2018) 1262.
- X. Han, Y. Zhou, W. Liu, Precision cardio-oncology: understanding the cardiotoxicity of cancer therapy, *NPJ Prec. Oncol.* 1 (2017) 31.
- S.E. Lipshultz, J.A. Alvarez, R.E. Scully, Anthracycline associated cardiotoxicity in survivors of childhood cancer, *Heart* 4 (2008) 525–533.
- D. Harake, V.I. Franco, J.M. Henkel, T.L. Miller, S.E. Lipshultz, Cardiotoxicity in childhood cancer survivors: strategies for prevention and management, *Future Cardiol.* 8 (2012).
- J.-M. Nabholz, A. Riva, Taxane/anthracycline combinations: setting a new standard in breast cancer? *Oncol.* 6 (2001) 5–12.
- Y. Sun, Chemosensitization by emodin, a plant-derived anti-cancer agent: mechanism of action, *Canc. Biol. Ther.* 7 (2008) 476–478.
- X. Huang, J. Wang, C. Huang, Y. Chen, G. Shi, Q. Hu, J. Yi, Emodin enhances cytotoxicity of chemotherapeutic drugs in prostate cancer cells: the mechanisms involve ROS-mediated suppression of multidrug resistance and hypoxia inducible factor-1, *Canc. Biol. Ther.* 7 (2008) 468–475.
- S.-C. Hsu, J.-G. Chung, Anticancer potential of emodin, *Biomedicine* 2 (2012) 108–116.
- W.-T. Wei, S.-Z. Lin, D.-L. Liu, Z.-H. Wang, The distinct mechanisms of the antitumor activity of emodin in different types of cancer (Review), *Oncol. Rep.* 30 (2013) 2555–2562.
- K. Rygiel, Benefits of antihypertensive medications for anthracycline- and trastuzumab-induced cardiotoxicity in patients with breast cancer: insights from recent clinical trials, *Ind. J. Pharmacol.* 48 (2016) 490–497.
- Y. Kwon, Mechanism-based management for mucositis: option for treating side effects without compromising the efficacy of cancer therapy, *OncoTargets Ther.* 9 (2016) 2007–2016.
- C. Henninger, G. Fritz, Statins in anthracycline-induced cardiotoxicity: Rac and Rho, and the heartbreakers, *Cell Death Dis.* 8 (2018), e2564.
- R.S. Cvetković, L.J. Scott, Dexrazoxane: a review of its use for cardioprotection during anthracycline chemotherapy, *Drugs* 65 (2005) 1005–1024.
- A. Jabłonska–Trypuc, G. Swiderski, R. Kretowski, W. Lewandowski, Newly synthesized doxorubicin complexes with selected metals—synthesis, structure and anti-breast cancer activity, *Molecules* 22 (2017) 1106.
- H. Mizutani, A. Nishimoto, S. Hotta, K. Ikemura, M. Imai, D. Miyazawa, K. Ohta, Y. Ikeda, T. Maeda, M. Yoshikawa, Y. Hiraku, S. Kawanishi, Oxidative DNA damage induced by pirarubicin, an anthracycline anticancer agent, in the presence of Copper(II), *Anticancer Res.* 38 (2018) 2643–2648.
- K.D. Mjos, J.F. Cawthray, G. Jamieson, J.A. Fox, C. Orvig, Iron(iii)-binding of the anticancer agents doxorubicin and vosaroxin, *Dalton Trans.* 44 (2015) 2348–2358.
- P. Das, C.K. Jain, S.K. Dey, R. Saha, A.D. Chowdhury, S. Roychoudhury, S. Kumar, H.K. Majumder, S. Das, Synthesis, crystal structure, DNA interaction and *in vitro* anticancer activity of a Cu(ii) complex of purpurin: dual poison for human DNA topoisomerase I and II, *RSC Adv.* 4 (2014) 59344–59357.
- S. Mukherjee, P.K. Gopal, S. Paul, S. Das, Acetylation of 1,2,5,8-tetrahydroxy-9,10-antraquinone improves binding to DNA and shows enhanced superoxide formation that explains better cytotoxicity on JURKAT T lymphocyte cells, *J. Anal. Oncol.* 3 (2014) 122–129.
- P. Das, D. Bhattacharya, P. Karmakar, S. Das, Influence of ionic strength on the interaction of THA and its Cu(ii) complex with DNA helps to explain studies on various breast cancer cells, *RSC Adv.* 5 (2015) 73099–73111.
- S. Roy, P. Mondal, P.S. Sengupta, D. Dhak, R.C. Santra, S. Das, P.S. Guin, Spectroscopic, computational and electrochemical studies on the formation of the copper complex of 1-amino-4-hydroxy-9,10-antraquinone and effect of it on superoxide formation by NADH dehydrogenase, *Dalton Trans.* 44 (2015) 5428–5440.
- B. Mandal, S. Singha, S.K. Dey, S. Mazumdar, T.K. Mondal, P. Karmakar, S. Kumar, S. Das, Synthesis, crystal structure from PXRD of a Mn<sup>II</sup>(purp)<sub>2</sub> complex, interaction with DNA at different temperatures and pH and lack of stimulated ROS formation by the complex, *RSC Adv.* 6 (2016) 51520–51532.
- P. Das, C.K. Jain, S. Roychoudhury, H.K. Majumder, S. Das, Design, Synthesis and *in vitro* anticancer activity of a Cu(II) complex of Carminic Acid: a novel small molecule inhibitor of human DNA topoisomerase I and topoisomerase II, *ChemistrySelect* 1 (2016) 6623–6631.
- B. Mandal, S. Singha, S.K. Dey, S. Mazumdar, S. Kumar, P. Karmakar, S. Das, CuII complex of emodin with improved anticancer activity as demonstrated by its performance on HeLa and Hep G2 cells, *RSC Adv.* 7 (2017) 41403–41418.
- S. Mukherjee–Chatterjee, C.K. Jain, S. Singha, P. Das, S. Roychoudhury, H.K. Majumder, S. Das, Activity of Co<sup>II</sup>-Quinalizarin: a novel analogue of anthracycline-based anticancer agents targets human DNA topoisomerase, whereas quinalizarin itself acts via formation of semiquinone on acute lymphoblastic leukemia MOLT-4 and HCT 116 cells, *ACS Omega* 3 (2018) 10255–10266.
- J. Butler, B.M. Hoey, A.J. Swallow, Reactions of the semiquinone free radicals of anti-tumour agents with oxygen and iron complexes, *FEBS Lett.* 182 (1985) 95–98.
- E.J. Land, T. Mukherjee, A.J. Swallow, J.M. Bruce, Possible intermediates in the action of adriamycin—a pulse radiolysis study, *Br. J. Canc.* 51 (1985) 515–523.
- P. Nandy, S. Das, Interaction of electrochemically generated reduction products of Ornidazole with nucleic acid bases and calf thymus DNA, *J. Indian Chem. Soc.* 95 (2018) 1009–1014.
- B. Mandal, H.K. Mondal, S. Das, *In situ* reactivity of electrochemically generated semiquinone on Emodin and its Cu<sup>II</sup>/Mn<sup>II</sup> complexes with pyrimidine based nucleic acid bases and calf thymus DNA: insight into free radical induced cytotoxicity of anthracyclines, *Biochem. Biophys. Res. Comm.* 515 (2019) 505–509.
- P. Nandy, S. Das, *In situ* reactivity of electrochemically generated nitro radical anion on Ornidazole and its monomeric Cu(II) complex with nucleic acid bases and calf thymus DNA *Inorg. Chim. Acta.* 501 (2020), 119267119267.
- P.S. Guin, S. Das, P.C. Mandal, Sodium 1, 4-dihydroxy-9, 10-antraquinone-2-sulphonate interacts with calf thymus DNA in a way that mimics anthracycline antibiotics: an electrochemical and spectroscopic study, *J. Phy. Org. Chem.* 23 (2010) 477–482.
- P. Das, P.S. Guin, P.C. Mandal, M. Paul, S. Paul, S. Das, Cyclic voltammetric studies of 1,2,4-trihydroxy-9,10-antraquinone, its interaction with calf thymus DNA and anti-leukemic activity on MOLT-4 cell lines: a comparison with anthracycline anticancer drugs, *J. Phy. Org. Chem.* 24 (2011) 774–785.
- O. Wangpradit, A. Rahaman, S.V.S. Mariappan, G.R. Buettner, L.W. Robertson, G. Luthé, Breaking the dogma: PCB-derived semiquinone free radicals do not form covalent adducts with DNA, GSH, and amino acids, *Environ. Sci. Pollut. Res. Int.* 23 (2016) 2138–2147.
- A. Tubbs, A. Nussenzweig, Endogenous DNA damage as a source of genomic instability in cancer, *Cell* 168 (2017) 644–656.
- W.P. Roos, A.D. Thomas, B. Kaina, DNA damage and the balance between survival and death in cancer biology, *Nat. Rev. Canc.* 16 (2016) 20–33.
- S.P. Jackson, J. Bartek, The DNA-damage response in human biology and disease, *Nature* 461 (7267) (2009) 1071–1078.

- [47] P. Strzyz, Cell thriving despite DNA damage, *Nat. Rev. Mol. Cell Biol.* 17 (2016) 396.
- [48] N.J. Curtin, DNA repair dysregulation from cancer driver to therapeutic target, *Nat. Rev. Canc.* 12 (2012) 801–817.
- [49] J.M. Floberg, L. Wang, N. Bandara, R. Rashmi, C. Mpoy, J.R. Garbow, B.E. Rogers, G.J. Patti, J.K. Schwarz, Alteration of cellular reduction potential will change  $^{64}\text{Cu}$ -ATSM signal with or without hypoxia, *J. Nucl. Med.* 61 (2020) 427–432.
- [50] M. Goldstein, M.B. Kastan, The DNA damage response: implications for tumor responses to radiation and chemotherapy, *Annu. Rev. Med.* 66 (2015) 129–143.
- [51] M. Hayyan, M.A. Hashim, I.M. AlNashif, Superoxide ion: Generation and chemical implications, *Chem. Rev.* 116 (2016) 3029–3085.
- [52] J.K. Glenn, L. Akileswaran, M.H. Gold, Mn(II) oxidation is the principal function of the extracellular Mn-peroxidase from *Phanerochaete Chrysosporium*, *Arch. Biochem. Biophys.* 251 (1986) 688–696.
- [53] T. Saha, P. Kumar, N. Sepay, D. Ganguly, K. Tiwari, K. Mukhopadhyay, S. Das, Multitargeting antibacterial activity of a synthesized  $\text{Mn}^{2+}$  complex of Curcumin on gram-positive and gram-negative bacterial strains, *ACS Omega* 5 (2020) 16342–16357.
- [54] G.E. Borgstahl, H.E. Parge, M.J. Hickey, W.F. Beyer, R.A. Hallewell, J.A. Tainer, Human mitochondrial manganese superoxide dismutase polymorphic variant Ile58Thr reduces activity by destabilizing the tetrameric interface, *Cell* 71 (1992) 107–118.
- [55] M. Saha, S. Singha, M. Chakraborty, S. Mazumdar, P. Karmakar, S. Das, Characterization of a  $\text{Mn}^{\text{II}}$  complex of alizarin suggests attributes explaining a superior anticancer activity: a comparison with anthracycline drugs, *Polyhedron* 173 (2019) 114104.
- [56] P.S. Guin, S. Das, P.C. Mandal, Electrochemical reduction of sodium 1,4-dihydroxy-9,10-anthraquinone-2-sulphonate in aqueous and aqueous dimethyl formamide mixed solvent: a cyclic voltammetric study, *Int. J. Electrochem. Sci.* 3 (2008) 1016–1028.
- [57] P.S. Guin, S. Das, P.C. Mandal, Electrochemical reduction of quinones in different media: a review, *Int. J. Electrochem.* 2011 (2011), 816202, 22.
- [58] M. Quan, D. Sanchez, M.F. Wasylkiw, D.K. Smith, Voltammetry of quinones in unbuffered aqueous solution: Reassessing the roles of proton transfer and hydrogen bonding in the aqueous electrochemistry of quinones, *J. Am. Chem. Soc.* 129 (2007) 12847–12856.
- [59] S.I. Bailey, I.M. Ritchie, A cyclic voltammetric study of the aqueous electrochemistry of some quinones, *Electrochim. Acta* 30 (1985) 3–12.
- [60] E. Laviron, Electrochemical reactions with protonations at equilibrium: Part X. The kinetics of the p-benzoquinone/hydroquinone couple on a platinum electrode, *J. Electroanal. Chem.* 164 (1984) 213–227.
- [61] J.E.B. Randles, A cathode ray polarograph. Part II.—the current-voltage curves, *Trans. Faraday Soc.* 44 (1948) 327–338.
- [62] A.J. Bard, L.R. Faulkner, *Electrochemical Methods Fundamental and Applications*, second ed., John Wiley & Sons, New York, 2001.
- [63] H.C. Birnboim, J.J. Jevcak, Fluorometric method for rapid detection of DNA strand breaks in human white blood cells produced by low doses of radiation, *Cancer Res.* 41 (1981) 1889–1892.
- [64] S. Das, A. Saha, P.C. Mandal, Radiation-induced double-strand modification in calf thymus DNA in the presence of 1, 2-dihydroxy-9, 10-anthraquinone and its Cu (II) complex, *Environ. Health Pers.* 105 (1997) 1459–1462.
- [65] S. Das, P.C. Mandal, Anthracyclines as radiosensitizers: a Cu(II) complex of a simpler analogue modifies DNA in Chinese Hamster V79 cells under low-dose  $\gamma$  radiation, *J. Radioanal. Nucl. Chem.* 299 (2014) 1665–1670.
- [66] R.C. Santra, D. Ganguly, D. Bhattacharya, P. Karmakar, A. Saha, S. Das,  $\gamma$  radiation-induced damage of nucleic acid bases, calf thymus DNA and DNA within MCF-7 breast cancer cells by  $[\text{Cu}_2(\text{OAc})_4(\text{tnz})_2]$ : a potential radiosensitizer, *New J. Chem.* 41 (2017) 11679–11685.
- [67] S. Tremblay, J.R. Wagner, Dehydration, deamination and enzymatic repair of cytosine glycols from oxidized poly(dG-dC) and poly(dI-dC), *Nucleic Acids Res.* 36 (2008) 284–293.







# A Cobalt<sup>II</sup>/Cobalt<sup>III</sup> complex of alizarin that was analyzed from the stand point of binding with DNA, for ROS generation and anticancer drug prospecting was identified as an analogue of anthracyclines

Mouli Saha<sup>a</sup>, Soumen Singha<sup>b</sup>, Deblina Ghosh<sup>c</sup>, Sanjay Kumar<sup>b</sup>, Parimal Karmakar<sup>c</sup>, Saurabh Das<sup>a,\*</sup>

<sup>a</sup> Department of Chemistry (Inorganic Section), Jadavpur University, Kolkata, 700 032, India

<sup>b</sup> Department of Physics, Jadavpur University, Kolkata, 700 032, India

<sup>c</sup> Department of Life Science & Biotechnology, Jadavpur University, Kolkata, 700 032, India

## ARTICLE INFO

### Article history:

Received 12 February 2022

Revised 2 April 2022

Accepted 4 April 2022

Available online 6 April 2022

### Keywords:

Alizarin

[Co<sup>II</sup>(alz)<sub>3</sub>]<sup>-</sup>/[Co<sup>III</sup>(alz)<sub>3</sub>]

Semiquinone

ROS

SIHA

HepG2

## ABSTRACT

A coordination compound of Co<sup>II</sup> with alizarin was prepared to see if it resembles various activities that are reported for anthracyclines as anticancer agents. Alizarin, which has a comparatively simpler structure than anthracyclines, contain the same hydroxy-9,10-anthraquinone as found in anthracyclines. Hence, if tried in cancer chemotherapy, it is expected to show some advantages related to cost and for all those reasons that become applicable in using a relatively simpler compound. However, to be acceptable, it must show comparable efficacy as known for anthracyclines. Like anthracyclines, alizarin forms the semiquinone radical anion that generates superoxide radical anion, responsible for cardiotoxicity. Complex formation decreases generation of superoxide, that was verified by an enzyme assay that might help to decrease toxic side effects. Although hydroxy-9,10-anthraquinones (here alizarin), resemble anthracyclines, biophysical and/or biochemical interactions of the former at the cellular level are less efficient than the latter. Besides, under physiological conditions alizarin is anionic. Hence, increase in pH affects DNA binding adversely. The prepared complex, which is anionic, when it has Co<sup>II</sup> and neutral when Co<sup>III</sup>, binds DNA better than alizarin under varying conditions of ionic strength and pH. Since reactive oxygen species are present in cells, there is a high probability that the Co<sup>II</sup> complex could either completely or partially convert to Co<sup>III</sup>. The Co<sup>III</sup> species would then manifest in several biological responses affecting the growth of cells. Experiments pertaining to ROS were performed on three human cell lines (SIHA, HepG2, WI 38) that suggest a shift in mechanism for the complex/complexes from that known for anthracyclines or hydroxy-9,10-anthraquinones. An expected loss in efficacy due to decreased semiquinone formation is compensated by the Co<sup>II</sup>/Co<sup>III</sup> couple owing to the metal ion being present in two oxidation states in cellular medium thus promoting cytotoxicity. The Co<sup>II</sup>/Co<sup>III</sup> complex tried on cells reveal several attributes that enable it/them to overcome some of the shortcomings of alizarin to become comparable to anthracyclines.

© 2022 Published by Elsevier B.V.

## 1. Introduction

Several studies reveal complex formation of anthracyclines by metal ions lead to decreased semiquinone formation in electron transfer reactions that in turn generate less superoxide radical anion [1–5]. Such complexes were usually found to possess higher efficacy than anthracyclines [1–5]. Complex formation decreases the general tendency of anthracyclines to show cardiotoxic side effects,

a major limitation in their use as anticancer agents [4–12]. They modify anthracyclines' actions significantly. Another extremely relevant issue is the cost of such drugs used in treating cancer, considered another major obstacle in patient care for economically challenged families [13–15]. Administration of drugs being important in chemotherapy, hence, for extremely relevant reasons, there is a search for molecules that address several issues plaguing anthracyclines. Since searched molecules would constantly be compared for efficacy against standard anthracyclines, such alternatives must possess a close resemblance to anthracyclines with regard to efficacy [16–22]. Several studies show, in spite of a considerable similarity in structure and electronic properties between the

Abbreviations: ROS, reactive oxygen species; SOD, superoxide dismutase.

\* Corresponding author.

E-mail address: [dasrsv@yahoo.in](mailto:dasrsv@yahoo.in) (S. Das).

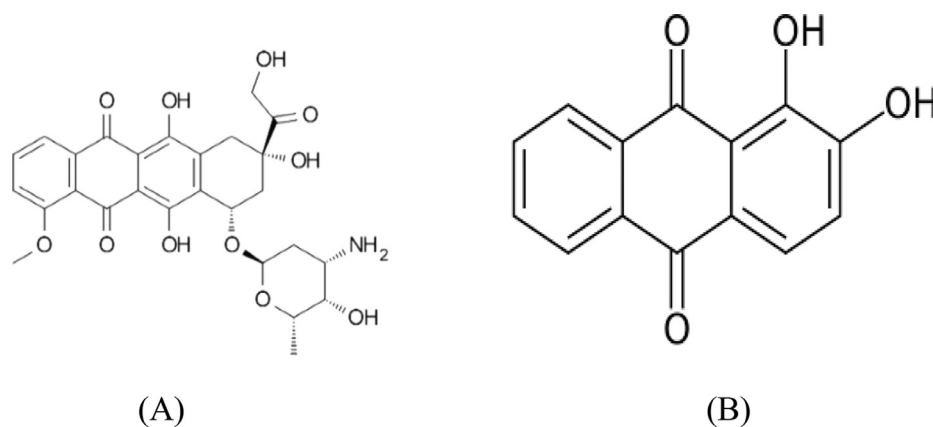


Fig. 1. Structure of (A) an anthracycline anticancer drug and (B) alizarin.

anthracyclines and hydroxy-9,10-anthraquinones, biophysical interactions and biochemical reactions of the latter trail behind that of the anthracyclines [16–24]. Apart from emodin and to some extent quinalizarin, not much is reported on other hydroxy-9,10-anthraquinones, either in clinical trials or in advanced bio-medical research, although good amount of laboratory based data exists [23–29]. Going by the information available, the overall efficacy of hydroxy-9,10-anthraquinones and their complexes in comparison to anthracyclines, is far from being called satisfactory. However, the encouraging part is that hydroxy-9,10-anthraquinones show an almost similar ability to participate in electron transfer reactions like anthracyclines [16–22,30,31]. Studies with hydroxy-9,10-anthraquinones have also revealed a distinct role for glycosyl group (sugar) in anthracyclines [12,16–22,30,31]. Hence, by choosing to work with hydroxy-9,10-anthraquinones (the aglycone of anthracyclines), one actually sacrifices some of the benefits of the glycosyl unit; hence this needs to be made up in some way. This is another major reason for the observed differences between anthracyclines and hydroxy-9,10-anthraquinones [16–22,30,31]. Although the representative aglycones are a lot less costly, the purpose behind selecting them to replace anthracyclines could well be missing [16–22,30,31]. Therefore, on the one hand, while simpler hydroxy-9,10-anthraquinone analogues are cheaper, their efficacy is also less.

Like that known for anthracyclines, complex formation of simpler analogues also control the generation of the superoxide radical anion that help to decrease toxic side effects [1,2,16–21]. Increasing the efficacy of such simpler analogues to the level reported for anthracyclines remain a challenge that accompanies drug simplification efforts. What is encouraging is that metal complexes of several hydroxy-9,10-anthraquinones show several attributes owing to the combined presence of a metal ion and quinone that together make them better anticancer agents [1,2,4–6,16–22]. Some of these properties enable the complexes to show better or comparable efficacy as those of the standard anthracyclines in use today [12].

The present study attempts to identify if complex formation of a hydroxy-9,10-anthraquinone results in an improvement in activity from a biological point of view, that is better than the parent hydroxy-9,10-anthraquinone. Although the possibility for a decrease in efficacy in the free radical pathway exists, complexes of hydroxy-9,10-anthraquinones are close in performance to anthracyclines and in a few cases better [12,16–22,30,31]. In fact, the mechanism of anticancer activity due to anthracyclines or hydroxy-9,10-anthraquinones are different from their metal complexes [4,9,18–22]. Although the complete mechanism for anthracycline functioning is still not very clear, several things have emerged [3,7–11]. These may not be the same for the complexes. This study suggests they would be different depending significantly on the metal ion. Hence, to realize the role of the metal ion over those used previ-

ously,  $\text{Co}^{\text{II}}$  was chosen [2,4,5,18–22].  $\text{Co}(\text{II})$  is bio-friendly and possesses a stable higher oxidation state unlike  $\text{Cu}^{\text{II}}$  or  $\text{Fe}^{\text{III}}$ . Therefore, a  $\text{Co}^{\text{II}}$  complex of a hydroxy-9,10-anthraquinone might be different from that of  $\text{Cu}^{\text{II}}$  or  $\text{Fe}^{\text{III}}$  complexes of anthracyclines/ hydroxy-9,10-anthraquinones [1,2,4,6,15,18–22,32–34].

## 2. Experimental

### 2.1. Materials

Alizarin (>90% pure) was obtained from TCI, Japan. It was purified by re-crystallization from ethanol-water mixtures. Since the compound is photosensitive, solutions prepared in ethanol ( $\sim 10^{-4}$  M) were stored in the dark so that there isn't any change in concentration due to storage. Cobalt(II) chloride hexahydrate,  $\text{NaNO}_3$  (AR) and  $\text{NaCl}$  (AR) were purchased from MERCK (India) and used to maintain the ionic strength of the medium. Calf thymus DNA, procured from Sisco Research Laboratories, India was dissolved in triple distilled water containing 120 mM  $\text{NaCl}$ , 35 mM  $\text{KCl}$  and 5 mM  $\text{CaCl}_2$ . A molar extinction coefficient of  $6600 \text{ M}^{-1} \text{ cm}^{-1}$  at 260 nm was used to determine the concentration of the solution. Absorbance was also recorded at 280 nm so that  $A_{260}/A_{280}$  could be obtained. The ratio found in the range 1.8 to 1.9 suggests DNA was sufficiently free of protein, requiring no further purification. A JASCO V-630 spectrophotometer was used for the purpose. The quality of calf thymus DNA was also checked by recording its CD spectrum at 260 nm using a CD spectropolarimeter (J815, JASCO) (Fig 1).

### 2.2. Methods

#### 2.2.1. Determination of stoichiometry of interaction of $\text{Co}^{\text{II}}$ and alizarin using mole ratio and Job's method of continuous variation

Determination of the composition of the complex was done in solution. In the mole ratio method,  $\text{Co}^{\text{II}}$  was kept constant while alizarin was varied. The absorbance at 429 nm was plotted against  $(T_L/T_M)_{\text{TM}}$  (Fig. 2A);  $T_M$  refers to a fixed concentration of  $\text{Co}^{\text{II}}$  while  $T_L$  indicates varying concentrations of alizarin. Data points were fitted to a linear equation yielding two straight lines, the intersection of which indicates stoichiometry of complex formation.

In the Job's method of continuous variation (Fig. 2B), complementary mixtures were prepared. Absorbance was recorded at 429 nm and plotted against volume of alizarin (DHA). Stoichiometry of  $\text{Co}^{\text{II}}$  to alizarin was found to be 1:3 from both methods. In Job's method, formation of a 1:1 metal to alizarin species and a 1:2 metal to alizarin species were also seen.

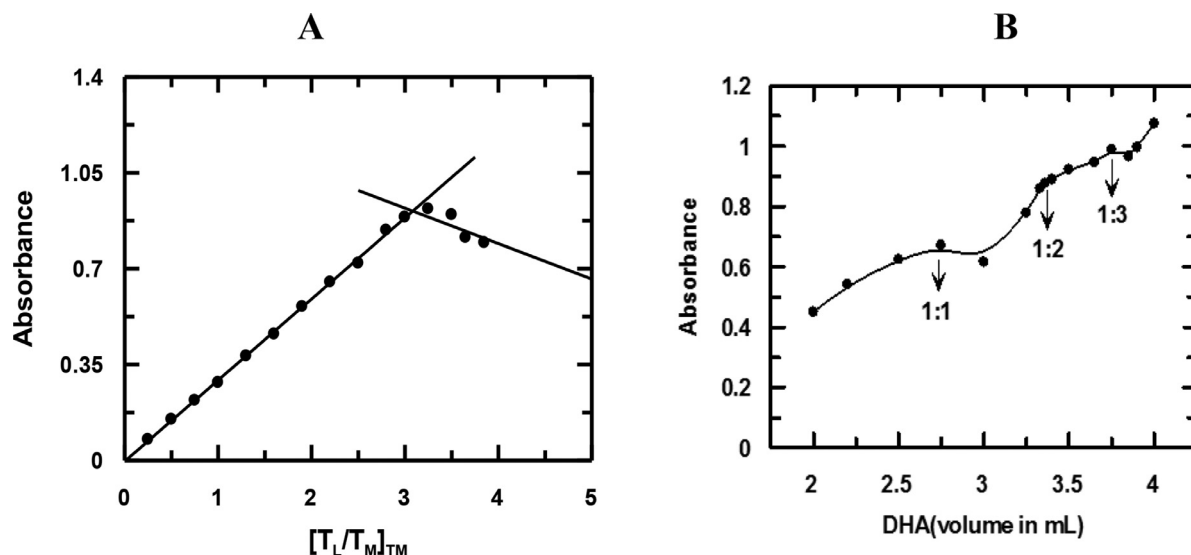


**Fig. 2.** Plots showing variation in absorbance at 429 nm for (A), a change in the ratio of alizarin to  $\text{Co}^{\text{II}}$  for a fixed concentration of  $\text{Co}^{\text{II}}$  ( $= 50 \mu\text{M}$ ) and (B) a continuous variation of the concentration of alizarin (DHA) and  $\text{Co}^{\text{II}}$  at physiological pH ( $\sim 7.4$ ). For (B), strength of stock solutions of  $\text{Co}^{\text{II}}$  and alizarin were  $100 \mu\text{M}$ ;  $[\text{NaNO}_3] = 0.01 \text{ M}$ , Temperature =  $298 \text{ K}$ .

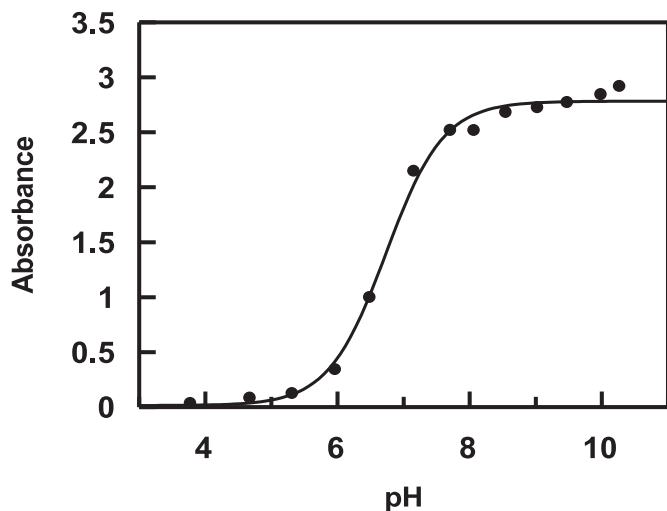


**Fig. 3.** Spectrophotometric titration of alizarin in presence of  $\text{Co}^{\text{II}}$ , shown by a variation in absorbance at  $540 \text{ nm}$ ;  $[\text{alizarin}] = 60 \mu\text{M}$ ,  $[\text{Co}^{\text{II}}] = 20 \mu\text{M}$ ,  $[\text{NaNO}_3] = 0.01 \text{ M}$ ,  $T = 301 \text{ K}$ .

### 2.2.2. Dissociation of proton per alizarin in presence of $\text{Co}^{\text{II}}$

Alizarin and  $\text{Co}^{\text{II}}$  were mixed in the ratio reported above and a spectrophotometric titration was performed in the pH range 3.0 - 12.0. pH was measured using a digital pH meter (LMPH-10, LAB-MAN). The change in absorbance of alizarin with pH in the presence of  $\text{Co}^{\text{II}}$  was recorded at  $540 \text{ nm}$ . The data was fitted to Eq. 1.

$$A_{\text{obs}} = A_1 / (1 + 10^{\text{pH} - \text{p}K_1}) + A_2 / (1 + 10^{\text{p}K_1 - \text{pH}}) \quad (1)$$

$A_1$  and  $A_2$  refer to absorbance of  $\text{LHH}_1$  and  $\text{LH}^-$  for alizarin respectively. Alizarin is denoted as  $\text{LHH}_1$  since hydrogens present on the two phenolic-OH groups are not equivalent. Fitting the experimental data (Fig. 3),  $\text{p}K_1$ , i. e. dissociation of  $\text{LHH}_1$  in presence of  $\text{Co}^{\text{II}}$  was found to be  $6.75 \pm 0.30$  at  $25 \text{ }^\circ\text{C}$ .



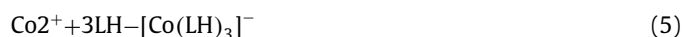
Alizarin ( $\text{LHH}_1$ ) interacts with  $\text{Co}^{\text{II}}$  according to Eq. 3, where H represents the hydrogen on OH at  $\text{C}_2$  and  $\text{H}_1$  denotes the hydrogen on OH at  $\text{C}_1$ . Formation of a complex between  $\text{Co}^{\text{II}}$  and alizarin

may be summarized with the help of the following equations.



Formation constants  $\beta$  and  $\beta^*$  may be evaluated using Eqs. (4-7).

$$\beta^* = \frac{[\{\text{Co}(\text{LH})_3\}^-][\text{H}_1^+]^3}{[\text{Co}^{2+}][\text{LHH}_1]^3} \quad (4)$$



$$\beta = \frac{[\{\text{Co}(\text{LH})_3\}^-]}{[\text{Co}^{2+}][\text{LH}^-]^3} \quad (6)$$

$$\beta = \frac{\beta^*}{K_2^3} \quad (7)$$

$K_2$  is the equilibrium constant for the dissociation of the proton of alizarin when present alone as shown in Eq. (2) [34].  $\text{p}K$  for the dissociation of phenolic OH at  $\text{C}_1$  of alizarin in the presence of  $\text{Co}^{\text{II}}$  was used to calculate stability constant of  $[\text{Co}(\text{LH})_3]^-$  in solution. Value for formation constant  $\beta$  for  $[\text{Co}(\text{LH})_3]^-$  was  $9.09 \times 10^{19}$  ( $\log \beta = 19.96$ ).

### 2.2.3. Preparation of $\text{Na}[\text{Co}^{\text{II}}(\text{alz})_3]$

$0.2 \text{ mmol CoCl}_2 \cdot 6\text{H}_2\text{O}$  dissolved in a minimum quantity of distilled water was added drop wise to a solution of  $0.6 \text{ mmol}$  alizarin in methanol. pH of the solution was adjusted to a value between 6.5 and 7.0 and warmed gently under reflux for approximately five hours. A dark violet amorphous compound was obtained. Anal. Calc. percentage for  $\text{C}_{42}\text{H}_{21}\text{O}_{12}\text{CoNa}$  is C, 63.03; H, 2.65. Found: C, 63.37; H, 2.69. Molecular ion peak  $(m/z)_{\text{calc}}$  for  $[\text{Co}(\text{alz})_3]^- = 776.63$ ;  $(m/z)_{\text{obs}} = 776.75$ ;  $\lambda_{\text{max}} = 535 \text{ nm}$  in DMSO.

### 2.2.4. Interaction of the complex with reactive oxygen species

Like most  $\text{Co}^{\text{II}}$  complexes in octahedral geometry,  $\text{Na}[\text{Co}^{\text{II}}(\text{alz})_3]$  should be susceptible to oxidation and convert to a  $\text{Co}^{\text{III}}$  species if conditions are favorable. If in the immediate vicinity of  $\text{Na}[\text{Co}^{\text{II}}(\text{alz})_3]$ , reactive oxygen species (ROS) are present there is high probability of  $\text{Co}^{\text{III}}(\text{alz})_3$  forming. This was very seriously considered because we had plans of performing experiments in cellular media where ROS would be present. Further, as a part of

this study since an effort would be made to understand the performance of alizarin and its Cobalt complex in the presence of ROS (generated artificially) and follow the interactions of the compounds thereafter, hence the impact ROS might have on the compounds had to be realized. Therefore, a proper knowledge on the composition of the complex was crucial. We needed to know what happens to  $\text{Na}[\text{Co}^{\text{II}}(\text{alz})_3]$  under such circumstances. Again, in a reducing environment within the cell there exists the possibility of a  $\text{Co}^{\text{III}}$  species becoming  $\text{Co}^{\text{II}}$ . Hence, for all these reasons, a  $\text{Co}^{\text{II}}$  complex species was prepared. Both forms of Co complexes were considered as they might exist simultaneously for reasons mentioned above differing in oxidation state of the metal ion. Both were tried in several experiments. Cobalt present in any one oxidation state was not considered exclusively since in presence of ROS (within cells), each complex would have its role towards cytotoxicity.

### 2.2.5. Preparation of $\text{Co}(\text{alz})_3$

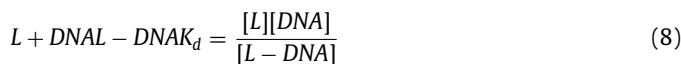
The prepared complex,  $\text{Na}[\text{Co}^{\text{II}}(\text{alz})_3]$  was treated with  $\sim 1\%$   $\text{H}_2\text{O}_2$  and warmed under mild heat in air for an hour to generate  $\text{Co}^{\text{III}}(\text{alz})_3$  which was characterized. In general,  $\text{Co}^{\text{II}}$  is oxidized to  $\text{Co}^{\text{III}}$  under mild heat by purging air through the reaction media. The solution was kept for a fortnight to allow the solvent to evaporate. Following a change in oxidation state, spectroscopic parameters and mass spectrometry data of  $\text{Co}^{\text{III}}(\text{alz})_3$  remained more or less same as that of  $\text{Na}[\text{Co}^{\text{II}}(\text{alz})_3]$ ; if it did change, it was negligible. Magnetic susceptibility measurements and cyclic voltammetry were significantly different from  $\text{Na}[\text{Co}^{\text{II}}(\text{alz})_3]$  (discussed later).

### 2.2.6. Computational methodology for structure determination

Since an important aim of this study is to obtain proper knowledge on the interaction of the prepared complexes with different cell lines, hence to find out the extent to which a complex was either better than alizarin or comparable to standard anthracyclines on grounds of efficacy, it was essential to know the structure of the complex in cellular media for it could be both oxidizing and reducing. Since after preparing the complex, inspite of our best efforts we failed to obtain single crystals, we were left with no other option but to arrive at a structure using computational techniques. As already mentioned, since  $\text{Co}^{\text{II}}$  complexes are prone to oxidation, it is only likely that a significant amount of the prepared complex,  $\text{Na}[\text{Co}^{\text{II}}(\text{alz})_3]$ , might convert to  $\text{Co}^{\text{III}}(\text{alz})_3$  in the presence of ROS in cellular medium. Hence, we decided to obtain the structure of  $\text{Co}^{\text{III}}(\text{alz})_3$  using computation supported by experimental evidence. Calculations were performed with Gaussian 09 program employing DFT method [35]. Becke's three parameter hybrid functional, [36] Lee–Yang–Parr's gradient corrected correlation functional (B3LYP) along with 6-31+ G(d,p) basis set were adopted for C, H and O. For Co, SDD basis set was chosen [37]. Grimmes third order correction for dispersion and Becke-Johnson damping was employed to take into account long range dispersion effects. Ground state ( $S_0$ ) geometries were fully optimized using very tight convergence criteria of the respective program in gas phase and in DMSO (solvent). Frequencies were calculated on optimized geometries. Nature of the stationary point was confirmed by carrying out a normal mode of analysis where all vibrational frequencies were found to be positive i.e. the optimized structure was considered to be at one of the minima of the potential energy surface. In solution phase, calculations were computed in DMSO, simulated by conductor-like polarizable continuum model (CPCM) [38]. Frontier molecular orbitals and molecular electrostatic potential (MEP) surface analyses were done with Gauss View while MO composition analysis was done with Gauss Sum program [39].

### 2.2.7. Interaction of the complex with calf thymus DNA monitored by UV-Vis spectroscopy

To get a correct picture on the interaction of the complex with DNA, titrations were performed using both forms; that of the initially prepared  $\text{Na}[\text{Co}^{\text{II}}(\text{alz})_3]$  and converted to  $[\text{Co}^{\text{III}}(\text{alz})_3]$  by treatment with  $\sim 1\%$   $\text{H}_2\text{O}_2$  (mentioned earlier). Binding studies were carried out at constant pH and constant ionic strength of the medium. Considering the following equilibrium (Eq. 8), interaction of the complexes with calf thymus DNA was realized [16–22,30,31].



In Eq. (8), L represents complexes.  $K_d$  is the dissociation constant for the interaction considered in a direction reverse to that in equilibrium. Eq. (9) is a double reciprocal equation where reciprocal of the change in absorbance was plotted against reciprocal of  $(C_D - C_L)$ .  $C_D$  is the concentration of calf thymus DNA and  $C_L$ , the concentration of the complexes. From the double reciprocal plot [Eq. 9],  $\Delta A_{\text{max}}$  and  $K_{\text{app}}$  ( $1/K_d$ ) were calculated from intercept and slope respectively.

$$\frac{1}{\Delta A} = \frac{1}{\Delta A_{\text{max}}} + \frac{K_d}{\Delta A_{\text{max}}(C_D - C_0)} \quad (9)$$

Decrease in absorbance ( $\Delta A$ ) during interaction of complexes with DNA was used to create the binding isotherms.  $\Delta A_{\text{max}}$  denotes the maximum change in absorbance following interaction of either form of the complex with calf thymus DNA. A plot of  $\Delta A/\Delta A_{\text{max}}$  against concentration of DNA was fitted by non-linear square fit analysis [Eq. 11] and  $K_d$  was evaluated.

$$k_d = \frac{[C_0 - (\frac{\Delta A}{\Delta A_{\text{max}}})C_0][C_D - (\frac{\Delta A}{\Delta A_{\text{max}}})C_0]}{(\frac{\Delta A}{\Delta A_{\text{max}}})C_0} \quad (10)$$

$$C_0 - \left(\frac{\Delta A}{\Delta A_{\text{max}}}\right)^2 - (C_0 + C_D + K_d)\left(\frac{\Delta A}{\Delta A_{\text{max}}}\right) + C_D = 0 \quad (11)$$

Overall binding constant ( $K^*$ ) was determined by multiplying  $K_{\text{app}}$  with " $n_b$ ". A modified form of the original Scatchard equation [40] was used to analyze titration results. Overall binding constant ( $K^*$ ) and binding stoichiometry " $n$ " =  $n_b^{-1}$  were obtained from Eq. 12.

$$\frac{r}{C_f} = K^* (n - r) \quad (12)$$

$r = \frac{C_b}{C_D}$ ; " $C_b$ " denotes the concentration of the bound form of both complexes while " $C_f$ " denotes the free form. " $n$ " refers to binding stoichiometry in terms of number of bound complex per nucleotide while " $n_b$ " reciprocal of " $n$ " denotes binding site size in terms of the number of nucleotides bound to each complex [16–22,30,31].

### 2.2.8. Estimation of superoxide radical anion by NADH dehydrogenase assay

An enzyme assay was performed at 298 K where NADH was the electron donor, cytochrome c, the electron acceptor and reaction was catalyzed by NADH dehydrogenase [1,2,18,19,21,30,31,34,41]. Alizarin and  $\text{Na}[\text{Co}^{\text{II}}(\text{alz})_3]$  were subjected to assay for NADH-cytochrome c reductase activity. Reduction of cytochrome c was followed at 550 nm. Phosphate buffer (pH  $\sim 7.4$ ), 80.0  $\mu\text{M}$  cytochrome c, 160.0  $\mu\text{M}$  NADH, 3.0 U/lit NADH dehydrogenase were used. Concentration of compounds was varied from 0 to 80.0  $\mu\text{M}$ . Activity of NADH dehydrogenase is expressed in units where one unit of activity reduces 1.0  $\mu\text{mole}$  oxidized cytochrome c per minute at 298 K. Formation of superoxide radical anion catalyzed by alizarin and  $\text{Na}[\text{Co}^{\text{II}}(\text{alz})_3]$  was measured from the reduction of cytochrome c inhibited by superoxide dismutase (SOD) (0 or

40.0  $\mu\text{g/ml}$ ) in the presence of NADH and NADH dehydrogenase [1,2,18,19,21,30,31,34,43]. The kinetics software of JASCO V-630 was used for the purpose.

### 2.2.9. Biological Experiments

**2.2.9.1. Cell culture.** Cervical cancer cells (SIHA), human hepatocellular carcinoma cells (Hep G2) and normal WI-38 lung fibroblast cells were cultured in DMEM medium (GIBCO, Invitrogen, Carlsbad, CA, US) supplemented with 10% fetal bovine serum (GIBCO), 100 IU/mL penicillin and 100  $\mu\text{g/ml}$  streptomycin at 37°C in a humid atmosphere containing 5%  $\text{CO}_2$  (Heraeus, Thermo Scientific, MA, USA). Cell lines were purchased from National Centre for Cell Science in Pune, India. Before treatment with compounds, cells were seeded in 96 well plates for 24 hours [42,43].

**2.2.9.2. Cell viability assay.** After 24 hours, each cell line was treated with alizarin and  $\text{Na}[\text{Co}^{\text{II}}(\text{alz})_3]$ , previously dissolved in DMSO. Concentration of DMSO was less than 0.5%. Cell viability was noted 48 hours after treatment with 3-(4,5-dimethylthiazol-2-yl)-2,5-diphenyltetrazolium bromide (MTT). Cells were washed with  $1 \times$  PBS and treated with MTT for 4 hours at 37°C. Crystals were dissolved in DMSO and plates scanned on Thermo MULTISKAN EX plate reader at 595 nm.

**2.2.9.3. Estimation of ROS by  $\text{H}_2\text{DCFDA}$  assay.** A fluorogenic dye, 2',7'-dichlorofluorescein diacetate ( $\text{H}_2\text{DCFDA}$ ) was used to detect reactive oxygen species (ROS) present in cells [42,44–46]. Once  $\text{H}_2\text{DCFDA}$  is de-acetylated by cellular esterases to a non-fluorescent compound ( $\text{H}_2\text{DCF}$ ), it is unable to show fluorescence until the non-fluorescent form is again oxidized. If ROS is present in cells, it oxidizes this non-fluorescent unit to 2',7'-dichlorofluorescein (DCF), a fluorescent compound, showing green fluorescence [44,46]. Using a fluorescence spectrophotometer (Hitachi, Japan), excitation was done at 504 nm and emission was recorded at 529 nm. A stock solution of  $\text{H}_2\text{DCFDA}$  (10 mM) was prepared in methanol which was diluted further to 100  $\mu\text{M}$  using culture medium. Two carcinoma cells (SIHA and Hep G2) and normal human lung fibroblast (WI 38) cells were treated with  $\text{IC}_{50}$  dose (obtained from MTT assay) of alizarin and its  $\text{Co}^{\text{II}}$  complex and allowed to stand for 30 minutes. ROS was generated by the free radical generator  $\text{H}_2\text{O}_2$  (70  $\mu\text{M}$ ). Cells were washed with ice cold Hanks balanced salt solution (HBSS) and incubated with 100  $\mu\text{M}$   $\text{H}_2\text{DCFDA}$  for 30 minutes at 37°C. Cells were lysed with an alkaline solution and fluorescence was measured.

## 3. Results and Discussion

### 3.1. Characterization of $\text{Na}[\text{Co}^{\text{II}}(\text{alz})_3]$

#### 3.1.1. Comparison of UV-Vis spectra of alizarin and $\text{Na}[\text{Co}^{\text{II}}(\text{alz})_3]$

Absorption spectrum of alizarin was recorded in methanol showing  $\lambda_{\text{max}}$  at 521 nm (Fig. S1, SI). Owing to poor solubility of the complex in water, its spectrum was recorded in aqueous-DMSO showing  $\lambda_{\text{max}}$  at 536 nm.

#### 3.1.2. IR spectra of alizarin and $\text{Na}[\text{Co}(\text{alz})_3]$

Analysis of FTIR data of alizarin and  $\text{Na}[\text{Co}^{\text{II}}(\text{alz})_3]$  (Fig. S2 and Fig. S3, SI respectively) obtained on a spectrophotometer (Perkin Elmer) using KBr pellets reveal that the sharp peak obtained for phenolic-OH at 3357  $\text{cm}^{-1}$  for alizarin was detected as a broad band for the complex (3413  $\text{cm}^{-1}$ ). Carbonyl stretching peaks at 1665  $\text{cm}^{-1}$  to 1586  $\text{cm}^{-1}$  for alizarin (Fig. S2, SI) was obtained at 1580  $\text{cm}^{-1}$  for the complex (Fig. S3, SI) [47]. The response for carbonyl stretching did not disappear completely in the complex since of the two carbonyls present on each alizarin, only one was involved in complex formation. Peaks obtained in the region 1452

$\text{cm}^{-1}$  to 775  $\text{cm}^{-1}$  for alizarin and between 1341  $\text{cm}^{-1}$  to 718  $\text{cm}^{-1}$  for the complex (due to -OH and -CH bending vibrations) were slightly different. Response for Co-O stretching expected between 450  $\text{cm}^{-1}$  to 390  $\text{cm}^{-1}$  [5,47,48] could not be detected for a limitation in the instrument used to detect responses in that region accurately.

#### 3.1.3. Analysis of the mass spectrum of $\text{Na}[\text{Co}^{\text{II}}(\text{alz})_3]$

Evidence from physico-chemical experiments and elemental analysis suggests formation of a 1:3  $\text{Co}^{\text{II}}$ -alizarin complex  $[\text{Co}^{\text{II}}(\text{alz})_3]^-$  whose mass is 776.63. Hence, the peak in the mass spectrum at  $m/z = 776.76$  (Fig. 4), recorded on a Micromass Q-ToF micro<sup>TM</sup>, Waters Corporation is the molecular ion of the complex. From the molecular ion, if one ligand and an -OH group from another ligand departs followed by entry of DMSO (used in analysis) in the coordination sphere, a species with  $m/z = 599.03$  is expected. The peak at  $m/z = 601.08 (+2\text{H})$  could be this species. From the molecular ion, since loss of one alizarin vacates two coordination sites, if they are subsequently occupied by two molecules of water (either present as an impurity in the solvent or from moisture) then the fragment should show up at  $m/z = 573.03$  (theoretical); an experimental peak at  $m/z = 574.28$  could be this species. The mass spectrum of the oxidized form of the complex  $[\text{Co}^{\text{III}}(\text{alz})_3]$  was pretty much the same.

#### 3.1.4. Thermo-gravimetric analysis

Fig. S4, SI, suggests, by 100°C there is a decrease in weight that corresponds to a 4.3% loss in weight. By  $\sim 140^\circ\text{C}$ , the decrease in weight is about 15.63%. While that at 100°C could be due to loss of absorbed water molecules, by 140°C, it could be due to additional loss of three unbound OH groups from the complex. Otherwise the complex is reasonably stable.

#### 3.1.5. Magnetic moment of $\text{Na}[\text{Co}^{\text{II}}(\text{alz})_3]$ and $[\text{Co}^{\text{III}}(\text{alz})_3]$

Magnetic susceptibility was measured by the Gouy method and  $\mu_{\text{eff}}$  was found to be 3.67 BM for  $\text{Na}[\text{Co}^{\text{II}}(\text{alz})_3]$  suggesting the presence of three unpaired electrons.  $[\text{Co}^{\text{III}}(\text{alz})_3]$  was diamagnetic.

#### 3.1.6. Electrochemical studies

To examine the electrochemical properties of the mono-anionic complex, cyclic voltammetry was performed over the potential range 0 to  $-1500$  mV (Fig. 5). A single cathodic quasi-reversible wave was obtained at customary scan rates. Keeping in mind some of our experiments would expose the mono-anionic complex to reactive oxygen species, we needed to know how it might behave following an exposure. Hence, an understanding of electrochemical processes was necessary to be sure on issues related to the performance of the complex in experiments pertaining to ROS and cell viability studies to be able to look for a correlation between them. Since  $\text{Co}^{\text{II}}$  complexes are prone to oxidation in the presence of oxidizing agents like  $\text{H}_2\text{O}_2$ , we thought it necessary to have some prior knowledge on what might happen if  $\text{Na}[\text{Co}^{\text{II}}(\text{alz})_3]$  is exposed to  $\text{H}_2\text{O}_2$ . In every likelihood, a  $\text{Co}^{\text{III}}(\text{alz})_3$  species would form which we verified electrochemically (Fig. 6a). Under exactly similar conditions as that employed for Fig 5, we found that the quasi reversible nature of  $\text{Na}[\text{Co}^{\text{II}}(\text{alz})_3]$  had changed completely when subjected to  $\sim 1\%$   $\text{H}_2\text{O}_2$  (Fig. 6a). Fig. 6b is the CV trace of the previously prepared  $\text{Co}^{\text{III}}$  complex  $[\text{Co}^{\text{III}}(\text{alz})_3]$  (Section 2.2.5).

Figures 6a and 6b clearly indicate that the species formed in solution upon addition of  $\sim 1\%$   $\text{H}_2\text{O}_2$  to a solution of  $\text{Na}[\text{Co}^{\text{II}}(\text{alz})_3]$  is the same as that characterized earlier as  $\text{Co}^{\text{III}}(\text{alz})_3$ . It may therefore be said that in presence of  $\text{H}_2\text{O}_2$ , the predominant species present in solution is  $\text{Co}^{\text{III}}(\text{alz})_3$ . This is important for realizing the form in which the complex is most likely to exist in a medium where  $\text{H}_2\text{O}_2$  or other forms of ROS are present since that would be useful in interpreting the results of ROS based experiments

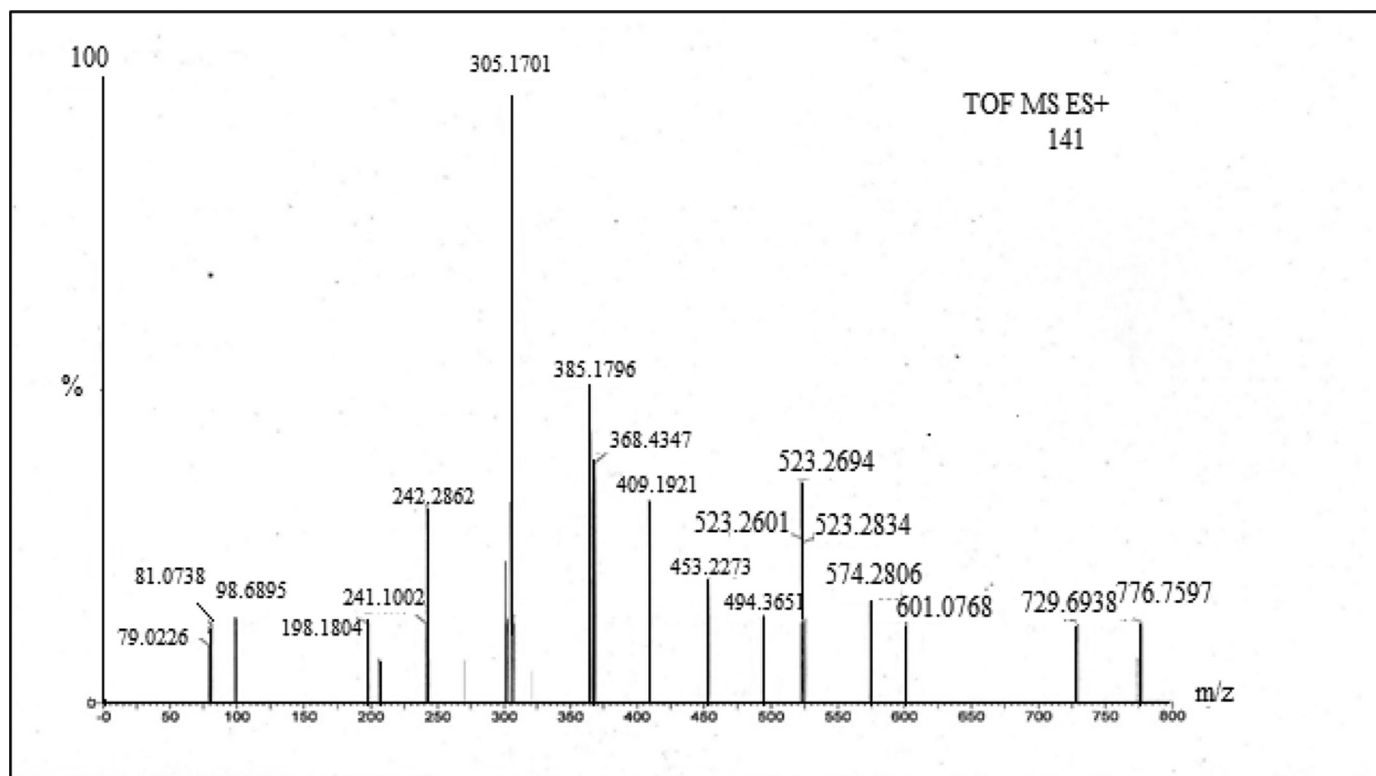


Fig. 4. Mass spectrum of Na[Co(alz)<sub>3</sub>].

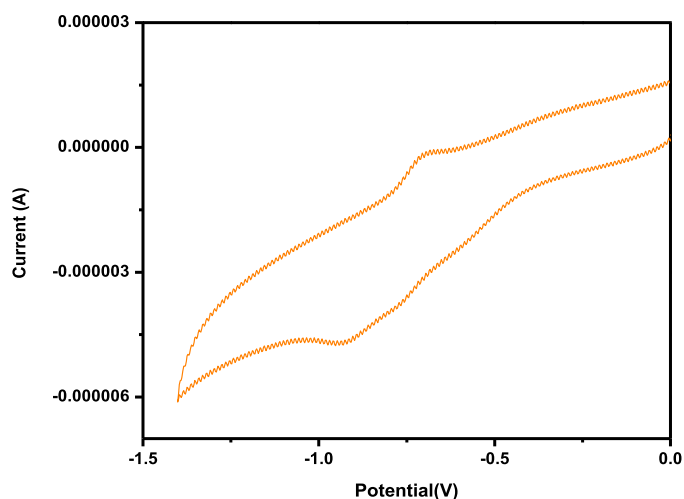


Fig. 5. Cyclic voltammogram of a 0.01 mM Na[Co<sup>II</sup>(alz)<sub>3</sub>] at pH ~ 7.4 showing a single step one electron reduction of quinone in aqueous solution containing 0.12 M KCl using a glassy carbon electrode (surface area 0.1256 cm<sup>2</sup>); Scan rate 100 mV/sec.

performed on different cell lines. As expected, following a treatment of Na[Co<sup>II</sup>(alz)<sub>3</sub>] with H<sub>2</sub>O<sub>2</sub> or on the previously prepared Co<sup>III</sup>(alz)<sub>3</sub>, the single reduction peak for the complex moved to more positive potential.

### 3.1.7. Structure of Co<sup>III</sup>(alz)<sub>3</sub> by computation

**3.1.7.1. DFT calculations based on spectroscopy and other evidence.** Molecular geometry of octahedral Co<sup>III</sup>(alz)<sub>3</sub> was optimized at its electronic ground state (S<sub>0</sub>) in gaseous and DMSO medium with appropriately labelled coordination environments as depicted in Fig. 7. Some selected bond lengths and bond angles are listed in

Table 1 while coordinates of optimized structures are provided in Table 1S, SI. Final optimized structures of the ground state configuration show an octahedral coordination environment both for gas and solution (in DMSO) phase calculations. Two oxygen atoms of each alizarin are connected to Co<sup>III</sup> (Fig. 7).

**3.1.7.2. Frontier Molecular Orbital analysis.** Frontier orbitals of the Co complex with orbital energies, optimized in gas and solution phases, are shown in Fig. 8 [49]. Assignment of both occupied and virtual MOs were made on the basis of their composition in terms of atomic contribution and visual inspection of their three-dimensional representation. The complex was assumed to be made of four constituents, Co, alizarin (L1), alizarin (L2), alizarin (L3). Composition from fragments is shown in Table 2.

Both for gas and solution phase optimized geometries we observed that HOMO and subsequent occupied orbitals up to HOMO-4 has major contributions from different alizarin moieties with varying ratios while contribution from metal atom/ion was negligible. Similar observations were found for LUMO upto LUMO +2. However, LUMO+3 and LUMO+4 orbitals had contributions from “Co d orbitals” along with some contribution from each alizarin but in different proportion. In both cases, the calculated HOMO-LUMO energy gap was found to be 2.69 eV. Some selected MOs of Co<sup>III</sup>(alz)<sub>3</sub> along with their energies and percentage composition are provided in Table 2.

**3.1.7.3. MEP Surface Analysis.** Molecular electrostatic potential surfaces calculated over optimized geometries both for gas and solvent phases are presented in Fig. 9 using the reverse rainbow color scheme and chosen iso-value of 0.02 a.u. for the envelope. The red color indicates regions of negative potential while blue represents those having positive potential. It is understood that hydrogen atoms of O–H bonds are the most positive region while hydrogen atoms of C–H bonds are only slightly positive. The most

**Table 1**  
Coordinated bond distances (in Å) and bond angles (in °) of Co(alz)<sub>3</sub>.

Bond	Gaseous phase	In DMSO	Angle	Gaseous phase	In DMSO
Co19–O15	1.897	1.898	O15–Co19–O17	94.35	98.77
Co19–O17	1.877	1.877	O15–Co19–O36	87.79	88.37
Co19–O34	1.892	1.887	O15–Co19–O52	88.05	88.59
Co19–O36	1.875	1.879	O15–Co19–O54	89.42	88.92
Co19–O52	1.912	1.910	O17–Co19–O36	89.50	89.27
Co19–O54	1.894	1.894	O17–Co19–O34	88.69	88.80
			O17–Co19–O54	88.67	89.11
			O36–Co19–O34	94.14	93.37
			O36–Co19–O52	88.58	88.96
			O34–Co19–O54	88.74	89.41
			O52–Co19–O54	93.37	92.77

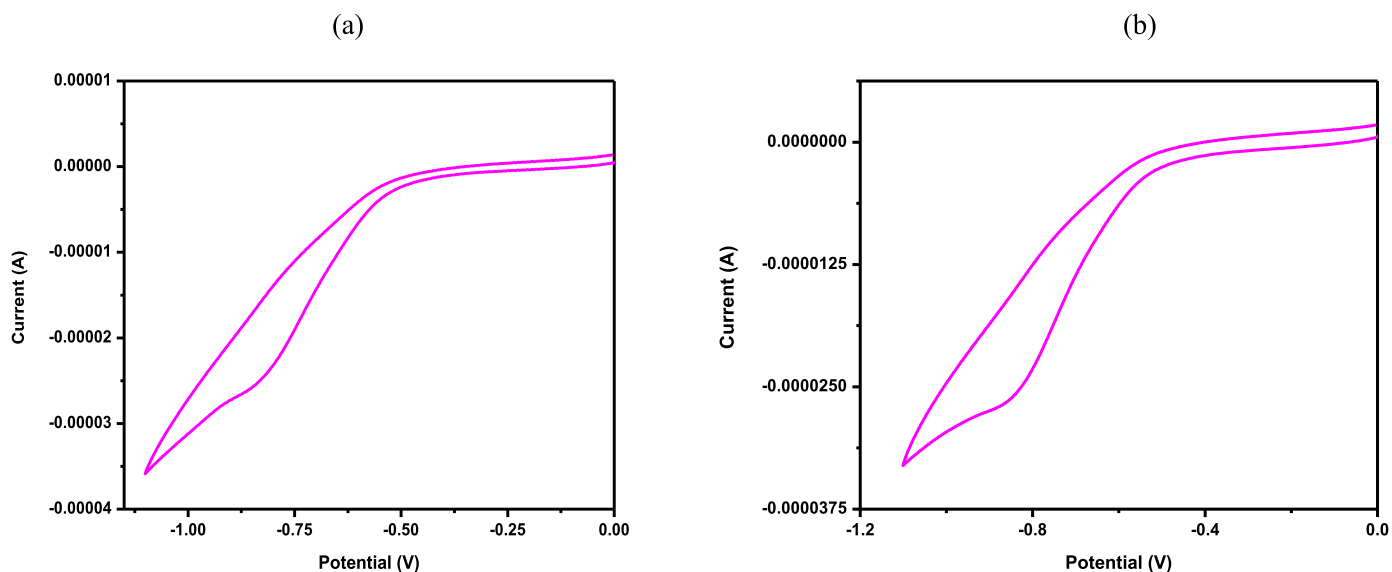


**Fig. 6.** (a) Cyclic voltammogram of a 0.01 mM Na[Co<sup>II</sup>(alz)<sub>3</sub>] at pH ~ 7.4 taken approximately 20 minutes after being treated with ~ 1% H<sub>2</sub>O<sub>2</sub> under gently warm conditions, showing a single step one-electron irreversible reduction; (b) Cyclic voltammogram of a 0.01 mM previously prepared and characterized [Co<sup>II</sup>(alz)<sub>3</sub>] at pH ~ 7.4 also shows a single step one-electron irreversible reduction. In both cases, the solution was aqueous-DMF (50:50) containing 0.12 M KCl; Temperature: 301 K. A glassy carbon electrode (surface area 0.1256 cm<sup>2</sup>) was used. Scan rate: 100 mV/sec.

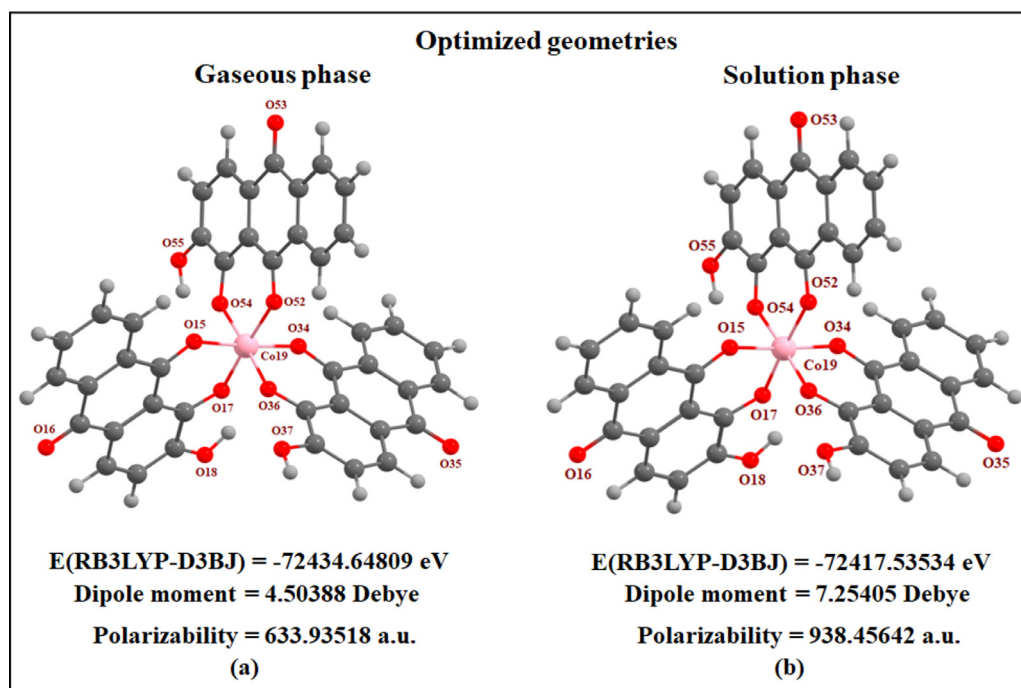


**Fig. 7.** Ground state optimized geometries of the complex with three alizarin ligands (L1, L2 and L3).

**Table 2**  
Some of selected MOs of the complex  $\text{Co(II)-(Alizarin)}_3$  in high spin state along with their energies and percentage compositions from four fragments in both gaseous phase and DMSO medium.

Sl. No.	MO	% Composition											
		Energy (eV)		Co		Alizarin (L1)		Alizarin (L2)		Alizarin (L3)			
		Gas	DMSO	Gas	DMSO	Gas	DMSO	Gas	DMSO	Gas	DMSO		
198	L+4	-2.42	-2.54	68	68	5	5	13	13	13	13		
197	L+3	-2.57	-2.68	69	70	16	16	9	9	6	6		
196	L+2	-3.26	-3.57	0	0	64	13	0	21	35	66		
195	L+1	-3.32	-3.60	0	0	29	49	20	49	51	1		
194	LUMO	-3.41	-3.67	1	1	6	37	79	29	14	33		
193	HOMO	-6.10	-6.36	3	2	68	0	0	83	29	14		
192	H-1	-6.11	-6.37	2	3	29	14	1	10	68	73		
191	H-2	-6.21	-6.41	2	1	1	84	96	4	1	11		
190	H-3	-7.19	-7.39	1	1	94	7	1	1	4	91		
189	H-4	-7.23	-7.41	1	1	3	60	0	36	95	3		

negative potential regions are located around oxygen atoms of carbonyls (C=O). Oxygen atoms of O–H bonds also depict negative potential energy whereas  $\pi$  rings of anthraquinone moieties were found to have higher MEP values than carbonyl oxygens. Thus it can be inferred there is a high possibility of molecules to form hydrogen bonding interactions between hydroxyl-H and carbonyl O that subsequently stabilize such systems.

**3.1.7.4. DORI analysis.** To distinguish between attractive and repulsive interactions within molecular systems “Density Overlap Regions Indicator” (DORI) analysis was performed that enables one to visualize covalent and non-covalent interactions simultaneously by mapping them as iso-surfaces over the molecular system (Fig 10). The plot of reduced density gradient versus sign of the second Hessian eigen value times the electron density [ $\text{sign}(\lambda_2)\rho$  in a.u.] enables one to differentiate between attractive/stabilizing (thus favourable) and repulsive (thus unfavourable) interactions. Strength of interactions are portrayed with the help of the red-green-blue color scheme where blue iso-surface represents strong attractive interactions; a red iso-surface, strong repulsive interactions and a green iso-surface, weak attractive interactions. As expected, coordination as well as covalent bonds are represented as blue iso-surfaces. Intra-molecular weak hydrogen bonding interactions between carbonyl-O and C–H hydrogens are presented as green iso-surfaces while for alizarin (L1) and alizarin (L3) presence of strong O–H...O intra-molecular hydrogen bonding interactions between hydroxyl-H and carbonyl-O are visualized by blue iso-surfaces.

### 3.2. Analysis of the interaction of complexes with calf thymus DNA

The performance of several anticancer drugs are affected owing to fluctuation in ionic strength or pH of the medium [50–52]. Hence, it is important to investigate interactions of drugs or “molecules that could become potential drugs” with a biological target, under varying conditions of ionic strength and pH. An essential criterion for good performance is that the molecules should be able to hold onto their efficacy over a substantial range of pH and ionic strength of the medium. For this reason, both forms of the Cobalt complex,  $\text{Na[Co}^{\text{II}}(\text{alz})_3]$  and  $\text{Co}^{\text{III}}(\text{alz})_3$  were considered for interaction with calf thymus DNA. Titrations were performed either at constant pH and varying ionic strength (by a variation of NaCl) or at a constant ionic strength and varying pH.

#### 3.2.1. At different ionic strengths of the medium

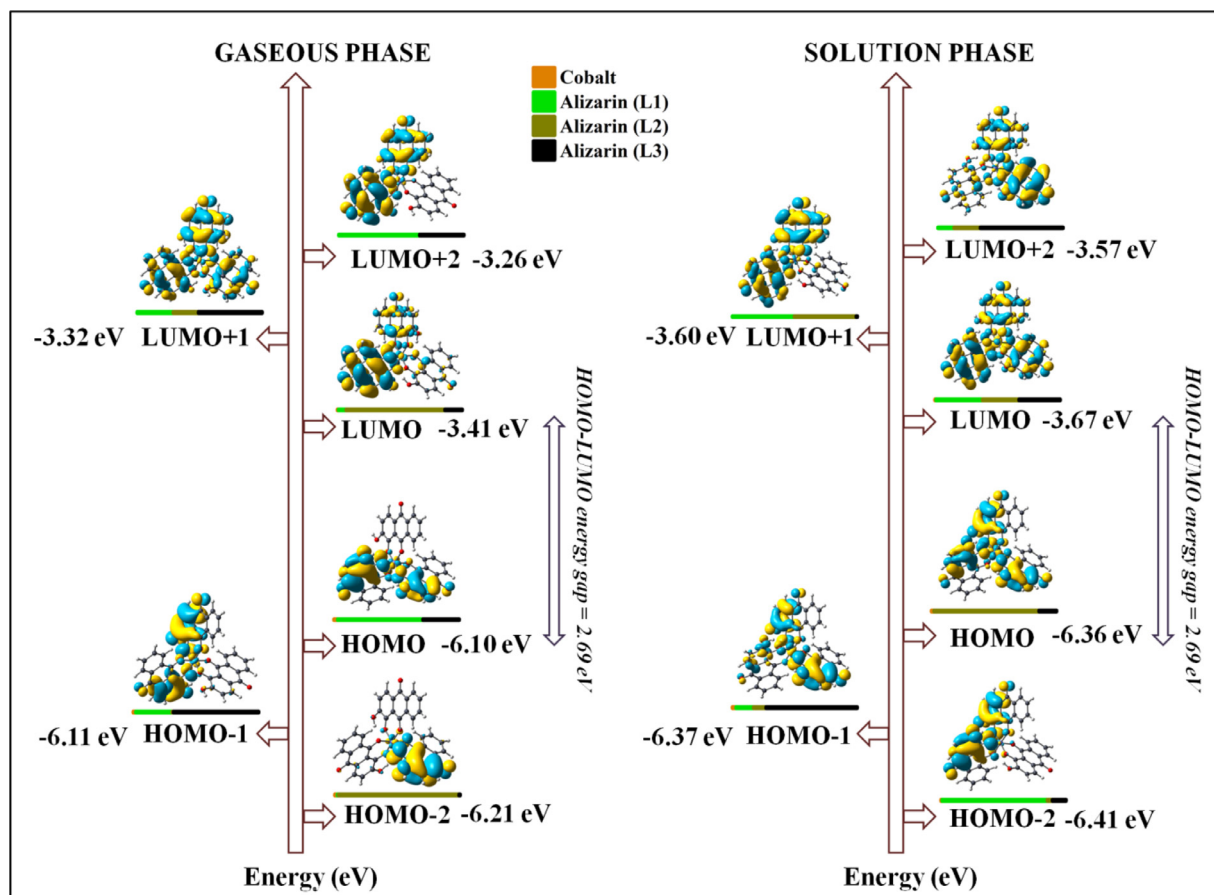
Titrations were performed at pH 7.4, at varying ionic strengths. For  $\text{Na[Co}^{\text{II}}(\text{alz})_3]$ , since the dissociation of free phenolic –OH on each alizarin (the one not bound to  $\text{Co}^{\text{II}}$ ) was beyond physiological pH, hence at pH  $\sim 7.4$ , the complex was largely mono-anionic. Titrations were followed at 536 nm. Fig. S5, SI, depicts a titration of  $\text{Na[Co}^{\text{II}}(\text{alz})_3]$  at an ionic strength of 0.12 M NaCl. Fig. 11 is a plot obeying Eq. (9) for titrations performed at ionic strength = 0.3 M NaCl. The apparent binding constants ( $K_{\text{app}}$ ) were evaluated from such plots (Table 3).

Fig. 12(A) is a plot fitted to Eq. (11) from where apparent binding constant ( $K_{\text{app}}$ ) was evaluated following interaction of the complex with calf thymus DNA. Table 3 provides values for binding parameters at different ionic strengths of the medium at which titrations were performed. Fig. 12(B) provides  $n_b$ , number of nucleotides bound to the complex (Table 3). If a comparison of site size of interaction ( $n_b$ ) for alizarin and  $\text{Na[Co}^{\text{II}}(\text{alz})_3]$  is made, it is seen that  $n_b$  for the complex at each ionic strength is approximately double that obtained for alizarin itself at an almost similar ionic strength. Considering evaluated values for  $K_{\text{app}}$  and  $n_b$  (Table 3), overall binding constant ( $K^*$ ) was obtained using the relation  $K_{\text{app}} \times n_b = K^*$ . Overall binding constant was also determined using the modified Scatchard equation (Eq. (12), Fig. 13).



**Table 3**Binding constant values obtained for the interaction of Na[Co(alz)<sub>3</sub>] with calf thymus DNA at varying ionic strengths of the medium.

Compound	[NaCl] in M	K <sub>app</sub> (M <sup>-1</sup> )			Site size	K <sub>app</sub> × n <sub>b</sub> = K* (M <sup>-1</sup> )	K* from Scatchard	n <sub>b</sub> calculated from Scatchard n <sub>b</sub> = (n <sup>-1</sup> )
		From double-reciprocal plot (a)	From Non-linear plot (b)	Average = (a+b)/2				
Na[Co(alz) <sub>3</sub> ]	0.12	1.06 × 10 <sup>4</sup>	1.35 × 10 <sup>4</sup>	1.20 × 10 <sup>4</sup>	12	1.44 × 10 <sup>5</sup>	1.09 × 10 <sup>5</sup>	8
	0.20	1.88 × 10 <sup>4</sup>	3.58 × 10 <sup>4</sup>	2.73 × 10 <sup>4</sup>	13	3.54 × 10 <sup>5</sup>	2.30 × 10 <sup>5</sup>	9
	0.30	2.15 × 10 <sup>4</sup>	3.89 × 10 <sup>4</sup>	3.02 × 10 <sup>4</sup>	14	4.26 × 10 <sup>5</sup>	4.37 × 10 <sup>5</sup>	10
	0.36	1.72 × 10 <sup>4</sup>	6.18 × 10 <sup>4</sup>	3.95 × 10 <sup>4</sup>	15	5.92 × 10 <sup>5</sup>	5.77 × 10 <sup>5</sup>	10

**Fig. 8.** Frontier molecular orbitals (FMOs) of optimized geometries of Co(II)-(alzarín)<sub>3</sub> and the graphical contribution from the four fragments to FMOs.**Table 4**Variation in overall binding constant of Na[Co<sup>II</sup>(alz)<sub>3</sub>] with calf thymus DNA at different ionic strength of the medium (pH ~ 7.4).

[NaCl] in M	-log[Na <sup>+</sup> ]	K* = K <sub>app</sub> × n <sub>b</sub> (M <sup>-1</sup> )	log K*	K*(M <sup>-1</sup> ) from Scatchard plot	log K*
0.12	0.921	1.44 × 10 <sup>5</sup>	5.15	1.09 × 10 <sup>5</sup>	5.04
0.20	0.699	3.54 × 10 <sup>5</sup>	5.55	2.30 × 10 <sup>5</sup>	5.36
0.30	0.523	4.26 × 10 <sup>5</sup>	5.63	4.37 × 10 <sup>5</sup>	5.64
0.36	0.444	5.92 × 10 <sup>5</sup>	5.77	5.77 × 10 <sup>5</sup>	5.76

Values for overall binding constant from Scatchard plots were close to those that were obtained by multiplying K<sub>app</sub> and n<sub>b</sub> (Table 3).

In general, the binding constant values increased for the complex. In fact, they were higher than we expected, i.e. if one considers only the suppression of dissociation of unbound phenolic -OH on each alizarin at physiological pH due to increased ionic strength of the medium (Tables 3 & 4). Fig. 14 shows an increasing trend for binding constant values for Na[Co<sup>II</sup>(alz)<sub>3</sub>] with calf thymus DNA, significantly higher than alizarin under similar conditions; a consequence of the presence of the metal ion showing its contribu-

tion towards interaction with nucleic acid bases, enabling better targeting of DNA. The values obtained for the complex are in close agreement with those obtained earlier for several anthracyclines that are either being used as drugs in cancer chemotherapy or are in clinical trials [12,16,53].

Both findings mentioned above i.e. (i) number of nucleotides bound to the complex being almost double that found bound to alizarin and (ii) that there is an increase in the tendency of the complex to bind to DNA, particularly at high ionic strength suggests, as the complex approaches DNA, probably one of the three

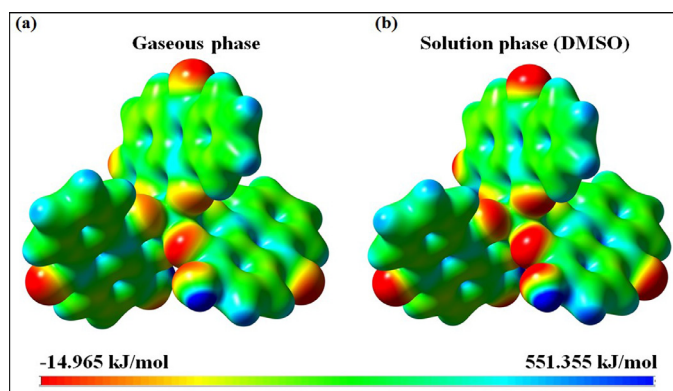


Fig. 9. Molecular electrostatic potential surface of  $\text{Co}(\text{alz})_3$  (a) gas phase (b) solution phase.

ligands break away resulting in a change in geometry from octahedral to square planar, thus allowing for better interaction with DNA as reported for several complexes of similar molecules that are either square planar or have water molecules on the third (z) axis [18,20,21,30]. Such re-organization on the part of the complex could be driven by an affinity of the nucleic acid bases located on DNA, trying to coordinate the metal centre at its fifth and sixth

coordination sites, somewhat similar to that reported for dimeric rhodium (II) acetates, enabling them to act as effective DNA destabilizing agents [54,55,56].

Titration performed with  $\text{Co}^{\text{III}}(\text{alz})_3$  at similar ionic strengths provide binding constant values that are close to those obtained for  $\text{Na}[\text{Co}^{\text{II}}(\text{alz})_3]$ , but slightly higher at each ionic strength of the medium. However, at the highest ionic strength of 0.36 M (with respect to NaCl), binding of neutral  $\text{Co}^{\text{III}}(\text{alz})_3$  to calf thymus DNA was substantially high compared to  $\text{Na}[\text{Co}^{\text{II}}(\text{alz})_3]$ . This is attributed to  $\text{Co}^{\text{III}}(\text{alz})_3$  being neutral and the fact that Co is in a higher oxidation state (Fig. S6, SI).

### 3.2.1. At different pH of the medium

Titration of  $\text{Na}[\text{Co}^{\text{II}}(\text{alz})_3]$  with calf thymus DNA was also followed at different pH (from 6.8 to 8.0). Fig. S7, SI is a plot obtained by fitting the data to Eq. (9) while Fig. 15 was obtained using Eq. (11) for a titration performed at pH 7.50. From the plots,  $K_{\text{app}}$  was evaluated. Inset of Fig. 15 indicates site size of interaction ( $n_b$ ) for  $\text{Na}[\text{Co}^{\text{II}}(\text{alz})_3]$  interacting with calf thymus DNA. Titrimetric data was analyzed using Eq. (12) that provide values for overall binding constant ( $K^*$ ) and site size of interaction “n” ( $n_b^{-1}$ ) using the modified Scatchard equation (Table 5). Fig. S8, SI is a modified Scatchard plot for  $\text{Na}[\text{Co}^{\text{II}}(\text{alz})_3]$  interacting with calf thymus DNA at pH 7.50. Similar titrations were performed at other pH as well and results are shown in Table 5. Titrations were also performed with  $\text{Co}^{\text{III}}(\text{alz})_3$ . However, interaction of calf thymus DNA

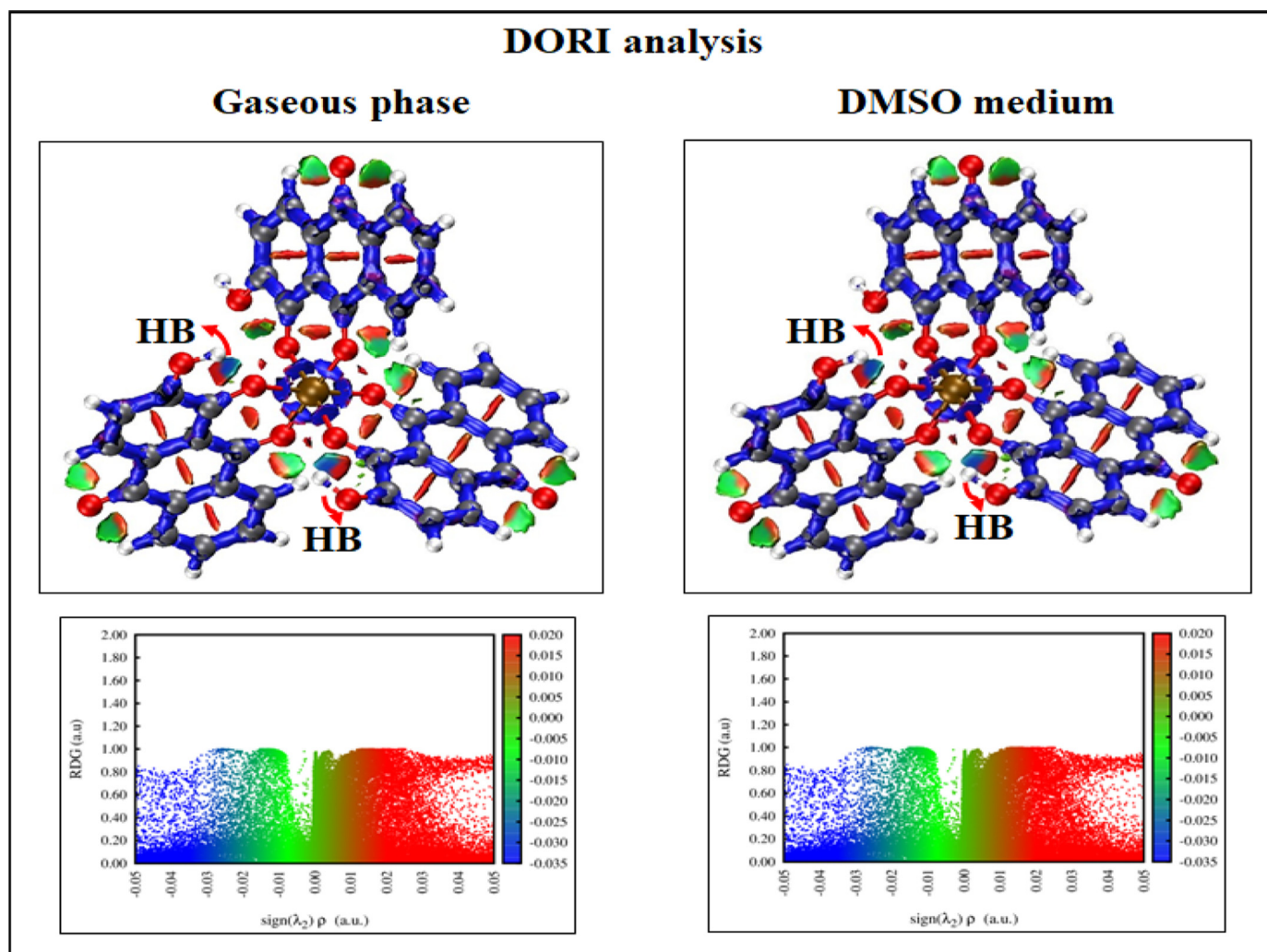
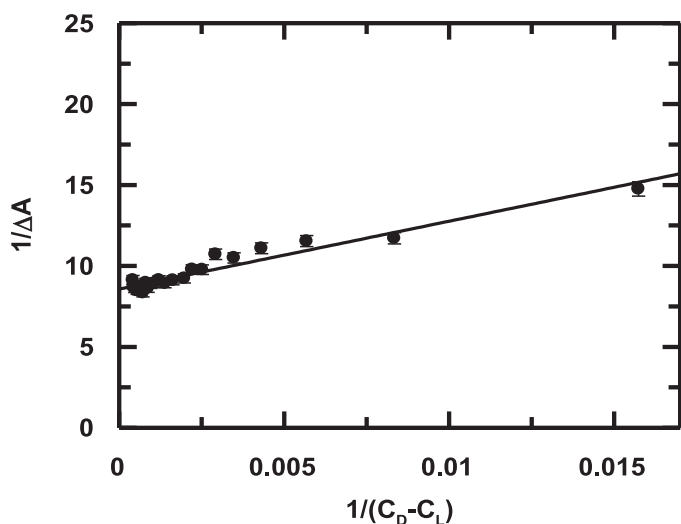


Fig. 10. Density Overlap Regions Indicator (DORI) analysis of  $\text{Co}(\text{alz})_3$ .

**Table 5**  
Variation in binding constant values of  $\text{Na}[\text{Co}(\text{alz})_3]$  with calf thymus DNA at different pH.

Compound	pH	$K_{\text{app}}(\text{M}^{-1})$			Site size	$K_{\text{app}} \times n_b = K^* (\text{M}^{-1})$	$K^*$ from Scatchard	$n_b$ calculated from Scatchard $n_b = (n^{-1})$
		From double-reciprocal plot (a)	From Non-linear plot (b)	Average = (a+b)/2				
$\text{Na}[\text{Co}^{\text{II}}(\text{alz})_3]$	6.80	$0.98 \times 10^4$	$1.18 \times 10^4$	$1.08 \times 10^4$	10	$1.08 \times 10^5$	$0.84 \times 10^5$	08
	7.11	$0.80 \times 10^4$	$1.17 \times 10^4$	$0.98 \times 10^4$	12	$1.18 \times 10^5$	$1.19 \times 10^5$	12
	7.50	$0.87 \times 10^4$	$1.16 \times 10^4$	$1.02 \times 10^4$	13	$1.33 \times 10^5$	$1.12 \times 10^5$	11
	7.81	$0.95 \times 10^4$	$1.00 \times 10^4$	$0.98 \times 10^4$	10	$0.98 \times 10^5$	$1.28 \times 10^5$	14



**Fig. 11.** A typical double reciprocal plots for the interaction of  $\text{Na}[\text{Co}^{\text{II}}(\text{alz})_3]$  with calf thymus DNA that enables evaluation of  $K_{\text{app}}$  at ionic strengths of 0.30 M, of  $\text{Na}[\text{Co}(\text{alz})_3] = 50 \mu\text{M}$ , pH = 7.40, Temp. = 300 K.

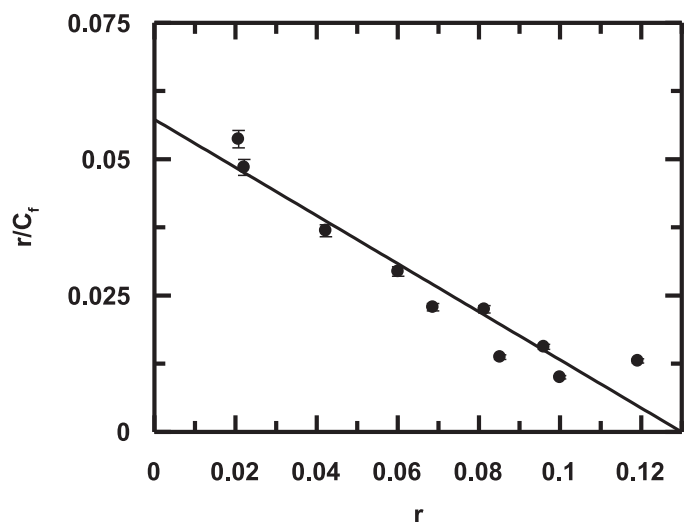


**Fig. 13.** A typical Scatchard plot (modified form of the original equation) showing interaction of  $\text{Na}[\text{Co}^{\text{II}}(\text{alz})_3]$  with calf thymus DNA that was followed by UV-Vis spectroscopy at 537 nm.  $\text{Na}[\text{Co}^{\text{II}}(\text{alz})_3] = 50 \mu\text{M}$ ;  $[\text{NaCl}] = 0.30 \text{ M}$ , pH = 7.40, Temperature = 301 K.

with  $\text{Co}^{\text{III}}(\text{alz})_3$  at different pH did not yield binding constant values any different from those of  $\text{Na}[\text{Co}^{\text{II}}(\text{alz})_3]$ .

Evaluation of binding constant values for alizarin with calf thymus DNA had earlier indicated a decreasing trend with increase in the pH of the medium [57,58]. In case of alizarin, an increase in pH leads to greater generation of anionic species and DNA being a negative polymer, its binding was affected. The same is

true for other hydroxy-9,10-anthraquinones as well [17,18,58]. For  $\text{Na}[\text{Co}^{\text{II}}(\text{alz})_3]$  however, binding constant values were higher than alizarin in the same pH range and importantly they were more or less constant over the entire range of pH over which titrations were performed (Table 5 & Fig. 16). This is significant because complex formation is able to arrest the decreasing trend observed in

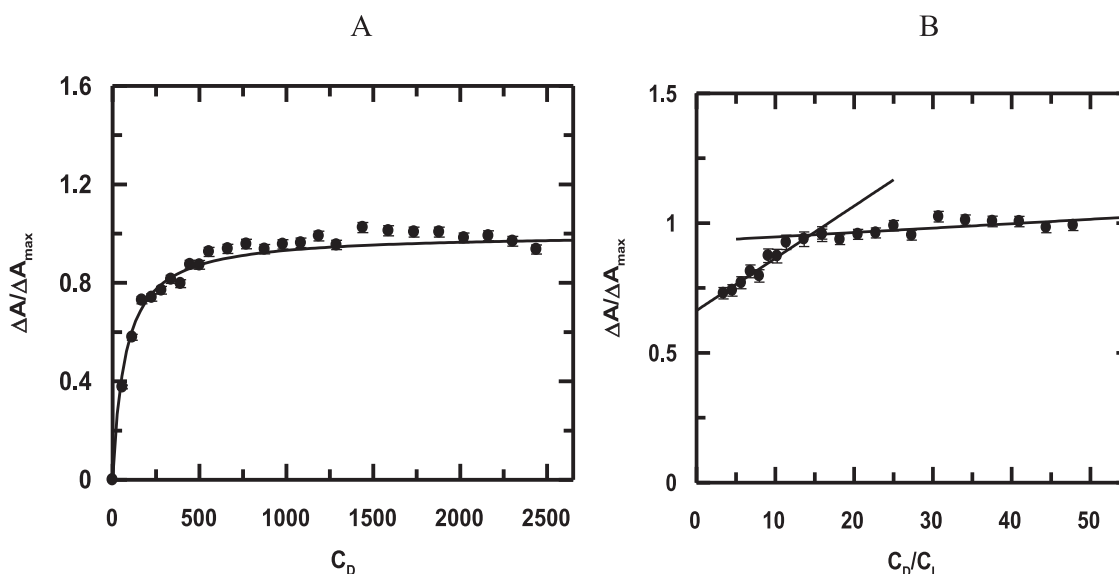


**Fig. 12.** (A) Binding isotherm of  $\text{Na}[\text{Co}(\text{alz})_3]$  with calf thymus DNA at an ionic strength of 0.30 M with respect to NaCl. The corresponding non-linear fit (Eq. 11) (B) Plot of normalized increase in absorbance as a function of the ratio of calf thymus DNA to  $\text{Na}[\text{Co}(\text{alz})_3]$ .  $\text{Na}[\text{Co}(\text{alz})_3] = 50 \mu\text{M}$ , pH = 7.40, T = 301K.

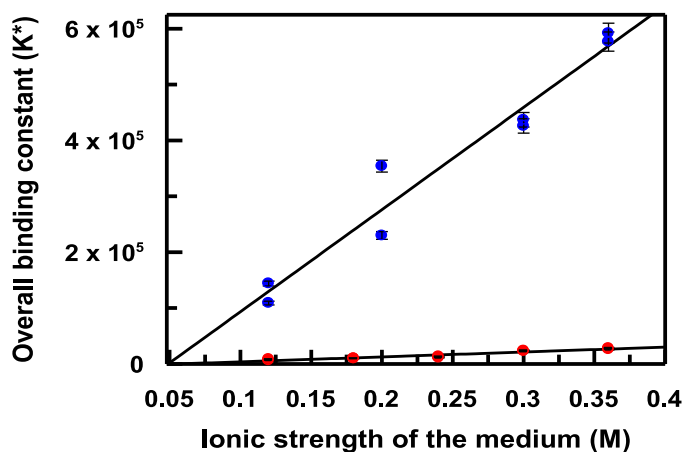


Fig. 14. Variation of overall binding constant of alizarin (·) and  $\text{Na}[\text{Co}^{\text{II}}(\text{alz})_3]$  (·) with calf thymus DNA at different ionic strength of the medium at pH  $\sim 7.4$ ; Temperature = 301K.

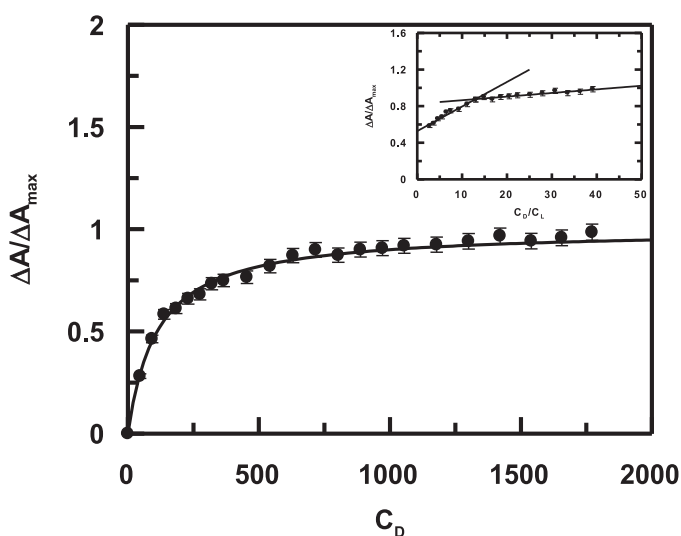


Fig. 15. Binding isotherm of  $\text{Na}[\text{Co}^{\text{II}}(\text{alz})_3]$  interacting with calf thymus DNA at pH 7.50. The corresponding non-linear fit is shown for the titration followed by UV-Vis spectroscopy. Inset: Plot of normalized increase in absorbance as a function of the ratio of calf thymus DNA to  $\text{Na}[\text{Co}^{\text{II}}(\text{alz})_3]$ .  $\text{Na}[\text{Co}^{\text{II}}(\text{alz})_3]$  = 50  $\mu\text{M}$ ,  $[\text{NaCl}]$  = 120 mM, Temperature = 301 K.

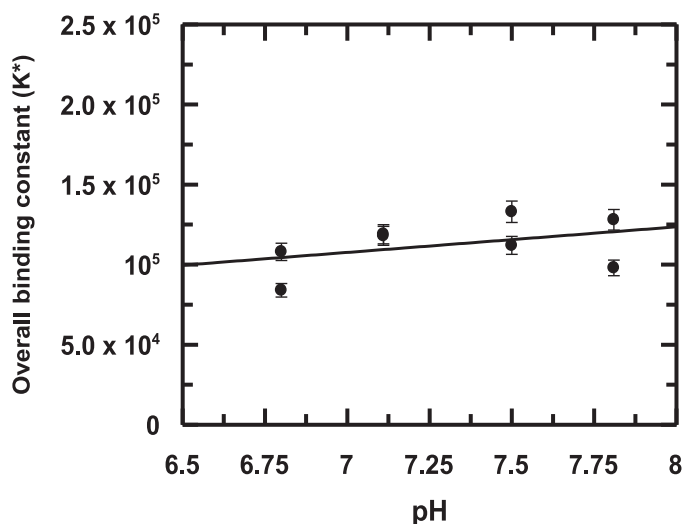


Fig. 16. Plot of a variation of overall binding constant of  $\text{Na}[\text{Co}(\text{alz})_3]$  interacting with calf thymus DNA at different pH (maintained using tris buffer) at 301 K and an ionic strength of 0.12 M with respect to NaCl. [Results of two independent experiments at each pH is shown].

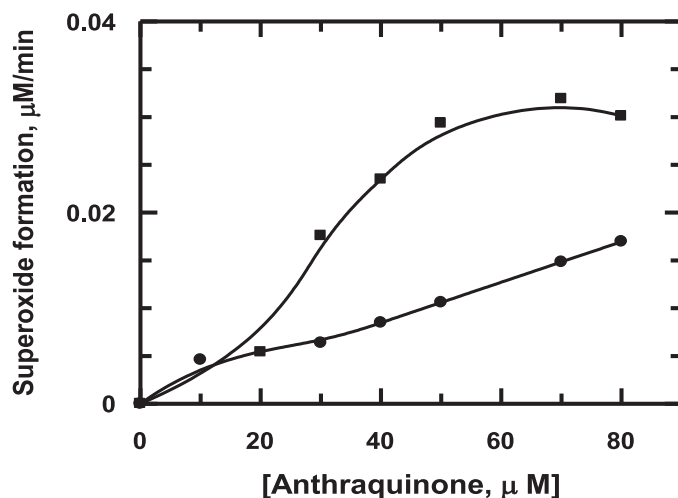


Fig. 17. A plot showing lack of stimulated superoxide formation by  $\text{Na}[\text{Co}(\text{alz})_3]$  in comparison to alizarin in NADH dehydrogenase catalyzed reduction of cytochrome c by NADH.

binding constant values for alizarin for an increase in the pH of the medium [57,58]. This is therefore an attribute of complex formation and important from a biological point of view since in some forms of cancer, patients experience a fluctuation in pH in body fluids [59–61].

Thus the complexes are able to overcome some of the problems reported for alizarin pertaining to binding with DNA. Since binding constant values for complexes are close to those known for standard anthracyclines [12,16,53], this substantially improves the chances of the complexes to be considered as potential anticancer agents that would be less costly than anthracyclines.

### 3.5. Alizarin and $\text{Na}[\text{Co}(\text{alz})_3]$ in NADH dehydrogenase assay to detect the generation of semiquinone

A serious drawback of hydroxy-9,10-anthraquinone based anthracycline anticancer agents is the generation of semiquinone radical anion, capable of forming superoxide radical anion, that are cardiotoxic and affects cancer patients adversely. At the same time, semiquinone and superoxide radical anions are necessary for cytotoxic activity having a role in mechanism of drug action [1,2,7–11,16–22]. Hence, owing to both positive and negative aspects associated with the formation of reduced oxygen species there is a need to have a correct balance in the generation of such intermediates so that efficacy and toxic side effects are such that it goes in favor of drug action benefitting the patient, i.e. minimizes adverse effects [1,2,7–11,16–22,24,33]. This is a major reason why complexes of hydroxy-9,10-anthraquinones (here alizarin) are studied; to be able to modulate the generation of semiquinone in a manner that cardiotoxicity is checked [33]. The compromise that a complex makes regarding efficacy in the free radical pathway is made up by some of its other attributes; facts that have compelled researchers to prepare metal complexes of hydroxy-9,10-anthraquinones and try them in enzyme assays. Monitoring the generation of superoxide radical anion inhibited by superoxide dismutase (SOD) is important to realize how much is achieved through complex formation. In our case, generation of superoxide radical anion in the presence of alizarin and its  $\text{Co}^{\text{II}}$  complex was followed by measuring reduction of cytochrome c inhibited by SOD [1,2,18,19,21,30,31,32,41]. As concentration of compounds increased, yield of  $\text{O}_2^{\cdot-}$  due to alizarin increased (Fig. 17) suggesting it catalyzes the flow of electrons from NADH to molecular oxygen in presence of NADH dehydrogenase. For the complex, however, formation of  $\text{O}_2^{\cdot-}$  was a lot less at similar concentrations. At

**Table 6**  
IC<sub>50</sub> values of compounds on three different cell lines.

Compounds	Normal human lung fibroblasts (WI 38)IC <sub>50</sub> value (μM)	SIHA cells IC <sub>50</sub> value (μM)	Hep G2 cells IC <sub>50</sub> value (μM)
Alizarin	126.0	79.0	108.0
Na[Co(alz) <sub>3</sub> ] or Co <sup>III</sup> (alz) <sub>3</sub>	98.0	38.0	67.0
*cisplatin [64]	30.0 ± 0.3	24.10 ± 0.15	(14.87 ± 1.22)
*Doxorubicin [63,65]	0.01	0.02	(4.68 ± 1.08)

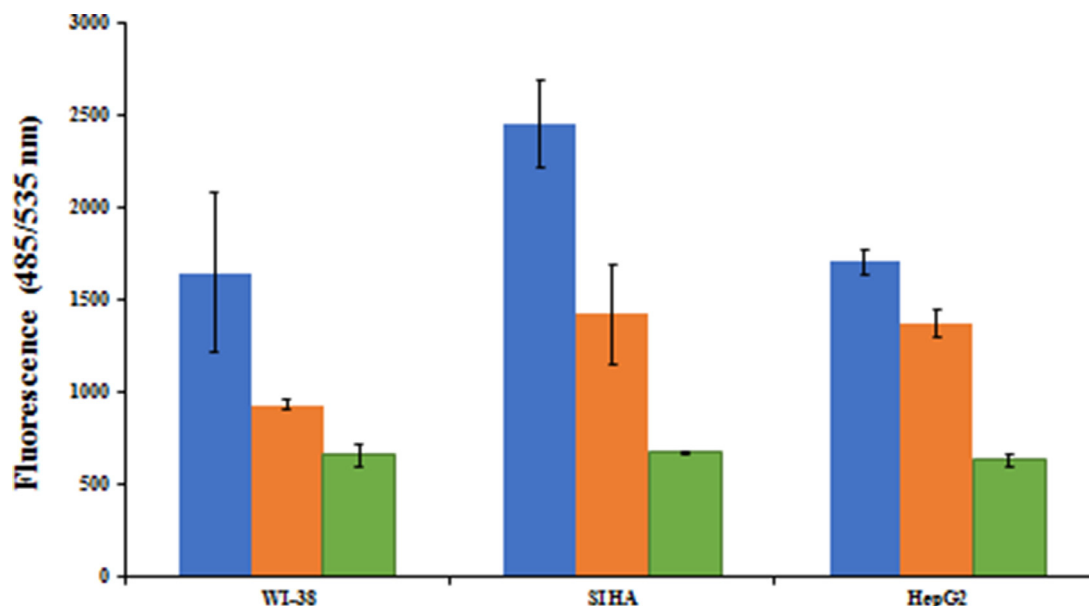


**Fig. 18.** Modulation of ROS generated by H<sub>2</sub>O<sub>2</sub> (~ 70 μM) in presence of alizarin (■) and Na[Co<sup>III</sup>(alz)<sub>3</sub>] (■). Presence of ROS in the absence of any compound is shown by (■). Difference in height for bars in blue is because the three cell lines are different and ROS due to the cell's own contribution being different gets added to ROS introduced from outside; Temperature = 301 K.

the same time, it should be mentioned here that the decrease was not as much as that obtained with complexes of metal ions having a stable lower oxidation state [1,2,18–20]. Co<sup>II</sup>, lacking a stable lower oxidation state, the decrease in its case was like that observed for Mn<sup>II</sup> complexes of hydroxy-9,10-anthraquinones reported earlier and not like Cu<sup>II</sup> or Fe<sup>III</sup> complexes [1,2,18–20]. For this complex, the carbonyl at C<sub>9</sub> of alizarin is involved in coordinating Co. Hence, the carbonyl not coordinated to the metal centre can form semiquinone (Fig. 17). However, immediately after such formation, the electron is transferred on to a metal centre located on an adjacent complex leading to its decrease [56]. As a result, semiquinone formation due to the complex decreases considerably, that is eventually successful in preventing them from being cardiotoxic (however, this couldn't be verified through experiments on cardiac muscle cells).

### 3.6. Effect of alizarin and complex on different cell lines

Cell viability assay performed with the compounds on normal human lung fibroblast (WI 38) cells and different cancer cell lines (SIHA and Hep G2) (Fig. S9, A–C, S1) indicate that the complex is more effective on all three cell lines. From the data in Table 6, it is clear that the performance of the complex on cancer cells was significantly better than on normal cells which is encouraging from the point of view of considering it as an anticancer agent. MTT assay indicates the complex is more effective on cervical cancer (SIHA) cells than Hep G2 cells and that although significantly weaker in performance in comparison to doxorubicin or cisplatin,

it is comparable to the reported activity of carboplatin and significantly better than Gemcitabine, all established drugs used in the treatment of cervical cancer [62–64]. Hence, findings suggest that Cobalt complexes of alizarin might have the potential to be an anticancer agent.

### 3.6. Detection of reactive oxygen species by H<sub>2</sub>DCFDA assay

An elegant approach to realizing the formation of ROS and its scavenging activity due to the complex was used by detecting them within cells by the H<sub>2</sub>DCFDA assay [40,44–46]. The complex and alizarin were investigated on cancer cell lines SIHA and HepG2 and on normal human lung fibroblast (WI-38) cells. As mentioned earlier, cells were previously treated with compounds at their respective IC<sub>50</sub> dose, determined by the MTT assay. For such treatment of cells, ROS was induced by adding H<sub>2</sub>O<sub>2</sub> (~ 70 μM).

ROS related experiments, where cells were not treated with any compound but only with H<sub>2</sub>O<sub>2</sub>, served as the control. In all three cell lines, depletion of ROS was greater for alizarin than for the complex. A result like this on the presence of ROS has a role related to the activity of compounds on a chosen cell line i.e. if we consider the free radical pathway to play a major role in the mode of action by compounds. Experiments on ROS clearly demonstrate why the complex performs better than alizarin on all three cell lines although the extent of damage is different. Although on all chosen cell lines ROS was found to be quenched to a maximum extent by alizarin, difference in presence of ROS due to compounds was larger and in favor of the complex on the two cancer cell lines.

Hence, Fig. 18 provides evidence why the complex performs better on cancer cells than on normal human lung fibroblast (WI-38) cells. Besides, biophysical interactions have also very clearly suggested why results on MTT assay are in favor of the complex. Going by the findings shown in Fig. 18, a prediction for the activity of the complex and of alizarin on normal human lung fibroblast (WI-38) cells should be the same if one considers the free radical pathway only, since difference in the presence of ROS is extremely small.

There is thus good correlation between sustenance (presence) of ROS on carcinoma (SIHA and HepG2) cells due to alizarin and the complex (Fig. 18) and that such trends were maintained in the results of the MTT assay (Table 6). This further suggests that free radical induced damage of cells is an important pathway for cytotoxic activity. Although not investigated as a part of this study, we reported earlier that a number of metal complexes of hydroxy-9,10-anthraquinones are effective inhibitors of human DNA topoisomerase I and human DNA topoisomerase II [18,19,21]. Therefore, this complex that is structurally similar to such previously reported metal-hydroxy-9,10-anthraquinone complexes, could well be a human DNA topoisomerase I and human DNA topoisomerase II inhibitor and this might serve as further reason for its superior anticancer activity.

#### 4. Conclusion

Complexes of alizarin with Co<sup>II</sup> and Co<sup>III</sup> were synthesized and characterized with the intention of realizing their performance on cancer cells and normal cells. Biophysical studies on interaction of alizarin and its Co<sup>II</sup>/Co<sup>III</sup> complex with calf thymus DNA and studies on ROS generation help us correlate results obtained in the MTT assay on SIHA, HepG2 (carcinoma) cells and on normal human lung fibroblast (WI 38) cells. Better efficacy due to the complex on cancer cells than on normal cells suggest there is some specificity towards cancer cells. This is encouraging from the aspect of cancer research. The complex was found to be clearly ahead on SIHA cells both with regard to ROS (identified by H<sub>2</sub>DCFDA assay) and with regard to findings of the MTT assay indicating the free radical pathway to be an important contributor to the overall mechanism responsible for anticancer activity. Besides, other attributes of complex formation like stronger binding to DNA, that unlike alizarin, tendency of the complexes to bind to DNA does not decrease with increase in pH or ionic strength of the medium might also explain better performance by the complex on cancer cells. Studies indicate normal cells are not much affected. Decrease in semiquinone radical anion by electron transfer from an electron donor (mimicking mitochondrial electron transfer) in case of the complex suggests it is likely to be less cardiotoxic. Hence, investigations with a cobalt complex pertaining to parameters that are usually followed to understand activities of anticancer agents help us realize antitumor activity keeping in mind aspects like induction of autophagy, cell cycle arrest, inhibition of cell invasion and P-glycoprotein (P-gp) activity.

Through this study, we were able to demonstrate that Na[Co<sup>II</sup>(alz)<sub>3</sub>] binds DNA better, thereby inducing cytotoxicity in cancer cell lines (SIHA and HepG2) compared to normal human lung fibroblast (WI-38) cells and that by scavenging ROS to a lesser extent than alizarin, the complex allows ROS to accumulate bringing about ROS mediated apoptosis.

#### Author statement

The following is an author statement outlining all authors' individual contributions using the relevant CRediT roles

**Mouli Saha, Soumen Singha, Deblina Ghosh:** Performed the experiments; analyzed and interpreted the data.

**Sanjay Kumar:** Conceived and designed the experiments; analyzed and interpreted the data.

**Parimal Karmakar:** Conceived and designed the experiments; analyzed and interpreted the data.

**Saurabh Das:** Conceived and designed the experiments; analyzed and interpreted the data; wrote the paper.

#### Declaration of Competing Interest

There are no conflicts of interest to declare.

#### Acknowledgements

MS acknowledges with gratitude UGC, New Delhi for a "Rajiv Gandhi National" fellowship (JRF & SRF). SD gratefully acknowledges UGC-DAE-CSR Collaborative Research Scheme for a project having sanction number UGC-DAE-CSR-KC/CRS/1 9/RC11/0985. He wishes to thank RUSA 2.0 program of the Government of India, operating at Jadavpur University, for a project having Sanction Ref. no. R-11/438/19 dated 30.05.2019 under the scheme "Research Support to Faculty Members" on the thrust area "Research in Sustainable Development". SD is grateful to DST-PURSE and UGC-CAS programs of the Government of India for financial support to Jadavpur University and the Department of Chemistry, Jadavpur University respectively from where funds were utilized for this work. Authors also acknowledge Govt. of India, for a grant to Department of Chemistry, Jadavpur University utilising which a mass spectrometer (Micromass-Q-Tofmicro<sup>TM</sup>, Waters Corporation) was purchased that was used in this study. MS is grateful to Mr. Tanmoy Saha for his help in organizing some portions of this manuscript.

#### Supplementary materials

Supplementary material associated with this article can be found, in the online version, at doi:[10.1016/j.molstruc.2022.133011](https://doi.org/10.1016/j.molstruc.2022.133011).

#### References

- [1] M.M.L Fiallo, A. Garnier-Suillerot, Physicochemical studies of the iron(III)-carminomycin complex and evidence of the lack of stimulated superoxide production by NADH dehydrogenase. *Biochim, Biophys. Acta.- Gen. Subj* 840 (1985) 91–98, doi:[10.1016/0304-4165\(85\)90165-5](https://doi.org/10.1016/0304-4165(85)90165-5).
- [2] M.M.L Fiallo, A. Garnier-Suillerot, Metal anthracycline complexes as a new class of anthracycline derivatives. Palladium(II)-adriamycin and palladium(II)-daunorubicin complexes: physicochemical characteristics and antitumor activity, *Biochemistry* 25 (1986) 924–930.
- [3] M. Volkova, R. Russell III, Anthracycline cardiotoxicity: Prevalence, pathogenesis and treatment, *Curr Cardiol Rev* 7 (2011) 214–220, doi:[10.2174/157340311799960645](https://doi.org/10.2174/157340311799960645).
- [4] A. Jabłońska-Trypuć, G. Swiderski, R. Krętoński, W. Lewandowski, Newly synthesized doxorubicin complexes with selected metals—Synthesis, structure and anti-breast cancer activity, *Molecules* 22 (2017) 1106, doi:[10.3390/molecules22071106](https://doi.org/10.3390/molecules22071106).
- [5] M. Kozsup, O. Domotor, S. Nagy, E. Farkas, E.A. Enyedy, P.Synthesis Bulyo, characterization and albumin binding capabilities of quinizarin containing ternary cobalt(III) complexes, *J. Inorg. Biochem* 204 (2020) 110963.
- [6] M.M.L Fiallo, A. Garnier-Suillerot, B. Matzanke, H. Kozłowski, How Fe<sup>3+</sup> binds anthracycline antitumor compounds, *J. Inorg. Biochem.* 75 (1999) 105–115, doi:[10.1016/s0162-0134\(99\)00040-9](https://doi.org/10.1016/s0162-0134(99)00040-9).
- [7] C. Vergely, S. Delemasure, Y. Cottin, L. Rochette, Preventing the cardiotoxic effects of anthracyclines: From basic concepts to clinical data, *Heart Metab* 35 (2017) 1–7.
- [8] S.E. Lipschultz, J.A. Alvarez, R.E. Scully, Anthracycline associated cardiotoxicity in survivors of childhood cancer, *Heart* 4 (2008) 525–533, doi:[10.1136/hrt.2007.136093](https://doi.org/10.1136/hrt.2007.136093).
- [9] M. Štěrbá, O. Popelová, A. Vávrová, E. Jirkovský, P. Kovaříková, V. Geršl, T. Šimůnek, Oxidative stress, redox signaling, and metal chelation in anthracycline cardiotoxicity and pharmacological cardioprotection, *Antioxid Redox Signal* 18 (2013) 899–929.
- [10] A.A. Lohade, R.R. Jain, K. Iyer, S.K. Roy, H.H. Shimpi, Y. Pawar, M.G.R. Rajan, M.D. Menon, A novel folate-targeted nanoliposomal system of doxorubicin for cancer targeting, *AAPS PharmSciTech* 17 (2016) 1298–1311, doi:[10.1208/s12249-015-0462-2](https://doi.org/10.1208/s12249-015-0462-2).

- [11] D. Cardinale, F. Iacopo, C.M. Cipolla, Cardiotoxicity of anthracyclines, *Front. Cardiovasc. Med* 7 (2020) 26, doi:10.3389/fcvm.2020.00026.
- [12] F. Perveen, N. Arshad, R. Qureshi, J. Nowsherwan, A. Sultan, B. Nosheen, et al., Electrochemical, spectroscopic and theoretical monitoring of anthracyclines' interactions with DNA and ascorbic acid by adopting two routes: Cancer cell line studies, *PLoS ONE* 13 (10) (2018) e0205764, doi:10.1371/journal.pone.0205764.
- [13] K. Shee, A.T. Kono, S.P. D' Anna, M.A. Seltzer, X. Lu, T.W. Miller, M.D. Chamberlin, Maximizing the benefit-cost ratio of anthracyclines in metastatic breast cancer: case report of a patient with a complete response to high-dose doxorubicin, *Case Rep Oncol* 9 (2016) 840–846.
- [14] M. Braun, V.R. Jacobs, S. Wagenpfeil, D. Sattler, N. Harbeck, U. Nitz, R. Bernard, W. Kuhn, A. Ihbe-Heffinger, Cost analysis comparing an anthracycline/docetaxel regimen to CMF in patients with early stage breast cancer, *Onkologie* 32 (2009) 473–481, doi:10.1159/000226211.
- [15] S.Y. van der Zanden, X. Qiao, J. Neeffjes, New insights into the activities and toxicities of the old anticancer drug doxorubicin, *FEBS J* (2020), doi:10.1111/febs.15583.
- [16] P.S. Guin, P.C. Mandal, S. Das, A comparative study on the interaction with calf thymus DNA of a Ni(II) complex of the anticancer drug adriamycin and a Ni(II) complex of sodium 1,4-dihydroxy-9,10-anthraquinone-2-sulphonate, *Jour. Coord. Chem* 65 (2012) 705–721.
- [17] S. Mukherjee, P.K. Gopal, S. Paul, S. Das, Acetylation of 1,2,5,8-tetrahydroxy-9,10-anthraquinone improves binding to DNA and shows enhanced superoxide formation that explains better cytotoxicity on JURKAT T lymphocyte cells, *Jour. Anal. Oncol.* 3 (2014) 122–129, doi:10.6000/1927-7229.2014.03.03.2.
- [18] P. Das, C.K. Jain, S.K. Dey, R. Saha, A.D. Chowdhury, S. Roychoudhury, S. Kumar, H.K. Majumder, S. Das, Synthesis, crystal structure, DNA interaction and *in vitro* anticancer activity of a Cu(II) complex of purpurin: dual poison for human DNA topoisomerase I and II, *RSC Adv* 4 (2014) 59344–59357.
- [19] P. Das, C.K. Jain, S. Roychoudhury, H.K. Majumder, S. Das, Design, synthesis and *in vitro* anticancer activity of a Cu(II) complex of carminic acid: A novel small molecule inhibitor of human DNA topoisomerase I and topoisomerase II, *ChemistrySelect* 1 (2016) 6623–6631.
- [20] B. Mandal, S. Singha, S.K. Dey, S. Mazumdar, S. Kumar, P. Karmakar, S. Das, Cu<sup>II</sup> complex of emodin with improved anticancer activity as demonstrated by its performance on HeLa and Hep G2 cells, *RSC Adv* 7 (2017) 141403–141418.
- [21] S. Mukherjee-Chatterjee, C.K. Jain, S. Singha, P. Das, S. Roychoudhury, H.K. Majumder, S. Das, Activity of Co<sup>III</sup>-Quinalizarin: A novel analogue of anthracycline-based anticancer agents targets human DNA topoisomerase, whereas quinalizarin itself acts via formation of semiquinone on acute lymphoblastic leukemia MOLT-4 and HCT 116 cells, *ACS Omega* 3 (2018) 10255–10266.
- [22] P. Das, D. Bhattacharya, P. Karmakar, S. Das, Influence of ionic strength on the interaction of THA and its Cu(II) complex with DNA helps to explain studies on various breast cancer cells, *RSC Adv* 5 (2015) 73099–73111.
- [23] N. Özenver, M. Saeed, L.Ö. Demirezer, T. Efferth, Aloe-emodin as drug candidate for cancer therapy, *Oncotarget* 9 (2018) 17770–17796, doi:10.18632/oncotarget.24880.
- [24] E.K. Akkol, I.I. Tatli, G.S. Karatoprak, O.T. A'gar, Ç. Yücel, E. Sobarzo-Sánchez, R. Capasso, Is emodin with anticancer effects completely innocent? Two sides of the coin, *Cancers* 13 (2021) 2733, doi:10.3390/cancers13112733.
- [25] Wei-Tian Wei, Sheng-Zhang Lin, Dian-Lei Liu, Zhao-Hong Wang The distinct mechanisms of the antitumor activity of emodin in different types of cancer (Review), *Oncology Reports* 30 (2013) 2555–2562, doi:10.3892/or.2013.2741.
- [26] G. Cozza, A. Venerando, S. Sarno, L.A. Pinna, The selectivity of CK2 inhibitor quinalizarin: A re-evaluation, *Biomed Res. Int.* 734127 (2015), doi:10.1155/2015/734127.
- [27] X. Li, H. Wang, J. Wang, Y. Chen, X. Yin, G. Shi, H. Li, Z. Hu, X. Liang, Emodin enhances cisplatin-induced cytotoxicity in human bladder cancer cells through ROS elevation and MRP1 down regulation, *BMC Cancer* 16 (2016) 578, doi:10.1186/s12885-016-2640-3.
- [28] YQ. Zang, YY. Feng, YH. Luo, YQ. Zhai, XY. Ju, YC. Feng, YN. Sheng, JR. Wang, CQ. Yu, CH. Jin, Quinalizarin induces ROS-mediated apoptosis via the MAPK, STAT3 and NFκB signaling pathways in human breast cancer cells, *Mol. Med. Rep.* 20 (2019) 4576–4586.
- [29] Y. Zhou, K. Li, S. Zhang, Q. Li, Z. Li, F. Zhou, X. Dong, L. Liu, G. Wu, R. Meng, Quinalizarin, a specific CK2 inhibitor, reduces cell viability and suppresses migration and accelerates apoptosis in different human lung cancer cell lines, *Ind. Jour. Cancer* 52 (2015) 119–124.
- [30] P.S. Guin, S. Das, P.C. Mandal, Studies on the formation of a complex of Cu(II) with sodium 1,4-dihydroxy-9,10-anthraquinone-2-sulphonate – An analogue of the core unit of anthracycline anticancer drugs and its interaction with calf thymus DNA, *Jour. Inorg. Biochem* 103 (2009) 1702–1710.
- [31] S. Roy, P. Mondal, P.S. Sengupta, D. Dhak, R.C. Santra, S. Das, P.S. Spectroscopic Guin, computational and electrochemical studies on the formation of the copper complex of 1-amino-4-hydroxy-9,10-anthraquinone and effect of it on superoxide formation by NADH dehydrogenase, *Dalton Trans* 44 (2015) 5428–5440.
- [32] B.R.J. Abdella, J. Fisher, A chemical perspective on the anthracycline antitumor antibiotics, *Environ. Health Pers.* 64 (1985) 3–18.
- [33] E. Monti, L. Paracchini, F. Piccinini, V. Malatesta, F. Morazzoni, R. Supino, Cardiotoxicity and antitumor activity of a copper(II)-doxorubicin chelate, *Cancer Chemother. Pharmacol.* 25 (1990) 333–336, doi:10.1007/BF00686232.
- [34] S. Das, A. Saha, P.C. Mandal, Studies on the formation of Cu(II) and Ni(II) complexes of 1,2-dihydroxy-9, 10-anthraquinone and lack of stimulated superoxide formation by the complexes, *Talanta* 43 (1990) 95–102.
- [35] Gaussian 09, Revision A.02 M.J. Frisch, G.W. Trucks, H.B. Schlegel, G.E. Scuseria, M.A. Robb, J.R. Cheeseman, G. Scalmani, V. Barone, G.A. Petersson, H. Nakatsuji, Gaussian, Inc, Li, X., Caricato, M., Marenich, A. V., Bloino, J., Janesko, B. G., Gomperts, R., Mennucci, B., Hratchian, H. P., Ortiz, J. V., Izmaylov, A. F., Sonnenberg, J. L., Williams-Young, D., Ding, F., Lipparini, F., Egidi, F., Goings, J., Peng, B., Petrone, A., Henderson, T., Ranasinghe, D., Zakrzewski, V. G., Gao, J., Rega, N., Zheng, G., Liang, W., Hada, M., Ehara, M., Toyota, K., Fukuda, R., Hasegawa, J., Ishida, M., Nakajima, T., Honda, Y., Kitao, O., Nakai, H., Vreven, T., Throssell, K., Montgomery, Jr., J. A., Peralta, J. E., Ogliaro, F., Bearpark, M. J. Heyd, J. J., Brothers, E. N., Kudin, K. N., Staroverov, V. N., Keith, T. A., Kobayashi, R., Normand, J., Raghavachari, K., Rendell, A. P., Burant, J. C., Iyengar, S. S., Tomasi, J., Cossi, M., Millam, J. M., Klene, M., Adamo, C., Cammi, R., Ochterski, J. W., Martin, R. L., Morokuma, K., Farkas, O., Foresman, J. B. and Fox, D. J Wallingford CT, 2016.
- [36] A.D. Becke, Density-Functional Thermochemistry. III. The role of exact exchange, *Jour. Chem. Phys.* 98 (1993) 5648–5652, doi:10.1063/1.464913.
- [37] C.T. Lee, W.T. Yang, R.G. Parr, Development of the Colle-Salvetti correlation-energy formula into a functional of the electron density, *Phys. Rev. B* 37 (1988) 785–789.
- [38] A.D. Becke, A new mixing of Hartree-Fock and local density functional theories, *J. Chem. Phys.* 98 (1993) 1372–1377.
- [39] S. Mandal, G. Das, H. Askari, Experimental and quantum chemical modeling studies of the interactions of L-phenylalanine with divalent transition metal cations, *J. Chem. Inf. Model.* 54 (2014) 2524–2535 Epub 2014 Sep 10, doi:10.1021/ci500500k.
- [40] G. Scatchard, The attractions of proteins for small molecules and ions, *Annals of the New York Academy of Sciences* 51 (1949) 660–672, doi:10.1111/j.1749-6632.1949.tb27297.x.
- [41] H.R. In Mahler, in: *Methods in Enzymology* 11, Academic Press, New York, USA; 1955, pp. 668–672. S. P. Colowick and N. O. Kaplan, eds.).
- [42] A. Pramanik, D. Laha, S. Chattopadhyay, S.K. Dash, S. Roy, P. Pramanik, P. Karmakar, Targeted delivery of “copper carbonate” nanoparticles to cancer cells *in vivo*, *Toxicol. Res.* 4 (2015) 1604–1612.
- [43] M. Dinda, U. Dasgupta, N. Singh, D. Bhattacharyya, P. Karmakar, PI3K-mediated proliferation of fibroblasts by Calendula officinalis tincture: implication in wound healing, *Phytother. Res.* 29 (2015) 607–616.
- [44] H. Wang, Joseph, Quantifying cellular oxidative stress by dichlorofluorescein assay using microplate reader, *Free Radical Biol. Med.* 27 (1999) 612–616.
- [45] O. Myhre, J.M. Andersen, H. Aarnes, F. Fonnum, Evaluation of the probes 2',7'-dichlorofluorescein diacetate, luminol, and lucigenin as indicators of reactive species formation, *Biochem. Pharmacol.* 65 (2003) 1575–1582.
- [46] A. Gomes, E. Fernandes, J.L. Lima, Fluorescence probes used for detection of reactive oxygen species, *J. Biochem. Biophys. Methods* 65 (2005) 45–80.
- [47] K. Nakamoto, Infrared and Raman spectra of inorganic and coordination compounds, 3rd edn., Wiley-Interscience, New York, USA, 1978.
- [48] O.L. Alves, Y. Hase, The infrared spectra of cobalt(II) halide complexes with trimethylphosphine oxide (TMPO), *Spect. Lett.* 15 (1982) 423–433.
- [49] V.I. Vovna, A.S. Chekh, V.V. Korochentsev, S.A. Tikhonov, I.S. Samoilov, Photoelectron spectra and electronic structure of Zn(II)bis-bidketonates with aromatic substituents by the PES, DFT, and OVGf, methods, *Jour. Mol. Struct* 1223 (2021) 128815.
- [50] F. Andrade, M.M. Roca-Melendres, E.F. Durán-Lara, D. Rafael, S. Schwartz Jr., Stimuli-responsive hydrogels for cancer treatment: The role of pH, light, ionic strength and magnetic field, *Cancers* 13 (2021) 1164, doi:10.3390/cancers13051164.
- [51] S. Senapati, A.K. Mahanta, S. Kumar, P. Maiti, Controlled drug delivery vehicles for cancer treatment and their performance, *Sig Transduct Target Ther* 3 (2018) Article 7, doi:10.1038/s41392-017-0004-3.
- [52] B. Manocha, A. Margaritis, Controlled release of doxorubicin from doxorubicin-polyglutamic acid ionic complex, *J. Nanomaterials*, 2010 (2010) 9 pages Article ID 780171, doi:10.1155/2010/780171.
- [53] F. Frezard, A. Garnier-Suillerot, Comparison of the binding of anthracycline derivatives to purified DNA and to cell nuclei, *Biochim. Biophys. Acta* 1036 (1990) 121–127 121–127.
- [54] J.M. Asara, J.S. Hess, E. Lozada, K.R. Dunbar, J. Allison, Evidence for binding of dirhodium bis-acetate units to adjacent GG and AA sites on single-stranded DNA, *J. Am. Chem. Soc.* 122 (2000) 8–13.
- [55] H.T. Chifotides, J.M. Koomen, M. Kang, S.E. Tichy, K.R. Dunbar, D.H. Russell, Binding of DNA purine sites to dirhodium compounds probed by mass spectrometry, *Inorg. Chem.* 43 (2004) 6177–6187.
- [56] J.L. Bear, H.B. Gray Jr, L. Rainen, et al., Interaction of Rhodium(II) carboxylates with molecules of biologic importance, *Cancer Chemotherapy Reports* 59 (1975) 611–620.
- [57] M. Saha, P. Nandy, M. Chakraborty, P. Das, S. Das, The importance of pK<sub>a</sub> in an analysis of the interaction of compounds with DNA, *Biophys. Chem.* 236 (2018) 15–21.
- [58] M. Saha, S. Singha, M. Chakraborty, S. Mazumdar, S. Kumar, P. Karmakar, S. Das, Characterization of a Mn<sup>II</sup> complex of alizarin suggests attributes explaining a superior anticancer activity: A comparison with anthracycline drugs, *Polyhedron* 173 (2019) 114104.
- [59] S. Mukherjee, P. Das, S. Das, Exploration of small hydroxy-9,10-anthraquinones as anthracycline analogues: Physicochemical characteristics and DNA binding for comparison, *Jour. Phys. Org. Chem.* 25 (2012) 385–393.
- [60] S.M. Noh, Measurement of peritoneal fluid pH in patients with non-serosal invasive gastric cancer, *Yonsei Med J* 44 (2003) 45–48, doi:10.3349/ymj.2003.44.1.45.

- [61] G. Hao, Z.P. Xu, L. Li, Manipulating extracellular tumour pH: an effective target for cancer therapy, *RSC Adv* 8 (2018) 22182–22192, doi:10.1039/C8RA02095.
- [62] S. GDas, A. Bhattacharya, P.C. Mandal, M.C. Rath, T. Mukherjee, One-electron reduction of 1,2-dihydroxy-9,10-anthraquinone and some of its transition metal complexes in aqueous solution and in aqueous isopropanol–acetone-mixed solvent: a steady-state and pulse radiolysis study, *Rad. Phys. Chem.* 65 (2002) 93–100.
- [63] R. Koivusalo, S. Hietanen, The cytotoxicity of chemotherapy drugs varies in cervical cancer cells depending on the p53 status, *Cancer Biol. Ther.* 3 (2004) 1177–1183, doi:10.4161/cbt.3.11.1340.
- [64] C.W. Lewis, R.M. Golsteyn, Cancer cells that survive checkpoint adaptation contain micronuclei that harbor damaged DNA, *Cell Cycle* 15 (2016) 3131–3145.
- [65] L.A. Lambert, N. Qiao, K.K. Hunt, D.H. Lambert, G.B. Mills, L. Meijer, K. Keyomarsi, Autophagy: a novel mechanism of synergistic cytotoxicity between doxorubicin and roscovitine in a sarcoma model, *Cancer Res* 68 (2008) 7966–7974.